



UNIVERSITY OF
BIRMINGHAM



Development of Corrosion Fatigue Testing in Sour Oilfield Environments

EngD Thesis

Dean Horspool

Dr Brian Connolly – Academic Supervisor

Dr Chris Fowler – Industrial Supervisor

Industrial Sponsor – Exova (*formerly Bodycote Testing Group*)

Date: 06/05/2011

UNIVERSITY OF
BIRMINGHAM

University of Birmingham Research Archive

e-theses repository

This unpublished thesis/dissertation is copyright of the author and/or third parties. The intellectual property rights of the author or third parties in respect of this work are as defined by The Copyright Designs and Patents Act 1988 or as modified by any successor legislation.

Any use made of information contained in this thesis/dissertation must be in accordance with that legislation and must be properly acknowledged. Further distribution or reproduction in any format is prohibited without the permission of the copyright holder.

Contents	Page No
1. Introduction	1
2. Business Context of the Project	5
3. Literature Review	9
3.1 Flexible Risers/Pipelines	9
3.1.1 Introduction	
3.1.2 Flexible Riser Wall Structure	
3.1.2.1 Carcass	
3.1.2.2 Liner	
3.1.2.3 Annulus	
3.1.2.4 Pressure Armour	
3.1.2.5 Tensile Armour	
3.1.2.6 Outer sheath	
3.1.2.7 Anti Wear Tape	
3.1.3 Failure Mechanisms for Tensile Armour	
3.1.3.1 General	
3.1.3.2 Wear	
3.1.3.3 Fatigue and Corrosion Fatigue	
3.1.3.4 Hydrogen Induced Cracking (HIC)	
3.1.4 Fatigue Design of Flexible Risers	
3.2 Materials used in Sour Oilfield Environments	26
3.2.1 Plain Carbon Steels	
3.2.1.1 Transformations and Crystal Structures of iron	
3.2.1.2 The iron-carbon equilibrium diagram	
3.2.1.3 Heating	
3.2.1.4 Cooling	
3.2.1.5 Formation of Pearlite	
3.2.1.6 Formation of Bainite	
3.2.1.7 Formation of Martensite	
3.2.1.8 Retained Austenite	

3.2.2 Materials used for Sour Service Applications

- 3.2.2.1 Carbon and Low Alloy Steel
- 3.2.2.2 Quench and tempered carbon steels
- 3.2.2.3 Cold Drawn Steels

3.3 Corrosion in Oil and Gas Production

38

3.3.1 Corrosion in the Annulus of a Flexible Pipe

3.3.2 Sour Gas Service

- 3.3.2.1 Mechanism of H₂S Corrosion
- 3.3.2.2 Corrosion of Carbon Steel
- 3.3.2.3 Promotion of Hydrogen absorption in the presence of H₂S
- 3.3.2.4 Types of Cracking in Wet H₂S-Containing Environments
- 3.3.2.5 Sulphide Stress Cracking (SSC)
- 3.3.2.6 Hydrogen Pressure Induced Cracking (HPIC) or Stepwise Cracking (SWC)
- 3.3.2.7 Stress Orientated Hydrogen Induced Cracking (SOHIC)/ Soft Zone Cracking (SZC)
- 3.3.2.8 Environmental Factors Affecting Cracking in H₂S-Containing Environments

3.3.3 CO₂ Corrosion

- 3.3.3.1 Introduction
- 3.3.3.2 Mechanism of CO₂ Corrosion
- 3.3.3.3 Corrosion of Carbon Steel
- 3.3.3.4 Partial Pressure of CO₂
- 3.3.3.5 Influence of Temperature
- 3.3.3.6 Influence of pH
- 3.3.3.7 Effects of H₂S Contamination

3.4 Stress Corrosion Cracking (Environmentally Assisted Cracking) 59

3.4.1 Stress Corrosion Crack-Propagation Mechanisms

- 3.4.1.1 Dissolution Models
 - 3.4.1.2 Mechanical Fracture Models
-

3.5 Fatigue and Corrosion Fatigue (CF)	68
3.5.1 Stress versus Life (S-N) Curves and Surface Effects	
3.5.2 Corrosion Fatigue Mechanisms	
3.5.3 Stages of Corrosion Fatigue	
3.5.3.1 Smooth Specimen $\Delta\sigma$ -Life method for High Cycle Fatigue	
3.5.3.2 Testing Techniques	
3.5.3.3 Data Acquisition	
3.5.4 Growth of Corrosion Fatigue Cracks	
3.5.4.1 Corrosion Fatigue Crack Growth Models	
3.5.4.2 Fracture Mechanics Characterisation of CF	
3.5.4.3 CF experimentation	
3.5.4.4 Variables Influencing CF	
3.5.5 Corrosion Fatigue in Carbon Steel Armour Wires for Flexible Oil and Gas Pipelines	
4. Scope of Work	92
4.1 Baseline Data - Lab Air Fatigue Test Series	
4.1.1 Axial Tension – Lab Air Fatigue Testing	
4.1.2 Four Point Bend - Lab Air Fatigue Testing	
4.2 Atmospheric Pressure Corrosion Fatigue Testing (Vs ‘Lab-air’ data)	
4.2.1 Artificial Seawater/1bar CO ₂ Investigation (Wire-1 & 2)	
4.3 Atmospheric Pressure Corrosion Fatigue Parameter Investigations	
4.3.1 Investigation of the Effect of Confinement (Wire-1)	
4.3.2 Investigation of the Effect of Test Frequency (Wire-2)	
4.3.3 Investigation of the Effect of Welded Samples (Wire-2)	
4.4 High Pressure Corrosion Fatigue Testing Parameter Investigation	
4.4.1 HPCF Qualification Test Series	
4.4.1.1 Introduction	
4.4.1.2 Deaeration Qualification Test	
4.4.1.3 Corrosion Fatigue Qualification Test Series	
4.4.2 Elevated Pressure CO ₂ with Trace Amounts of H ₂ S (7.08bar CO ₂ /0.15mbar H ₂ S) – Wire-1	

5. Methodology	113
5.1 Materials Characterisation Methodology	113
5.1.1 Metallographic Preparation	
5.1.2 Optical microscopy & SEM	
5.1.3 Tensile Testing	
5.1.4 Hardness Testing	
5.2 Generation of Baseline Fatigue Data in ‘Lab Air’	115
5.2.1 Axial Tension Test Configuration	
5.2.2 Four Point Bend Fatigue Testing in Lab Air	
5.3 Atmospheric Pressure Corrosion Fatigue (APCF) Testing	123
5.3.1 Requirements of Experimental Setup	
5.3.2 Test Method	
5.3.2.1 Load Method	
5.3.2.2 Sample Preparation	
5.3.2.3 Test Environment	
5.3.2.3.1 Preparation of a Test for Unconfined Conditions	
5.3.2.3.2 Preparation of a Test for Confined Conditions	
5.3.2.4 Fatigue Loading Parameters	
5.3.2.5 Testing Procedure	
5.4 High Pressure Corrosion Fatigue (HPCF) Testing	137
5.4.1 Requirements of Experimental Setup	
5.4.2 Test Method	
5.4.3 Load Method	
5.4.4 Sample Preparation	
5.4.5 Test Environment	
5.4.6 Elevated Pressure pH Measurements	
5.4.7 Fatigue Loading Parameters	
5.4.8 Testing Procedure	
5.4.9 Calculation of Gas Mix required to simulate pH ₂ S at Elevated Pressures	

6. Results and Discussion (Design and Development of Test Facilities)	150
6.1. Atmospheric Pressure Corrosion Fatigue Rig	150
6.1.1 Description of Test Facility	
6.1.1.1 General Description	
6.1.1.2 Actuating System	
6.1.1.3 Specimen fixture and Loading Chain	
6.1.1.4 Environmental Control and Containment System	
6.1.1.5 Materials Selection	
6.1.1.6 Data Acquisition and Monitoring	
6.1.2 Confinement Investigation Trial Testing	
6.2 High Pressure Corrosion Fatigue Rig	164
6.2.1 HPCF Testing Facility	
6.2.1.1 General Layout of HPCF Facility	
6.2.1.2 Extraction System	
6.2.1.3 Gas Lines	
6.2.1.4 Gas Detection/Alarm System	
6.2.1.5 H ₂ S Scrubber System	
6.2.2 General HPCF Test Machine Description	
6.2.3 Actuating System	
6.2.4 Specimen fixture and Loading Chain	
6.2.5 Environmental Control and Containment System (Autoclave)	
6.2.6 Materials Selection	
6.2.7 Data Acquisition and Monitoring	
7. Results and Discussion (Fatigue Testing)	197
7.1 Materials Characterisation	197
7.1.1 Microstructure	
7.1.2 Tensile Testing	

7.2 Fatigue Testing	206
7.2.1 Lab Air Fatigue Testing	206
7.2.1.1 Wire-1	
7.2.1.2 Wire-2	
7.2.2 Atmospheric Pressure Corrosion Fatigue Testing	223
7.2.2.1 Synthetic Seawater/1barCO ₂ Testing – Wire-1	
7.2.2.2 Synthetic Seawater/1barCO ₂ Testing – Wire-2	
7.2.2.3 Effect of Confinement (Wire-1)	
7.2.2.4 Investigation of Frequency Effect (Wire-2)	
7.2.2.5 Investigation of the effect of Welded Samples (Wire-2)	
7.2.3 High Pressure Corrosion Fatigue Testing	278
7.2.3.1 Qualification of High Pressure Corrosion Fatigue Test Rig	
7.2.3.2 Elevated Pressure CO ₂ with Trace Amounts of H ₂ S (7.08bar CO ₂ /0.15mbar H ₂ S) – Wire-1	
8. Summary & Conclusions	297
9. Further Work	301
10. Acknowledgements	303
11. References	304

Appendix 1 – Atmospheric Pressure Corrosion Fatigue Test Machine Drawings

Appendix 2 –High Pressure Corrosion Fatigue Test Machine Drawings

Thesis Layout

Thesis Layout

Environmental degradation of carbon steel tensile armour wires in the annulus of flexible Oil and Gas pipelines can pose a threat to their safe and continuous operation. (The annulus is the protective cavity within the wall of the pipe in which the load bearing armour wires are located). Specifically, the integrity of the wires is at risk when corrosive conditions prevail in the annulus environment which can result in premature fatigue failures compared to what would be expected in a benign environment such as air. Investigation of the corrosion fatigue behaviour of such components in corrosive oilfield conditions will aid the design of flexible pipelines and allow more accurate service life calculations.

This dissertation describes an investigation into the fatigue behaviour of tensile armour wires under corrosive oilfield conditions. Initially, a literature review will be presented discussing the design and application of flexible Oil and Gas pipelines and risers (Chapter 3.1). Corrosion issues associated with the Oil and Gas industry and specifically, the annulus of flexible pipelines will then be described in more detail to provide the reader some familiarity with the specific environmental conditions and to establish the terminology that will be used in the remainder of this document (Chapters 3.2-3.5).

In order to investigate the corrosion fatigue behaviour of the tensile armour wires, the first objective in the current research project was to develop test facilities and test

Thesis Layout

procedures capable of conducting commercial test programs in highly corrosive environments at both atmospheric and elevated pressure to the requirements of the Oil and Gas industry (Chapter 6). Particular emphasis is given to describe the testing equipment and testing procedure that has been developed, since this was an important aspect of this thesis and provided the framework that enabled the experimental programme which has been undertaken.

It should be noted that the worldwide experience of corrosion fatigue testing under such specific conditions as that encountered during Oil and Gas production is limited. What little information is available has been summarized and includes some research from a Joint Industry Project (JIP) sponsored by the flexible pipeline manufacturers and other oil majors (Section 3.5.5).

The bulk of the thesis discusses an experimental programme designed to investigate the effects simulated corrosive oilfield environments have on fatigue life as well as an investigation of the effects of different parameters of the corrosion fatigue test method (Chapter 7). An outline of the scope of work and experimental programme is provided in Chapter 4 (Figure 4-1).

1. Introduction

Increasing demands for fossil fuels throughout the developed and developing world has promoted the Oil and Gas industry to implement recovery strategies to oil reserves once thought to be economically unviable. These ‘new’ reserves are typically located offshore in deepwater (400-1500m) and ultra-deepwater (>1500m) fields. New technologies and associated materials advancements are required for installation of platforms, umbilicals, risers, flowlines and subsea pipelines in these severe, deepwater offshore environments. According to the International Energy Agency (World Energy Outlook 2009), estimates of known reserves located in such waters range from 160bn to 300bn barrels. Most of these reserves are in the waters of Brazil, Angola, Nigeria and the US. Progress towards extracting these reserves has been surprisingly rapid with deepwater production increasing from less than 200,000 barrels per day in 1995 to in excess of 5m in 2007. Ultra-deepwater production only began in 2004 and will reach 200,000 barrels per day by 2012. This number is only set to continue with huge investment in offshore facilities such as the \$500m Dalian Pioneer, the biggest offshore rig yet, currently under construction in China’s Liaoning Province which is capable of safely operating in waters up to 3048m deep (The New Economy, Spring 2011).

The development of flexible pipelines and risers has played a major role in enabling such rapid progression. Installation of these dynamic production components has been essential in allowing the Oil and Gas industry to develop fields in deeper and deeper waters, utilising floating production technologies (Figure 1-1).

1. Introduction

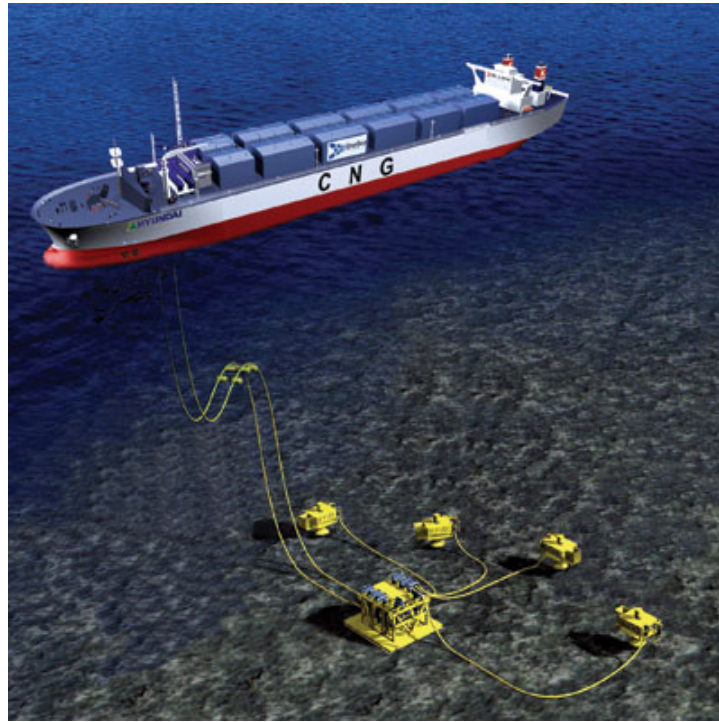


Figure 1-1 – Flexible flowline and riser system. Illustrating how flexible pipelines and risers are used to connect subsea production equipment to floating production facilities [1].

Structural integrity of the load supporting armour wires within the flexible pipe remains a concern within the industry. During service, the annulus environment located between the two polymer layers of the flexible pipe may become corrosive. Permeation of corrosive species from the produced fluids along with permeation and subsequent condensation of water in the annulus of the pipe may result in the development of an acidic aqueous environment.

If this situation occurs in service the structural integrity of the supporting carbon steel tensile armour wires located in the annulus may be at risk. The subsequent corrosion loss results in significant reductions in fatigue life as well as maximum tensile load bearing

1. Introduction

capacity. Such armour wires are also highly susceptible to hydrogen embrittlement and cracking in the presence of H_2S , which will significantly reduce fatigue life.

Fatigue has long been the limiting factor for the design life of these structures. Furthermore, effects of the environment within the pipe annulus have been largely overlooked and assumed to be benign resulting in fatigue design based on experimental results obtained via testing in air.

Therefore, the overall aims and objectives of the current research are, firstly to develop test equipment for commercial testing of components for flexible Oil and Gas pipelines at both atmospheric and elevated pressure, secondly to subsequently develop a repeatable testing procedure for corrosion fatigue testing under simulated oilfield conditions and, finally to investigate the corrosion fatigue behavior of tensile armour wire components of flexible Oil and Gas pipelines via fatigue life (S-N) experiments in simulated sour (i.e., H_2S rich production gas/fluids) and sweet (CO_2 rich production gas/fluids) oilfield environments.

A significant element of the current research project has been the design and development of the corrosion fatigue testing facilities along with the development of suitable testing procedures to meet the requirements of flexible Oil and Gas pipeline manufacturers.

The initial stages (i.e. the first two years) of the current research focused largely on the development of a test machine and procedures for corrosion fatigue testing in simulated

1. Introduction

sweet oilfield environments at atmospheric pressure and temperature. This machine has subsequently generated corrosion fatigue data in several different simulated Oil and Gas environments, the results of which form a major part of this thesis.

Following the success of the atmospheric corrosion fatigue test method, the second phase (i.e. years three and four) of the present research involved the design and development of a High Pressure Corrosion Fatigue test facility. This was driven by strong demand from within the Oil and Gas industry for corrosion fatigue data representative of service environments expected to be encountered on deepwater projects and in high pressure/high temperature reservoirs. In order to closely simulate complex environmental conditions inherent to such challenging production locations, test machines capable of testing up to 50 bar and 100°C in simulated oilfield environments (i.e. H₂S and CO₂ rich, produced fluids) have been developed and installed into a unique state-of-the-art Corrosion Fatigue Facility at Exova's Fatigue and Fracture Mechanics laboratory in Daventry, Northamptonshire, UK. These newly designed test facilities have enabled investigation of fatigue-life properties over a wide range of service environments and the data generated has contributed towards the technological advancement of flexible pipelines and risers.

2. Business Context of the Project

2. Business Context of the Project

The industrial sponsor of the current research project is Exova Group Ltd, formerly Bodycote Plc - Bodycote Testing Group, which operates more than 100 laboratories worldwide. As part of the Materials Testing division Exova Corrosion Centre is a world leading laboratory in the testing of pipeline materials for sour service environments. The laboratory offers an extensive array of corrosion testing and consultancy to the Oil and Gas industry ranging from small scale electrochemistry and hydrogen induced cracking tests through to full scale testing on pipelines up to 50 inch in diameter (i.e., full ring test). In addition to this, Exovas Fatigue and Fracture Mechanics facility provides the necessary expertise required to service such a multidisciplinary area as corrosion fatigue testing. The current research project aims to draw on the extensive experience of Exova and work in collaboration with both the corrosion and fatigue testing laboratories, located in Dudley and Daventry respectively.

As a world leader in materials testing for the Oil and Gas Industry, Exova have responded to increasing demand within the flexible Oil and Gas pipeline market for validation of the fatigue life of metallic components within the wall structure of the pipe (Fig 2-1) when exposed to a corrosive environment.

2. Business Context of the Project



Fig. 2-1 – Typical Cross Section of a Flexible Pipe Wall Structure [1].
(1) Stainless Steel carcass, (2) Thermoplastic Liner, (3) Carbon Steel Pressure Armour, (4) Carbon Steel Tensile Armour – 2 counter wound layers, (5) Thermoplastic Outer Sheath

This market demand has arisen due to the fact that in the as-fabricated state, void space in the pipe annulus (i.e., cavity between the two thermoplastic layers (5) and (2) in Figure 2-1) is filled with atmospheric air. As a result fatigue design of carbon steel armour wires in the annulus has been based on the assumption that the environment is benign [1]. However, during service the chemical composition and corrosivity of the annulus environment may change, due to several possible reasons which include:

1. Leakage due to damage of the outer polymer sheath, caused during installation or operation. This would lead to sea water flooding of the annulus. Depending on the nature of the leak, sea water in the annulus could be depleted of

2. Business Context of the Project

oxygen, or possibly saturated with air. Sea water may be combined with H₂S and/or CO₂ due to permeation from the bore fluid within the pipe.

2. Permeation of species from the product flow (hydrocarbons), notably water (H₂O) which may condense and accumulate in the annulus, and may become acidified by permeation and subsequent dissolution of acidic corrosive species such as; hydrogen sulphide (H₂S), carbon dioxide (CO₂) and methane (CH₄)

Each of these environments may have a significant effect on the fatigue life of carbon steel components and need to be considered in operation and design.

From a business perspective, the main task of the present research project was to enable Exova to exploit this niche in the market and be in a position to offer corrosion fatigue testing for life prediction as a commercial test method to flexible pipeline manufacturers.

As a result of the facility development work carried out as part of this thesis, Exova now work in collaboration with the two major manufacturers of flexible Oil and Gas pipelines (i.e., Technip Flexi France and Wellstream International) and have delivered several contracts where a significant amount of corrosion fatigue testing has been performed. Indeed, the development work carried out during the atmospheric pressure corrosion fatigue testing phase is now offered commercially as a standard in-house test method which has the potential to make a significant impact upon Exova's business objectives.

2. Business Context of the Project

This initial development work also led to Exova entering the market of High Pressure Corrosion Fatigue (HPCF) testing. Representing the second phase of the current research project, the development of HPCF testing machines culminated with the installation of a brand new, state-of-the-art Corrosion Fatigue Facility. This unique facility houses 8 bespoke HPCF test rigs capable of testing at up to 50bar and 100°C in simulated oil and gas environments. Commercially, the HPCF test method has already had an impact for Exova with the entire suite of newly built test machines occupied with long term, multi-million pound projects for the foreseeable future.

Indications from within the industry are that with more and more deepwater and sour projects on the horizon this demand is only set to increase. With corrosion fatigue facilities in place, Exova should be well placed to bid for such testing contracts, whether production based or research and design. The test method has proven to be a successful addition to the range of testing services offered by Exova.

3. Literature Review

3.1 Flexible Risers/Pipelines

3.1.1 Introduction

Unbonded dynamic flexible risers are a key integrating technology used for connecting subsea installations with surface Oil and Gas production facilities. The development of such pipes has allowed the industry to move away from the traditional fixed platform configuration to more modern floating production facilities, which are more viable for deepwater applications and marginal fields (Figure 3-1).

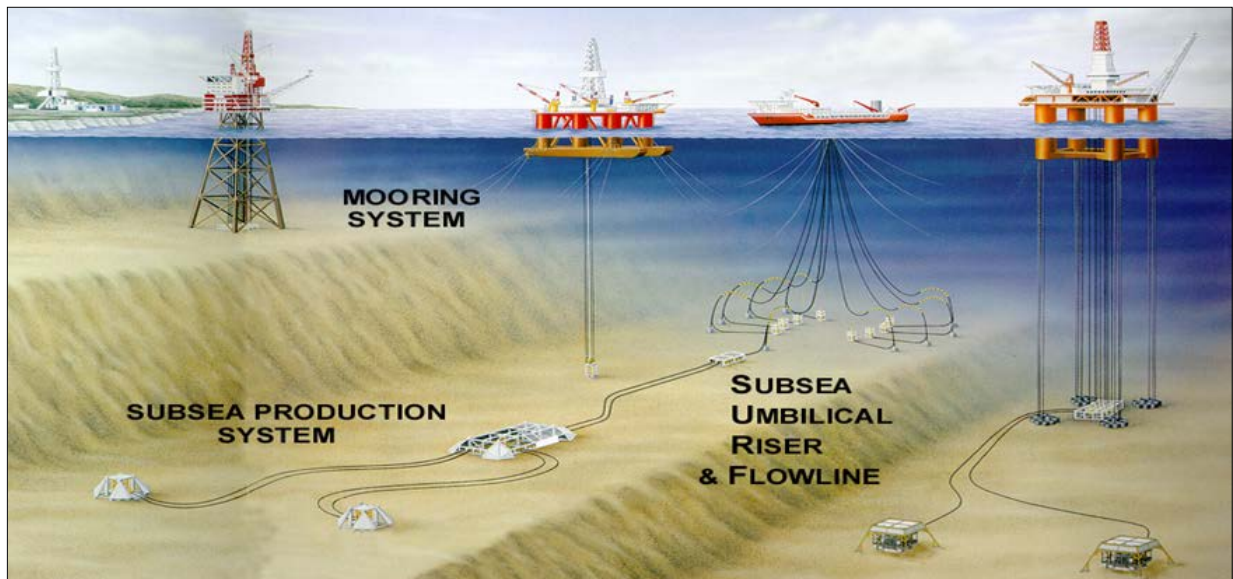


Fig 3-1 – Image showing a typical field layout utilising flexible dynamic risers to connect subsea installations with floating production facilities.

Flexible risers are used for a range of functions including; traditional flexible riser systems for floating production, storage and offloading (FPSO) developments, fluid transfer lines connecting offset riser systems to floating production units and export systems, or offloading lines connecting floating production units to offloading buoys.

3. Literature Review

The versatility of flexible pipelines to provide this range of applications is largely a result of their structure (Figure 3-2) which comprises the helical application of wires and tapes, and extruded thermoplastics to form a composite pipe structure which is designed to address field specific constraints such as, pressure, depth, temperature and produced fluid characteristics.

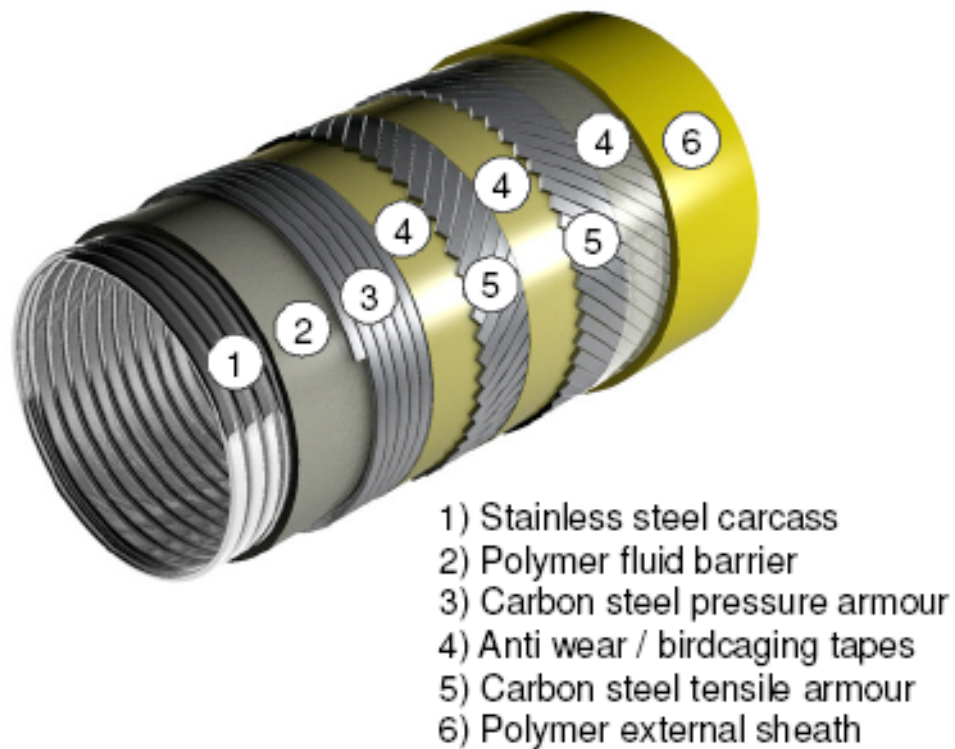


Fig 3-2 – Structure of an unbonded flexible pipe. Note the annulus void is located between the two polymeric sheaths (layers 2 and 6). It is the environment which develops in this location that will be simulated during the testing phase of this thesis [2].

3. Literature Review

There are numerous advantages to this strategy of combining the flexibility of polymer pipe with the strength and weight of a steel pipe, these include; relatively faster and easier installation and accommodation of misalignments, the option to remove and reinstall a pipeline due to changes in field architecture or for use on a marginal field, and the fact that external corrosion is minimised by encapsulating the steel armouring layers inside a continuous extruded polymer outer sheath.

Flexible pipelines used for production, injection or export are subjected to a number of conditions that may compromise the integrity of the riser. Due to the complicated nature of the wall structure where layers of different materials with very different properties are interacting, a large number of failure modes are possible. Many of these modes of failure are related to material properties. In this section the different layers of a flexible pipeline are outlined with respect to function, structure, material and possible modes of failure.

3.1.2 Flexible Riser Wall Structure

Figure 3-3 shows a cross section of the different layers contained within a flexible pipe.

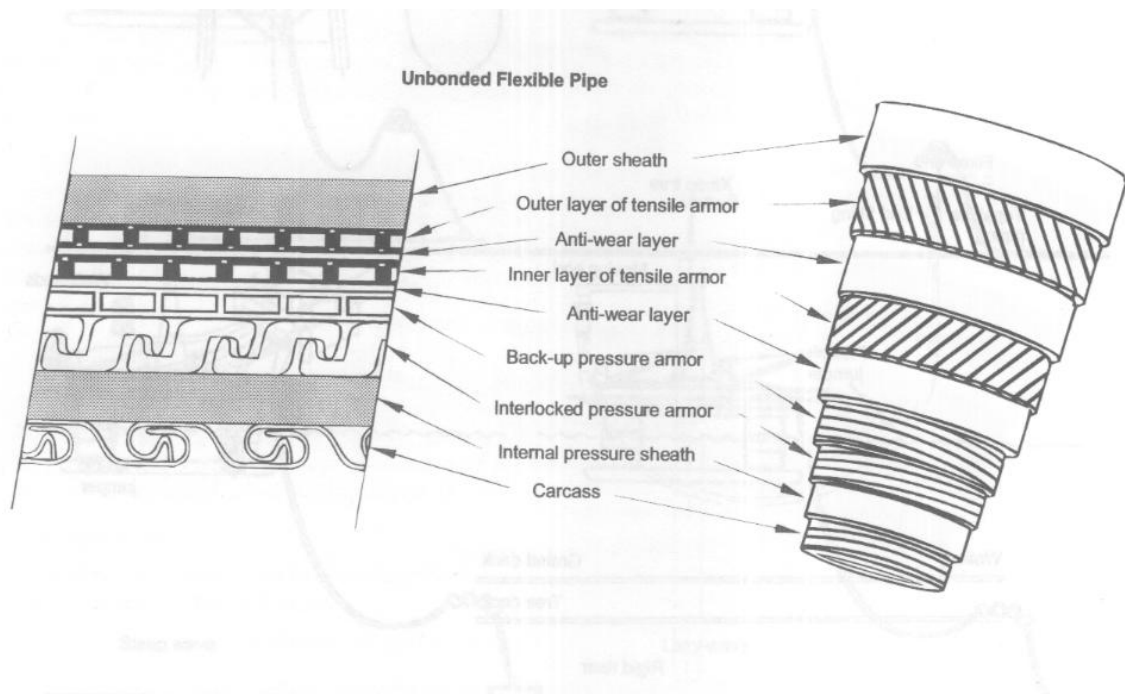


Fig 3-3 – Schematic showing the configuration of the different layers of a flexible pipe

3.1.2.1 Carcass

The carcass is the innermost layer of a pipe, and the only metallic component that is in direct contact with the production fluid in the bore. The carcass material is stainless steel, the exact grade will depend on the corrosivity of the produced fluids but typically AISI 316L or similar, which needs to be resistant to the chemical constituents of the transported liquids and/or gases.

The function of the carcass is to provide strength against external hydrostatic pressure and crushing loads to prevent collapse of the bore and loss of production. At large water

3. Literature Review

depths (deep, >400m/ultradeep water fields >1500m) hydrostatic and crushing loads are greatly increased to 243 Atm at a water depth of 1500m. This external hydrostatic pressure limits the size of pipe that can be used at such depths and also requires high strength materials however it is the internal bore pressure of the produced fluids which influences annulus pressures and therefore calculated test pressures and fluid compositions.

The carcass is an open structure and does not provide any containment of internal pressure, i.e. oil and gas can flow freely across the carcass. Flexibility in the structure is achieved by each profile being able to slide with respect to adjoining profiles.

If the outer sheath were damaged, the external pressure would act directly on the liner and must then be resisted by the carcass alone

3.1.2.2 Liner

The liner is the sealing layer, made from a thermoplastic by extrusion over the carcass. In some applications a multi-layer liner is used, with sacrificial layers on the inside and/or outside of the sealing layer. The purpose of the sacrificial layers is to provide protection against the metallic components. The liner is exposed to the fluid in the bore, and limits the upper service temperature of the riser and the chemical composition to the various fluids that may be transported through the line.

Different materials may be used depending on the design code. Three general classes of materials used as liner are;

- high density polyethylene (HDPE) and cross linked polyethylene (XLPE)

3. Literature Review

- Polyamide (nylon) (PA11 or PA12)
- Poly vinylidene fluoride (PVDF)

Within each class of materials a large range of properties are achievable. Some of the materials used are brand names, protected by patents or licenses e.g. Rilsan® (PA11 + plasticizer).

A major design parameter for selection of liner material is the design temperature of the riser system. In general, HDPE has very good chemical resistance and maintains good mechanical properties up to approximately 60°C. However, hydrocarbons like crude oil, methane and methanol are absorbed and may work as plasticizer. Therefore, if the bore fluid contains hydrocarbons, HDPE may be used at low and moderate temperatures only, generally below 20-30°C. Cross-linking may in general improve high temperature properties and in addition reduce the absorption of hydrocarbons, and thus XLPE may be used at somewhat higher temperatures than HDPE.

Polyamide materials may be used at higher temperatures but is very sensitive to humidity. In the case of a high water content, polyamide suffers from hydrolysis at elevated temperatures. The main mechanism of hydrolysis of PA11 and PA12 is chain scissoring (reduced molecular weight), causing brittleness. PVDF may be used at higher temperatures, possible 130°C with present brands. Typically 20% plasticizer is added to improve processing properties and reduce the possibility of defects (blisters). When in contact with hydrocarbons, the plasticizer tends to be extracted from the PVDF, leading

3. Literature Review

to permanent shrinkage of the material which can contribute to several failure modes associated with the liner material.

3.1.2.3 Annulus

The section between the liner and the external sheath is called the annulus of the pipe and this is where the carbon steel armouring components of the pipe are located. It is this area of the pipe that this project aims to simulate very closely and as such it can be a very specific environment in which there is a very large ratio of steel surface area to free volume resulting in very confined conditions which affects the chemistry of the environment.

The operating environment in the annulus is in principal determined by the following factors:

1. Diffusion of corrosive species from the produced fluids into and out of the annulus through the polymer layers;
2. Presence of water in annulus, seawater ingress from external damage or possible permeation from the bore and subsequent condensation;
3. Corrosion reactions.

Detailed descriptions of predicted annulus environments and prediction models have previously been given [3]. The main conclusions are:

3. Literature Review

1. The annulus of a flexible pipe may fill with condensed water due to permeation from the produced fluids in the bore through the polymer liner into the annulus. Alternatively, the annulus may also be filled with seawater as a result of damage to the outer sheath.
2. If the corrosive gases CO₂ and H₂S are present in the produced fluid they will permeate through the polymer liner. Once dissolved in any water present in the annulus an aggressive corrosive environment can form which puts the integrity of carbon steel armouring components at risk.
3. The pH in the annulus is found to be higher than predicted by normal corrosion models. A well established theory for this elevated pH is oversaturation of the solution with iron ions (Fe²⁺) due to the large ratio of steel surface area compared to solution volume in the annulus (V/S ratio) [4,5,6]. This is known as a confined environment and in the annulus of a flexible pipe this is a very important factor in determining the chemical composition of the corrosive environment. This effect has been investigated in the development phase of the test procedure, and is described in more detail in the confinement investigation section (section 6.1.7).

In summary, the annulus of a flexible pipe during normal operation can become corrosive as a result of the factors outlined above. In such situations the effect of the environment on the properties of the carbon steel armour wires, particularly fatigue life, needs to be investigated. This is the aim of the experimental plan in the current research project.

3.1.2.4 Pressure Armour

The primary function of the pressure armour is to resist the hoop stress generated as a result of internal pressure. The pressure armour is also a strength component with respect to external forces, e.g. crushing forces due to handling or accidental loading.

The pressure armour is an interlocking profile made from rolled carbon steel with tensile strength in the range 700-900 MPa. Three different profiles are currently in use, Zeta/Flexlok, C-clip and Theta. The interlocking of the pressure armour is a limiting factor for the minimum bending radius of the riser. If this limit is exceeded, the flexible line will suffer irreversible damage, resulting in perforation of the liner when subjected to internal pressure.

3.1.2.5 Tensile Armour

Tensile armouring wires for unbonded flexible pipes are produced from carbon or low alloy steels. Wire rods are cold drawn followed by a number of cold rolling steps resulting in a very accurate shape with a near rectangular cross section. This means that the final manufactured wire has a radius on the drawn edge of the wire and a rolled flat, smoother finish on the rolled surfaces (Figure 3-4).

3. Literature Review

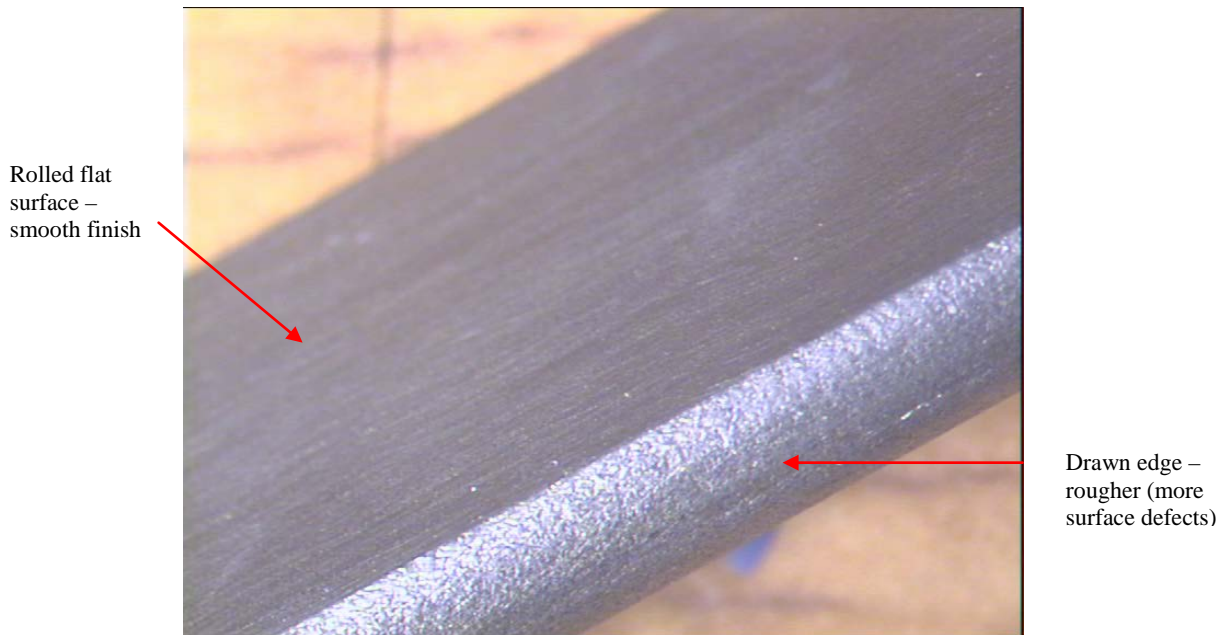


Figure 3-4 – Image of a tensile armour wire, showing the final manufactured wire. Note the as-drawn edges of the wire and the rolled flat, smoother finish on the rolled faces.

The flat carbon steel wires are counter wound in pairs and they provide strength against axial stress caused by internal pressure and by external loads as well as providing torsional strength and stiffness. However, for torsional loads in a direction leading to unwinding of the outer layer of armour wire, the strength and stiffness is poor.

Tensile armour wire can be produced in several different grades depending on the operating conditions the pipe is expected to experience. In general they are classified into one of three groups depending on strength (Table 3-1).

Table 3-1 – Different classes of tensile armouring wires [7]

Strength class	Yield strength (MPa) (approximate ranges)
Sour service	600-700
Basic sweet service	750-850
High strength sweet service	1100-1400

It is clear from table 1 that if the pipeline is expected to operate under sour conditions then the strength of the carbon steel armour wires needs to be limited in order to maintain resistance against hydrogen embrittlement. Under non-sour conditions where the flux of hydrogen into the steel is considerably less, the strength level can be correspondingly higher.

It is this component of the flexible pipe that is the test material for the current research project. As such, a detailed discussion of possible failure modes associated with tensile armour wires can be found in later sections.

3.1.2.6 Outer sheath

The primary function of the outer sheath is to provide a seal against sea water in order to prevent corrosion and to give mechanical protection to the steel armour wires. The loads typically applied on the outer sheath are: impact, erosion and tearing as well as, in certain cases, external or internal pressure. The material is extruded thermoplastic – HDPE or Rislant® (Polyamide PA-11).

3.1.2.7 Anti Wear Tape

In a flexible riser subjected to cyclic bending the steel armour will slide cyclically. If two layers of steel armour are in direct contact, wear may take place. For this reason anti wear tape is applied between layers of steel armour. The tape is not leak proof and fluids in the annulus may flow through the tape. The materials used are thermoplastic tape approximately 1mm thick. The tape is subjected to significant contact stress and large slip

amplitudes. Cumulative slip for a 20 year design life may be of the order $50 \cdot 10^3$ m. The tape must retain a minimum strength at the temperature of the armour wire and be wear resistant.

3.1.3 Failure Mechanisms for Tensile Armour

3.1.3.1 General

Potential failure mechanisms for tensile armour wire may be listed as:

- Overload in tension, causing tensile failure
- Overload in bending or compression causing wire disarray or ‘birdcaging’
- Overload in torsion causing unwinding of armour
- Fatigue
- Corrosion fatigue
- Fretting fatigue
- Wear
- Hydrogen Induced Cracking (HIC)
- Corrosion

Overload mechanisms of failure are related to design and operational conditions. The remaining modes can be related to material properties and may be linked.

3.1.3.2 Wear

Early designs of flexible risers consisted of tensile armour wires being laid directly against each other resulting in metal-metal contact. With this design philosophy, wear

was considered to be the limiting factor for service life of the riser. Wear life was assessed by rotating bend tests, which was a somewhat conservative test. Since around 1990 manufacturers have applied layers of polymer tape between layers of metallic armour. Provided this anti-wear tape can withstand contact pressure, this has proved to be effective, and wear is no longer considered a problem for tensile armour. However, the long term durability of anti-wear tape in demanding conditions has not been proved. If the anti-wear tape is compromised and significant wear is able to occur this would result in failure as a stress concentration would be produced. Failure could either be due to reduced cross section resulting in tensile overload, or due to fatigue/corrosion fatigue initiating at such stress concentrations.

3.1.3.3 Fatigue and Corrosion Fatigue

Design analysis has shown that fatigue of tensile armour wires may be critical with respect to design life [7]. In the as-manufactured condition, void space in the annulus of the riser is filled with atmospheric air. Due to this, fatigue strength criteria have been developed on the basis of fatigue tests in air, assuming the environment in the annulus of the riser to be benign. Service experience has shown that during operation the chemical composition of the annulus is likely to become corrosive [8] as a result of the following possible scenarios:

1. Leakage by damage of the outer sheath, caused during installation or operation, leading to sea water ingress into the annulus. Sea water in the annulus may be

3. Literature Review

- oxygen depleted or possibly saturated with air depending on the nature of, and distance from the leak. The flooded annulus may also be combined with hydrogen sulphide and carbon dioxide permeating from the product flow. Microbial Induced Corrosion (MIC) is also a possibility as sulphide reducing bacteria (SRB's) may develop in stagnant seawater.
2. Permeation of species from the bore, most importantly gaseous components hydrogen sulphide and carbon dioxide, possibly in combination with water from the produced fluids which may condense and accumulate in the annulus.
 3. Flexible pipelines which have been flooded with sea water have been repaired, flushed with inhibitor, and re-installed [8]. Inhibitor fluid, possibly with some residual sea water in combination with hydrogen sulphide and/or carbon dioxide permeating from the bore, could have an affect on residual fatigue life.

Carbon steel exposed to a hydrogen sulphide and/or carbon dioxide containing aqueous environment is susceptible to corrosion, and as a consequence, fatigue strength is likely to be affected. Figure 3-5 shows an example of the type of corrosion damage to the tensile armour wires that has been observed in service [8]. The image shows the tensile armour wires from a recovered riser where the annulus had been flooded with seawater which had been acidified by the presence of CO₂. This type of localised corrosion damage developed over a period of up to 2 years and it is clear that damage to this extent will have a significantly detrimental effect on fatigue life of the tensile armour wires. It is

3. Literature Review

operational experience such as this that has made the current research project of utmost importance to the Oil and Gas industry.



Figure 3-5 - Localised corrosion damage found on the tensile armour wires of a recovered riser. In this case the annulus had been flooded with seawater acidified by the presence of CO_2 . The wires may have been exposed for a period of up to 2 years [8].

3.1.3.4 Hydrogen Induced Cracking (HIC)

Carbon steel tensile armour wires are susceptible to HIC in H_2S and/or CO_2 containing aqueous environments. Tensile armour wires are generally classified on the basis of ‘sweet’ or ‘sour’ service, according to the criteria given by the National Association of Corrosion Engineers (NACE) in ISO15156 [9]. Sweet service refers to an environment containing only CO_2 whilst an environment is termed sour when H_2S is present.

3. Literature Review

Sour service wire generally has strength below 700 MPa. Sweet service wire has a tensile strength in the range 800-1400 MPa. Some operators will take a conservative approach to their specification for tensile armour, utilising sour service wire even if the well flow is initially sweet according to the NACE criteria. This conservatism is well founded since many wells that are initially sweet become sour throughout production life. The predominant cause of H₂S development is the use of sea water for re-injection, resulting in the development of sulphide reducing bacteria (SRB) inside the formation and subsequent reservoir souring.

3.1.4 Fatigue Design of Flexible Risers

In a typical dynamic application, flexible pipes are used as risers or jumpers connecting a floating production facility with the subsea architecture of the field. The floating production facility is moved by the action of; wind, waves and the tides resulting in bending and tension being transferred to the flexible pipes connected to the facility. Such dynamic loading results in alternating stresses being generated in the pipe where analysis and testing has shown that in general the steel armour wires are the most fatigue critical component with a near rectangular cross section.

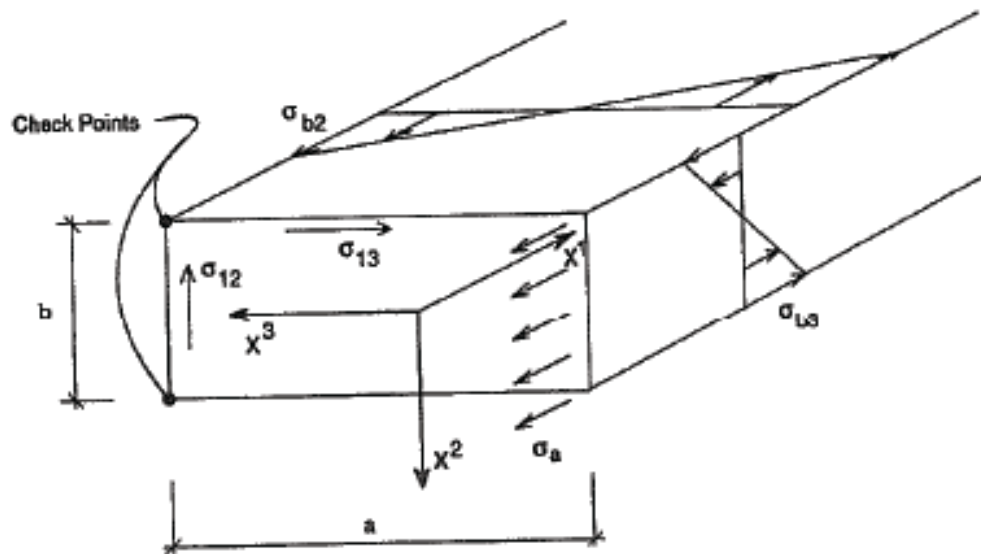


Figure 3-6 -Schematic showing the dynamic stress components on a tensile armour cross section [7]

The resulting stress on the flexible riser is a combination of cyclic loading and tensile stress, Berge et al (2003). When analysing a component, various check points are identified as typical initiation sites for on the tensile armour, an example shown in figure 3-6 [7]. Fatigue is identified at the corners of the sample; other companies have identified the initiation site at the apex of the edge, seen when the edges of the sample have been rounded. Prediction of alternating stresses within a flexible pipe is a complicated process and beyond the scope of the current research however the main conclusion is that S-N data for the tensile armour wire component is needed in relevant annulus service environments to accurately predict the service life of a flexible pipe.

3.2 Materials used in Sour Oilfield Environments

Materials used in sour service environments generally fall into two main categories; 1) Carbon or Low alloy steels and 2) Corrosion Resistant Alloys (CRA). The use of CRAs such as 13Cr and duplex stainless steels all the way up to Ni-based alloys has increased in the oil and gas industry due to a combination of pressures including; the production of more corrosive fluids, more hostile operating conditions, a requirement for improved reliability with associated, increasing, safety and environmental considerations. In addition to this there is constant pressure on the industry to reduce costs hence increasingly the trend is to seek the lowest overall cost of equipment ownership, rather than just its lowest initial cost. Whilst CRAs may offer the lowest life cycle cost they carry a heavy initial cost penalty. For this reason along with its availability, plain carbon steels remain the material of first choice for construction of oil and gas field production facilities.

3.2.1 Plain Carbon Steels

3.2.1.1 Transformations and Crystal Structures of iron

On heating pure iron from room temperature to its melting point it undergoes a number of crystalline transformations and exhibits two different allotropic modifications. When cooled these transformations take place in reverse order at approximately the same temperatures as on heating.

The two allotropic modifications are termed ferrite and austenite. Ferrite is stable below 911 °C as well as between 1392 °C and its melting point, under the names α -iron and δ -iron respectively. Austenite, designated γ -iron, is stable between 911 °C and 1392 °C.

3. Literature Review

The atoms in metals are arranged in a regular three-dimensional pattern, known as a crystal structure. In the case of iron it may be pictured as cubes stacked side by side and on top of each other. The corners of the cubes are the atoms and each corner atom is shared by eight cubes or unit cells. Other than the corner atoms the unit cell of iron contains additional atoms, the number of positions of which depends on the phase being studied.

Ferrite, has an additional atom at the intersection of the cube body diagonals, this is referred to as a body-centered cubic lattice (BCC). The length of the unit cube edge or lattice parameter is 2.87 \AA at $20 \text{ }^\circ\text{C}$. Austenite has a face-centered cubic lattice (FCC) which has an additional atom on each face of the cubic structure resulting in a lattice parameter 3.57 \AA (extrapolated to $20 \text{ }^\circ\text{C}$). Since the γ -iron unit cell contains more atoms it has a greater density than that of the α -iron cell, being 8.22 g/cm^3 and 7.93 g/cm^3 respectively.

3.2.1.2 The iron-carbon equilibrium diagram

The most important alloying element in steel is carbon. Its presence reduces the ductility but increases the strength and the susceptibility to hardening when rapidly cooled from elevated temperatures. At room temperature the solubility of carbon in α -iron is very low and therefore the carbon atoms are found very infrequently between individual iron atoms. Instead the carbon is combined to form iron carbide, (Fe_3C) also known as cementite. Cementite may be present as lamellae alternating with lamellae of ferrite, which together form a constituent called pearlite, which has a mean carbon content of

3. Literature Review

0.8%. The amount of pearlite found in the structure increases with the carbon content of the steel up to 0.8%. Carbon in excess of this amount separates as grain-boundary carbides. A steel containing 0.8% carbon is said to be eutectoid.

The phase transformations of the iron-carbon system are shown in the iron-carbon phase diagram, figure 3-7 For the sake of completeness the phase diagram shows up to 6.67% C where it can be observed that the solubility of carbon is much greater in austenite than in ferrite. It is evident from the lower left hand part of the iron-carbon equilibrium diagram that a steel with 0.17% carbon contains about 80% ferrite and 20% pearlite, while 0.5% and 0.8% carbon steels contain 60% and 100% pearlite respectively.

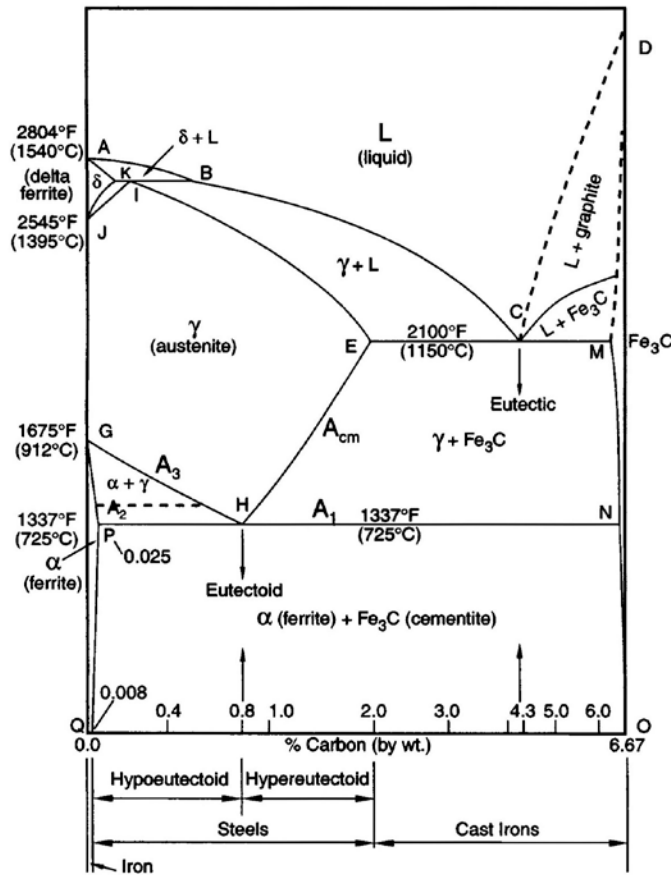


Figure 3-7- Fe-Fe₃C phase diagram [10]

3.2.1.3 Heating

As mentioned earlier, α -iron transforms to γ -iron on being heated to 912 °C. This can be seen by looking at the left hand vertical axis on Fig 2.1.3. In a steel containing 0.8% C (eutectoid), the transformation to austenite takes place around 725 °C. The temperature at which α -iron, γ -iron and cementite are at equilibrium is designated A_1 steels with less than 0.8% carbon, termed hypo-eutectoid steels, begin to transform from pearlite to austenite at the same temperature, approximately 725 °C. The test material for the current research project, the tensile armouring wire components are classified as hypo-eutectoid steels. In the equilibrium region between PH and GH there is austenite, formed from pearlite, and unchanged ferrite. The transformation is not complete until temperature A_3 given by the line GH is reached. Above this line austenite is the only stable phase. If the carbon content is more than 0.8% the steel is referred to as hyper-eutectoid. The pearlite in these steels also begins to transform to austenite at 725 °C but the cementite does not go into solution completely until the temperature rises above the equilibrium line HE, designated A_{cm} .

The course of events taking place during heating is thus, as follows. At 725 °C the transformation to austenite begins to take place in steels containing more than 0.025% carbon. This means that the atomic configuration changes from ferrite to austenite in which the carbon atoms are more soluble. At temperatures above G-H-E there is austenite only, all the carbon having been dissolved and evenly distributed throughout the austenite.

3.2.1.4 Cooling

As the temperature of a fully austenitized eutectoid plain carbon steel is slowly lowered below 725 °C the transformation from γ -iron to α -iron begins to take place and as a consequence the carbon is forced out of the lattice, due to the solubility in ferrite being less than that of austenite, and results in the formation of cementite. On complete cooling to room temperature the steel has once again its pearlitic structure.

The general appearance of the structure created during cooling is dependent on the temperature of transformation and on the time taken for the transformation to start. The transformation of a steel at a certain temperature can be investigated by cooling it from the austenitic state to the temperature concerned, allowing the transformation to take place and then quenching to room temperature. Using this technique the structure is locked in place and results in formation of various structural components such as martensite and bainite. In the following sections the formation of these structural constituents of steel will be discussed in further detail.

3.2.1.5 Formation of Pearlite

If a eutectoid steel is cooled from an austenitizing temperature of around 850 °C to 750 °C and held at this temperature, no transformation will take place. If the temperature is lowered to 650 °C pearlite will start to form and the transformation will be complete in 10 seconds. As the pearlite transformation temperature is lowered the pearlite lamellae become increasingly finer and the whole structure becomes harder. If the transformation of a hypo-eutectoid steel takes place at 750 °C, only ferrite separates and a state of

equilibrium is reached between ferrite and austenite. If the transformation takes place at 650 °C ferrite separates first followed by pearlite. Similarly, with hyper-eutectoid steels, cementite separates first followed by pearlite.

Pearlite formation is initiated at the austenite grain boundaries. Pearlite growth proceeds by branching and formation can be initiated on either ferrite or cementite. Platelets of cementite grow in juxtaposition since carbon transport from the austenite to the edges of the cementite platelets results in a simultaneous carbon impoverishment of the edges of the ferrite platelets.

3.2.1.6 Formation of Bainite

At temperatures below about 550 °C another constituent begins to separate along with pearlite, this is known as bainite. Its formation is assumed to be initiated on ferrite nuclei which grow as platelets from the grain boundaries. The carbon content of the surrounding austenite increases continuously until it has reached a limiting value, when platelets of cementite form in juxtaposition with platelets of ferrite.

Depending on the temperature of formation of bainite it is classified as upper or lower bainite, where upper bainite is relatively brittle and lower bainite is relatively tough.

3.2.1.7 Formation of Martensite

If cooling takes place rapidly, austenite will begin to form ferrite on reaching line M_S . As cooling proceeds below M_S there is a very small amount of carbon migration while the austenite is transforming. As a result the carbon atoms remain in solid solution in the α -

iron. Since the space available for carbon atoms is less in α -iron than in γ -iron the carbon atoms will expand the lattice. The resulting state of stress increases the hardness of the steel and the new constituent martensite is a supersaturated solution of carbon in α -iron.

3.2.1.8 Retained Austenite

Most of the austenite of a eutectoid steel will be transformed to martensite upon quenching to room temperature. Any austenite left untransformed is known as retained austenite. The amount of retained austenite in an unalloyed steel increases with carbon content. If the temperature is lowered to below room temperature the transformation to martensite continues by a process called subzero treatment. In a process called martempering the cooling is interrupted just above M_S and then the steel is allowed to cool to room temperature. By interrupting the cooling in this manner the austenite is stabilized, which causes the martensite formation to begin at a lower temperature, thereby resulting in a higher proportion of retained austenite at room temperature. Thus, a martempered or air hardened steel has in general a greater amount of retained austenite than an oil-hardened one.

As will be discussed in following sections low temperature transformation constituents such as martensite, bainite etc, may not be of practical use without first tempering them. This process results in a further change in microstructure which will give the steel a better combination of mechanical properties.

3.2.2 Materials used for Sour Service Applications

3.2.2.1 Carbon and Low Alloy Steels

Carbon and low alloy steels may be susceptible to cracking when exposed to corrosive H₂S containing environments, usually referred to as sour service. Failures of various items of H₂S containing production equipment and pipelines by various cracking mechanisms have led to requirements and recommendations being set for carbon and low alloy steels when exposed to corrosive H₂S containing environments, these guidelines form the international standard NACE MR0175/ISO15156 [9]. Among these sour service resistant material criteria the influence of hardness is most remarkable on sulphide stress cracking (SSC). The standard states that base carbon steels should feature a max hardness of HRC 22 as well as contain less than 1% Ni. These requirements can be relaxed in mildly sour environments where fit-for-purpose testing demonstrates adequate sour service resistance. NACE MR0175/ISO15156 also specifies that quenched and tempered Cr-Mo steel can be used in any sour environment provided that its hardness is below HRC 26 and its maximum yield strength is restricted to 760 MPa.

Since quench and tempering are the most common heat treatment for carbon steels for sour service including the armour wires tested in this project [4], as such these materials will be focused on in more detail in the following section.

3.2.2.2 Quench and tempered carbon steels

Carbon steel is usually heat treated by raising it through the eutectoid transformation temperature, approximately 50°C into the single phase austenitic field, holding it there long enough to dissolve the cementite and disperse the carbon uniformly, and then cooling to room temperature. Speed of cooling is critical to obtain the desired properties and most carbon steels for sour service are rapidly cooled or ‘quenched’ in a liquid bath, which is then followed up by a tempering treatment. The purpose of giving the steel such a heat treatment is to give it a fine grained ferritic-pearlitic structure which will result in higher strength and toughness values than what a simple normalizing treatment will give. In the as-quenched condition martensite is too brittle for practical use. The steel must be tempered to improve its toughness. At higher temperatures (above 400°C) this tempering treatment also substantially softens carbon steel and in practice a balance has to be struck between requirements of toughness and hardness. For treatments of about 1 hour duration the first stage of tempering is the precipitation of ϵ -carbide at about 100°C with a corresponding drop in the carbon content of the martensite to approximately 0.25 wt% C. At about 250°C retained austenite decomposes, and at about 350°C particles of cementite (Fe_3C) begin to form replacing the ϵ -carbide and reducing the low carbon martensite to ferrite. This is particularly important in carbon steels intended for use in sour service since the guidelines for materials requirements in EFC 16 [11] specify that the microstructure must be homogenous and free from regions of untempered martensite. The control of microstructure is vital due to the hardness limits placed on sour service carbon steel. To eliminate deleterious crack sensitive microstructures strength needs to be limited

and measuring bulk hardness is a convenient way to check the strength of materials having homogenous microstructures. EFC 16 recommends that hardness is limited to values in the range ≤ 250 HV30 (22 HRC). However, the hardness at which a steel is resistant to H₂S cracking mechanisms is dependent upon the severity of the environment and loading profile. Therefore, the guidelines for allowable hardness levels may be relaxed in mildly sour environments provided appropriate testing demonstrates adequate resistance. This is likely to be the case when testing carbon steel armour wires, as the partial pressures of H₂S usually encountered in the annulus environment of a flexible pipe are relatively low (mbar) compared to the 1bar H₂S conditions that the guidelines refer to.

3.2.2.3 Cold Drawn Steels

Carbon steel armouring wires for unbonded flexible pipes are produced from cold drawn wire rods followed by a number of cold rolling steps each reducing the cross section of the wire by both axial tensile stresses and transverse compressive stresses to give the desired dimensions very accurately. This manufacturing process (cold drawing) induces strong plastic deformations able to cause important microstructural changes [12, 13] and induce progressive anisotropy in the material which can influence fracture behaviour and stress corrosion performance of the steel.

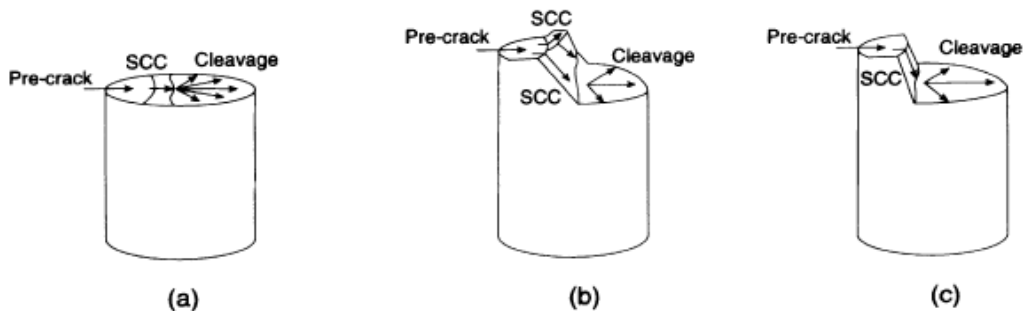
The cold drawing process consists of passing the wire rod through a series of dies until the required cross sectional area is achieved. Each reduction in area is achieved by

3. Literature Review

plastically deforming the steel resulting in a corresponding increase in ultimate tensile strength (UTS). Using this procedure it is possible to obtain yield strengths that range

from 686 MPa in an undrawn material up to 1506 MPa in a fully drawn material [14]. In this case the microstructures can be seen to be clearly different between the undrawn and fully drawn material in the longitudinal direction (parallel to the drawing direction). Although all of the steels consisted of fine pearlite the undrawn material has a randomly oriented microstructure and no preferential orientation angle with respect to the loading axis. In contrast, in the fully drawn steel the pearlite plates tend toward an alignment in the drawing direction. Transverse sections of the same material maintain a randomly oriented appearance regardless of the extent of cold drawing applied [13].

The microstructural orientation effects associated with cold drawn steels described above enhance the classical mechanical properties of the steel but also have an influence on the time dependant behaviour in a corrosive environment. This may seriously affect the fracture behaviour which is potentially dangerous when these materials are exposed to a corrosive environment. This is summarised in figure 3-8 where it shows how the crack growth path changes in a corrosive environment as the level of cold drawing is increased.



3. Literature Review

Fig 3-8 – Change in the SCC crack growth path as the level of cold drawing is increased, a) low, b) intermediate and c) high levels of cold drawing [15].

For isotropic materials with low levels of cold drawing (fig 3.2.2.3-a) the SCC crack growth path was in the same plane as the fatigue crack in a direction perpendicular to the loading axis. As the level of cold drawing increases (figs 3.2.2.3-b&c) the fracture propagation direction changes and grows at an increasing angle to the fatigue plane. This suggests a relationship between the microstructural orientation process of the pearlitic plates and the crack propagation path [15].

3.3 Corrosion in Oil and Gas Production

Hydrocarbon production is often associated with corrosive species such as the acid gases; H_2S and CO_2 . The first condition for any corrosion process to develop is the presence of water, which almost always co-exists with hydrocarbons in the reservoir. The ratio of water to the produced fluid is known as the 'water cut'. With increasing water cut, water wetting of production pipelines is increased and as a result the produced fluid becomes more corrosive.

When considering corrosion in oil and gas production, one key characteristic of the environment is the absence of oxygen which results in a less noble corrosion potential compared to that of atmospheric and seawater environments. The lack of oxygen in the produced fluids relates to the fact the oxygen has all been consumed in the formation of minerals and oxides as a result of reactions with reducing chemicals such as hydrocarbons and hydrogen sulphide.

The corrosivity of a production pipeline is generally governed by the presence of corrosive elements contained within the produced fluids in particular the acid gases H_2S and CO_2 . Where this is the case corrosion mitigation needs to be engineered into the development scheme or the effect of environment needs to be considered at the design stage when calculating design lifetimes. H_2S and CO_2 partial pressures reaching several tens of MPa are encountered in oil and gas production. General and localised corrosion are key issues in CO_2 environments, whereas embrittlement and cracking is of major concern in H_2S environments. Each of these environments or a combination of the two can potentially develop in the annulus of a flexible pipe in the presence of an aqueous

3. Literature Review

phase and therefore shall be discussed further in the following sections. Firstly, it is appropriate to review some of the literature specific to the unique conditions encountered in the annulus of flexible oil and gas pipelines and risers.

3.3.1 Corrosion in the Annulus of a Flexible Pipe

The annulus void of a flexible pipe lies between the pressure sheath (liner) and the outer polymeric sheath of the structure and is the area of the pipe where the carbon steel armouring components are located (Figure 3-9).

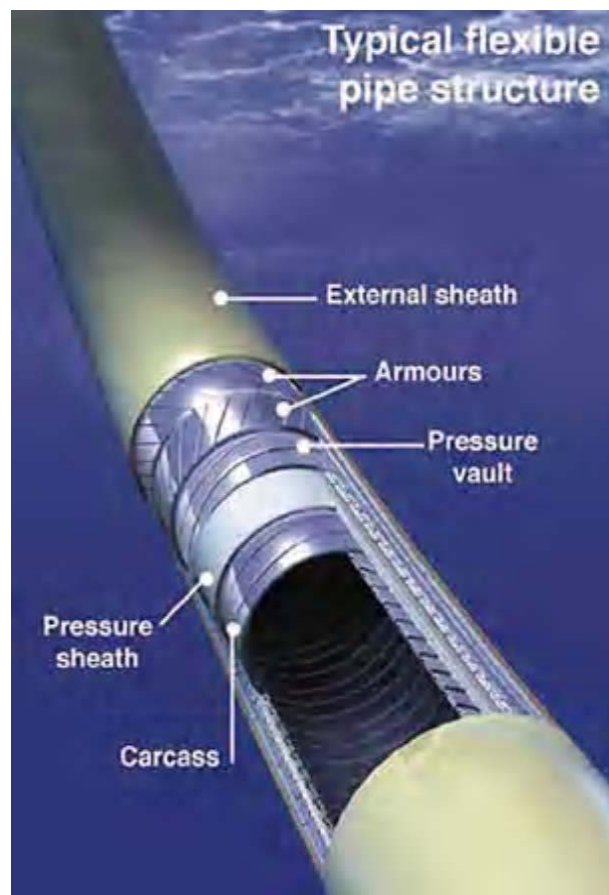


Fig 3-9 – The structure of an unbonded flexible pipe. The annulus environment is located between the two polymeric components of the pipe - the liner and the outer sheath [Image courtesy of Technip Flexi-France]

3. Literature Review

The unique conditions in the annulus of a flexible pipe create a very specific environment in which corrosion can occur. The confinement (the ratio of electrolyte free volume to free corrosion surface area on the armour wires) of the steel wires in the annulus contributes to the creation of this specific environment and it has been shown to have a significant effect on annulus corrosion rates [5]. Corrosion can be caused by permeation of CO₂ and/or H₂S from the bore of the pipe through the polymer barrier into the annulus along with water permeation and subsequent condensation resulting in an acidic fluid environment. As noted in previous work which assessed the corrosivity of this environment [4-6, 16-17] the corrosion conditions in the annulus of a flexible pipe can be very corrosive and determination of an applicable corrosion rate was necessary. Each of the papers in the public domain had a different focus to the research but aspects can be compared to try and understand the corrosion in the annulus of a flexible pipe.

A paper presented at Eurocorr (2000) [5] provided important information about the effect of confinement on the corrosion rate. Further work from the Nace Corrosion conference (2006) [4] investigated corrosion behaviour with very low levels of confinement, building on and validating the previous research. Work presented at OMAE (Offshore Mechanical Arctic Engineering) in both CO₂ and H₂S conditions investigated the effect of a transition between a gaseous saturated environment and a liquid environment [16], and went on to perform longer term liquid environment tests in a sour environment [17]. Testing also artificially acidified the test solution making the test more conservative, but did not take into account the confinement ratio.

3. Literature Review

Previous Work by Technip Flexi-France [5]

Data from this research indicates the corrosion rate (mm/yr) decreases in a logarithmic form versus the confinement V/S (ml/cm^2), figure 3-10. Minimum confinement tested was $0.25 \text{ ml}/\text{cm}^2$ which is still a lot higher than the actual estimated confinement value of $0.03 \text{ ml}/\text{cm}^2$ in the annulus. Test environments and durations used in this research were not consistent so there may be a margin of error in these results however the overall trend of reducing corrosion rate with increased confinement is clear and was the major finding of the study.

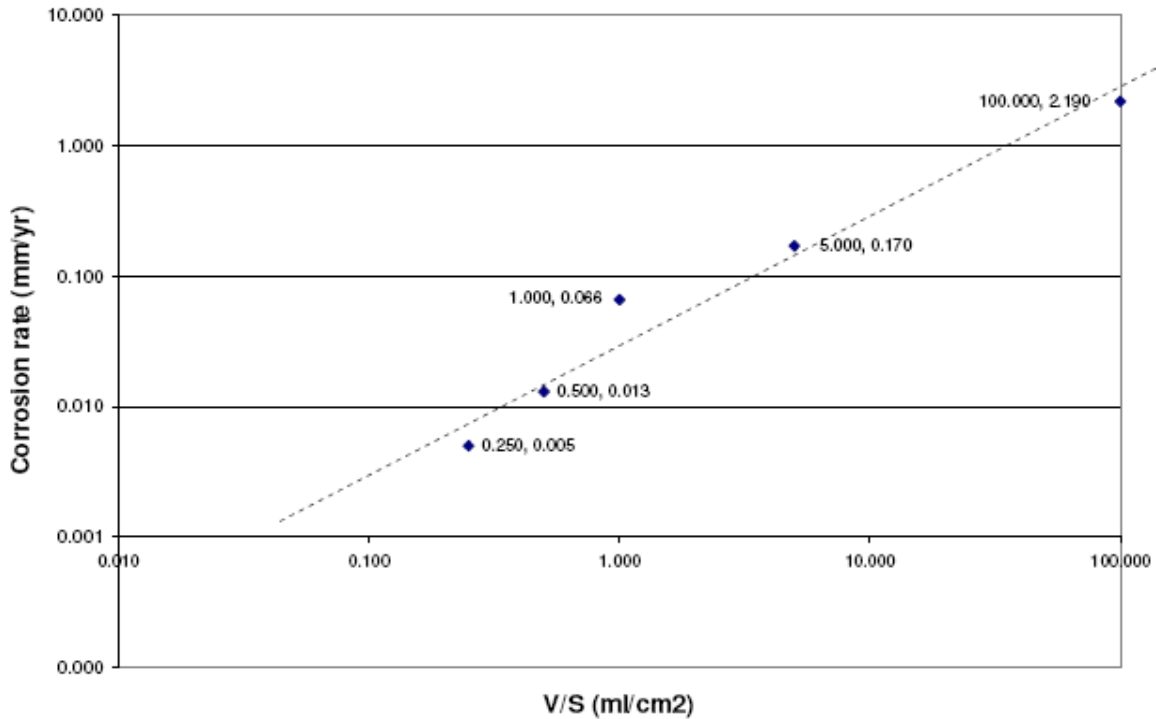


Fig 3-10 – Findings of Eurocorr 2000 paper [5], showing the trend of reduced corrosion rates with high levels of confinement.

3. Literature Review

Previous Work by NKT Flexibles [4]

Results from this research show similar corrosion rates as reference [5]. Importantly the two studies conduct the testing using similar volume to surface area ratios. The results demonstrate a slight difference between deionised water and seawater fluid environments, and also clearly show that with the same confinement the corrosion rate decreases over time. The greater confinement levels used in this study, likely contributed to the greater difference between the fluid environments that reported in OMAE 2003 [17]. With much higher confinement the solution chemistry would be different with significantly higher iron concentrations and different pH values which could alter scale formation rates, resulting in different corrosion rates.

Previous Work by Wellstream International [17]

Data was generated at a single confinement (V/S) of 4.6 ml/cm^2 (>150 less than estimated values for an annulus of an actual pipe). The wires were exposed to deionised water buffered to pH4 with HCl and sodium acetate and corrosion rates started at 0.16 mm/year after the first week decreasing over time to 0.07 mm/year after 24 weeks. This appears high compared with the other data, however the confinement is low and the pH buffering make the corrosion rate rather conservative.

In summary, the published data on corrosion in the annulus of a flexible pipe indicates that corrosion rates are higher in the early stages of exposure and then reduce over a period of time as dissolved iron builds up in solution and corrosion products form on the

3. Literature Review

surface of the steel, inhibiting further corrosion. The supersaturation of iron in solution is observed along with a corresponding increase in pH which also contributes to lower corrosion rates after a period of exposure. A second conclusion from the literature is that the final corrosion rate is significantly affected by confinement level. Indeed one further study aimed to review results of initial and final corrosion rates from research in the public domain in order to establish a realistic value for both parameters [2]. This review combines all of the data on the basis that for carbon and low alloy steels there is no effect from changes in carbon or manganese contents of the steel; key alloy elements (Cr, Ni, Mo) content will start to affect the corrosion resistance as they increase beyond those typical for low alloy steels. Since all of the materials were carbon or low alloy steels there will be little or no effect from differences in the chemistries of the wires tested. It was concluded that the long term corrosion rate for a confined flexible pipe annulus could be approximated as initially 0.015 mm/yr, decreasing over the first few months of exposure to 0.15 μ m/yr meaning that testing in less confined conditions or short test durations could lead to overly conservative results.

3.3.2 Sour Gas Service

3.3.2.1 Mechanism of H₂S Corrosion

H₂S is a gas under standard conditions of pressure and temperature; it is heavier ($d = 1.539 \text{ kg m}^{-3}$, at 0°C, 0.1 MPa) than air ($d = 1.293 \text{ kg m}^{-3}$), and its critical temperature and pressure are 100.4°C and 9 MPa, respectively. H₂S liquefying pressure is 2 MPa at 20°C and is very toxic even at low concentrations.

3. Literature Review

The different chemical and electrochemical reactions involved in the H₂S corrosion mechanism are listed below.

H₂S dissolution



H₂S dissociation

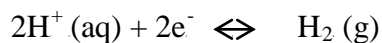


HS⁻ dissociation



The H₂S containing environments associated with oil and gas production are generally oxygen free so the controlling cathodic reaction usually involves the evolution of hydrogen by the following reaction;

H₂ evolution



An additional cathodic reaction involves the direct reduction of H₂S, which again results in the evolution of hydrogen.

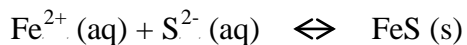
H₂S reduction



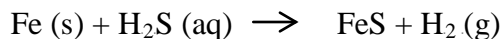
3. Literature Review

Once the environmental conditions become favourable iron sulphide films (FeS) may be produced on the metal surface via one of two reactions.

FeS produced by precipitation



FeS produced by solid state reaction



Environmental conditions will dictate the rate and characteristics of film formation, which in turn will determine the protective properties of the layer.

The Fe^{2+} species in the above precipitation reaction is a product of the corresponding anodic dissolution reaction of the steel;

Iron oxidation



3.3.2.2. Corrosion of Carbon Steel

In H_2S containing environments the amount of hydrogen entering the steel is very large. As a result the critical type of material degradation in carbon and low alloy steels is sulphide stress cracking (SSC) and embrittlement as opposed to general or localised corrosion. The corrosion rate of steel in H_2S environments is usually lower than in that of CO_2 [18] a phenomenon explained by the formation of a stable ferrous sulphide film

which protects the steel surface from further attack. Indeed, trace amounts (<3.44mbar) of H₂S have also been shown to reduce the CO₂ corrosion rate by this mechanism [19]. As a result weight loss corrosion is rarely a problem, the major degradation mechanism results from a large influx of hydrogen into the steel and subsequent cracking.

3.3.2.3 Promotion of Hydrogen absorption in the presence of H₂S

In the presence of H₂S the amount of hydrogen entering the steel can be increased by up to two orders of magnitude compared to seawater environments depending on the partial pressure encountered. The reasons for this observation are firstly, the rate of the cathodic reduction of hydrogen is increased in the presence of H₂S resulting in an increase in the amount of evolved hydrogen. This enhances the coverage of hydrogen atoms adsorbed onto the steel surface (H_{ad}).

Secondly, H₂S (or other compounds containing elements such as arsenic or cyanide) inhibits the recombination reaction of hydrogen atoms to form the hydrogen molecule. In this situation the reaction from H_{ad} to form hydrogen absorbed in the steel (H_{ab}) is increased.

Reaction without presence of H₂S



Reaction with H₂S present



The hydrogen atoms that enter the steel cause Hydrogen Pressure induced cracking (HPIC) and SSC degradation mechanisms and are essentially a hydrogen embrittlement phenomenon. As a result non-sour grade material can exhibit very low critical stress for cracking in the presence of H₂S.

3.3.2.4 Types of Cracking in Wet H₂S-Containing Environments

In a wet H₂S containing environment it is characteristic of the corrosion process that atomic hydrogen, resulting from an electrochemical reaction between the metal and the H₂S-containing electrolyte, enters the steel at the corroding surface.

The presence of hydrogen in the steel may cause embrittlement and possibly cracking depending on such factors as; type of steel, hardness, microstructure and inclusion distribution, and tensile stress distribution (applied and residual). In the following sections a description of the three main types of H₂S cracking mechanisms related to carbon steels will be presented.

3.3.2.5 Sulphide Stress Cracking (SSC)

This type of cracking occurs when atomic hydrogen diffuses into the metal but remains in solid solution in the crystal lattice. This reduces the ductility and deformability of the metal which is termed hydrogen embrittlement. Under tensile loading, be it applied or residual from welding or cold working etc, the embrittled material readily cracks to form

3. Literature Review

sulphide stress cracks (Figure 3-11). The cracking process may be very rapid and has been shown to take as little as a few hours for a crack to be initiated and cause failure.

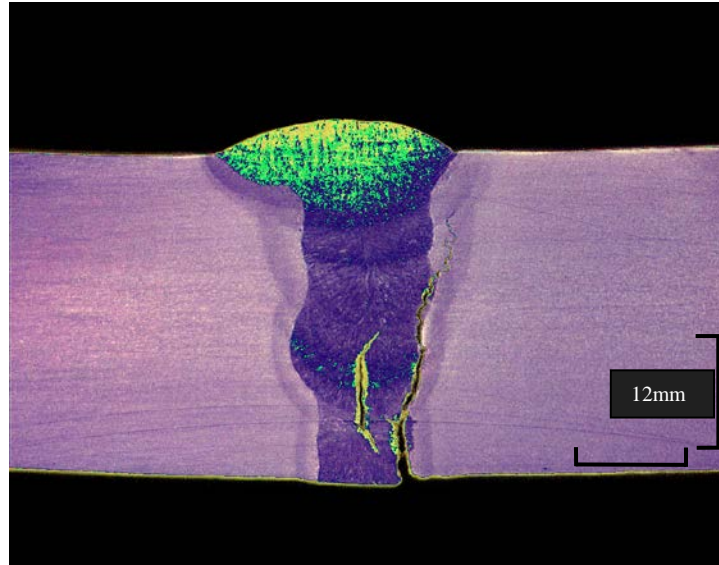


Fig 3-11 – Image of SSC through the weld of an X65 pipeline steel. Plate thickness is 30mm [Exova Corrosion Centre]

The presence of hard microstructures such as untempered or partly tempered low temperature transformation products (martensite, bainite) increases the susceptibility of the metal to SSC. These microstructures may be inherently present in high strength low alloy steels or could arise due to incorrect or inadequate heat treatment. Hard microstructures may also arise in welds, particularly in the heat affected zones (HAZ) of low heat input welds. Controlling hardness within the limits set by industry standards NACE MR0175/ISO 15156 [9] and EFC 16 [11] has been found to correlate with prevention of SSC in sour environments.

3.3.2.6 Hydrogen Pressure Induced Cracking (HPIC) or Stepwise Cracking (SWC)

Hydrogen pressure induced cracking is the name given to surface blistering and cracking parallel to the rolling plane of the steel plate which can arise without any externally applied or residual stress. This type of cracking occurs when atomic hydrogen diffuses into the metal and then recombines as molecular hydrogen at trap sites within the steel matrix. Favourable trap sites typically found in rolled products are elongated inclusions and segregated bands of microstructure. The molecular hydrogen is trapped within the metal at interfaces between inclusions and the matrix and in microscopic voids, with first a crack initiation phase and then propagation along the metallurgical structures sensitive to this form of hydrogen embrittlement. As more hydrogen enters these trap sites the pressure begins to rise, deforming the surrounding steel so that blisters may become visible at the surface. The steel around the crack becomes highly strained and this can cause linking of adjacent cracks to form SWC. The arrays of such cracks have a characteristic stepped appearance. Whilst individual hydrogen induced cracks do not affect the integrity of equipment, they are a clear indication of a cracking problem which will continue to develop unless the corrosion is prevented. At the point when cracks link up to cause SWC damage the load bearing capacity of the equipment may be seriously affected. Failures caused by this cracking mechanism may take months or sometimes years depending on the severity of the environment and the susceptibility of the steel. Control of the cleanliness of the steel and the microstructure is critical to avoiding SWC since this reduces the availability of crack initiation sites and thus the likelihood of SWC damage.

3.3.2.7 Stress Orientated Hydrogen Induced Cracking (SOHIC)/ Soft Zone Cracking (SZC)

SOHIC and SZC are related to both SWC and SSC. With SOHIC damage staggered small cracks are formed approximately perpendicular (through-wall) to the principal stress (applied or residual) resulting in a ladder-like crack formation. The cracking mechanism can be described as SSC caused by a combination of external stress and the local straining around hydrogen pressure induced cracks.

3.3.2.8 Environmental Factors Affecting Cracking in H₂S-Containing Environments

The above mentioned cracking mechanisms all result from corrosion in the presence of H₂S followed by hydrogen uptake in the steel. For each cracking mechanism there is a critical hydrogen uptake rate and/or hydrogen concentration in the steel below which cracking does not occur.

The extent of hydrogen uptake into the steel is dependant on a number of factors, the most important of which are; 1) hydrogen sulphide concentration 2) pH and 3) temperature. There are many other parameters such as; CO₂ content, water content and composition, flow rates, surface condition, and presence of corrosion inhibitors etc, which may affect directly or indirectly the extent of hydrogen uptake and thus the risk of cracking.

For practical purposes the environmental parameters affecting SSC can be simplified to H₂S concentration and pH. Environments in which SSC can occur are called sour and this can be illustrated by a domain diagram (Fig 3-12).

3. Literature Review

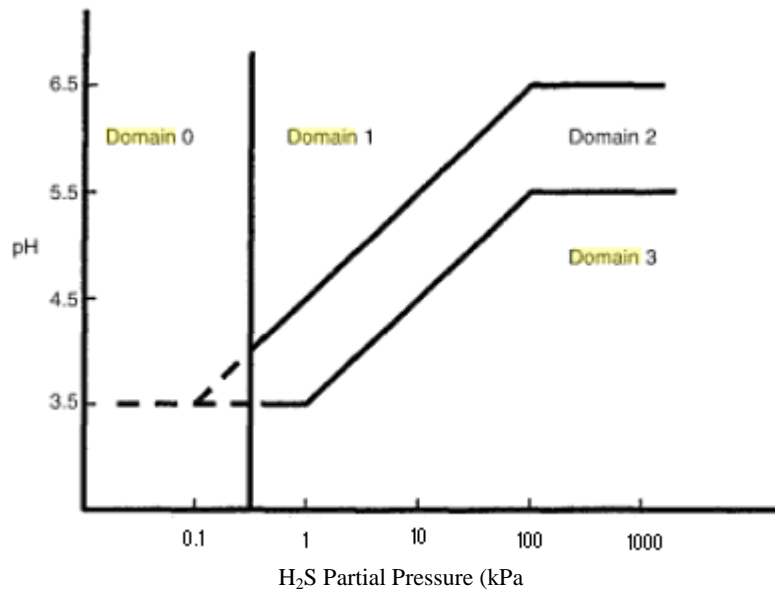


Fig 3-12– NACE MR0175/ISO 15156 [9] sour service definition, domain showing pH versus H₂S Partial Pressure (kPa).

For SWC and SOHIC, a general guide to limiting environmental parameters below which cracking will not occur is difficult to provide because these cracking mechanisms are strongly dependent on the internal steel quality, i.e. number and types of inclusions, micro-segregations etc. If the quality of the steel is less than desirable even trace levels of H₂S can result in cracking.

3. Literature Review

3.3.3 CO₂ Corrosion

3.3.3.1 Introduction

CO₂ is a gas under standard conditions of pressure and temperature; it is heavier ($d = 1.977 \text{ kg m}^{-3}$, at 0°C, 0.1 MPa) than air ($d = 1.293 \text{ kg m}^{-3}$) and its critical temperature and pressure are 31.1°C and 7.8 MPa, respectively. The liquefying pressure of CO₂ at 20°C is 5.72 MPa.

The problem of CO₂ corrosion has long been recognised and as a result of extensive studies the mechanisms are relatively well understood. Dry CO₂ gas is itself not corrosive at the temperatures associated with oil and gas production (<250°C) but once dissolved in an aqueous phase it can promote an electrochemical reaction between the steel and the contacting solution.

3.3.3.2 Mechanism of CO₂ Corrosion

Several mechanisms have been proposed to explain the corrosion process but they all involve the formation of carbonic acid and the bicarbonate ion upon dissolution of CO₂ in water. CO₂ dissolves in water and forms carbonic acid so that its aqueous solution exhibits weak acidity. The carbonic acid reaction is outlined in the following steps:

CO₂ hydration



Carbonic Acid Dissociation

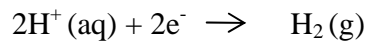
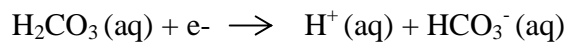


3. Literature Review

Bi-carbonate ion Dissociation



Perhaps one of the best known mechanisms was proposed by de Waard [20] which included direct reduction of carbonic acid as an additional cathodic reaction via the following equation



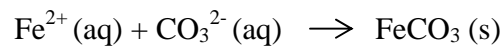
CO₂ containing environments in hydrocarbon production are usually oxygen free. Since the cathodic reaction in this case is a hydrogen forming reaction, the corrosion potential is rather less noble (less severe).

The corresponding anodic reaction can be described as:

Iron Oxidation



If super-saturation of corrosion products Fe²⁺ and CO₃²⁻ is achieved then iron carbonate precipitation can occur according to the following reaction:



Depending upon the nature of this iron carbonate scale it has been shown to afford the steel a significant level of corrosion protection [21] by presenting a diffusion barrier for the species involved in the corrosion process and by covering a portion of the steel thus preventing further oxidation [22]. This shall be discussed further in later sections as this

3. Literature Review

super-saturation of corrosion products is shown to occur in the annulus of a flexible pipe due to the large amount of steel surface area compared with a small volume of electrolyte [4, 5, 6].

3.3.3.3 Corrosion of Carbon Steel

Carbonic acid is a weak acid. Under the same pH that is, based on the same concentration of H^+ , the availability of H^+ by dissociation of carbonic acid and bi-carbonate ion is far greater with carbonic acid than with strong acids such as HCl. H^+ can be made rapidly available by carbonic acid dissociation at the metal surface where H^+ is consumed into cathodic sites. In the case of strong acids, which are fully dissociated, H^+ must diffuse from the bulk solution to the metal surface.

Due to the fact that carbonic acid exhibits high availability of H^+ and suppresses the pH rise as a result of corrosion, the corrosion rate of carbon steel in CO_2 environments is much greater than that in strong acids with the same pH.

3.3.3.4 Partial Pressure of CO_2

CO_2 corrosion results from CO_2 dissolving in aqueous media to form carbonic acid which, then reacts with the steel surface. The level of dissolved CO_2 is dependent upon the partial pressure of CO_2 in the gas phase in equilibrium with the aqueous phase. Thus as the CO_2 partial pressure of the system increases, so to does the concentration of dissolved CO_2 . As a result this is a key parameter to consider when determining the severity of a particular environment and is often used in the estimation of corrosion rates [20].

3.3.3.5 Influence of Temperature

Carbon steels, in CO₂ containing environments experience their worst case corrosion rates at around 100°C [23]. This form of localised attack is commonly known as “mesa-corrosion”. CO₂ corrosion phenomenon can be explained by considering corrosion product stability and can be broadly grouped into three main types:

- Type 1. General corrosion, <60°C
- Type 2. Mesa-corrosion, around 100°C
- Type 3. Corrosion resistant type, >150°C

It has been shown that the corrosion product formed under aqueous CO₂ conditions contains Iron Carbonate (FeCO₃) regardless of temperature [23]. Consequently, it is the kinetics of the corrosion product formation that determines its ability to mitigate further corrosion. At lower temperatures <60°C classified as general corrosion, the FeCO₃ corrosion product, which features either no corrosion film or a soft and non-adherent film on the surface, can be easily removed under flowing conditions.

Above 150°C, lower corrosion rates can be attributed to the fact that both initial metal dissolution and FeCO₃ formation rates are very high resulting in the deposition of a uniform, dense corrosion product. Consequently, the metal is protected by a passive corrosion film which consists of thin, homogenous and adhesive FeCO₃ [24].

Around intermediate temperatures (100°C) where carbonate films can form but are not strongly stable is where mesa-corrosion behaviour can be expected to occur [25].

Due to the lower temperature the kinetics of film formation are assumed to be different resulting in a thicker, porous film of FeCO₃ on the metal surface. The presence of pores

3. Literature Review

or spalling of corrosion product after reaching a critical thickness [26] can result in severe localised attack in the form of pitting since the small pit is anodic to the remaining (much larger) area of protective corrosion product. This can lead to very high local rates of penetration of the surface and in extreme cases will result in the perforation of pipes or the formation of stress raisers that can initiate cracking.

3.3.3.6 Influence of pH

Solution pH is an important parameter in the corrosion of carbon and low alloy steels. It provides a measure of the availability of the hydrogen ion in solution and it affects both the electrochemical reactions and the precipitation of corrosion products. In specific production conditions the solution may contain salts which will buffer the pH, e.g. bicarbonate ion (HCO_3^-). This will generally result in a decrease in corrosion rate and lead to conditions where precipitation of a protective film is more likely to occur.

The effect of pH on the formation of a protective corrosion film is shown in Figure 3-13 where it can be seen that pH has a significant effect on the solubility of FeCO_3 . As pH increases the solubility of FeCO_3 decreases and thus it becomes super-saturated on the steel surface. As a result the formation and precipitation of a protective FeCO_3 corrosion film is accelerated leading to reduced corrosion rates at pH levels above 5.5. [27].

3. Literature Review

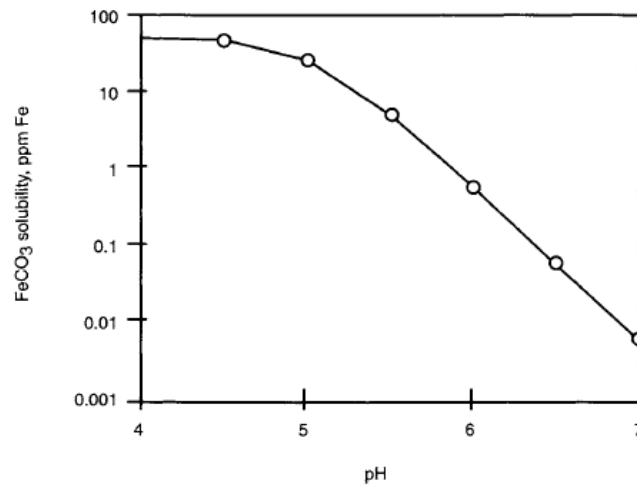


Figure 3-13 – Solubility of FeCO₃ released in the corrosion process at 2bar CO₂ and 40°C [27].

3.3.3.7 Effects of H₂S Contamination

The presence of H₂S in CO₂ environments can have a beneficial effect on the CO₂ corrosion behaviour of carbon steels [18, 19]. The reduction in corrosion rate under such conditions is often attributed to the formation of sulphide scales which form on the surface of the steel and suppress corrosion [28]. The formation of such sulphide films is dependent upon many parameters including the ratio of H₂S/ CO₂ where it has been shown that the corrosion product formed is dependent on the competitiveness of iron carbonate and iron sulphide (makinawite) [28]. This study showed that at high H₂S concentrations and low Fe²⁺ concentrations makinawite was the dominant scale to form on the surface of the steel, whilst at lower H₂S concentrations and high Fe²⁺ concentrations both makinawite and iron carbonate form [28]. The protectiveness of these layers will be dependent upon operating conditions and it is important to note that H₂S contamination under certain conditions can also increase the CO₂ corrosion rate [29] by

3. Literature Review

promoting anodic dissolution through sulphide adsorption or by forming a sulphide film that is less protective than an iron carbonate corrosion product. In addition to this it is vital to ensure that materials exposed to any level of H₂S containing environment are resistant to sour cracking mechanisms (HIC, SSC) as hydrogen entry into the steel will be significantly promoted even by low levels of H₂S contamination.

3.4 Stress Corrosion Cracking (Environmentally Assisted Cracking)

The visible manifestations of stress corrosion are cracks that create the impression of inherent brittleness in the material, since the cracks propagate with little attendant macroscopic plastic deformation. The combination of circumstances that cause a normally ductile metal to behave in this way are the presence of a specific environment, a tensile stress of sufficient magnitude and, usually, a specific metallurgical requirement in terms of the composition and structure of the alloy [30].

Environments that cause SCC are usually aqueous and can be either condensed layers of moisture or bulk solutions. SCC is alloy/environment specific and is frequently the result of a specific chemical species in the environment. For example, the SCC or SSC (sulphide stress cracking) of carbon steels used in the oil and gas industry is usually due to the presence of H_2S in the environment causing increased hydrogen uptake in the steel resulting in embrittlement. Chloride ions cause or exacerbate cracking in corrosion resistant alloy (CRA) material where breakdown of the passive film is required.

3.4.1 Stress Corrosion Crack-Propagation Mechanisms

Many different mechanisms have been proposed to explain the synergistic stress-corrosion interactions that occur at the crack tip, and there may be more than one process that causes SCC. The proposed mechanisms can be classed into two basic categories: anodic mechanisms and cathodic mechanisms. That is, during corrosion, both anodic and

cathodic reactions must occur, and the phenomenon that results in crack propagation may be associated with either type. A specific mechanism must be able to explain the actual crack-propagation rates, the fractographic evidence, and the mechanism of formation or nucleation of cracks [31].

SCC mechanisms usually assume that breaking of the interatomic bonds of the crack tip occurs either by chemical salvation and dissolution or by mechanical fracture (ductile or brittle). Mechanical fracture includes normal fracture processes that are assumed to be stimulated or induced by interaction between the material and the environment such as; adsorption of environmental species, surface reactions, reactions in the metal ahead of the crack tip, or surface films [31].

The proposed mechanisms for crack propagation fall into two basic classifications: those based on dissolution and those that involve mechanical fracture.

3.4.1.1 Dissolution Models

In so far as the occurrence of stress corrosion in a susceptible material requires the conjoint action of a tensile stress and a dissolution process, it follows that the boundary conditions within which stress corrosion occurs will be those defined by failure under a stress in the absence of corrosion, and failure by corrosion in the absence of stress. Between these extremes, wherein stress corrosion occurs, it is necessary to consider how corrosion processes may be influenced by the application of stress to a metal and how fracture may be facilitated by corrosion [30].

Slip / Film Rupture / Dissolution Model

The film rupture or slip dissolution SCC model assumes that the stress at the crack tip acts to open the crack tip and rupture the protective surface film. The bare metal then dissolves rapidly, resulting in crack growth. The idea that the breaking of a protective film could be an essential mechanistic feature of the cracking process was first outlined by Champion [32] and Logan [33].

Slip processes were first identified by Swan [34] as being crucial to the cracking process, however these original ideas were related to dislocation interactions within the metal.

The role of the slip step emergence and film rupture in the early stages of stress corrosion cracking of austenitic iron-nickel-chromium alloys has been outlined by Smith and Staehle [35]. Essentially the protective film ruptures at the crack tip enabling some amount of material to be dissolved. After an appropriate period, a new protective film forms. The amount of material which is irretrievably lost amounts to the incremental advance of chemical penetration, or cracking, see Figure 3-14.

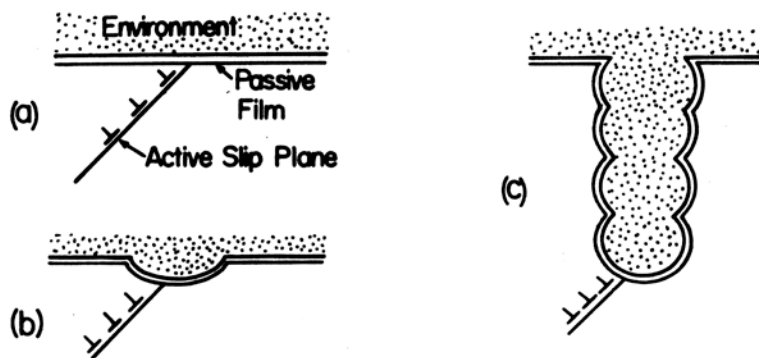


Figure 3-14 – Schematic illustrating the film rupture model. (a) metal protected by a surface film, (b) stress causes film to rupture permitting transient anodic dissolution before repassivation, (c) continued film rupture and repassivation results in crack advance [35].

Vermilyea [36] pursued the possibility that creep in the metal ahead of the advancing film can introduce increasing elastic strain in the brittle film, eventually leading to fracture. The creep process was considered to be transient because of the low temperatures at which stress corrosion cracking can occur. This approach assumes that dislocations do not play a direct role in the film rupture process.

Crack advance by the film rupture mechanism is proposed to be correlated with the charge associated with the dissolution and passivation of the bare metal surface exposed to the solution as a result of the rupture [37]. In order to retain crack geometry the rate of anodic reaction on adjacent walls must be sufficiently low relative to the rate of growth of the crack. From Faraday's law the average crack growth velocity will be given by,

$$\frac{da}{dt} = \frac{MQ_f}{zF\rho\varepsilon_f} \dot{\varepsilon}_{ct}$$

where, M and ρ are respectively the atomic weight and density of the metal, F is Faraday's constant, z is the number of electrons involved in the overall oxidation of the metal atom, Q_f is the oxidation charge density passed between oxide rupture events, ε_f is the strain to fracture of the oxide and $\dot{\varepsilon}_{ct}$ is the crack-tip strain rate [38].

Variables affecting the localised crack tip system can be separated into mechanical and chemical/electro-chemical factors. The mechanical factors (e.g., stress and strain states, creep rate, yield stress, oxide ductility, crack growth rate, grain boundary structure at the

crack tip) control the crack tip strain rate and thereby the periodicity of the oxide rupture events. The chemical factors (e.g., material composition at the crack tip and crack tip water chemistry, which is influenced by corrosion potential, impurities, flow rate etc.) determine the repassivation response of the crack tip [39].

3.4.1.2 Mechanical Fracture Models

SCC mechanisms which fall under the mechanical fracture category are described below.

Adsorption-Enhanced Plasticity

It is believed that similarities between the different types of failure, SCC, liquid metal embrittlement (LME), and hydrogen embrittlement (HE), may be explained by the adsorption-enhanced plasticity model [40]. This model assumes that environmentally induced cleavage of normally ductile materials (during liquid-metal embrittlement, hydrogen assisted cracking, stress-corrosion cracking, and corrosion fatigue) can be explained on the basis that chemisorption of environmental species facilitates nucleation of dislocations at the crack tip, promoting the shear processes responsible for brittle, cleavage fracture [41], Figure 3-15.

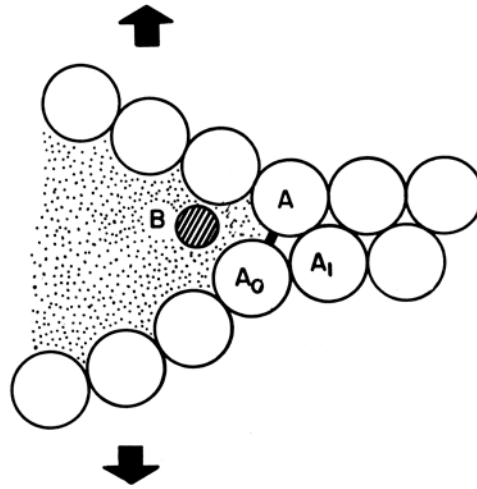


Figure 3-15 – Illustration of the adsorption-enhanced plasticity mechanism. The model requires a specific ion from the environment, B, to interact and reduce the cohesive strength between the strained bond A-A₀ at the tip of a brittle crack. [42].

Adsorption-Induced Brittle Fracture

The adsorption-induced brittle fracture mechanism is based on the assumption that adsorption of species from the environment can lower the interatomic bond strength and the stress required for cleavage fracture [43]. Similar mechanisms have been proposed for LME and HE [44]. According to this model the crack propagates continuously, with the crack propagation rate controlled by the rate at which the embrittling species arrives at the crack tip. The model does not explain how a sharp crack tip can be maintained in an otherwise ductile material. Uhlig [45] also considers that a sharply defined potential exists below which the adsorption of damaging ions, and hence cracking, does not occur.

Film-Induced Cleavage Model

The film-induced cleavage model proposes that dealloying and/or vacancy injection could induce brittle fracture. Sieradzki and Newman [46] developed this concept into a model where a surface film could induce transgranular cleavage fracture by assuming that a thin film forms on the surface. According to this model, a brittle crack nucleates in this film and propagates through the film across the film-substrate interface into the ductile metal substrate. Once the crack enters the ductile metal, it will continue to propagate in a brittle manner for some time and will eventually blunt and stop, after which the process of film formation and brittle fracture repeat itself. This model can account for the crack-arrest markings, the cleavage-like facets on the fracture surface, and the discontinuous nature of crack propagation.

Hydrogen Embrittlement

Stress corrosion cracking in some material/environment combinations is the result of hydrogen-induced subcritical crack growth. Hydrogen can enter an alloy lattice from both gaseous and aqueous phases. In an aqueous phase where corrosion reactions take place, both anodic and corresponding cathodic reactions occur. In many cases, hydrogen ion reduction is the cathodic reaction where hydrogen atoms are formed on the surface. While some of the hydrogen atoms combine to form hydrogen gas, other hydrogen atoms remain adsorbed to the surface. Because of the high partial hydrogen pressure or fugacity in H₂S containing environments, there exists a driving force for the hydrogen atoms to be

absorbed into the lattice [47]. Once hydrogen has been absorbed by a material, its effect, whether from a gaseous or cathodic source, is essentially the same [48].

Four principal fracture mechanisms have been proposed for hydrogen embrittlement:

(a) *The pressure theory (HPIC).* This approach assumes that embrittlement of steels results from high internal pressures produced by the formation of molecular hydrogen within voids or fissures [49]. This model however, does not address the basic question of how the normally ductile metal undergoes brittle failure rather than deforming plastically or failing by local ductile rupture [42].

(b) *The surface energy theory.* This theory links cracking susceptibility to a reduction in surface energy, which in turn is related to surface chemisorption through the Gibbs adsorption equation [50]. Various objections have been raised over the Petch-Stables theory, from the use of the Griffith crack stability relationship, to the nature of the link between changes in surface energy and changes in fracture toughness. Heady [51] reviewed the various objections to the Petch-Stables theory of hydrogen embrittlement and concluded that the theory is fundamentally sound, however is incapable of explaining the large decreases in fracture toughness observed in high strength structural steels subjected to hydrogen containing environments.

(c) *The decohesion theory.* This theory utilises a stress criterion, postulating that dissolved hydrogen in iron at a sufficiently large concentration decreases the maximum cohesive force between the iron atoms [52, 53]. Recognising that embrittlement does not arise from hydrogen uniformly distributed in solid solution, these authors proposed that the interstitial element diffuses to regions of large triaxial stress ahead of the crack, thus producing local concentrations [42].

(d) *The enhanced plasticity model.* This model suggests that the presence of sufficiently concentrated hydrogen dissolved in the lattice just ahead of the crack tip aids whatever deformation processes the microstructure will allow, including intergranular, quasicleavage, or microvoid coalescence fracture [54]. The enhanced plasticity model has been supported experimentally by Birnbaum's work on thin foils using an environmental cell in a high-voltage transmission electron microscope [55].

3.5 Fatigue and Corrosion Fatigue (CF)

Corrosion fatigue is a term which is commonly used to describe the damage and failure of a material under the combined action of cyclic stresses and any embrittling medium, although in the majority of cases it is in the context of aqueous environments [56]. This phenomenon is known to occur in many engineering alloys over a broad range of environments and has been recognised as an important cause for failure of engineering structures [57]. The majority of this section describes corrosion fatigue mechanisms, the different stages of corrosion fatigue and a discussion of corrosion fatigue data on carbon steel armour wires for flexible Oil and Gas pipelines. Firstly however, an introduction to fatigue in a broader sense, in particular stress-life (S-N) curves and the impact of surface effects on such curves is presented.

3.5.1 Stress versus Life (S-N) Curves and Surface Effects

When a test specimen or an engineering component is subjected to a sufficiently large cyclic stress, a fatigue crack will develop resulting in complete rupture of the sample/component. If the same test is repeated at a higher stress range the number of cycles for the rupture to occur will be reduced. The results from such testing conducted at a number of different stress ranges can be plotted to form a stress-life curve which is also referred to as an S-N curve. The stress range ($\Delta\sigma$) is commonly plotted against the number of cycles to failure (N_f) (see Figure 3-17). A whole test series of such fatigue samples giving an S-N curve may all be run at zero mean stress or at a specific non-zero

3. Literature Review

mean stress. It is also common to perform S-N curves with a constant value of the stress ratio, R . The number of cycles to failure changes rapidly according to stress level and may range over several orders of magnitude. For this reason, the cycle numbers are often plotted on a logarithmic scale.

In some materials, notably plain carbon steels there appears to be a distinct stress level below which fatigue failures will not occur under normal (i.e., non embrittling) conditions. At this point the S-N curve approaches a horizontal asymptote at a given stress level, this stress level is known as the endurance limit. This fatigue behaviour (i.e., an S-N curve) for un-notched specimens is generally considered to be a material property where information is derived from fatigue tests until failure or a large number of cycles is achieved (i.e., at run-out). Observations on crack growth are not included in stress-life experiments on un-notched specimens since this period is relatively short. In other words, in most systems the lifetime until failure is only slightly larger than the crack initiation lifetime when testing un-notched samples. This indicates that the fatigue life in un-notched S-N experiments is initiation driven. Since the crack initiation period is a surface phenomenon, various kinds of surface effects can have a significant impact on fatigue life. Surface effects include all conditions (e.g., surface roughness, surface defects, surface damage and surface modifications such as anodisation) which can reduce the crack initiation period (i.e., enhance the crack initiation mechanism).

Surface roughness and surface damage imply that the surface is no longer perfectly flat, resulting in localised stress concentrations. The significance of this surface effect on fatigue life is shown in Figure 3-16 where samples were tested with two different surface

3. Literature Review

finishes. The effect of surface roughness on crack initiation and crack growth was investigated by incrementally stopping a test to look for possible crack initiation and subsequent growth.

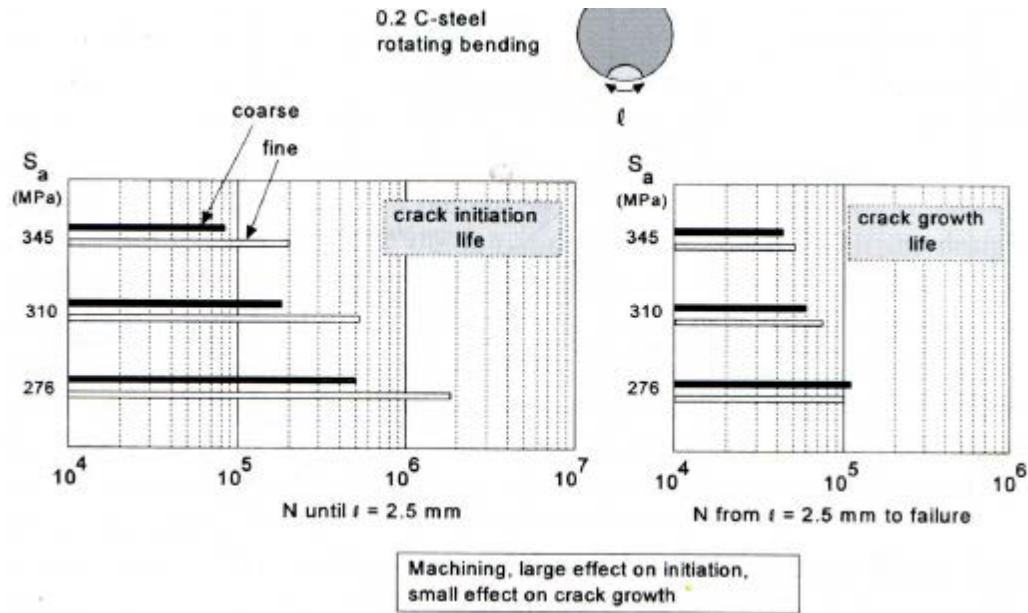


Figure 3-16- Effects of surface roughness on crack initiation and crack growth period [Schijve 2003].

It is clear that crack initiation life is significantly shorter for the coarse surface finish compared to fine finish. However, the crack growth period is hardly affected by surface roughness. It is also clear from the graphs that the crack growth period is much shorter than the crack initiation period and that the biggest increase in crack initiation period is observed at the lowest stress level. This is illustrated in Figure 3-17, where the impact of surface effects on the S-N curve is demonstrated. It should be noted that in some systems,

the most detrimental consequence of an undesirable surface effect is the large reduction of the endurance (fatigue) limit.

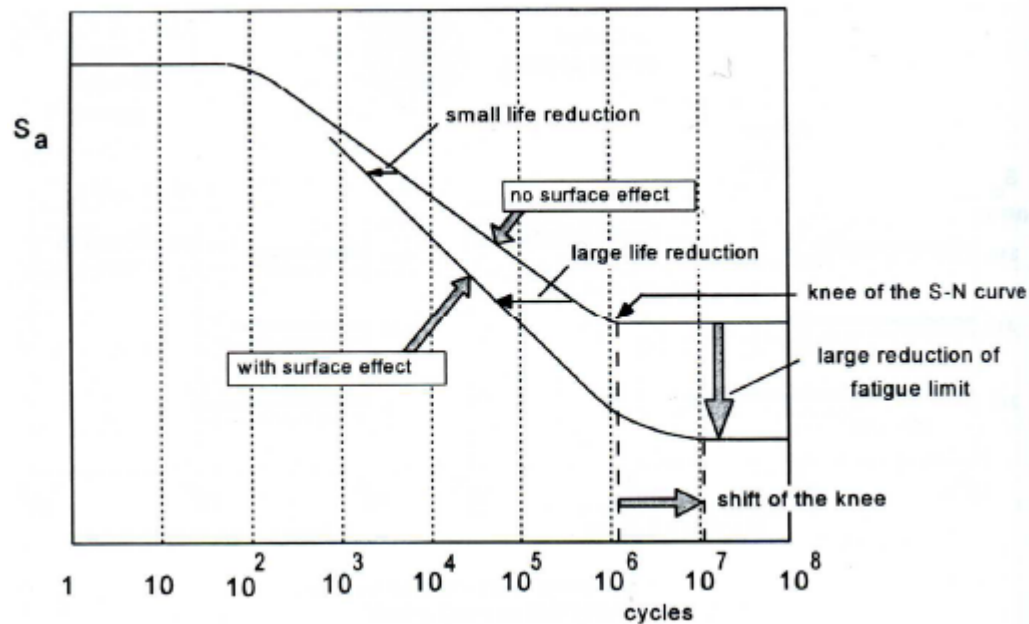


Figure 3-17- Impact of surface effects on the S-N curve. [Schijve 2003].

3.5.2 Corrosion Fatigue Mechanisms

Similar to SCC, the mechanism for CF may involve hydrogen embrittlement; film rupture, dissolution and repassivation; enhanced localised plasticity; interactions of dislocations with surface dissolution, films or adsorbed atoms; and complex combinations of these processes [58]. For ductile alloy/aqueous environment systems subjected to both monotonic and cyclic loads, interpretation of embrittlement involves the mechanism of electrochemical reaction at freshly formed slip steps or at the crack tip. This process includes two principal candidate mechanisms of environmental damage: anodic slip

3. Literature Review

dissolution or hydrogen embrittlement [58]. The advance of fracture by slip dissolution occurs by the diffusion of the active species (such as water molecules or halide ions), the rupture of the protective oxide film at a slip step or in the immediate wake of a crack tip by strain concentration or fretting contact between the crack faces, respectively, the dissolution of the exposed surface, and the nucleation and growth of oxide on the bared surface [58].

For the alternative mechanism of hydrogen embrittlement in aqueous environment (Fig 3-18) which is particularly relevant in H_2S containing environments since hydrogen uptake into the steel is significantly increased, the critical steps involve; the diffusion of water molecules or hydrogen ions between the crack walls toward the crack tip, the reduction of these species to create adsorbed hydrogen atoms at the crack tip surface, surface diffusion of adsorbed atoms to preferential surface locations, and absorption of the atoms to a critical location e.g., a grain boundary or the region of high triaxiality ahead of a crack tip, or a void [58].

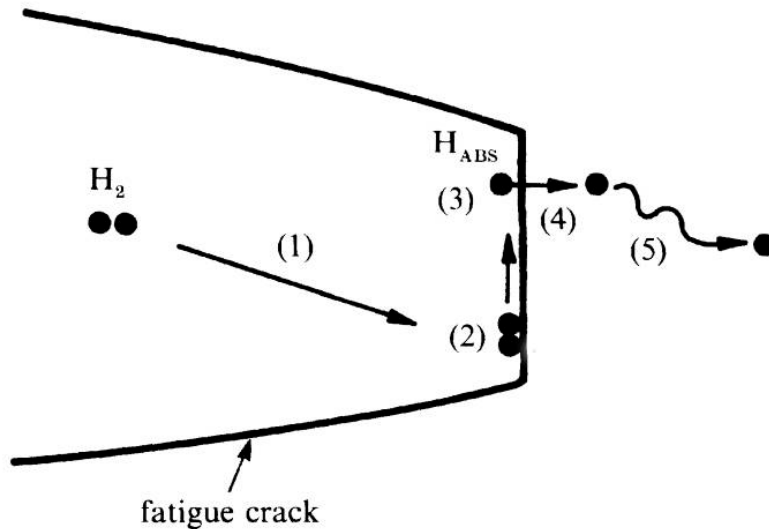


Figure 3-18- Hydrogen Embrittlement mechanism in aqueous environment (Schematic) [56]

3.5.3 Stages of Corrosion Fatigue

Corrosion Fatigue damage accumulates with increasing load cycle count (N) in four distinct phases: 1. cyclic plastic deformation, 2. micro-crack initiation, 3. small crack growth, linkup and coalescence, and 4. macro-crack propagation. A key objective is to design a corrosion fatigue experiment to isolate and quantitatively characterise one of these phases.

Methods detailed in the following sections include:

1. Smooth specimen life for high cycle fatigue (HCF) described by $\Delta\sigma$ versus N_f (S-N) data.
2. Fatigue crack propagation kinetics described by da/dN versus the fracture mechanics ΔK

3.5.3.1 Smooth Specimen $\Delta\sigma$ -Life method for High Cycle Corrosion Fatigue

Considering smooth specimens, the range of applied stress controls the fatigue or corrosion fatigue responses of metals for HCF. Smooth specimen corrosion fatigue life increases with decreasing elastic stress range, at cycles in excess of the transition fatigue life, N_T , according to the Basquin equation

$$\Delta\sigma = \sigma'_f (N_f)^{-b}$$

3. Literature Review

The material property parameters σ'_f and b depend on metallurgical, environmental and time variables. Data from Figure 3-19 show how the HCF life of AISI 4140 steel is degraded by aerated neutral NaCl solution, compared to similar fatigue lives for dry and moist air as well as deaerated chloride.

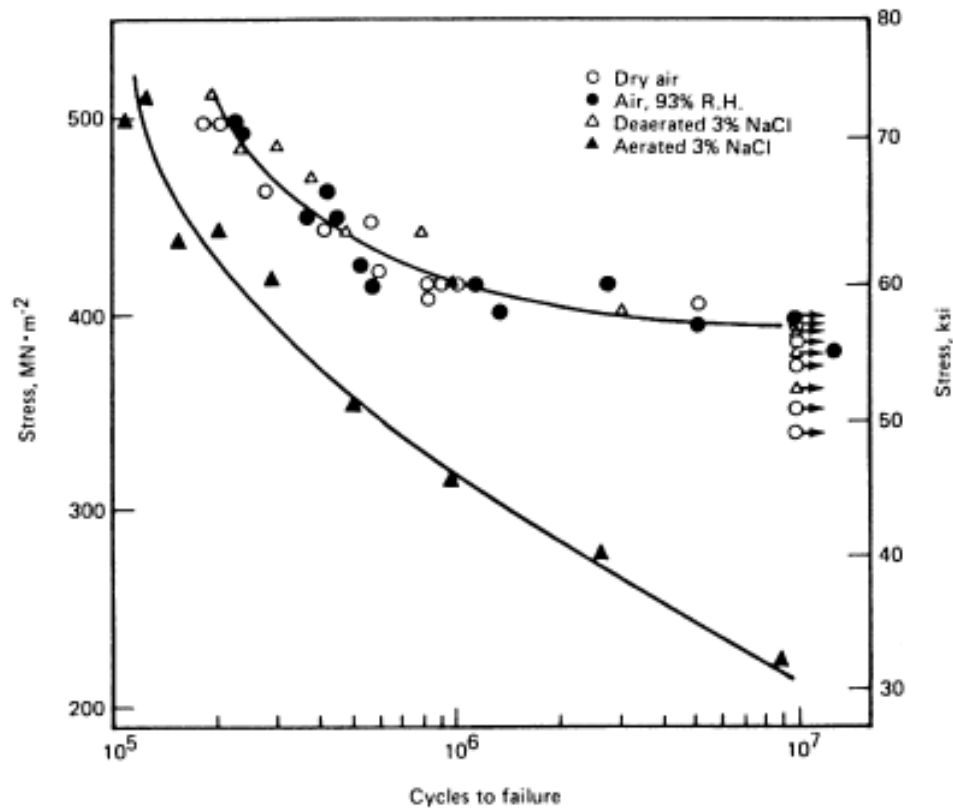


Fig. 3-19- S-N plot showing the damaging effect of an aerated seawater environment on a tempered martensitic steel [58].

The Basquin relationship is generally obeyed for fatigue in electrochemical environments, however, multiple power law segments may occur. Critically, the HCF endurance limit can be eliminated by the action of the electrolyte as illustrated in Figure

3-20. A popular explanation for this phenomenon is pitting based corrosion fatigue crack initiation [58].

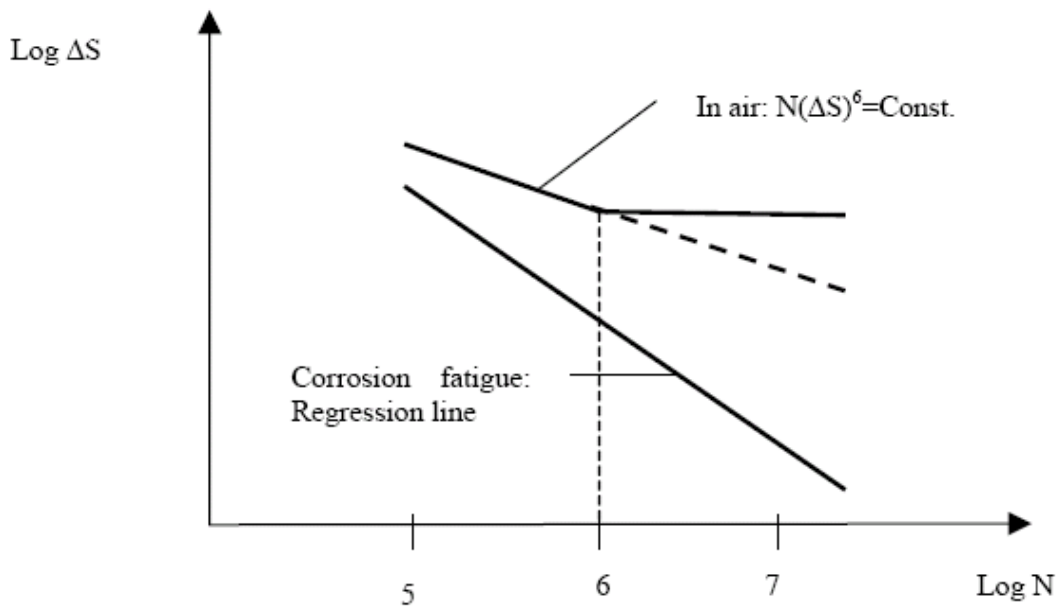


Fig. 3-20 – Schematic illustration showing the possible effects of a corrosive environment on fatigue life. Note the corrosion fatigue curve shows no endurance limit [1].

3.5.3.2 Testing techniques

Experiments to characterise high cycle corrosion fatigue according to the Basquin Law follow from ASTM standards for metals in moist air. High cycle corrosion fatigue specimens focus failure in a carefully prepared reduced uniform or mild-blend radius gage section, often of circular cross-section and with ends for gripping in the fatigue

3. Literature Review

machine. HCF specimens are loaded in uniaxial tension or bending (three-point, four-point and cantilevered) with electromechanical, servohydraulic, or rotating wheel/mass machines and grips of various designs. Elastic straining is load or displacement controlled; involves either negative, zero, or positive mean stress; and varies with time symmetrically in a sinusoidal or linear-ramp waveform. Since corrosion fatigue is sensitive to electrochemical surface damage, N_f could decrease and variability may increase with increasing surface area that is stressed.

HCF experiments are conducted for 10^5 to 10^9 cycles to failure, generally at a relatively high frequency of 25 to 100Hz due to time constraints. (N_f of 10^6 cycles requires 5.5 hours, while 10^9 cycles require 230 days of continuous loading at 50 Hz).

Caution is required when extrapolating the results of relatively rapid frequency experiments, to lower frequencies and/or the very long life regime in excess of 10^9 cycles. This is a particular limitation to the current research project since the corrosion fatigue testing in simulated oilfield environments needs to be carried out at relatively low frequencies of 0.5Hz up to a maximum of 2Hz if this is shown to produce realistic results compared to the recommended lower frequency. For test series carried out at 0.5Hz it would take 231 days to reach 10^7 cycles, which is prohibitively long when only one test machine is available.

3.5.3.3 Data Acquisition

The maximum and minimum applied loads (or alternatively, displacements) are measured with a load cell (or remotely attached extensometer/LVDT) and controlled during a HCF experiment. $\Delta\sigma$ is calculated from standard elastic solutions for bars under uniaxial tension, or beams subjected to bending. Elastic strain range is calculated from $\Delta\sigma/E$ and gauge displacement is not typically measured. Total load cycles to failure are measured, but crack initiation and growth are not monitored during a HCF experiment. Data on these stages of HCF is critical, but difficult to obtain.

3.5.4 Growth of Corrosion Fatigue Cracks

It is convenient to characterise the effects of environment on the rates of fatigue crack growth by considering different combinations of crack growth rates measured under purely mechanical fatigue and under stress corrosion conditions [56]. Figure 3-21 schematically illustrates the sigmoidal variation of fatigue crack growth as a function of stress intensity factor range under purely mechanical cyclic loading conditions (i.e., inert environment).

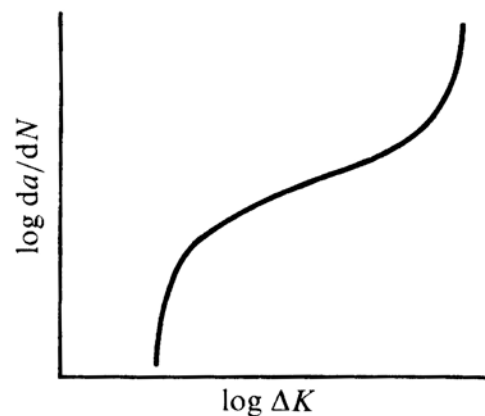


Figure 3-21 – Fatigue crack growth behaviour in inert environment [56]

3. Literature Review

The typical variation in crack velocity da/dt as a function of the applied stress intensity factor K is illustrated in figure 3-22 for sustained load crack growth of metallic materials in the presence of an environment. The environment has no effect on the fracture behaviour of the material below a static stress intensity factor value K_{ISCC} , where the subscript denotes stress corrosion cracking in mode I. Above K_{ISCC} , the crack velocity exhibits a precipitous increase with increasing stress intensity factor K (region I). This is followed by a region of growth (region II) in which the crack increment per unit time is essentially independent of the applied K . As the stress intensity factor values approach the fracture toughness of the material (region III), there is a steep rise in crack velocity [56].

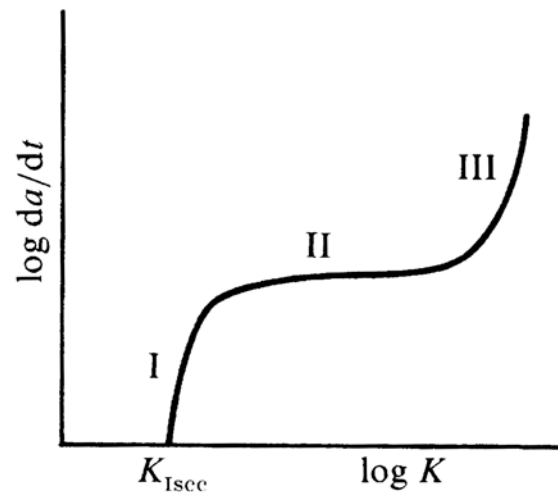


Figure 3-22 – Stress corrosion crack growth under sustained loads [56].

3. Literature Review

The corrosion fatigue crack growth of materials may be broadly characterised in terms of three general patterns of behaviour [56, 59]. Type (a), figure 3-23, represents the interaction of corrosion and fatigue at stress intensity factor values less than K_{ISCC} as evidenced by the reduction in cyclic threshold stress intensity and the increase in the rate of crack growth. This behaviour is called “true corrosion fatigue”. Type (b) behaviour, figure 3-21, is typical of those systems where there is a substantial environment-enhanced sustained-load crack growth component. The process is a simple superposition of mechanical fatigue and stress corrosion cracking. This behaviour is called “stress corrosion fatigue”. Environment effects are quite strong above the threshold K_{ISCC} for stress corrosion cracking and are negligible below this level. The hump in the “cyclic stress corrosion” curve is rather difficult to characterise. Type (c) behaviour is a combination of true corrosion fatigue and stress corrosion fatigue resulting in a mixed corrosion behaviour.

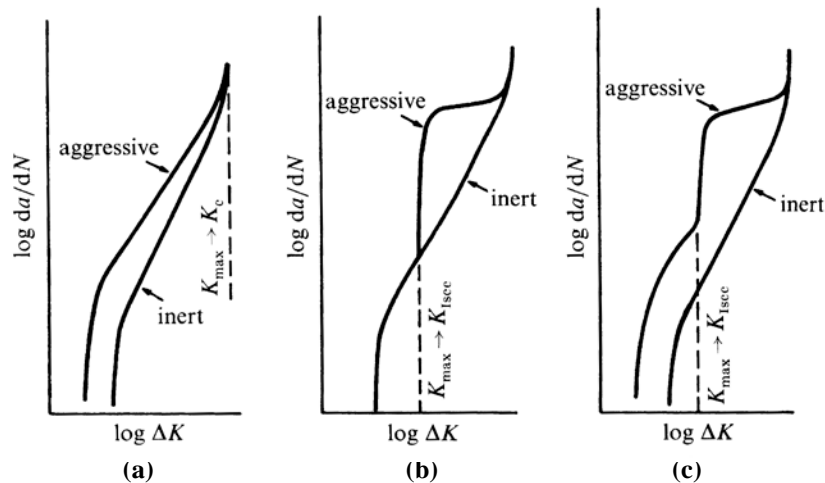


Figure 3-23 (a) True corrosion fatigue arising from synergistic effects of cyclic loads and aggressive environments. (b) Stress corrosion fatigue behaviour obtained from a superposition of mechanical fatigue. (c) Mixed corrosion behaviour obtained from a combination of (a) and (b). [56]

3.5.4.1 Corrosion Fatigue Crack Growth Models

Corrosion fatigue is a process which is an outcome of synergistic interactions among the environment, material microstructure, and cyclic loads. The mechanisms of corrosion fatigue are specific to a particular material-environment-load system. Therefore, a single model which is capable of quantitatively predicting the essential features of environmentally assisted fatigue for broad classes of materials and environments does not exist [56]

A simple approach to modelling corrosion fatigue is the *superposition model* of Wei and Landes [60]. This model accounts for the effects of environment, test frequency, wave form, and load ratio on corrosion fatigue crack propagation. The superposition model approximates the total crack extension rate $(da/dN)_r$ under corrosion fatigue conditions by a simple superposition of the intrinsic fatigue crack growth rate $(da/dN)_{fat}$ (determined in an inert atmosphere) and the stress corrosion crack growth rate $(da/dN)_{sc}$ due to a sustained load applied in an aggressive environment [61].

The linear character of the superposition model implies that there is no interaction (or synergism) between the purely mechanical and environmental components. The model also depends on the assumption that the same mechanisms control the fracture process in both stress corrosion and corrosion fatigue [61].

If however, the fatigue and stress corrosion crack growth processes are mutually competitive, and the crack propagates at a faster rate pertinent to the prevailing stress

intensity, then the *process competition model* developed by Austen and Walker [62] can be used.

Corrosion fatigue crack growth rates are strongly influenced not only by the specific combinations of cyclic loads, material and environment, but also by the crack size. This implies that the critical steps in corrosion processes which depend on crack size, such as the rate of transport of the embrittling species to the crack tip, the rate of pumping the environment by the opening and closing of the crack walls, and the development of crack closure and fretting contact along the crack flanks, must be incorporated into any complete model for environmentally assisted fatigue [56].

3.5.4.2 Fracture Mechanics Characterisation of CF

Fracture mechanics is based on the concept of similitude, wherein the stress-intensity factor (K) defines the near-tip driving forces for crack growth and thus is able to characterise crack growth for different geometries and loads. The fracture mechanics approach isolates crack propagation from initiation in terms of a precise near-tip mechanical driving force, ΔK , which is defined as the difference between maximum and minimum stress intensities for any time-dependent loading. Crack growth rates are related directly to the kinetics of mass transport and chemical reaction that constitute embrittlement [63]. Although the relationship between crack growth rate, (da/dN) , versus ΔK may be complex, an effective approach for region two is based on a power law (or Paris) relationship [64] of the form,

$$\frac{da}{dN} = A\Delta K^m$$

The advantage of using a fracture mechanics approach is that corrosion fatigue crack growth ($da/dN - \Delta K$) data from laboratory testing is in many cases useable in stress-intensity solutions for practical prediction of component life [63].

3.5.4.3 Corrosion Fatigue Crack Growth Experimentation

Three problem areas are relevant to corrosion fatigue experimentation [63]. (1) The environment must be contained about the cracked specimen without affecting loading, crack monitoring, or specimen environment composition; (2) the deleterious effect of low cyclic frequency dictates that the crack growth rates must be measured at low (often <0.2 Hz) frequencies, which lead to long test times, often from several days to weeks. Load-control and crack-monitoring electronics and environment composition must be stable throughout long-term testing; (3) crack length must also be measured for calculations of stress intensity and crack growth rate. Optical methods are often precluded by the environment and test chamber. Indirect methods based on specimen compliance or electrical potential difference, have been applied successfully to monitor crack growth. Experimental and analytical requirements, however, are complex for indirect crack monitoring.

Experimental characterisations of corrosion fatigue crack propagation are complicated by the numerous variables that influence the failure process. Both the mechanics of loading

and the composition of the environment must be controlled [65]. Experimental methods of corrosion fatigue crack growth in terms of a linear elastic fracture mechanics approach have been standardised in ASTM E 647-95a [66], and BS ISO 11782-2:1998 [67].

3.5.4.4 Variables Influencing Corrosion Fatigue

Many variables can influence corrosion fatigue crack growth. Some are unique to specific materials and environments, such as temperature, load history and waveform, stress state, and environment compositions. Others are known to repeatedly influence crack growth rate. A number of papers [58, 63] have reviewed these variables, and have been summarised below.

Stress Intensity Range

For embrittling environments, crack growth rate generally increases with increasing stress intensity; however, the precise dependence varies markedly. It is incorrect to assume that the three regimes (near threshold, power law, and fast fracture) of fatigue cracking observed for benign environments simply shift to higher crack speeds at all ΔK levels.

Load Frequency

Cyclic load frequency is the most important variable that influences corrosion fatigue for most material, environment, and stress-intensity conditions. The rate of brittle cracking, above that produced in vacuum, generally decreases with increasing frequency. The dominance of frequency is related directly to the time dependence of mass transport and

3. Literature Review

chemical reaction steps required for brittle cracking. Basically, insufficient time is available for chemical embrittlement at rapid loading rates; fatigue damage is only mechanical, equivalent to crack growth in vacuum. It is impossible to predict the frequency range at which corrosion fatigue is severe, due to the numerous chemical processes.

Stress Ratio

Rates of fatigue crack propagation generally are enhanced by increased stress ratio, R , which is the ratio of the minimum stress to the maximum, $R = \sigma_{\min} / \sigma_{\max}$. Stress ratio only slightly influences fatigue crack growth rate for benign environments, but can have a significant deleterious effect in corrosion fatigue.

Aqueous Environment Electrode Potential

Like loading frequency, electrode potential strongly influences rates of corrosion fatigue crack propagation for alloys in aqueous environments. Controlled changes in the potential of a specimen can result in either the complete elimination or the dramatic enhancement of brittle fatigue cracking. The precise influence depends on the mechanism of the environmental effect and on the anodic or cathodic magnitude of the applied potential. Electrode potential can suppress corrosion fatigue for alloys that crack through anodic dissolution/film rupture or anion adsorption mechanisms.

Environmental Contamination

Environment composition and purity can influence corrosion fatigue crack propagation. The composition and purity of the corrosion fatigue test environment must be carefully controlled, documented, and, when possible, equivalent to the intended application.

Metallurgical Variables

Microstructure and alloy strength influence fatigue crack propagation in embrittling gases and liquids. In general, brittle corrosion fatigue cracking is accentuated by:

Impurity (phosphorous or sulphur, for example) segregation at grain boundaries.

Solute depletion or sensitisation (chromium, for example) about grain boundaries.

Planar deformation associated with ordering or peak aged coherent precipitates.

Increased yield strength or hardness.

Large inclusions (manganese sulphide, for example).

Crack Closure

Premature crack surface contact during unloading, or “crack closure,” can greatly reduce rates of fatigue crack propagation. The true (or effective) crack-tip driving force is reduced below the applied ΔK because of the reduced crack-tip displacement range. Closure phenomena are produced by a variety of mechanisms and are particularly relevant to fatigue crack propagation in the near-threshold regime, after large load excursions, or for corrosive environments.

3. Literature Review

Two mechanisms of crack closure are relevant to corrosion fatigue. Rough intergranular surfaces, typical of environmental embrittlement, promote crack closure, because uniaxially loaded cracks open in a complex three-dimensional mode, thus allowing for surface interactions and load transfer. Roughness-induced closure is most relevant to corrosion fatigue at low ΔK and at stress-ratio levels where absolute crack opening displacements (0.5 to 3 μm) are less than fractured grain heights (5 to 50 μm). Alternatively, crack closing is impeded by dense corrosion products within the pulsating fatigue crack. For mildly oxidising environments, such as moist air, this closure mechanism is relevant at low stress-intensity levels and contributes to the formation of a “threshold” [65].

As a diagnostic, if CF crack growth rate depends strongly on R, if the environmental ΔK_{TH} value is high and increases with decreasing loading frequency, or if crack arrest occurs during CF propagation at constant applied ΔK , then environment-sensitive crack closure should be suspected. A bilinear specimen compliance trace (of applied load versus crack mouth or load line displacement) confirms the presence of crack closure [58].

3.5.5 Corrosion Fatigue in Carbon Steel Armour Wires for Flexible Oil and Gas Pipelines

Flexible pipeline manufacturers are operating in an extremely competitive market and as a result technological advancements in design and materials are kept as well protected

3. Literature Review

secrets. For this reason corrosion fatigue data in oilfield environments is somewhat limited, since suppliers carry out most of the work in-house and very little of this is public domain information. Despite this situation there are a limited number of papers in this area and a Joint Industry Project (JIP), which all of the manufacturers are involved in along with some major oil companies, was set up and has been running for approximately 8 years. The aim of the JIP is to generate some much needed data in order to advance the reliability and robustness of the final product. Results from the JIP have been kept largely confidential, however a paper has recently been published [7] releasing some interesting results. One of the key findings in the research was that testing at 2Hz rather than the recommended 0.5Hz [68] gives realistic, comparable results in the environments tested, which were aerated seawater, anaerobic seawater saturated with 2bar CO₂ and anaerobic seawater with 10mbar H₂S/balance CO₂. This is an important finding when it comes testing at relatively low frequencies as the testing time to 10⁷ cycles at 0.5Hz is 230 days, which is somewhat prohibitive particularly when a large amount of data needs to be generated. Increasing the frequency to 2Hz to effectively speed up testing schedules is therefore an attractive prospect, but not without risk, since corrosion fatigue is a time-dependant process involving chemical reactions, transport of products through the electrolyte and hydrogen absorption into the steel. It is clear that if loading frequency is increased too much in a corrosion fatigue test, the effect of the environment may be reduced as the test data tends towards that seen 'in air'. For this reason the conclusion of the JIP that a frequency 2Hz gives realistic results is a key finding and Figure 3-24 shows some the results from this study.

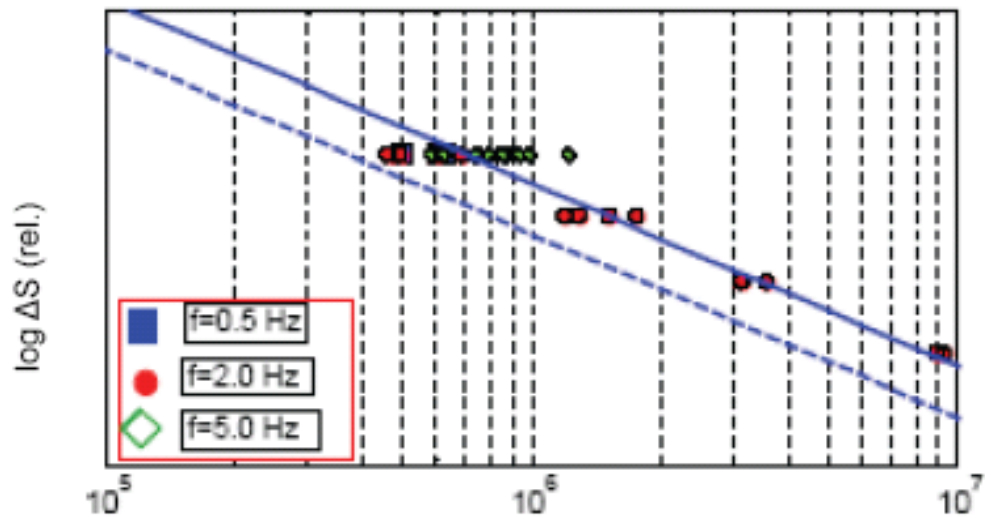


Fig 3-24 – SN data from the JIP study for wire tested in aerated seawater, at loading frequencies of 0.5, 2 and 5Hz [7].

Further interesting findings of this study include the results of testing in CO_2 and $\text{CO}_2+\text{H}_2\text{S}$ environments. Testing in CO_2 was carried out at 2bar pressure in deaerated artificial seawater. Results from this test series showed that fatigue life in the finite life region was largely unaffected by the corrosive environment compared to the in-air data (Figure 3-25), indicating that at these stress ranges fatigue life was still dictated by mechanical variables rather than the environment.

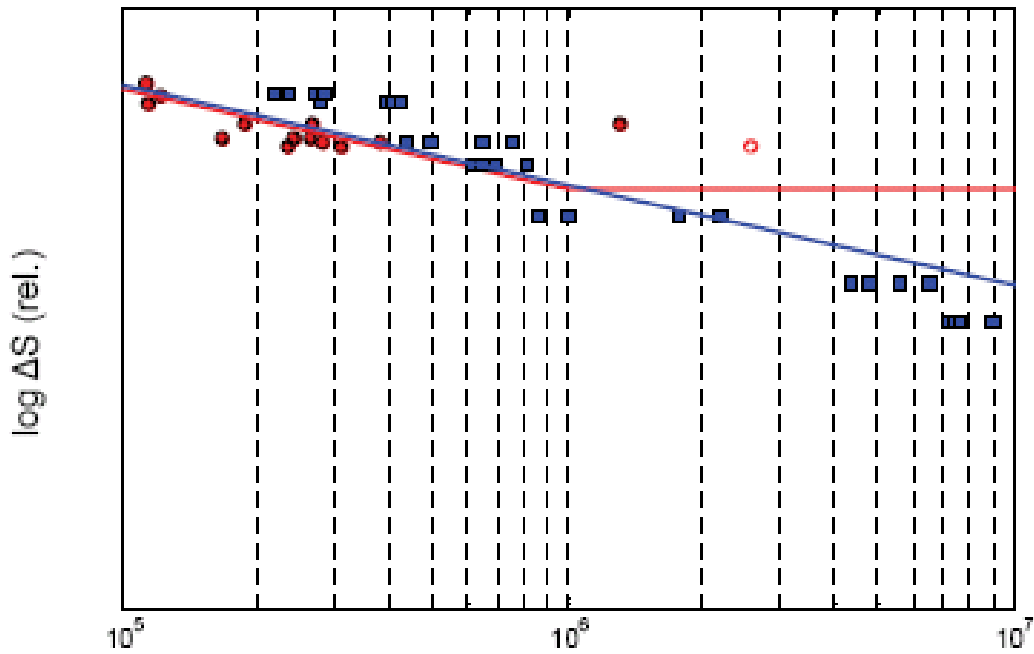


Fig 3-25 – SN data from the JIP study for armour wire tested in air and deaerated seawater with 2bar CO₂ [7], (circles are in air data and squares are CF data)

Data from this test series also shows that the action of the corrosive environment results in the removal of an endurance limit indicating that the effect of the environment is more pronounced at lower stress ranges and hence longer test durations.

Data from testing in mixed gas environments showed that the addition of a small amount of H₂S to a CO₂ environment exacerbated the detrimental effect on fatigue life compared to a purely CO₂ environment. In this test 0.1 mbar H₂S was balanced with CO₂ to 1bara total pressure and compared against the results of the 2bar CO₂ tests. These comparative results showed that the further decrease in fatigue life could be attributed to the addition of H₂S and increased hydrogen uptake into the steel.

3. Literature Review

Further work in the field to date has included corrosion fatigue data generated in both ‘sweet’ (CO₂ only) and mixed gas (CO₂/H₂S) environments. Such data on carbon steel armour wire has been generated via several different fatigue loading configurations, for example, a test program performed using uniaxial tensile specimens machined from wireline material has shown that corrosive environments containing 0.1bar and 0.01bar CO₂ reduced fatigue life by approximately 1/10 and 1/50 respectively [69] compared to that derived in air, indicating that corrosion fatigue becomes more pronounced as the corrosivity of the environment increases. Other work utilising a cantilever bending fatigue setup has reported decreased corrosion fatigue life when the strength of the wireline material is increased and when the sample contains a weld [70]. Data from this test program also reported that a 5% addition of H₂S to a CO₂ environment at ambient pressure resulted in a decrease in fatigue life compared to a 10% CO₂/N₂ environment however this data was generated at different frequencies of 0.5 and 10Hz respectively. This work also found that cathodic protection appeared to provide some improvement in the corrosion fatigue resistance of wireline material.

It has been shown that within the same strength class of armour wire there are no significant differences in fatigue strength [7]. Some research that investigated the corrosion fatigue behaviour of two different grades has been performed, one a sour grade wire with a specified minimum yield stress (SMYS) of 640 MPa and the other a non sour grade with a SMYS of 800 MPa. These grades were tested in 0.1bar and 0.02bar H₂S balanced with CO₂ to 1bar total pressure respectively. This data was generated using a four point bend configuration and testing was carried out in a deaerated artificial seawater

3. Literature Review

solution. The authors concluded that two linear regimes were present. One regime up to approximately 10^6 cycles, corresponding to stress ranges of 300MPa and above, and another regime from 10^6 and beyond corresponding to stress ranges below approximately 300MPa [4]. This conclusion possibly indicates a shift in the governing failure mechanism depending on stress range.

4. Scope of Work

4. Scope of Work

Chapters 2 & 3 detail the industrial need for fatigue data in corrosive environments representative of those found in the annulus of flexible oil and gas pipelines and risers. In Chapter 4, an outline of the key milestones and the evolution of the current research project is presented together with the experimental programme undertaken. (A detailed description of the experimental method is provided in Chapter 5).

Work conducted as part of this thesis consisted of two distinct phases:

Phase I: corrosion fatigue facility development and testing in simulated corrosive environments at atmospheric pressure (Sections 4.2-4.3).

Phase II: corrosion fatigue facility development and testing in simulated corrosion environments at elevated pressures associated with deepwater oil production (Section 4.4).

The first major objective of Phase I of this thesis was to develop the testing facilities in order to carry out corrosion fatigue testing at atmospheric pressure on tensile armour wire components of flexible Oil and Gas pipelines. Once this milestone was reached the next objective was to subsequently develop a corrosion fatigue test procedure which met all of the requirements of testing in a specific corrosive environment. Following successful pilot testing to validate the data generated the third objective of Phase I was now possible which was to investigate the corrosion fatigue behaviour of tensile armour wires via S-N experiments in simulated oilfield environments. This has been achieved via investigations

4. Scope of Work

into the effect of testing in artificial seawater saturated with 1bar CO₂ compared to in-air data. Further investigations were performed to identify the effect of environment confinement and test frequency on armour wire fatigue life. In addition, testing was performed to compare the effect of the corrosive environment on the fatigue properties of welded test pieces.

It should be noted that most of the testing in the programme has been completed as part of contracts with the flexible pipeline manufacturers (Exovas client) and has at times restricted the research aspect of the project. The test conditions have often been specified by client project work and this has restricted machine time availability for other aspects which would have otherwise demanded further detailed investigation.

The positive aspect of completing successful testing programmes for the clients in Phase I, was that it led to a big development in the current research project (Phase II), which was high pressure corrosion fatigue testing (HPCF). This second phase of the current research project wasn't an initial objective, but was driven by strong demand from the flexible oil and gas pipeline manufacturers. Through the good track record of corrosion fatigue testing at atmospheric pressure during Phase I of the current research project Exova secured a large testing contract consisting of several years' worth of work. This represented the natural, industry driven progression for this EngD programme and the process of test machine development and test procedure development started again, this time for elevated pressure corrosion fatigue testing. This multi-million pound investment

4. Scope of Work

culminated with the installation of a unique state-of-the-art HPCF facility to house 8 bespoke test machines. Corrosion Fatigue results from the initial testing using the HPCF facility are included in Section 7.2.3.2 of this thesis. The development of the HPCF test facility and the ability to present results from such unique test conditions is a major achievement for the current EngD research project. The data generated can be regarded as novel and extremely valuable to the technological advancement of flexible Oil and Gas pipelines.

In the following sections of chapter 4 the experimental programme is outlined in more detail, including test matrices for each test condition. An overview of the experimental plan is given in Figure 4-1.

4. Scope of Work

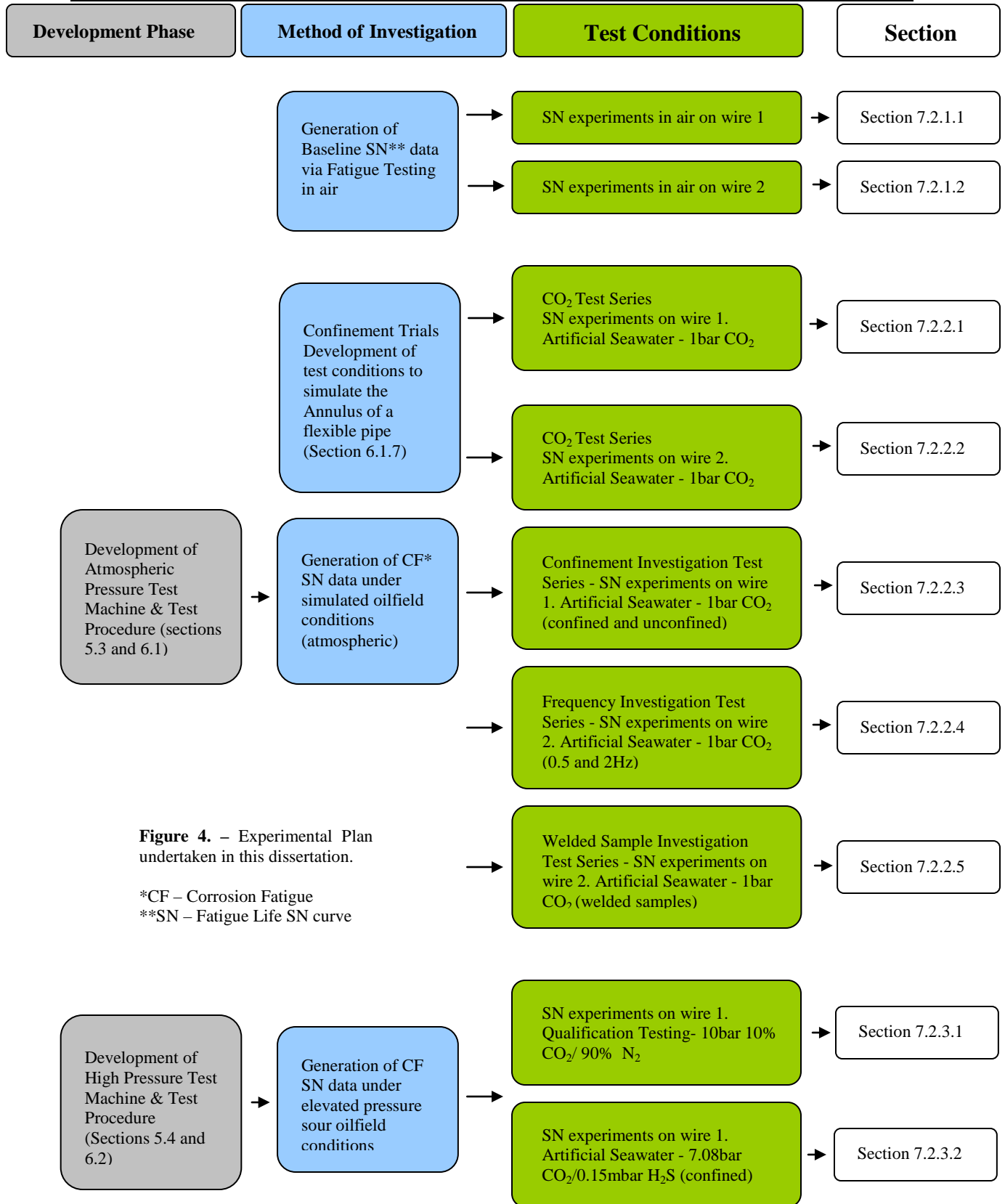


Figure 4. – Experimental Plan undertaken in this dissertation.

*CF – Corrosion Fatigue

**SN – Fatigue Life SN curve

4. Scope of Work

4.1 Baseline Data - Lab Air Fatigue Test Series

4.1.1 Axial Tension – Lab Air Fatigue Testing

At the request of the client, baseline data was generated in lab air using an axial tension configuration. This is standard practice in the industry since it is consistent with test results from the manufacturers existing database.

Fatigue testing in lab air was performed on two grades of tensile armour wire (i.e., Wire-1 and Wire-2) supplied by different flexible pipeline manufacturers. All testing was performed with constant amplitude loading, however, the fatigue loading parameters differ slightly for each wire according to how each manufacturer had generated their previous database. Table 4-1 presents the testing matrix for the lab-air test series on Wire-1 which was tested with a constant mean stress of 400MPa. Using the mechanical properties from the tensile testing data, appropriate stress ranges were selected to produce an S-N curve and ascertain the endurance limit within a limited number of samples.

4. Scope of Work

Table 4-1 – Testing matrix for the lab air test series on wire 1. This curve is performed with a constant mean stress of 400MPa

Sample ID	Steel Grade	Size (mm ²)	Curve	Frequency (Hz)	Environment	Mean Stress (MPa)	Stress Range (MPa)
1	Wire 1	15x5	In-Air Test Series	10	Air	400	760
2							
3							
4							
5							700
6							
7							
8							
9							600
10							
11							
12							
13							500
14							
15							
16							
17							400
18							
19							
20							

Similarly, Table 4-2 presents the testing matrix for Wire-2. Wire-2 was tested using a constant r-ratio of 0.1. When using this baseline in-air data for comparative purposes against the corrosion fatigue data it is important that the test parameters in the corrosive environment are consistent with that generated in lab air. To ensure this is the case, all corrosion fatigue testing on Wire-1 was conducted with constant mean stress whilst that on Wire-2 was done with constant r-ratio.

4. Scope of Work

Table 4-2 – Testing matrix for the lab air test series on wire2. This curve is performed with a constant r-ratio of 0.1

Sample ID	Steel Grade	Size (mm ²)	Curve	Frquency (Hz)	Environment	r-ratio	Stress Range (MPa)	Percentage of Yield
1	Wire 2	9x3	In-Air	10	Air	0.1	1000	77.3
2								
3								
4								
5							900	69.6
6								
7								
8								
9							800	61.8
10								
11								
12								
13							750	58
14								
15								
16								
17							600	46.5
18								
19								
20								

4.1.2 Four Point Bend – Lab Air Fatigue Testing

Despite the industry generally requesting air fatigue data to be generated in axial tension the experimental approach in this thesis is to compare directly between lab air data and data generated in a corrosive environment. For this reason it is important to have baseline data in lab air that has been generated in four-point bend for comparison with corrosion fatigue data, which is all generated in four-point bend. By taking this into account, possible effects on fatigue life induced by a different testing geometry will be avoided.

4. Scope of Work

Table 4-3 shows the test matrix for the air fatigue test series in four-point bend on Wire-1. It should be noted that due to availability of test material, lab air fatigue data on Wire-2 was only generated in axial tension.

Table 4-3 – Testing matrix for the four point bend lab air test series on wire 1. This curve is performed with a constant mean stress of 400 MPa.

Sample ID	Steel Grade	Size (mm ²)	Curve	Frequency (Hz)	Environment	Mean Stress	Stress Range
1	Wire 1	15x5	Air Test Series (Four Point Bend)	5	Air	400	760
2							
3							
4							
5							700
6							
7							
8							
9							600
10							
11							
12							

4.2 Atmospheric Pressure Corrosion Fatigue Investigation (Vs Lab-air Data)

4.2.1 Artificial Seawater/1bar CO₂ Investigation (Wire-1 & 2)

Fatigue design of the tensile armour wire component of flexible oil and gas pipe lines was originally based on the assumption that the annulus environment was benign with respect to corrosion and consequently the fatigue data used for design purposes was generated in air. Service experience has since proven that the annular environment of the flexible pipe

4. Scope of Work

can become corrosive. When this situation occurs in service the integrity of the carbon steel elements of the pipe (tensile armours) are at risk and therefore fatigue life may be affected.

The aim of the first phase of the corrosion fatigue testing was to investigate the effect of the corrosive environment on the fatigue life compared to that of data generated in lab air.

In this test series, termed ‘CO₂ test series’, the testing environment consists of artificial seawater saturated with 1bar CO₂. The test matrices for these test series are shown in

Tables 4-4 and 4-5 where the test conditions are outlined for testing on both Wire-1 and

2. The test parameters for each wire are consistent with the loading parameters used on that particular grade during the air fatigue testing phase.

Table 4-4 – Test matrix outlining the corrosion fatigue testing carried out during the CO₂ test series. The purpose of this test series is to assess the effect of the corrosive environment on fatigue life compared to the data generated via in air testing. Test matrix for wire 1.

Sample ID	Steel Grade	Size (mm ²)	Curve	Frequency	Approximate Start pH	CO ₂ in bar	Environment	Mean Stress (MPa)	Stress Range
low pH 1	Wire 1	15x3 machined	CO ₂ Test Series (unconfined - lower pH)	0.5Hz	5.0-5.2	1	Synthetic Seawater (ASTM D1141) unconfined	400	600
2									
3									
4									
5									
6									500
7									
8									
9									
10									400
11									
12									
high pH 1	Wire 1	15x3 machined	CO ₂ Test Series (confined - higher pH)	0.5Hz	5.8	1	Synthetic Seawater (ASTM D1141) confined	400	600
2									
3									
4									
5									
6									500
7									
8									
9									
10									400
11									
12									

4. Scope of Work

Table 4-5 – Test matrix outlining the corrosion fatigue testing carried out during the CO₂ test series. The purpose of this test series is to assess the effect of the corrosive environment on fatigue life compared to the data generated via in air testing. Test matrix for wire 2.

Sample ID	Steel Grade	Size (mm ²)	Curve	Frequency (Hz)	Environment	Approx Start pH	CO ₂	r-ratio	Stress Range (MPa)
1	Wire 2	9x3	CO ₂ Test Series	2	ASTM D1141 (synthetic seawater) Unconfined	5-5.2	1bar	0.1	880
2									
3									
4									
5									750
6									
7									
8									
9									600
10									
11									
12									
13									400
14									
15									
16									
17									250
18									
19									
20									

4.3 Atmospheric Pressure Corrosion Fatigue Parameter Investigations

4.3.1 Investigation of the Effect of Confinement

As described in Section 3.3.1, the confined conditions (high ratio of steel surface area to electrolyte volume) found inside the annulus of flexible oil and gas pipelines are one of the most important parameters dictating the corrosivity of the prevailing environmental conditions. It has been demonstrated [4,5,6] that corrosion rates differ significantly between confined and unconfined conditions and that under confined conditions the chemistry of the environment is altered. Specifically, elevated pH and iron saturation of the electrolyte is to be expected under confined test conditions which have the effect of

4. Scope of Work

making the test environment less severe from a corrosion standpoint. In this test series the current research project aims to investigate the effect of such confined environmental conditions on fatigue life. This parameter was investigated by following the methodology outlined in the following sections, essentially performing a series of corrosion fatigue tests under unconfined conditions (no additional steel surface area) where solution pH and dissolved iron content will be lower than that of the confined test conditions. A further test condition was also investigated which was under confined conditions with a 4-day pre exposure period of the samples prior to initiating the fatigue loading. During this 4 day period the pH of the test solution had to reach a value of 5.8 in order to be representative of confined test conditions. All three of the corrosion fatigue conditions in this test series were conducted at a frequency of 0.5Hz and a constant mean stress of 400 MPa. All of the tests have been carried out on the same batch, heat and spool of tensile armour wire material designated 'Wire-1'. An outline of the testing matrix is shown in Table 4-6.

4. Scope of Work

Table 4-6 – Test matrix outlining the corrosion fatigue testing carried out during the confinement investigation test series.

Sample ID	Steel Grade	Size (mm ²)	Curve	Approximate Start pH	CO ₂ in bar	Environment	Mean Stress (MPa)	Stress Range (MPa)	
low pH 1	Wire 1	15x3 machined	Unconfined	5.0-5.2	1	Synthetic Seawater (ASTM D1141)	400	600	
2									
3									
4									
5								400	500
6									
7									
8									
9									400
10									
11									
12									
high pH 1	Wire 1	15x3 machined	Confined (addition of steel wool)	5.8	1	Synthetic Seawater (ASTM D1141)	400	600	
2									
3									
4									
5								400	500
6									
7									
8									
9									400
10									
11									
12									
4day 1	Wire 1	15x3 machined	Confined (addition of steel wool) + 4 day pre exposure	5.8	1	Synthetic Seawater (ASTM D1141)	400	600	
2									
3									
4									

As shown in the test matrix, the environmental conditions were consistent between tests with the test solution always artificial seawater and the test gas always 1bar CO₂. This enabled the effect of confinement to be investigated as it was the only parameter being manipulated.

4.3.2 Investigation of the Effect of Test Frequency

Test frequency used in corrosion fatigue testing is another key parameter. API 17J [68] recommends that testing is conducted at a frequency representative of actual service conditions. In the case of flexible oil and gas pipes this frequency is 0.5Hz which is representative of marine structures subjected to wave loading. Despite such recommendations there is a desire to increase the test frequency in order to generate data within a reasonable timescale. This manipulation does come with the risk that the data generated at higher test frequencies will differ from that at lower frequencies since the faster the loading is applied the less time the environment has to affect the fatigue life. If test frequency is increased too far the effect of the corrosive environment may be overlooked as the data generated tends towards that seen 'in-air'.

In this frequency investigation test series the aim is to see whether testing at a frequency of 2Hz rather than 0.5Hz results in any significant effect on fatigue life. Table 4-7 outlines the testing matrix for this test series where it can be seen that all other parameters of the test are consistent with only the frequency of testing being manipulated. This test series was carried out on tensile armour Wire-2 with all of the samples in this test series from the same heat, batch and spool.

Testing in this test series has been carried out at a constant r-ratio of 0.1. Environmental conditions were the same between tests and consist of unconfined artificial seawater saturated with 1bar CO₂.

4. Scope of Work

Table 4-7 – Test matrix outlining the corrosion fatigue testing carried out during the frequency investigation test series.

Sample ID	Steel Grade	Size (mm ²)	Curve	Approximate Start pH	CO ₂ in bar	Environment	r-ratio	Stress Range (MPa)														
0.5Hz 1	Wire 2	9x3	0.5Hz (frequency investigation)	5.0-5.2	1	Synthetic Seawater (ASTM D1141) unconfined	0.1	550														
2																						
3																						
4																						
5								Wire 2	9x3	0.5Hz (frequency investigation)	5.0-5.2	1	Synthetic Seawater (ASTM D1141) unconfined	0.1	450							
6																						
7																						
8																						
9															Wire 2	9x3	0.5Hz (frequency investigation)	5.0-5.2	1	Synthetic Seawater (ASTM D1141) unconfined	0.1	350
10																						
11																						
12																						
2Hz 1	Wire 2	9x3	2Hz (frequency investigation)	5.0-5.2	1	Synthetic Seawater (ASTM D1141) unconfined	0.1															550
2																						
3																						
4																						
5								Wire 2	9x3	2Hz (frequency investigation)	5.0-5.2	1	Synthetic Seawater (ASTM D1141) unconfined	0.1								450
6																						
7																						
8																						
9															Wire 2	9x3	2Hz (frequency investigation)	5.0-5.2	1	Synthetic Seawater (ASTM D1141) unconfined	0.1	350
10																						
11																						
12																						

4.3.3 Investigation of the Effect of Welded Samples

During the manufacture of flexible Oil and Gas pipelines it is necessary to include welded sections when installing the tensile armour wire component of the wall structure. The welds are usually strategically located to sections of the pipe expected to see less severe loading conditions in order to limit their impact on the overall design. However

4. Scope of Work

they are still located in the annulus environment and subjected to loading conditions that are often unpredictable in nature so a comparison of the fatigue life of welded and parent sections of tensile armour wire is a relevant investigation. The weld investigation test series was conducted on the same batch of wire as was tested in the frequency investigation test series (Wire-2). Table 4-8 outlines the test matrix for the welded samples test series where it can be seen that the test parameters are the same as in the frequency investigation test series in order to allow a direct comparison between the data sets where the only manipulation is the addition of a welded rather than a parent test sample.

Table 4-8 – Test matrix outlining the corrosion fatigue testing carried out during the weld investigation test series.

Sample ID	Steel Grade	Size (mm ²)	Curve	Frequency	Approximate Start pH	CO ₂ in bar	Environment	r-ratio	Stress Range (MPa)	
Weld 1	Wire 2 (welded samples)	9x3	Welded Samples (effect of a weld)	2Hz	5.0-5.2	1	Synthetic Seawater (ASTM D1141) unconfined	0.1	550	
2										
3										
4										
5									0.1	450
6										
7										
8										
9										
10										
11										
12										
Weld 0.5Hz 1	Wire 2 (welded samples)	9x3	Welded Samples (effect of a weld)	0.5Hz	5.0-5.2	1	Synthetic Seawater (ASTM D1141)	0.1	450	
2										
3										
4										

4. Scope of Work

Most of the testing for the weld investigation test series was conducted at a test frequency of 2Hz along with one stress range tested at 0.5Hz to look for any possible effect of frequency within welded test samples.

4.4 High Pressure Corrosion Fatigue Testing

4.4.1 HPCF Qualification Test Series

4.4.1.1 Introduction

Following completion of the design and build stages of the high pressure corrosion fatigue facility (see Chapter 6.2 for details) it was necessary to conduct a qualification test series for comparison with existing data in order to establish a high level of confidence in the data being generated. Hence, the aim of the qualification test series was twofold, firstly to prove that the testing procedure and the experimental setup, including the containment vessel (autoclave) were oxygen tight and secondly, for the corrosion fatigue testing results of a known material (Wire-1) to fall within the general scatter band of the existing database from the industrial client.

4.4.1.2 Deaeration Qualification Test

For the initial stage of qualification a test was setup as normal except for the absence of steel wool in the autoclave. This was to ensure that if any O₂ was present it would not be consumed via reaction with Fe²⁺ and therefore not measured by the O₂ measurement

4. Scope of Work

equipment. During these tests two oxygen sensors were utilised, one measured dissolved O₂ in the solution in the deaeration vessel and the second sensor was fitted to the autoclave so that O₂ measurements could be taken continuously whilst the rig was cycling over a minimum of 48 hours. Results from the deaeration qualification tests are extremely important to the accuracy of the simulated environments since Oil and Gas corrosive conditions are strictly anaerobic and even small increases in O₂ content would significantly increase the severity of the environment.

4.4.1.3 Corrosion Fatigue Qualification Test Series

Testing for the high pressure corrosion fatigue qualification was performed on a 15x5mm wire (Wire-1) which is classified as a ‘sweet service wire’ on the basis of its mechanical properties. In fact, this is this same grade of material that was tested in the ambient pressure corrosion fatigue test series (see Section 4.2-4.3). It is from the same heat, batch and spool so the results provide a direct comparison on this particular grade of tensile armour wire. Table 4-9 presents the test matrix for the HPCF qualification test series which summarises the test conditions used in this stage of testing.

4. Scope of Work

Table 4-9– Test matrix outlining the testing conditions for the HPCF qualification test series. Test has been performed on the same grade of material as used in the atmospheric pressure confinement investigation test series so a constant mean stress of 400MPa is again used.

Sample ID	Steel Grade	Size (mm ²)	Curve	Frequency (Hz)	Gas Mix	Test Pressure (bar)	Environment	Mean Stress (MPa)	Stress Range (MPa)
1	Wire 1	15x5	HPCF Qualification test series	2	10% CO ₂ balance N ₂	10	ASTM D1141 (synthetic seawater) Confined	400	400
2									
3									

Test Conditions

The gas mix used for the qualification tests consisted of 90% N₂ / 10%CO₂ at a total test pressure of 10bar. With this gas mixture and a total system pressure of 10bar test conditions simulate the conditions of testing with pure CO₂ at atmospheric pressure. This is the environment that has been used in all of the atmospheric corrosion fatigue tests performed in the current research project. In addition to this the manufacturers of the flexible pipes have existing results on this environment/material combination from various independent test houses. The results from the HPCF qualification were required to fall within the general scatter of this existing database.

The test qualification procedure is in accordance with the methodology section on HPCF (see Section 5.4). Three samples were tested at a constant mean stress of 400MPa and a stress range of 400MPa at 2Hz. All three of these samples were required to fail between

4. Scope of Work

550,000 and 4,000,000 cycles with two out of the three failing between 740,000 and 3,000,000.

4.4.2 Elevated Pressure CO₂ with Trace amounts of H₂S - (7.08bar total CO₂ pressure with pH₂S of 0.15mbar)

For the high pressure corrosion fatigue (HPCF) test series the aim was to simulate as closely as possible the predicted annulus environment when the pipe is subjected to elevated pressures due to both high internal bore pressure and external hydrostatic pressures encountered during deepwater oil production. The predicted pressures and partial pressures of chemical species within the annulus will alter the local chemistry and thus the corrosivity of the environment.

In order to accurately simulate such complex environments pre-mixed gas cylinders were used containing the correct amounts of corrosive species to achieve the desired test partial pressures. Table 4-10 shows the relationship between the required H₂S partial pressure (pH₂S), total CO₂ pressure and the required gas mix. The gas mix was calculated by multiplying the required pH₂S in mbar by 1000 and then dividing by the total system pressure to give a value in ppm, which is the gas mix (ppm H₂S) needed to provide a specific pH₂S at a given test pressure.

4. Scope of Work

Table 4-10- Table showing the relationship between p_{H_2S} , total CO_2 pressure and required gas mixture. The values used for the HPCF test series are highlighted at the bottom of the table

Required p_{H_2S} (mbar)	Total System/ CO_2 Pressure (bar)	Gas Mix required (ppm)
0.1	1	100
1	1	1000
10	1	10000
0.1	1	100
0.1	10	10
0.1	100	1
0.15	7.08	21.19

For example, in the HPCF test series the annulus conditions were predicted to be 7.08 bar total CO_2 pressure with a p_{H_2S} of 0.15mbar. So from Table 4-10 it can be seen that the required gas mixture was 21.19ppm H_2S balanced with CO_2 . The gas mixes were ordered from BOC Gases Ltd and were certified to +/-5% of the requested value. In order to ensure that the chemistry was not below the required value, a 5% error margin was added to the required value giving a gas mix of 22.3ppm. This value was then rounded to 22ppm which was the gas mixture used for the HPCF test series.

Table 4-11 outlines the testing matrix for the HPCF test series. This test series was conducted on Wire-1, which is the same grade used in the HPCF qualification and confinement investigations. As such, the HPCF test series were also been carried out with a constant mean stress of 400MPa.

4. Scope of Work

Table 4-11 - Test matrix outlining the test details for the HPCF test series.

Sample ID	Steel Grade	Size (mm ²)	Curve	Frequency (Hz)	CO ₂ Pressure (bar)	pH ₂ S (mbar)	Environment	Mean Stress (MPa)	Stress Range (MPa)
1	Wire 1	14x6	HPCF test series	2	7.08	0.15	ASTM D1141 (synthetic seawater) Confined	400	700
2									
3									
4									
5									500
6									
7									
8									
9									400
10									
11									
12									
13									300
14									
15									
16									

The test environment in the HPCF test series consisted of artificial seawater with the addition of steel wool to create confined test conditions. This test solution was then saturated with the test gas as outlined above and then pressurised to 7.08 bar.

5. Methodology

In order to generate the required fatigue data (i.e., stress-life or S-N curves) in simulated oilfield environments, key stages of the current research project have involved the design and manufacture of a prototype atmospheric pressure environmental/corrosion fatigue (APCF) rig and a bespoke high pressure environmental/corrosion fatigue (HPCF) facility for testing carbon steel armour wire components of flexible Oil and Gas pipelines and risers. It should be noted that the following sections in Chapter 5 give brief mention to the general requirements of the corrosion fatigue rig designs for both the atmospheric and elevated pressure facilities, however a detailed discussion of the design and construction of the experimental setup shall be included in the first chapter of the results (Chapter 6) as this was a key, ongoing task throughout the current research project. In this chapter, after a brief description of materials characterisation methodology, a detailed description of the use of these two facilities to obtain fatigue and corrosion fatigue data is provided.

5.1 Materials Characterisation Methodology

5.1.1 Metallography

Specimens were prepared and polished to a mirror finish in order to characterize the grain structure of the as-received steel armour wire. The polishing process begins with grinding using specific abrasive papers attached to a grinding wheel. The grades of paper used are as follows; 200, 400, 800, 1200, 1200/1400 and 4000. Following each grinding stage the sample was washed with distilled water, wiped with a cotton bud, rinsed in acetone and dried using a hairdryer. The sample was intermittently observed under a microscope to

5. Methodology

ensure that the previous abrasion had been polished away. Once the sample had been sufficiently ground the sample was then polished down to a 3 μm then a 1 μm finish.

Etching

A 2% Nital etchant was used to determine structural characteristics of the armour wire. The etchant was applied via a cotton bud swab. The tensile armour wires were sectioned transverse and parallel to the rolling/drawing direction in order to maximize visualization of grain morphology.

5.1.2 Optical microscopy & SEM

Optical microscopy was used to observe the as received microstructure and to view tested samples where a detailed view of surface corrosion phenomenon was deemed useful. Scanning Electron Microscopy (SEM) was used for fracture surface analysis of the ruptured fatigue specimens from the S-N experiments in both air and corrosive environments. The fractographic analysis in the SEM provided further information on the crack initiation site that could not be observed via macro and optical imaging of the fracture surface.

5.1.3 Tensile Testing

Before fatigue testing the armour wire material it was necessary to perform tensile tests to obtain information about its mechanical properties. This data, specifically the yield strength, was then used to determine relevant stress ranges for fatigue testing. The tensile

5. Methodology

testing was performed using a 500kN servo-hydraulic test machine. The test sample was instrumented with strain gauges on either side of the as received armour wire specimens allowing strain to be recorded against load. As received samples were gripped using a tabbing technique which is discussed in detail in section 5.2.

5.1.4 Hardness Testing

Hardness testing provides an indication to the materials resistance to permanent deformation. The hardness of the sample will depend on the ease of deformation and therefore can be related to the yield stress of the sample. Hardness testing was performed across the transverse face of the armour wire specimen utilizing the Vickers method (HV10). Results are presented using Vickers Pyramid number (HV).

5.2 Generation of Baseline Fatigue Data in ‘Lab Air’

In the early stage of the programme, it was necessary to generate baseline stress-life fatigue data on the tensile armour wires via testing in lab air. This data was later used to assess the effect the corrosive environment has on fatigue life from the corrosion fatigue test data. This section aims to outline the methodology used and provide details of the lab air fatigue testing performed. In line with recommendations from the JIP studies [1,7] and at the request of the flexible pipeline manufacturers, the in air fatigue data was generated utilising an axial tension test configuration. The armour wire has been tested with full cross sections using a ‘tabbing’ technique which aims to avoid premature failures at the

5. Methodology

hydraulic gripping locations. Testing full cross sections meant that no machining and subsequent polishing was required allowing the as-received surface to be tested. It should be noted that fatigue testing in lab air was also conducted on Wire-1 in a four point bend configuration (Section 5.2.3) as a direct comparison with the corrosion fatigue data in this dissertation, which has all been generated utilising a four point bend test configuration.

5.2.1 Axial Tension Test Configuration

Samples tested in the 'lab-air' test series were fatigued under load control using a 100kN servo-hydraulic test machine with closed loop feedback to maintain the test loads accurately. Samples were located and held in place using hydraulic grips (Figure 5-1).

As can be seen from Figure 5-1 the samples were loaded in axial tension and the test was deemed valid if the rupture initiated from inside the gauge length which was at least 50mm in length. The gauge length is the area between the two tabbed regions of the sample (see Figure 5-2).

5. Methodology

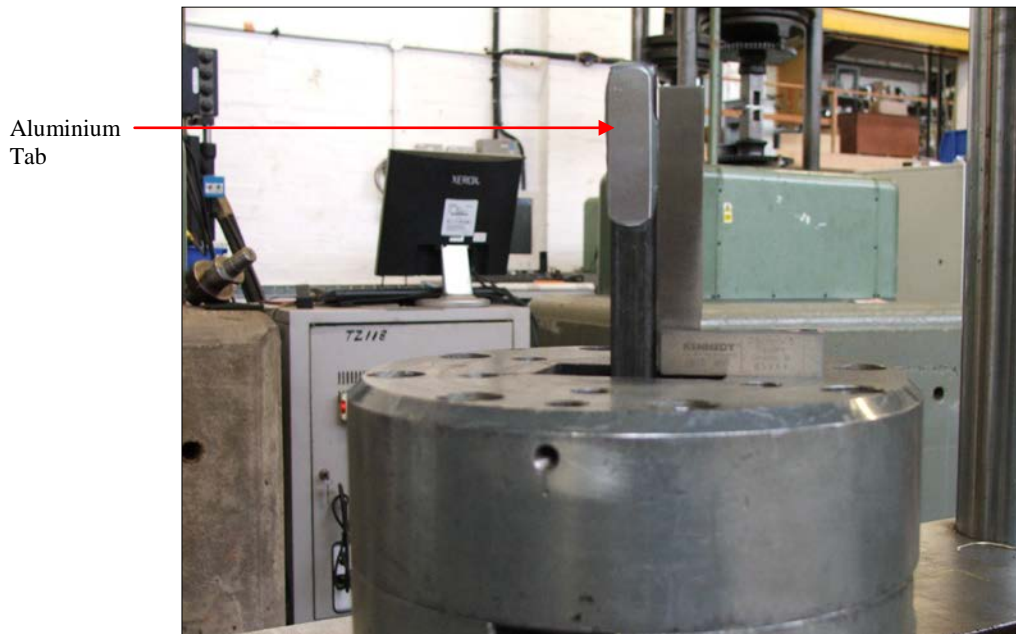
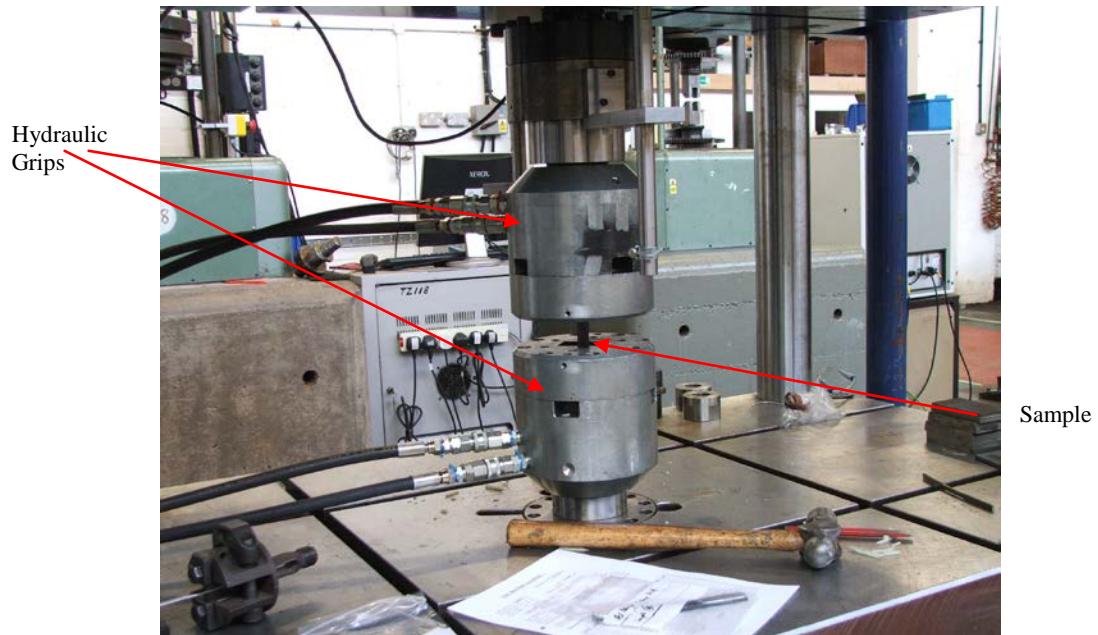


Fig 5-1 – Image of the test machine used during the ‘lab-air’ test series. Hydraulic grips were utilised to load the test sample and failures at the grip were avoided by using an aluminium tabbing technique which can be seen on the sample being aligned in the grip.

5. Methodology

Sample Preparation

Samples tested in the lab air fatigue test series have all been tested as-received, full cross section with no machining process applied. As noted above, the test samples for this test series have been tested in axial tension which often presents problems with sample failures at the gripping locations, particularly in samples without a reduced section gauge length. To overcome this issue and successfully test full section test samples a ‘tabbing’ technique was used.

Samples were prepared by cutting to length (approx 160mm) and if necessary being straightened in a four point bend jig. Samples tested in the axial tension configuration need to be relatively straight to ensure good alignment when tested in axial tension.

Tabs were prepared from 3mm thick sheets of aluminium, these were cut to size and abraded with coarse paper to ensure no rough edges remained that could cause fretting during the test (Figure 5-2).

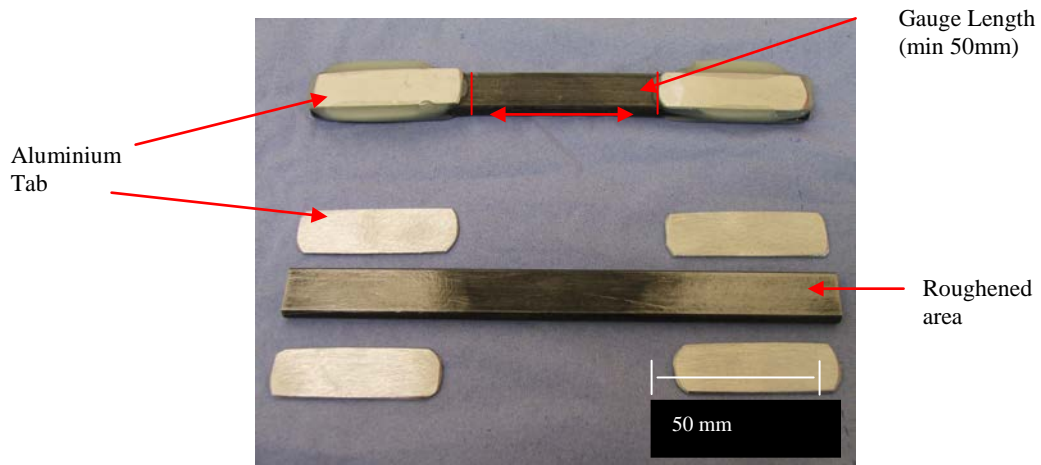


Fig 5-2 – Image of fully prepared axial tension fatigue sample and a sample ready for installation of aluminium tabs.

5. Methodology

As can be seen in Figure 5-2 both the aluminium tabs and the area of the test sample where the tabs will be located were prepared by abrading the surface with a coarse sand paper to ensure good keying and aid adhesion. These surfaces were then thoroughly degreased with acetone before a thin layer of araldite was applied to both the tab and the surface of the sample.



Fig 5-3 – Images of the bespoke jig used to prepare tabbed axial tension samples used in the air fatigue test series.

Once all tabs were roughly in position the sample was inserted into a specially designed jig (Figure 5-3) to ensure that the tabs stay parallel with the sample as the adhesive cured. Samples were left in the jig for at least 2 hours and given at least 24 hours of curing time before testing. By installing these aluminium tabs to the areas of the sample which will see high gripping pressures when loaded via the hydraulic grips any local damage to the test piece which could lead to an early failure and an invalid test result is prevented. The aluminium tabs absorb any damage from the gripping mechanism as the sample is not in

5. Methodology

direct contact with the grip jaw faces which reduces the likelihood of a premature rupture at the gripping location.

Fatigue Loading Parameters

The general methodology for the axial fatigue testing in lab air was the same for both Wire-1 and Wire-2. The specific parameters for the fatigue testing of each wire material are outlined in Chapter 4 (Section 4.1).

All testing was performed with constant amplitude. Within a sequence of testing to generate an S-N curve the tests were performed either with constant mean stress or with a constant R ratio (i.e., constant ratio between minimum and maximum stress). Most of the testing was dictated to an extent by the flexible pipe manufacturers (i.e., Exova's contractual clients) and as such two testing programs were carried out, one material with constant mean (Wire-1 Chapter 4 (Sections 4.1 and 4.1.1)) and another with constant R ratio (Wire-2 Chapter 4 (Sections 4.1)) depending on how the clients comparative data had been generated. Throughout all further testing in the current research project these parameters have been kept the same to ensure consistency and to allow comparison between datasets generated in different environments.

5.2.2 Four-Point Bend Fatigue Testing in Lab Air

Fatigue testing in lab air was also performed on Wire-1 in a four point bend configuration. Figure 5-4 shows the experimental setup where testing was performed on

5. Methodology

an as received sample. This test series was performed in load control in a servo-hydraulic test machine and the test loads were calculated using standard elastic solutions for beams in bending (Fig 5-5). These calculated loads were also verified utilising a strain gauged specimen.

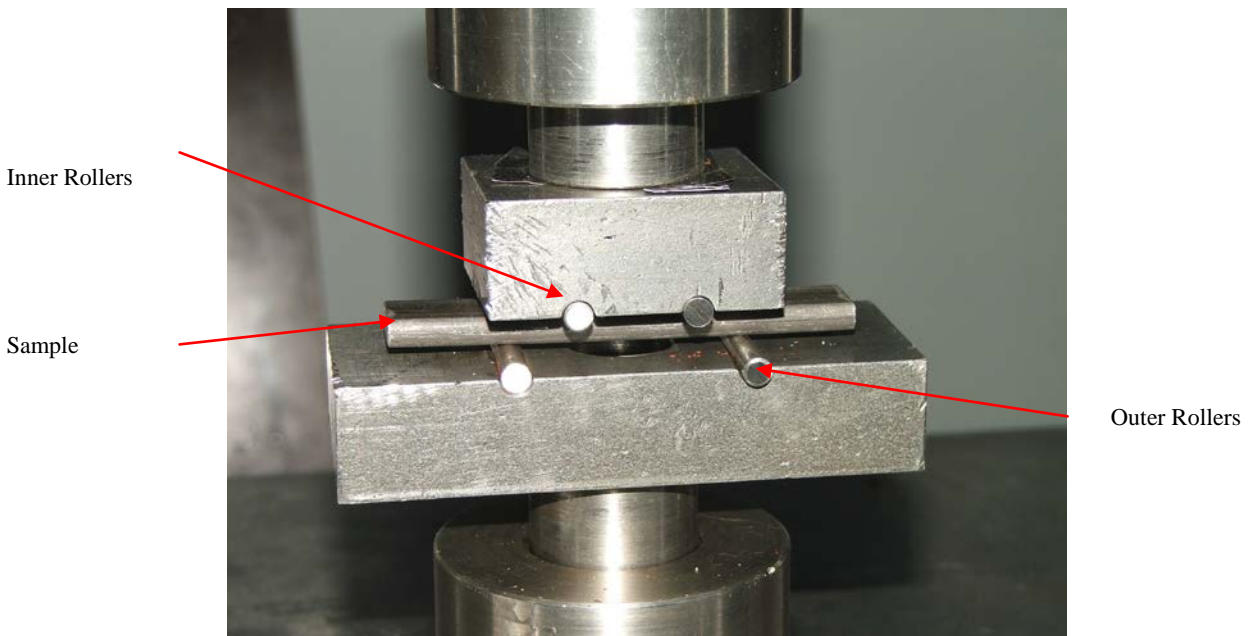
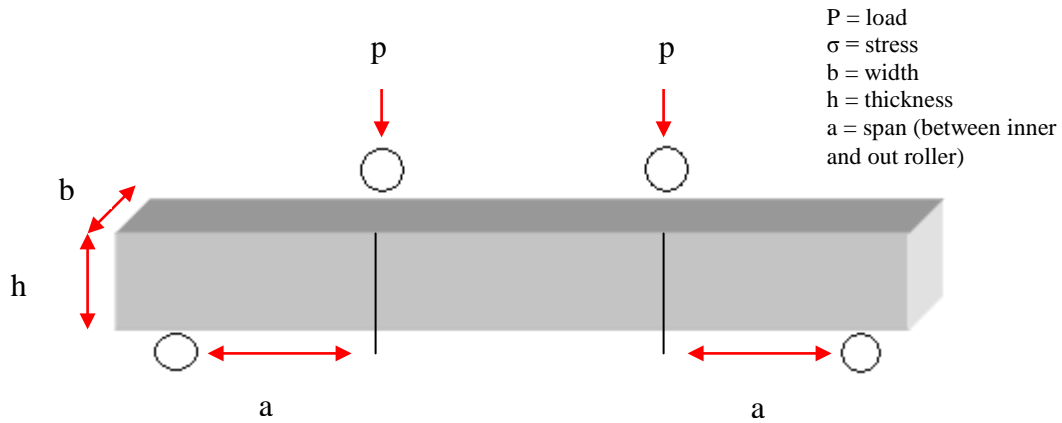


Fig 5-4 – Test setup for the four point bend lab air test series on Wire-1. The four point bend fatigue testing in lab air is performed with a constant mean stress of 400 MPa.

5. Methodology



$$p = \sigma b h^2 / 3a$$

Fig 5-5 - Schematic of the load calculations for the four-point bend configuration. Includes equation used to determine test loads.

The armour wire material used for the experimental programme in this thesis is received with a certain amount of curvature from the manufacturing and production processes. For testing in four-point bend the samples were cut to length but not straightened. The convex face of the sample was always the test face of the sample i.e. the face which has seen tensile strains during manufacture is the face that is subjected to tension during the fatigue testing. Throughout this thesis the convex surface will be termed the ‘tensile’ face and the concave surface the ‘compressive’ face of the sample. In terms of residual stresses induced during manufacture the opposite terminology would be true i.e., the convex face of the armour wire would exhibit compressive residual stresses. The terminology used in this thesis refers to the strain that the face of the sample has been exposed to rather than the residual stress induced by manufacture.

Details of the specific test parameters used for the four-point bend testing in lab air can be found in Chapter 4 (Section 4.1.1).

5.3 Atmospheric Pressure Corrosion Fatigue (APCF) Testing

5.3.1 Requirements of Experimental Setup

Following discussion with the flexible pipeline manufacturers it was clear that the development of a corrosion fatigue prototype machine was required to meet certain test requirements according to their specifications/procedures. Some of the key requirements that the rig had to meet were as follows:

1. Apply loading to the samples in bending, either four point bend or cantilevered
2. Apply sine shaped loading
3. Capability of testing four samples simultaneously in a communal environment
4. Adjustable displacement/stroke length
5. Capability to expose samples to deaerated simulated oilfield environments saturated with controlled partial pressures of H₂S and CO₂.
6. Apply loading frequency between 0.1 and 2Hz

A detailed description of the manufactured prototype APCF testing machine is given in Chapter 6. The following sections discuss the corrosion fatigue test methodology that was developed for atmospheric pressure.

5.3.2 Test Method

The test protocol used for corrosion fatigue testing in the current research project is in general accordance with the requirements given in the JIP test protocol [1] and with specific requirements within several flexible pipeline manufacturers test procedures.

5.3.2.1 Load Method

Fatigue testing is generally performed in one of two ways; axial tension or bending. Axial loading would have presented problems in testing multiple samples simultaneously as well as being performed in relatively complex load control. Since bending appeared to be the more favourable option three potential methods/test configurations were identified; three-point bending, cantilever bending and four-point bending. Each method will result in different stress patterns being generated in the sample however all three methods will only generate tensile strains to one side of the sample. Four-point bending was chosen as the principal method although the rig design allowed the option of all three by simply changing the sample fixture installed in the rig (see Chapter 6). The four-point bend configuration was chosen since the area of the sample between the two central rollers is exposed to maximum uniform tensile strains as opposed to hotspots being generated at the grip in cantilever bending and at the centre contact point in three-point bending. This is important as it will generate realistic results taking into account defects and imperfections along the length of the tested sample. Furthermore, in the four-point bend configuration samples can be tested in the as-received condition or machined easily by simply reducing the thickness. If samples are machined, the machining process is

5. Methodology

conducted on the compressive side (concave face) of the sample making sure that the tensile face is kept in as-received condition.

5.3.2.2 Sample Preparation

The fatigue life properties of many materials are sensitive to the surface condition of the sample as well as the level of residual stress induced during manufacture. These are key parameters to consider during corrosion fatigue testing since both can also have a significant impact upon the way in which the sample reacts to the corrosive environment.

It is important to generate data that is simulating the materials in service performance. In the case of testing armour wires, the tensile surface of the wire must be kept in the as-received condition so that any effect on the fatigue behaviour of the manufactured surface is included in the test. Any machining of the wire must be conducted on the compressive side of the sample. In Phase-1 of the CO₂ trials (see Section 4.2.1 (Wire-1)) the 15mm x 5mm wire was machined down to 3mm thickness over a test area of 75mm (Figure 5-6).

5. Methodology

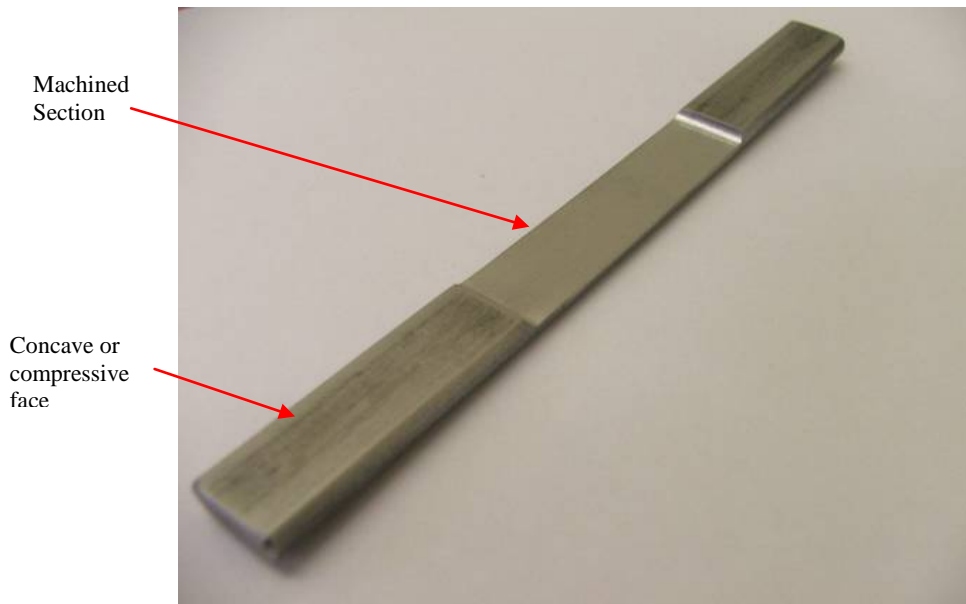


Fig 5-6 – Image of the compressive face of a machined corrosion fatigue sample – Wire-1 – CO₂ test phase (carbon steel armour wire material). Sample 160mm long, machined section 70mm. Note the residual curvature inherent to the armour wire.

Since the armour wire material is usually taken from a coil there was a certain level of residual stress contained within each sample. The preparation of a corrosion fatigue sample involved cutting the armour wire to the required length and then machining the test area. Machining depended on the thickness of the wire since the atmospheric pressure rig has some load limitations due to certain components of the loading chain, and can only test up to 3mm thick wire with full thickness. For the larger wires that are machined (i.e., 15mm x 5mm) the compressive side of the sample was marked prior to cutting to ensure that the correct side was machined, this way the side that has seen tensile stresses in manufacture and reeling is tested in tension.

The samples were thoroughly cleaned using soap and detergent and degreased with

5. Methodology

acetone prior to testing. One specimen for every batch or different machining process was instrumented with a strain gauge and load cell readings were verified against strain gauge measurements to ensure that the strain levels were all within 5% of the theoretical strain at a given load (Fig 5-7).

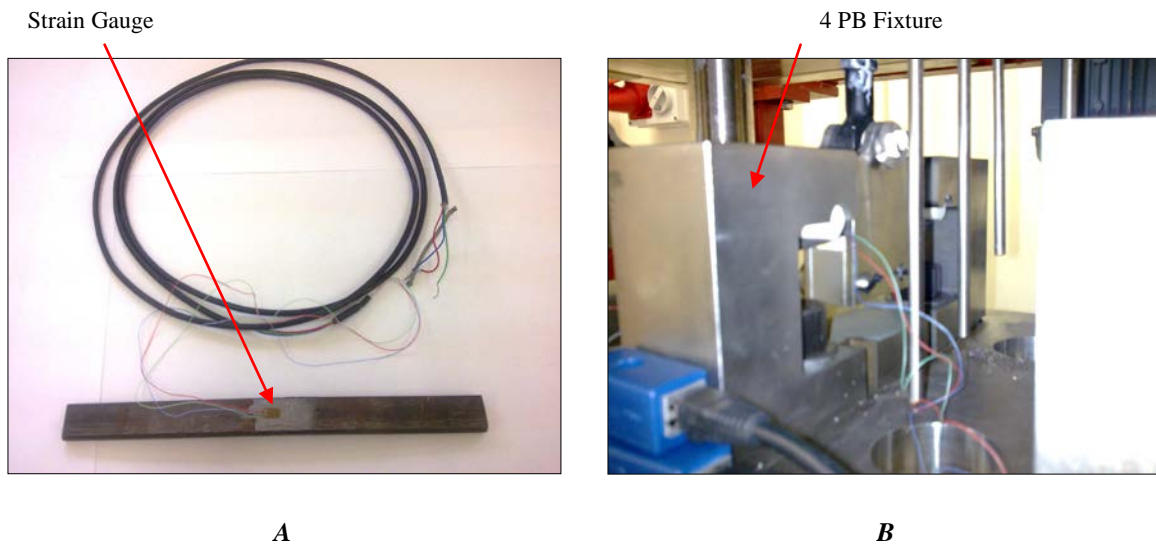


Fig 5-7 – a) instrumented dummy sample, b) instrumented sample mounted inside the four point bend fixture.

5.3.2.3 Test Environment

The electrolyte used in the corrosion fatigue tests was a standard ASTM D1141 (without heavy salts) artificial seawater solution [71], see Table 5-1. Corrosion conditions in Oil and Gas production are oxygen free so the solution is strictly deaerated to levels below 5 ppb. The artificial seawater solution is used in Oil and Gas related experiments is typically saturated with a mixture of H_2S and CO_2 as a test gas although only CO_2 conditions have been investigated at atmospheric pressure in the current research project. Since the annulus of a flexible pipe is densely packed with carbon steel armouring

5. Methodology

components, there is little free volume for the electrolyte which results in extremely confined conditions. The ratio of free volume to steel surface area (V/S) in the annulus environment is typically below $0.1\text{ml}/\text{cm}^2$ [2]. In order to simulate the confined conditions in the annulus of an unbonded flexible pipe steel wool was added to the test solution in order to increase the surface area of steel. The result of this is that as the steel wool corrodes Fe^{2+} and an equivalent amount of alkalinity is released into the electrolyte causing the pH to increase and the solution to become super-saturated with Fe^{2+} . It should be noted that where steel wool was added into the test rig it was not in galvanic contact with the specimens. Furthermore, other than the addition of steel wool to the environmental chamber, the pH was allowed to settle freely.

Not all testing was conducted under confined environmental conditions as this allowed for the effect of this parameter on fatigue life to be investigated. Therefore the test environment preparation procedure varies slightly depending on whether or not confinement is being simulated, this shall be described further in the following sections. Chapter 4 (Section 4.3.1) outlines the test matrix where confinement is investigated.

5. Methodology

Table 5-1 - ASTM D1141 Substitute ocean seawater components [71]

Reagents	Amount (g/L)	Volume (mL/L)	Comments
NaCl	24.53		Components to make up any required volume of ASTM D1141 (without heavy salts)
NaS (anhydrous)	4.09		
Stock Solution 1		20	
Stock Solution 2		10	
The stock solutions are made up separately and added in the above amounts			
MgCl ₂ 6H ₂ O	555.6	Stock Solution 1	
CaCl ₂ (anhydrous)	405.6		
SrCl ₂ 6H ₂ O	14.8		
KCl	69.5	Stock Solution 2	
NaHCO ₃	20.1		
KBr	10		
H ₃ BO ₃	2.7		
NaF	0.3		
Ba(NO ₃) ₂	0.0994	Stock Solution 3	Add 1 mL/L to make substitute ocean seawater with heavy metals
Mn(NO ₃) ₂ 6H ₂ O	0.0546		
Cu(NO ₃) ₂ 3H ₂ O	0.0396		
Zn(NO ₃) ₂ 6H ₂ O	0.0151		
Pb(NO ₃) ₂	0.0066		
AgNO ₃	0.00049		

5.3.2.3.1 Preparation of a Test for Unconfined Conditions

The artificial seawater was made up to a pH of 8.2 which is within the limits of ASTM D1141 [71]. The solution was added to the deaeration vessel (Fig 5-8) where it was purged with inert gas (N₂) until the oxygen level was below 5 ppb. This was measured via a Hach Lange Orbisphere oxygen sensor. Once the solution had been sufficiently deaerated the test solution was ready for transfer to the test rig which has also been sealed and purged with inert gas (N₂) for at least 12 hours. The solution transfer took place with constant bubbling of N₂ to ensure that there was no ingress of oxygen during the transfer procedure (Fig 5-9). Once the solution transfer was complete the gasflow to the test chamber was switched over to the CO₂ test gas and the solution was purged until

5. Methodology

saturation was reached. Saturating the solution with CO₂ results in a drop in pH from 8.2 to approximately 5.00-5.20 and saturation was indicated by a stabilisation of pH.

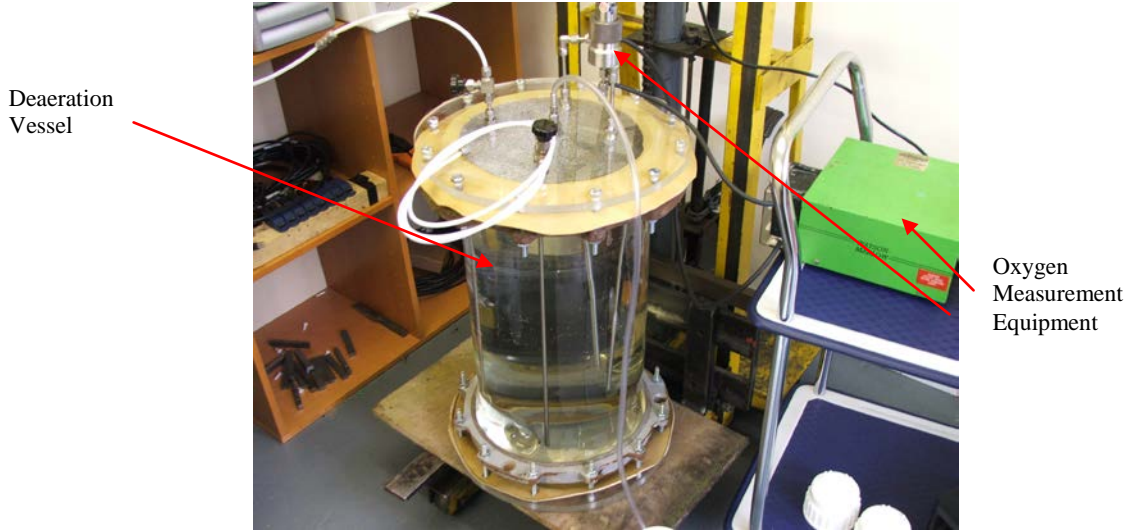


Fig 5-8 – Image of the deaeration vessel containing the test solution, note the gas inlets and outlets along with the ports for the oxygen measuring equipment.

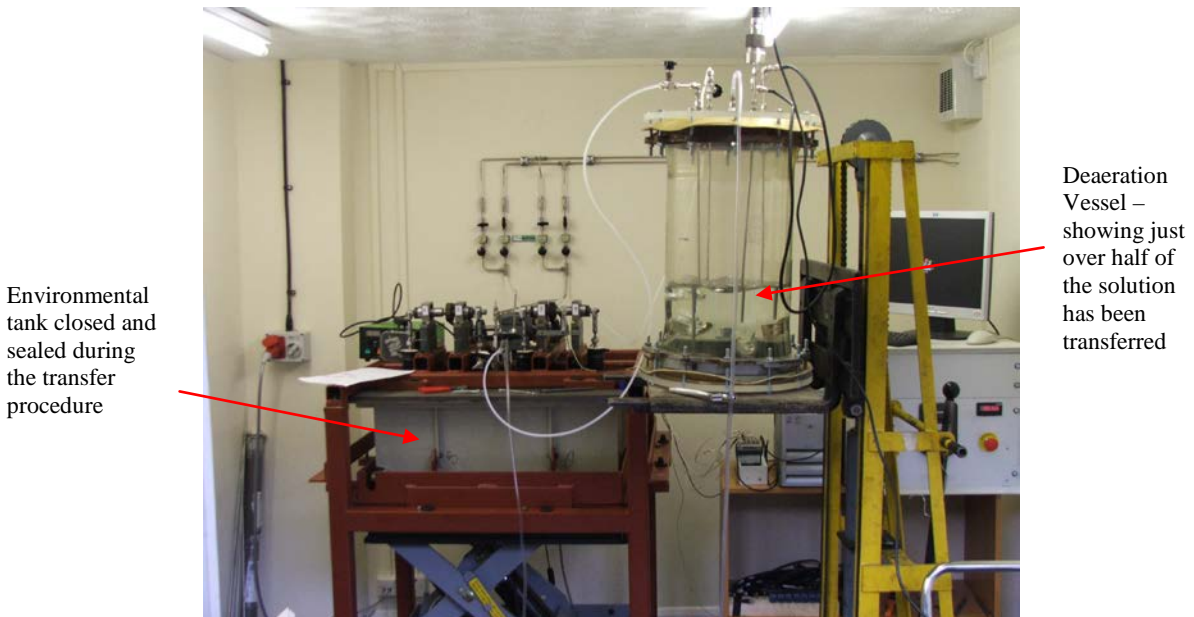


Fig 5-9 – Image of the deaeration vessel and sealed test rig during the solution transfer procedure.

5. Methodology

5.3.2.3.2 Preparation of a Test under Confined Conditions

The test solution was made up in the same way as for the unconfined conditions and placed into the deaeration vessel. Steel wool/steel swarf was then added to the test solution in the deaeration vessel. This was then purged with CO₂ as part of the deaeration process. In this case CO₂ is used for the deaeration process as it will also speed up the corrosion rate of the steel wool to help evolve a test solution representative of confined conditions, i.e. increased pH and super-saturation with Fe²⁺, which was measured via a colorimetric method (Fig 5-10). Once the minimum pH value was reached the solution was transferred into the deaerated test rig which was also packed with steel wool to ensure that confined conditions were maintained throughout the duration of a test.



Fig 5-10 – Image of the colorimetric method used to measure Fe²⁺ content in solution, note the test stick indicates a level in excess of 500 ppm.

5. Methodology

The confined test solution decreased to approximately the same level as the unconfined solution (pH 5.2) upon saturation with CO₂ however, as the steel wool corrodes the pH of the solution will begin to rise. For the confined test conditions a minimum solution pH of 5.8 was set before the solution could be transferred to the test chamber and the dynamic loading started. This value was selected following discussions and advice from flexible pipe manufacturers. The timescale for the solution pH to reach 5.8 is dependant on the volume of solution and the amount of steel wool used. If the ratio is such that it is close to V/S ratio seen in the annulus of a flexible pipe this pH evolution can take as little as a few hours. For the testing under confined conditions carried out in the current research project the V/S ratio used has been sufficient to ensure that confined conditions are obtained within a 4 day pre-conditioning period. Table 5-2 outlines the approximate confinement ratios used for the experimental work in the current research project.

Table 5-2 – Approximate confinement levels used under confined test conditions at both atmospheric and elevated pressure.

Test	Solution Volume (mL)	Approx Surface Area of Steel (cm ²)	Approx confinement Ratio (mL/cm ²)
HPCF	3800	400	9.5
APCF	30000	3000	10

5.3.2.4 Fatigue Loading Parameters

All testing was performed with constant amplitude. Within a sequence of testing to generate an S-N curve the tests were performed either with constant mean stress or with a constant R ratio (i.e., constant ratio between minimum and maximum stress). Most of the

5. Methodology

testing was dictated to an extent by the flexible pipe manufacturers (i.e., Exova's contractual clients) and as such two testing programs were carried out, one material with constant mean (Wire-1 Chapter 4 (Sections 4.2.1 and 4.3.1)) and another with constant R ratio (Wire-2 Chapter 4 (Sections 4.2.1, 4.3.2 and 4.3.3)) depending on how the clients comparative data had been generated. Throughout all further testing in the current research project these parameters have been kept the same to ensure consistency and to allow comparison between datasets generated in different environments.

The frequency of loading is an important parameter to consider in corrosion fatigue testing since corrosion is largely a time dependant process. Manufacturers are keen to accelerate fatigue testing to reduce timescales and costs, however there is a danger that the effect of the corrosive environment on fatigue life is reduced or even eliminated as the test duration is reduced. The API specification [68] recommends that loading frequency should represent conditions seen in-service and advises 0.5Hz as the maximum frequency. Despite this the JIP results have shown that testing at 2Hz is not unrealistic and it was concluded that it does not result in non-conservative fatigue lives in comparison to testing at 0.5Hz [7].

Initial testing on the atmospheric test rig was conducted at a frequency of 0.5Hz. This data includes the investigation of the effect of confinement (Wire-1). Further testing on Wire-2 was conducted at 0.5 and 2Hz to investigate the frequency effect as outlined in Chapter 4. Following the results of this test series together with results from the JIP study [7] most of the subsequent testing was conducted at 2Hz.

5.3.2.5 Testing Procedure

Having described in earlier sections the main the requirements of the test (Section 5.3.1) it is clear to see that there is a considerable effort involved in executing a corrosion fatigue test under such specific conditions. This section aims to describe the different steps involved during the test setup.

1. **Sample Preparation** – Samples are prepared as described in section 5.3.2.2.
2. **Setting Load Levels** – Samples are loaded into their individual fixtures and the eccentricity of the spindle in each loading chain is adjusted to achieve the required load levels (see Figure 6-1, 6-2 or (Appendix 1 – DR/1611-D1 - D4)). Live readings from the load cell on each station show the maximum and minimum values as the samples are cycled during setup.
3. **Pre-cycling** – In order to avoid any relaxation of residual stresses during the test the specimens are pre-cycled in air. This is particularly important as the rig is running with constant displacement so any relaxation during a test would result in a decrease in applied load.

The samples are pre-cycled before any contact with the test environment and are cycled up to 20,000 cycles. After the pre-cycling phase the maximum and minimum load levels are checked and re adjusted if necessary.

5. Methodology

4. ***Sealing and Deaeration of Test Rig*** – Once the sample setup is complete the test rig is then closed and sealed. The rig is then deaerated by purging with nitrogen for at least 12 hours.

5. ***Preparation of Test Solution*** – Test solution is prepared as described in section 5.3.2.3. Depending on the required test environment the solution may need to be prepared 4 days prior to starting the test (confined conditions).

6. ***Solution Transfer*** – Once oxygen content has reached a sufficient level the solution can be transferred to the already deaerated test rig/chamber. The transfer of solution is conducted under constant bubbling of test gas where the flow rate is increased to the deaeration vessel and decreased in the test rig. This, together with increasing the pressure very slightly in the deaeration vessel results in a smooth transfer of solution from vessel to test rig with no ingress of oxygen. Once the transfer is complete the gas supply to the test rig is switched from nitrogen to the required test gas.

7. ***Start of Fatigue Loading*** – Following solution transfer the fatigue loading can begin. This is carried out under constant bubbling of test gas. Signals from each load cell are monitored and logged during the test and pH measurements are also taken during the test

5. Methodology

8. *End of Test* – When all samples have failed as indicated by the load cell readings the test gas supply is switched off and the loading mechanism stopped. If the test requirements specify a sour environment the system is flushed with nitrogen for at least 12 hours before the setup is taken apart. The fractured samples can then be removed and cleaned ready for investigation.

5.4 High Pressure Corrosion Fatigue (HPCF) Testing

As production from the more easily accessible oil reserves begins to decline the industry needs to develop the technology to extract resources from more challenging locations. One aspect is moving production into deep and ultra-deep waters which can have a significant effect on the environmental conditions the flexible pipe needs to withstand due to high hydrostatic and internal bore pressures and/or temperatures dictating the corrosivity in the annulus of a flexible pipe. Accordingly, the next phase of the current research project was to develop capability and perform corrosion fatigue testing at elevated pressure and temperature in order to closely simulate the complex environmental conditions inherent to such challenging production locations.

5.4.1 Requirements of Experimental Setup

Following discussion with flexible pipeline manufacturers it was clear that a high pressure corrosion fatigue (HPCF) test facility was required to meet certain requirements if it were to be capable of conducting tests according to their specifications/procedures. Specifically, the key requirements from the industry that the HPCF test rig had to meet were as follows:

1. Apply loading to the samples in four point bending
2. Apply sine shaped waveform
3. Operate in load control (rather than displacement control used on the APCF rig)

5. Methodology

4. Capability to expose samples to deaerated simulated oilfield environments saturated with controlled partial pressures of H₂S and CO₂.
5. Apply loading frequency between 0.1 and 2Hz
6. Measurement of test solution pH at elevated (test) pressure

5.4.2 Test Method

The test protocol used for high pressure corrosion fatigue testing in the current research project is in general accordance with the requirements given in the JIP test protocol [1] and manufacturers test procedures.

5.4.3 Loading Method

Fatigue testing is generally performed in one of two ways; axial tension or bending. Since most of the development work on the ambient pressure rig was conducted in four-point bending this was the preferred option when developing the HPCF facility. It should be noted that four-point bending was chosen since the area of the sample between the two central rollers is exposed to maximum uniform tensile strains as opposed to loading hotspots being generated at the grip in cantilever bending and at the centre contact point in three point bending. This is important as it will generate results taking into account a realistic population of defects and imperfections along the length of the tested sample. Furthermore, samples tested in the four-point bend configuration can be tested in the as-received condition or machined easily by simply reducing thickness. If samples are

machined the machining process is conducted on the compressive load side of the sample making sure that the tensile face is kept in as-received condition.

5.4.4 Sample Preparation

The fatigue properties of a given material are sensitive to the surface condition of the sample as well as the level of residual stress induced during manufacture. These are key parameters to consider during corrosion fatigue testing since both can also have a significant impact upon the way in which the sample reacts to the corrosive environment.

It is important to generate data that is simulating the materials in service performance. In the case of testing armour wires the tensile surface of the wire must be kept in as-received condition so that any effect of the manufactured surface is included in the test.

Since the armour wire material is delivered on coils there is a certain level of residual stress contained within each sample. The preparation of a corrosion fatigue sample involved cutting the armour wire material to the required length and clearly marking the tensile face of the sample. Since we operated the test in load control, load capacity on the test machine was designed to cope with even the largest size of tensile armour wire currently used by the industry. For this reason all samples in the HPCF test series were tested in as received condition (full thickness) with no machining required.

The samples were then thoroughly cleaned using soap and detergent and degreased with acetone prior testing. One calibration sample for every batch was instrumented with a strain gauge and load cell readings were subsequently checked against strain gauge

5. Methodology

measurements to ensure that the strain levels are within 5% of the theoretical strain at a given load (Fig 5-11).

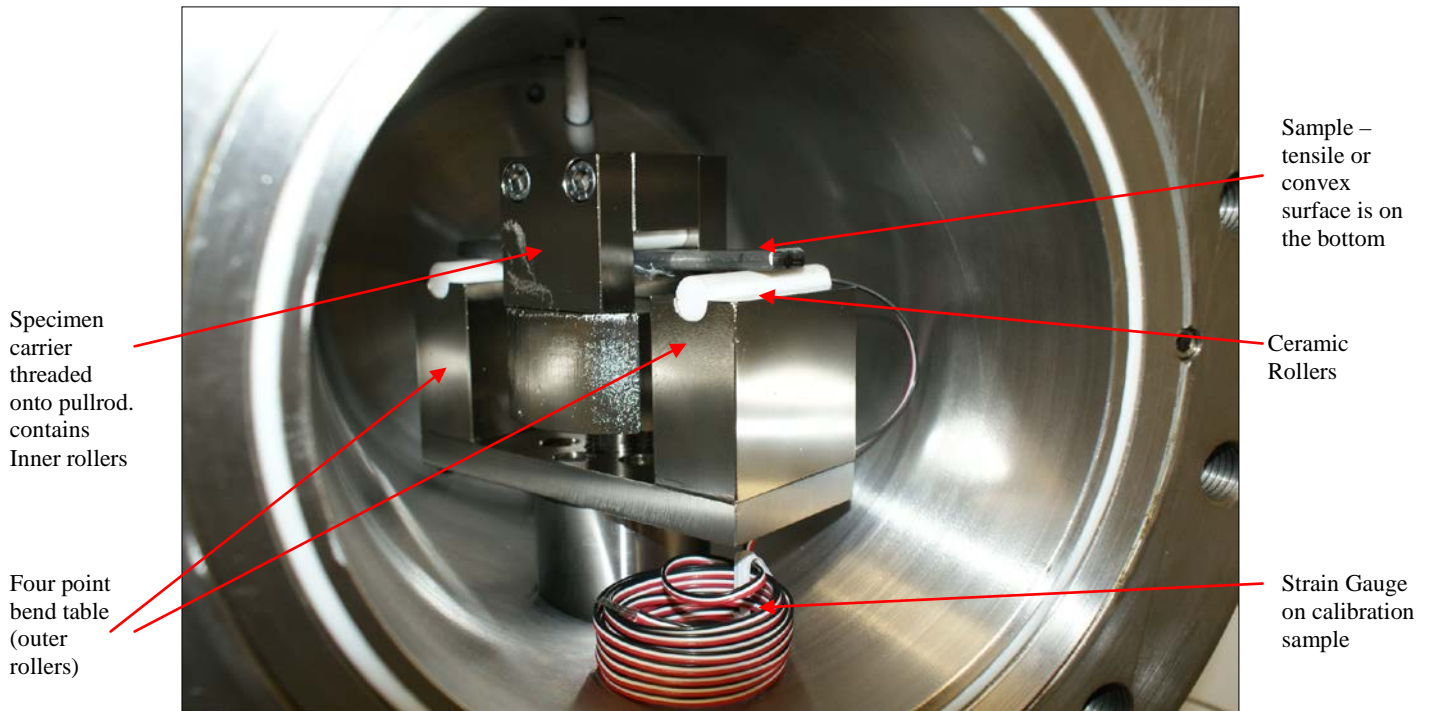


Fig 5-11 – instrumented sample mounted inside the four point bend fixture.

5.4.5 Test Environment

The electrolyte used in the corrosion fatigue tests was a standard ASTM D1141 (without heavy salts) artificial seawater solution [71]. Corrosion conditions in oil and gas production are oxygen free so the solution was strictly deaerated to levels below 5 ppb. The artificial seawater solution is typically saturated with a mixture of H₂S and CO₂ as a test gas and then pressurised to the required test pressure. Since the annulus of a flexible

5. Methodology

pipe is densely packed with carbon steel armouring components there is little free volume for the electrolyte which results in extremely confined conditions. The ratio of free volume to steel surface area (V/S) in the annulus environment is typically below $0.1\text{ml}/\text{cm}^2$. In order to simulate the confined conditions in the annulus of an unbonded flexible pipe steel wool was added to the test solution in order to increase the surface area of steel. Consequently, as the steel wool corrodes Fe^{2+} and an equivalent amount of alkalinity was released into the electrolyte causing the pH to increase and the solution to become super-saturated with Fe^{2+} [3,4,5]. All testing in the HPCF test series was conducted under confined conditions. Steel wool was added into the test rig contained within polymer netting so that it is not in galvanic contact with the specimens. Other than the addition of steel wool the pH was allowed to settle freely. The steel wool was weighed into 40g parcels and 6 of these were added into the autoclave for each test giving a total weight of 240g, equivalent to a surface area of 0.4m^2 (Figure 5-12) and an approximate confinement ratio of $9.5\text{mL}/\text{cm}^2$.

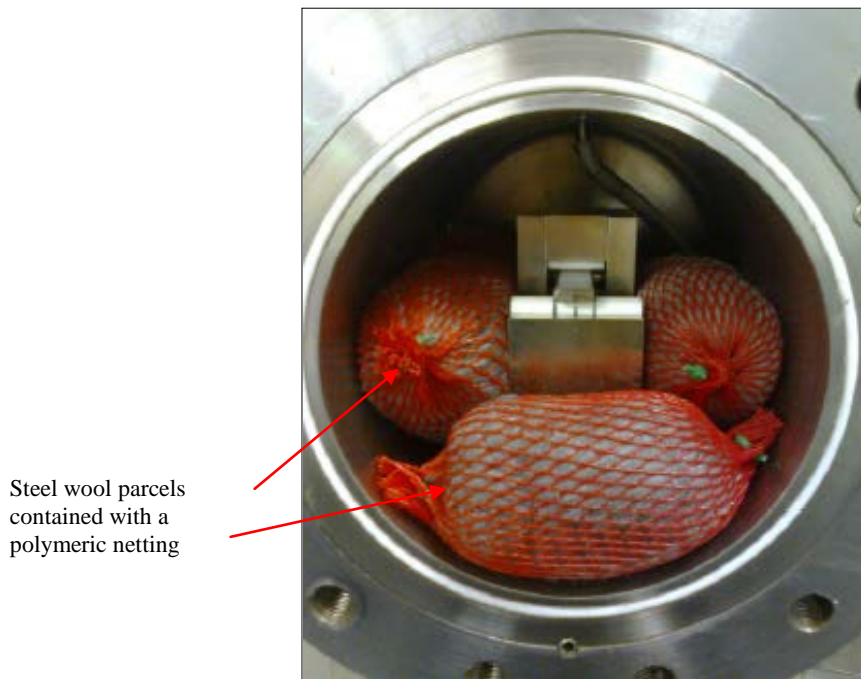


Figure 5-12 – Inside of the autoclave showing the sample in the fixtures and the densely packed arrangement of the steel wool parcels in order to ensure confined test conditions.

The artificial seawater was made up to a pH of 8.2 within the limits of ASTM D1141 [71]. The solution was added to the deaeration vessel where it was purged with inert gas (N_2) until the oxygen level was below 5 ppb. Once this level was reached the test solution was ready to transfer to the autoclave which had also been sealed and purged with inert gas for at least 2 hours. The solution transfer took place with constant bubbling of inert gas to ensure there was no ingress of oxygen during the transfer procedure (Fig 5-13).

Once the solution was inside the autoclave it was purged with inert gas for a further 15 minutes before being switched over to the test gas and pressurised to the required test pressure. This point marks the start of a 4 day pre-exposure period where the samples

5. Methodology

were held in position with a low static load (0.3kN). At the end of this 4 day period a pH measurement was taken at test pressure and if it had reached a value of pH 5.6 then the fatigue loading portion of the testing could begin.

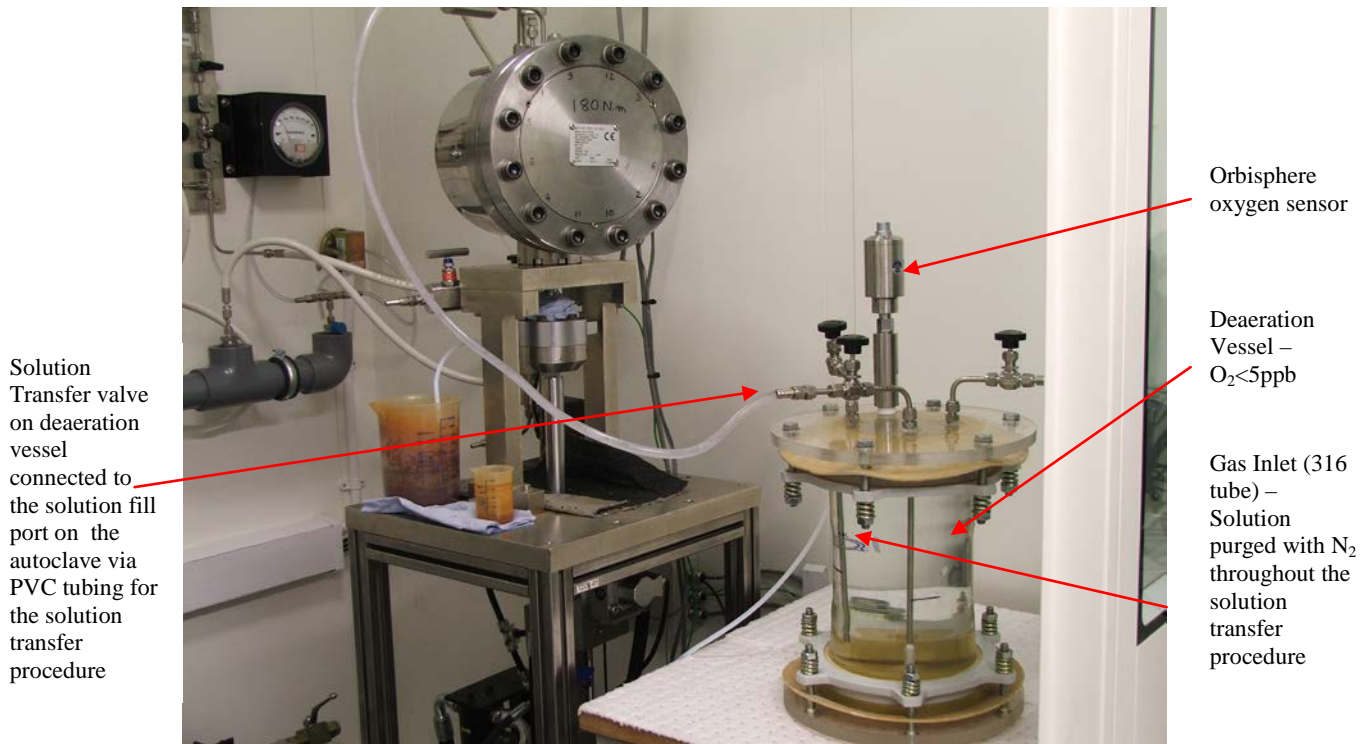


Fig 5-13 – Image of the deaeration vessel and sealed test rig during the solution transfer procedure

5.4.6 Elevated Pressure pH Measurements

To meet the requirement of measuring test solution pH at elevated (test) pressures a bespoke secondary autoclave for pH measurements was manufactured (described in Section 6.2). The procedure used for making these measurements was as follows:

5. Methodology

1. Firstly, following calibration and insertion of the high pressure pH probe into the secondary autoclave, the vessel and all associated pipework and tubing must be deaerated by purging with N₂.
2. Once deaerated, the pH vessel is pressurised to the same test pressure as the main autoclave, with the test gas mix.
3. When the pH vessel is at equal pressure to the main autoclave the needle valve which connects the pH sampling port on the main autoclave to the solution in port on the pH vessel can be opened allowing the vessels to be at equilibrium.
4. The needle valve on gas outlet of the pH vessel can then be opened a ¼ turn which will allow the test solution to flow from the main autoclave into the pH vessel. Once the LED light from the liquid level sensor is energised the valves can be closed and an elevated pressure pH measurement can be taken.
5. Following the measurement at test pressure the pH vessel can be depressurised by opening the gas outlet fully. After 3 minutes a second pH measurement can be recorded at ambient pressure.
6. Finally, the pH vessel is purged with N₂ for 15 minutes to ensure that all H₂S is removed before the solution is drained away and the vessel and probe can be cleaned.

5.4.7 Fatigue Loading Parameters

All HPCF testing was performed with constant amplitude and with a constant mean stress of 400MPa. The frequency of loading is an important parameter to consider in corrosion fatigue testing since it is a time dependant process. Manufacturers are keen to accelerate testing to reduce testing timescales and costs however the danger is that the effect of the corrosive environment on fatigue life is reduced or even eliminated. The JIP results [7] along with the frequency investigation work carried out on the atmospheric pressure CF rig in the current research project have shown that testing at 2Hz is not unrealistic and it was concluded that it does not result in non-conservative fatigue lives in comparison to testing at 0.5Hz. As a result, all testing in the HPCF test series was performed with a test frequency of 2Hz.

5.4.8 Testing Procedure

Having described in earlier sections the main requirements of the test it is clear to see that there are a lot of stages involved in executing a corrosion fatigue test under such specific conditions. This section aims to describe the different steps involved during the test setup.

Sample Preparation – Samples are prepared as described in section 5.4.4.

Setting Load Levels – Samples are loaded into the bend fixture ensuring the correct orientation and alignment then a small load (0.1kN) is applied to the sample to hold it in

5. Methodology

place whilst it is secured at either end with elastic bands to prevent any ‘walking’ of the sample. The required loads are then input to the software for the pre-cycling phase in air.

Pre-cycling – In order to avoid any relaxation of residual stresses during the test the specimens are pre-cycled in air. The samples are pre-cycled before any contact with the test environment and are cycled up to 20,000 cycles. Once pre-cycled the samples are then held in place in load control at 0.3kN throughout the 4 day pre exposure period.

Sealing and Deaeration of Autoclave – Once the sample setup is complete the autoclave is packed with the steel wool parcels then closed and sealed. The autoclave is then deaerated by purging with nitrogen for at least 2 hours.

Preparation of Test Solution – Test solution is prepared as described in section 5.4.5.

Test solution will be purged with inert gas until oxygen levels are less than 5ppb.

Solution Transfer – Once oxygen content has reached a sufficient level the solution can be transferred to the already deaerated autoclave. The transfer of solution is conducted under constant bubbling of inert gas where the flow rate is increased to the deaeration vessel and decreased in the autoclave. This, together with increasing the pressure very slightly in the deaeration vessel results in a smooth transfer of solution from vessel to autoclave with no ingress of oxygen. Once the transfer is complete the autoclave is

5. Methodology

purged with nitrogen for a further 15 minutes (this duration has been verified as sufficient during the qualification phase) before being switched to the required test gas and then pressurised to the test pressure.

4 day Pre-exposure – Samples are exposed to the test solution at test pressure for a period of 4 days before the fatigue loading is started. This is to allow time for the test sample to become saturated or ‘charged’ with hydrogen and also for the confined conditions to develop before any dynamic loading is initiated. After the 4 day exposure period a pH is taken at test pressure. If the measured pH is above 5.6 then the fatigue loading can be started.

Start of Fatigue Loading – before starting the fatigue phase the test loads are recalculated to take account of the effect of the test pressure reacting against the pullrod and specimen carrier, thus affecting the load cell readings. This is done by subtracting the value of load that is observed at the test pressure (measured during qualification and calibration phase) from the required test loads. This ensures that test loads do not exceed the targeted values.

End of Test – When the sample has failed as indicated by a trip on one of the preset limits (load and/or displacement) the test machine will stop automatically. At the end of each test a pH measurement is taken at test pressure and then at ambient pressure. If the

test requirements specify a sour environment then the system is flushed with nitrogen for at least 2 hours before the experimental setup is taken apart. The fractured sample can then be removed and cleaned ready for investigation.

5.4.9 Calculation of Gas Mix required to simulate p_{H_2S} at Elevated Pressures

For the high pressure corrosion fatigue (HPCF) test series the aim is to simulate as closely as possible the predicted annulus environment when the pipe is subjected elevated pressures due to both high internal bore pressure and external hydrostatic pressures. The predicted pressures and partial pressures of species within the annulus will alter the chemistry and thus the corrosivity of the environment.

In order to accurately simulate such complex environments pre-mixed gas cylinders were used containing the correct amounts of corrosive species to achieve the desired test partial pressures. Table 5-3 shows the relationship between the required H_2S partial pressure (p_{H_2S}), total CO_2 pressure and the required gas mix. The gas mix was calculated by multiplying the required p_{H_2S} in mbar by 1000 and then dividing by the total system pressure to give a value in ppm, which is the gas mix (ppm H_2S) needed to provide a specific p_{H_2S} at a given test pressure.

5. Methodology

Table 5-3- Table showing the relationship between pH₂S, total CO₂ pressure and required gas mixture. The values used for the HPCF test series are highlighted at the bottom of the table.

Required pH ₂ S (mbar)	Total System/CO ₂ Pressure (bar)	Gas Mix required (ppm)
0.1	1	100
1	1	1000
10	1	10000
0.1	1	100
0.1	10	10
0.1	100	1
0.15	7.08	21.19

For example, in the HPCF test series annulus conditions are predicted to be 7.08 bar total CO₂ pressure with a pH₂S of 0.15mbar. So from table 5.4.9 it can be seen that the required gas mixture is 21.19ppm H₂S balanced with CO₂. The gas mixes are ordered from BOC Gases Ltd and come certified to +/-5% of the requested value. In order to ensure that levels are not below the required value, the 5% error margin is added to the required value giving a gas mix of 22.3ppm. This value is then rounded to 22ppm which was the gas mixture that has been used for the HPCF test series.

6. Results and Discussion (Design and Development of Test Facilities)

6. Results and Discussion (Design and Development of Test Facilities)

6.1 Atmospheric Pressure Corrosion Fatigue Rig

The aim of the initial stages of the current research project was to design and manufacture a prototype atmospheric pressure corrosion fatigue (APCF) test rig capable of commercially testing flexible pipe tensile armour wires to the specification and requirements outlined in Chapter 5. As such it is logical to include such work in the first section of the results since this was a key task/milestone throughout the current research project. Tasks for this work along with a list of the associated project team involved are outlined in Table 6-1.

Table 6-1 – Overview of the different phases of work during the design and development stage of this thesis.

Atmospheric Pressure Corrosion Fatigue Design and Development stages		
Phase	Task	Project Team
Preliminary Work	Confinement Investigation Trials	DH
	Design of Deaeration Vessel	DH
	Development of deaeration/transfer procedures	DH
	Component Testing, resistance to Environment	DH
Test Room Design	Specification of Gas Lines	DH
	Specification of Extraction	DH
	Specification of Electrical Supply	DH
Test Rig Design	General Layout to meet Test requirements	DH, OR
	Design of Top and Bottom Plate	DH, OR
	Design of Loading Chain	DH, OR
	Design of Bend Fixtures	DH, OR
	Design of Environmental Tank	DH, OR
	Specification of Corrosion Related Ports	DH
	Pipework Design for connection of gaslines	DH
	Specification of Inverter/Electric Motor	OR
Data Acquisition Software development	OR	
Manufacture	Machining of all components (in-house machine shop)	machine shop
	Fabrication of box section frame (welded)	MP
Assembly	Scissor lift, Environmental tank to main frame	MP
	Loading Chains	DH
	Bending fixtures	DH
	top and bottom plates	DH
	corrosion fittings, valves and pipework	DH
	Sealing components, rubber bellows, o-ring	DH
Inverter/Electric Motor	OR	
Qualification Testing	Deaeration qualification Testing	DH
	1bar CO2 qualification testing	DH

DH – Dean Horspool (EngD Student)

OR – Olivier Ravier (Project Engineer – Exova)

MP – Mick Parton (Senior Fitter – Exova)

6. Results and Discussion (Design and Development of Test Facilities)

6.1.1 Description of Test Facility

A description of the main characteristics of the designed and manufactured experimental corrosion fatigue setup is given in the following section. Figure 6-1 gives a global overview of the manufactured test rig while detailed drawings can be found in Appendix

1.

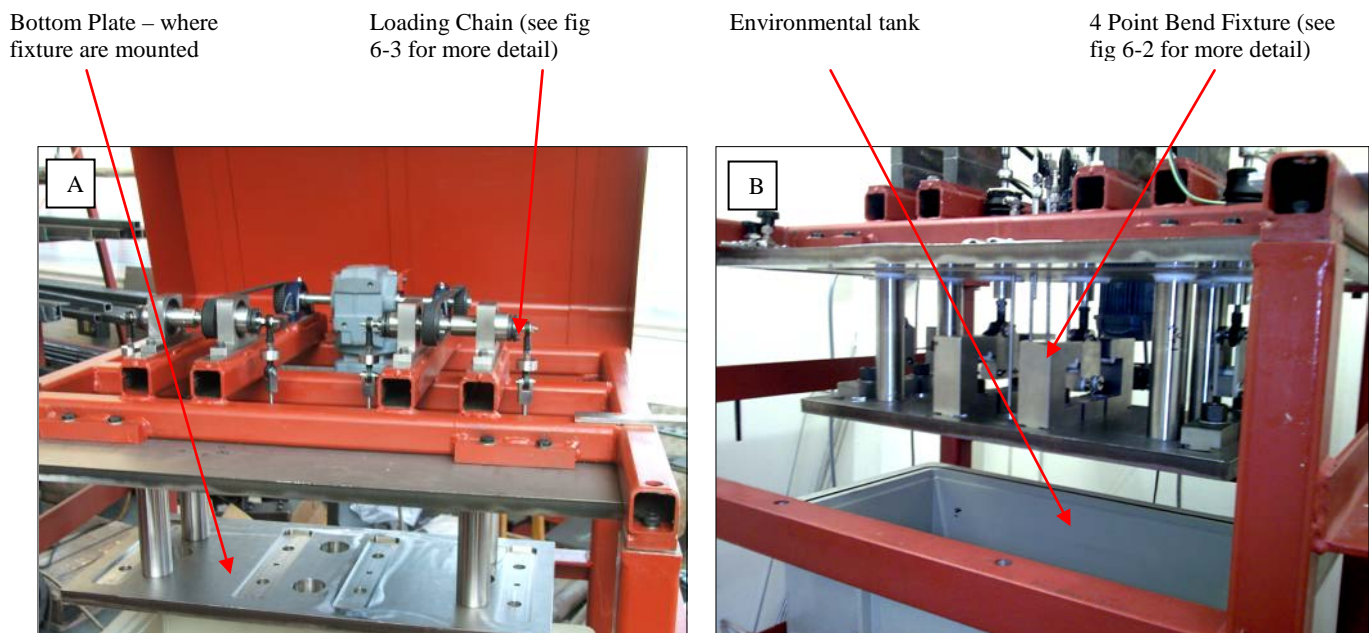


Fig 6-1 –Overview of Rig Construction (Appendix 1 – Drawing title - Layout of Test Machine), a) showing top assemblies and bottom plate (Appendix 1 – DR/1611-D21) with locations machined for specimen fixtures , b) showing containment tank and bottom plate with four point bend specimen fixtures in place.

6.1.1.1 General Description

The constructed machine is a fixed displacement atmospheric pressure corrosion fatigue rig. It has four independently adjustable stations, each station having an individual load

cell incorporated into the loading chain allowing load readings to be continuously monitored. Displacement is achieved via a combination of a rotating eccentric cam and an eccentric spindle giving displacements ranging from 0-6mm (see Appendix 1 – DR/1611-D1 - D4). The four stations are then submerged into a communal tank which can be raised on a scissor lift and seals on to the top plate via an o-ring (Fig 6-1) giving an air tight seal for environmental containment.

6.1.1.2 Actuating System

A popular and versatile method for the application of alternating loads is via servo hydraulic actuators. However, such systems can be very complex and also rather expensive. As a result an alternative actuating system has been utilised and since the required loading pattern is sinusoidal shaped it makes sense that the system is based on a rotating shaft. In order to adjust stroke length on such a fixed displacement machine an adjustable eccentric spindle was designed to fit into the bore of an eccentric cam. Displacement is then controlled by offsetting the eccentricity of the spindle relative to the cam. The eccentric shaft is then driven by an electric motor controlled by a frequency inverter which allows accurate control of the loading frequency.

6.1.1.3 Specimen fixture and Loading Chain

Loading is applied in four-point bending by supporting each end of the sample and deflecting the sample via two central contact points acting on the opposite side of the

6. Results and Discussion (Design and Development of Test Facilities)

specimen. Cylindrical rods of 15mm diameter were selected as the roller contact points which are fixed in place on the specimen fixture (outer contact points) and located in machined holders on the specimen carrier (inner contact points). The specimen fixture is shown in Figure 6-2.

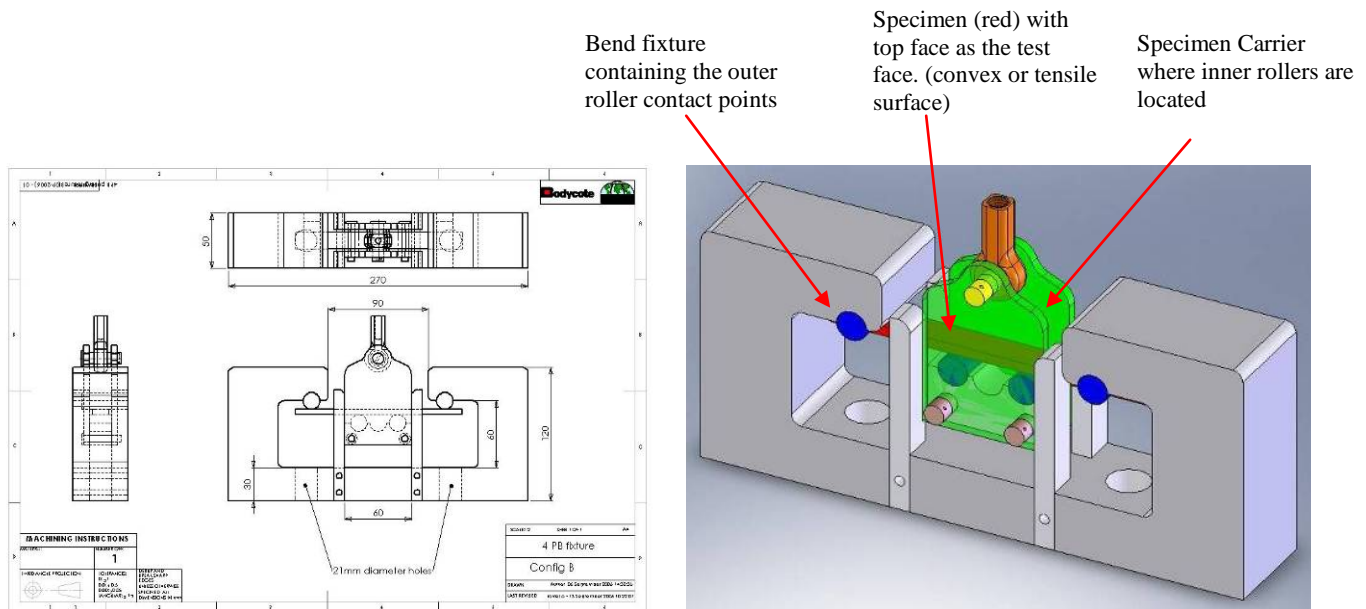


Fig 6-2 –Specimen fixture Construction, a) Solidworks drawing, b)CAD picture illustrating the specimen carrier (green), roller contacts (blue) and the specimen (red) locations in the experimental setup.

The material used for the roller contact point must be resistant to environmental degradation from test solutions in which it operates. It must have high wear resistance and electrically insulate the specimens so that galvanic corrosion effects are avoided. Therefore, a ceramic material was chosen for the contact points since it meets all of the above requirements and is readily available.

Load transfer is accomplished by the specimen carrier pulling the top face of the sample

6. Results and Discussion (Design and Development of Test Facilities)

into tension as the eccentric shaft rotates. This method of load transfer is self aligning since the specimen carrier is attached to the loading chain via a rod end bearing on which it can pivot (Fig 6-2b). This is important as the alignment of the specimens results in deflection which is perpendicular to the length of the specimens in order to produce the predicted stress pattern from four-point bending. Further detail of the loading chain is shown in Figure 6-3

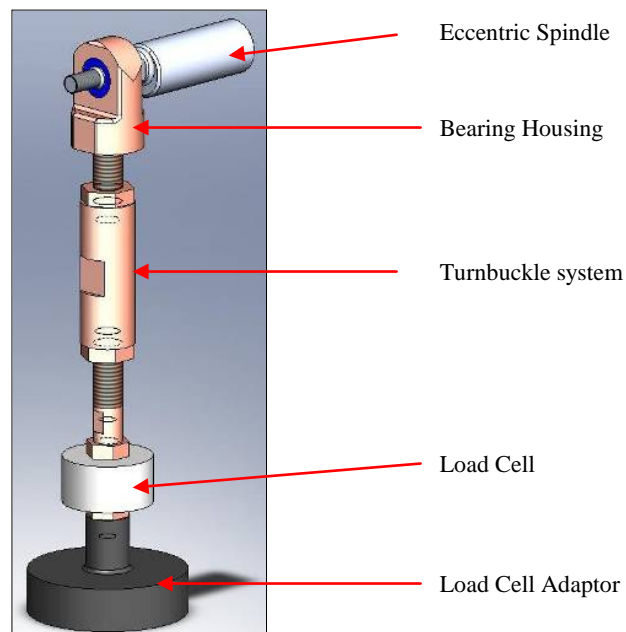


Fig. 6-3 – CAD illustration of the components within the loading chain.

6. Results and Discussion (Design and Development of Test Facilities)

From top to bottom the loading chain consists of:

1. Bearing Housing – contains a needle roller bearing that fits directly onto the shaft of the eccentric spindle with a right hand threaded section that fits into the turnbuckle barrel.
2. Turnbuckle system – consists of a barrel with a right handed thread on the top and a left handed thread on the bottom. This allows adjustment of the height of the specimen carrier which is essential when setting the required loads on a sample.
3. Load Cell – incorporated for continuous monitoring and logging of load data. The load cell will also be used to detect failure and trip the system software when a decrease in load is observed.
4. Load Cell Adaptor – component made from super duplex (as are all components in direct contact with the environment). A rubber bellow seals around this component making the rig air tight.

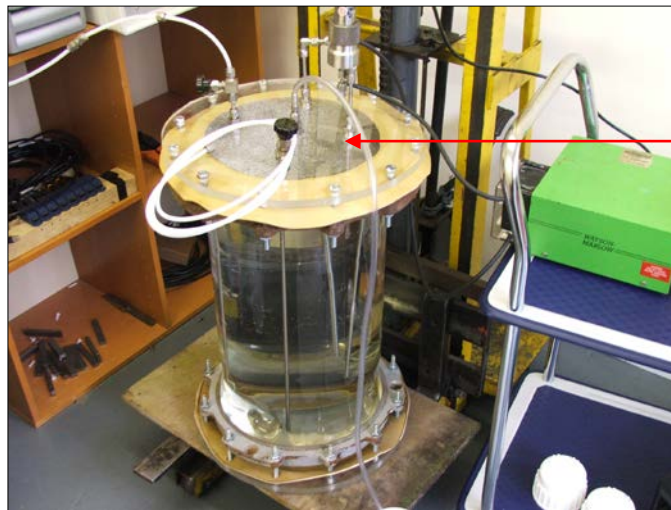
6.1.1.4 Environmental Control and Containment System

To meet the requirements of the test procedure, test samples needed to be exposed to a controlled corrosive environment whilst being fatigue loaded. Components used in the experimental setup for the corrosion fatigue tests needed to be resistant to the simulated service environments. These components are outlined in the following section.

Deaeration Vessel – The purpose of the deaeration vessel was to prepare the test solution prior to transfer to the test rig and contact with the test samples. The deaeration vessel

6. Results and Discussion (Design and Development of Test Facilities)

was constructed to contain up to approximately 50L of test solution however 30L was typically used. Figure 6-4 shows an image of the constructed deaeration vessel made up of tapering glass cylindrical walls with a top and bottom flange. A plexiglass base was then fitted and sealed against the bottom flange using a rubber gasket. For the top of the deaeration vessel a plexiglass lid was machined to contain all of the necessary ports including; gas inlet, gas outlet, solution transfer and ports for the orbisphere oxygen analysis equipment.



Deaeration vessel – plexiglass base and lid with ports for gas inlet, outlet and oxygen measurements. Also a solution transfer port

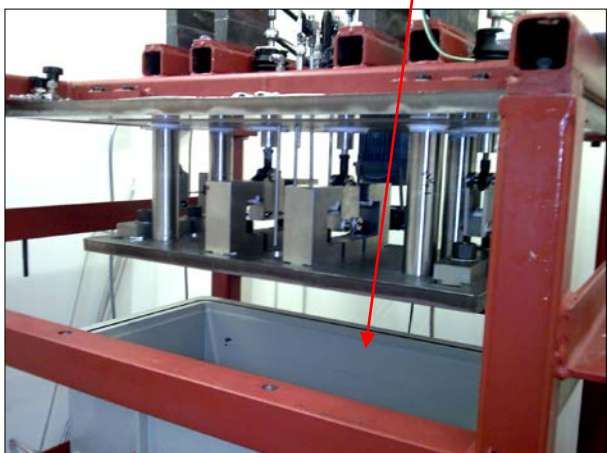
Fig. 6-4 – Image of the constructed deaeration vessel used in the experimental setup, Note the ports and fittings on the lid of the vessel needed for the deaeration procedure.

Test Chamber/Tank – The test chamber was built to encapsulate all four specimen fixtures so that each sample was exposed to the same environment within each test run. The test chamber is shown in Figure 6-5 and construction consists of rectangular tank

6. Results and Discussion (Design and Development of Test Facilities)

with a top flange which has an o-ring groove machined into it (see Appendix 1 – DR/1611-12 – 16 for details).

Tank in its open position revealing the bottom plate and associated bend fixtures



Tank in its closed position where the o-ring seals against the top plate



Fig. 6-5 – Images of the constructed test chamber used in the experimental setup, a) tank is in its lowered position allowing the specimen fixtures to be seen, b) tank in its raised position, sealed against the top plate and containing the sample fixtures (see Appendix 1 – DR/1611-12 – 16).

The tank sits on a hydraulic scissor lift which was used to raise and lower the tank into its test and off test positions, respectively (Fig 6-5). Once in its raised position the tank was mechanically locked in place using bolts and c-washers ensuring that there was enough force applied to deform the o-ring which seals onto the top plate (see Appendix 1 – DR/1611-D8) providing an air tight seal.

Gas Supply System– Gas lines were installed to allow for supply of all gases used during the test procedure. Nitrogen was generally used as the deaeration gas with CO₂ or CO₂+H₂S used as test gases which were supplied in pre-mixed pressurised cylinders. The

gas supply system was set up in such a way that you could switch from one gas to another without disconnecting any of the lines which prevents oxygen ingress. Flow rates to the test rig were very finely controlled through the use of flow meters. It should be noted that the the prototype test rig was designed to operate at ambient pressure only.

Following manufacture and assembly of the experimental setup a qualification trial was conducted in order to verify that the environmental conditions generated during testing met the necessary requirements, specifically control of oxygen levels during a test. This qualification test consisted of setting up a test as normal under unconfined conditions (Section 5.2.2.3.1) and following the usual deaeration procedure. Following the transfer of solution to the test chamber the orbisphere oxygen analysis equipment was also transferred onto the test rig and oxygen levels monitored over a 24 hour period to ensure that levels remained below 5 ppb during a test.

6.1.1.5 Materials Selection

All components of the experimental setup that are in direct contact with the corrosive test solution must be manufactured from materials that are resistant to degradation by the environmental conditions produced. For this prototype rig that environment is typically anaerobic artificial seawater saturated with 1bara CO₂ or some mbara of H₂S balanced with CO₂ to a total pressure of 1bar. This rig has been designed for testing at ambient temperature and pressure.

A glass vessel and plexiglass base and lid have been used for the deaeration vessel since these are not reactive with the test solution. The test chamber is constructed of

polycarbonate and specimen fixtures are manufactured from duplex stainless steel type 2205. In fact all components located within the test chamber in its raised position are made from duplex stainless steel including; top and bottom plates, support columns, specimen carriers, pull-rods and all nuts and bolts. Rollers used as the specimen contact points for support and deflection are made from a ceramic material ensuring there is no galvanic coupling between the test samples and other alloys in the test chamber. All pipework, Swagelok fittings and valves are made in stainless steel type 316.

6.1.1.6 Data Acquisition and Monitoring

The control and monitoring systems form a very important part of the corrosion fatigue setup. All systems are electronic and integrated in a computer system. The system and user interface was built in National Instruments LabView. This data acquisition system was used to monitor and log individual load cell readings for each station as well as a cycle counter for each station. This cycle counter is tripped when the peak load value drops below a certain level and is used to detect failure of a sample during the test.

Frequency control of the system is based on controlling the rotating speed of the electric motor with a frequency inverter. Based on the frequency the system calculates the number of cycles during a test. In addition to the frequency based system a mechanical counter is applied to measure the number of cycles directly.

6. Results and Discussion (Design and Development of Test Facilities)

6.1.2 Confinement Investigation Trial Testing

In order to simulate as closely as possible the environmental conditions encountered during service in the annulus of a flexible oil and gas pipeline, corrosion fatigue tests need to be carried out in Fe^{2+} saturated solutions. This is due to the fact that there is very little solution volume compared to surface area of steel wires in the annulus of a flexible pipe and there is evidence to show that under such conditions solutions quickly become saturated with Fe^{2+} ions which may have a beneficial effect on corrosion and corrosion fatigue [2,5,6]. Under such conditions the solution pH is higher than calculated by standard CO_2 corrosion models and the beneficial effect is attributed to a combination of this and precipitation of a protective iron carbonate scale (FeCO_3) on the surface of the steel wires both acting to decrease corrosion rates within the annulus.

Preliminary tests on the effect of confinement on solution chemistry and pH have been conducted to verify this phenomenon (Figure 6-6).

Vessel used for confinement trials – steel wool inside with ASTM D1141 saturated with 1bar CO_2 . Jacket to maintain ambient temperature



Fig. 6-6 – (left) Confinement investigation trials experimental setup, (right) samples of test solution taken at intervals between 1 and 48 hours, visually showing the increasing levels iron saturation as pH increases.

6. Results and Discussion (Design and Development of Test Facilities)

In these tests the Fe^{2+} rich solutions have been obtained by corroding commercially available steel wool [1] in artificial seawater [71] saturated with 1bar CO_2 . pH (Fig 6-7) and Fe^{2+} (Fig 6-8) concentrations were then monitored periodically over a duration of 30 days.

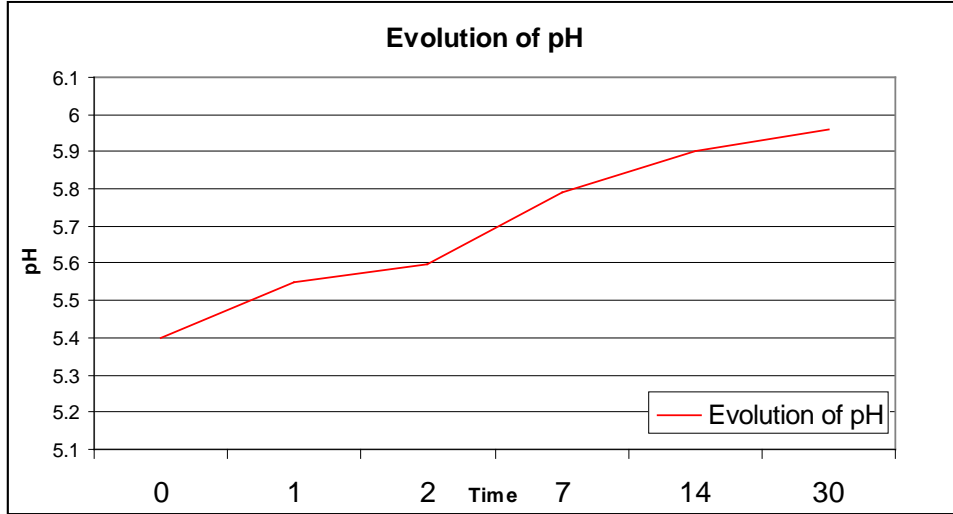


Fig. 6-7 – Graph showing pH evolution of ASTM D1141 saturated with 1bar CO_2 under confined conditions (using steel wool).

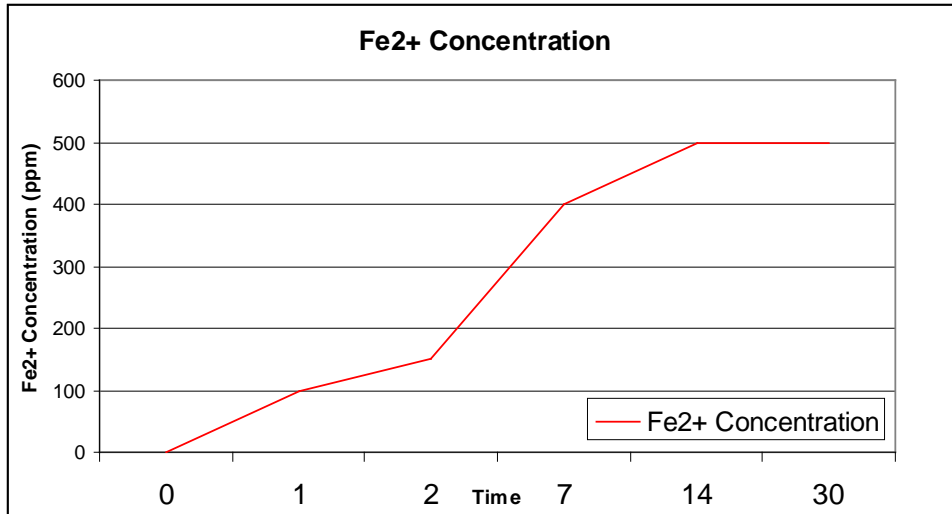


Fig. 6-8– Graph showing Fe^{2+} concentration of ASTM D1141 saturated with 1bar CO_2 under confined conditions (using steel wool).

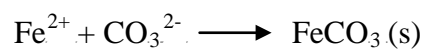
6. Results and Discussion (Design and Development of Test Facilities)

The results of these tests clearly show that pH and Fe^{2+} levels increase throughout the duration of the test. pH appears to stabilise between pH 5.9-6 which is in agreement with previous work [6] . Equally Fe^{2+} concentration increases to supersaturated levels in excess of 500ppm over the duration of the test. The speed at which pH and Fe^{2+} reach saturation is dependant on the ratio of solution volume to surface area of steel (V/S). At V/S ratios approaching that seen in the annulus of a flexible pipe saturation can take as little as a few hours to occur. For the fatigue testing under confined conditions carried out in the current research project the V/S ratio used has been sufficient to ensure that confined conditions are obtained within a 4 day pre-conditioning period. Table 6-2 outlines the approximate confinement ratios used for the experimental work in the current research project.

Table 6-2 – Approximate confinement levels used under confined test conditions at both atmospheric and elevated pressure.

Test	Solution Volume (mL)	Approx Surface Area of Steel (cm ²)	Approx confinement Ratio (mL/cm ²)
HPCF	3800	400	9.5
APCF	30000	3000	10

Once the concentrations of Fe^{2+} and CO_3^{2-} (carbonate) ions exceed the solubility limit, precipitation of a potentially protective FeCO_3 scale can occur [72].



6. Results and Discussion (Design and Development of Test Facilities)

The solubility of FeCO_3 is strongly dependent on pH and CO_2 partial pressure. This is demonstrated in Figure 6-9 where the amount of Fe^{2+} needed to be produced by corrosion to reach FeCO_3 saturation is plotted as a function of pH at the start of the corrosion process.

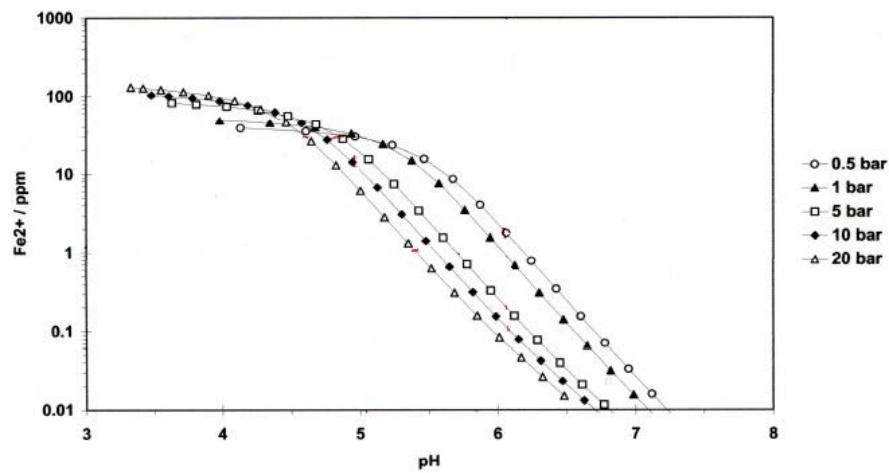


Fig. 6-9 – Amount of Fe^{2+} needed to be produced by Corrosion to reach FeCO_3 saturation, plotted as a function of pH. pH is the pH before corrosion has started. [72].

It can be seen that at pH 6 and 1bar CO_2 partial pressure $[\text{Fe}^{2+}]_{\text{sat}}$ is approximately 1-2 ppm and is reduced 100 times per unit pH increase. This indicates that in the corrosion fatigue testing under confined conditions, saturation levels are well above the solubility limit for Fe^{2+} under those specific conditions. This means that FeCO_3 precipitation can occur and potentially provide the steel with a level of corrosion protection.

6.2 High Pressure Corrosion Fatigue (HPCF) Design and Rig Setup

Following successful pilot testing and completion of the initial corrosion fatigue test matrix generated on the atmospheric pressure prototype rig, the flexible pipeline manufacturers were keen to extend the scope of service environments that could be simulated within the corrosion fatigue test facility. Such testing requirements evolved due to demand from within the Oil and Gas industry which resulted in the design and manufacture of facilities at Exova capable of corrosion fatigue testing at elevated temperature and pressure (HPCF). Specifically, test machines have been designed to enable corrosion fatigue testing at up to 50bar and 100°C in simulated sour oilfield environments. These newly designed test facilities enable the investigation of properties over a wide range of service environments and the data generated will contribute towards the technological advancement of flexible pipelines and risers.

The following sections aim to discuss the main aspects of the design and installation of this unique, state of the art HPCF facility along with details of the main characteristics of the designed and manufactured HPCF experimental setup. Table 6-3 outlines the work carried out in the design and development stages for Phase II of this thesis.

6. Results and Discussion (Design and Development of Test Facilities)

Table 6-3 – Overview of the different phases of work during the design and development stage of this thesis.

High Pressure Corrosion Fatigue (HPCF) Design and Development Stages		
Phase	Task	Project Team
Design of HPCF Facility	General Layout of Building/Gas Cylinder Building	DH,OR,LB
	Specification of Gas Lines	DH, OR
	Specification of Extraction System	DH, OR
	Specification of Gas Alarm System	DH, OR
	Specification of H2S Scrubber System	DH
	Specification of Hydraulic System	MP
	Specification of Electrical Supply	DH, OR
Build Phase	Build and Installation of Services/systems	sub-contracted
Test Rig Design	General Layout to meet Test requirements	DH, OR
	Specification of Autoclave Design/Corrosion Ports	DH, OR
	Design of Dynamic Seal Cartridge System	DH, OR
	Secondary Autoclave Design/Corrosion Ports	DH, OR
	Design of Bend Fixtures	DH, OR
	Test Frame Design	DH, OR
	Actuator Specification	DH, OR
	Loading Chains Design	DH, OR
Servo-controller and data acquisition system	bought in (Tiab)	
Manufacture	Manufacture of Autoclaves/Dynamic Seal Cartridge	Baskevilles R&A Ltd
	Machining of all components (in-house machine shop)	machine shop
Assembly	Test Frame build	DH
	Autoclave assembly- fittings, valves and pipework	DH
	Secondary autoclave assembly- fittings, valves and pipework	DH
	Connection to Corrosion related services	DH
	Connection to electrical services	sub-contracted
	Sealing components, Dynamic seal cartridge, o-ring	DH, OR
	Hydraulic Power Supply	MP
Qualification Testing	Deaeration qualification Testing	DH
	10bar 10%CO2/90%N2 qualification testing	DH, OR

DH – Dean Horspool (EngD Student), OR – Olivier Ravier (Project Engineer – Exova)

MP – Mick Parton (Senior Fitter – Exova), LB – Lee Best (General Manager – Exova Daventry)

6.2.1 HPCF Testing Facility

The new High Pressure Corrosion Fatigue facility is located at Exova’s Fatigue and Fracture Mechanics site in Daventry, UK. This facility has been purpose built to house the suite of 8-12 bespoke HPCF testing machines developed as part of the current research project (Section 6.2.2).

6.2.1.1 General Layout of HPCF Facility

Figure 6-10 shows the general layout of the facility where it can be seen that it consists of 6 testing cells alongside which runs a corresponding control room. At the end of the facility next to the exterior wall is the 'regulator' room which houses the regulators for all of the gas lines which feed into the facility from the gas cylinder building located directly opposite on the external side of the exterior wall. This building also houses the dry-chemical H₂S scrubber, which has pipework running back through the length of the facility with a number of inlets in each of the test cells allowing for direct removal of used test gas from the gas outlets of the HPCF test rigs.

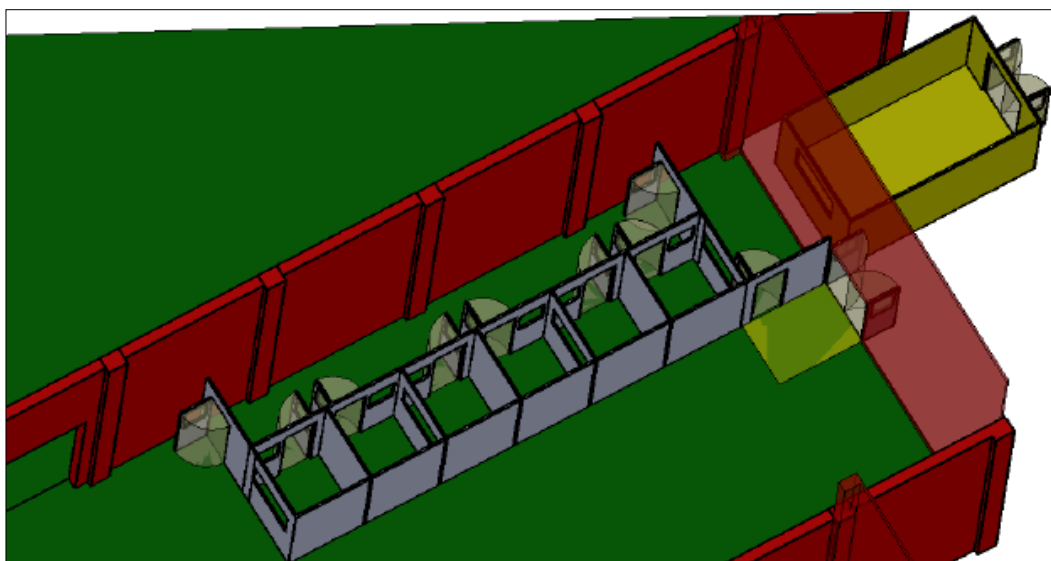


Fig 6-10 – Overview of the structure of the HPCF facility. It is made up of 6 test cells, a control room, regulator room and external gas cylinder/scrubber building.

The HPCF facility has been built inside the existing laboratory and is constructed with interconnecting panels made from a composite structure consisting of two sheets of powder coated steel with a honeycomb structure in between. Figure 6-11 shows the area

6. Results and Discussion (Design and Development of Test Facilities)

of the existing laboratory where the facility has been constructed, along with some images of the facility during the build phase of the initial shell of the building.



Fig 6-11 – Images of the HPCF facility during the initial building phase. This self contained structure allows for accurate control and monitoring of the environment within the testing rooms which is essential when handling toxic gases such as H_2S .

6.2.1.2 Extraction System

The design of the facility and installation of services and monitoring equipment was largely driven by health and safety considerations which have to be paramount when handling toxic gases such as H₂S. The extraction system installed in the HPCF facility primarily ensures that the control room is always at positive pressure relative to the testing cells and the regulator room. This is achieved by an air intake fan blowing air from the main laboratory into the control room, whilst the test cells and regulator room are constantly extracted via a separate extraction fan. The extraction system is also linked into the gas alarm system such that if an alarm is triggered in one of the test cells the extraction system automatically switches to high speed where the number of air changes per hour is doubled. If the extraction system was to fail, this link with the gas alarm system would also ensure that all gas lines carrying H₂S are shut off via the de-energisation of an electro-pneumatic solenoid which would revert the pneumatic shut-off valves to their normally closed position.

6.2.1.3 Gas Lines

Stainless steel (316) gas lines are used to supply the chemically aggressive gases required during corrosion fatigue testing in order to simulate sour oilfield environmental conditions. The lines start in the gas cylinder building outside of the main facility and are piped into the regulator room. From the outlet of the regulators, the lines run up and across the roof of the facility and then drop down into each individual test cell (Figure 6-12). All joints are orbitally welded and each line is pressure tested as standard procedure.

6. Results and Discussion (Design and Development of Test Facilities)

Figure 6-12b shows the gas lines terminated at a stainless steel panel used for mounting the point of use valves for operating the line. There are 3 panels in each test room and 4 gas lines per panel. In each test room there are two HPCF test machines both of which are permanently connected to one of these panels, leaving the third panel to be used to supply gas to the secondary pH autoclave when taking elevated pressure pH measurements.

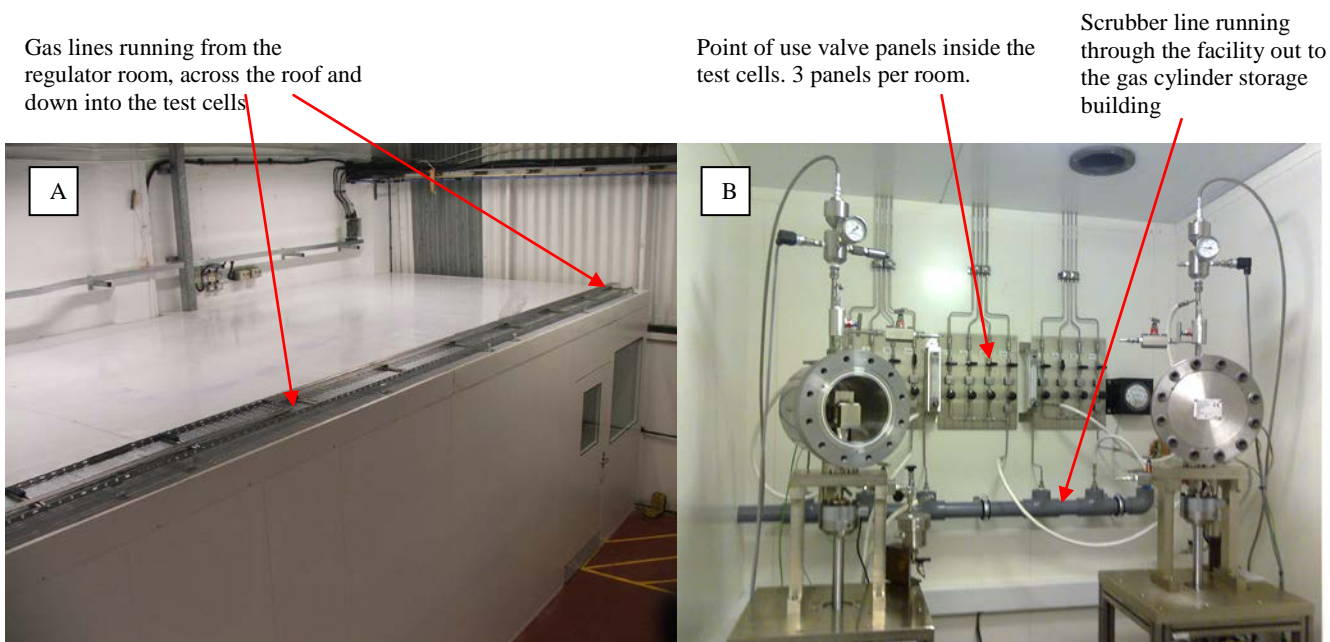


Fig 6-12 – Images of a) gas lines mounted in a cable tray running from the regulator room, across the roof and down in each test cell, b) gas lines connecting to stainless steel panels which are used to mount, non-return, ball and needle valves for each gas line.

Each panel can switch between nitrogen, carbon dioxide and mixed gas ($\text{CO}_2+\text{H}_2\text{S}$) without any disconnections ensuring that no oxygen is introduced when switching between gases. Nitrogen and carbon dioxide are communal lines that feed into all of the

6. Results and Discussion (Design and Development of Test Facilities)

test cells whilst there is an individual mixed gas line per test cell (for every 2 autoclaves). There is also a communal mixed gas line which feeds into each test cell giving the flexibility to run tests using two different gas mixes (in each autoclave) within one room if needed.

For all of the mixed gas (test gas) lines there is also a nitrogen purge system incorporated into the manifold block where the pre-mixed gas cylinder connects to the main gas line via a flexible stainless steel hose. The nitrogen purge system is a very important element of the gas lines since it allows a cylinder of test gas to be changed during a test without introducing any oxygen inside the autoclave. This system consists of a nitrogen line that is teed into the manifold of each mixed gas line and via a series of valves and a vent line. The entire manifold and flexible hose can be purged with nitrogen prior to opening the new cylinder (Figure 6-13). Once purged with nitrogen, the manifold pipework can be pressurised with test gas by opening the new gas cylinder. Closing the cylinder and venting the pressure in the manifold completes the cylinder changeover procedure. The cylinder can then be re-opened and the needle valve opened to allow gas to run through the entire gas line and into the autoclave.

6. Results and Discussion (Design and Development of Test Facilities)

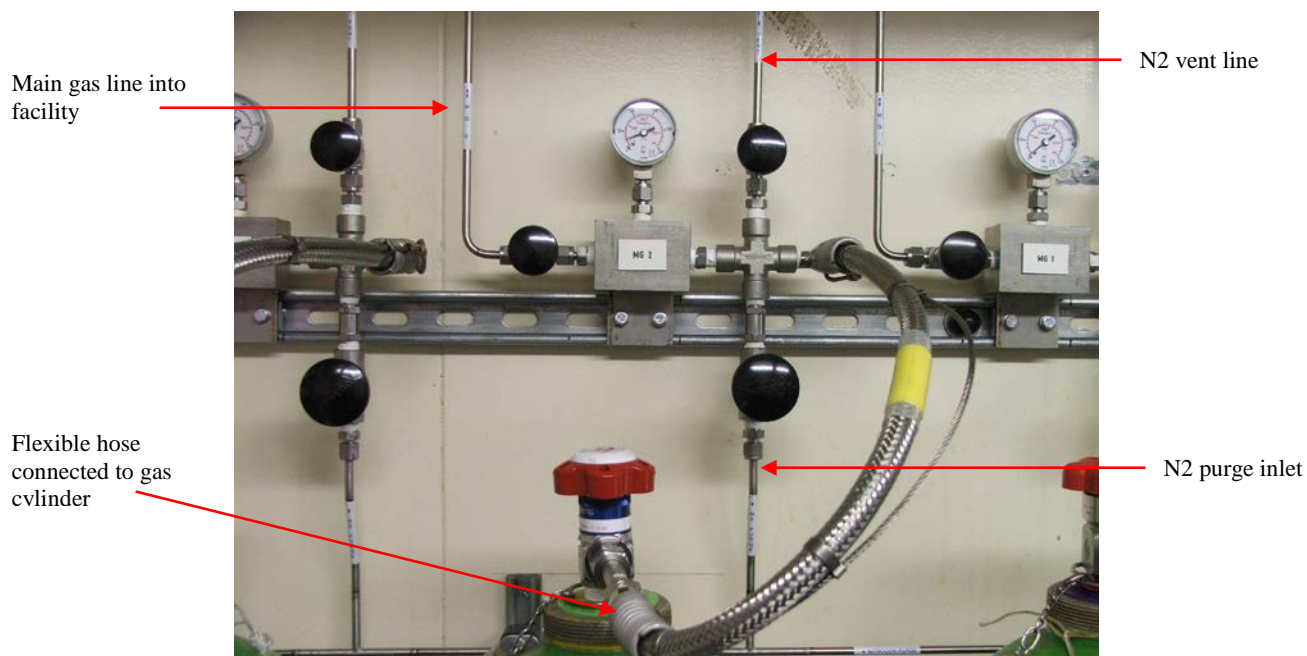


Fig 6-13 – Image of the cylinder connection manifold for the mixed gas lines, showing the setup of valves, fittings and gas lines which make up the nitrogen purge system. Shows nitrogen purge inlet, vent line, Swagelok cross fitting, flexible hose cylinder connector and a needle valve allowing gasflow to the main line.

6.2.1.4 Gas Detection/Alarm System

In order to closely simulate the corrosive oilfield environments that flexible oil and gas pipelines see in service requires the use of hydrogen sulphide gas (H_2S). This has very serious implications from a health and safety point of view and means that sophisticated detection, alarm and shut-off systems need to be in place in order to maintain a safe working environment within the facility at all times.

Each of the test cells is equipped with a gas alarm sensor which provides constant monitoring of the H_2S level within that room. Should any gas leak develop, audio-visual (amber light) alarms will give an initial warning if the level of H_2S reaches 5ppm. If the

6. Results and Discussion (Design and Development of Test Facilities)

concentration inside the test cell reaches 10ppm then the audio-visual alarm shows a red light and this automatically shuts off the H₂S supply to the test cell in which the sensor was triggered. The shut off mechanism works by using electro-pneumatic solenoids which use compressed air to keep the pneumatic shut-off valves (normally closed) open under safe conditions but shut off the supply when an alarm state is triggered causing the valve to close. Figure 6-14 shows the solenoid control panel which acts as the link between the gas alarm system and the pneumatic shut-off valves. It can be seen that feeding into this panel are a compressed air supply and inputs from each of the gas sensors that are linked to the shut-off valves. Coming out the bottom of the panel from each of the solenoids is an air line which connects to the shut-off valve enabling the valve to open when under normal operating conditions.

Compressed air supply out of electro-pneumatic solenoid valves going to inlet of pneumatic shut off valves

Compressed air supply into electro-pneumatic solenoid valves

Compressed air supply into shut off valves. Valve energised into its open position

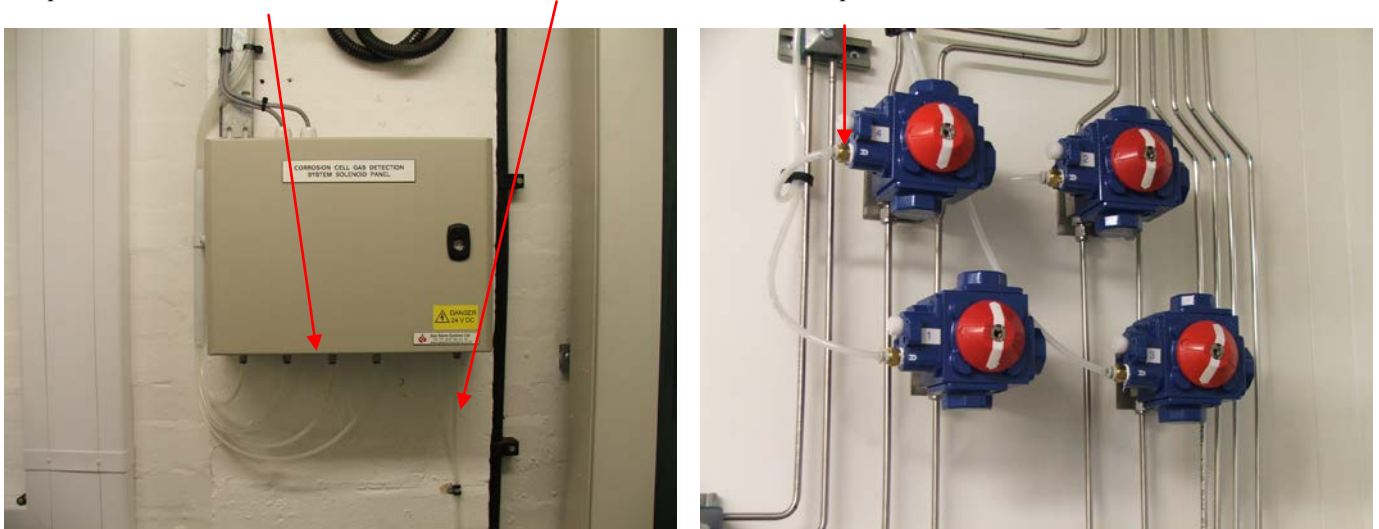


Fig 6-14 – Image of the of the solenoid panel which provides the link between the gas alarm system and the pneumatic shut-off valves. The second image shows the pneumatic shut-off valves in their open position indicating that they are being energised by the compressed air supply from the electro pneumatic solenoids.

This system ensures that H₂S levels cannot exceed 10ppm without the gas supply being shut off. Combined with the extraction system inside each test cell and the positive air pressure in the control room, the operator should never be exposed to levels above the recommended exposure limits. Personal H₂S alarms are also always worn when entering a test cell as a further precaution, these alarms ensure that any ‘local pockets’ of higher concentrations are detected and subsequent exposure avoided.

Oxygen sensors are also installed as a further precaution in the confined space of the test cell. Again, alarms will sound if the oxygen level in the test cell drops as could happen in the event of a substantial N₂ or CO₂ leak which would not be detected by H₂S sensors alone.

6.2.1.5 H₂S Scrubber System

When testing under sour environmental conditions, the waste H₂S gas from the outlet of the autoclaves needs to be contained and then dealt with or ‘scrubbed’ appropriately. Traditionally this meant utilising wet scrubbers containing sodium hydroxide to absorb the waste H₂S. This is not the safest, most practical or environmentally friendly method of extracting the waste H₂S and this method also requires a local scrubber for each test machine which would need changing regularly, increasing the potential for H₂S exposure when the scrubbers become saturated.

The H₂S scrubber system installed in the HPCF facility is a dry-chemical scrubber which is capable of dealing with waste gas from the entire facility. A communal scrubber line runs the length of the facility through every test cell, where the outlet from each

6. Results and Discussion (Design and Development of Test Facilities)

autoclave is connected to an inlet port on the scrubber line. The scrubber is located in the gas cylinder building outside the main laboratory so the scrubber line is fed through a galvanised steel tunnel (Figure 6-15) which links the regulator room and the cylinder storage building. This is the same route the gas lines take out into the gas cylinder building.

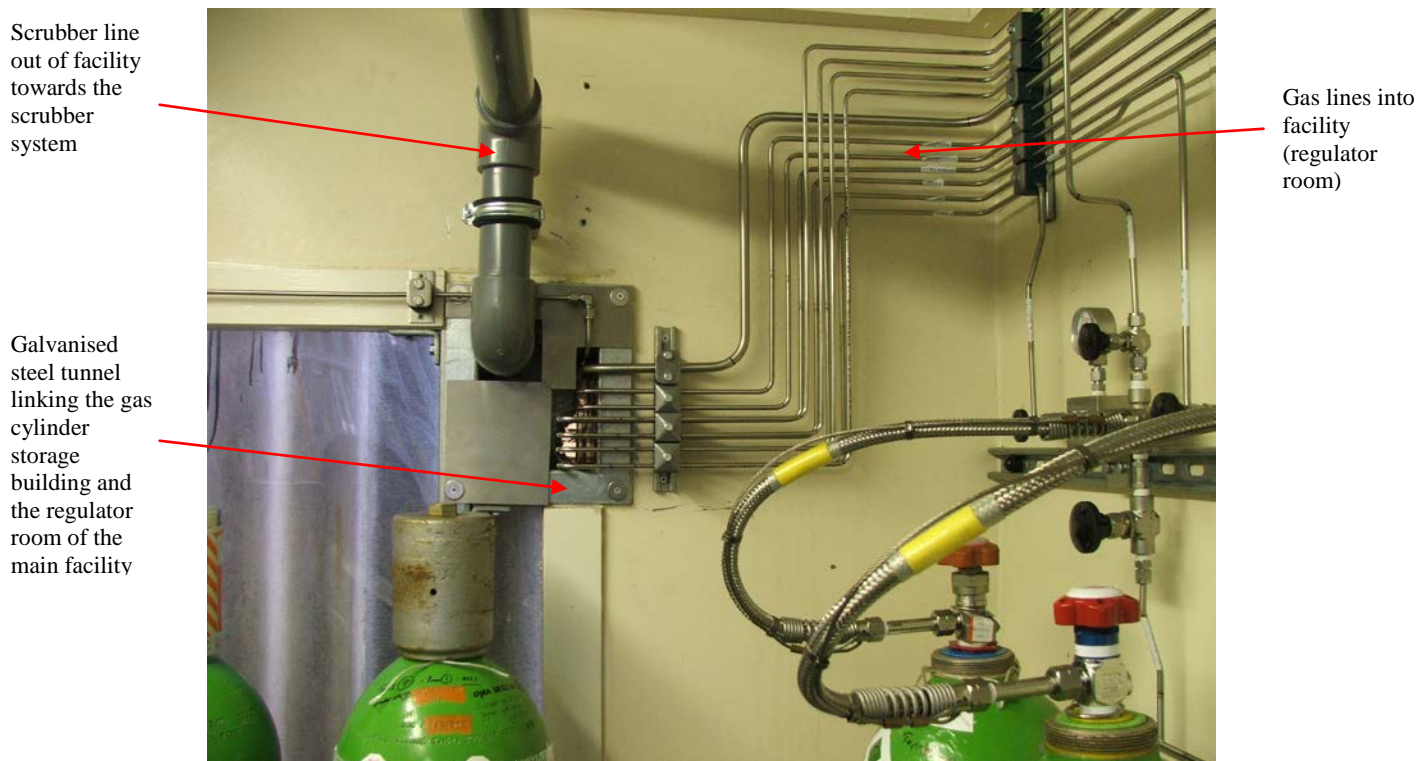


Fig 6-15 – Image of the H₂S scrubber line (grey ABS pipe) and all other gas lines exiting the gas cylinder building via a galvanised steel tunnel. This tunnel runs for approximately 1m straight into the regulator room of the main HPCF facility.

Figure 6-16 shows the wall mounted components of the scrubber system along with the barrels containing the chemical absorption medium.

6. Results and Discussion (Design and Development of Test Facilities)

The scrubber system incorporates a motorised fan ensuring that there is always negative pressure in the scrubber line so that the waste gas is drawn down the line towards the scrubber barrels containing the pelletised absorption medium. The fan also draws in fresh air via an air intake and this is mixed with the waste gas from the scrubber line before it enters the scrubber barrels. The amount of dilution can be adjusted via a needle valve which also adjusts the level of negative pressure inside the scrubber line.



Fig 6-16 – Image of the H₂S scrubbing system installed for the HPCF facility. The setup operates a lead-lag system using a series of valves to ensure that it is never offline.

6. Results and Discussion (Design and Development of Test Facilities)

From figure 6-16, it can also be seen that there is a wall mounted panel supporting a series of valves and pipework. This allows the setup to operate a lead-lag system where the flow of waste gas passes through a lead barrel and a lag barrel before being exhaust to atmosphere. This means that the scrubber is never offline or shutdown for changeovers. Once the lead barrel reaches breakthrough as it becomes saturated, this will be detected by a H₂S sensor mounted inside the outlet of the lead barrel. By switching the associated valves, the flow of waste gas can be diverted into the lag barrel whilst the saturated lead barrel is removed and replaced. Once in place the valves can be reopened so that the fresh barrel becomes the lag barrel. There is a second H₂S sensor mounted inside the outlet pipework for the second barrel so that saturation can also be detected in this barrel indicating that the changeover procedure needs to be repeated.

6.2.2 General HPCF Test Machine Description

The aim of the next stage of the research project was to design and manufacture a high pressure corrosion fatigue test rig capable of commercially testing flexible pipeline tensile armour wires to specifications and requirements dictated by the industrial clients (outlined in Chapter 5). A description of the main characteristics of the designed and manufactured experimental HPCF setup is given in the following section. Figure 6-17 provides a global overview of the manufactured test rig and detailed drawings can be found in Appendix 2.

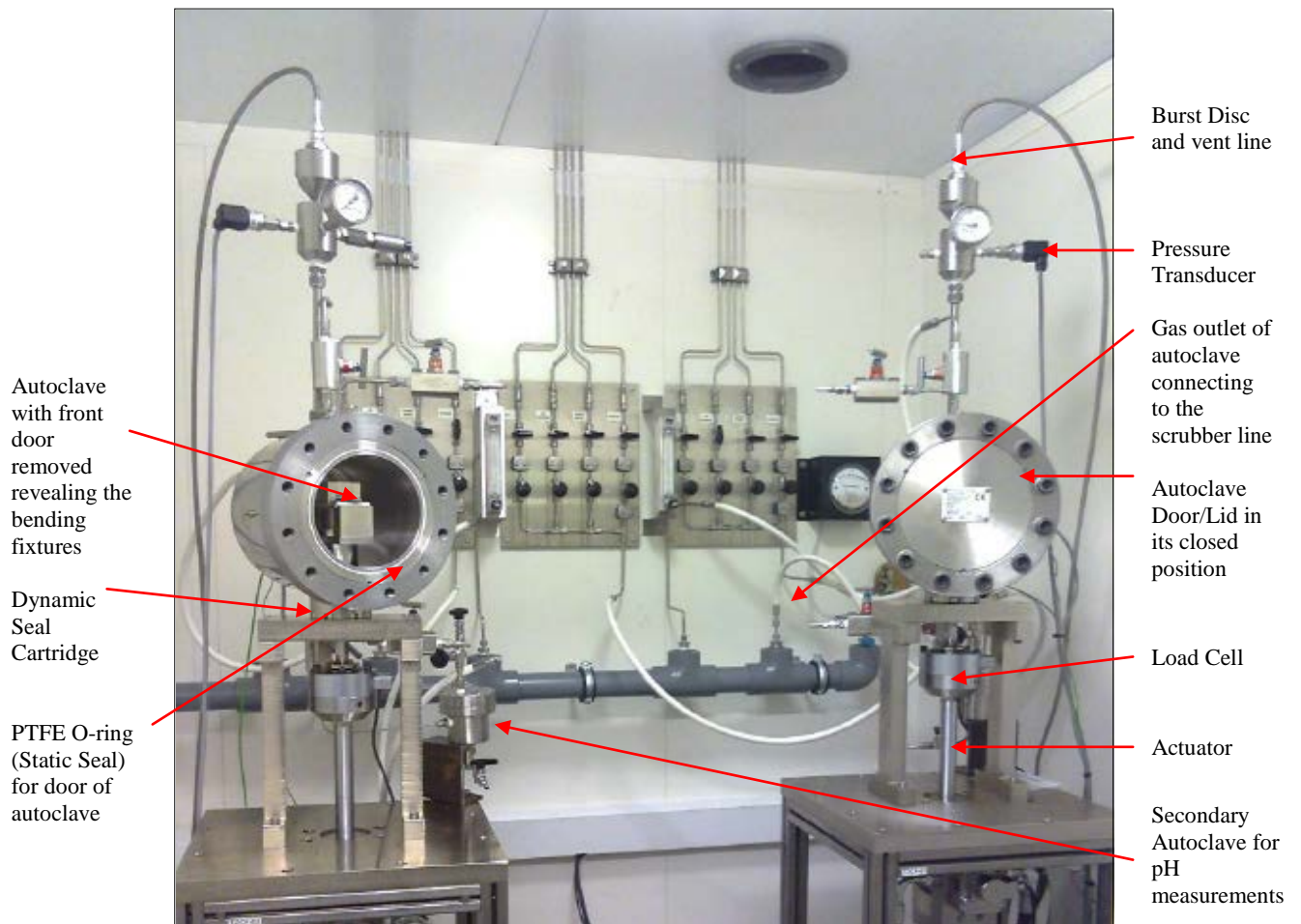


Fig 6-17 –Overview of Rig Construction, showing the autoclave mounted on a support stand on top of a servo-hydraulic test frame.

Each constructed testing machine is a servo hydraulic fatigue rig which incorporates an autoclave into the design setup allowing samples to be loaded dynamically at elevated temperature and pressure in a controlled simulated oilfield environment. The hydraulic actuator connects to a load cell which in turn is connected to a pullrod which enters the autoclave through a complex dynamic sealing cartridge system. This dynamic sealing setup allows containment of the simulated corrosive environment whilst the pullrod is cycled through the body of the autoclave. This experimental setup is capable of temperatures up to 100°C and pressures up to 50bar under sour gas conditions. Although tests can be performed in both load or displacement control, the ability to run tests in load control is seen as a key benefit of servo hydraulic controlled test machines where closed loop feedback to the controller can ensure constant test loads.

6.2.3 Actuating System

The method used for the application of alternating loads is a servo hydraulic actuator. Custom stainless steel actuators supplied by Helipebs Plc have been utilised to afford resistance to the operating environments the test rig is likely to encounter. The actuators have a load capacity of 20kN which is considered ample for even the largest sizes of tensile armour wire. An LVDT is incorporated into the actuator and this, together with the load cell signal is fed into a Tiab servo-controller unit which provides a closed loop system where load and displacement can be automatically adjusted by the controller depending on the input settings resulting in a load controlled system (Figure 6-18).

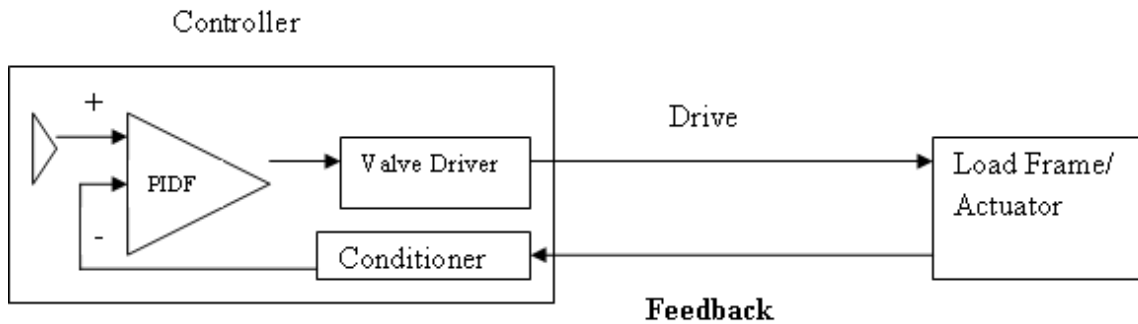


Figure 6-18 – Schematic showing the control system used on the test machines to obtain closed loop control of the actuator.

6.2.4 Specimen fixture and Loading Chain

Loading is applied in four-point bending by supporting each end of the sample and deflecting the sample via two central contact points acting on the opposite side of the specimen. Cylindrical rods of 15mm diameter were selected as the roller contact points which are fixed in place on the specimen fixture (outer contact points) and located in machined holders on the specimen carrier (inner contact points). The specimen fixture is shown in Figure 6-19.

6. Results and Discussion (Design and Development of Test Facilities)

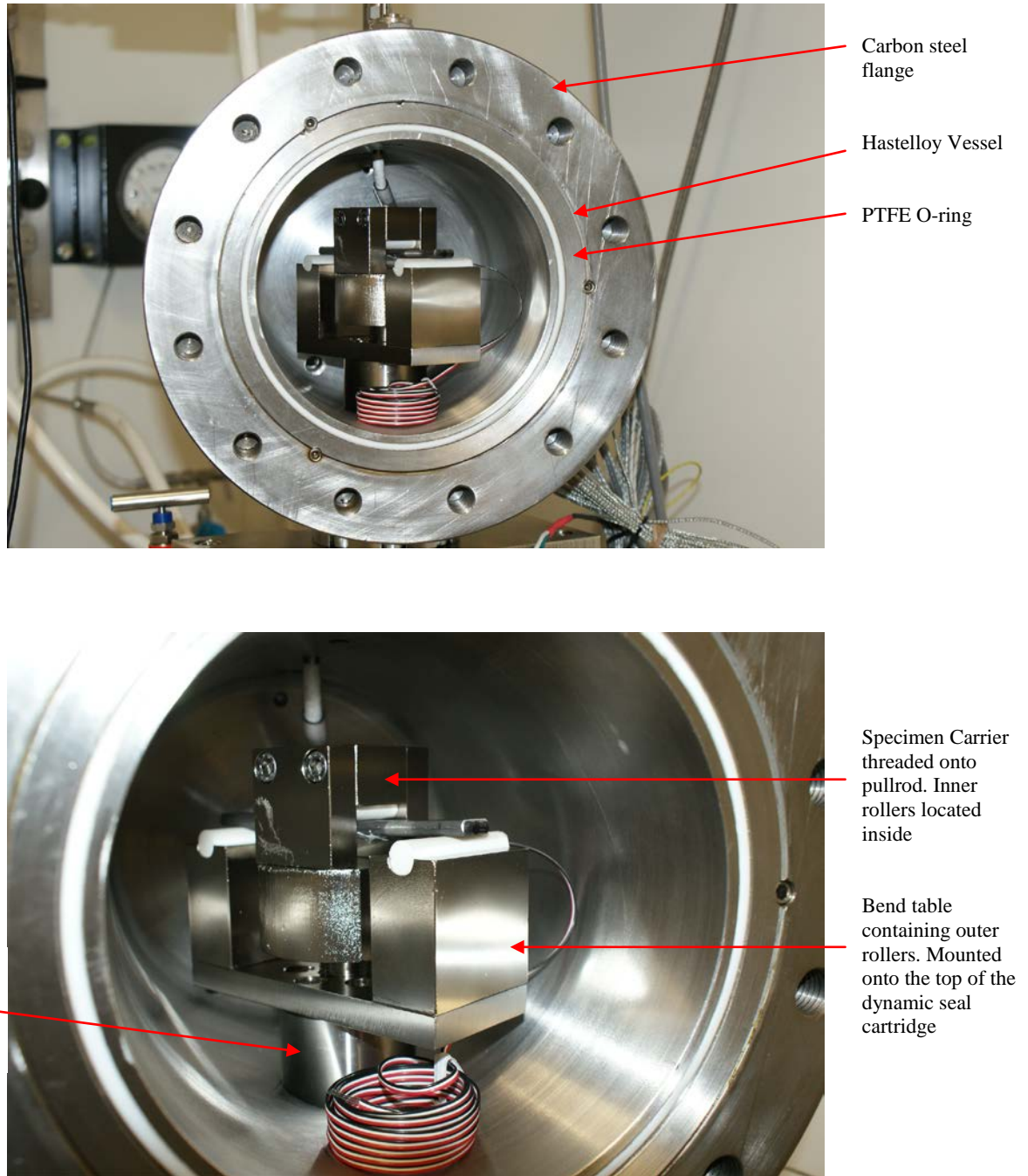


Fig 6-19 –Specimen fixture Construction, a) bend table mounted onto the top of the dynamic seal cartridge, b) specimen carrier threaded onto the end of the pullrod applying load to a strain gauged sample.

6. Results and Discussion (Design and Development of Test Facilities)

The material used for the roller contact point must be resistant to environmental degradation from test solutions in which it operates. It must have high wear resistance and electrically insulate the specimens so that galvanic corrosion effects are avoided. A ceramic material was chosen for the contact points since it meets all of the above requirements and is readily available.

Load transfer is accomplished by the specimen carrier pulling down on the sample forcing the bottom face of the sample into tension as the actuator retracts. The bend table is designed to bolt onto the top of the dynamic seal cartridge and is not in contact with the main body of the autoclave. With this set up, when the specimen carrier puts load onto the sample, this load reacts against the body of the dynamic seal cartridge and the associated mounting framework rather than against the main body of the autoclave. This was a key aspect in the design stage since it made certification of the autoclaves to the required pressures much easier.

6.2.5 Environmental Control and Containment System (Autoclave)

To meet the requirements of the test procedure, test samples need to be exposed to a controlled corrosive environment at elevated pressure whilst being fatigue loaded. The parts used in the simulation of oilfield environmental conditions for the HPCF experimental setup are outlined in the following sections.

6. Results and Discussion (Design and Development of Test Facilities)

Deaeration Vessel – The purpose of the deaeration vessel is to prepare the test solution prior to transfer to the test rig and contact with the test samples. The deaeration vessel is constructed to contain up to approximately 5L of test solution however 4L is typically used. Figure 6-20 shows an image of the constructed deaeration vessel made up of tapering glass cylindrical walls with a top and bottom flange. A plexiglass base is then fitted and sealed against the bottom flange using a rubber gasket. For the top of the deaeration vessel a plexiglass lid is machined to contain all of the necessary ports including; gas inlet, gas outlet, solution transfer and ports for the orbisphere oxygen analysis equipment.

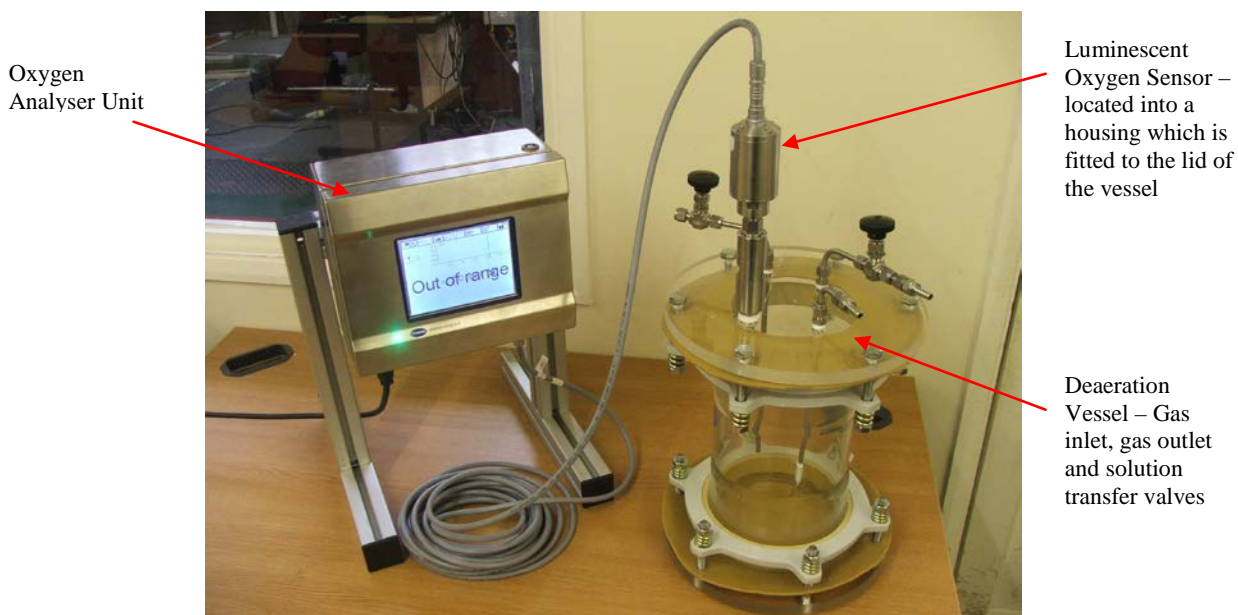


Fig. 6-20 – Image of the constructed deaeration vessel used in the experimental setup, Note the ports and fittings on the lid of the vessel needed for the deaeration procedure (reads out of range since O_2 level is above the upper sensing limit of 2ppm).

Autoclaves

The autoclaves in the experimental setup are used to contain the simulated corrosive oilfield environment which is at elevated pressure and/or temperature. The autoclave design is completely bespoke for the application of corrosion fatigue testing, and the dynamic sealing cartridge system is also an in-house design. The manufacture of the autoclaves was outsourced to Baskervilles R & A Ltd who are specialists in the machining of Hastelloy C276 and autoclave manufacture.

As a general note the autoclaves have been machined from a solid 8” bar of hastelloy C276 which is then bored out to the required dimensions. Each autoclave is certified to test up to 50bar and 100°C and is horizontally aligned with the pullrod centrally and axially aligned about the vessel centreline and lower quadrant.

Figure 6-21 shows the general design and a CAD drawing of the autoclave fully assembled within the test rig to aid the description given in the text. The following sections will give a detailed description of the different sealing systems used and also describe the arrangement of the various ports on the autoclave which enable simulation of a controlled corrosive oilfield environment.

6. Results and Discussion (Design and Development of Test Facilities)

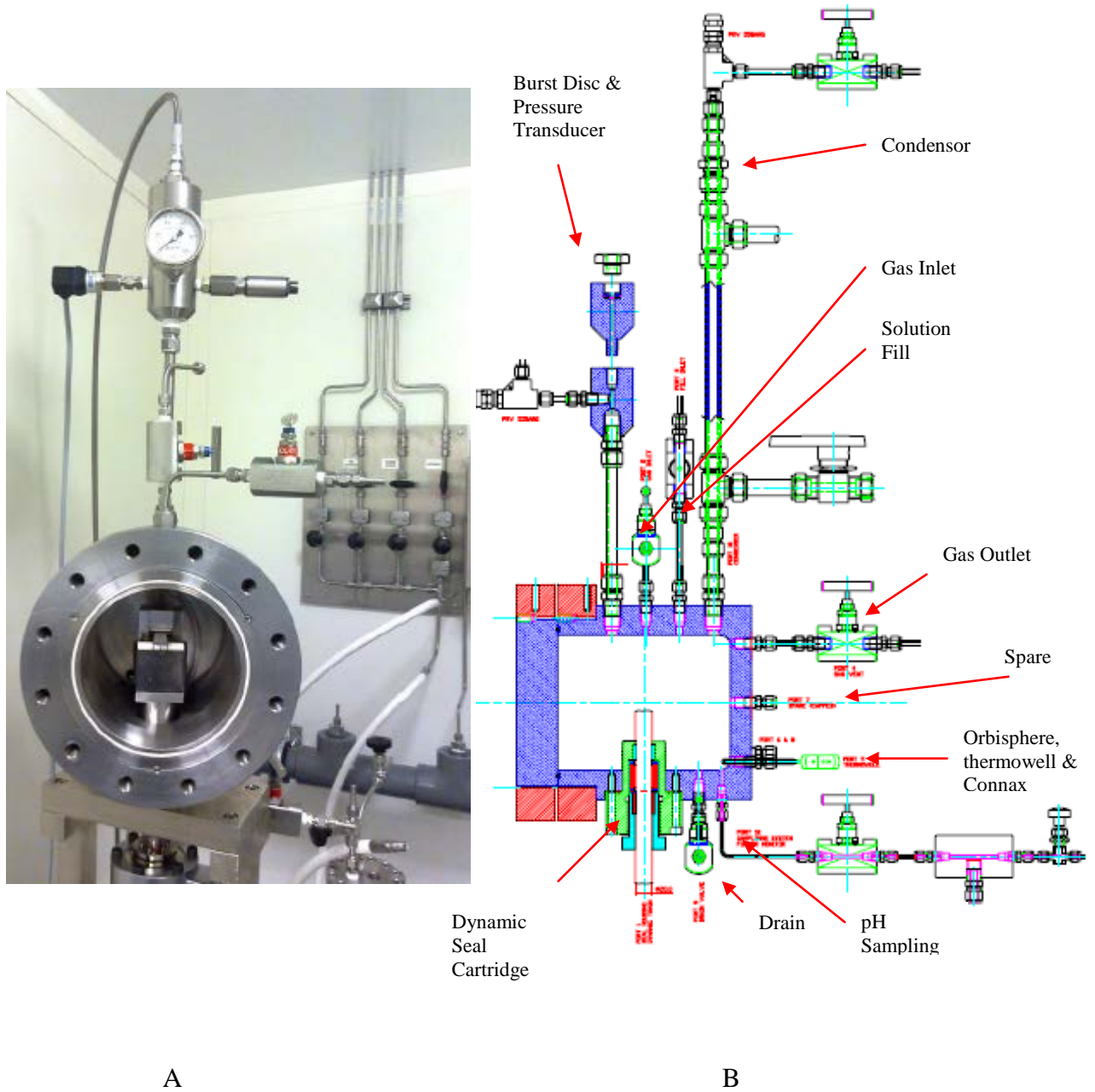


Figure 6-21 – a) overview of the general setup of the assembled autoclave (Appendix 2 – DR 65767), b) CAD drawing of the assembled autoclave (see following text for detailed explanation).

6. Results and Discussion (Design and Development of Test Facilities)

Dynamic Sealing Cartridge System

Developing and designing a dynamic sealing system to withstand the particular conditions of the test procedure used in this thesis was one of the key technical challenges to overcome in order to load a sample dynamically within an autoclave at elevated pressure.

Figure 6-22 shows a CAD drawing of how the hastelloy dynamic seal cartridge attaches to the main body of the autoclave. It bolts onto the base of the autoclave and a seal is achieved via a standard PTFE o-ring (static). The dynamic seal cartridge component was deliberately designed to detach from the rest of the assembly so that seals could be changed quickly and easily when necessary and also allowed some flexibility if the seal design needed to be changed (Appendix 2 – DR 65763).

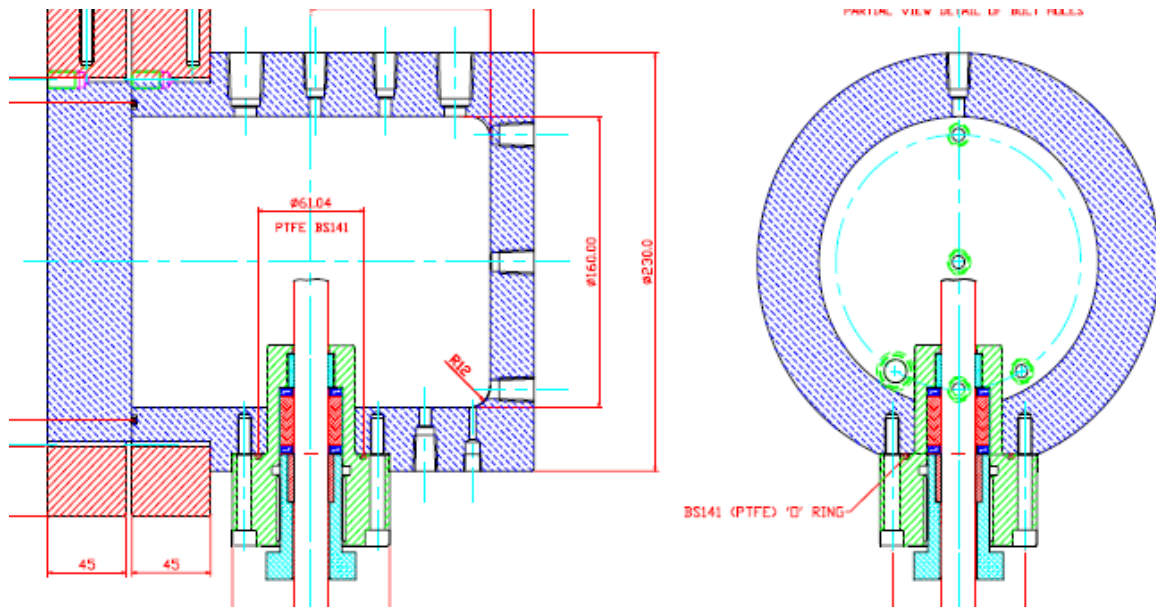


Figure 6-22 – CAD drawings showing the location, attachment and sealing method of the dynamic seal cartridge (green) with regard to the main body of the autoclave (Appendix 2 – DR 65761).

6. Results and Discussion (Design and Development of Test Facilities)

The dynamic seal is located within a plastic seal carrier (Figure 6-23) which fits inside the bore of the dynamic seal cartridge along with two PTFE linear guidance bushes and hastelloy washers, located either side of the seal carrier. The outside of the seal carrier seals against the bore of the dynamic seal cartridge via a static o-ring which fits into a groove machined on the seal carrier. The seal carrier is then held in place by a gland nut which is threaded into the base of the dynamic seal cartridge (Figure 6-23b).



Fig 6-23 – a) seal carrier containing the dynamic seals, b) hastelloy dynamic seal cartridge (note the tapped hole pattern on the top of the cartridge is for attachment of the bend fixture). Detailed drawing of the dynamic seal cartridge can be found in Appendix 2 – DR 65763.

Inside the seal carrier are two additional machined grooves which are where the two dynamic rod seals are located. Firstly, an o-ring is placed into each groove, then the rod seal component which has a lip on it which has to be positioned so that it faces the

'pressure side' of the system. When the autoclave is pressurised this rod seal will be energised and seal against the pullrod as it moves up and down. The general arrangement is not unlike that found in a hydraulic actuator where a rod seal is used to seal against a piston to contain high pressure oil. For the application of corrosion fatigue a H₂S resistant grade of seal material has been utilised in order to extend the service life as far as possible. It is worth noting at this point that a hastelloy pullrod was used in the early stages of the design phase as a result of its superior corrosion resistance, however after extensive trials on the seal/rod combination it was observed that this rod material was too soft and a wear scar would develop after 1-2 days of cycling severe enough to cause an unacceptable rate of leakage through the seals. It was clear from these trials that a much harder rod surface was required whilst maintaining adequate corrosion resistance to the anticipated testing environments. The solution was to manufacture a stainless steel rod and then have it chrome plated and cylindrically ground much the same as the piston of an actuator. The manufacture of these components was outsourced to Helipebs Plc who are specialists in these processes. In fact, they also supplied the stainless steel actuators used on the test machines which have undergone the same process. With this new rod material the resulting hardness is much more suitable for the application of a dynamic sealing system.

Static PTFE O-ring Seal (Front door)

With the autoclave horizontally aligned it was decided to only flange the vessel at one end since access was only needed from one side. This also allowed more space on the

6. Results and Discussion (Design and Development of Test Facilities)

back of the vessel for the different corrosion related ports that were required. Figure 6-24 shows a CAD drawing of the flanged end (front door) of the vessel. The flanged rings are manufactured from carbon steel and are screwed onto both the main body of the vessel and onto the hastelloy door (see Appendix 2 – DR 65760). The o-ring groove is machined onto the main body of the autoclave so that when the door is bolted into position the PTFE O-ring is compressed by the hastelloy section of the front door.

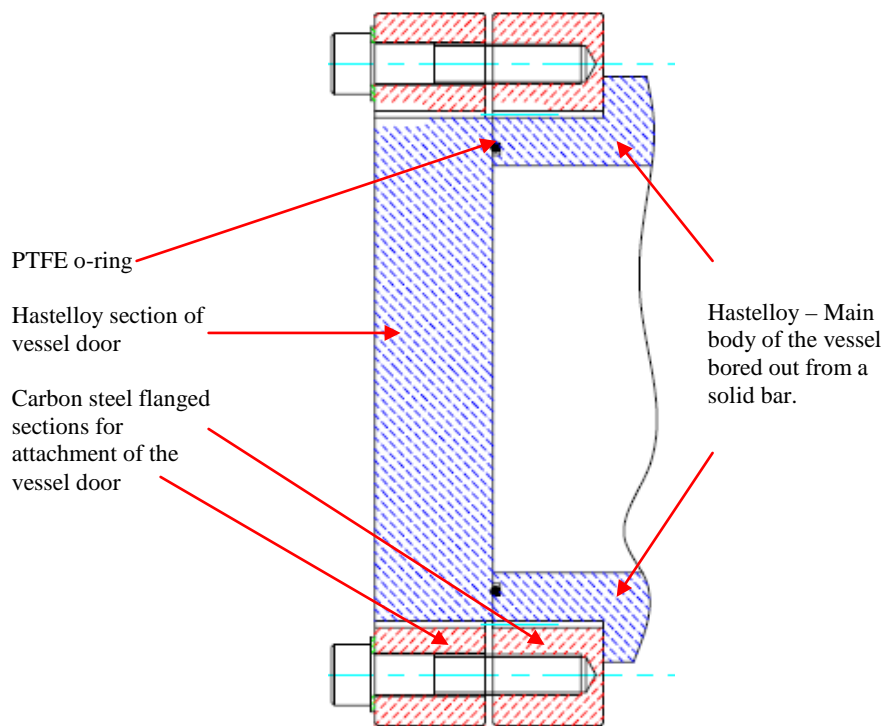


Figure 6-24– CAD drawing of the flanged end of the autoclave, showing the static sealing system. (blue is hastelloy and red is the steel flanges). Appendix 2 – DR 65761

Autoclave Ports (see Appendix 2 – DR 65767 for additional detail)

Port 1 – Gas Inlet

Gas inlet needle valve connected to upper quadrant of the vessel shell by a ¼” NPT male connector. Inside the vessel, flexible tubing extends the gas inlet down to the bottom of the vessel ensuring that test gas is always bubbled into the bottom of the liquid phase (test solution).

Port 2 – Solution Fill

Solution fill needle valve connected to the upper quadrant of the vessel shell via a ¼” NPT male connector.

Port 3 – Gas Outlet

Gas outlet needle valve connected to the upper quadrant of the back wall of the vessel via a ¼” NPT male connector.

Port 4 – Thermowell

Ø ¼” thermocouple in well connected to the lower quadrant of the back wall of the vessel via a ¼” NPT male connector.

Ports 6 & 7 Spare Ports

Spare ¼”NPT male connectors capped. Located on the back wall of the vessel in the lower quadrant.

6. Results and Discussion (Design and Development of Test Facilities)

Port 8 – Orbisphere (Oxygen Sensor)

½” NPT port for oxygen sensor housing. This is located on the back wall of the vessel in the lower quadrant as the sensor needs to be submerged in the liquid phase.

Port 9 – Drain

¼” drain needle valve connected to the underside (base) of the vessel shell via a ¼” NPT male connector.

Port 10 – Condenser

Hastelloy tube in tube condenser accommodating Ø ½” tube in Ø ¼” tube condenser approximately 300mm long and connected to the top of the vessel via a 1/2” NPT male connector with associated isolating ball valve and pressure relief valve.

Port 11 – Manifold (Bursting Disc)

Connected to the top of the vessel shell by a ½” NPT male connector and ½” tubing. Bursting disc body fitted with PTFE protected nickel bursting disc to the requirements of B.S 2915:1990, manufactured to 55barg. Also incorporated into the manifold is a dual scale pressure gauge and a pressure transducer (0.2% accuracy) which links back to the process meter in the electronic control panel.

Port 12 – pH Sampling

pH sampling 1/8” Needle valve connected to the base of the vessel shell via a 1/8” NPT male connector. This port allows a sample of solution to be extracted into a secondary ‘pH sampling autoclave’ for measurement of pH at test pressures. The secondary pH autoclave and associated components will be described in detail in the following sections.

Secondary Autoclave for pH measurements

The purpose of the secondary autoclave is to provide the capability of measuring test solution pH at elevated (test) pressures. This ‘pH’ autoclave is manufactured from stainless steel and is connected to the main autoclave via the 1/8” pH sampling port and some 1/8” hastelloy tubing. Figure 6-25 shows an assembled ‘pH’ autoclave with a cap on the port where the high pressure pH probe housing fits. The pH probe used for making the elevated pH measurements was a high pressure pH probe supplied by Mettler-Toledo with a working range of 0-60bar and up to 110°C.

6. Results and Discussion (Design and Development of Test Facilities)

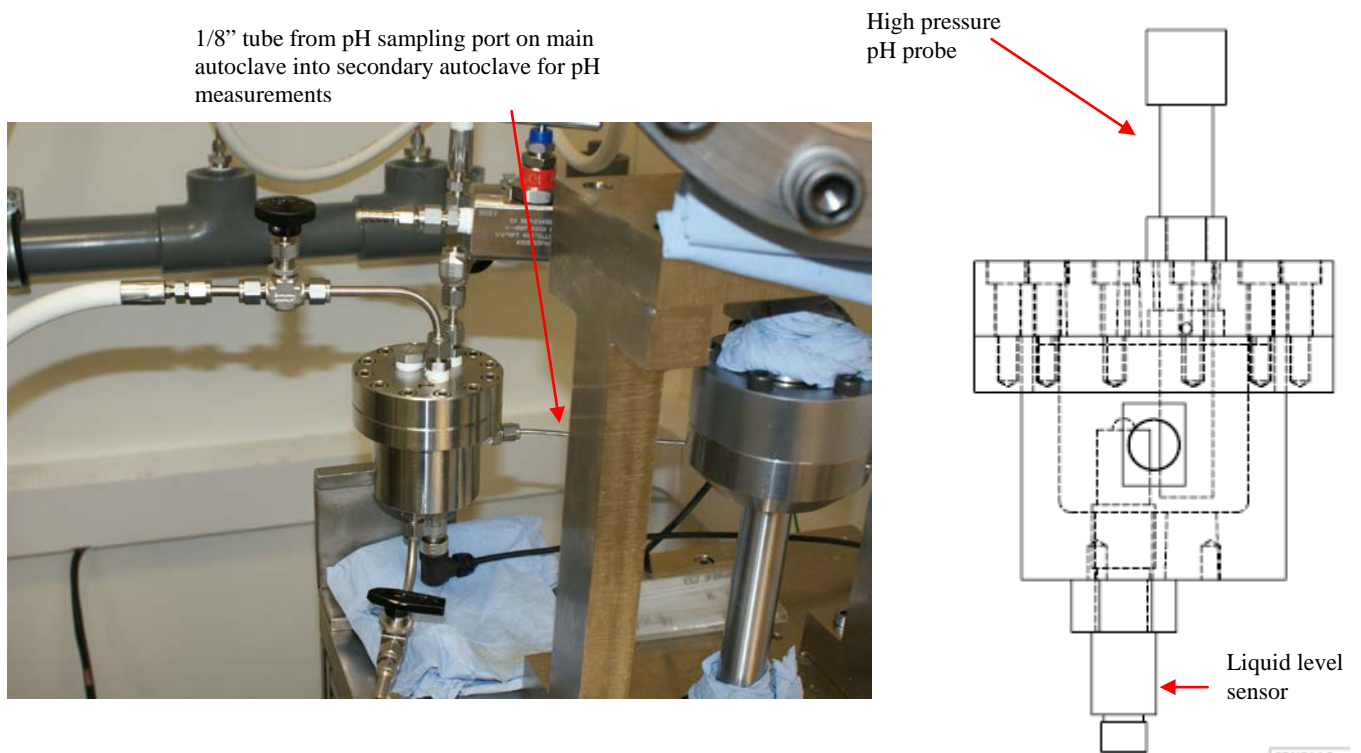


Figure 6-25 - a) Image of secondary autoclave mounted onto the test machine, b) CAD drawing of the pH vessel. (Appendix 2 – DR 65766)

The pH vessel also has a number of ports that are required to make the pH measurement as accurate as possible, these are outlined below.

Port 1 – Gas Inlet

1/4" NPT fitting and needle valve located in the lid of the vessel to allow deaeration of the vessel and pipe work and also pressurisation with test gas.

6. Results and Discussion (Design and Development of Test Facilities)

Port 2 – Gas Outlet

¼” NPT fitting and needle valve located in the lid of the vessel.

Port 3 – pH Probe

3/8” NPT tapped hole to accept the pH probe housing. This port will be capped when the vessel is not in use.

Port 4 – Solution In

1/8” NPT fitting located in the sidewall of the vessel shell. Connected to the 1/8” hastelloy needle valve from the pH sampling port on the main autoclave.

Port 5 – Level Sensor

3/8” BSP tapped hole in the base of the vessel for connection of a liquid level sensor. This sensor has been incorporated into the design so that it is clear how much test solution is extracted with each sample measurement.

Port 6 – Drain

¼” NPT fitting and ball valve located in the base of the vessel. Used to drain the sample solution after measurement and depressurisation.

Gas Supply System– Gas lines have been installed to allow for supply of all gases used during the test procedure. Nitrogen is generally used as deaeration gas with CO₂ or

6. Results and Discussion (Design and Development of Test Facilities)

CO₂+H₂S used as test gas which is supplied in pre-mixed pressurised cylinders. The gas supply system is set up in such a way that you can switch from one gas to another without disconnecting any of the lines which prevents any ingress of oxygen. Flow rates to the test rig can be very finely controlled through the use of flow meters. Following manufacture and assembly of the experimental setup a qualification trial was conducted in order to verify that the environmental conditions generated during testing met the necessary requirements, specifically control of oxygen levels during a test. Further information on the qualification test matrix of the HPCF test machines will be given in Section 7.2.3.1.

6.2.6 Materials Selection

All components of the high pressure/high temperature experimental setup that are in direct contact with the corrosive test solution must be manufactured from materials that are resistant to degradation by the environmental conditions produced. For this test method this environment is typically anaerobic artificial seawater saturated with CO₂ or some mbara of H₂S balanced with CO₂ or N₂ to a total pressure of up to 50bar.

A glass vessel and plexiglass base and lid have been used for the deaeration vessel since these are not reactive with the test solution. The autoclave, dynamic seal cartridge and specimen fixtures are manufactured from Hastelloy C276. In fact all components located within the test chamber are made from hastelloy C276 except for the pullrod which had to be re-evaluated and changed due to hardness/wear issues as outlined in Section 6.2.5 Rollers used as the specimen contact points for support and deflection are made from a

ceramic material ensuring there is no galvanic coupling between the test samples and other alloys in the test chamber.

6.2.7 Data Acquisition and Monitoring

The control and monitoring systems form a very important part of the corrosion fatigue setup. All systems are electronic and integrated in a computer system. The system and user interface is built in National Instruments LabView (Figure 6-26). This data acquisition system is incorporated into a Tiab servo-controller to monitor and log individual load and displacement readings as well as controlling the applied loads during the test. The cycle counters are tripped when the controller detects a reading that exceeds a preset limit value, which could be either load or displacement limits. This is used to detect failure of a sample but also to protect the sample against any anomalies within the hydraulic power system.

6. Results and Discussion (Design and Development of Test Facilities)



Figure 6-26– Image of the servo-controller and data acquisition software used to control and monitor the HPCF test machines.

7. Results and Discussion

7.1 Materials Characterisation

7.1.1 Microstructure

Tensile armouring wires for unbonded flexible pipe are manufactured from carbon or low alloy steels. Table 7-1 shows the chemical composition for the grades of steel armour wires tested in the current research project.

Table 7-1 – Typical chemical composition of the two grades of carbon steel armour wires tested in the current research project (wt %)[Values provided by industrial client].

C	Mn	P	S
0.6	0.7	0.01	0.003

Wire-1

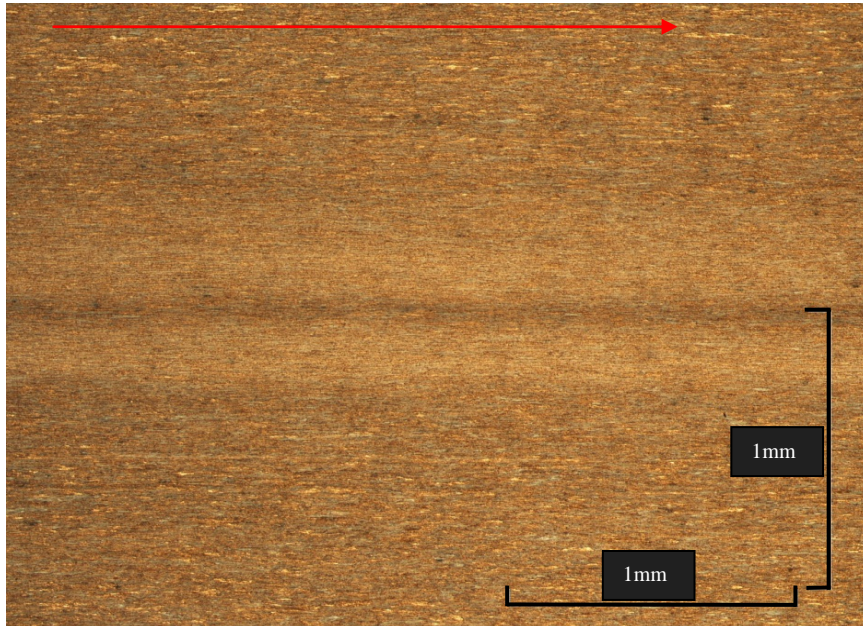
C	Mn	P	S
0.6-0.7	0.7-0.9	0.04 (max)	0.05 (max)

Wire-2 – AISI 1065

The wires have been supplied by two flexible pipe manufacturers. The wires are sweet service wires and on the basis of the JIP findings [7] can be classified as being in the same strength class. (The mechanical properties of the wires are given in Section 7.1.2). Figures 7-1 to 7-4 show the resulting microstructure for both wires, which is fine-grained ferrite and pearlite with grain directionality corresponding to the cold drawing and rolling manufacturing processes. This is most clearly seen with sections taken in the longitudinal direction, parallel to the rolling direction (Figures 7-1 and 7-3).

7. Results and Discussion

Rolling
direction



Rolling
direction

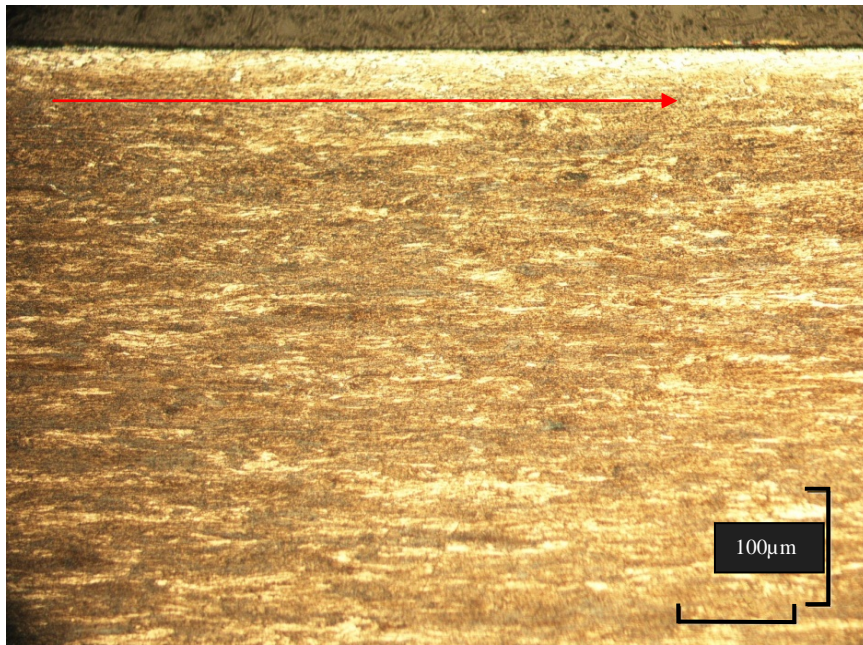


Fig. 7-1 – Wire-1- Longitudinal Section (parallel to the rolling direction of the wire). Fine grained ferritic-pearlitic microstructure showing grain elongation in the rolling direction, 2% Nital etch.



Fig. 7-2 – Wire-1 – Transverse Section (perpendicular to the rolling direction of the wire). 2% Nital etch.

7. Results and Discussion

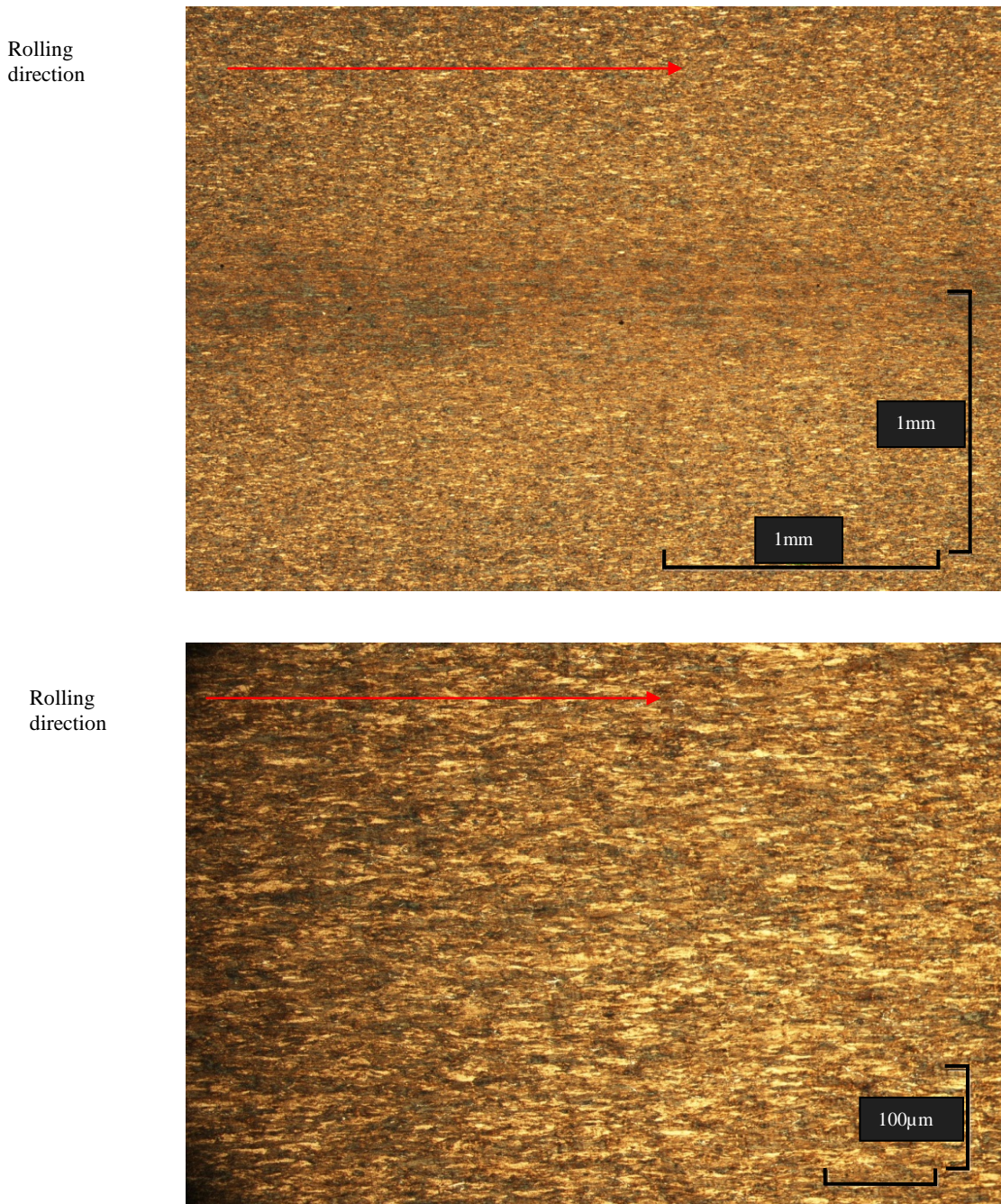


Fig. 7-3 – Wire-2 - Longitudinal Section (parallel to the rolling direction of the wire). Fine grained ferritic-pearlitic microstructure showing grain elongation in the rolling direction, 2% Nital etch.

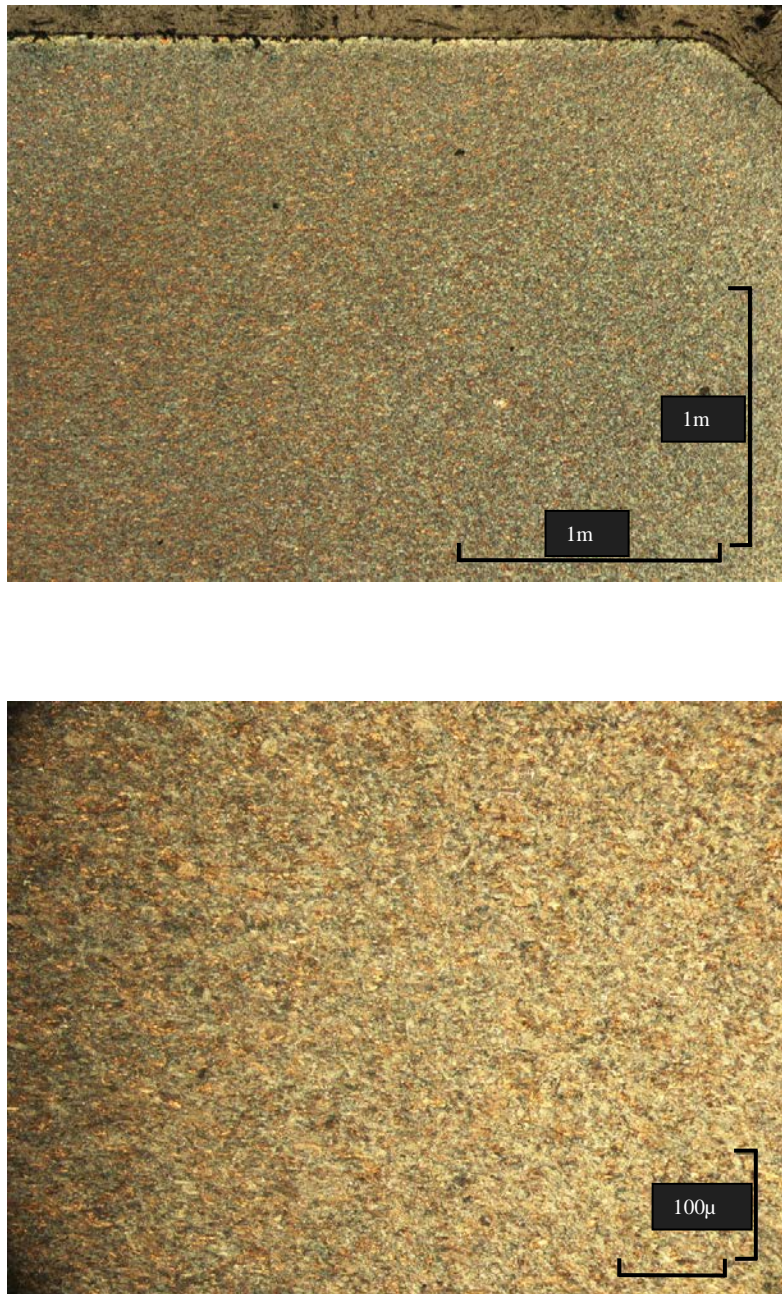


Fig. 7-4 – Wire-2 – Transverse Section (perpendicular to the rolling direction of the wire). 2% Nital etch.

7.1.2 Tensile and Hardness Testing

Before fatigue testing the armour wire material it is necessary to perform tensile tests to obtain information about its mechanical properties. This data, specifically the yield strength, can then be used to decide relevant stress ranges to begin fatigue testing. The tensile test was performed using a 500kN servo-hydraulic test machine (Fig 7-5a). The test sample was instrumented with strain gauges (Fig 7-5b) on either side of the armour wire material allowing strain to be plotted against load during data analysis.

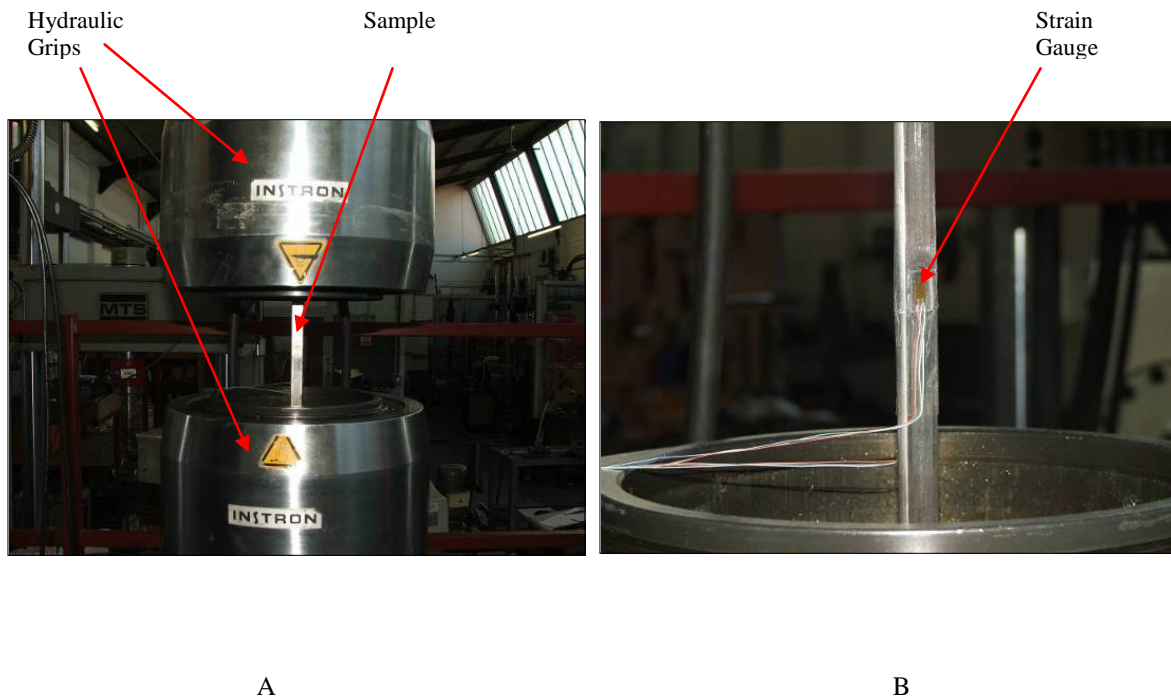


Fig. 7-5 – a) Image showing the wireline material in the hydraulic grips of the test machine, b) Close-up of the instrumented sample showing strain gauges on the sample surface

7. Results and Discussion

Having obtained this important information it allows relevant stress ranges to be selected in order to build an S-N curve. Figures 7-6 & 7-7 show the graphical representation of the tensile testing results for Wire-1 & Wire-2 and hardness values are displayed in table 7-2.

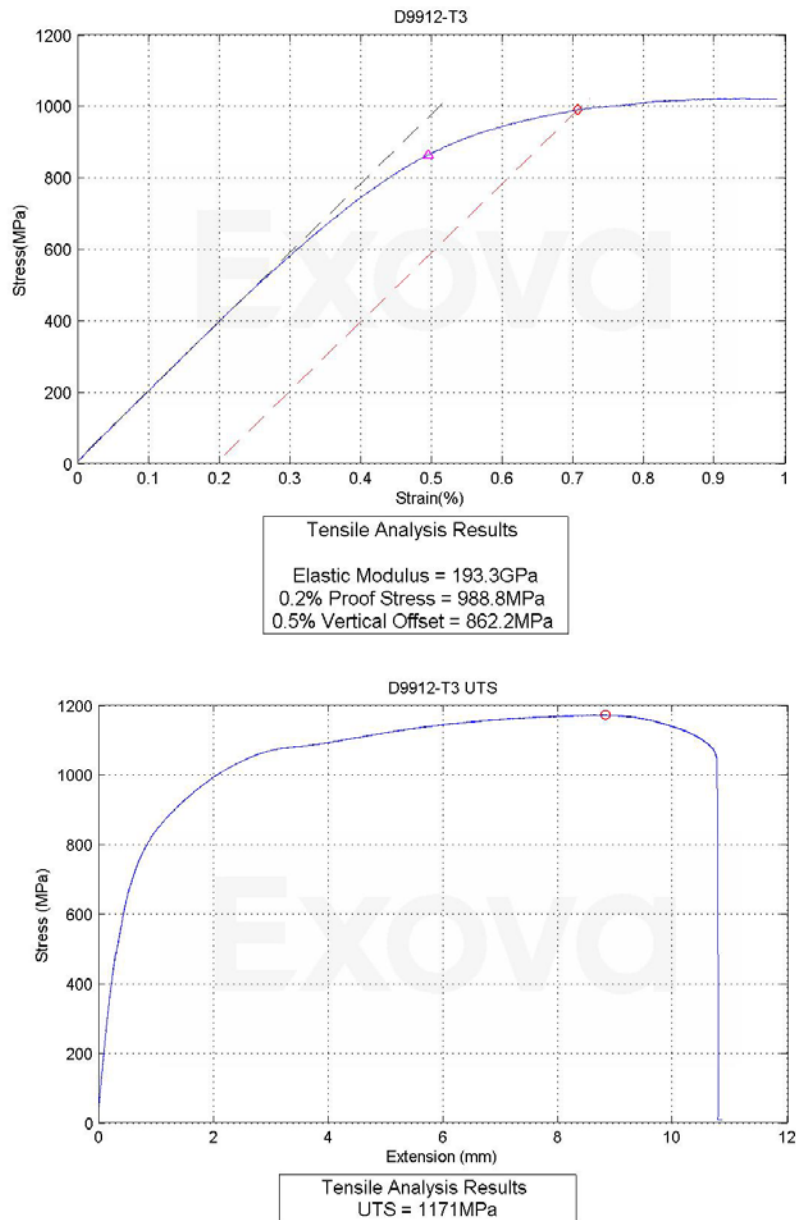


Fig. 7-6 – Tensile testing results for Wire-1 (15x5mm).

7. Results and Discussion

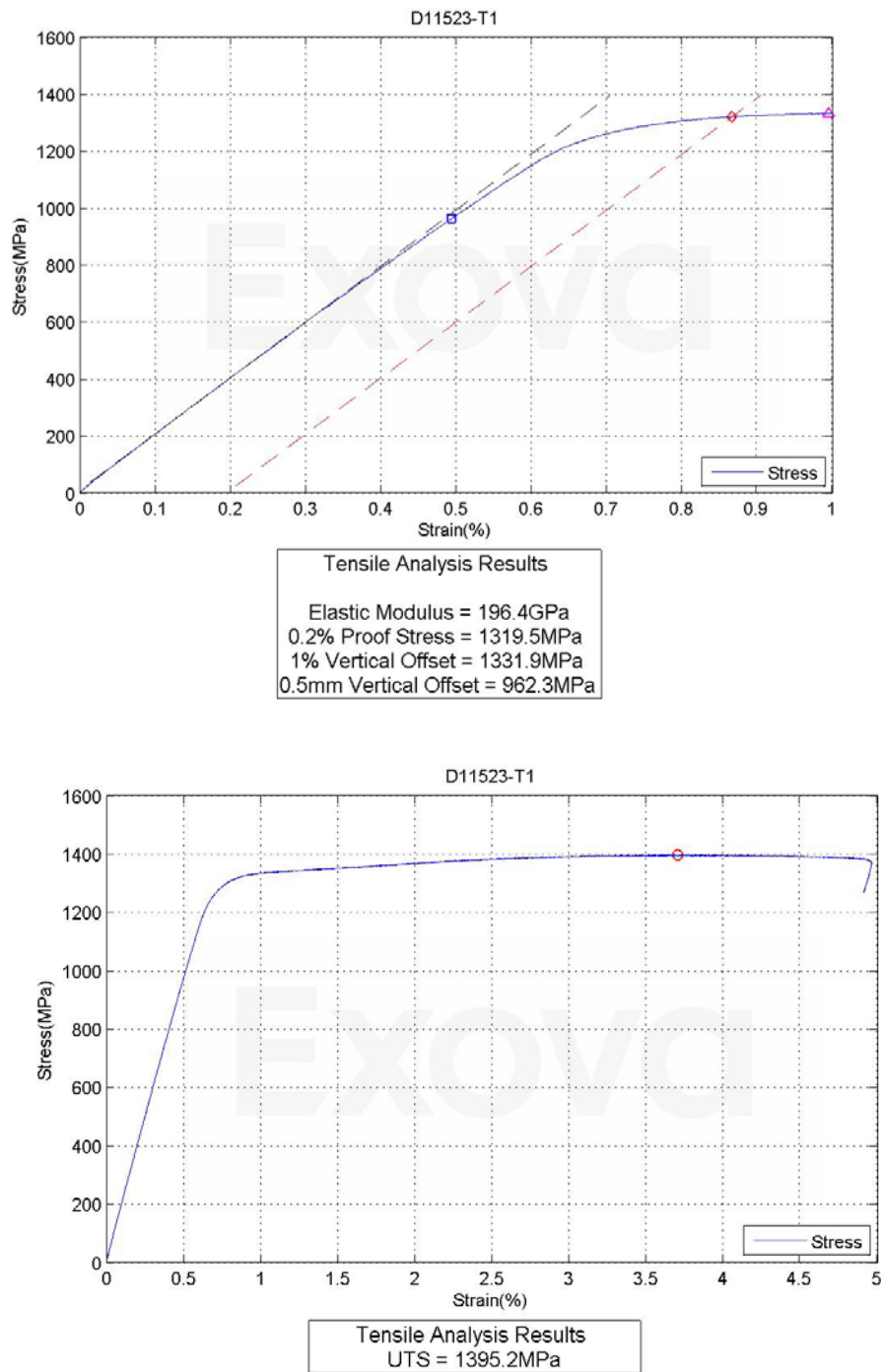


Fig. 7-7 – Tensile testing results for Wire-2 (9x3mm).

7. Results and Discussion

Table. 7-2 – Hardness testing results displayed as HV10 with corresponding UTS values for each grade of wire.

Wire Grade	UTS (MPa)	Hardness (HV10)
Wire 1	1171	376
Wire 2	1395	397

7. Results and Discussion (Fatigue Testing)

7.2 Fatigue Testing

7.2.1 Lab Air Fatigue Testing

7.2.1.1 Wire-1

To get an idea of the fatigue life and the endurance limit of the armour wire material, fatigue testing in lab air was carried out in order to generate some baseline fatigue data. This baseline data is used to highlight the effect on fatigue life of the corrosive environments discussed in the following sections.

Air fatigue testing on Wire-1 was conducted in axial tension at the request of the client since this is historically how they have generated their in-air data. For the purposes of this thesis some complementary lab air fatigue testing has been carried out in a four-point bending configuration so that the corrosion fatigue results could be compared like for like in terms of test configuration. The number of samples tested was limited however due to availability of test material. Table 7-3 presents the results for the lab air test series generated in axial tension.

Table 7-3 – Results of the air fatigue test series on Wire-1 (axial tension)

Sample	Max Load	Min Load	%age Yield	Peak Stress	Stress Range	Constant Mean	Frequency	No. Cycles to rupture	Fracture Location	Fracture Initiation	Straightened and Tabbed (AI)
	kN	kN		MPa	MPa	MPa	Hz				
AF01	59.94	0.76	90	780	760	400	10	124965	Gauge Length	Edge	Yes
AF02	59.67	0.76	90	780	760	400	10	62810	Gauge Length	Edge	Yes
AF03	59.63	0.75	90	780	760	400	10	133933	Gauge Length	Edge	Yes
AF04	56.27	3.75	80	700	600	400	10	211303	Gauge Length	Edge	Yes
AF05	56.43	3.76	80	700	600	400	10	103207	Gauge Length	Flat	Yes
AF06	56.61	3.77	80	700	600	400	10	130971	Gauge Length	Edge	Yes
AF07	54.57	5.65	75	650	500	400	10	2000000	N/A	N/A	Yes
AF08	54.76	5.67	75	650	500	400	10	336249	Gauge Length	Edge	Yes
AF09	54.42	5.63	75	650	500	400	10	159985	Gauge Length	Edge	Yes
AF10	59.47	0.75	90	780	760	400	10	100926	Gauge Length	Edge	Yes
AF11	56.61	3.77	80	700	600	400	10	150752	Gauge Length	Edge	Yes
AF12	54.70	5.66	75	650	500	400	10	163114	Gauge Length	Edge	Yes
AF13	52.48	7.50	70	600	400	400	10	1017711	Tabbing	Edge at defect	Yes
AF14	52.74	7.53	70	600	400	400	10	354962	Gauge Length	Edge at nick	Yes
AF15	52.76	7.54	70	600	400	400	10	270968	Gauge Length	Flat	Yes
AF16	52.76	7.54	70	600	400	400	10	N/A Sample Damaged			Yes
AF17	52.70	7.53	70	600	400	400	10	243447	Gauge Length	Flat	Yes

7. Results and Discussion (Fatigue Testing)

These results are displayed in an SN plot in figure 7-8.

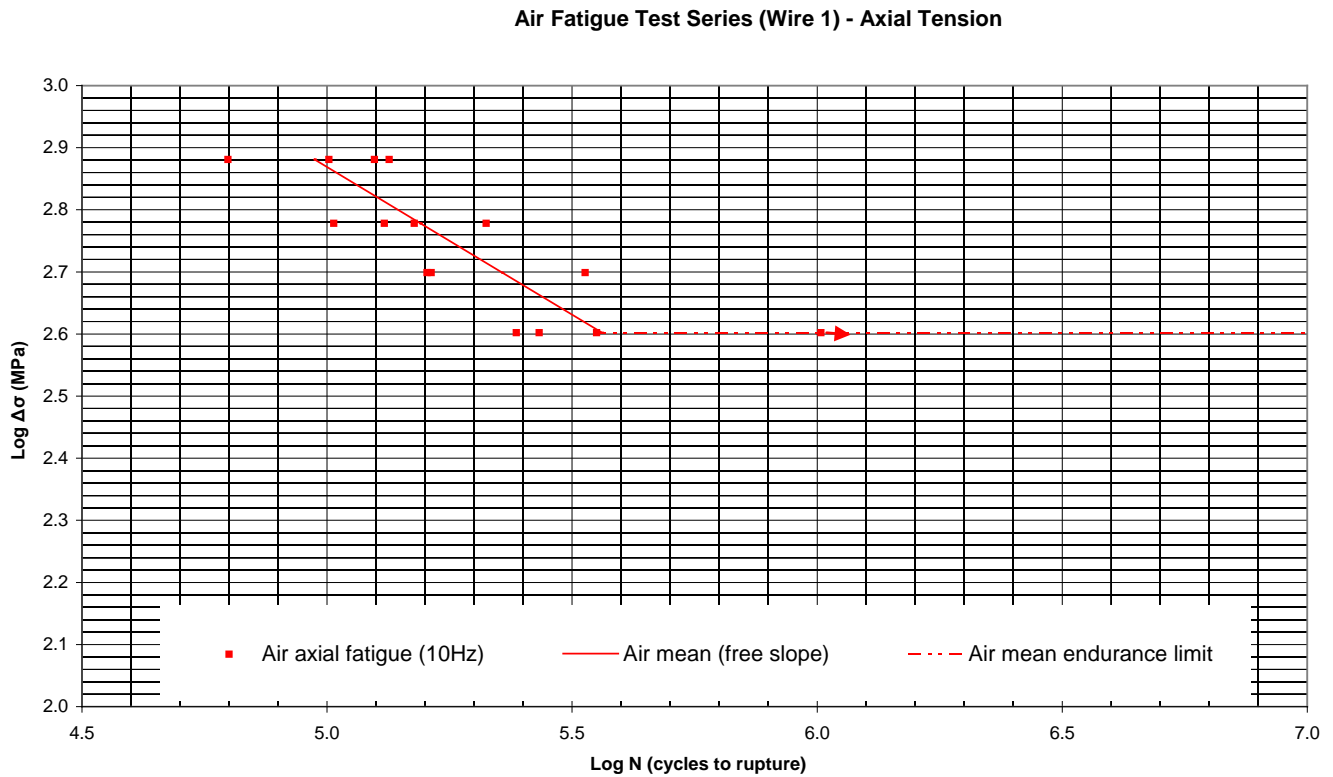


Figure 7-8 –SN plot presenting the results of the air fatigue test series on Wire-1 (axial tension).

Before discussing these results in more detail it makes sense to present the lab-air four-point bend data so that the discussion can focus on the differences between the test results in each configuration and then an explanation via SEM investigation of the different fracture surfaces.

As such Table 7-4 displays the results of the lab air fatigue test series in the four-point bend configuration.

7. Results and Discussion (Fatigue Testing)

Table 7-4 – Results of the lab air fatigue test series on Wire-1 (four-point bend)

Sample ID	Steel Grade	Size (mm ²)	Curve	Test Frequency	Stress Range (MPa)	Cycles to Rupture	Comments
1	Wire 1	15x5	Air Fatigue (Four point Bend)	5Hz	760	299531	Valid within constant stress area
2					760	193438	Valid within constant stress area
3					760	277433	Valid within constant stress area
4					760	587554	Valid within constant stress area
5					700	601243	Valid within constant stress area
6					700	814596	Valid within constant stress area
7					600	2000000	Valid within constant stress area
8					600	8000000	Valid within constant stress area
9					600	8000000	Valid within constant stress area
10					550	8000000	Valid within constant stress area
11					550	8000000	Valid within constant stress area

These results are displayed alongside the tension lab air fatigue data in an SN plot in

Figure 7-9.

In air data - Comparison of Axial Tension Configuration Vs 4 Point Bending Configuration (Wire 1)

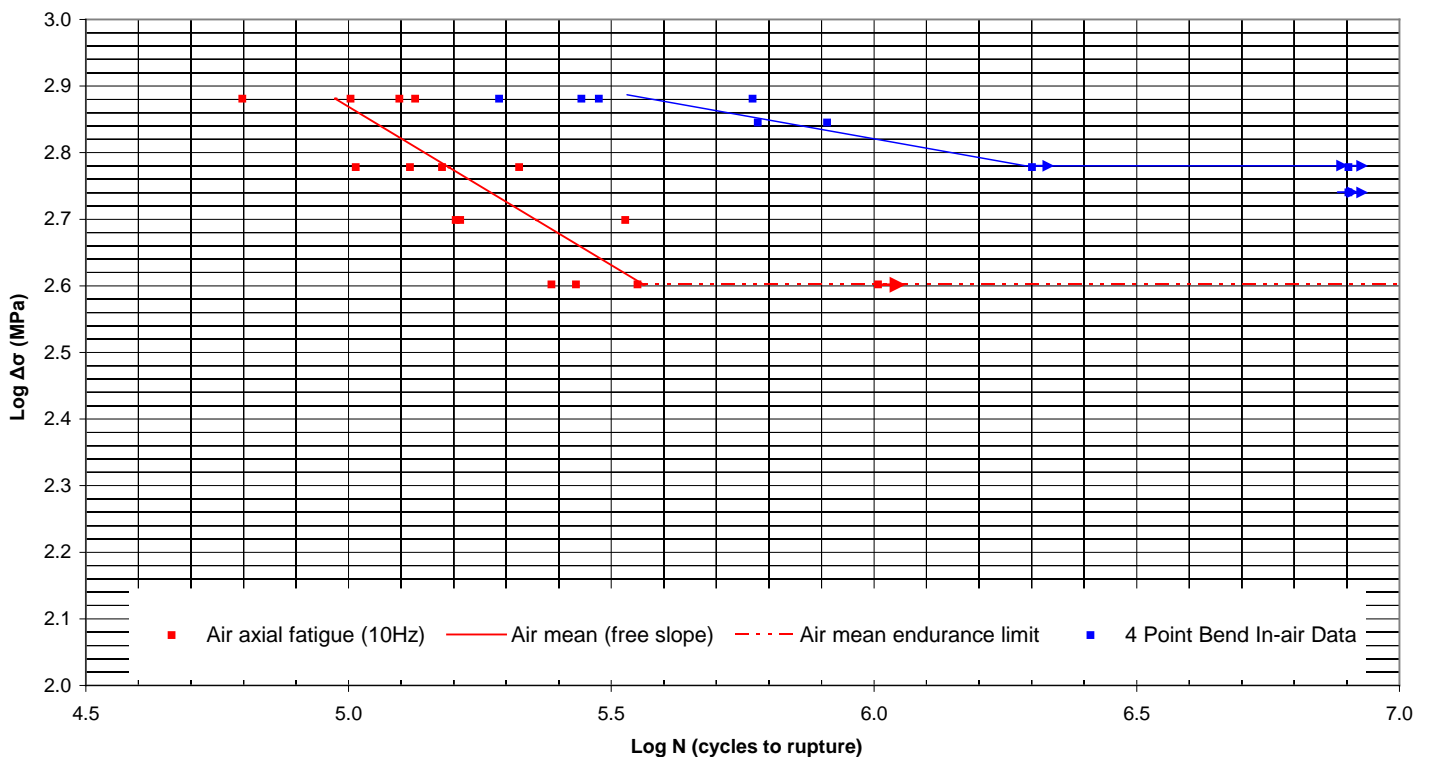


Figure 7-9 –SN plot presenting the results of the lab air fatigue test series on Wire-1. Comparison of tension and four-point bend test configuration. Data shows testing in tension results in significantly reduced fatigue life and endurance limit. (Arrows indicate run-outs)

7. Results and Discussion (Fatigue Testing)

It can be seen from Figure 7-9 that there is a significant difference in the fatigue results depending on the test configuration used. Testing in axial tension results in a significant reduction in fatigue life and a reduced endurance limit compared to testing in a four-point bend configuration. Testing in tension could be expected to be more conservative than four-point bend since in the tension configuration every surface of the sample over the gauge length is exposed to peak strains increasing the likelihood of initiation from a worst case surface defect. In the four-point bend test it is only the surface of the sample in tension (convex face) that sees maximum strains, reducing the chances of a worst case initiation site being subjected to the strains required for it to initiate a fatigue failure.

Investigation of the fracture faces from each of the test configurations appears to corroborate the above assessment and it is clear that the initiation point in each configuration is different. Figure 7-10 shows images from the SEM investigation on the fracture face of a sample from the axial tension air fatigue test series. Figure 7-11 shows a schematic of how the fracture face was oriented in the SEM chamber.

The top image shows a macro of the fracture face with the fatigue region highlighted. Closer inspection of this region in images (a), (b) and (c) reveal that the initiation point is from the drawn edge of the wire. This observation is consistent in the vast majority of samples tested in tension. Images (d), (e) and (f) provide information as to why this is the case when testing in tension. With the sample tilted to view the drawn edge of the wire, the nature of this surface of the sample is revealed and there is clear evidence of surface defects, one of which served as the initiation point for the fracture in this sample.

7. Results and Discussion (Fatigue Testing)

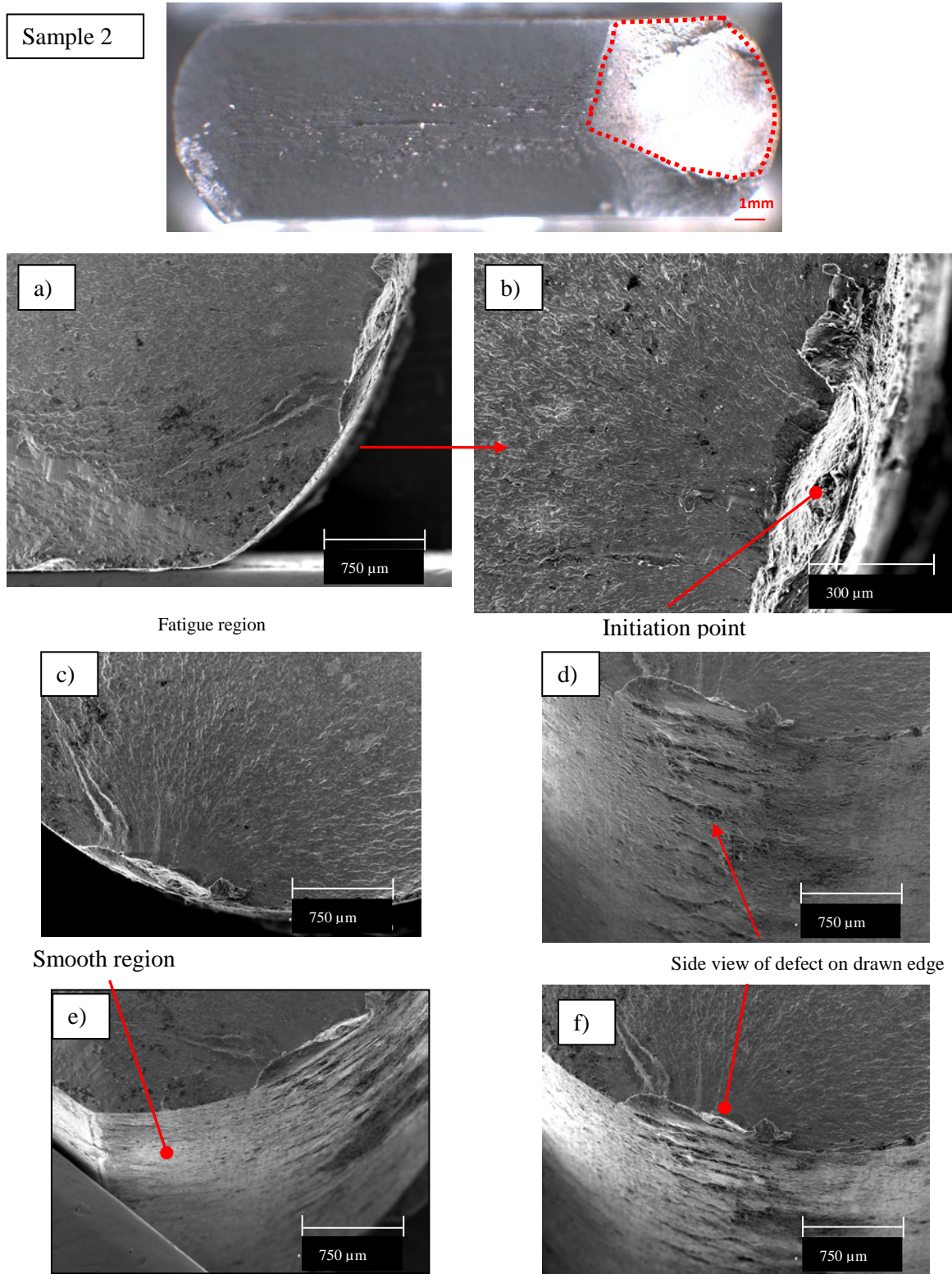


Figure 7-10 – SEM fractography of sample 2 from the axial tension lab-air test series. Typical initiation site is from the drawn edge of the wire where the surface finish is of poor quality and surface defects can be observed.

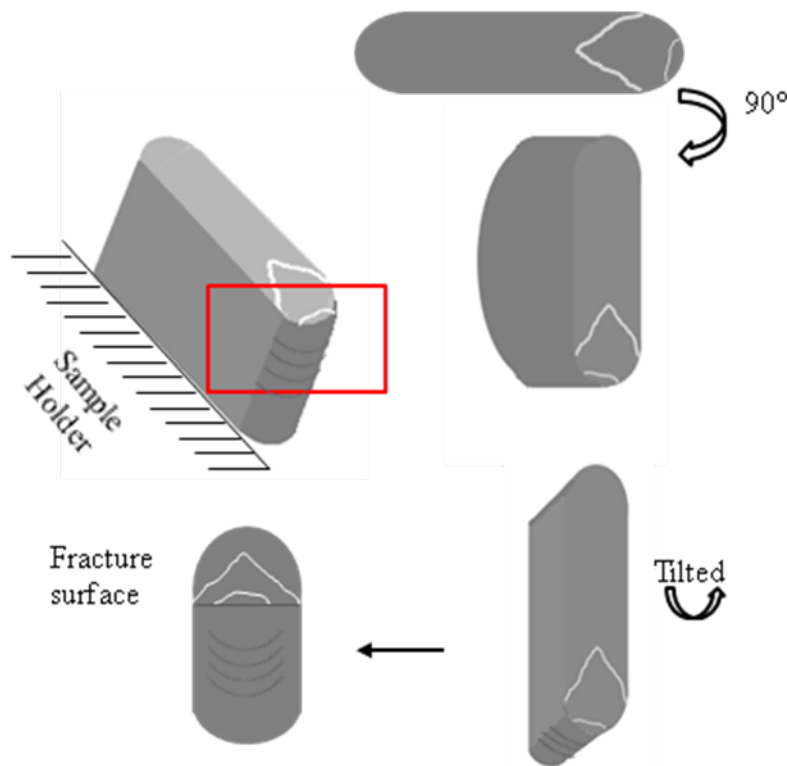


Figure 7-11 – Schematic showing how the axial tension fracture face was positioned during the SEM investigation.

In contrast to the fracture surface seen in tension, Figure 7-12 shows the fracture surface investigation from the lab-air four-point bend test series. It is clear from the macro image that the fracture surface is very different to that seen in the axial tension configuration. In this case the initiation point is from the rolled, flat surface of the wire which has seen the maximum tensile strains during testing. The better surface finish on this face of the sample results in the increased fatigue life shown in Figure 7-9 since the defects observed on the drawn edge of the wire are not subjected to critical strains in the four-point bend configuration.

7. Results and Discussion (Fatigue Testing)

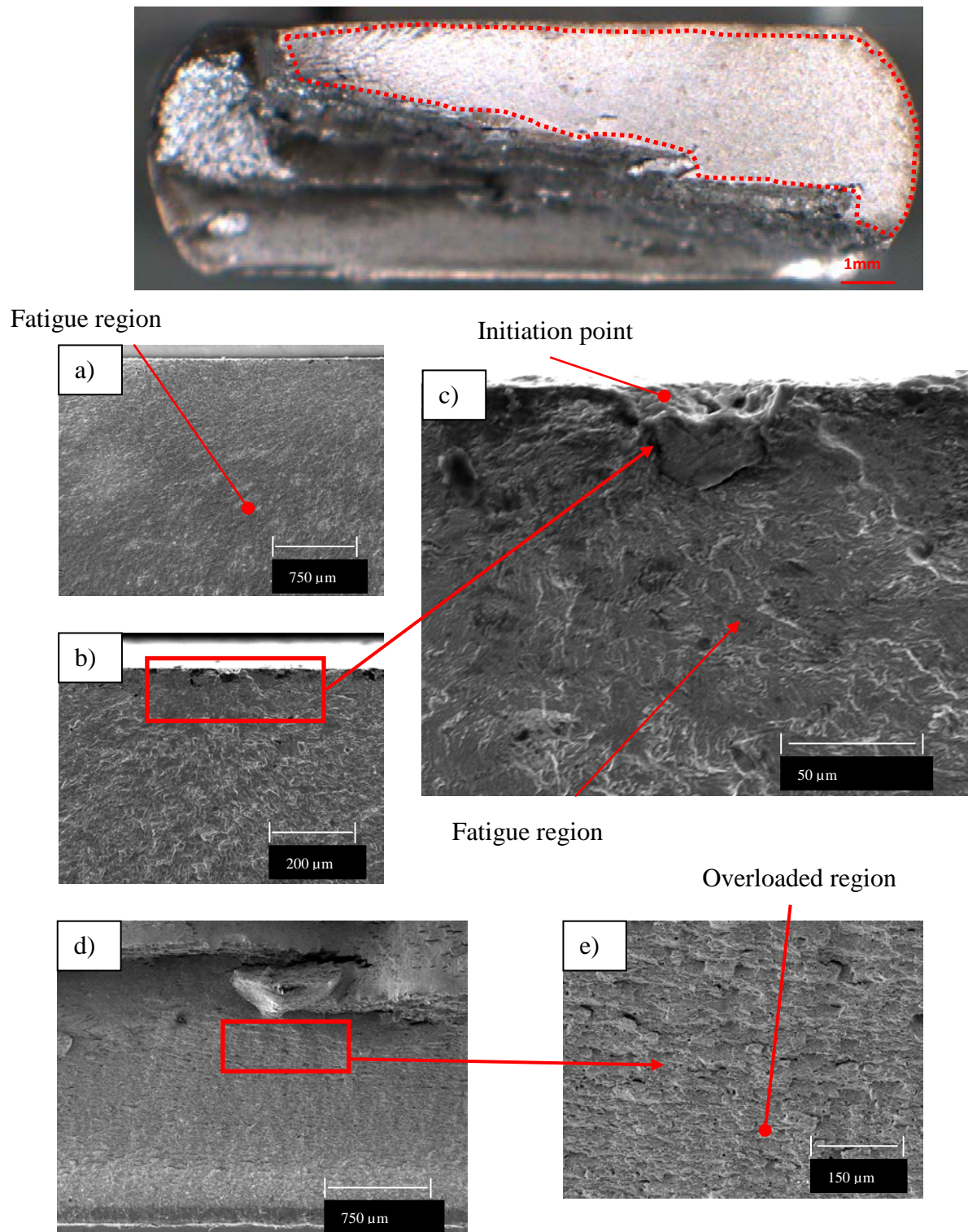


Figure 7-12 – SEM fractography from the four-point bend in-air test series. Note the significantly different appearance of the fracture face to that seen in axial tension. Initiation is from the rolled, flat surface of the wire which has seen maximum tensile strains.

7. Results and Discussion (Fatigue Testing)

In summary, the results in this thesis have shown that different fatigue results will be obtained in lab air depending on the configuration used in testing. This is due to the initiation point being different between test configurations as a result of changing stress pattern on the sample. In tension, the fatigue life is reduced as nearly all of the samples initiate from the rougher drawn edge of the wire. When this edge of the wire is not subjected to critical loading as in the four-point bend configuration the fatigue life is increased since cracks must now initiate from the relatively defect free rolled surface indicating that initiation and therefore fatigue life is largely determined by the surface condition of the wire.

When comparing fatigue data the effect of test configuration must be considered and data generated in axial tension should be treated as conservative relative to that in four-point bend.

In the following sections of this thesis (Sections 7.2.2.1 & 7.2.3.2) when comparing lab air data with that generated in a corrosive environment it will be lab air data generated in a four-point bend configuration that is presented. This way a like for like comparison can be drawn with the corrosion fatigue data removing any effects of testing configuration. Unfortunately in this thesis, for Wire-2, due to material availability only lab air data in tension has been generated for comparison with the four-point bend corrosion fatigue data.

7. Results and Discussion (Fatigue Testing)

7.2.1.2 Lab Air Fatigue Testing (Axial Tension) – Wire-2

Table 7-5 outlines the results for the lab air fatigue test series on Wire-2 along with other data from this phase of testing. This test series was conducted with a constant r ratio of 0.1.

Table 7-5 – Results of the lab air fatigue test series on Wire-2.

Sample	Max Load	Min Load	%age Yield	Stress Range	Frequency	No. Cycles to rupture	Fracture Location	Fracture Initiation	Tabbed and Straightened (AI)
	kN	kN		MPa	Hz				
AF 1	28.27	2.83	81.4	1050	5	27863	Gauge Length	Edge	Yes
AF 2	28.29	2.83	81.4	1050	5	18924	Gauge Length	Edge	Yes
AF 3	16.17	1.62	46.5	600	10	141375	Gauge Length	Edge	Yes
AF 4	16.16	1.62	46.5	600	10	139857	Gauge Length	Edge	Yes
AF 5	16.15	1.61	46.5	600	5	339172	Gauge Length	Edge	Yes
AF 6	16.20	1.62	46.5	600	5	111362	Gauge Length	Edge	Yes
AF 7	Not Tested								
AF 8	16.20	1.62	46.5	600	5	206114	Gauge Length	Corner	Yes
AF 9	16.12	1.61	46.5	600	5	240176	Gauge Length	Corner	Yes
AF 10	14.93	1.49	42.5	550	5	173602	Gauge Length	Corner	Yes
AF 11	16.26	1.63	46.5	600	5	10000000	N/A	run-out	Yes
AF 12	21.60	2.16	61.8	800	5	53105	Gauge Length	Corner	Yes
AF 13	21.62	2.16	61.8	800	5	66105	Gauge Length	Corner	Yes
AF 14	21.6	2.16	61.8	800	5	103373	Tabs	Edge	Yes
AF 15	24.31	2.43	69.6	900	5	65590	Gauge Length	Corner	Yes
AF 16	20.25	2.02	58.0	750	5	88499	Gauge Length	Corner	Yes
AF 17	20.24	2.02	58.0	750	5	94920	Gauge Length	Corner	Yes
AF 18	20.23	2.02	58.0	750	5	105085	Gauge Length	Corner	Yes
AF 19	20.18	2.02	58.0	750	5	93577	Gauge Length	Corner	Yes
AF 20	24.26	2.43	69.6	900	5	44059	Gauge Length	Corner	Yes
AF 21	24.27	2.43	69.6	900	5	39723	Gauge Length	Corner	Yes
AF 22	24.27	2.43	69.6	900	5	51068	Tabs	Corner	Yes
AF 23	27.06	2.71	77.3	1000	5	39677	Gauge Length	Corner	Yes
AF 24	26.92	2.69	77.3	1000	5	33369	Gauge Length	Corner	Yes
AF 25	26.97	2.70	77.3	1000	5	31885	Gauge Length	Corner	Yes
AF 26	26.95	2.69	77.3	1000	5	33937	Gauge Length	Corner	Yes
AF 27	24.31	2.43	69.6	900	5	46478	Gauge Length	Corner	Yes
AF 28	16.18	1.62	46.5	600	5	2000000	N/A	run-out	Yes
AF 29	21.60	2.16	61.8	800	5	51998	Gauge Length	Corner	Yes

7. Results and Discussion (Fatigue Testing)

Figure 7-13 and 7-14 display these results in the form of an SN plots. There are two features evident for the in air data; 1) the finite life region is less than 10^6 cycles and 2) the SN curve is quite flat. This has been shown to be the case for armour wire samples from several different suppliers where material within the same strength class has the same fatigue strength in air regardless of the brand [8].

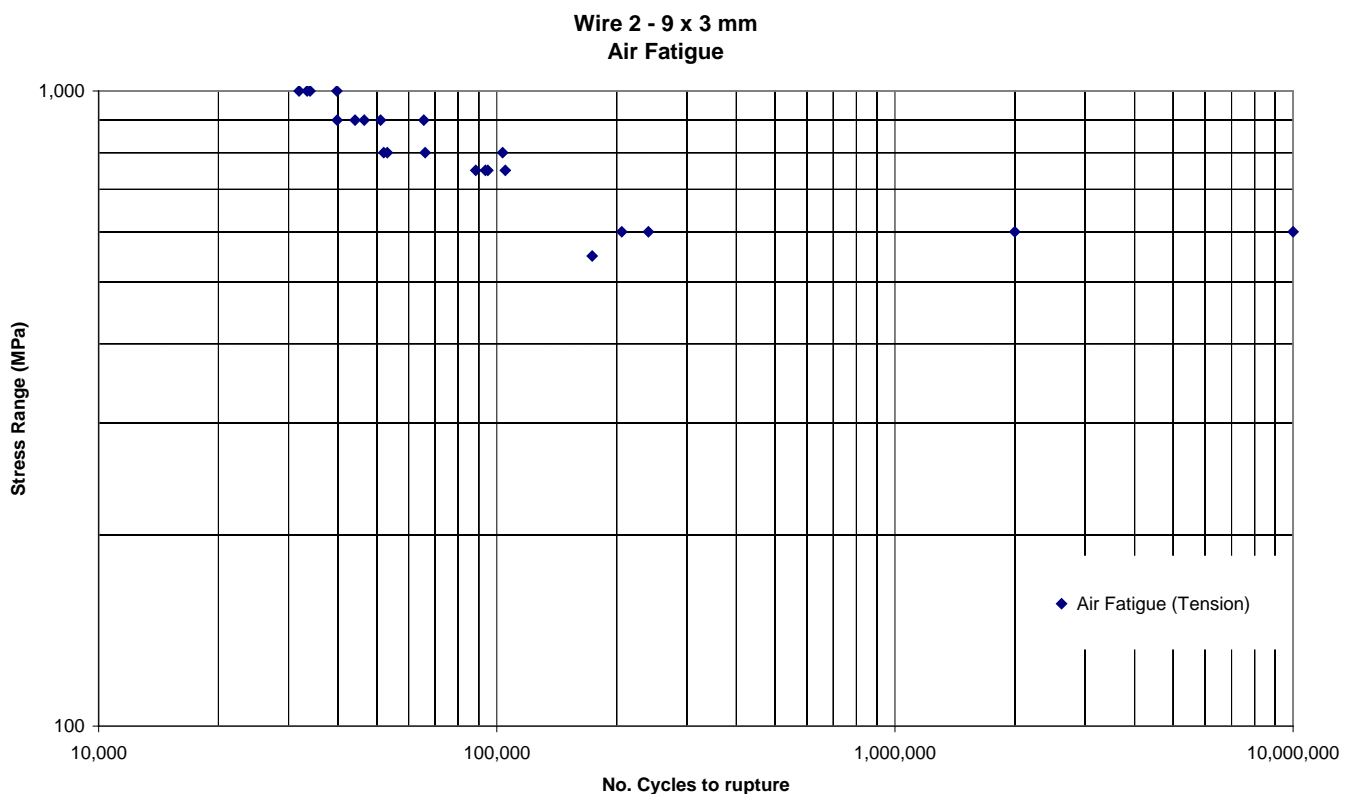


Figure 7-13 – Results of the lab air fatigue test series on Wire-2. SN plot displaying the in air fatigue data. Raw data plot shows stress range against cycles to failure

7. Results and Discussion (Fatigue Testing)

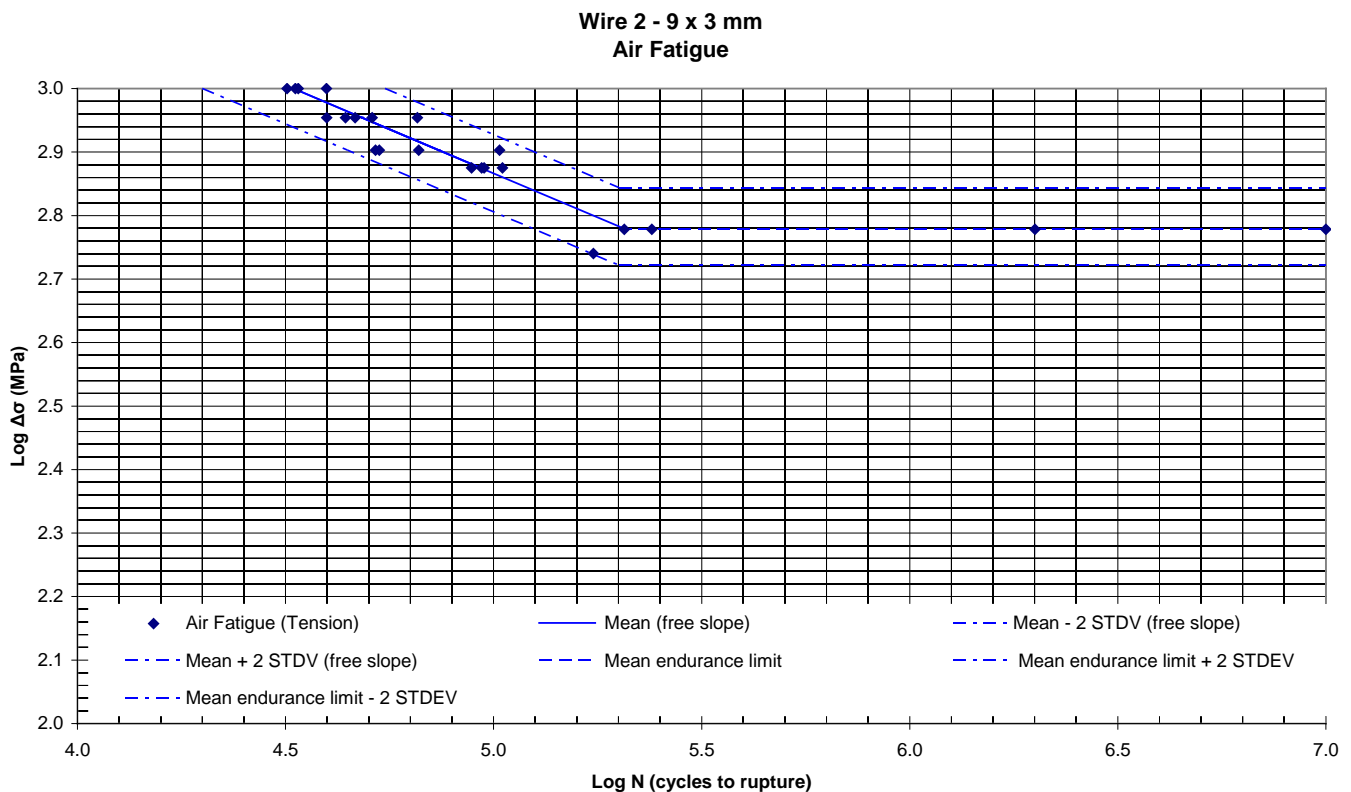


Figure 7-14 – Results of the lab air fatigue test series on Wire-2. SN plot displaying the in air fatigue data. Plot is a log-log graph showing the mean curve +/- 2 SD and the endurance limit.

Investigation of selected fracture surfaces via optical microscopy revealed typical fatigue failures initiating from the drawn edge of the armour wire sample which is consistent with the lab air fatigue test series utilising an axial tension configuration on Wire-1. Testing for this thesis was unable to include lab air fatigue testing in four-point bend on Wire-2 due to material availability. Based on the results of Wire-1 in four-point bending (Section 7.2.1.1) the lab air fatigue results on Wire-2 presented in this section can be considered conservative. The fracture faces from a selection of the valid ruptures from this test series are shown in Figures 7-15 to 7-17.

7. Results and Discussion (Fatigue Testing)

Invalid ruptures from the gripping points or beneath the aluminium tabs have not been used in the data analysis and therefore are not shown in this section.

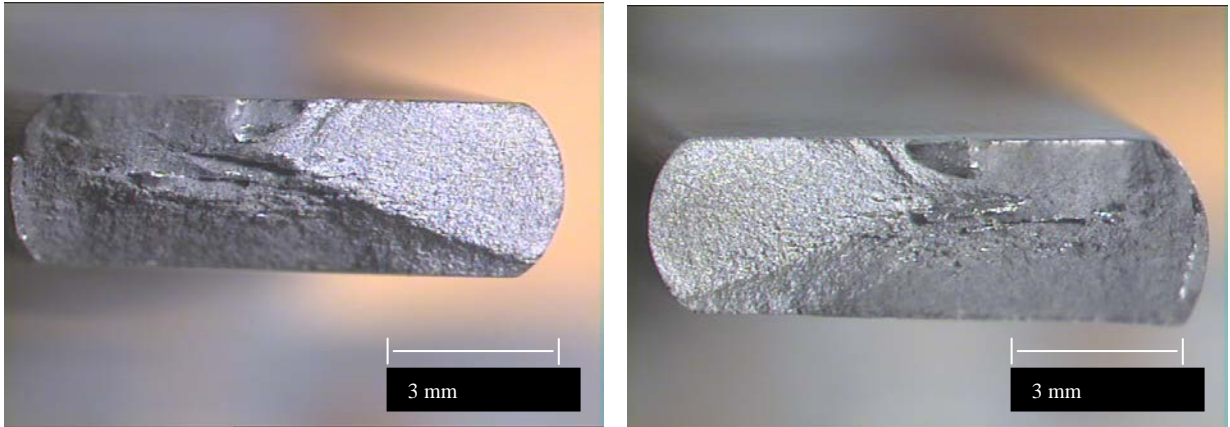


Figure 7-15- Sample AF 8 – 206,114 cycles

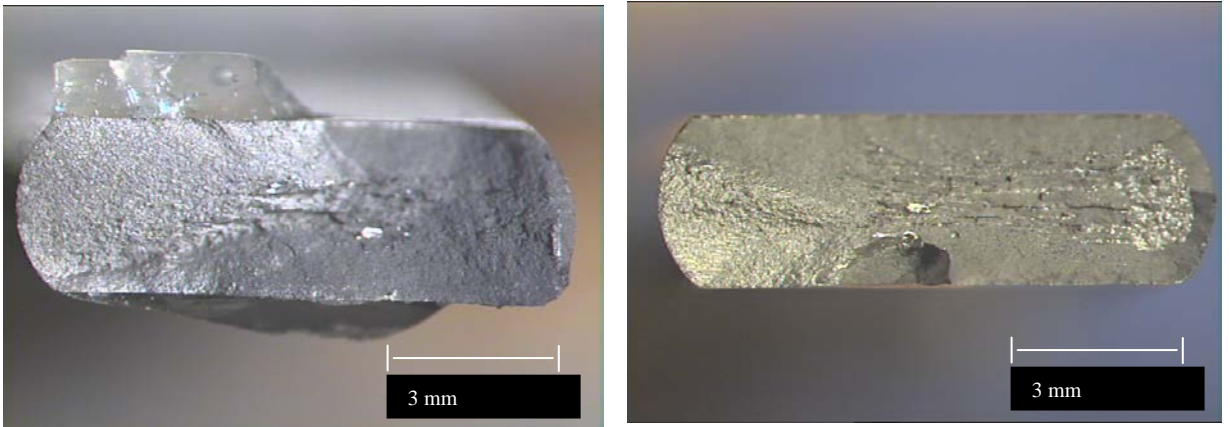


Figure 7-16- Sample AF 9 – 240,176 cycles

7. Results and Discussion (Fatigue Testing)

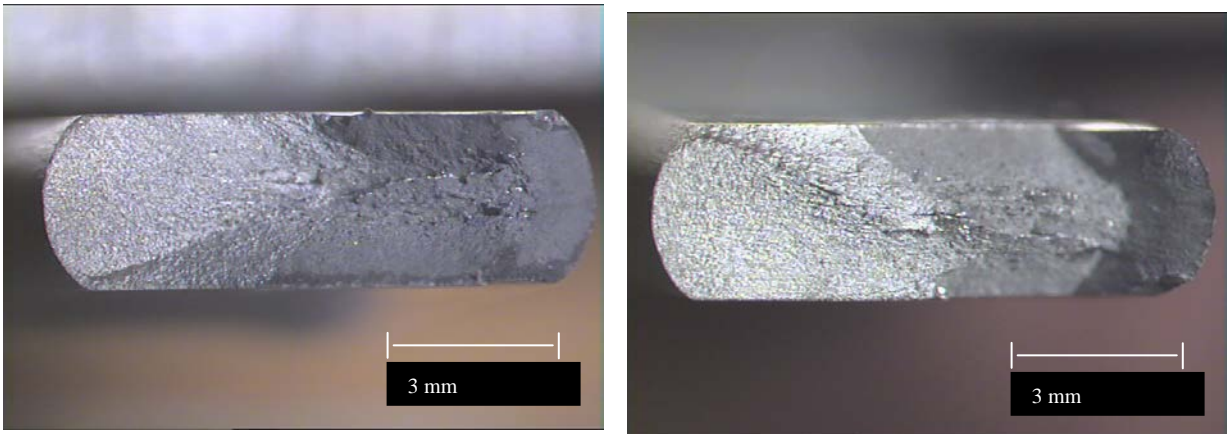


Figure 7-17- Sample AF 10 – 173,602 cycles

The fracture face of sample AF 8 (Figure 7-15) has also been investigated further using a SEM. Figure 7-18 shows the smooth fatigue portion of the fracture face with a single initiation point on the drawn edge of the wire (highlighted) which is consistent with that observed in the axial tension configuration lab-air testing on Wire-1.

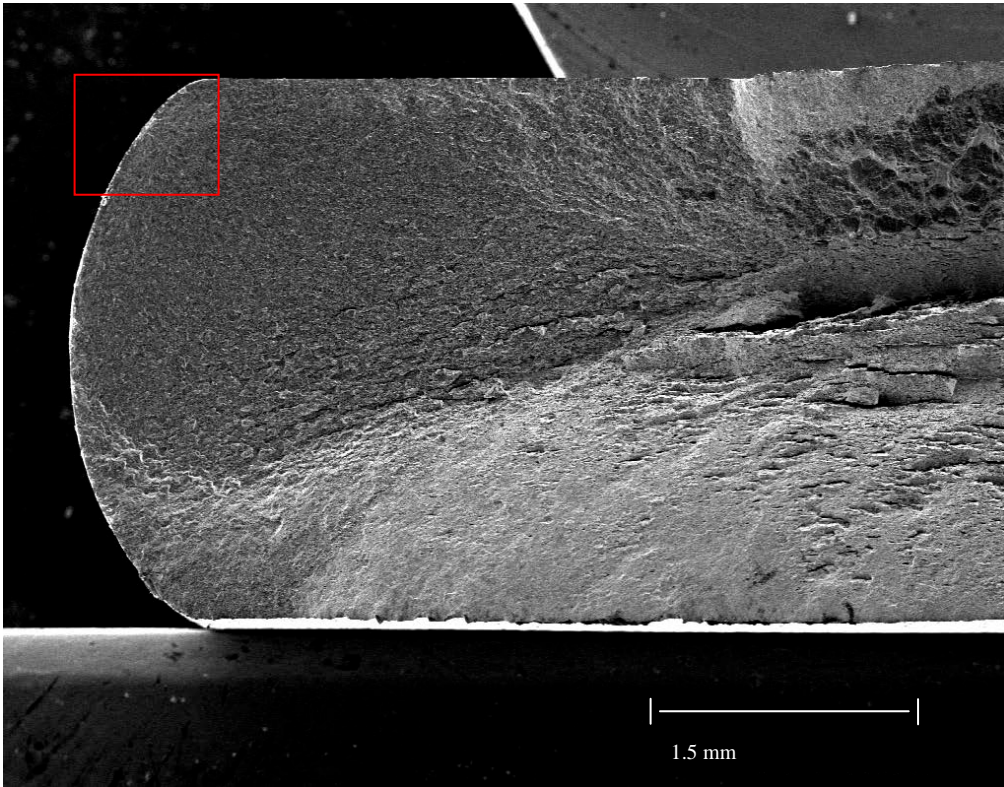


Figure 7-18- Sample AF 8- SEM Fractograph showing the smooth fatigue region of the fracture face with the initiation point highlighted on the drawn edge of the wire.

Figure 7-19 shows higher magnification images of the highlighted region from Figure 7-18, where the initiation point can be clearly identified.

7. Results and Discussion (Fatigue Testing)

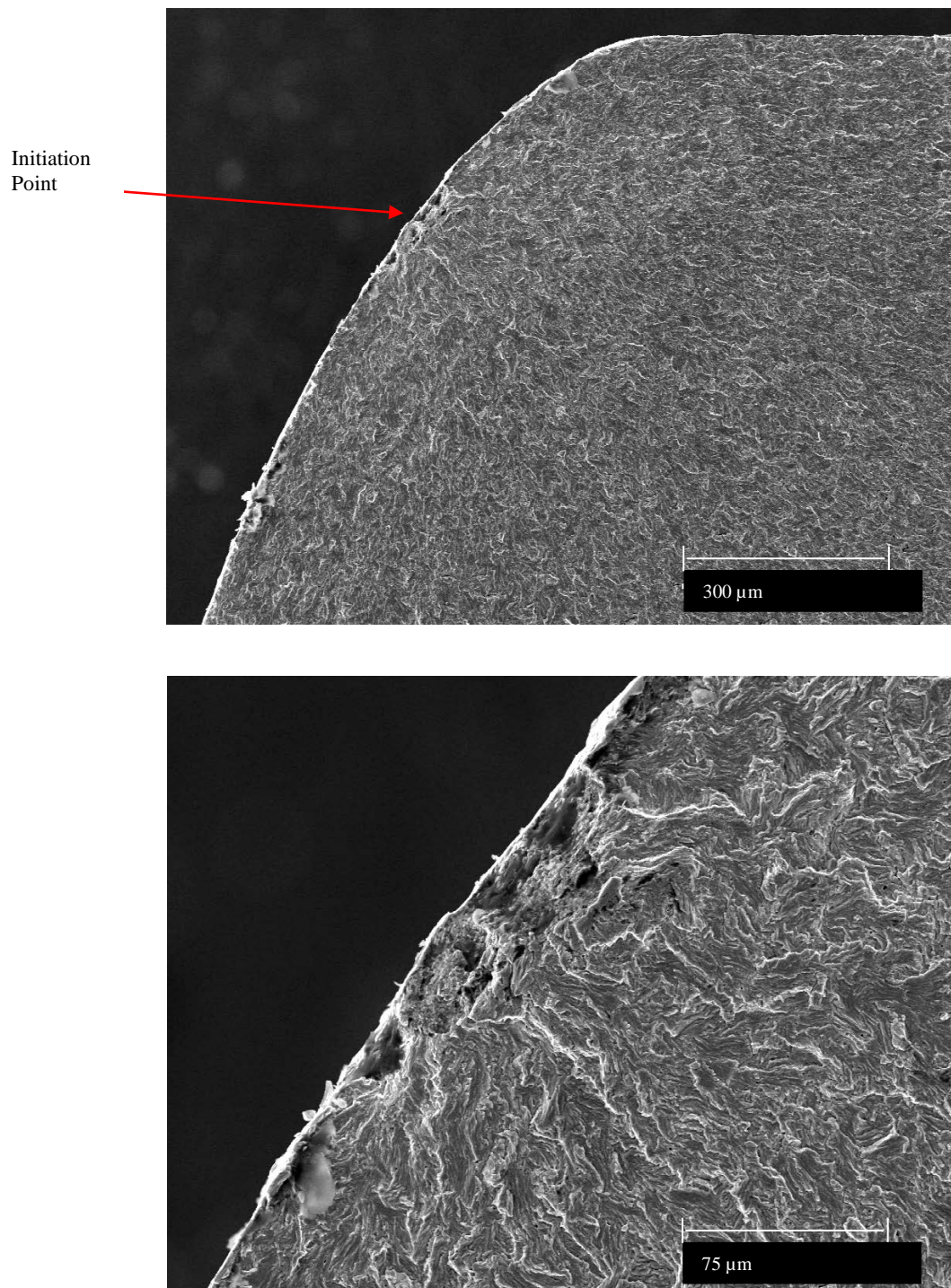


Figure 7-19- Sample AF 8- SEM Fractographs showing the initiation point highlighted on the drawn edge of the wire.

7. Results and Discussion (Fatigue Testing)

Figure 7-20 shows this initiation point from a different angle where it is also possible to see the surface condition of the drawn edge of the wire. As was observed with Wire-1 the drawn edge of the wire has surface defects associated with manufacture which serve to reduce fatigue life when this edge of the wire is exposed to maximum strains in the axial tension configuration.

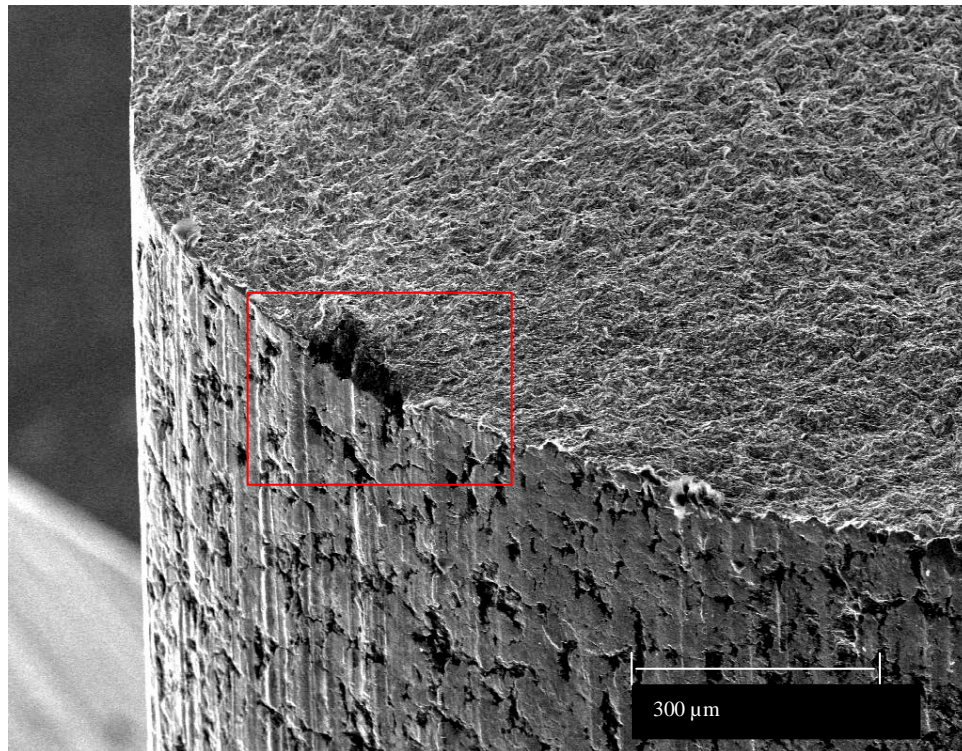


Figure 7-20- Sample AF 8- SEM Fractograph showing the initiation point highlighted on the drawn edge of the wire. The surface condition of the drawn edge is also evident where it can be seen that there are surface defects associated with manufacture.

Figure 7-21 shows the drawn edge of an untested section of Wire-2. This is presented to show that the surface condition of the drawn edge shown in Figure 7-20 is not caused during the fatigue testing and that it is present on the as-received wire.

7. Results and Discussion (Fatigue Testing)

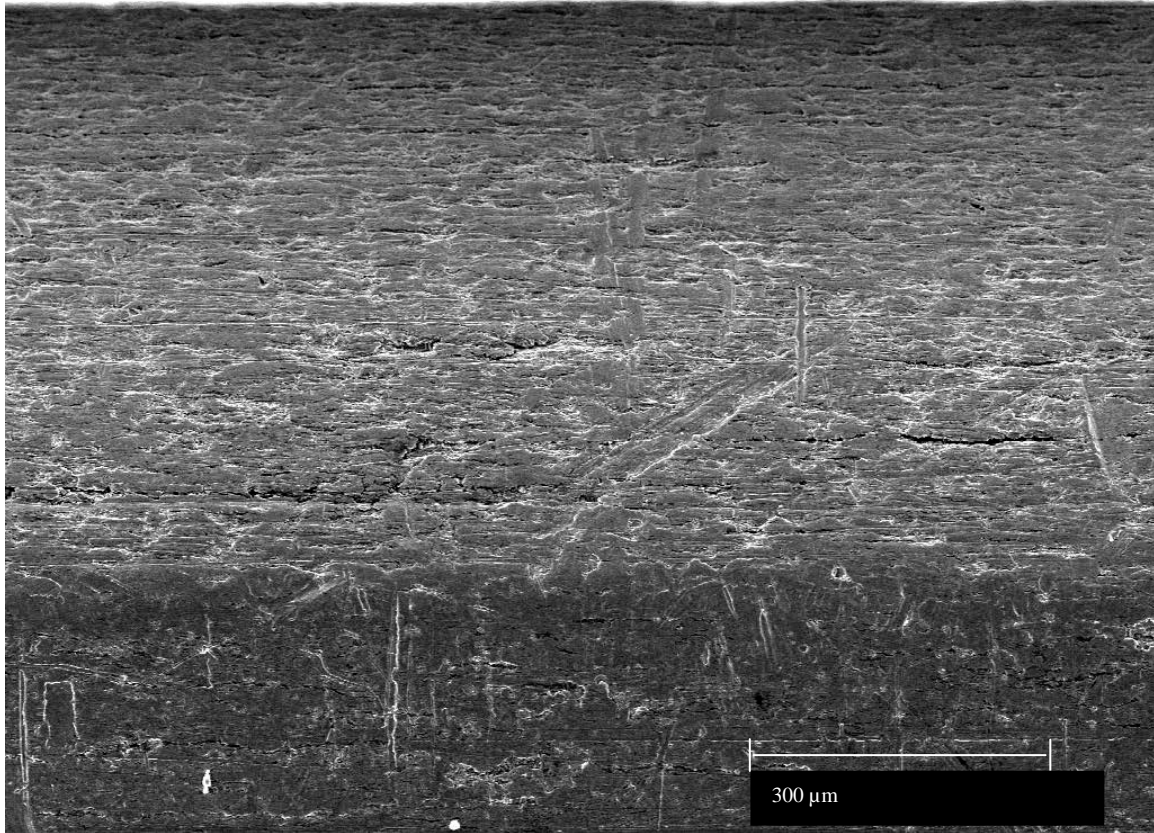


Figure 7-21-- SEM image showing the drawn edge of an as-received (untested) section of Wire-2. Shows clearly that the surface defects are present on the untested wire indicating that such damage is not caused during the fatigue testing.

7. Results and Discussion (Fatigue Testing)

7.2.2 Atmospheric Pressure Corrosion Fatigue Testing

7.2.2.1 Synthetic Seawater/1bar CO₂ – Wire 1

Table 7-6 outlines the test results for this test series along with other data from this phase of testing. This test phase was conducted at a constant mean stress of 400MPa so that the loading is consistent with the lab air fatigue test series on this wire (Wire-1). The results of this test series include data generated under both confined (high pH) and unconfined (low pH) test conditions since both are conducted at 1bar CO₂. In this section the two environments are treated as one population for comparison with the data generated in lab air. This same data is analysed again as the confinement investigation test series in Section 7.2.2.3 where a comparison is drawn between confined and unconfined test conditions.

Table 7-6 Outline of the test results from the CO₂ test series on Wire-1. Both unconfined and confined test environments are included in the results of this section since they are both tested at 1bar CO₂.

Sample ID	Steel Grade	Size (mm ²)	Curve	Approximate Start pH	Calculated Stress Range (MPa)	Cycles to Rupture	Comments
low pH 1	Wire 1	15x3 machined	1bar CO ₂ Unconfined	5.0-5.2	610	163490	Valid within constant stress area
2					585	219143	Valid within constant stress area
3					581	222118	Valid within constant stress area
4					657	137880	Valid within constant stress area
5					520	318140	Valid within constant stress area
6					515	617897	Valid within constant stress area
7					498	480791	Valid within constant stress area
8					501	585415	Valid within constant stress area
9					415	2006719	Valid within constant stress area
10					419	1944897	Valid within constant stress area
11					436	1927129	Valid within constant stress area
12					440	439395	Valid within constant stress area
high pH 1	Wire 1	15x3 machined	1bar CO ₂ Confined (addition of steel wool)	5.8	603	277156	Valid within constant stress area
2					607	188580	Valid within constant stress area
3					609	207229	Valid within constant stress area
4					599	212308	Valid within constant stress area
5					498	747941	Valid within constant stress area
6					487	524106	Valid within constant stress area
7					497	691006	Valid within constant stress area
8					482	660299	Valid within constant stress area
9					398	2101245	Valid within constant stress area
10					420	1834987	Valid within constant stress area
11					400	2445678	Valid within constant stress area
12					395	2537895	Valid within constant stress area

7. Results and Discussion (Fatigue Testing)

Figure 7-22 displays these results in the form of SN plots. The graph in this figure plots only the results from CO₂ test series on Wire-1 whilst Figure 7-23 superimposes the results of the air fatigue test series for Wire-1. As discussed in Section 7.2.1.1 when comparing fatigue data it is good practice to compare like for like. For this reason the air fatigue data generated in four-point bend will be used for comparison in this section.

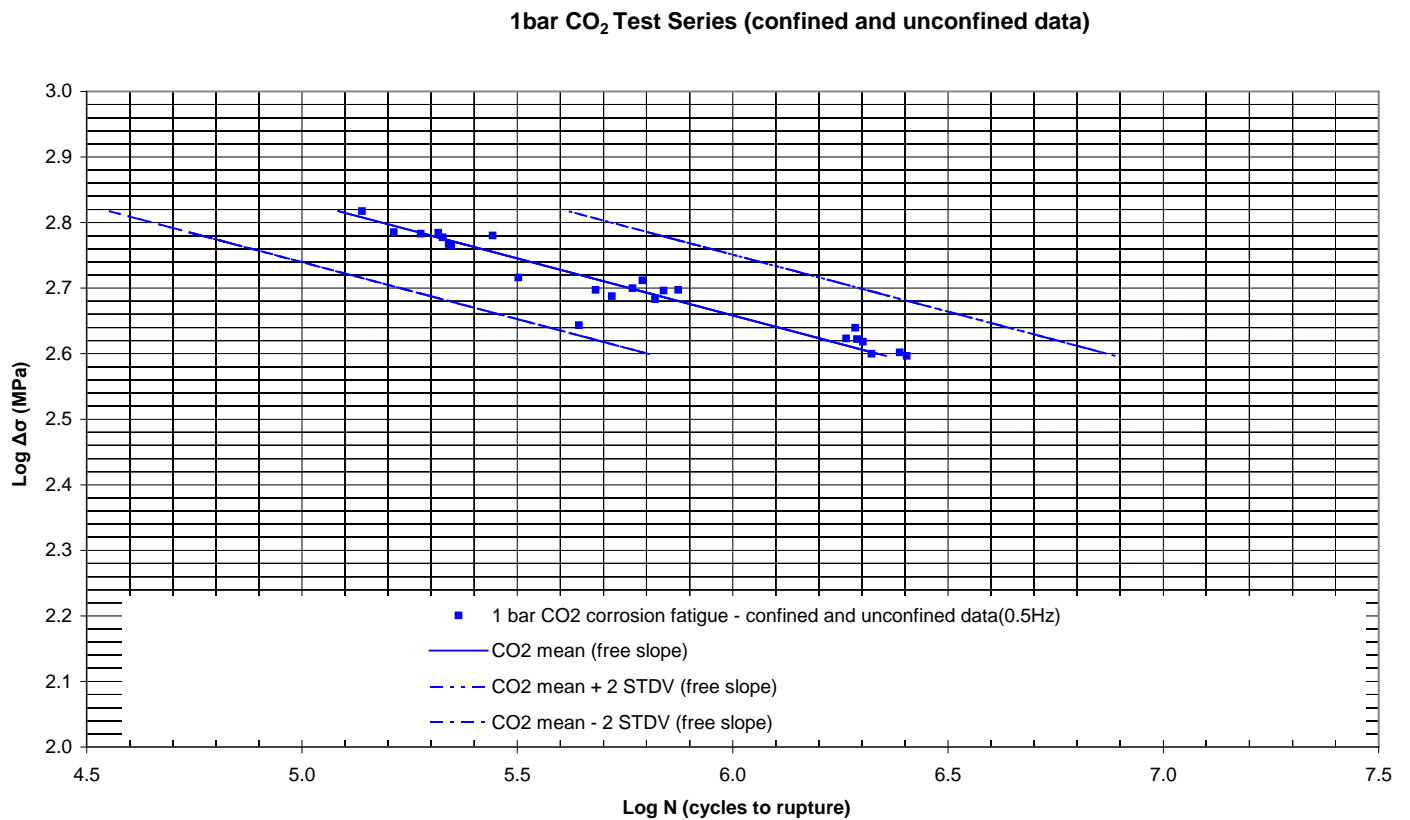


Figure 7-22 – Test results from the 1bar CO₂ test series in the form of an SN plot.

This comparison of SN curves clearly demonstrates the effect of testing in a corrosive environment on fatigue life, as compared to data generated in air. It can be observed that in the CO₂ test series there are failures at stress levels well below the in air endurance

7. Results and Discussion (Fatigue Testing)

limit which can be attributed to the action of the corrosive environment. It can also be observed from Figure 7-23 that there is a reduction of fatigue life in the finite life region when testing in a corrosive oilfield environment.

1bar CO₂ Test Series (confined and unconfined data) Vs Air Curve Test Series

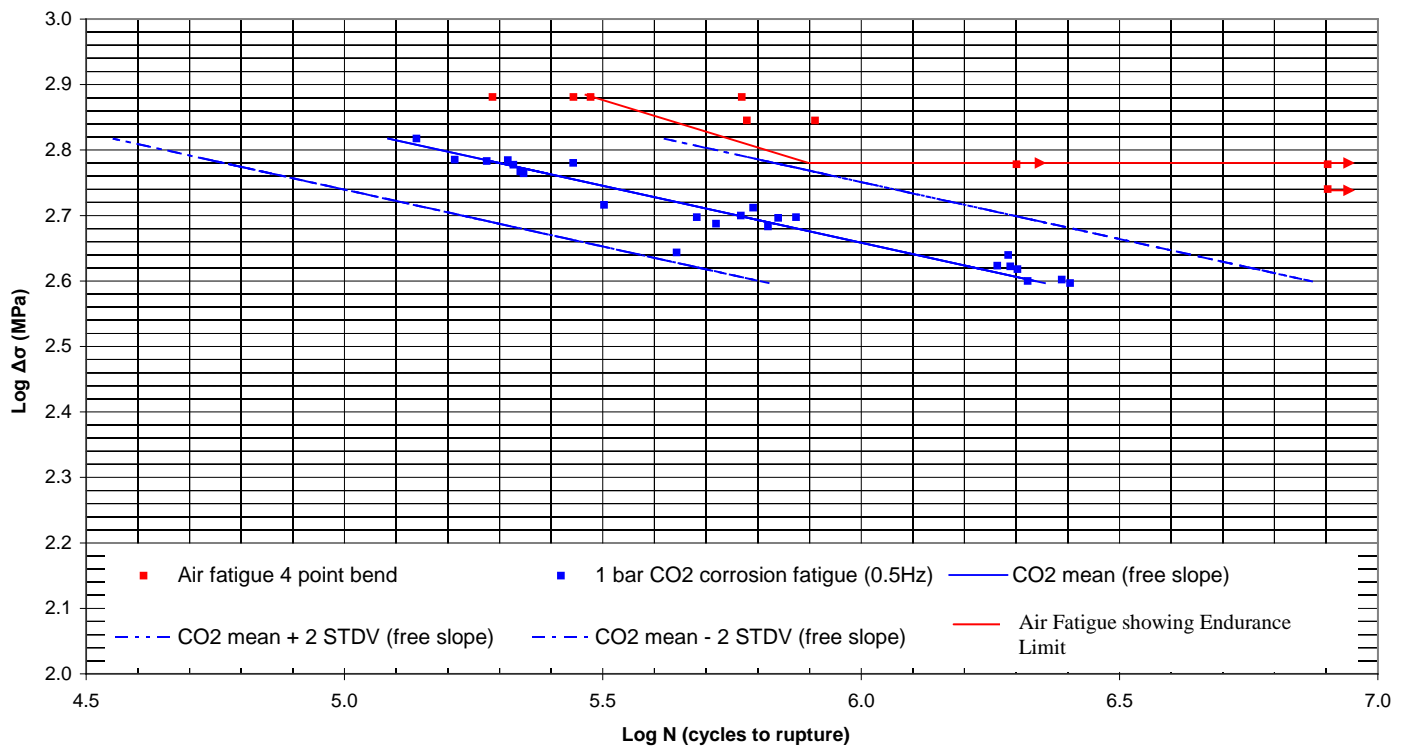


Figure 7-23 – Test results from the 1bar CO₂ test series along with the lab air fatigue (four-point bend) test series data to demonstrate the effect the corrosive environment has on fatigue life.

Investigation of some of the samples from the 1bar CO₂ test series reveals the cause of these effects of reduced fatigue life and elimination of an endurance limit when testing is performed under simulated corrosive oilfield conditions. Figure 7-24 shows the tensile surface of a tested sample in the area of constant stress between the two centre rollers.

7. Results and Discussion (Fatigue Testing)

There is clear evidence on the sample surface of secondary and hairline cracking over this area of the sample where it has seen maximum tensile strains. These phenomenon are not seen in samples tested in lab air so these features must be related to the exposure to an aggressive environment and therefore corrosion related.

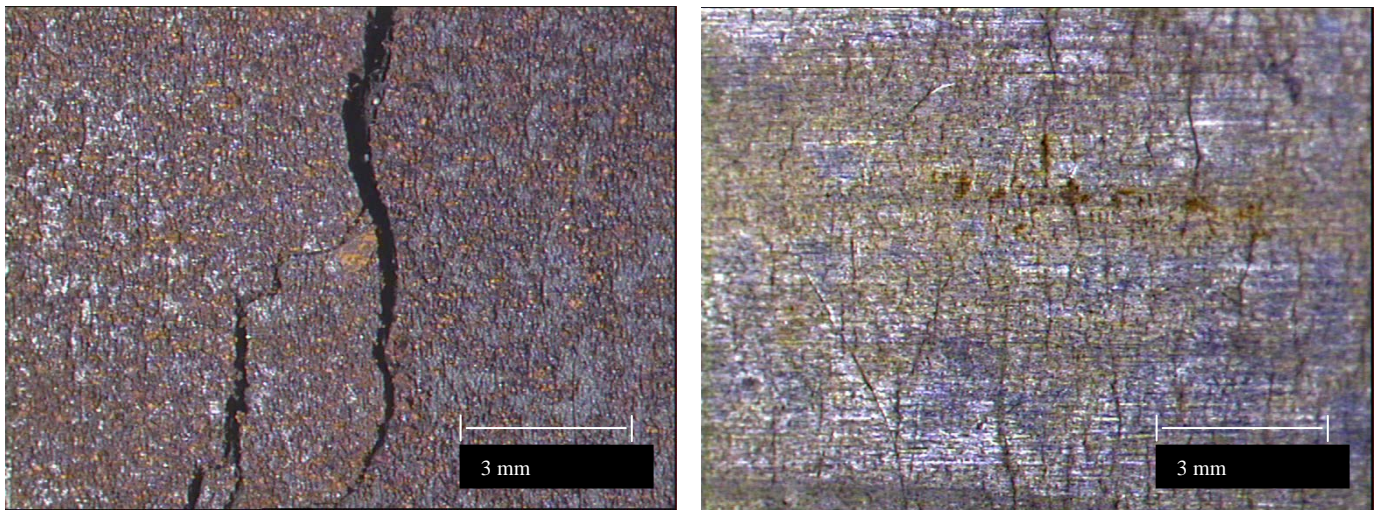


Figure 7-24 – Tensile surface of a ruptured sample from the CO₂ test series. Image shows the area of constant stress between the two rollers where there is evidence of secondary and hairline cracking on the surface of the sample. Low pH test sample.

To investigate further the source of these surface cracks and the reason for the effect of the environment on fatigue life the sample in Figure 7-24 was longitudinally sectioned through the constant stress area where the surface corrosion related features are located. The following Figures (7-25 to 27) show this sample after polishing and etching had revealed the surface corrosion features and subsequent cracking in more detail.

It is clear from these images that the reduction in fatigue life and elimination of an endurance limit is caused by corrosion related surface damage. Specifically, the

7. Results and Discussion (Fatigue Testing)

formation of small pits on the surface of the sample are a precursor to further cracking emanating from the base of such phenomenon as they act as a local stress raiser.

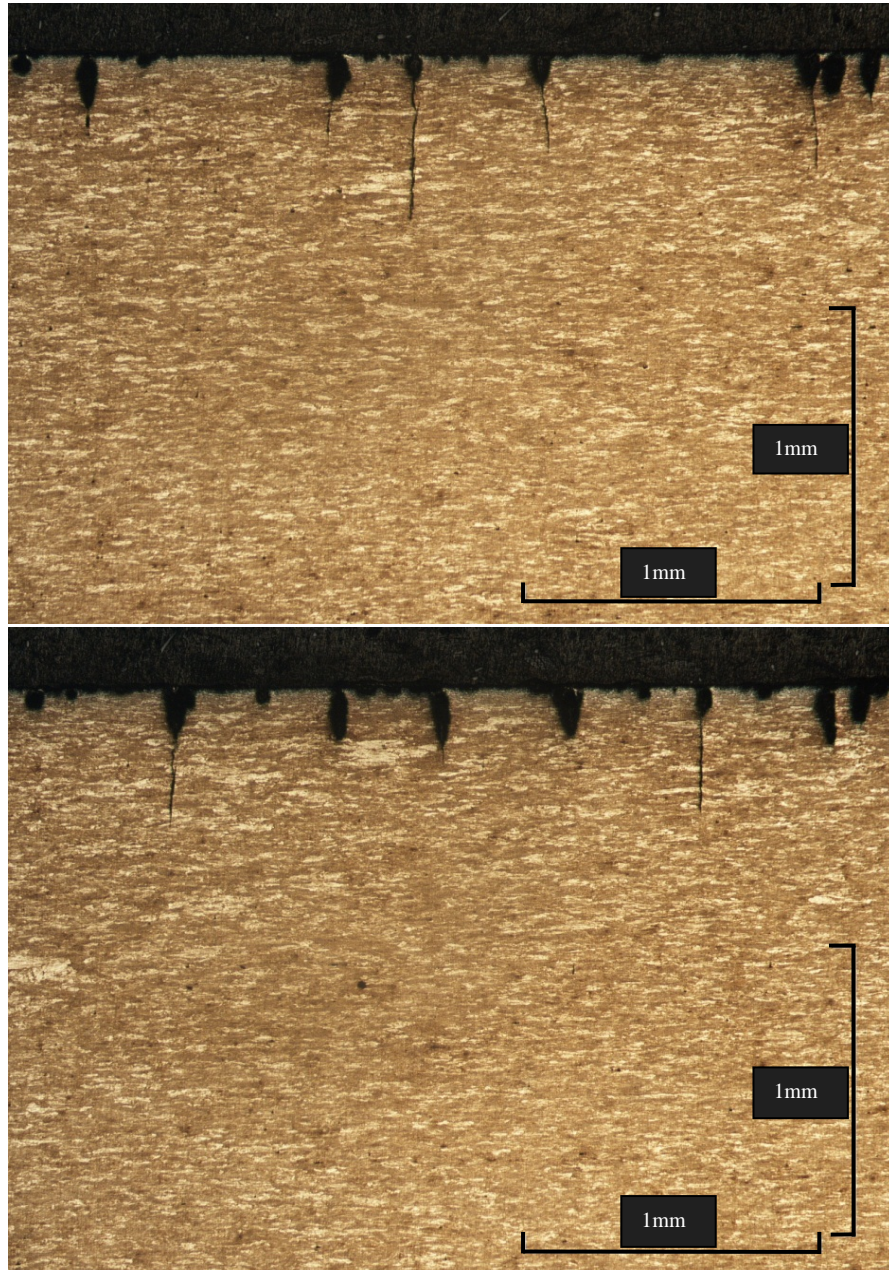


Figure 7-25 –Longitudinal section of the constant stress area of the sample post test. Selection of corrosion related pits with subsequent cracking emanating from the base of such phenomenon. (2% nital etch – Wire-1)

7. Results and Discussion (Fatigue Testing)

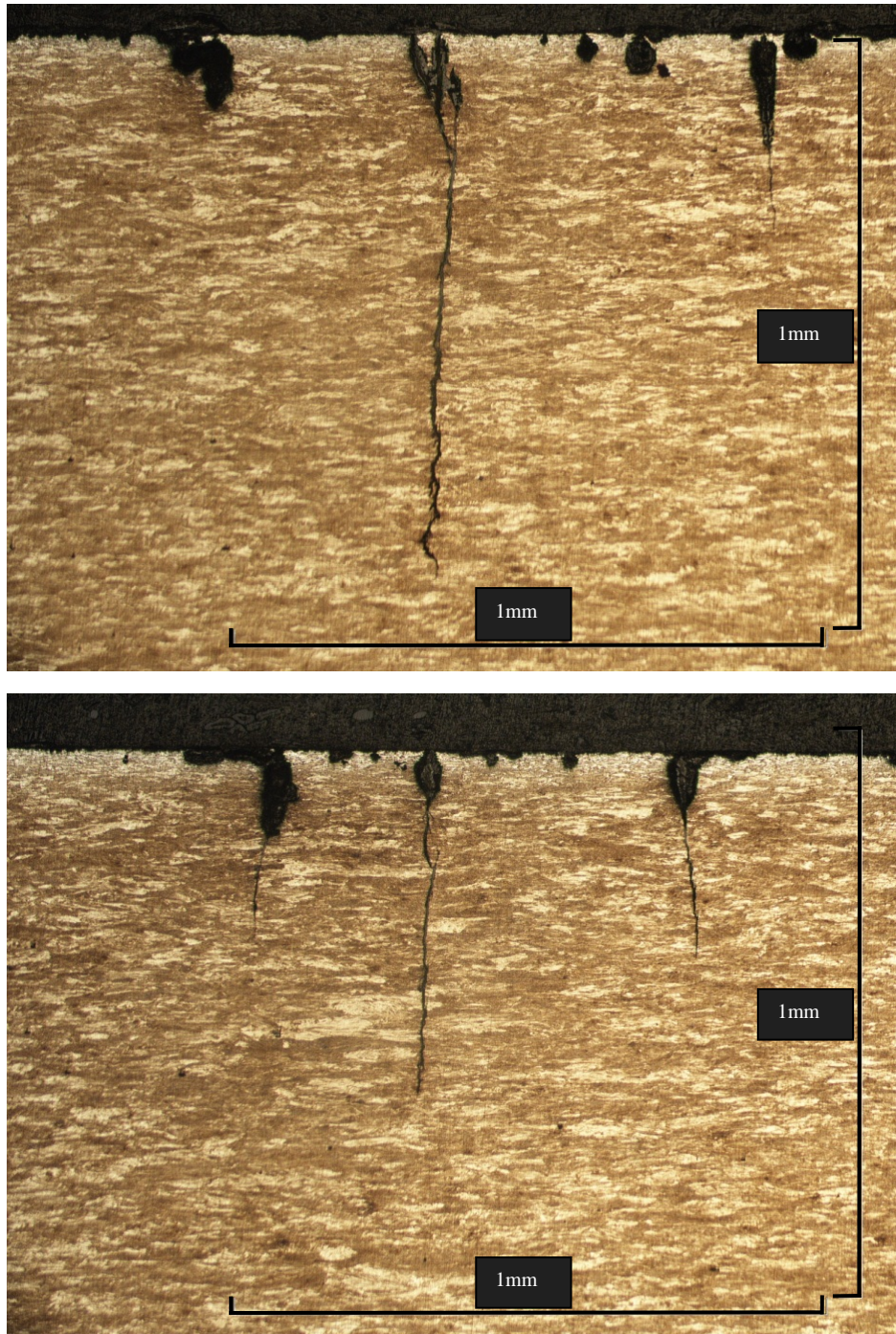


Figure 7-26 –Longitudinal section of the constant stress area of the sample post test. Higher mag selection of corrosion related pits with subsequent cracking emanating from the base of such phenomenon. (2% nital etch – Wire-1)

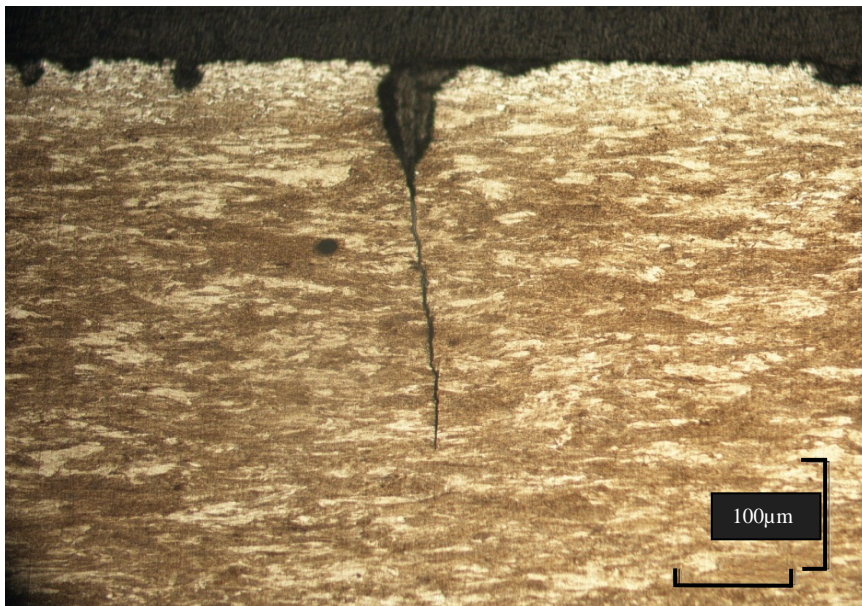
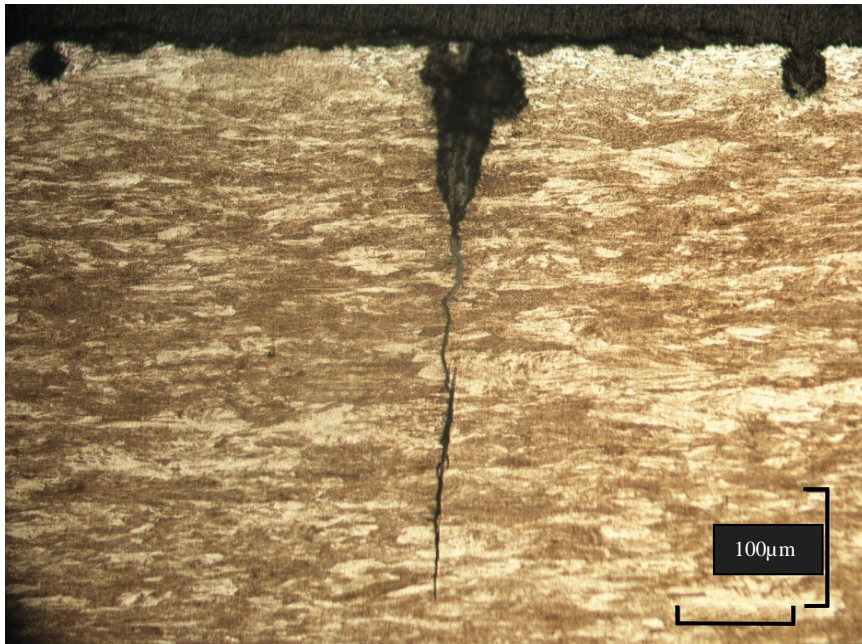


Figure 7-27 –Longitudinal section of the constant stress area of the sample post test. Higher mag selection of corrosion related pits with subsequent cracking emanating from the base of such phenomenon. (2% nital etch – Wire-1)

7. Results and Discussion (Fatigue Testing)

The fracture surface of one of the ruptured samples (low pH 3) was also subjected to an SEM investigation in order to view the initiation sites and possible links to pitting in more detail. Figure 7-28 shows these images. A macro image is shown at the top, the highlighted region shows the fatigue area of the fracture face where initiation is likely to be from the tensile (top) surface of the wire. A clear initiation point was not seen, however from the shape of the fracture face it is likely to have been in the top right corner of the sample. Pitting was identified along the specimen surface (figure a & b). A detailed image of these pitting sites is shown in images (c) and (d). This type of corrosion feature will act as a corrosion fatigue initiation site and as we have seen from the previous figures, such damage can eventually result in cracking.

7. Results and Discussion (Fatigue Testing)

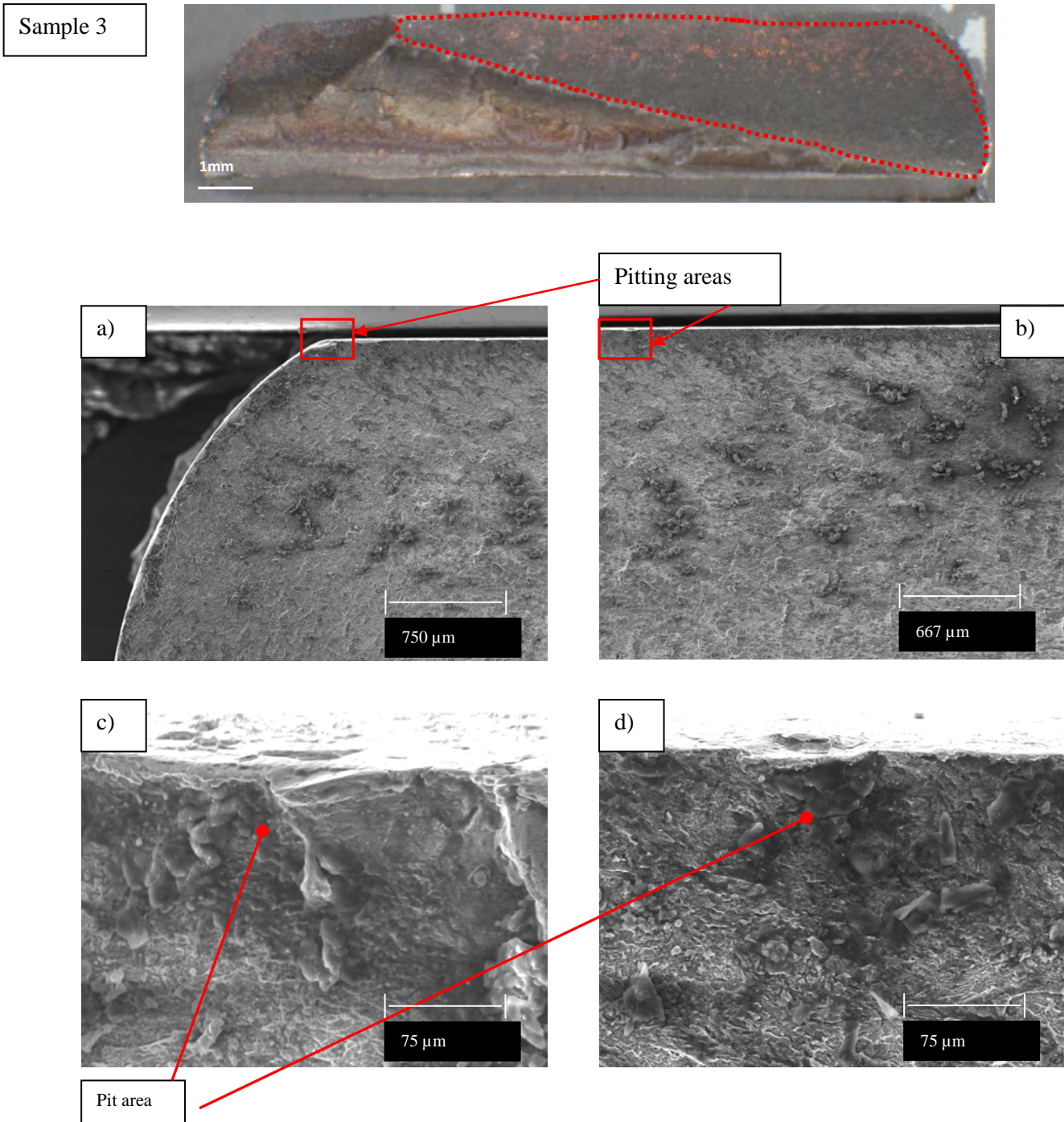


Figure 7-28 – SEM fractographs showing pitted areas along the tensile surface of the sample. Such corrosion features will act as corrosion fatigue initiation sites. (Wire-1) Low pH test sample.

7. Results and Discussion (Fatigue Testing)

7.2.2.2 Synthetic Seawater/1bar CO₂ – Wire-2

Tables 7-7 and 7-8 outline the test results for this test series along with other data from this phase of testing. This test phase was conducted at a constant r-ratio of 0.1 so that the loading is consistent with the lab air fatigue test series on this wire (Wire-2). This phase of testing provides an investigation into the effect of a corrosive environment on fatigue life compared to the baseline lab air data.

Table 7-7 Test results from the CO₂ test series on Wire-2.

Sample ID	Targeted stress range (MPa)	Targeted peak stress (MPa)	R ratio	Calculated stress range (MPa)	Cycles to rupture	Comments
CO ₂ - 1	880	977.78	0.1	838	65,019	Valid rupture within constant stress area.
CO ₂ - 2				849	75,431	Valid rupture within constant stress area.
CO ₂ - 3				865	51,348	Valid rupture within constant stress area. Possible edge initiation.
CO ₂ - 4				853	58,880	Valid rupture within constant stress area.
CO ₂ - 5	750	833.33	0.1	738	78,343	Valid rupture within constant stress area. Possible edge initiation.
CO ₂ - 6				741	99,380	Valid rupture within constant stress area.
CO ₂ - 7				747	68,019	Valid rupture within constant stress area. Possible edge initiation.
CO ₂ - 8				744	83,363	Valid rupture within constant stress area.
CO ₂ - 9	600	666.67	0.1	611	112,604	Valid rupture within constant stress area.
CO ₂ - 10				600	136,424	Valid rupture within constant stress area.
CO ₂ - 11				589	129,911	Valid rupture within constant stress area.
CO ₂ - 12				573	160,315	Valid rupture within constant stress area.
CO ₂ - 13	400	444.44	0.1	386	403,584	Valid rupture within constant stress area. Possible edge initiation.
CO ₂ - 14				378	434,596	Valid rupture within constant stress area. Possible edge initiation.
CO ₂ - 15				397	355,907	Valid rupture within constant stress area. Possible edge initiation.
CO ₂ - 16				410	358,982	Valid rupture within constant stress area.
CO ₂ - 17	250	277.78	0.1	262	1,185,995	Valid rupture within constant stress area. Possible edge initiation.
CO ₂ - 18				232	2,193,698	Valid rupture within constant stress area. Possible edge initiation.
CO ₂ - 19				244	2,010,360	Valid rupture within constant stress area. Possible edge initiation.
CO ₂ - 20				244	2,156,539	Valid rupture within constant stress area.

7. Results and Discussion (Fatigue Testing)

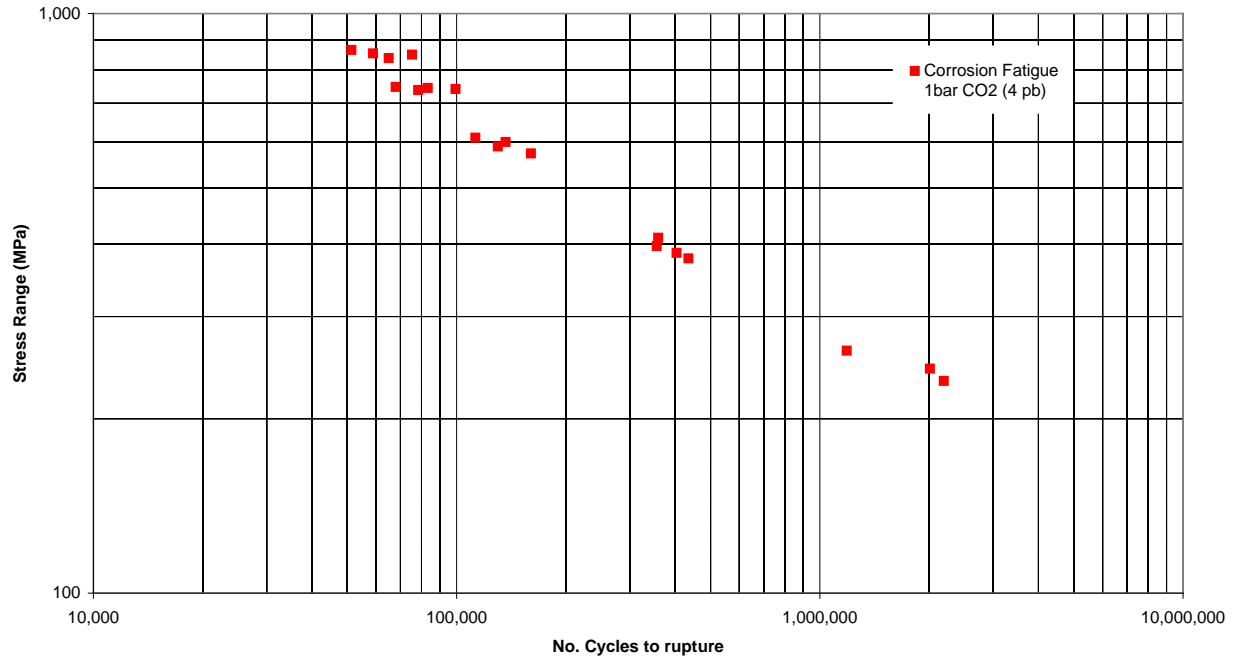
Table 7-8 - Test results from the CO₂ test series on Wire-2. pH measurements from this test series

Sample ID	Calculated stress range (MPa)	Cycles to rupture	pH measurements						
			start	day2	day3	day4	day5	week2	end of test
CO ₂ - 1	838	65,019	5.14	5.08	N/A	N/A	N/A	N/A	5.08
CO ₂ - 2	849	75,431							
CO ₂ - 3	865	51,348							
CO ₂ - 4	853	58,880							
CO ₂ - 5	738	78,343	5.00	5.03	N/A	N/A	N/A	N/A	5.03
CO ₂ - 6	741	99,380							
CO ₂ - 7	747	68,019							
CO ₂ - 8	744	83,363							
CO ₂ - 9	611	112,604	5.02	5.00	N/A	N/A	N/A	N/A	5.00
CO ₂ - 10	600	136,424							
CO ₂ - 11	589	129,911							
CO ₂ - 12	573	160,315							
CO ₂ - 13	386	403,584	4.99	5.00	5.00	N/A	N/A	N/A	5.01
CO ₂ - 14	378	434,596							
CO ₂ - 15	397	355,907							
CO ₂ - 16	410	358,982							
CO ₂ - 17	262	1,185,995	4.95	4.95	4.94	N/A	N/A	5.03	5.09
CO ₂ - 18	232	2,193,698							
CO ₂ - 19	244	2,010,360							
CO ₂ - 20	244	2,156,539							

Figure 7-29 displays these results in the form of SN plots. The graphs in this figure plot only the results from CO₂ test series on Wire-2 whilst figure 7-30 superimposes the results of the lab air fatigue test series for wire 2.

7. Results and Discussion (Fatigue Testing)

Corrosion Fatigue on 9 x 3 mm wire 2 - 1bar CO₂/Synthetic seawater (unconfined)



Corrosion Fatigue on 9 x 3 mm wire 2 - 1 bar CO₂ and synthetic seawater (unconfined)

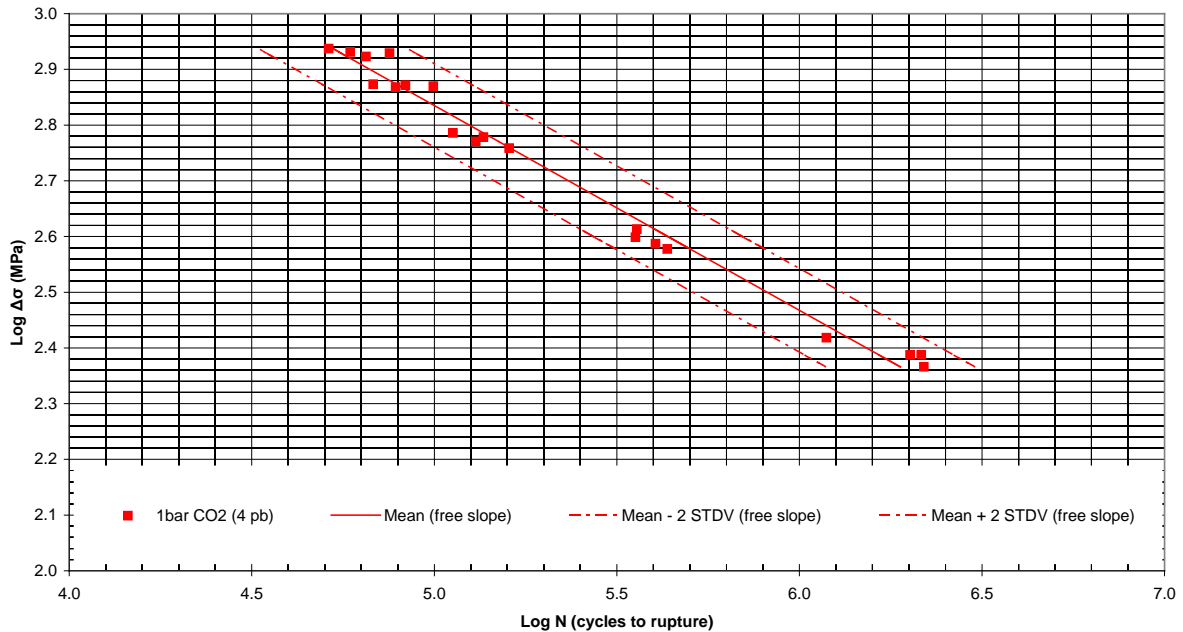


Figure 7-29 Test results from the CO₂ test series on Wire-2. SN plots displaying the CO₂ test series data. Top plot shows stress range against cycles to failure whilst the bottom plot is a log-log graph showing the mean curve +/- 2 SD. Note the absence of an endurance limit.

7. Results and Discussion (Fatigue Testing)

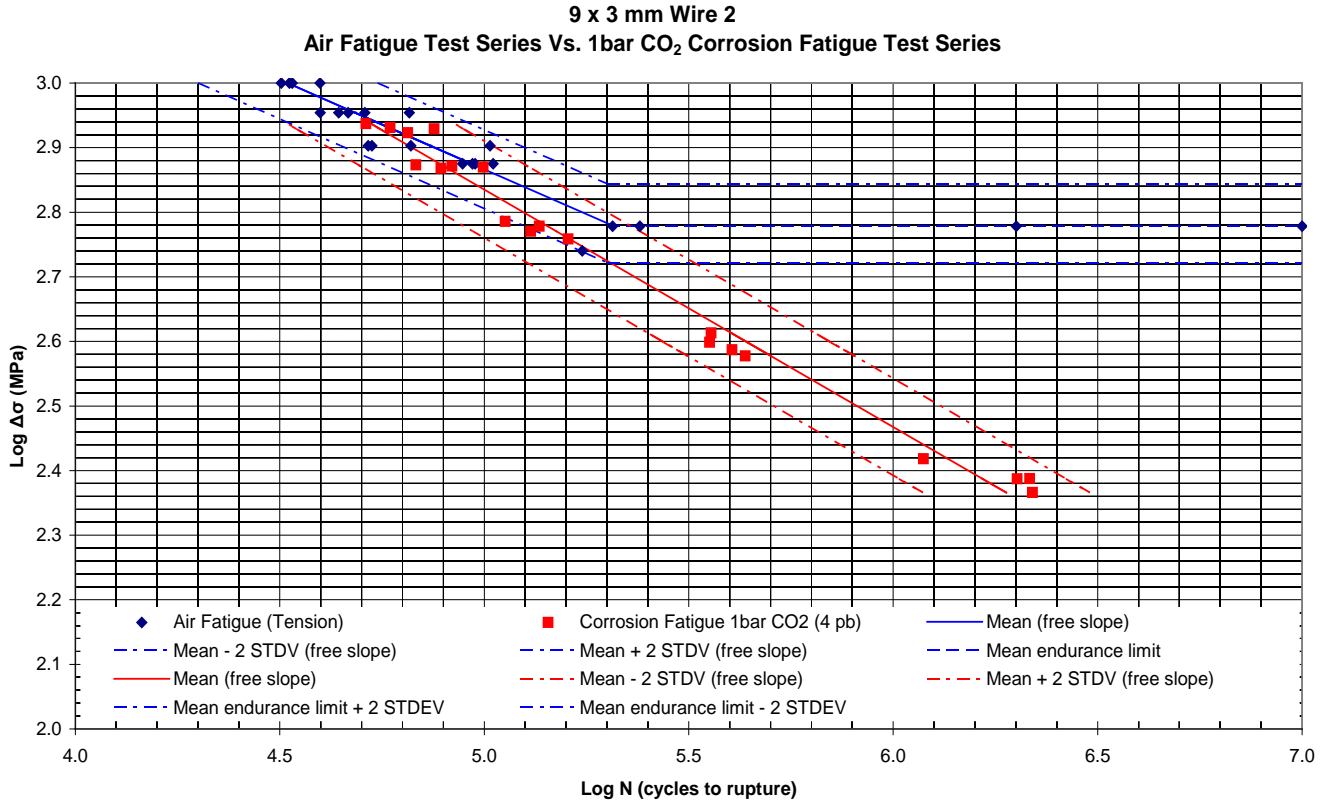


Figure 7-30 – SN plot showing the test results from the lab air fatigue and CO₂ test series on Wire-2. This plot shows clearly the effect of a corrosive environment from the CO₂ test series data. Note the presence of failures in the CO₂ test series at stress levels well below the in air endurance limit.

This comparison of SN curves clearly demonstrates the effect of testing in a corrosive environment on fatigue life, as compared to data generated in air. It can be observed that in the CO₂ test series there are failures at stress levels well below the lab air endurance limit which can be attributed to the action of the corrosive environment, this is consistent with the findings of the CO₂ test series on Wire-1 and with information in the literature [7]. It can also be observed from Figure 7-30 that there doesn't appear to be a reduction of fatigue life due to the corrosive environment in the finite life region with Wire-2 as was observed with Wire-1. As discussed in Section 7.2.1.1 the test configuration has an

7. Results and Discussion (Fatigue Testing)

effect of the fatigue results and for this reason it is good practice to compare like with like. This section compares lab air fatigue data generated in tension (Section 7.2.1.2) with corrosion fatigue data generated in four-point bend which explains the difference in the effect on fatigue life in the finite region between Wire-1 and Wire-2. Since the lab air fatigue data on Wire-2 (axial tension) can be regarded as conservative (based on Section 7.2.1.1) then a similar effect could be expected if the air fatigue data on Wire-2 was generated in four-point bend. The endurance limit that could be expected in four-point bend could also be higher than for that in tension based on the results of Wire-1 (Section 7.2.1.1)

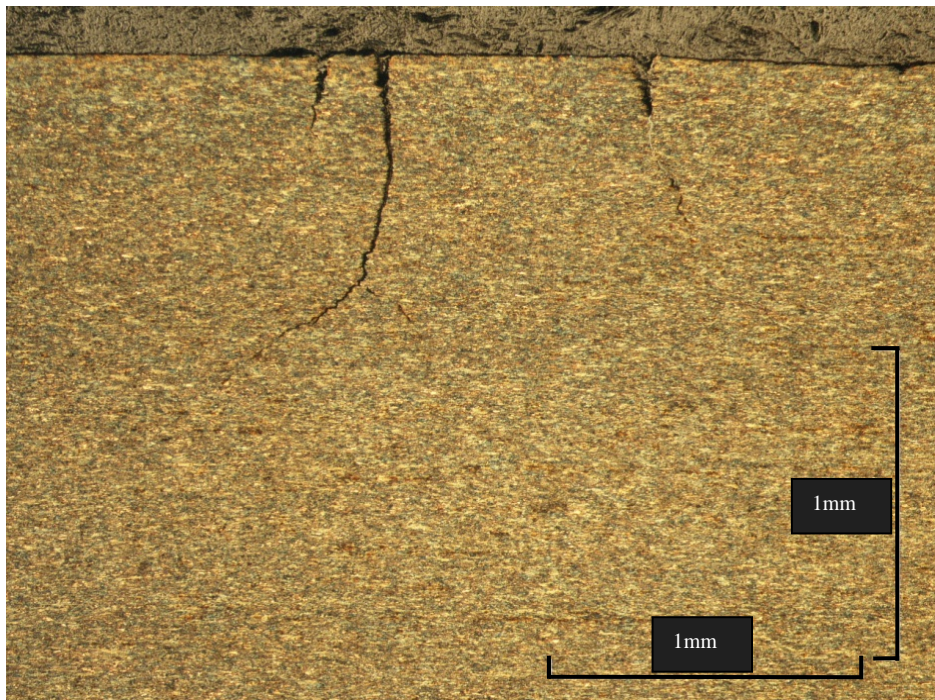
Post test investigation of a selection of samples from the 1bar CO₂ test series reveals the cause of the observed reduction in fatigue life and elimination of an endurance limit when testing is performed under simulated corrosive oilfield conditions. Figure 7-31 shows the tensile surface of a tested sample in the area of constant stress between the two centre rollers. There is clear evidence on the sample surface of secondary and hairline cracking over this area of the sample where it has seen maximum tensile strains. These phenomenon are not seen in samples tested in lab air so these features must be related to the exposure to an aggressive environment and therefore corrosion related.



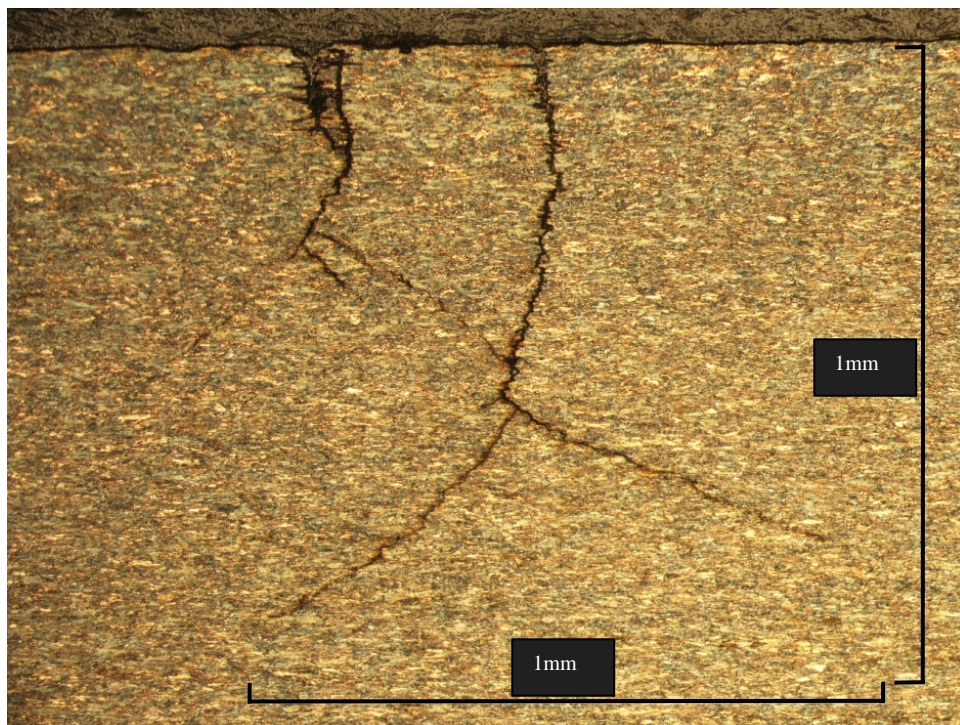
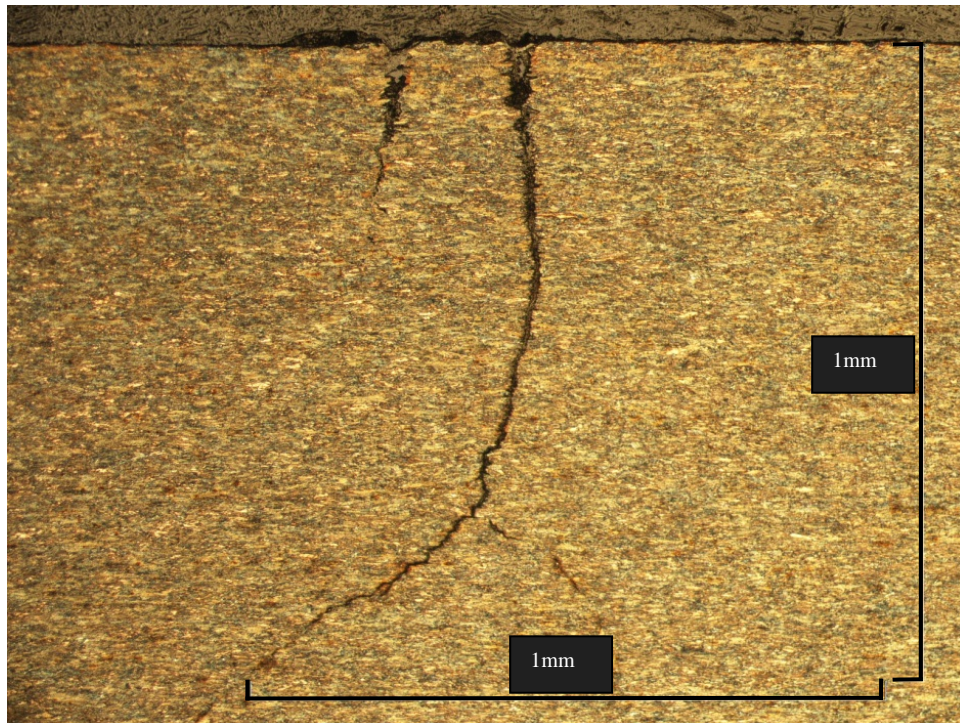
Figure 7-31 – Sample CO₂ – 6 – Rupture from tensile face, show secondary and hairline cracks on the surface.

7. Results and Discussion (Fatigue Testing)

To investigate further the source of these surface cracks and the reason for the effect of the environment on fatigue life the sample in Figure 7-31 was longitudinally sectioned through the constant stress area where the surface corrosion related features are located. The following images in Figure 7-32 show this sample after polishing and etching had revealed the surface corrosion features and subsequent cracking in more detail. It is clear from these images that the reduction in fatigue life and elimination of an endurance limit is caused by corrosion related surface damage. The formation of small pits on the surface of the sample lead to further cracking emanating from the base of such phenomenon as they act as a local stress raiser This is consistent with the findings on Wire-1 (Section 7.2.2.1)



7. Results and Discussion (Fatigue Testing)



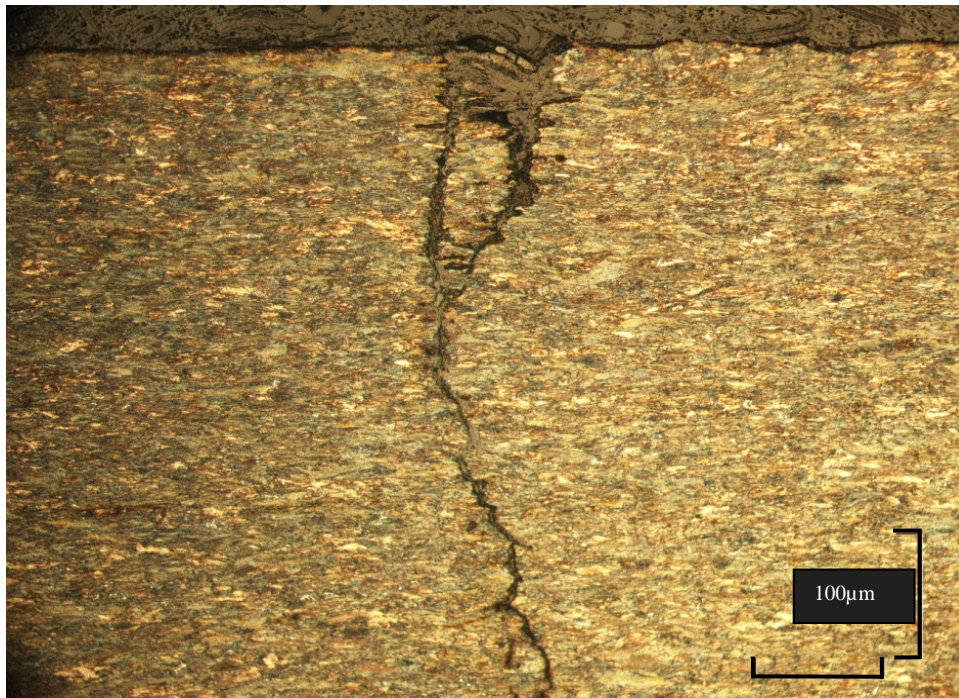
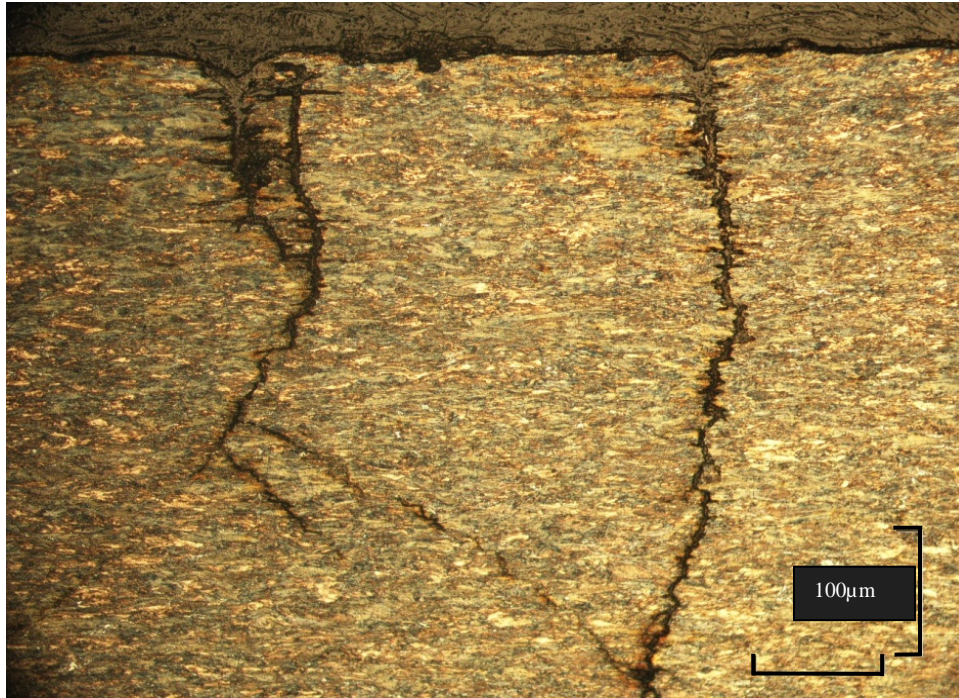


Figure 7-32 – Longitudinal section through the constant stress region of a tested sample. Evidence of secondary and hairline cracking associated with some metal dissolution at the surface. (2% nital etch). Selection of magnifications.

7. Results and Discussion (Fatigue Testing)

Figures 7-33 to 35 show the tensile face (subjected to tensile strains during testing) of a selection of samples in this test series from which the rupture was initiated. The fracture faces are also shown for each sample. SEM investigation on samples from this test series was not permitted since test samples were requested to be returned to the client post test.

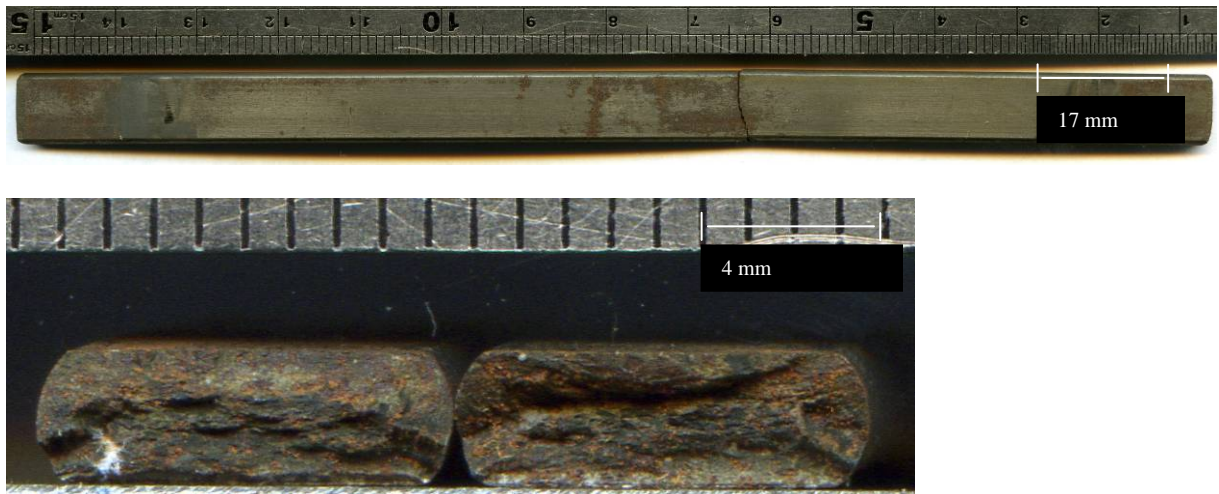


Figure 7-33 – Sample CO₂ – 1 – Rupture from tensile face, and fracture surfaces

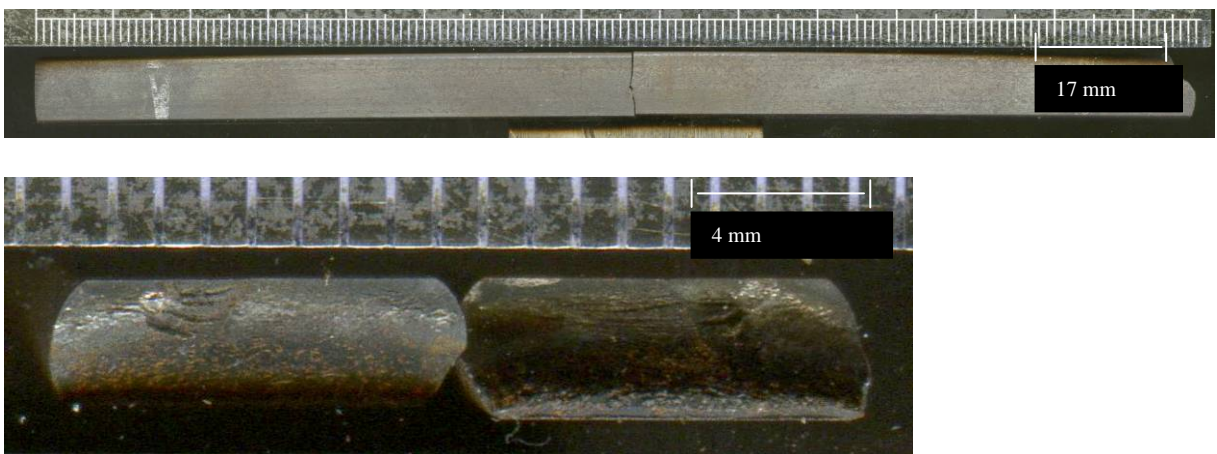


Figure 7-34 – Sample CO₂ – 13 – Rupture from tensile face, and fracture surfaces

7. Results and Discussion (Fatigue Testing)

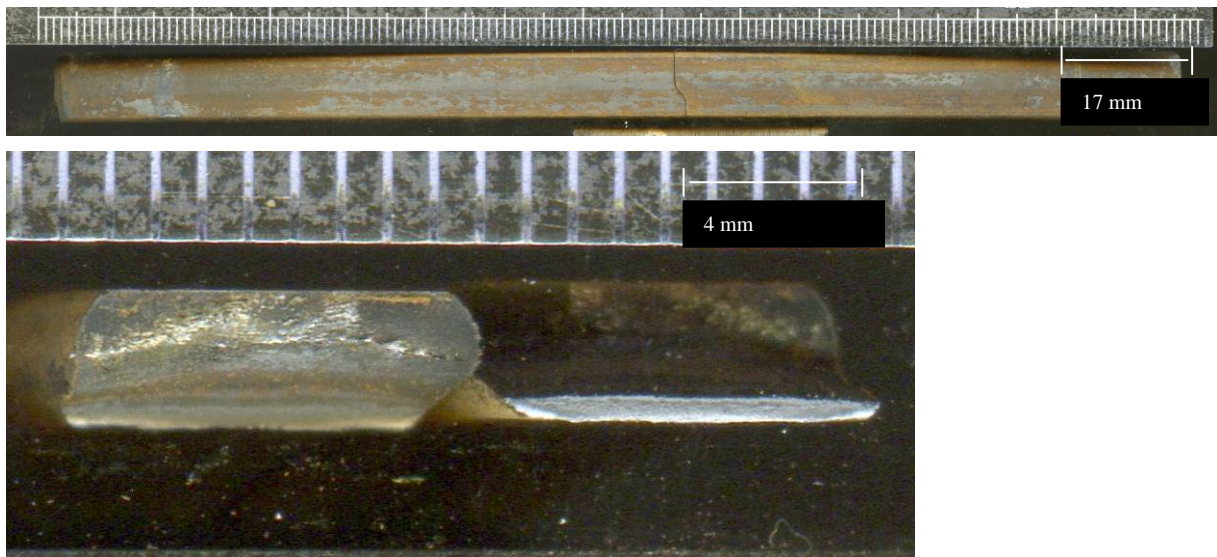


Figure 7-35 – Sample CO₂ – 18 – Rupture from tensile face, and fracture surfaces

7. Results and Discussion (Fatigue Testing)

7.2.2.3 Effect of Confinement (Wire 1)

The testing protocol for the confinement investigation test series is outlined in Section 4.3.1. This test series uses the same results for Wire-1 generated under 1bar CO₂ in Section 7.2.2.1 for comparison with the lab air fatigue test series data. In this section results are presented as an investigation into confined conditions i.e. higher test pH and iron saturated test solution compared to the unconfined test condition with a lower pH and no addition of steel wool. Results for the confinement investigation test series are shown in Tables 7-9 and 7-10.

Table 7-9 – Test results from the different test environments simulated in the confinement investigation test series.

Sample ID	Steel Grade	Size (mm ²)	Curve	Approximate Start pH	Calculated Stress Range (MPa)	Cycles to Rupture	Comments
low pH 1	Wire 1	15x3 machined	Unconfined	5.0-5.2	610	163490	Valid within constant stress area
2					585	219143	Valid within constant stress area
3					581	222118	Valid within constant stress area
4					657	137880	Valid within constant stress area
5					520	318140	Valid within constant stress area
6					515	617897	Valid within constant stress area
7					498	480791	Valid within constant stress area
8					501	585415	Valid within constant stress area
9					415	2006719	Valid within constant stress area
10					419	1944897	Valid within constant stress area
11					436	1927129	Valid within constant stress area
12					440	439395	Valid within constant stress area
high pH 1	Wire 1	15x3 machined	Confined (addition of steel wool)	5.8	603	277156	Valid within constant stress area
2					607	188580	Valid within constant stress area
3					609	207229	Valid within constant stress area
4					599	212308	Valid within constant stress area
5					498	747941	Valid within constant stress area
6					487	524106	Valid within constant stress area
7					497	691006	Valid within constant stress area
8					482	660299	Valid within constant stress area
9					398	2101245	Valid within constant stress area
10					420	1834987	Valid within constant stress area
11					400	2445678	Valid within constant stress area
12					395	2537895	Valid within constant stress area
4day 1	Wire 1	15x3 machined	Confined (addition of steel wool) + 4 day pre exposure	5.8	605	238327	Valid within constant stress area
2					602	248432	Valid within constant stress area
3					598	249336	Valid within constant stress area
4					602	236739	Valid within constant stress area

7. Results and Discussion (Fatigue Testing)

Table 7-10 – Test results from the different test environments simulated in the confinement investigation test series – pH measurements from the beginning and end of each set of four samples.

Sample ID	Calculated stress range (MPa)	Cycles to rupture	pH measurements	
			start	end of test
High pH 1	610	163490	5.88	6.03
2	585	219143		
3	581	222118		
4	657	137880		
5	520	318140	5.81	6.10
6	515	617897		
7	498	480791		
8	501	585415		
9	415	2006719	5.90	6.28
1	419	1944897		
11	436	1927129		
12	440	439395		
Low pH 1	603	277156	4.99	5.04
2	607	188580		
3	609	207229		
4	599	212308		
5	498	747941	5.02	5.09
6	487	524106		
7	497	691006		
8	482	660299		
9	398	2101245	5.05	5.16
10	420	1834987		
11	400	2445678		
12	395	2537895		
4 day 1	605	238327	5.89	6.05
2	602	248432		
3	598	249336		
4	602	236739		

In this phase of testing the environment is deaerated seawater saturated with 1bara CO₂. However, the solution chemistry has been manipulated slightly in order to investigate the effect of the confined conditions within the annulus of a flexible pipe as discussed in Chapter 3.

One set of data has been generated in unconfined (low pH) conditions, these data points refer to the lower start pH of the test solution at the start of the test. The other data set has been generated under confined conditions where the test solution has a higher start pH as a result of supersaturation with Fe²⁺ following the corrosion of steel wool into the environment [4,5,6]. Figure 7-36 (bottom) shows the corrosion fatigue data again, this time with mean life points included at each stress level. The first thing to note is that under confined conditions the mean life shows a modest shift to the right on the graph possibly as a combination of higher solution pH and precipitation of iron carbonate serve to create a less severe testing environment. Indeed, from the literature it is clear that under the specific confined conditions of the high pH test (confined) iron carbonate precipitation can take place [4, 5, 6, 72] and evidence of an adherent corrosion product is shown in Figure 7-37 which is present under confined conditions but absent when there is no confinement.

7. Results and Discussion (Fatigue Testing)

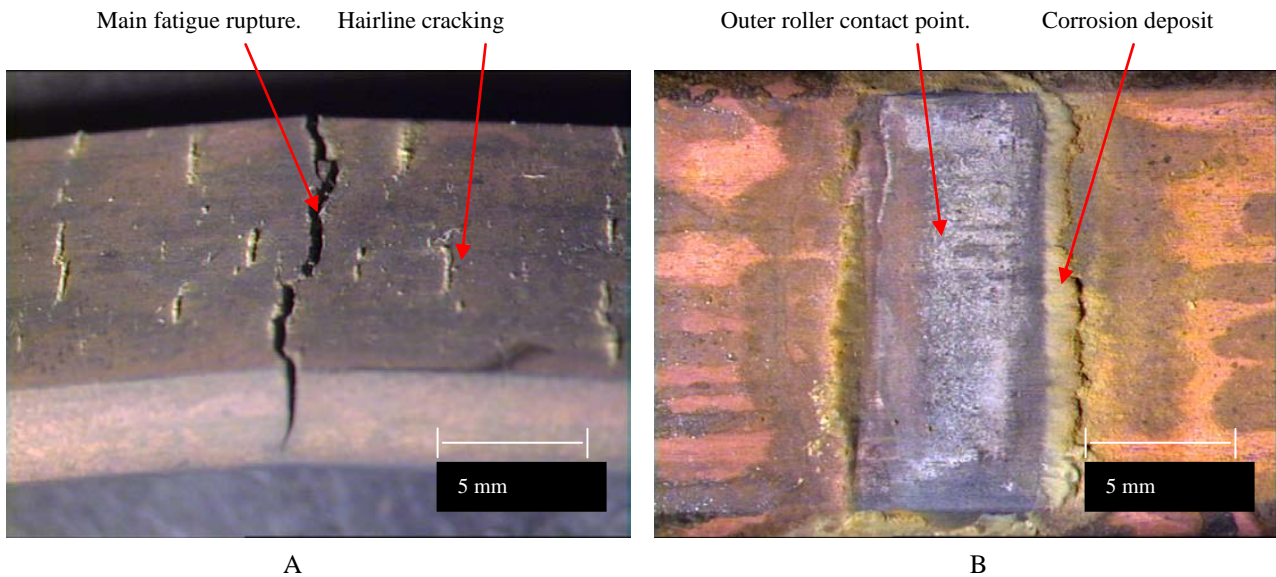


Fig.7-37 – Images of the iron carbonate corrosion product formed on a test sample under confined conditions a) product formed in surface cracks, b) product formed around the roller location. Sample 11 from the confined test condition (high pH)

Interestingly the increase in mean life in the confined condition as a percentage of fatigue life in unconfined conditions is least at the lowest stress range tested. It may be expected that the effect would be largest at lower stress levels since with a longer test duration the environment will play more of a role in dictating fatigue life, however the present set of results have not shown this.

The following figures show a selection of features from ruptured test samples and fracture surfaces from the confinement investigation test series where post test sample investigations have been carried out. In the majority of samples, cracking initiated from the corner of the wire, an example of which can be seen in Figure 7-38 indicating that keeping the as-received surface and radius on the edge of the tensile surface of the wire is essential.

7. Results and Discussion (Fatigue Testing)

However, in some of the test samples it could be observed that the fatigue crack initiated from the centre of the tensile face of the wire (Figure 7-39). This type of initiation point is a much less common observation from the testing in the current research project. This fracture initiation location phenomenon was present in both the confined and unconfined tests.

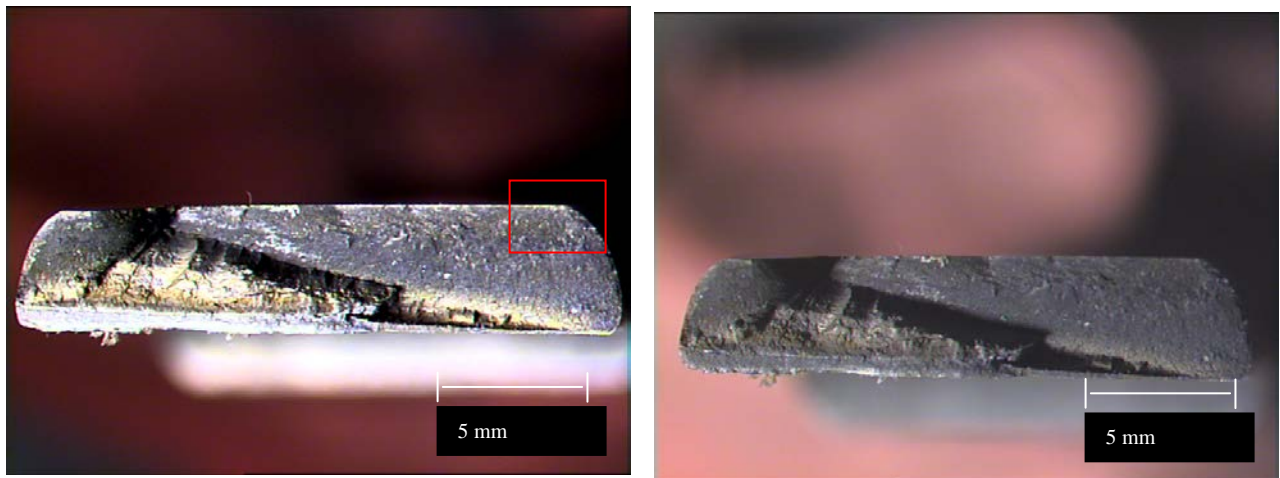


Figure 7-38 – Sample 3 from the unconfined test conditions. Example of fatigue initiation from the corner of the armour wire material.

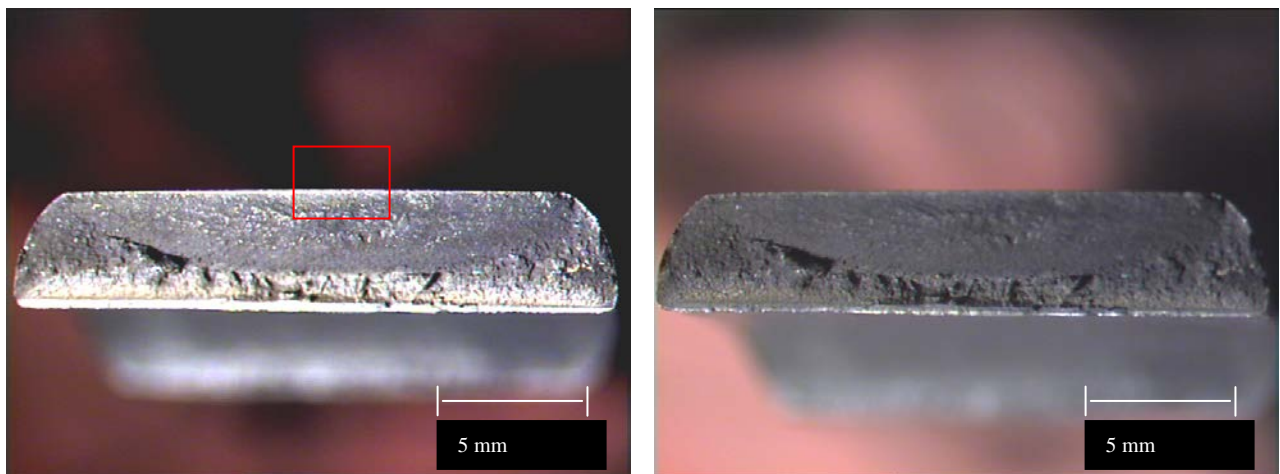


Figure 7-39 – Sample 2 from the unconfined test conditions. Example of fatigue initiation from the centre of the armour wire material. This initiation point is less common.

7. Results and Discussion (Fatigue Testing)

Figure 7-40 and 7-41 show the SEM investigations from a sample in both the confined and unconfined test conditions.

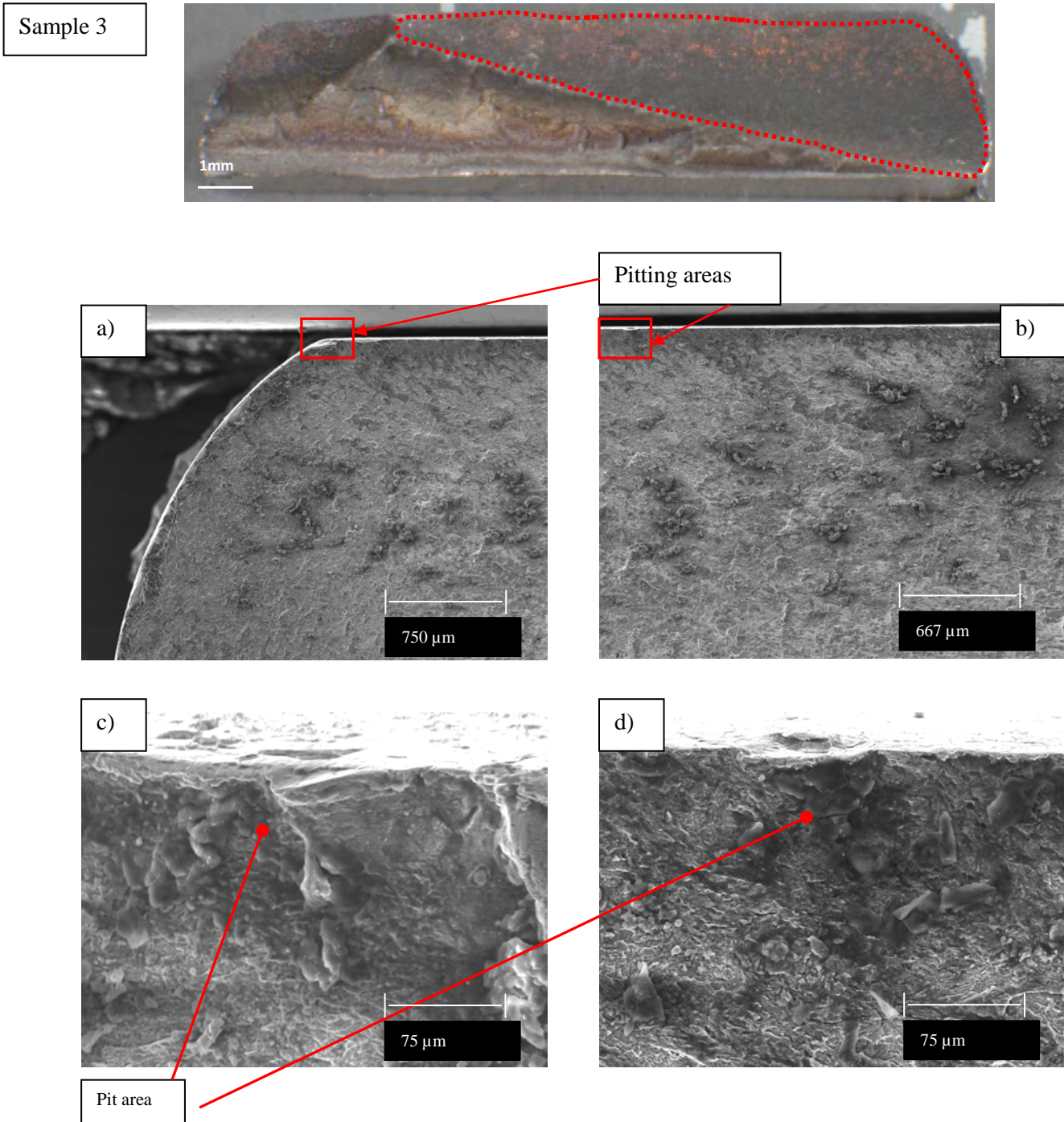


Figure 7-40 – SEM fractographs showing pitted areas along the tensile surface of the sample. Such corrosion features will act as corrosion fatigue initiation sites. (Wire-1) Low pH test sample (unconfined).

7. Results and Discussion (Fatigue Testing)

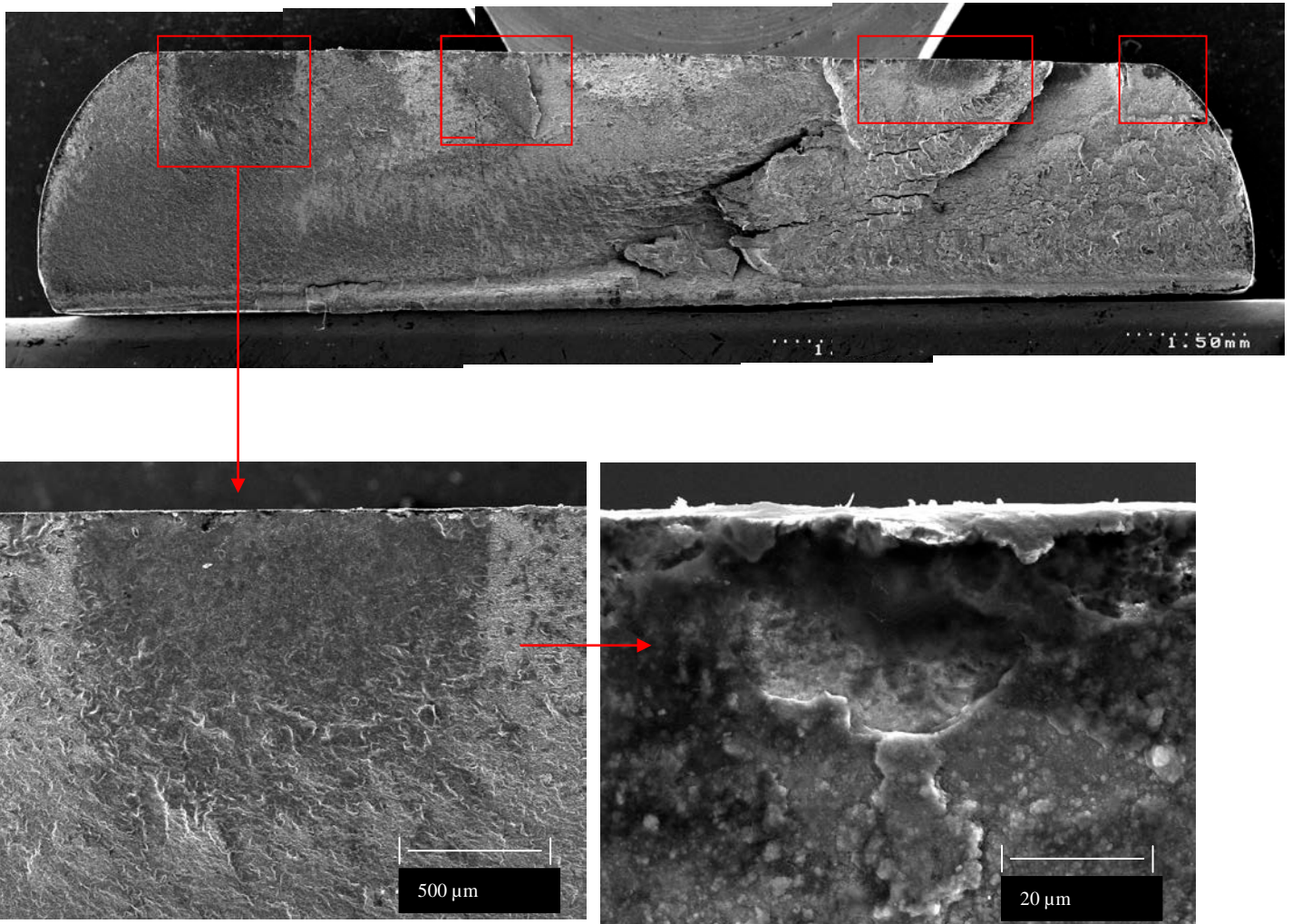


Figure 7-41 – SEM fractographs showing multiple initiation sites along the tensile surface of the sample. Higher magnification images of the initiation site on the left hand side of the fracture face. (Wire11) High pH test sample (confined).

The fracture faces were similar between test conditions with both showing the same initiation points and often multiple initiation sites were observed. SEM of the tensile face (flat rolled surface) of the samples did however reveal a difference between test conditions (Figure 7-42 and 7-43). The extent of corrosion to the tensile surface appears to be less in the high pH condition (Figure 7-42).

7. Results and Discussion (Fatigue Testing)

Images of the low pH test surface are shown in Figure 7-43 where it can be seen that the more severe environmental conditions have resulted in more significant surface damage.

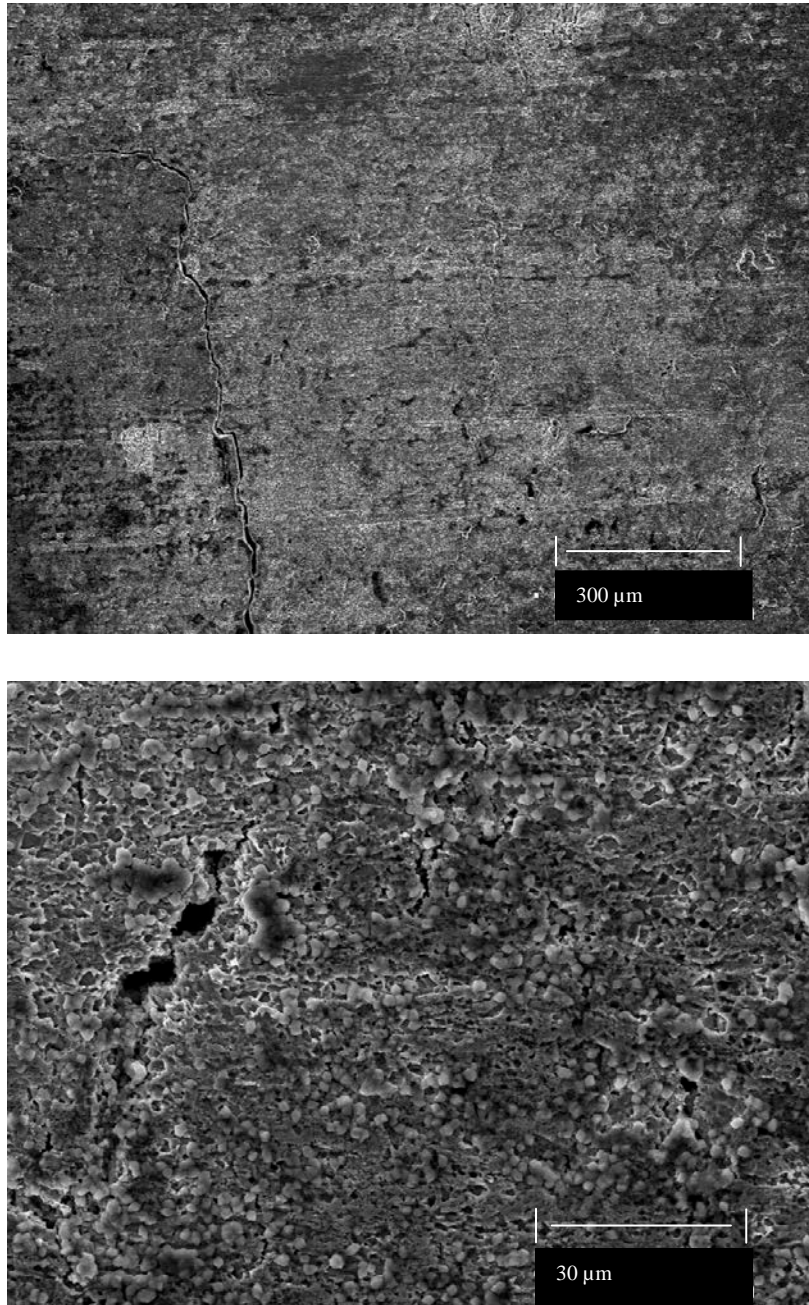


Figure 7-42 – SEM micrographs showing surface corrosion on the the tensile surface of the sample. Wire-1 Confined conditions (High pH). Corrosion damage is less severe than that observed in the low pH test condition (Fig 7-43).

7. Results and Discussion (Fatigue Testing)

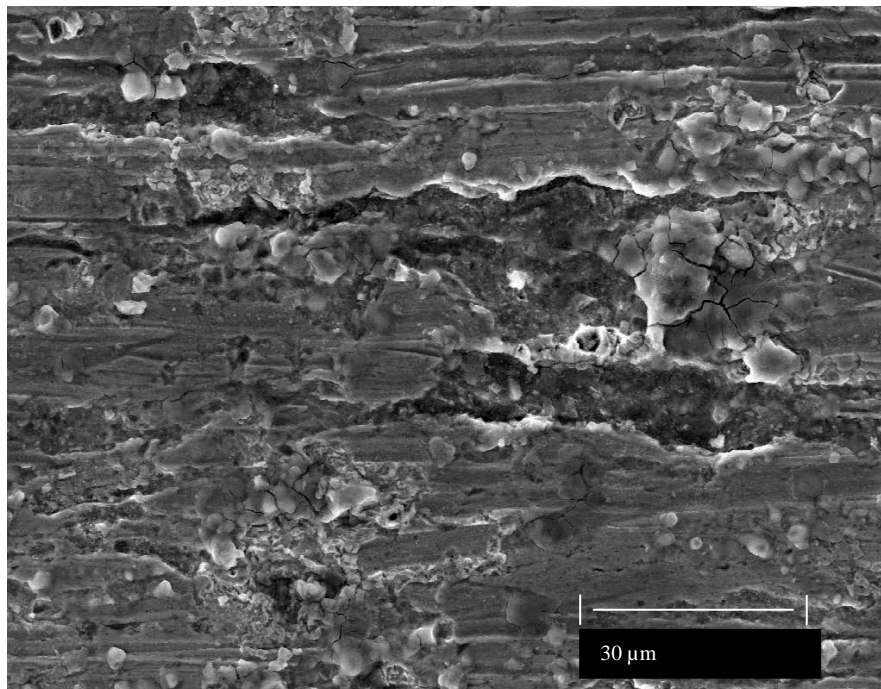
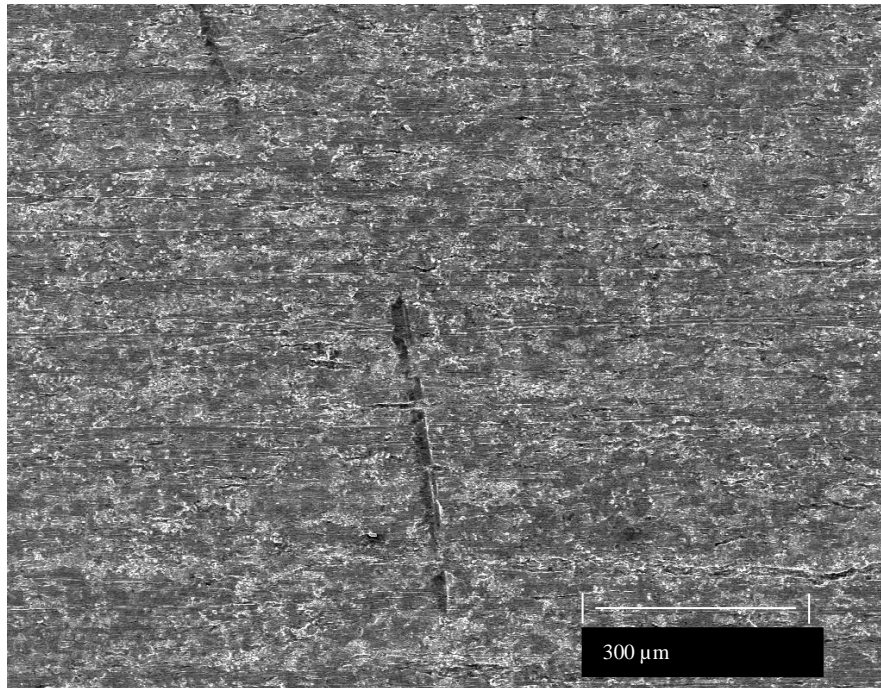


Figure 7-43 – SEM micrographs showing surface corrosion on the the tensile surface of the sample. Wire-1 Unconfined conditions (Low pH). Corrosion damage is more significant than that observed in the high pH (confined) test condtion (Fig 7-42).

7. Results and Discussion (Fatigue Testing)

Evidence of the combination of corrosion and maximum tensile strains can also be found on the tensile surface over a 40mm section corresponding to the constant stress region between the two centre rollers on some of the ruptured samples (Figure 7-44 and 7-45).

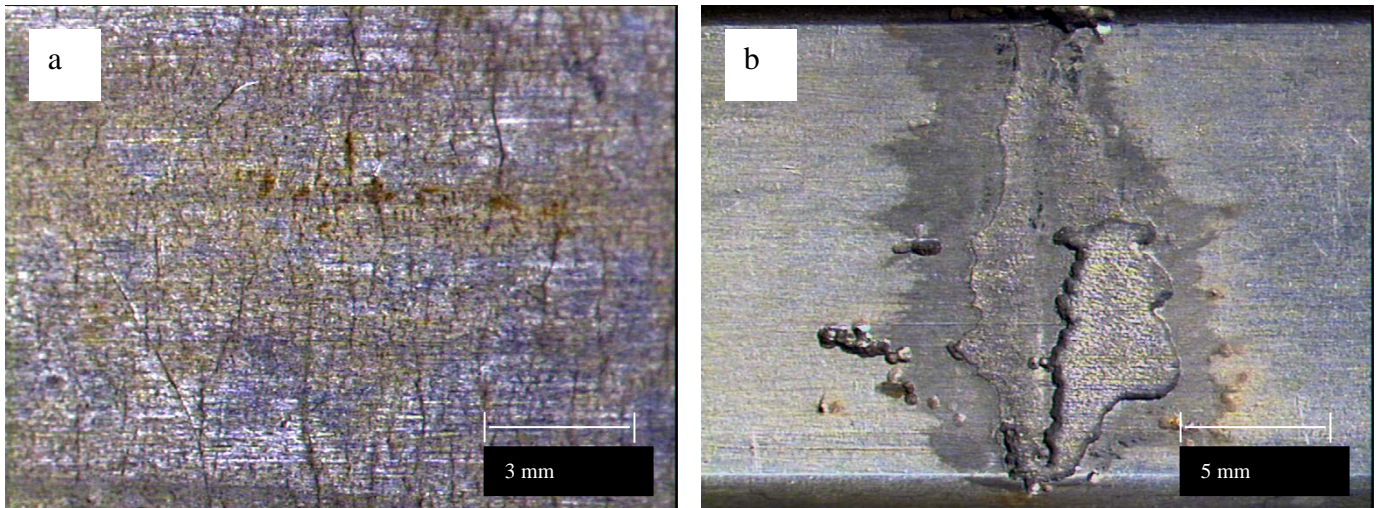


Figure 7-44 – Sample from the unconfined (low pH) test conditions. A) Showing evidence of the effect of maximum tensile strains causing secondary and hairline cracking in the constant stress region of the sample b) increased severity of corrosion in unconfined (low pH) test condition, shows crevice corrosion around the roller location.

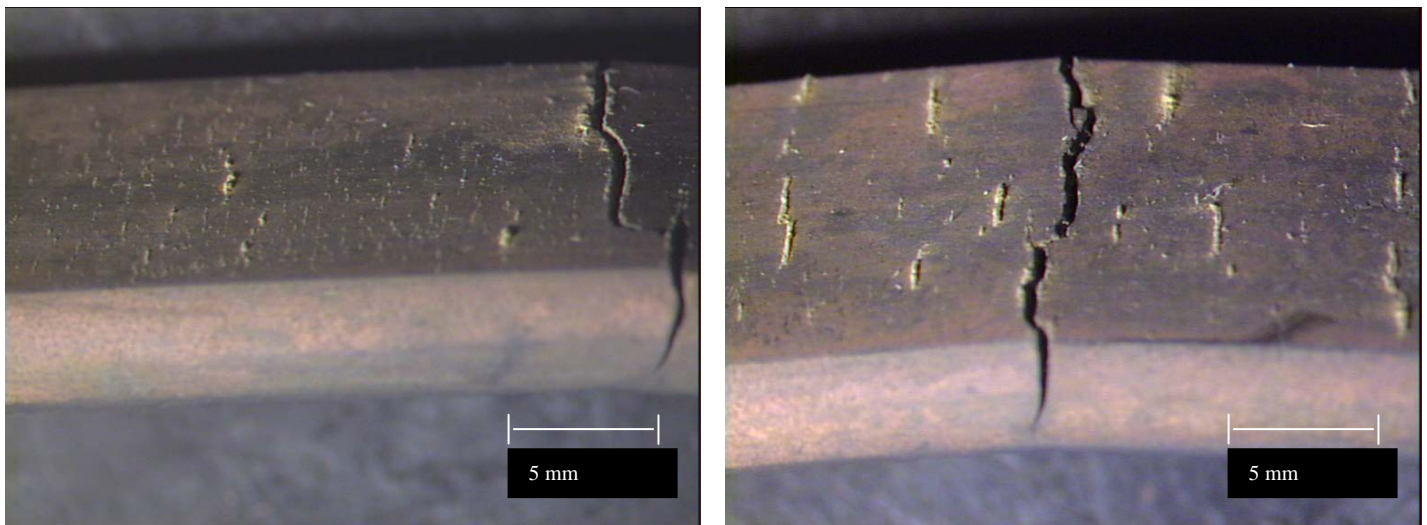


Figure 7-45 – Samples from the confined (high pH) test conditions. Showing evidence of the effect of maximum tensile strains causing secondary and hairline cracking in the constant stress region of the sample.

7. Results and Discussion (Fatigue Testing)

It can be seen from Figures 7-44 and 7-45 that the severity of corrosion damage is increased when tested under unconfined conditions where the solution pH is lower and there is no saturation with iron ions. This finding is in agreement with information on corrosion rates under such conditions within the literature [4,5,6].

To investigate this surface damage in more detail and investigate the reason for the effect of confinement on fatigue life the samples shown above for both confined and unconfined conditions were longitudinally sectioned through the constant stress area where the surface corrosion related features are located. The following Figures (7-46 & 7-47) show these samples after polishing and etching had revealed the surface corrosion features and subsequent cracking in more detail.

It is clear from these micrographs that the surface corrosion damage seen in unconfined test environments is more severe than that seen under the confined conditions of higher pH and iron ion saturation. The pits observed in the unconfined test condition are larger than that seen with confinement and this results in a greater tendency for such pits to form cracks due to the formation of a larger local stress concentration. As such, the cracks emanating from surface corrosion damage are larger in the unconfined sample which would explain the reduced fatigue life seen in this test condition.

7. Results and Discussion (Fatigue Testing)

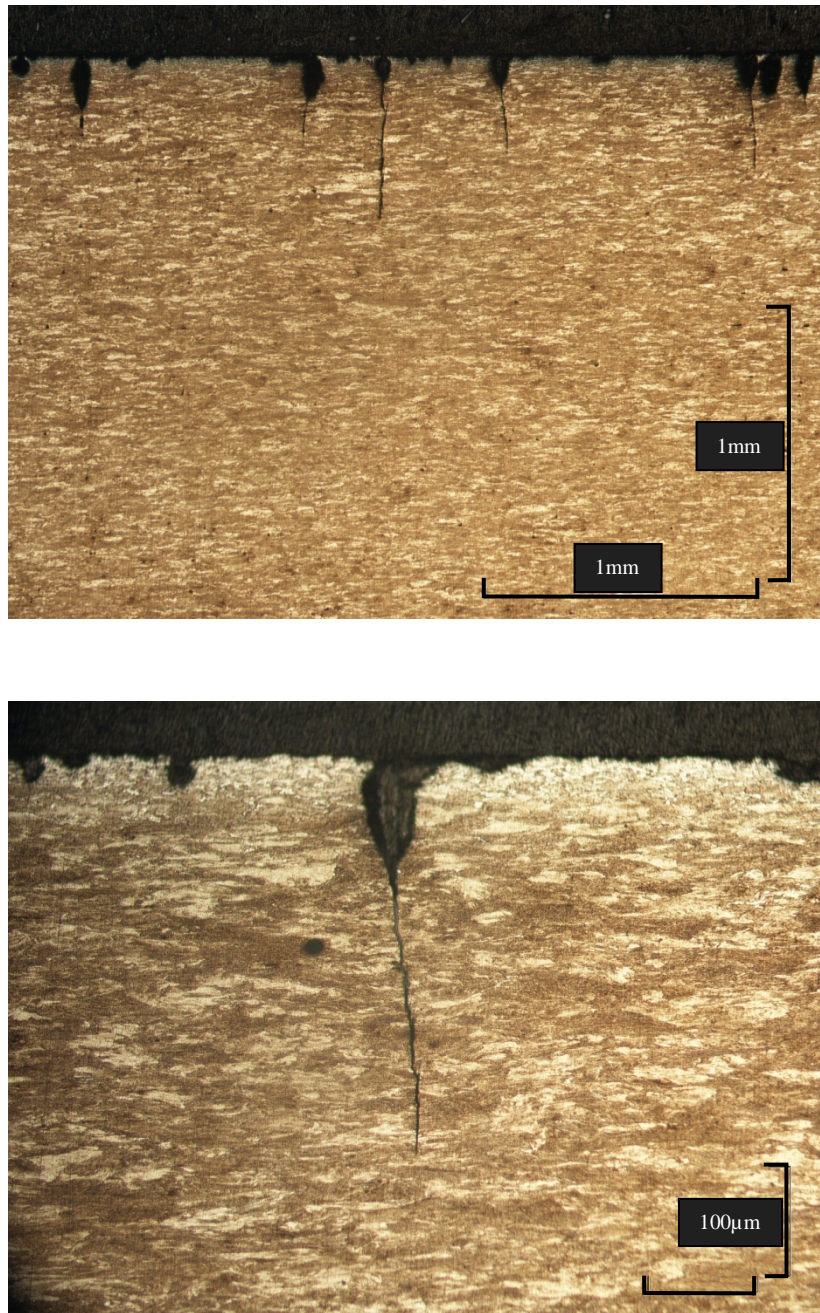


Figure 7-46– Sample from the unconfined (low pH) test conditions. Longitudinal section through the constant stress area of the sample shown in Fig 7-44a. Surface pitting leading to subsequent cracking.

7. Results and Discussion (Fatigue Testing)

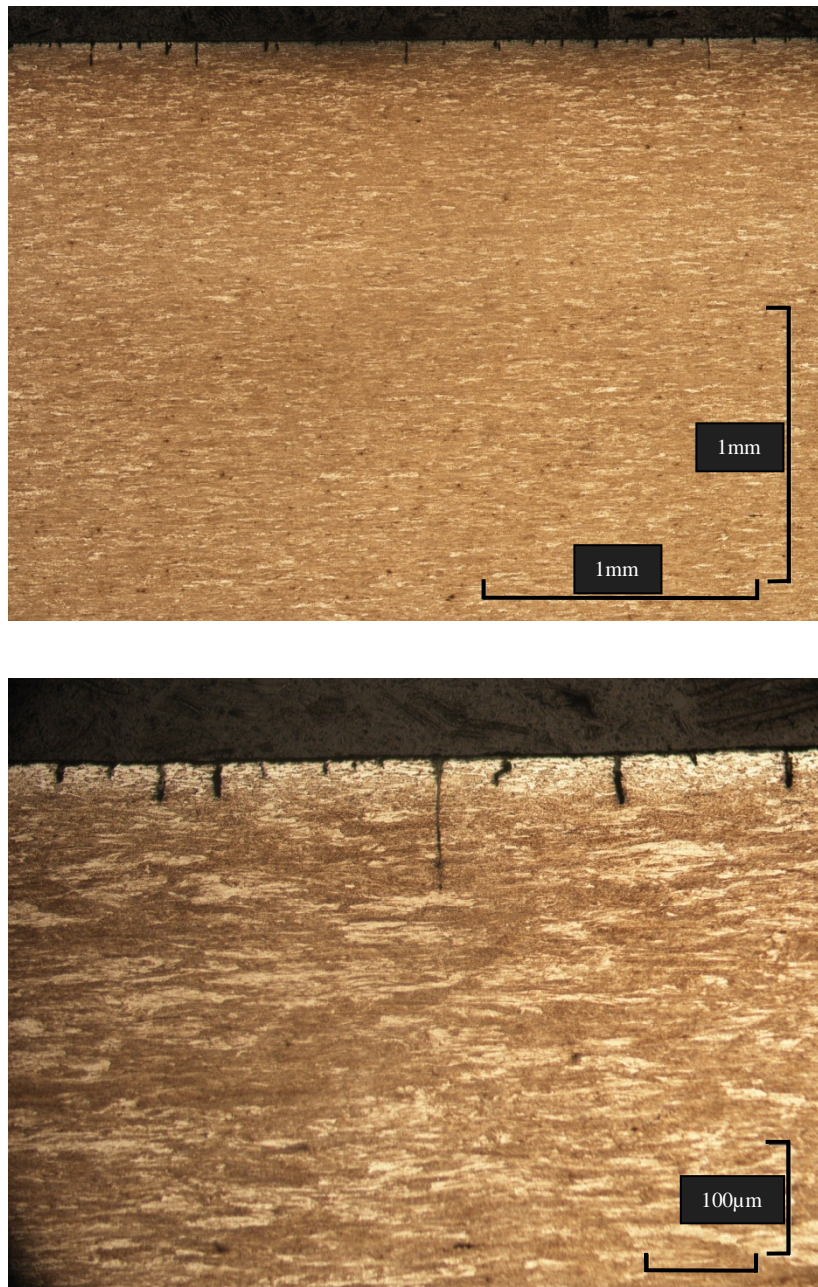


Figure 7-47– Sample from the confined (high pH) test conditions. Longitudinal section through the constant stress area of the sample shown in Fig 7-45a. Significantly smaller surface corrosion phenomenon than in the confined (low pH) test condition.

7. Results and Discussion (Fatigue Testing)

The depth of these observed pits were measured over a 10mm section within the constant stress area on a sample from each test condition. It was also noted the number of subsequent cracks formed from within each range of pit size. From Figure 7-48 it is clear to see that under unconfined (low pH) conditions the frequency of deeper pits is significantly higher although the total number of pits over the measured section is similar. More of the pits observed in the low pH condition also resulted in subsequent crack formation (Figure 7-49) however none of the deepest pits measured (151-250 μm) resulted in cracking indicating that it is not only pit depth that dictates the extent of the stress concentration that is created.

Pit Depth Distribution - Confined Vs Unconfined Test Conditions

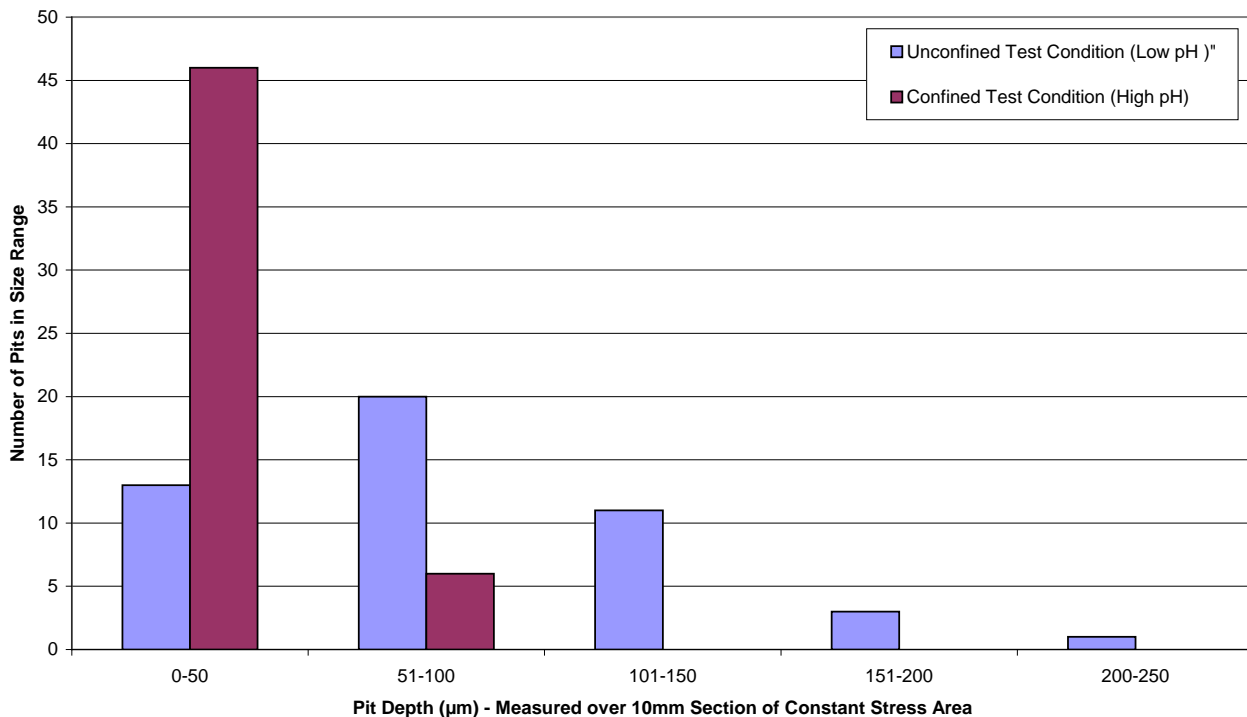


Figure 7-48– Sample of pit depths measured over a 10mm section within the constant stress area of the sample. Graph shows a higher frequency of deeper pits in the unconfined condition but the total number of pits observed is similar.

7. Results and Discussion (Fatigue Testing)

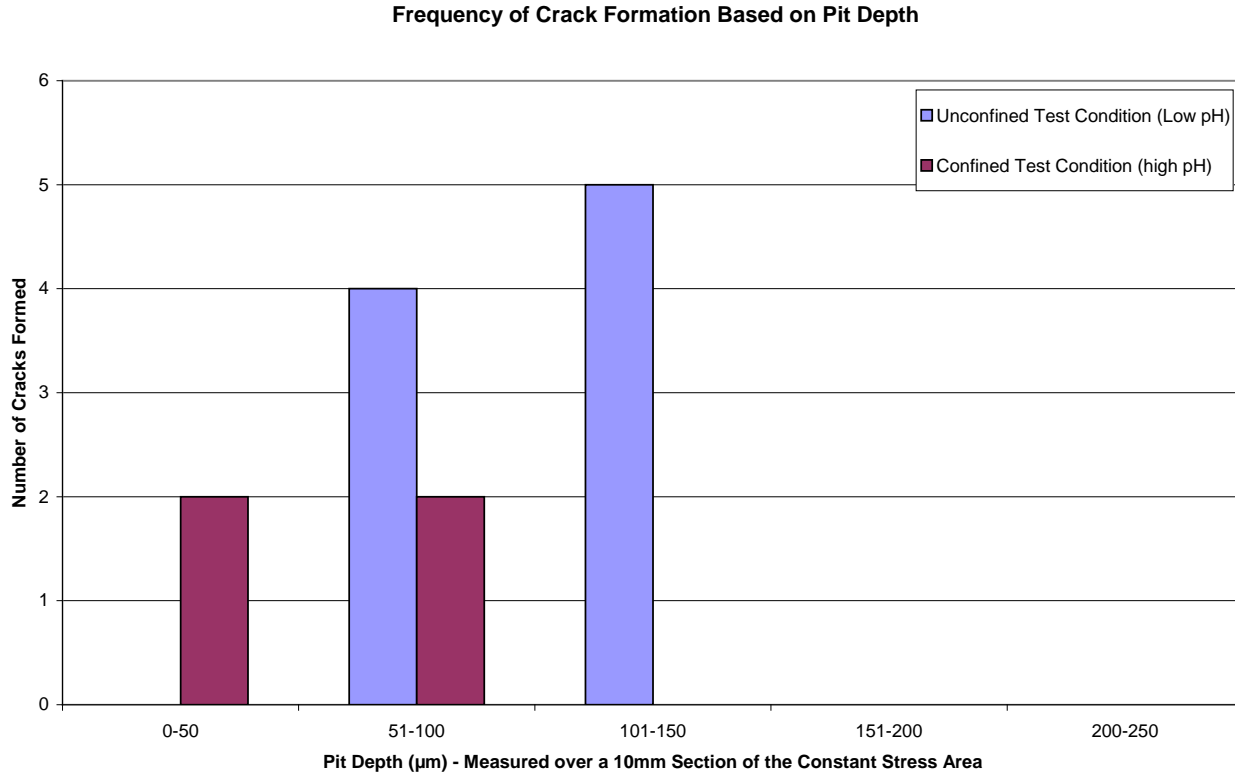


Figure 7-49– Sample of crack formation based on pit depth measured over a 10mm section within the constant stress area of the sample. Graph shows a higher frequency of crack formation in the unconfined condition with the highest percentage of pit to crack formation in the range 101-150μm (i.e., 45% of pits in this range formed cracks).

Under confined test conditions cracks were still observed forming from pits, however much less frequently and the subsequent average crack length was significantly shorter (74μm compared to 290μm under unconfined conditions).

In summary, the results from the confinement investigation test series in this thesis show that the chemistry of the simulated annulus environment can have an effect on fatigue life.

Under the more severe conditions of the low pH test (unconfined) mean fatigue life is reduced at all of the stress ranges tested. Further investigation has revealed that the cause

7. Results and Discussion (Fatigue Testing)

of this observation appears to be the formation of larger, more severe corrosion features on the surface of the sample under the unconfined test condition. Such corrosion phenomenon has been shown to be the cause of subsequent cracking.

A further finding was the observation of an adherent corrosion product (Iron Carbonate) over some areas of the samples under confined test conditions. Such scales, under the right conditions can be protective and mitigate further corrosion [21]. This feature was not observed in the unconfined test conditions so it may have had an impact on the results obtained in this thesis.

7. Results and Discussion (Fatigue Testing)

7.2.2.4 Investigation of Frequency Effect

Table 7-11 presents the results for the frequency investigation test series performed on Wire-2. This test series was carried out in accordance with the methodology outlined in Section 4.3.2 and aims to compare corrosion fatigue life data generated at test frequencies of 0.5 and 2Hz to investigate if this has an effect on the results obtained.

Table 7-11 – Results of the frequency Investigation test series performed on Wire-2. Testing conducted under the same conditions with the test frequency manipulated between 0.5 and 2Hz.

Sample ID	Steel Grade	Size (mm ²)	Curve	r-ratio	Test Frequency	Calculated Stress Range (MPa)	Cycles to Rupture	Comments
0.5Hz - 1	Wire 2	9x3	Frequency Investigation (Unconfined)	0.1	0.5Hz	553	210314	Valid within constant stress area
0.5Hz - 2						553	232000	Valid within constant stress area
0.5Hz - 3						551	215575	Valid within constant stress area
0.5Hz - 4						547	299481	Valid within constant stress area
0.5Hz - 5						450	300000	Valid within constant stress area
0.5Hz - 6						450	330000	Valid within constant stress area
0.5Hz - 7						450	370000	Valid within constant stress area
0.5Hz - 8						450	475000	Valid within constant stress area
0.5Hz - 9						350	421914	Valid within constant stress area
0.5Hz - 10						350	535115	Valid within constant stress area
0.5Hz - 11						350	461255	Valid within constant stress area
0.5Hz - 12						350	512275	Valid within constant stress area
2Hz - 1	Wire 2	9x3	Frequency Investigation (Unconfined)	0.1	2Hz	561	245946	Valid within constant stress area
2Hz - 2						559	236612	Valid within constant stress area
2Hz - 3						556	236695	Valid within constant stress area
2Hz - 4						558	310687	Valid within constant stress area
2Hz - 5						450	419594	Valid within constant stress area
2Hz - 6						451	411262	Valid within constant stress area
2Hz - 7						452	392202	Valid within constant stress area
2Hz - 8						447	467558	Valid within constant stress area
2Hz - 9						350	537000	Valid within constant stress area
2Hz - 10						350	649867	Valid within constant stress area
2Hz - 11						350	569456	Valid within constant stress area
2Hz - 12						350	505768	Valid within constant stress area

Figure 7-50 presents these results in the form of an SN plot. These tests were conducted to investigate the effect of variations in loading frequency and hence length of exposure to the corrosive environment. These tests have been carried out under unconfined conditions in deaerated artificial seawater saturated with 1bara CO₂ with loading frequencies of 0.5Hz and 2Hz. The data for both frequencies is plotted on Figure 7-50.

7. Results and Discussion (Fatigue Testing)

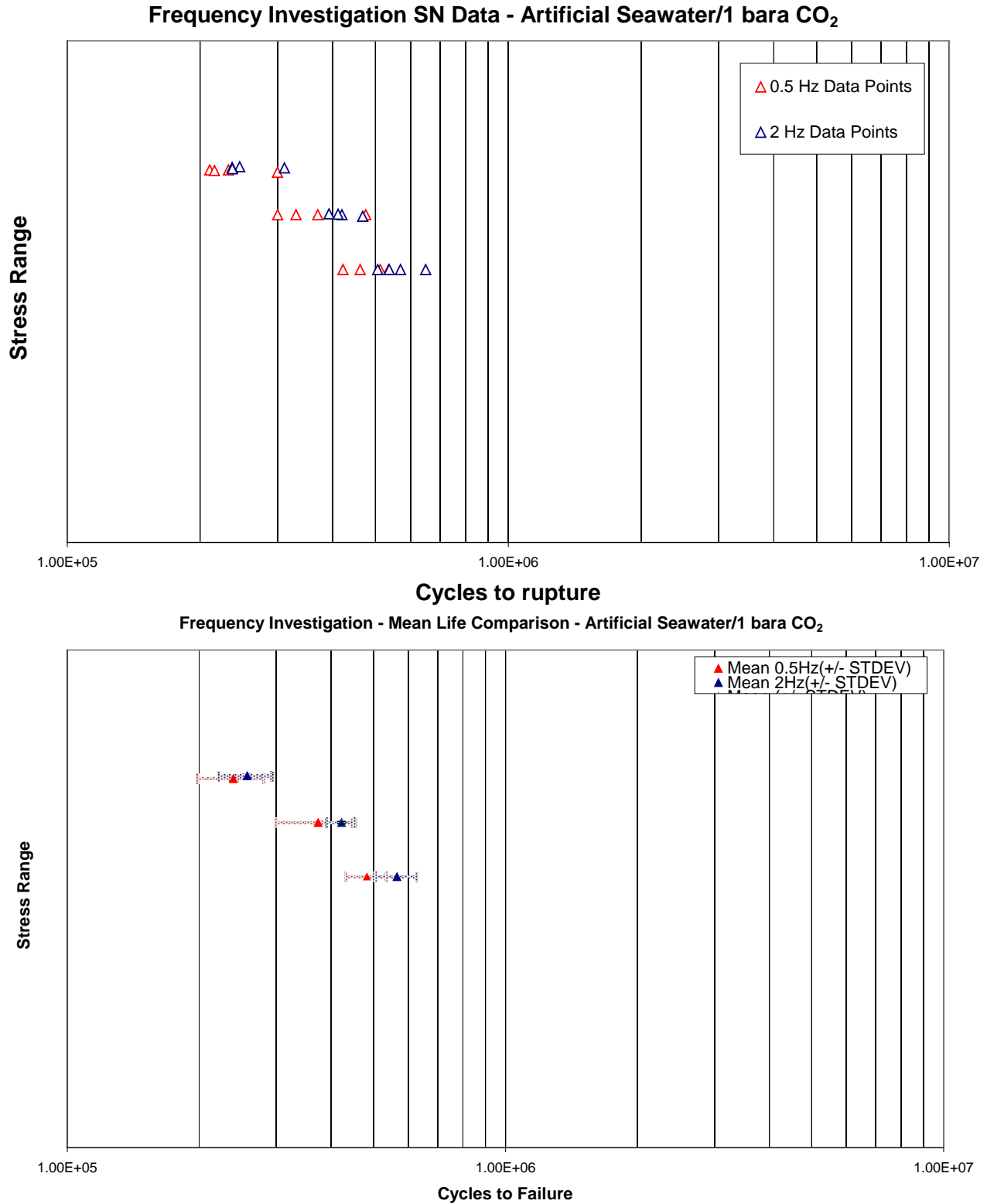


Figure 7-50 – Results of the frequency Investigation test series performed on Wire-2. SN plots showing a comparison between fatigue life generated at test frequencies 0.5 and 2Hz. Top) all data points, Bottom) mean life at each stress range.

7. Results and Discussion (Fatigue Testing)

Figure 7-50 shows the SN data for these set of tests. The 0.5 and 2Hz data fall largely within the same scatter band at all 3 of the stress ranges tested although there is a slight increase in mean life when testing at 2Hz. It is possible that we are seeing the minimum effect of frequency when testing at higher stress ranges. At lower stress ranges and hence longer test durations this apparent shift could become more pronounced.

Similar data from the literature has concluded that testing at 2Hz gives realistic results which are comparable to testing at 0.5Hz [8]. The results of the current tests would concur with this observation however the effect of frequency will be most evident at low stress ranges when testing out to higher fatigue lives.

Post test investigation of ruptured specimens revealed many of the same features as seen in the other corrosion fatigue test series. Figure 7-51 shows a ruptured sample where the main crack can be seen along with secondary cracking and surface hairline cracks.



Figure 7-51 - Image illustrating the effect of max tensile strains in the constant stress area of the sample, note the presence of the main crack, a secondary crack and surface hairline cracking

7. Results and Discussion (Fatigue Testing)

This Figure also illustrates the constant stress region of the four-point bend set up very clearly where there is a combination of corrosion and maximum tensile strains over a 40mm section corresponding to the region between the two centre rollers. Beyond this area of the sample there is no such evidence. This demonstrates that the loading is well controlled over the sample surface. This was the case for testing at both 0.5 and 2Hz although these features appeared clearer on the 2Hz samples since there was less general corrosion to the surface of the sample. At lower stress regimes and hence longer test durations the exposure time will be significantly larger for the 0.5 Hz test meaning that degradation of the surface condition could also be exacerbated having a knock on effect on fatigue life.

An interesting feature of the 9mm x 3mm (Wire-2) samples is the characteristic fracture geometry. Figure 7-52 shows some ruptured specimens post test where it can be seen that the failure is initiated parallel to the direction of the applied stress and the crack propagates in this direction until approximately mid-thickness at which point it changes direction leaving a characteristic diagonal fracture geometry. This observation was the same at both test frequencies.

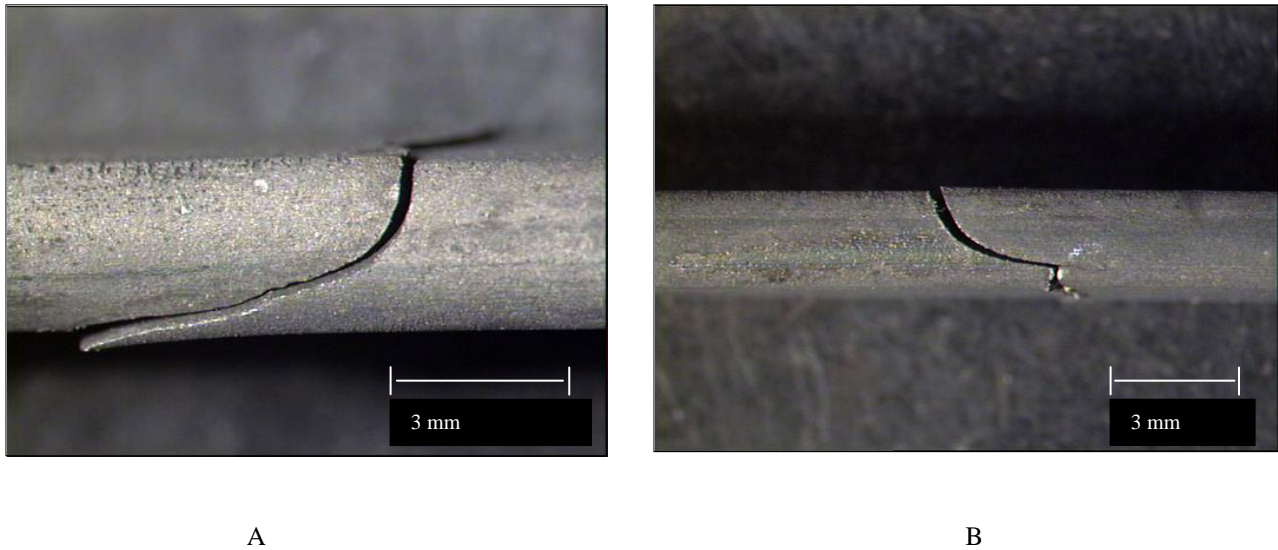


Figure 7-52 – Images of the characteristic fracture geometry on the Wire-2 (9x3mm), A- sample 2 (0.5Hz), B- sample 4 (2Hz)

This fracture path can be attributed to the directionality of the microstructure and the crack follows the grain orientation which has been elongated in the rolling direction. Section 7.1.1 shows the microstructure of the wire material where such grain elongation is clearly visible and appears to be most pronounced mid-thickness which would explain the change in direction of the failure path at this point on the sample [15].

The tensile face of the samples exhibited secondary and hairline cracking in both tests, although it did appear to be more pronounced in the 2Hz test (Figure 7-53).

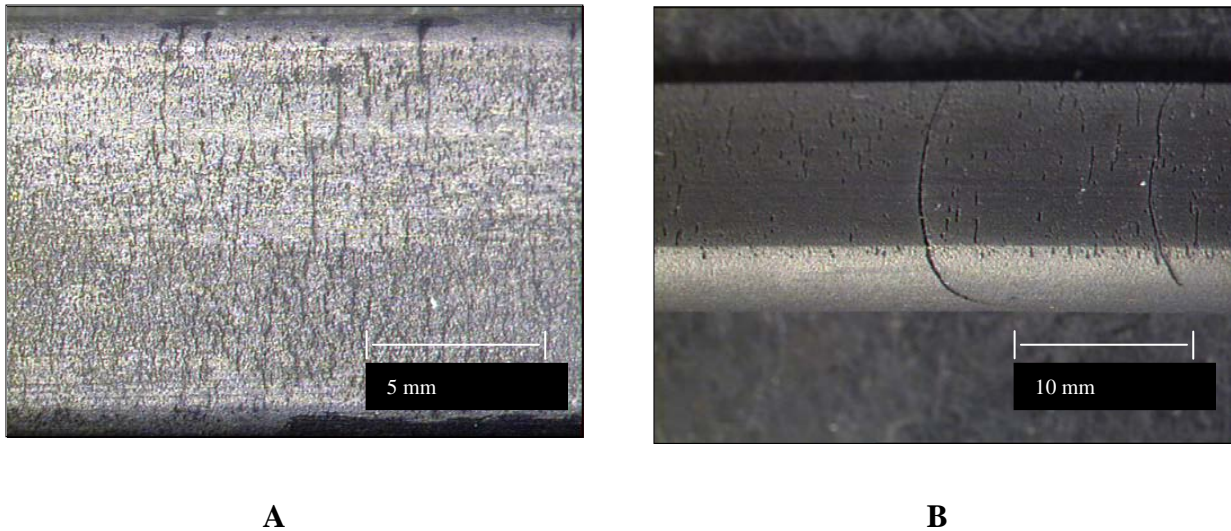


Figure 7-53 – Images showing secondary and surface cracking, A- sample 2 (0.5Hz), B- sample 2 (2Hz)

In the case of the 0.5 Hz samples there appeared to be more evidence of general surface corrosion in addition to some hairline cracking induced by the tensile strains. For the 2Hz test, such general surface corrosion was largely absent making the hairline cracks appear much clearer on the surface of the sample. This is one possible effect of frequency since the 0.5Hz samples are exposed to the environment for a much longer duration.

Figure 7-54 shows a closer view of the surface corrosion that was evident in the 0.5Hz test and also some evidence of crevice corrosion around a roller location. Again, this phenomenon was largely absent in the 2Hz test and there was no evidence of crevice corrosion.

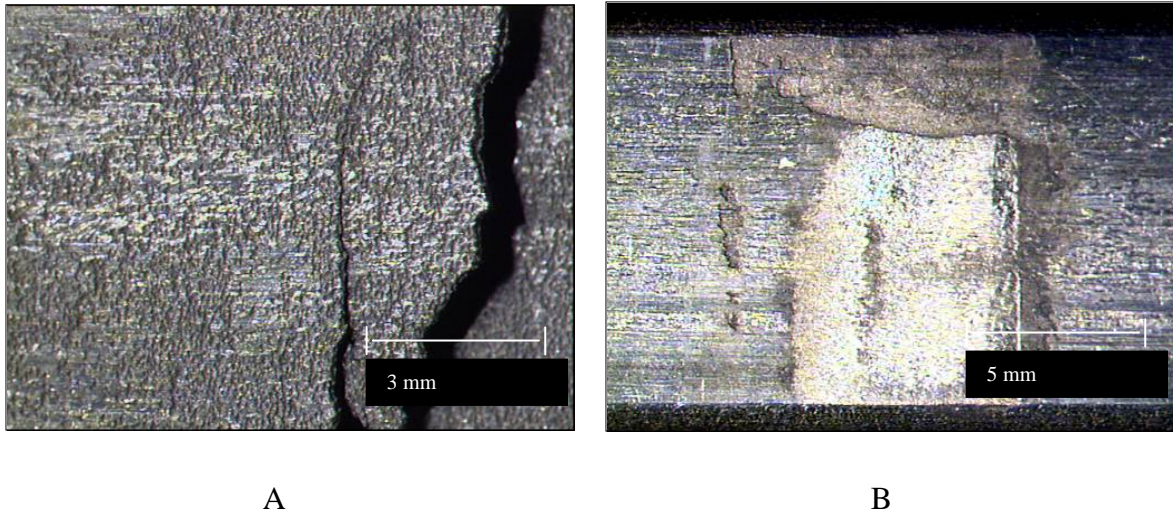


Figure 7-54 - Images of Sample 1 (0.5Hz test) - a) Surface corrosion around the rupture location, b) Crevice corrosion around the roller on the tensile face.

As a result of this investigation together with results from the literature [7] the flexible pipeline manufacturers concluded that testing at 2Hz could generate comparable data to that generated at 0.5Hz. The results presented in this thesis would agree with this conclusion at the stress ranges tested, although further work testing at 0.5Hz out to longer lives is needed to ensure that this remains the case at lower stress ranges. The remaining corrosion fatigue tests presented in the following Sections of this thesis contain data generated at a frequency of 2Hz since this was the preferred option of the client based on the results presented in this section along with supporting data in the literature [7].

7. Results and Discussion (Fatigue Testing)

7.2.2.5 Investigation of the Effect of Welded Samples

Table 7-12 presents the results for the welded sample investigation test series performed on Wire-2. This test series was carried out in accordance with the methodology outlined in Section 4.3.3 and the aim was to test as-received welded samples to investigate the effect on fatigue life compared to the results obtained with a parent (non welded) sample.

Table 7-12 – Results of the Welded Sample Investigation test series performed on Wire-2. Testing conducted under the same conditions as the frequency investigation test series. Testing performed at 2Hz. with one comparative dataset at 0.5Hz.

Sample ID	Steel Grade	Size (mm ²)	Curve	r-ratio	Test Frequency	Nominal Stress Range (MPa)	Cycles to Rupture	Comments
1	Wire 2 (Welded)	9x3	Welded Sample Investigation	0.1	2Hz	350	510000	Valid within constant stress area
2						350	286387	Valid within constant stress area
3						350	297726	Valid within constant stress area
4						350	165576	Valid within constant stress area
5						450	117396	Valid within constant stress area
6						450	175983	Valid within constant stress area
7						450	110678	Valid within constant stress area
8						450	142129	Valid within constant stress area
9						550	67566	Valid within constant stress area
10						550	83390	Valid within constant stress area
11						550	91935	Valid within constant stress area
12						550	34318	Valid within constant stress area
1	Wire 2 (Welded)	9x3	Welded Sample Investigation	0.1	0.5Hz	450	78433	Valid within constant stress area
2						450	75272	Valid within constant stress area
3						450	55635	Valid within constant stress area
4						450	111615	Valid within constant stress area

The welded sample investigation test series was carried out under the same test conditions as the frequency investigation test series, i.e. 1bar CO₂/artificial seawater and unconfined test conditions. This allowed for direct comparison with the results generated on parent samples as the only manipulation was the addition of a welded sample. The testing was performed on samples of Wire-2 which had a weld in the centre of the test

7. Results and Discussion (Fatigue Testing)

sample and was exposed to the maximum strains in the constant stress region of the sample. Figure 7-55 presents the results from this test series in the form of an SN plot.

Welded Samples Vs Plain Samples SN Data - Artificial Seawater/1 bara CO₂

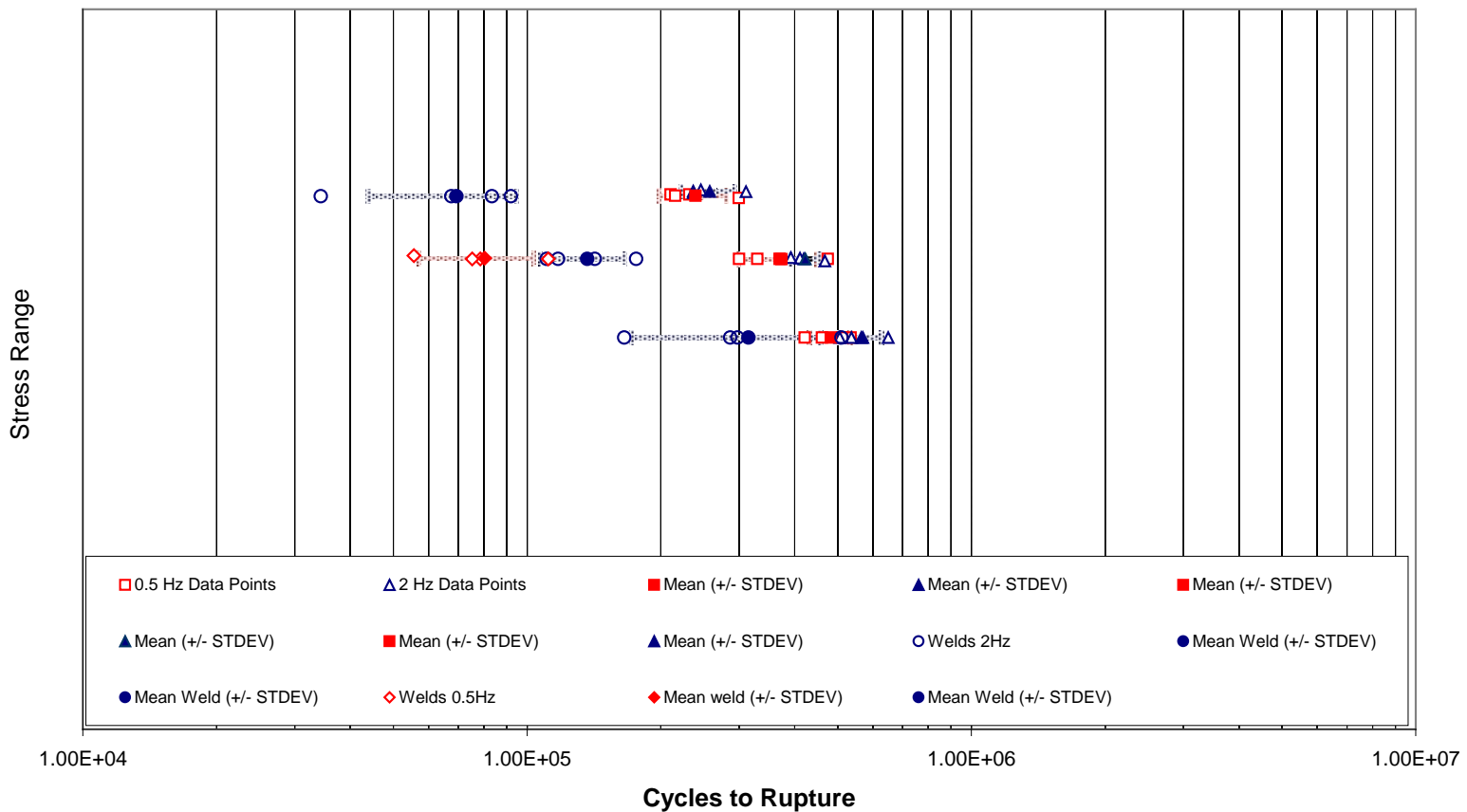


Figure 7-55 – Results of the Welded Sample Investigation test series performed on Wire-2. SN plot showing effect of a weld compared to the SN data of parent samples (from frequency investigation test series). Circle symbols are welded samples, red 0.5 Hz and blue 2Hz.

From Figure 7-55 it is clear to see that the presence of a weld appears to have a marked effect on fatigue life. In the current test series the mean fatigue life of the welded samples

7. Results and Discussion (Fatigue Testing)

was decreased significantly compared to parent samples. This result is in agreement with data in the literature [70]. The effect of frequency also seems to be more pronounced when testing welded samples. Mean life showed a 41% increase at 2Hz (compared to 0.5Hz) with welded samples. In comparison, testing with parent samples at 2Hz resulted in a mean life only 11% longer than that at 0.5Hz.

The results from the weld investigation test series also show a large amount of scatter compared to parent test samples. This is to be expected due to the condition of the welded samples and the fact that they have been tested in as-received condition. Due to the irregular and uneven nature of the welded section, each of the samples was significantly different in terms of geometry and/or cross-section as a result of the welding process (Figure 7-56). Since this would be the case in service, samples in this test series were tested at nominal load ranges corresponding to the stress ranges given. The local stresses due to the irregularities of the welded section could have been significantly higher so these results can be considered to be very conservative.

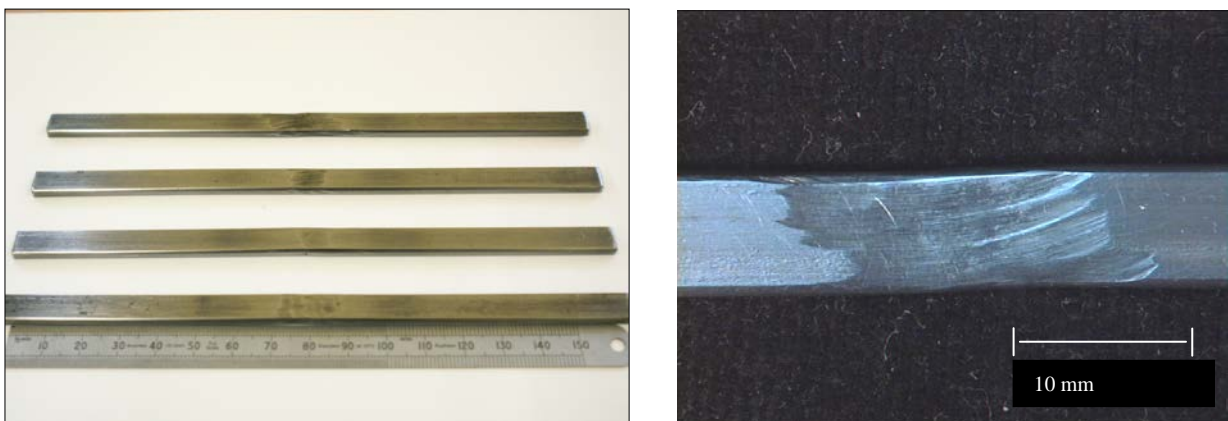


Figure 7-56 – Images of some test samples from the welded sample investigation test series. Note there is some mismatch between each side of the welded section and an irregular surface condition due to grinding away of flash during the welding process.

7. Results and Discussion (Fatigue Testing)

Another interesting feature of the welded samples is the different fracture geometry observed compared to parent samples. Figure 7-57 shows the two contrasting fracture paths between parent and welded samples.

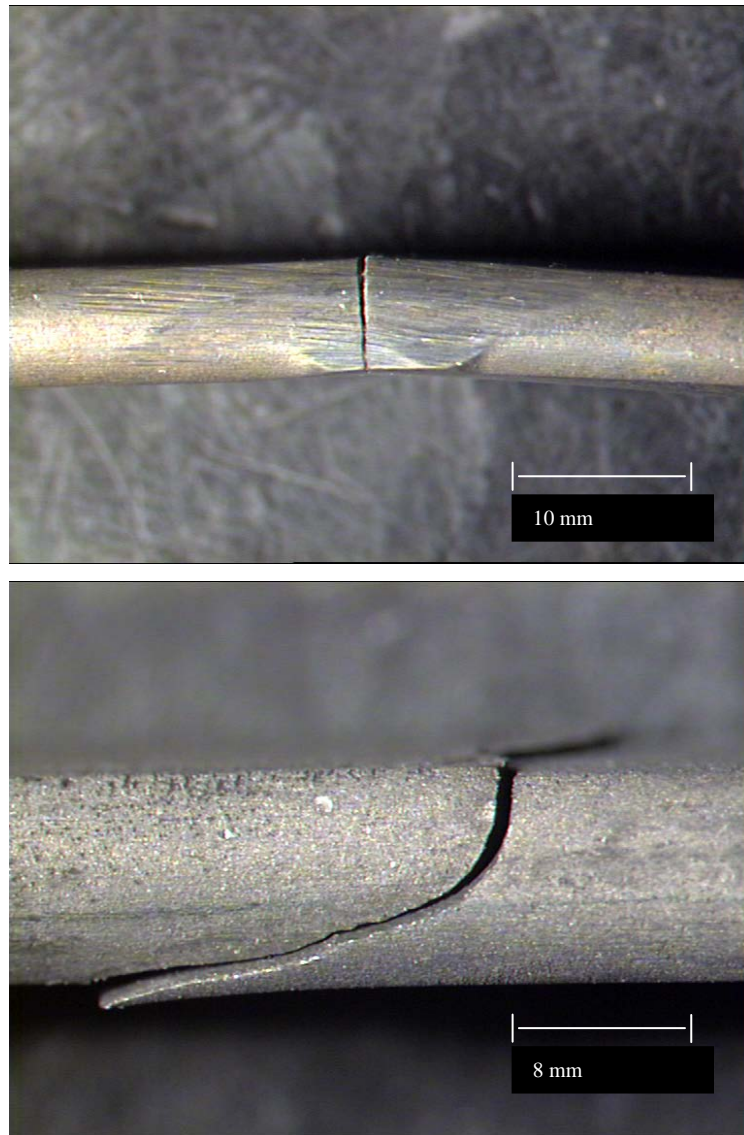


Figure 7-57 – Contrasting images of the fracture geometries from the welded sample investigation test series and a parent sample from the frequency investigation test series. Top) welded sample, bottom) parent sample.

7. Results and Discussion (Fatigue Testing)

The ruptured sample containing a weld shows a fracture path that runs straight down through the weld parallel to the direction of the alternating stress. In the parent sample the fracture path is dictated by the microstructural effects caused by the strong plastic deformations of the wire associated with the manufacturing processes. This results in a fracture that diverges off perpendicular to the direction of applied stress when the crack reaches approximately mid-thickness [15]. In the welded samples this directionality is disrupted during the joining process leading to the different fracture geometries observed (Figures 7-58 and 7-59).

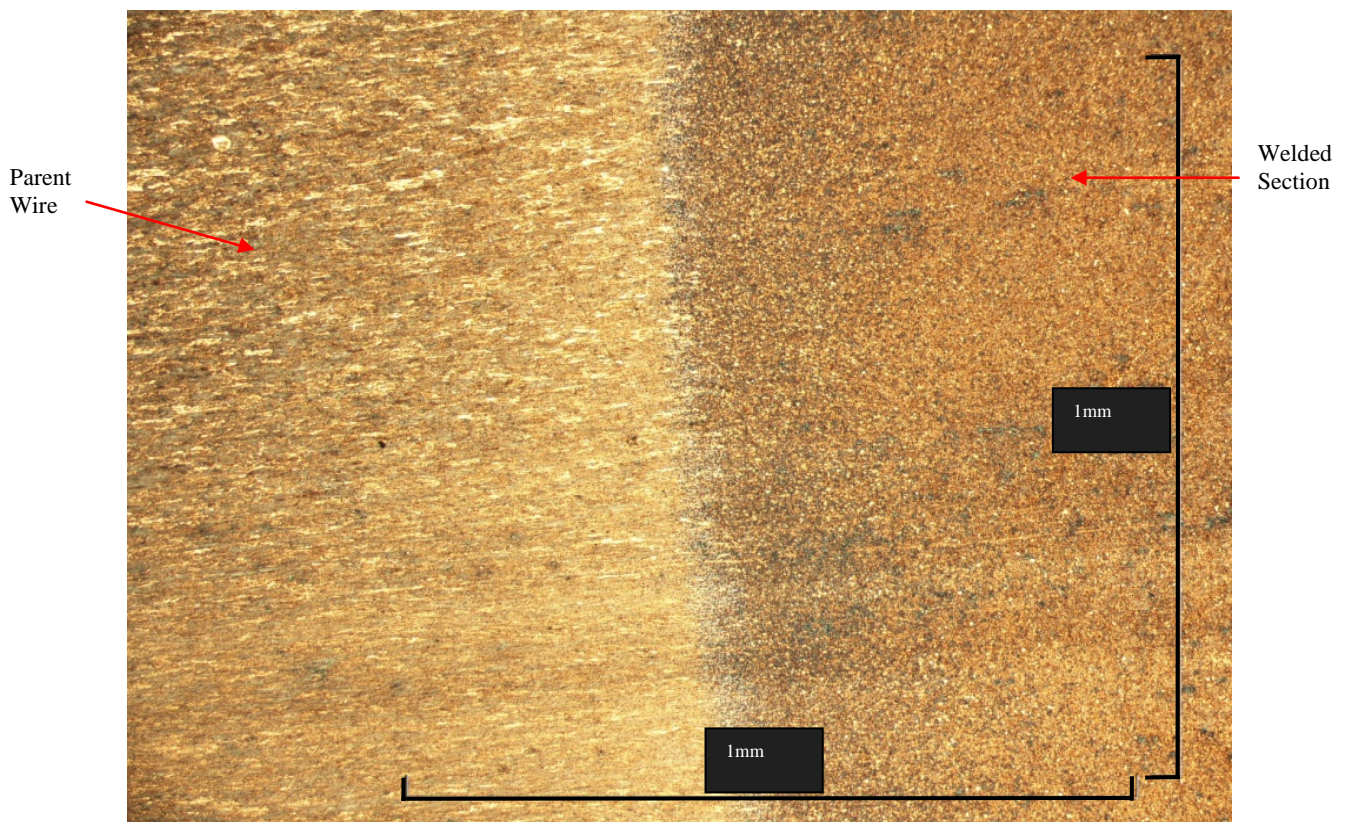


Figure 7-58 – Longitudinal section through a welded sample showing the contrast in microstructures between the oriented rolled parent wire and the more homogenous welded section.

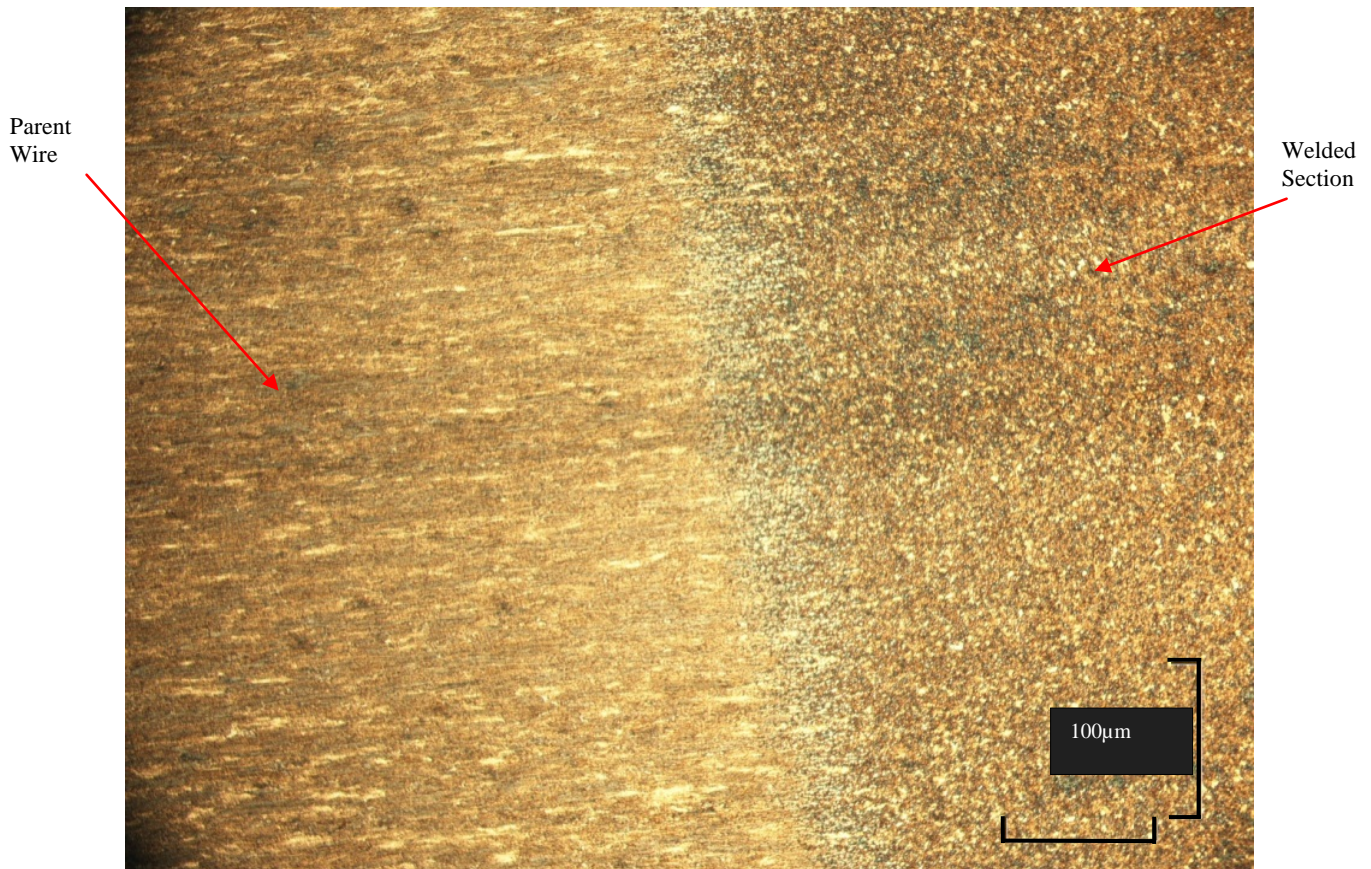


Figure 7-59 – Longitudinal section through a welded sample showing the contrast in microstructures between the oriented rolled parent wire and the more homogenous welded section.

A selection of fracture faces from samples in the welded sample investigation test series are shown in the following Figures (7-60 to 7-62). In each of the images the tensile face (surface subjected to maximum tensile strains) of the sample is at the top of the fracture face.

The majority of fracture faces are very flat suggesting that the ruptures are failing along the interface between the two sections of parent wire that have been welded together. This would also explain the very straight fracture geometry seen in Figure 7-57.

7. Results and Discussion (Fatigue Testing)

In summary, the results presented in this section of the present thesis suggest that welded sections of tensile armour wire require careful positioning within the overall pipe structure to areas that will not be subjected to the most severe loading conditions. Furthermore, careful control of the post weld surface finish will help to minimize the detrimental effect and restore fatigue life closer to that seen in parent samples.

7. Results and Discussion (Fatigue Testing)

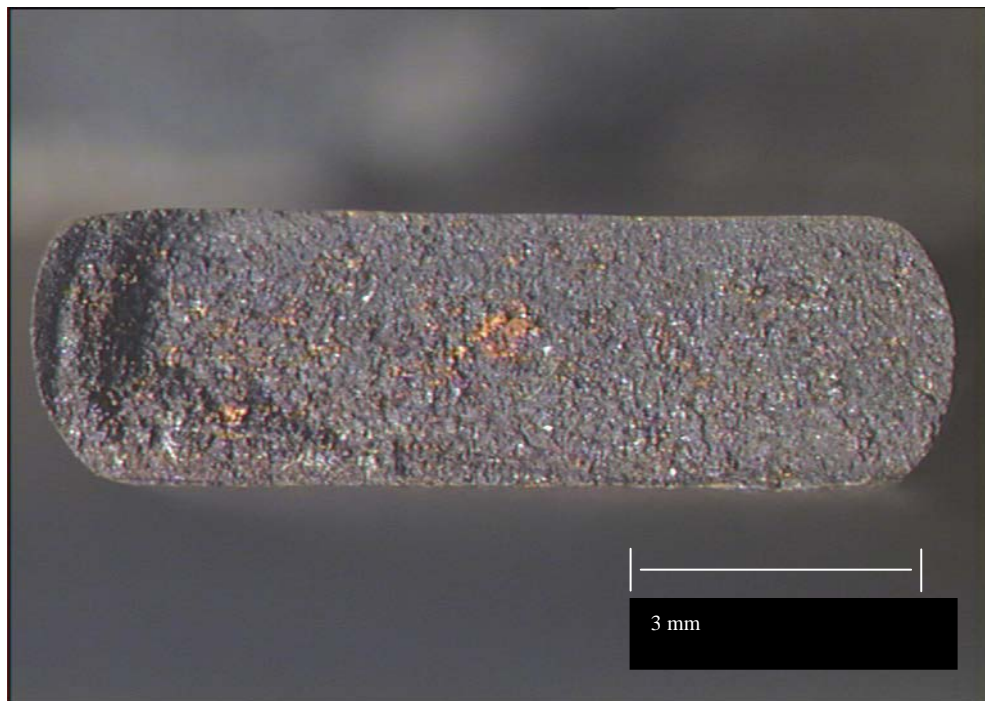
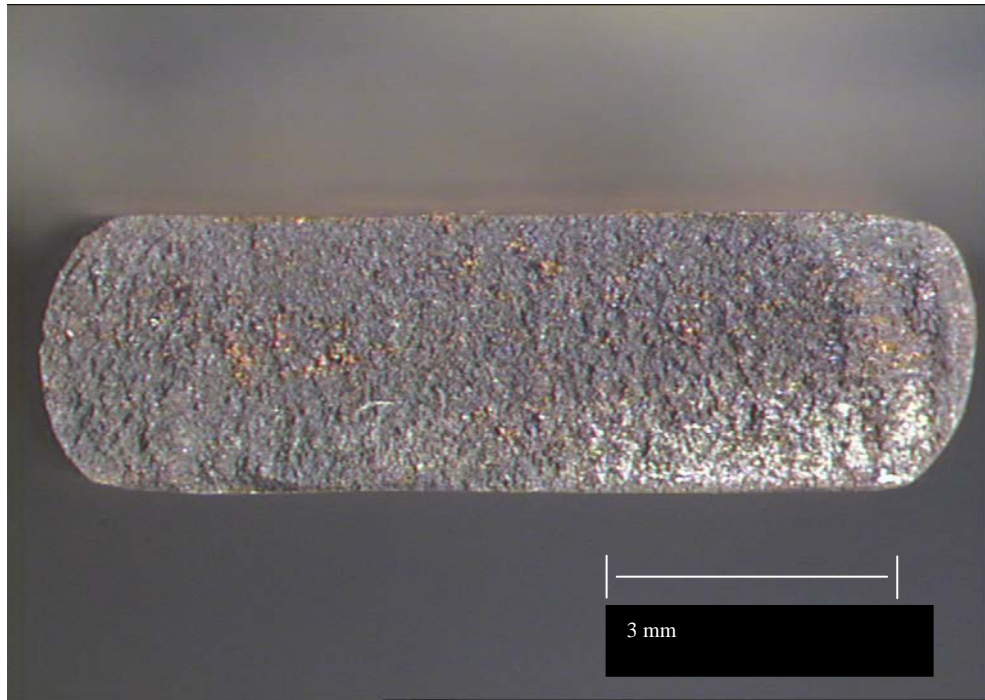


Figure 7-60 – Welded sample investigation test series. Sample 1, 510,000 cycles. (2Hz)

7. Results and Discussion (Fatigue Testing)



Figure 7-61 – Welded sample investigation test series. Sample 2, 286,387 cycles. (2Hz)

7. Results and Discussion (Fatigue Testing)

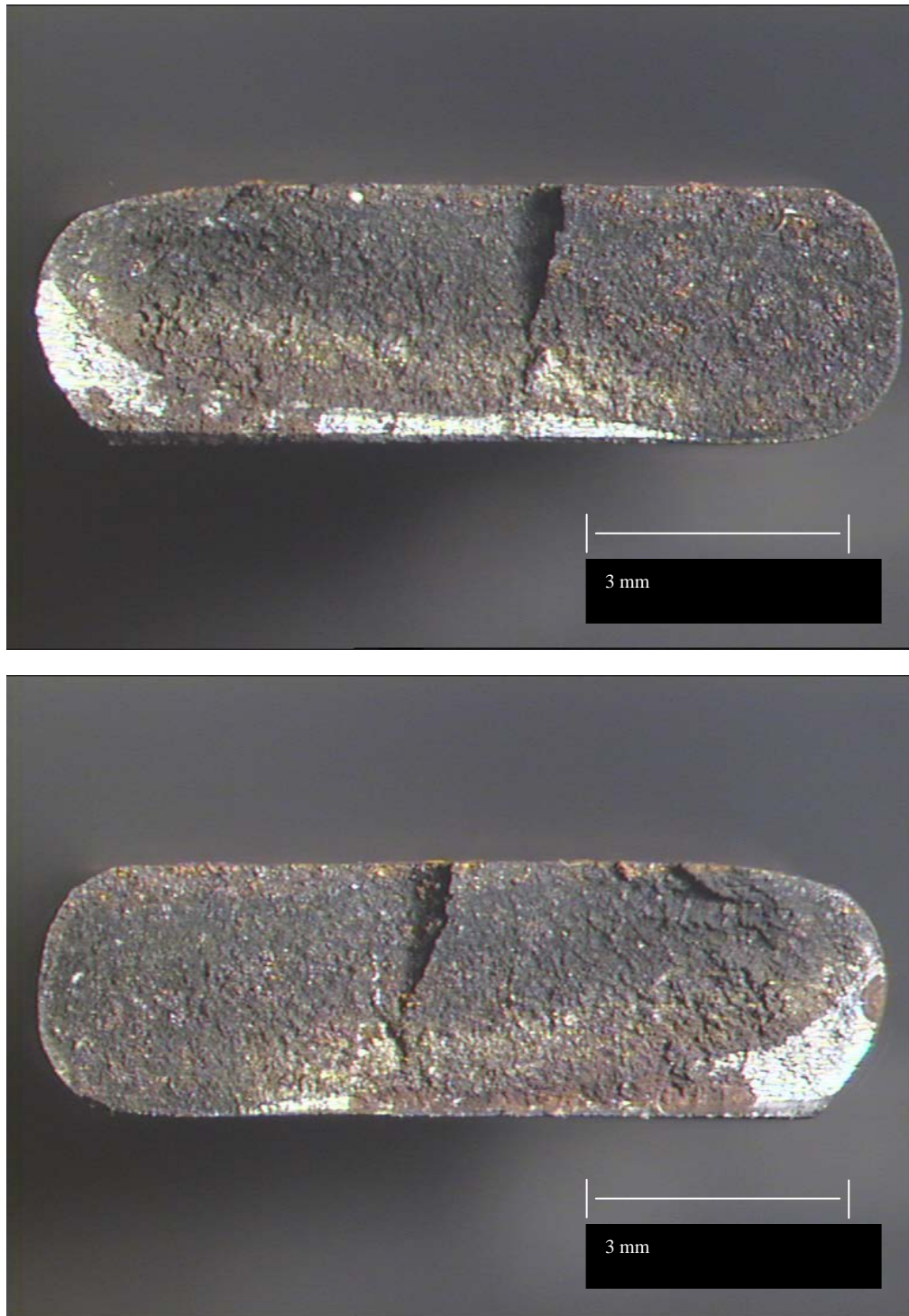


Figure 7-62 – Welded sample investigation test series. Sample 3, 297,726 cycles. (2Hz)

7. Results and Discussion (Fatigue Testing)

Further investigation was carried out on a sample via an SEM evaluation. Figure 7-63 Shows the full fracture surface where multiple initiation points are highlighted.

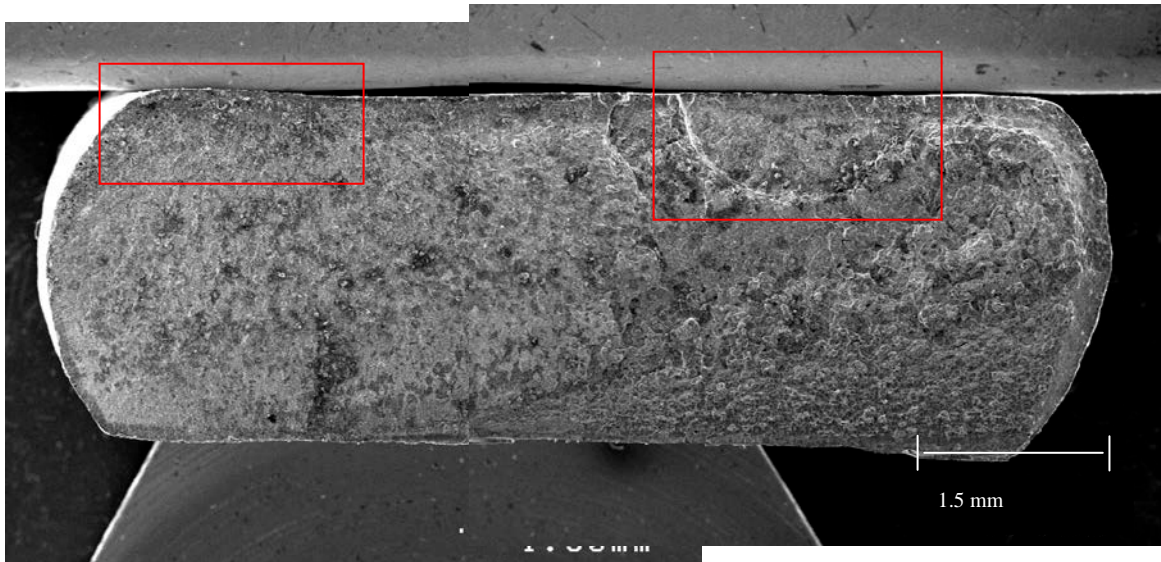


Figure 7-63 – Welded sample investigation test series. SEM fractographs showing a sample with multiple initiation points.

The following Figures (Figures 7-64 and 7-65) show higher magnification images of the highlighted initiation points in figure 7-63. Figure 7-64 shows the main initiation site on the left hand side of the sample close to the corner of the wire. Figure 7-65 shows the second initiation site on the right hand side of the fracture face in Figure 7-63.

7. Results and Discussion (Fatigue Testing)

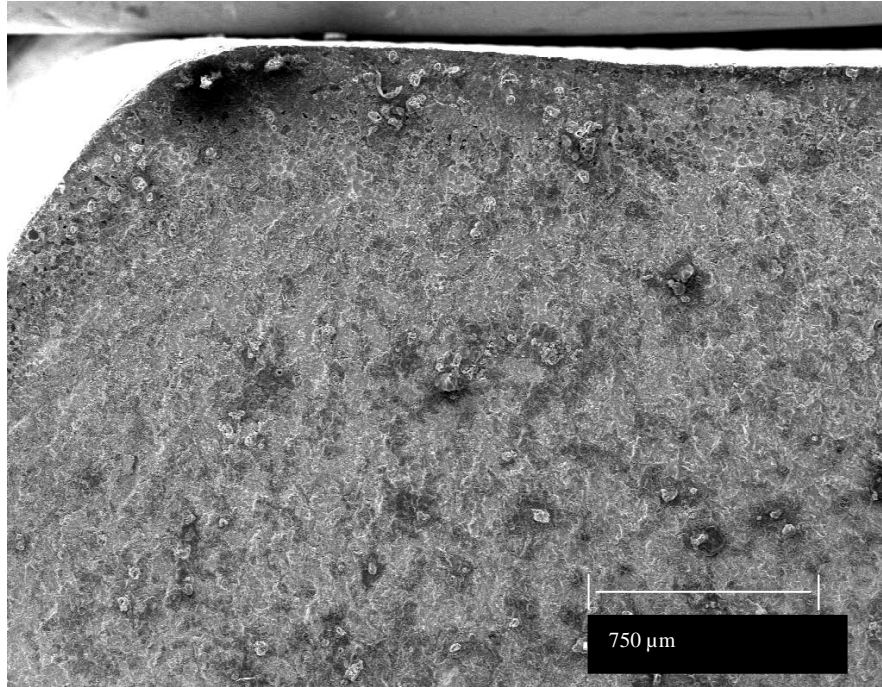


Figure 7-64 – Welded sample investigation test series. SEM fractograph showing main initiation site. Left hand initiation site from figure 7-63.

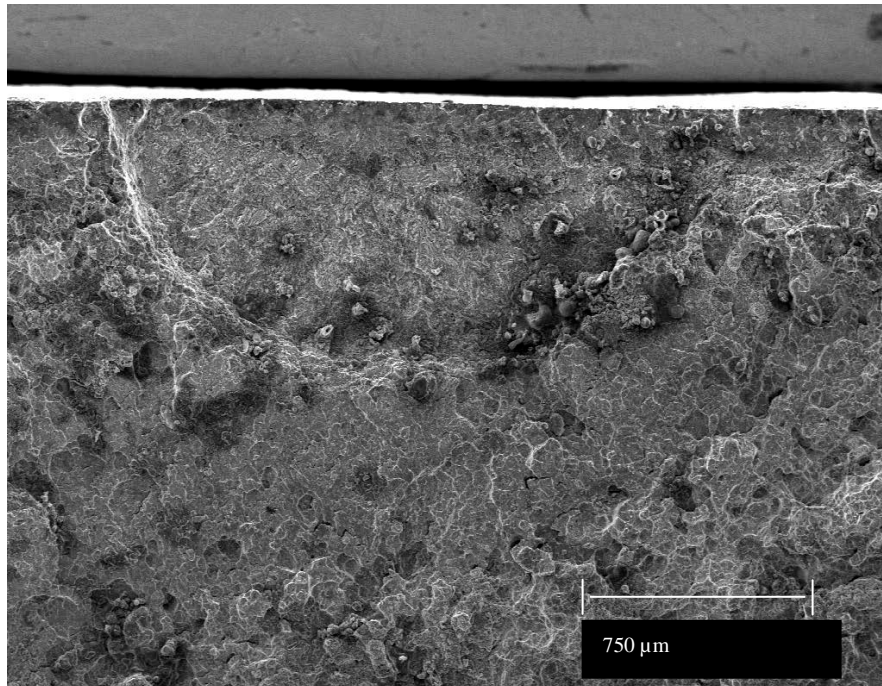


Figure 7-65 – Welded sample investigation test series. SEM fractograph showing the second initiation site. Right hand initiation site from figure 7-63.

7.2.3 High Pressure Corrosion Fatigue Testing

7.2.3.1 Qualification of High Pressure Corrosion Fatigue Test Rigs

Deaeration Qualification Test

For this phase of the qualification a test was setup as normal except that no steel wool was added to the autoclave to ensure that any O₂ would not be consumed and therefore not measured by the O₂ sensor equipment. During this phase two oxygen sensors were utilised, one measured dissolved O₂ in the solution in the deaeration vessel (Figure 7-66) and the second sensor was fitted to the autoclave so that O₂ measurements could be taken continuously whilst the rig was cycling over a minimum of 48 hours.

Figure 7-66 shows the plot from the O₂ sensor in the deaeration vessel during the nitrogen purging stage prior to being transferred into the autoclave. The plot starts at 2000 ppb which is the upper detection limit of the sensor and gradually falls to a level below 5 ppb when it is ready for transfer. Approximately 6L of ASTM D1141 was deaerated during the deaeration qualification test.

7. Results and Discussion (Fatigue Testing)

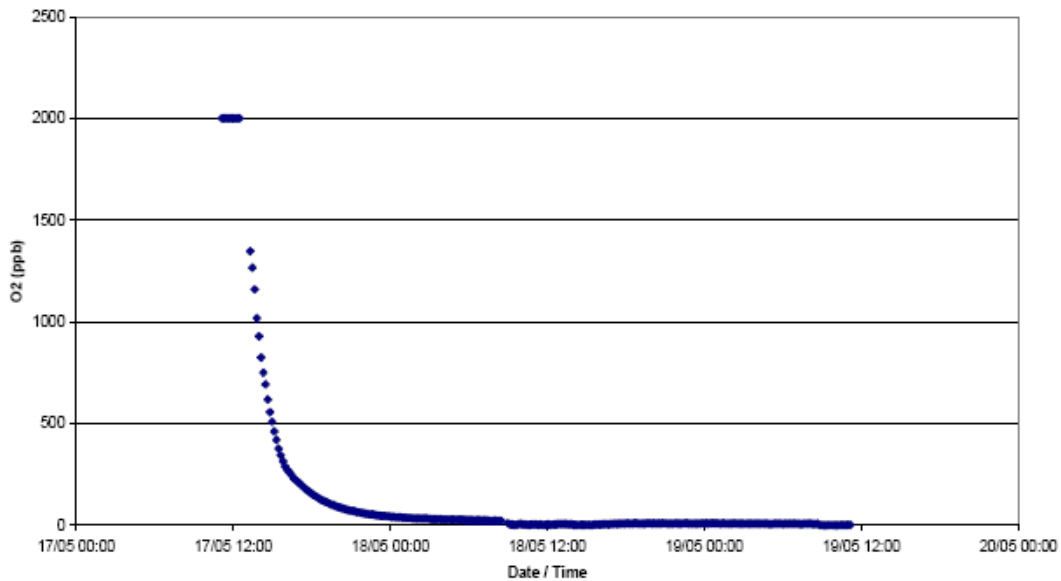


Figure 7-66 – Dissolved oxygen plot from the sensor located in the deaeration vessel. Test solution (ASTM D1141) is purged with nitrogen until levels reach less than 5 ppb.

Following transfer of the test solution and obtaining an O₂ level of less than 5ppb from the sensor located inside the autoclave, the autoclave was pressurised to 5bar using nitrogen. The test rig was then set to run in displacement control with the dynamic cycling of the pullbar set to a frequency of 2Hz.

Although the minimum duration for this qualification test was 48 hours, the rig was cycled over a period of 6 days where the pressure was maintained at 5bar with a gas flow rate of approximately 20mL/min. Oxygen measurements were continuously monitored and recorded over this period and are shown in Figure 7-67. It can be observed from the plot in Figure 7-67 that the oxygen level remained well below 5 ppb throughout the duration of the test confirming that there is no ingress of oxygen anticipated with the proposed experimental setup and testing procedure.

7. Results and Discussion (Fatigue Testing)

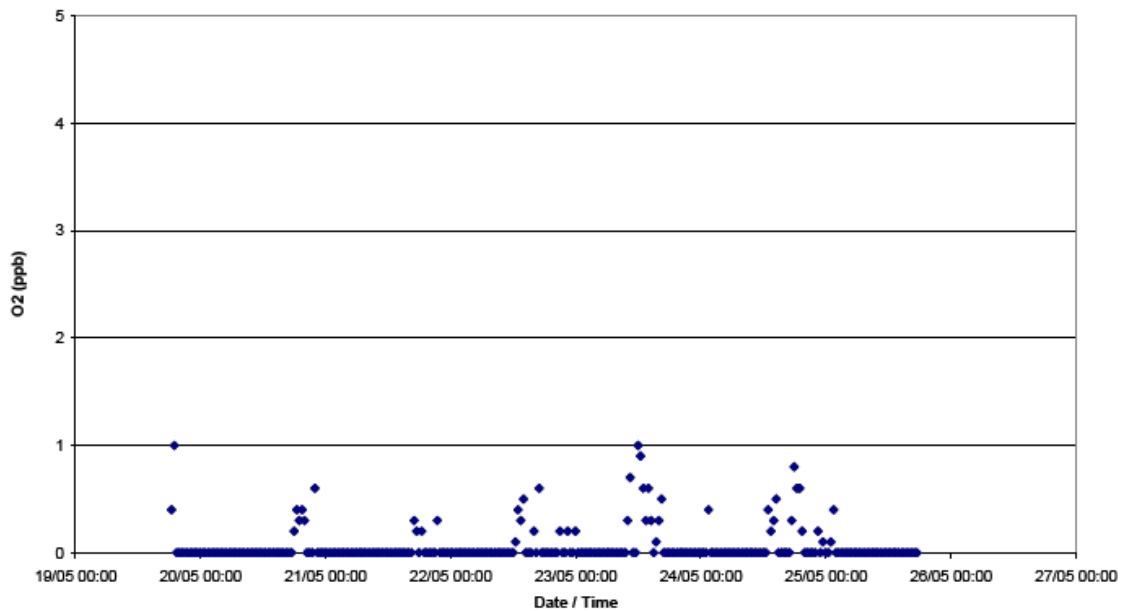


Figure 7-67 - Dissolved oxygen plot from the sensor located in the autoclave over a 6 day test where the pullrod is cycled dynamically at 2Hz. The autoclave is pressurised to 5bar with nitrogen with a gas flow rate of 20 mL/min. The plot demonstrates that there is no ingress of oxygen with the proposed experimental setup.

Corrosion Fatigue Qualification Test

Testing for the corrosion fatigue qualification phase has been performed on 15x5mm wire (Wire-1) which is classified as a ‘sweet service wire’ on the basis of its mechanical properties. In fact, this is this same grade of material that was tested in the ambient pressure corrosion fatigue test series. It is from the same heat, batch and spool so the results will provide a direct comparison on this particular grade of tensile armour wire.

Test Results

Results of the HPCF qualification test series are presented in the two tables in Table 7-13. These tables give details of the test conditions as well as the total number of cycles to failure.

7. Results and Discussion (Fatigue Testing)

Table 7-13 – Tables showing the results of the HPCF qualification test series along with all other details of the tests.

Exova ID	Material	Test gas	Width (mm)	Thickness (mm)	length (mm)	Stress (MPa)		Pressure (bar)	Cycles to rupture	Comments	
						Mean	Range				
D9912-Q-01	Wire 1 (15x5mm)	10% CO2 90% N2	15.00	4.99	116	400	400	10	N/A	Sample bent after 4,913,242 cycles due to hydraulic/controller problem	With TZCF-01, XS-ECOPUR seal and Hastelloy pull rod
D9912-Q-02			14.98	4.99	118				1,381,519	Edge initiation within the 20mm constant stress area	With TZCF-02, XS-ECOPUR seal and Hastelloy pull rod
D9912-Q-03			14.98	5.01	118				N/A	Sample bent after 348,130 cycles due to hydraulic/controller problem	With TZCF-02, S-ECOPUR seal and Hastelloy pull rod
D9912-Q-04			14.99	5.01	113				674,878	Edge initiation within the 20mm constant stress area	With TZCF-02, S-ECOPUR seal and Hastelloy pull bar
D9912-Q-05			15.00	5.00	115				1,484,345	Mid-width initiation within the 20mm constant stress area	With TZCF-01, S-ECOPUR seal and nickel plated pull bar

Exova ID	Material	Test gas	Pre-cycles	Pressure (bar)	pH at test pressure after						Number of Cycles	Comments
					1h	3h	4 days	5 days	6 days	End		
D9912-Q-01	Wire 1 (15x5mm)	10% CO2 90% N2	20,000	10	5.39	N/A	6.02	6.15	6.15	N/A	4,913,242	Non valid, leakage + sample bent
D9912-Q-02					N/A	5.73	6.16	N/A	6.16	6.28	1,381,519	Valid rupture
D9912-Q-03					5.68	N/A	6.25	N/A			348,130	Non valid, sample bent
D9912-Q-04					N/A		6.06	N/A		6.12	674,878	Valid rupture
D9912-Q-05					N/A		6.05	N/A		5.96	1,484,345	Valid rupture

Results of the qualification tests are also presented in an S-N plot in Figure 7-68. Three out of the five specimens tested provided valid ruptures within the designated range of fatigue life (as specified in Section 4.4.1) shown in Figure 7-69, with failures at 1,381,519, 674,878, and 1,484,345 cycles.

7. Results and Discussion (Fatigue Testing)

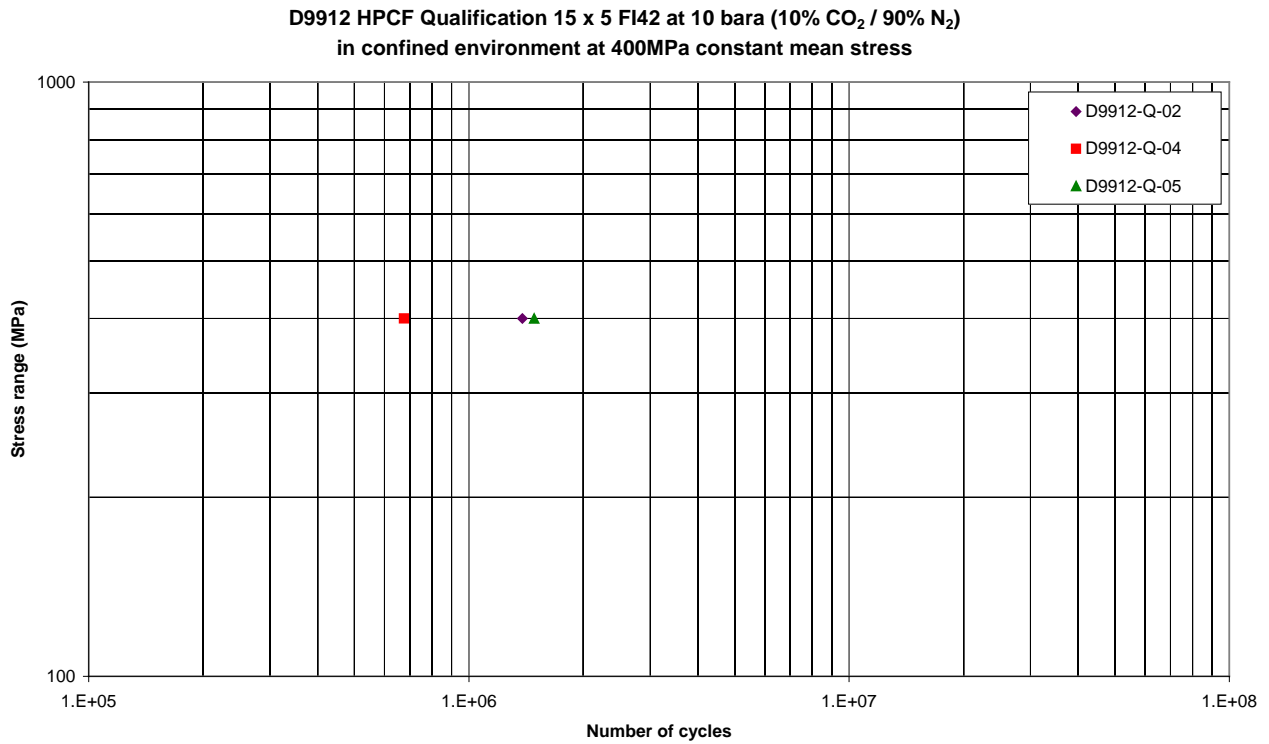


Figure 7-68 – S-N Plot showing the results of the Elevated Pressure corrosion fatigue qualification tests. ASTM D1141 saturated with a 10% CO₂/90% N₂ gas mix at a test pressure of 10bar. These data points fall within the scatter bands described in section 4.4.1 and illustrated in Figure 7-69.

7. Results and Discussion (Fatigue Testing)

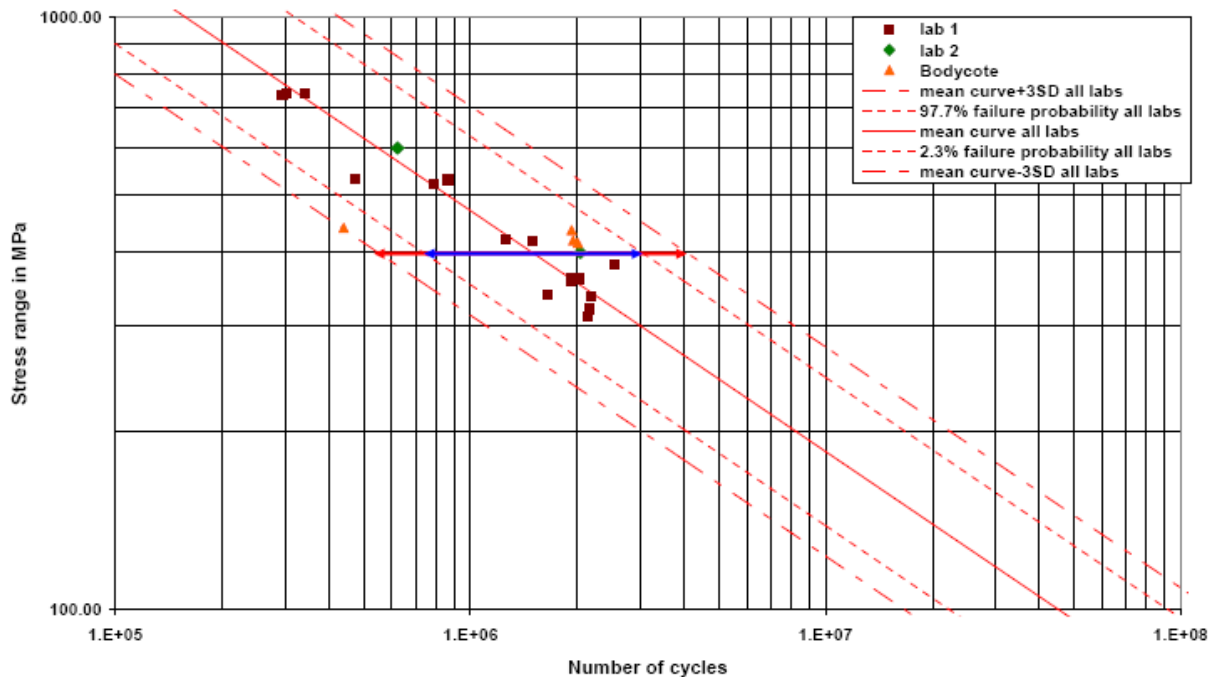
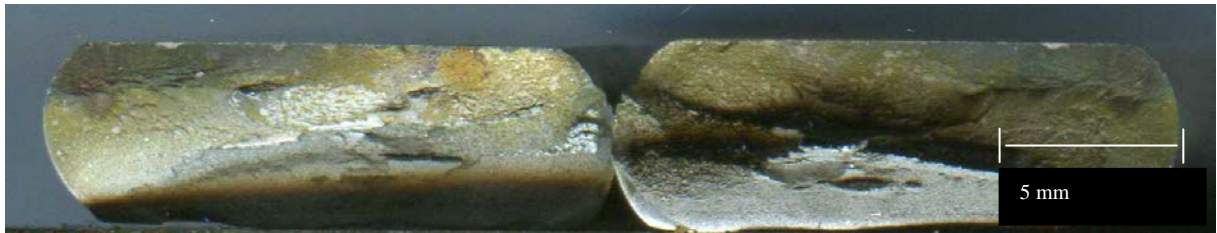


Figure 7-69 – S-N Plot showing the general scatter of results when testing at 1bar CO₂ (400MPa mean stress). The triangles (Bodycote) are data points generated in the current research project during the atmospheric pressure corrosion fatigue testing phase, the other points have been generated by other independent test labs. Note arrows at 400MPa stress range show the scatter bands that the qualification samples needed to fall into.

The fracture faces from the three valid qualification samples are shown in Figure 7-70. It can be observed from samples 02 and 04 that the fatigue crack began from an edge initiation point within the 20mm constant stress area. It can be seen from the fracture face on sample 05 that the fatigue crack initiated mid-width on the tensile face of the sample within the 20mm constant stress area.

7. Results and Discussion (Fatigue Testing)



Sample 02



Sample 04



Sample 05

Figure 7-70 –Fracture Faces from the qualification test series showing the two different initiation points. Initiation on samples 02 and 04 was from the edge of the wire and on sample 05 it was from the middle of the tensile face of the wire.

Samples 02 and 05 have also undergone an SEM investigation in order to view the initiation points in more detail. These images are shown in Figures 7-71 and 7-72.

For sample 02 (Figure 7-71) it is clear from the top image that the sample is corroded; the highlighted region is fatigue region and the area of focus, this is where the initiation point is situated somewhere along the top (tensile) surface. There was no clear initiation point.

7. Results and Discussion (Fatigue Testing)

However there were several pits along the top surface which are likely to act as stress raisers, image (a) and (c) show examples of some that were identified. The smooth fatigue region was clear, as shown in (d) this image was taken from below a pitted region. In the case of sample 05 (Figure 7-72) again it is clear that the sample is corroded; the highlighted region is the fatigue region, which is shown in further detail in image (c). The initiation point on this sample was in the centre of the tensile face of the sample where there was also evidence of several pits on the surface. Images (c), (d) and (e) show the initiation site at different magnifications. In images (b) and (d) the initiation site can be seen quite clearly at the tensile surface of the wire in the centre of a semi-circular shaped feature which shows the shape in which the fatigue crack grew.

7. Results and Discussion (Fatigue Testing)

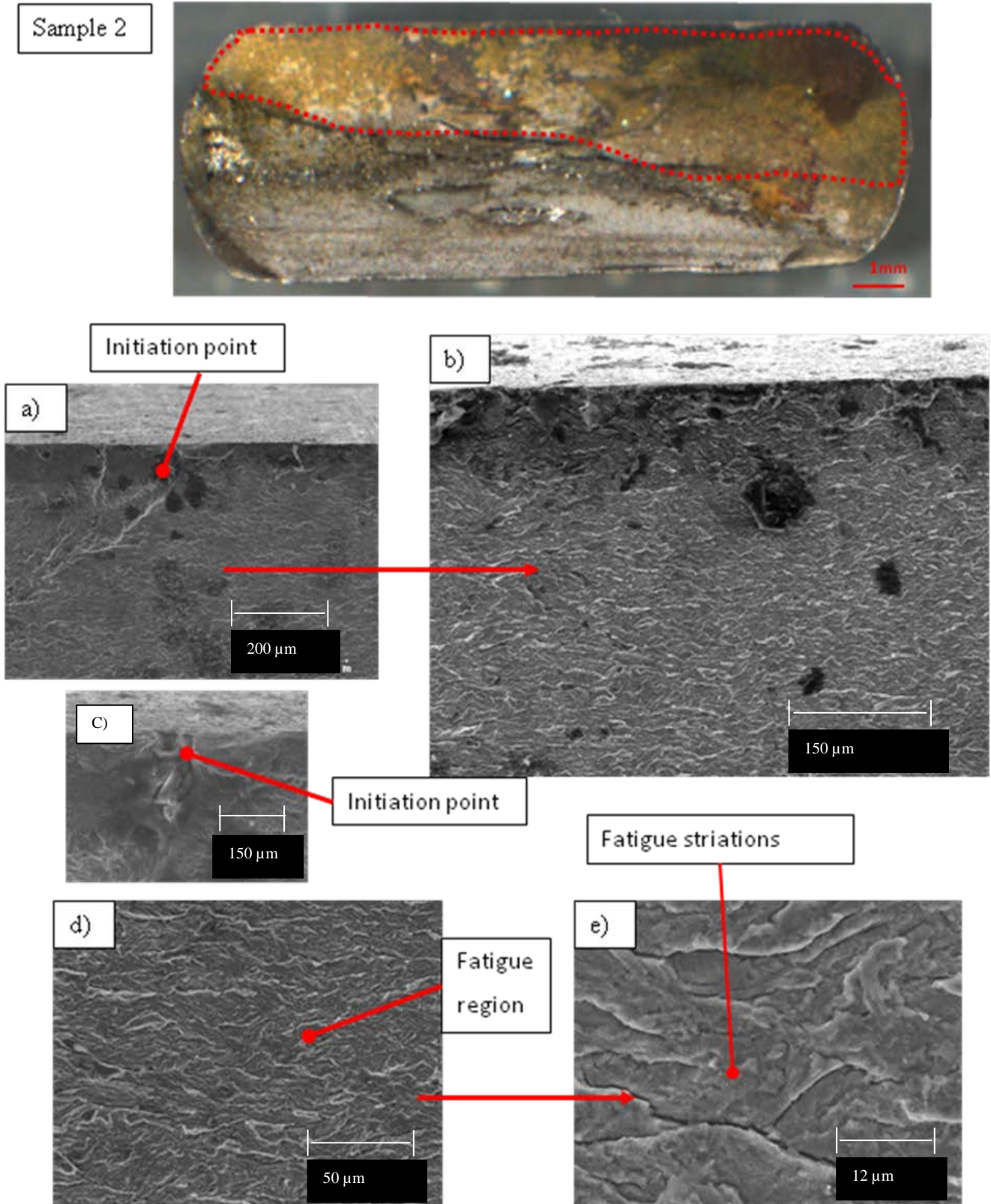


Figure 7-71 – SEM fractographs for sample 02 from the HPCF qualification test series.

7. Results and Discussion (Fatigue Testing)

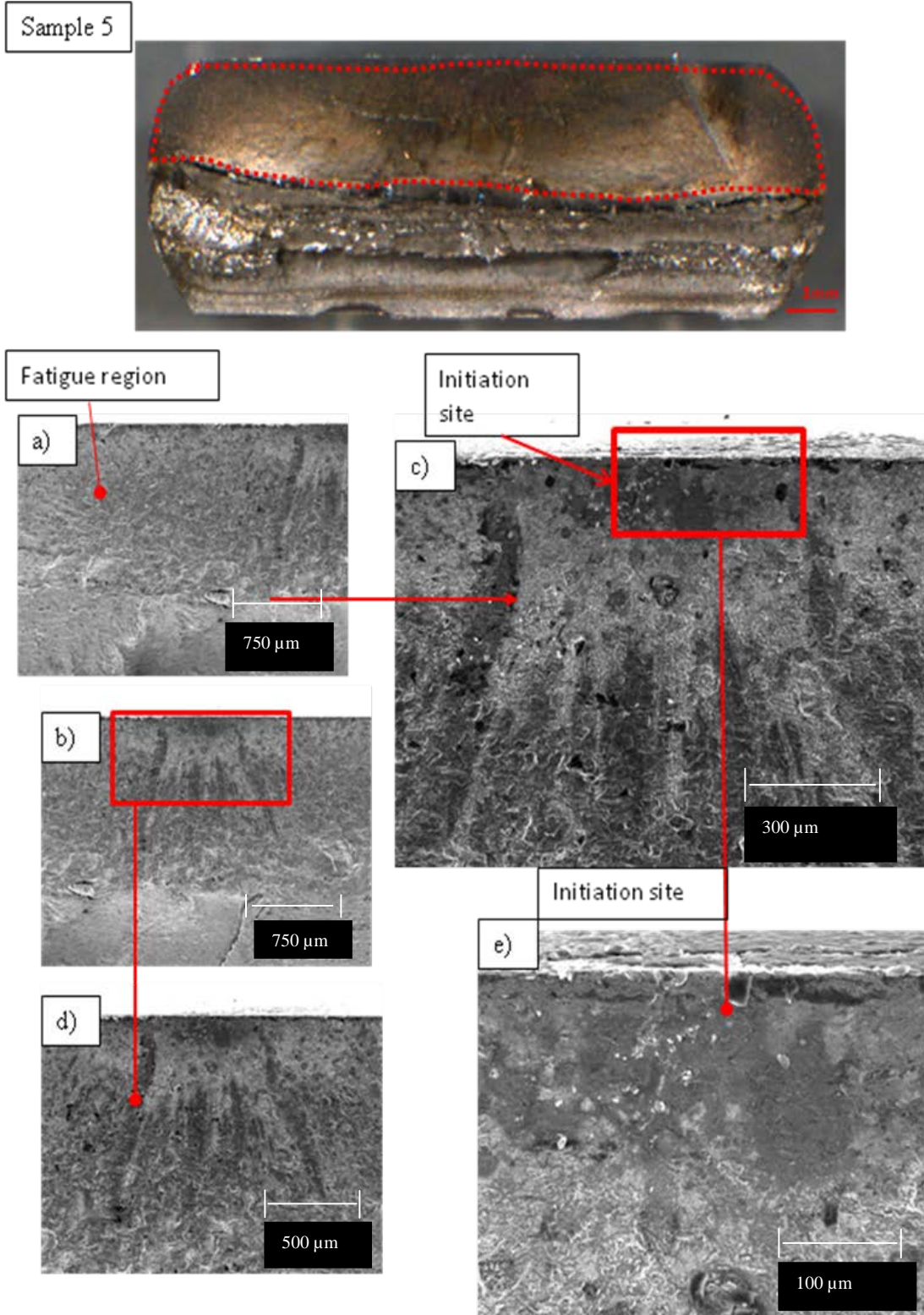


Figure 7-72 – SEM fractographs for sample 05 from the HPCF qualification test series.

7. Results and Discussion (Fatigue Testing)

7.2.3.2 Elevated Pressure CO₂ with Trace Amounts of H₂S (7.08bar CO₂/0.15mbar H₂S) – Wire-1

Measurements of the test samples from the elevated pressure test series are given in Table 7-14. This test series was conducted on Wire-1 with a constant mean stress of 400 MPa.

Table 7-14 – Sample measurements from the elevated pressure test series on Wire-1.

Exova ID	Width (mm)				Thickness (mm)			
	1	2	3	avg	1	2	3	avg
HP-01	14.07	14.08	14.07	14.07	6.04	6.04	6.04	6.04
HP-02	14.05	14.06	14.08	14.06	6.03	6.02	6.03	6.03
HP-03	14.06	14.05	14.03	14.05	6.02	6.04	6.02	6.03
HP-04	14.04	14.04	14.05	14.04	6.04	6.02	6.01	6.02
HP-05	14.07	14.07	14.07	14.07	6.04	6.05	6.04	6.04
HP-06	14.06	14.06	14.05	14.06	6.03	6.04	6.03	6.03
HP-07	14.07	14.04	14.05	14.05	6.04	6.04	6.03	6.04
HP-08	14.06	14.06	14.05	14.06	6.03	6.04	6.04	6.04
HP-09	14.06	14.07	14.06	14.06	6.04	6.03	6.03	6.03
HP-10	14.05	14.05	14.06	14.05	6.05	6.05	6.04	6.05
HP-11	14.05	14.07	14.05	14.06	6.03	6.04	6.04	6.04
HP-12	14.05	14.06	14.05	14.05	6.04	6.04	6.03	6.04
HP-13	14.02	14.04	14.05	14.04	6.03	6.03	6.03	6.03
HP-14	14.04	14.05	14.07	14.05	6.04	6.05	6.04	6.04
HP-15	14.07	14.08	14.05	14.07	6.03	6.04	6.03	6.03
HP-16	14.06	14.07	14.07	14.07	6.05	6.04	6.04	6.04
HP-17	14.04	14.05	14.03	14.04	6.05	6.04	6.05	6.05

Table 7-15 outlines the test results for this test series along with other data from this phase of testing. This test phase was conducted at a constant mean stress of 400 MPa so that the loading is consistent with the air fatigue test series and the CO₂ test series on this same grade of wire (Wire-1).

7. Results and Discussion (Fatigue Testing)

Table 7-15 – (Top) Test results from the elevated pressure test series. (Bottom) pH measurements from this test series.

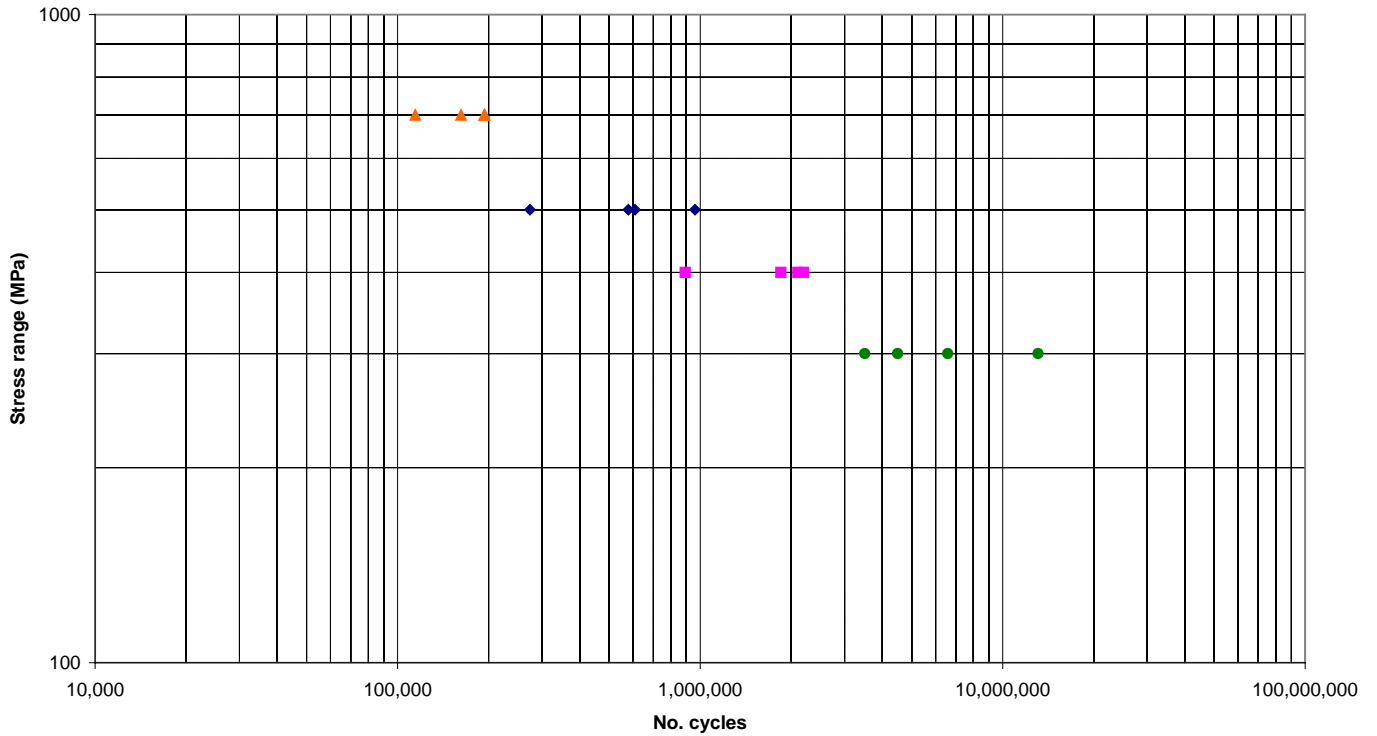
Exova ID	Steel Grade	Size (mm ²)	Curve	H2S in mbar	CO2 in bar	Mean Stress (MPa)	Stress Range (MPa)	No. cycles to rupture	Comments
HP-01	Wire 1	14 x 6	Elevated Pressure Test Series	0.15	7.08	400	500	273,891	Valid rupture within constant stress area
HP-02								609,048	Valid rupture within constant stress area
HP-03								961,444	Valid rupture within constant stress area
HP-04								578,827	Valid rupture within constant stress area
HP-05							400	2,197,048	Valid rupture within constant stress area
HP-06								2,104,329	Valid rupture within constant stress area
HP-07								892,840	Valid rupture within constant stress area
HP-08							1,848,110	Valid rupture within constant stress area	
HP-09							700	114,422	Valid rupture within constant stress area / High pH value
HP-10								193,986	Valid rupture within constant stress area
HP-11								N/A	sample damaged during setup (replaced with HP-17)
HP-12								193,328	Valid rupture within constant stress area
HP-13							162,019	Valid rupture within constant stress area	
HP-14							300	13,103,603	Valid rupture within constant stress area
HP-15								6,581,324	Valid rupture within constant stress area
HP-16								3,500,000	Valid rupture within constant stress area
HP-17								4,494,797	Valid rupture within constant stress area

Sample ID	Stress range (MPa)	Cycles to rupture	pH measurements			
			Start (after 4 days pre-exp)		End of Test	
			Test Pressure	Ambient	Test Pressure	Ambient
HP - 01	500	273,891	5.70	6.04	5.73	6.06
HP - 02		609,048	5.73	6.06	5.78	5.93
HP - 03		961,444	5.82	6.05	n/a	n/a
HP - 04		578,827	n/a	n/a	n/a	n/a
HP - 05	400	2,197,048	5.68	5.80	5.42	5.64
HP - 06		2,104,329	5.59	5.94	5.01	5.61
HP - 07		892,840	5.88	6.03	5.69	5.92
HP - 08		1,848,110	5.64	6.07	5.34	6.01
HP - 09	700	114,422	6.32	6.41	6.35	6.41
HP - 10		193,986	5.83	6.39	5.85	6.35
HP - 11		N/A	n/a	n/a	n/a	n/a
HP - 12		193,328	5.80	6.76	5.83	6.47
HP - 13	162,019	5.91	6.75	5.76	6.49	
HP - 14	300	13,103,603	5.89	6.50	5.26	5.88
HP - 15		6,581,324	5.80	6.29	5.28	5.98
HP - 16		3,500,000	5.58	6.03	5.71	6.00
HP - 17		4,494,797	5.60	5.85	5.54	6.12

Figure 7-73 displays these results in the form of SN plots. The first graph in this figure plots the raw data from this test series whilst the second graph plots a mean curve with +/- two standard deviations design curve.

7. Results and Discussion (Fatigue Testing)

Elevated Pressure Test Series - 7.08bar CO₂/0.15mbar H₂S



Elevated Pressure Test Series - 7.08bar CO₂/0.15mbar H₂S (free slope)

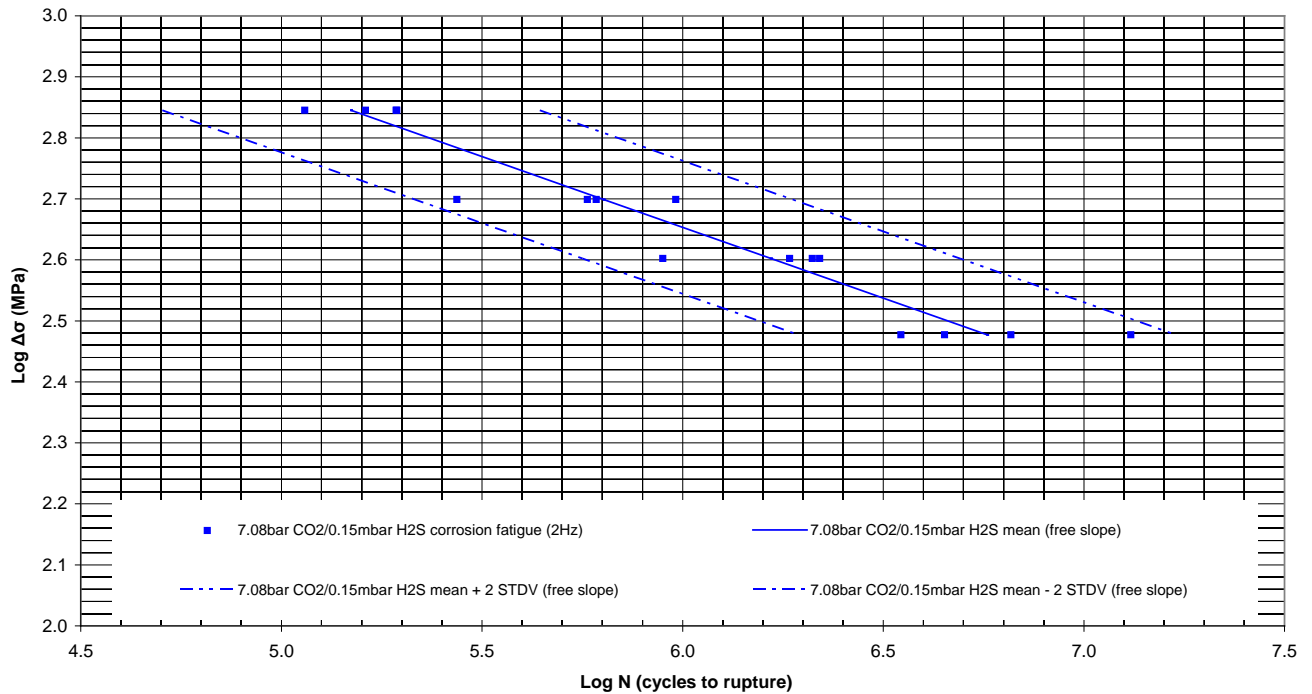


Figure 7-73 Test results from the elevated pressure test series. SN plot displaying the elevated pressure test series data. Test frequency for this test series is 2Hz.

7. Results and Discussion (Fatigue Testing)

Figure 7-74 superimposes the results of the air fatigue test series for Wire-1. This comparison of SN curves clearly demonstrates the effect of testing in a corrosive environment on fatigue life, as compared to data generated in lab air. It can be observed that in the elevated pressure test series there are failures at stress levels well below the lab air endurance limit which can be attributed to the action of the corrosive environment. There is also a reduction in fatigue life in finite life region when testing is conducted in the corrosive environment.

Elevated Pressure Test Series - 7.08bar CO₂/0.15mbar H₂S Vs Air Curve (4 Point Bend)

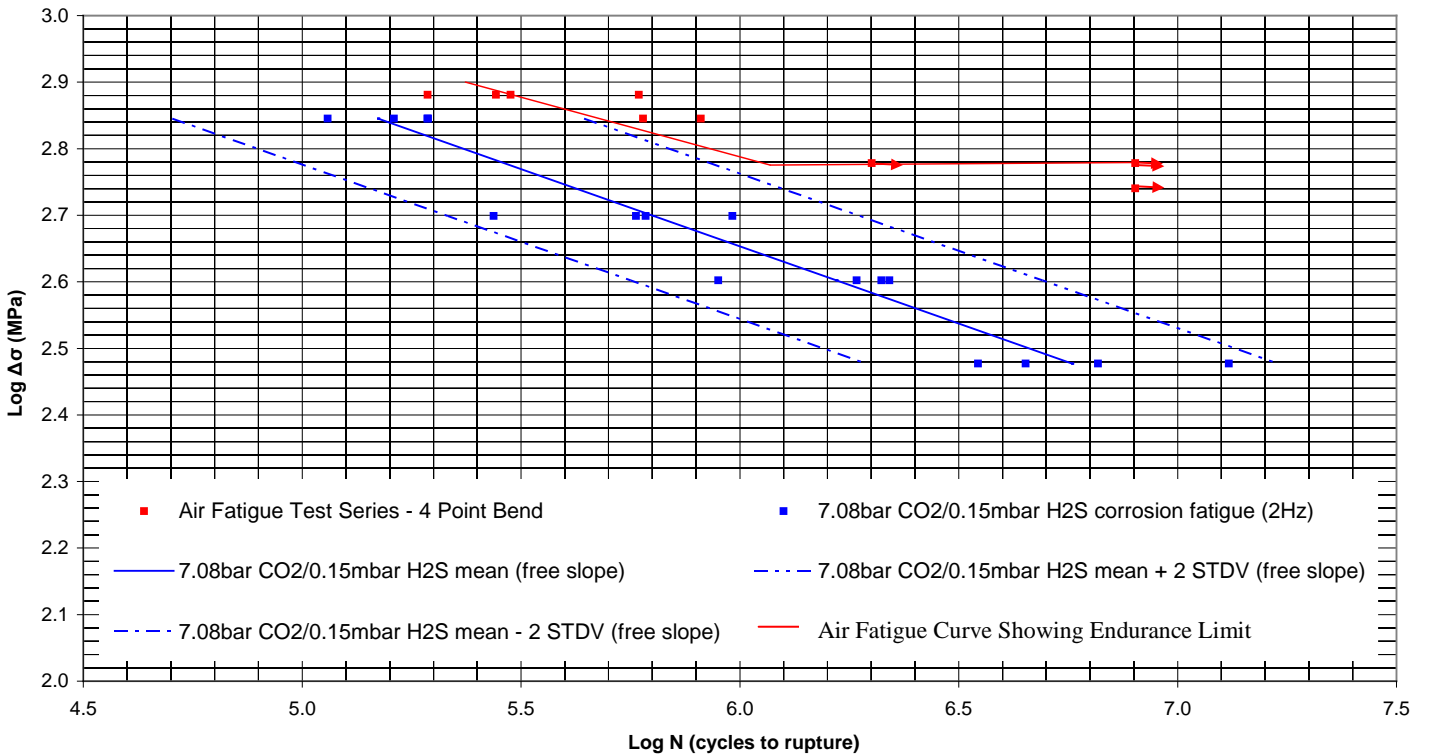


Figure 7-74 Test results from the elevated pressure test series. SN plot displaying the elevated pressure test series data compared to data generated in air. Note the reduction in fatigue life in the finite life region and the elimination of the endurance limit caused by the corrosive environment. (Arrows indicate runouts)

7. Results and Discussion (Fatigue Testing)

Figure 7-75 shows an interesting comparison of the elevated pressure test series data and data from the CO₂ test series generated at atmospheric pressure (1 bar CO₂ confined).

Elevated Pressure Test Series - 7.08bar CO₂/0.15mbar H₂S Vs 1bar CO₂ test Series (confined)

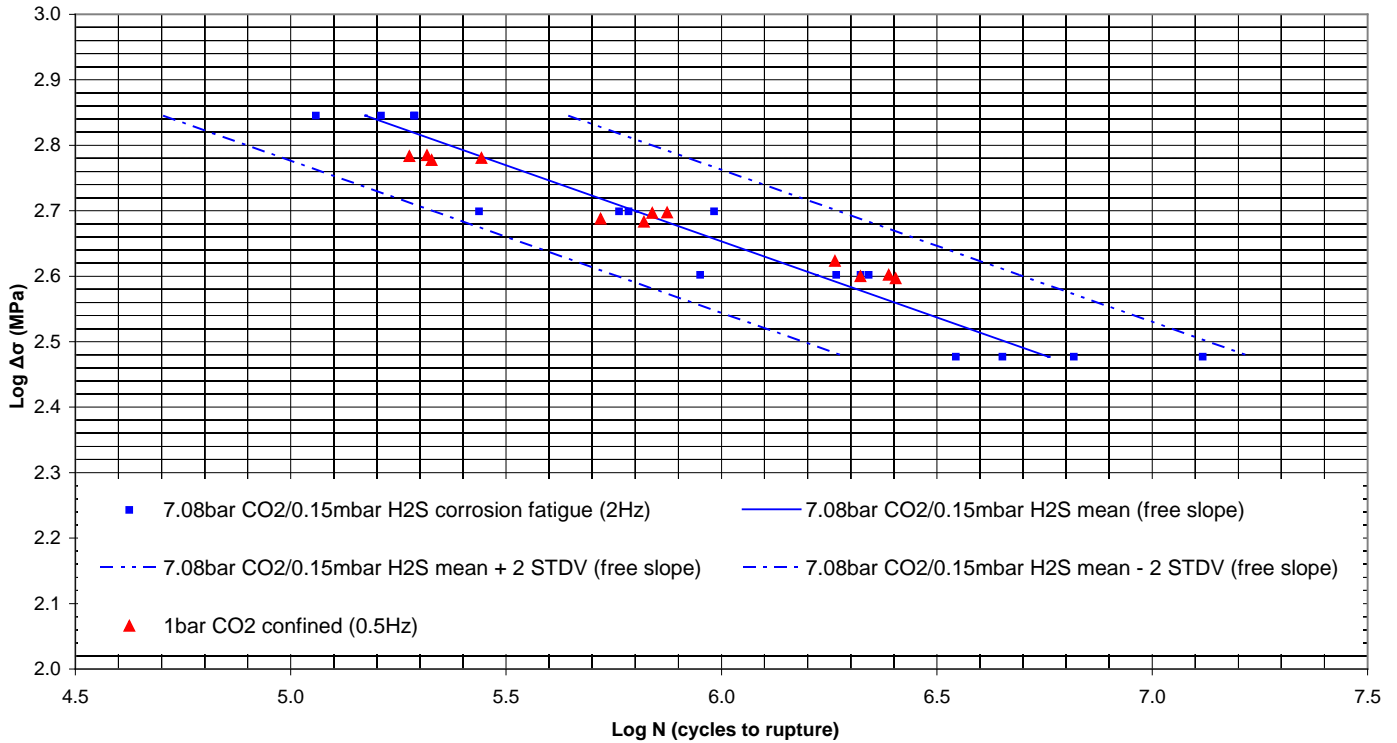


Figure 7-75 Test results from the elevated pressure test series. SN plot displaying the elevated pressure test series data compared to data generated at atmospheric pressure (1bar CO₂) under confined conditions. It must be noted that the 1bar CO₂ data was generated at 0.5Hz compared to 2Hz for the elevated pressure test series.

Both datasets are generated from the same material (Wire-1) and both are under confined test conditions. It is important to note that the atmospheric pressure testing (1bar CO₂) was generated at a frequency of 0.5Hz compared to 2Hz in the case of the elevated pressure test series. When plotted against one another the two datasets are very similar with all of the data points from the CO₂ test series located close to the mean curve of the

7. Results and Discussion (Fatigue Testing)

elevated pressure test series. This indicates that the more severe environmental conditions of the elevated pressure test series are not significantly affecting fatigue life compared to the CO₂ test series at atmospheric pressure and that both of these simulated oilfield conditions have a similar effect on fatigue life compared to data generated in lab air.

This is an important result and a major finding of this thesis. The results of the elevated pressure test series show that at this particular pressure and pH₂S with this grade of armour wire, the fatigue life is comparable to that of 1bar CO₂ conditions. This indicates that for this grade of wire a pH₂S of ≤ 0.15 mbar does not have an effect on fatigue life, which in turn suggests that the flux of hydrogen into the steel matrix is still below a critical level to cause an embrittling effect which would result in reduced fatigue life compared to a CO₂ only test environment. Further work should aim to increase the pH₂S level incrementally until an effect on fatigue life is observed. At this pH₂S the flux of hydrogen into the material will have reached a critical level in terms of having an embrittling effect on the steel.

Corrosion rates have been shown to be decreased under CO₂ corrosion conditions with trace amounts of H₂S [18,19] and with the exception of sample HP15 the corrosion damage observed was generally no more severe than that in the 1bar CO₂ testing, which indicates that increasing CO₂ pressure to 7.08 bar has little overall effect on the extent of corrosion. This could also have contributed to the similar fatigue life observed in the HPCF test series and the CO₂ test series.

7. Results and Discussion (Fatigue Testing)

The following Figures show the fracture faces of the samples from this test series where evidence of multiple crack initiation can be found. Post test investigation revealed evidence of multiple crack initiation and secondary cracking along the length of the constant stress area on some of the tested samples; Figure 7-80 as an example.

Sectioning and SEM analysis of samples from this test series was restricted for the current research project due this curve being included in an ongoing commercial test program. It is clear from Figure 7-80 that the tensile face would have shown significant corrosion and subsequent cracking similar to that seen in the other CF testing environments.

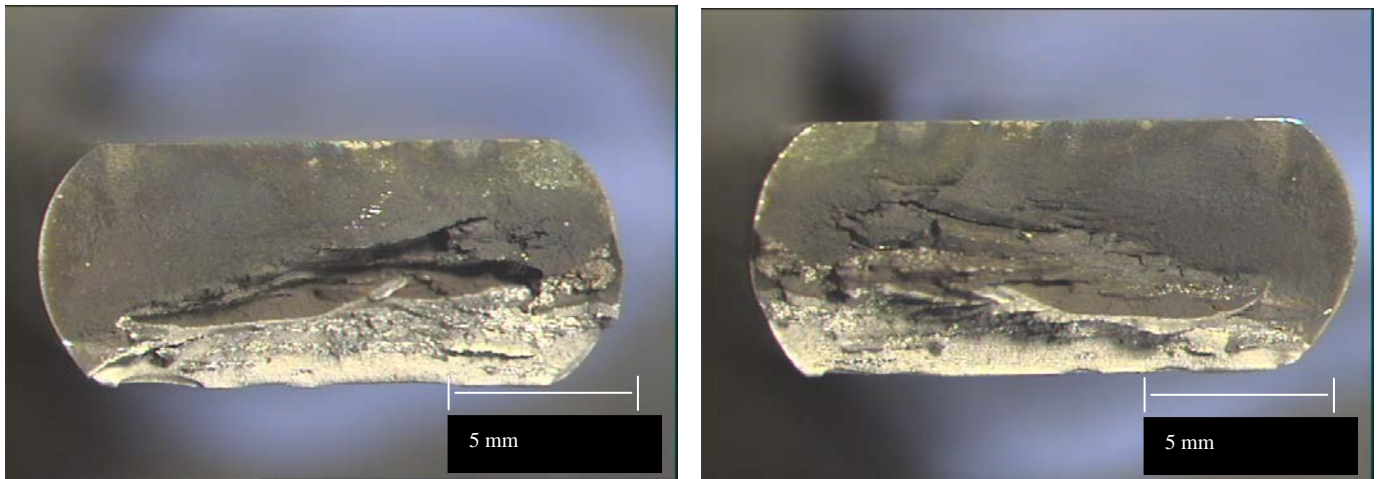


Figure 7-76 Fracture faces from the elevated pressure test series. Sample HP1 – 273,891 cycles

7. Results and Discussion (Fatigue Testing)

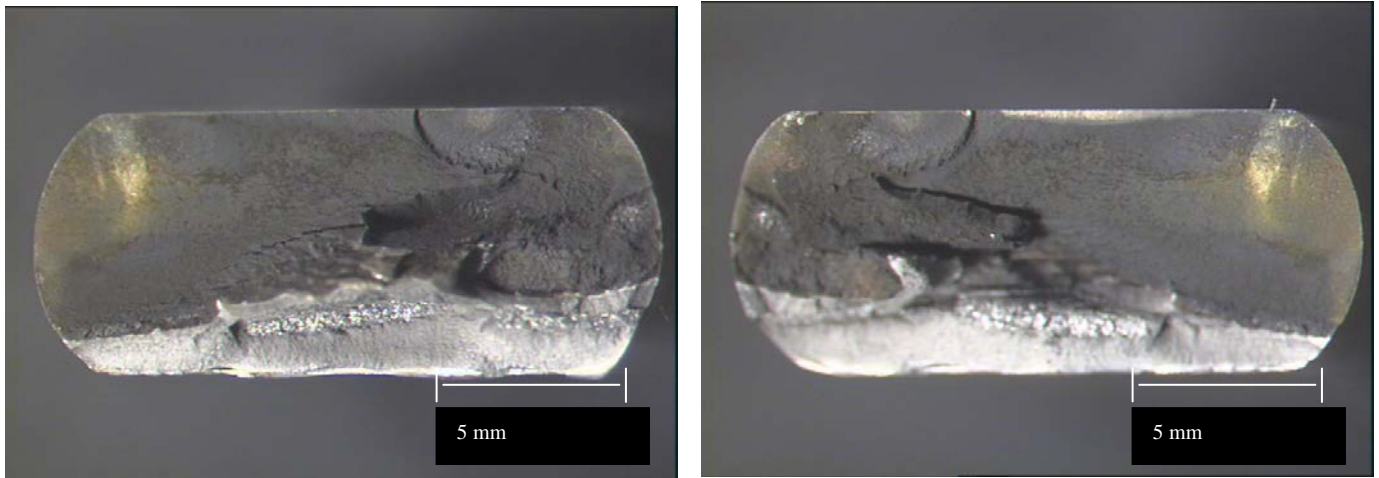


Figure 7-77 Fracture faces from the elevated pressure test series. Sample HP5 – 2,147,048 cycles

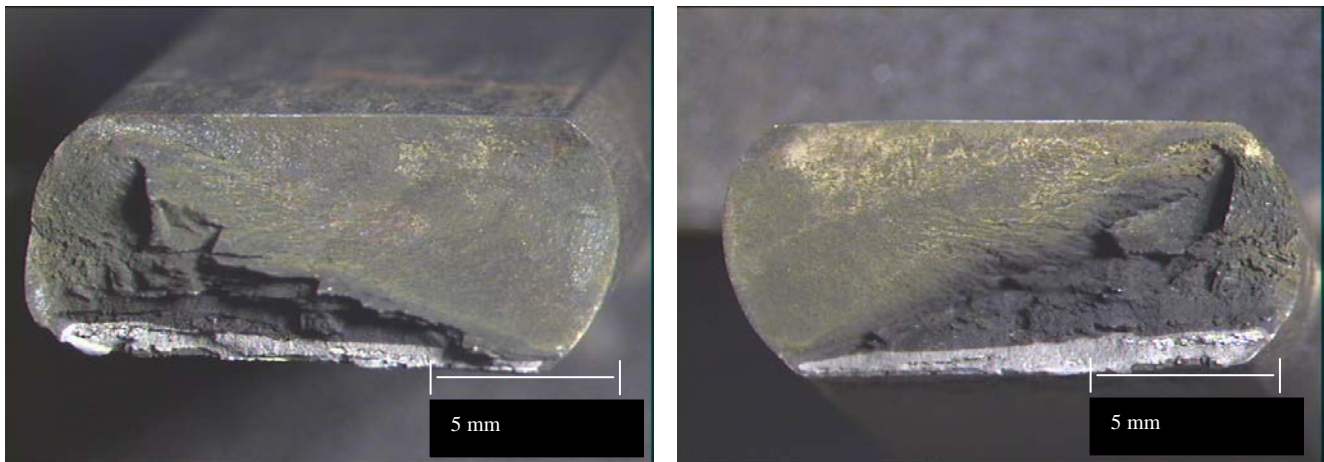


Figure 7-78 Fracture faces from the elevated pressure test series. Sample HP6 – 2,104,329 cycles

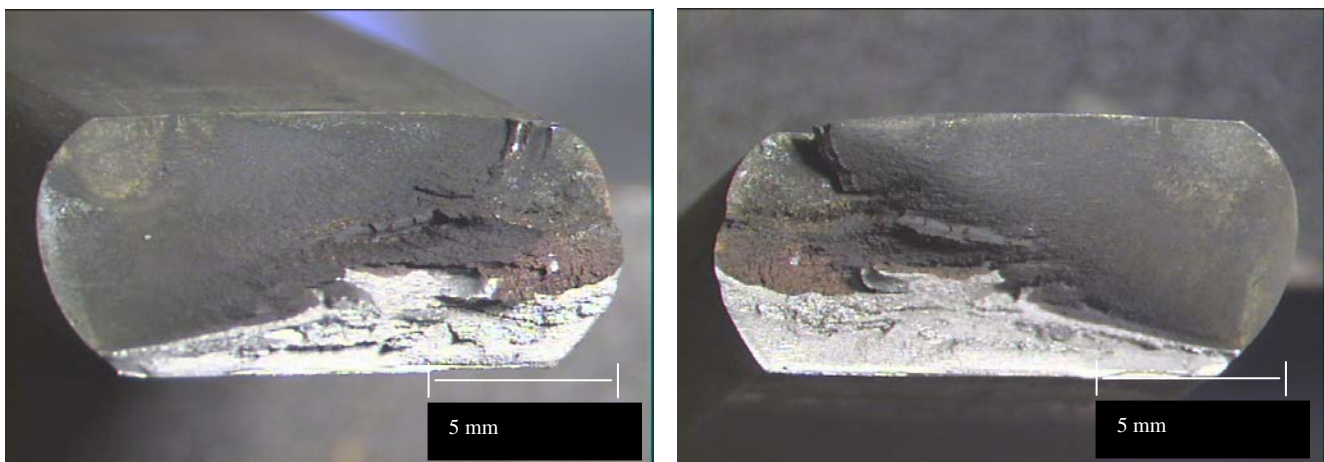


Figure 7-79 Fracture faces from the elevated pressure test series. Sample HP7 – 892,840 cycles

7. Results and Discussion (Fatigue Testing)

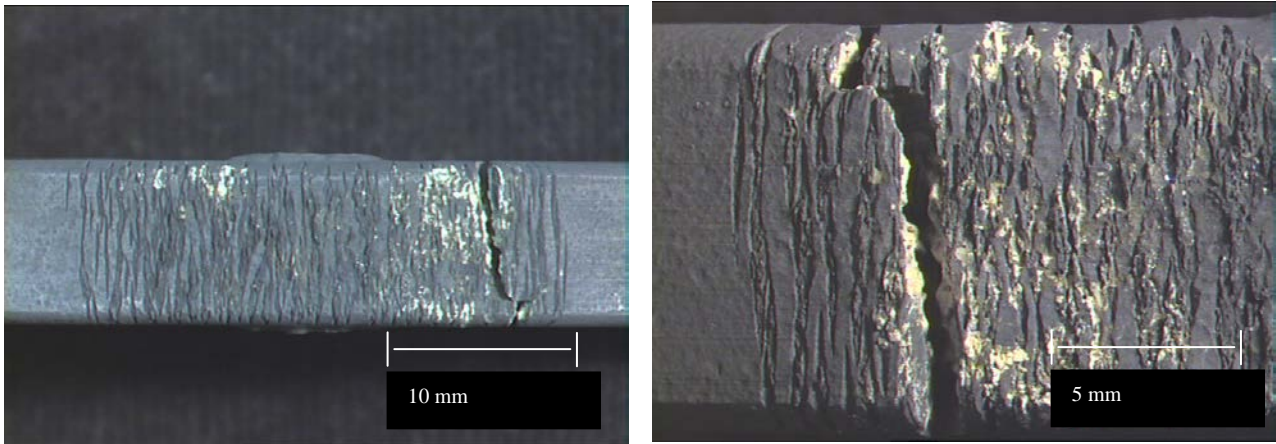


Figure 7-80 Tensile surface within the constant stress area, showing severe secondary cracking. Sample HP15 – 6,581,324 cycles

8. Summary and Conclusions

8. Summary and Conclusions

In order to summarize the current research project it is helpful to revisit the aims and objectives that this project set out to achieve. The first major objective in Phase I was to develop the testing facilities in order to carry out corrosion fatigue testing on tensile armour wire components of flexible Oil and Gas pipelines. Once this milestone was reached the next objective was to develop a repeatable corrosion fatigue test procedure which met all of the requirements of testing in such a specific corrosive environment. Following successful pilot testing to validate the data being generated, the third aim of the project was now possible, which was to investigate the corrosion fatigue behaviour of tensile armour wires via SN experiments in simulated oilfield environments. This has been achieved via investigations into the effect of testing in artificial seawater saturated with 1 bar CO₂ compared to in air data, confinement investigations, investigations of the effect of test frequency and the effect of using welded test pieces.

All of the testing mentioned above in Phase I was conducted at atmospheric pressure and some of it was completed for the flexible pipeline manufacturers (Exovas client). This has sometimes restricted the research aspect of the project since the test conditions have often been driven by client project work which has restricted machine time availability somewhat. The positive aspect of completing successful testing programmes for client driven projects was that it led to a big development in the current research project (Phase II), which was high pressure corrosion fatigue testing (HPCF). Phase II of the current research project wasn't an initial objective, but was driven by strong demand from the

8. Summary and Conclusions

flexible Oil and Gas pipeline manufacturers. With a good track record of corrosion fatigue testing at atmospheric pressure via the current research project Exova secured a large testing contract consisting of several years' worth of work. This represented the natural, industry driven progression for this EngD thesis and the process of test machine development and test procedure development started again, this time for elevated pressure corrosion fatigue testing. This multi-million pound investment culminated with the installation of a unique state of the art HPCF facility which houses 8-12 bespoke test machines. One test environment/SN curve from the HPCF test machines is included in the current research project (Section 7.2.3.2). This is a major achievement for the current research project and the data generated can be regarded as novel and has made a significant contribution to the technological advancement of flexible Oil and Gas pipelines.

Conclusions

1. Corrosion fatigue testing equipment has been developed for use at atmospheric and elevated pressures with the capability of commercially testing tensile armour wire components from flexible Oil and Gas pipelines (Sections 6.1 and 6.2).
2. A test method for the corrosion fatigue testing of tensile armour wires at atmospheric and elevated test pressures has been successfully developed to meet the requirements of the oil and gas industry and is now offered as a commercial testing service by Exova (Sections 5.3 and 5.4).

8. Summary and Conclusions

3. Investigations into the chemistry of confined annulus environments reveal that pH is higher than in unconfined conditions and test solutions are saturated with Fe^{2+} (Section 6.1.7).

4. Fatigue testing results in-air are sensitive to test configuration due to a shift in initiation point. Data generated in axial tension should be treated as conservative when testing as received samples due to initiation from the less fatigue resistant drawn edge of the wire. Four point bend data generated in air provide a more accurate comparison with four point bend corrosion fatigue data where any effect of test configuration is removed resulting in a like for like comparison (Section 7.2.1.1).

5. High strength steel armour wires tested in deaerated artificial seawater saturated with 1bara CO_2 exhibit failures beyond the in air endurance limit. The effects of the corrosive environment are evident with failures in excess of 10^6 cycles indicating the removal of an endurance limit under corrosive conditions. This reduction in fatigue life can be attributed to surface corrosion phenomenon caused by exposure to the environment and subsequent cracking from such phenomenon (Sections 7.2.2.1 and 7.2.2.2).

8. Summary and Conclusions

6. With the same grade of wire a confined environment appears to provide a modest increase in fatigue life compared to testing at a lower pH and without Fe^{2+} saturation under unconfined conditions (Section 7.2.2.3).
7. Investigation of the frequency effect revealed that despite a small increase in mean life when testing at 2Hz the standard deviation scatter bands were largely overlapping indicating that testing at 2Hz provided realistic results relative to testing at 0.5Hz, at least at the stress ranges tested in this thesis. Testing out to longer lives at 0.5Hz is needed to be more conclusive; however this was beyond the time constraints of the current research project since only one test machine was available (Section 7.2.2.4).
8. Testing a welded, as-received sample under the same conditions as a parent sample leads to a significant reduction in fatigue life. This can be attributed to the geometrical variations around the welded section leading to local stress concentrations (Section 7.2.2.5).
9. Testing at elevated pressure and with a small partial pressure of H_2S (7.08bar CO_2 /0.15mbar H_2S) appears to have no significant effect on fatigue life compared to testing at 1bar CO_2 . Both environments induce a similar effect on fatigue life compared to that seen in air (Section 7.2.3.2).

9. Further Work

Starting in May 2011 the author has been awarded a Knowledge Transfer Secondment (KTS) Research Fellowship (May 2011-April 2012) by the Engineering and Physical Sciences Research Council (EPSRC). During this research fellowship the author will be seconded to Exova with aim of expanding the corrosion fatigue facilities that were developed as part of this EngD thesis. Furthermore, this research fellowship will provide the opportunity to carry out relevant further work outlined below to supplement the results and discussion presented in this thesis.

1. To extend the frequency investigation trials out to longer fatigue lives i.e. $>10^7$ cycles at 0.5 Hz to ensure that fatigue testing at 2Hz isn't overly unconservative. This was not possible for the present thesis since 10^7 cycles at 0.5 Hz would take 231 days and with only one test rig this was not feasible.
2. To investigate the effect of the addition of different partial pressures of H₂S at atmospheric pressure on fatigue life. Incrementally increasing the partial pressure of H₂S until a threshold is reached where there is a marked effect on fatigue life.
3. To investigate the effect of increased partial pressures of H₂S at elevated pressure to that presented in this dissertation (section 7.2.3.2). Incrementally

9. Further Work

increasing the partial pressure of H₂S until a threshold is reached where there is a marked effect on fatigue life over and above that seen in the purely CO₂ environment. [Planned to be performed July 2011 onwards – testing in an environment with a 7 fold increase in p_{H₂S} to that presented in this thesis. p_{H₂S} of 1.03mbar, total system pressure of 5.4bar CO₂ with a gas mix of 200ppm H₂S.]

4. Conduct hydrogen melt extract measurements on coupons exposed to the above environments to link increased H₂S partial pressures with increased hydrogen uptake in the steel. The partial pressure at which uptake is significantly increased should also show signs of embrittlement via a reduction in fatigue life.

10. Acknowledgements

10. Acknowledgements

The author would like to acknowledge the advice and guidance of project supervisors Dr. B.J. Connolly (University of Birmingham) and Dr. C.M. Fowler (Exova). Author also wishes to thank Dr. C. Cooper of the University of Birmingham, Mr. P. Dent & Mr. O. Ravier along with all other colleagues at Exova Corrosion Centre and Exova Daventry Engineering & Technology. Thanks to Mr. R. Clements of Wellstream International Ltd and Mr. N. Desamais of Technip Flexi-France for their helpful discussions and issue of test materials.

Author also greatly acknowledges the support received from the EPSRC and Exova Ltd for the funding of this work. The author would also like to thank The School of Metallurgy and Materials, University of Birmingham, for the provision of research facilities and management of the EngD programme. The author would also like to thank the Nace Foundation and Nace Great Britain (UK Section) for the provision of travel assistance to attend the Corrosion 2010 conference in San Antonio, Texas.

11. References

11. References

¹ Berge, S., Clements, R., Bendiksen, E., Gudme, J. *Corrosion Fatigue Testing of Flexible Riser Armor, Procedures for Testing and Assessment of Design Criteria*, Proceedings of OMAE 2003, paper 37327, Cancun

² Clements, R. *Corrosion Assessment Prediction for a confined Flexible Pipe Annulus*, EuroCorr 2008

³ Z. Benjelloun-Dabaghi et al, *MOLDI: A fluid Permeation Model To Calculate the Annulus Composition in Flexible Pipes*, Oil and Gas Science Technology, Vol 57 (2002), pp. 177-192

⁴ Rubin, A., Gudme, J. *Qualification of Steel Wire for Flexible Pipes*. NACE Int. Conf. 2006, Paper 06149

⁵ Ropital, F., Taravel-Condat, C., Saas, J.N., Duret, C. *Methodology to study the General Corrosion of Steel Armors in Simulated Conditions of Flexible Pipe Annulus – Influence of Confinement and Evaluation of the pH*. EuroCorr (2000).

⁶ C. Taravel Condat, N. Desamais, *Qualification of High Strength Carbon Steel Wires for use in Specific Annulus Environment of Flexible Pipes containing CO₂ and H₂S*, OMAE 2006, paper No 92394

⁷ S. Berge, N. Langhelle, T. Gunnar Eggen, *Environmental Effects on Fatigue Strength of Armour Wire for Flexible Risers*, OMAE 2009, Paper No 80262

⁸ Taylor, T.S., Joosten, M.W and Smith, F. (2002). *Technical Solutions applied for the treatment of damaged Dynamic Risers*. Proc. Int. Conf. OMAE, Paper 28371, Oslo

⁹ NACE MR0175/ISO 15156, Petroleum and Natural Gas Industries – Materials for use in H₂S Containing Environments in Oil and Gas Production, first edition (2001/2002)

¹⁰ Lamb, S., *CASTI Handbook of Stainless Steels & Nickel Alloys*. Second ed. 2003: CASTI Publishing Inc.

¹¹ European Federation of Corrosion, Pub number 16, Guidelines for Material Requirements for Carbon and Low Alloy Steels for H₂S containing environments in oil and gas production (1995)

¹² Embury JD, Fisher RM. *The structure and properties of drawn pearlite*. Acta Metall 1966; 14:147-59

¹³ Toribio J, Ovejero E. *Microstructure evolution in a pearlitic steel subjected to progressive plastic deformation*, Material Sci Eng 1997;A234-236:579-82

¹⁴ Toribio J, Ovejero E. *Effect of cold drawing on microstructure and corrosion performance of high strength steel*. Mechanics of Time Dependant Materials, 1998, 1, 307-19

¹⁵ Toribio J, Ovejero E. *Failure analysis of cold drawn prestressing steel wires subjected to stress corrosion cracking*. Engineering Failure Analysis, 2005, 12, 654-661.

¹⁶ Underwood, NJ. *Corrosion Testing of Reinforcement in simulated annulus environments of flexible pipelines*, OMAE 2002, 28098

¹⁷ Clements, R. Etheridge A. *Corrosion testing of armour wire in simulated annulus environments of flexible pipelines – an update*. OMAE 2003 37473

11. References

- ¹⁸ Bijan Kermani, John Martin, Khlefa Esaklul, *Materials Design Strategy: Effects of H₂S/CO₂ Corrosion on Materials Selection*, NACE 2006, Paper 06121
- ¹⁹ **Bruce Brown, Shilpha Reddy Parakala, Srdjan Nestic, CO₂ Corrosion in the Presence of Trace Amounts of H₂S, NACE 2004, Paper 04736**
- ²⁰ C. de Waard and D. E. Milliams, *Carbonic Acid Corrosion of Steel*, *Corrosion*, 1975, 31, 131
- ²¹ A. Dugstad, *Formation of protective Corrosion Films during CO₂ Corrosion of Carbon Steel*, *Eurocorr* 97, vol 1, 15-20
- ²² W. Sun and S. Nestic, *Basics Revisited – Kinetics of Iron Carbonate Scale Precipitation in CO₂ Corrosion*, NACE 2006, Paper 06365
- ²³ A. Ikeda, M. Ueda and S. Mukai, *CO₂ corrosion Behaviour and Mechanism of Carbon and Alloy Steel*, *Corrosion*, 1983, Paper 45, Houston Texas, Nace (1983)
- ²⁴ A. Munoz and J. Genesca, *Mechanism of FeCO₃ formation on API X70 Steel in Brine Solutions Containing CO₂*, NACE 2005, Paper 05297
- ²⁵ European Federation of Corrosion Publications – Number 23, *CO₂ Corrosion Control in Oil and Gas Production – Design Considerations* (1997)
- ²⁶ G. Schmitt, T. Gudde and E. Strobel-Effertz, *Fracture mechanical properties of CO₂ Corrosion Product Scales and their Relation to Localised Corrosion*, *Corrosion* 96, Paper 96006, NACE 1996
- ²⁷ A. Dugstad, *The Importance of FeCO₃ supersaturation on the CO₂ corrosion of Carbon Steels*, *Corrosion* 92, Paper 14, NACE 1992
- ²⁸ W. Sun and S. Nestic, *Kinetics of Iron Sulphide and mixed Iron Sulphide/Carbonate Scale Precipitation in CO₂/H₂S Corrosion*, NACE 2006, paper 06644
- ²⁹ A. Ikeda, M. Ueda and S. Mukai, *Influence of Environmental Factors on Corrosion in a CO₂ Source Well*. NACE, 1985, paper 29
- ³⁰ Shreir, R.A., R.A. Jarman, and G.T. Burstein, *Corrosion - Metal/Environment Reactions*. Third ed. 1994.
- ³¹ Jones, R.H., *Stress Corrosion Cracking - Materials Performance and Evaluation*. 1992: ASM International.
- ³² Champion, F.A., *Symposium on Internal Stresses in Metals and Alloys*, 1948: p. 468.
- ³³ Logan, H.L., *Film rupture mechanism of stress corrosion*. United States Bureau of Standards -- Journal of Research, 1952. 48(2): p. 99-105.
- ³⁴ Swann, P.R., *Dislocation substructure vs transgranular stress corrosion susceptibility of single phase alloys*. *Corrosion*, 1963. 19(3): p. 102-112.
- ³⁵ Smith, T.J. and R.W. Staehle, *Role of slip step emergence in early stages of stress corrosion cracking in face centered iron-nickel-chromium alloys*. *Corrosion*, 1967. 23(5): p. 117-129.
- ³⁶ Vermilyea, D.A. *A Film Rupture Model for Stress Corrosion Cracking*. in *Stress Corrosion Cracking and Hydrogen Embrittlement of Iron Base Alloys*. 1973. Unieux-Firminy, France: NACE.
-

11. References

- ³⁷ Scully, J.C., *Stress corrosion crack propagation: A constant charge criterion*. Corrosion Science, 1975. 15(4): p. 207-24.
- ³⁸ Turnbull, A., *Modelling of environment assisted cracking*. Corrosion Science, 1993. 34(6): p. 921-960.
- ³⁹ Andresen, P.L. and T.M. Angeliu. *Evaluation of the role of hydrogen in SCC in hot water*. Corrosion NACE. 1997.
- ⁴⁰ Lynch, S.P., *Environmentally assisted cracking: overview of evidence for an adsorption-induced localised-slip process*. Acta Metallurgica, 1988. 36(10): p. 2639-61.
- ⁴¹ Lynch, S.P., *Cleavage fracture in face-centred cubic metals*. Metal Science, 1981. 15(10): p. 463-7.
- ⁴² Pugh, E.N., *A post conference evaluation of our understanding of the failure mechanisms*. International Corrosion Conference Series, 1977. NACE-5(Stress Corros. Cracking Hydrogen Embrittlement Iron Base Alloys): p. 37-51.
- ⁴³ Uhlig, H.H., *New perspectives in the stress corrosion problem*. Metallurgical Society Conferences [Proceedings], 1959. 4: p. 1-17.
- ⁴⁴ Stoloff, N.S., *Recent developments in liquid-metal embrittlement*. Environ.-Sensitive Fract. Eng. Mater., Proc. Symp., 1979: p. 486-518.
- ⁴⁵ Uhlig, H.H. *Stress Sorption Cracking and the Critical Potential. Stress Corrosion Cracking and Hydrogen Embrittlement of Iron Base Alloys*. 1973. Unieux-Firminy, France: NACE.
- ⁴⁶ Sieradzki, K. and R.C. Newman, *Brittle behaviour of ductile metals during stress-corrosion cracking*. Philosophical Magazine A (Physics of Condensed Matter, Defects and Mechanical Properties), 1985. 51(1): p. 95-132.
- ⁴⁷ Gerhardus, H.K., *Stress-Corrosion Cracking and Hydrogen Embrittlement*, in *ASM Handbook*, S.R. Lampman, Editor. 1996, ASM International.
- ⁴⁸ Jones, R.H., *Stress Corrosion Cracking - Materials Performance and Evaluation*. 1992: ASM International.
- ⁴⁹ Zapffe, C.A. and C.E. Sims, *Hydrogen embrittlement, internal stress and defects in steel*. American Institute of Mining and Metallurgical Engineers -- Transactions -- Iron and Steel Division, 1941. 145: p. 225-261.
- ⁵⁰ Petch, N.J. and P. Stables, *Delayed fracture of metals under static load*. Nature, 1952. 169: p. 842-843.
- ⁵¹ Heady, R.B., *The Petch-Stables Theory of hydrogen embrittlement*. Corrosion, 1977. 33(12): p. 441-7
- ⁵² Troiano, A.R., *The role of hydrogen and other interstitials in the mechanical behavior of metals*. Transactions of the American Society for Metals, 1960. 52: p. 54-80.
- ⁵³ Oriani, R.A., *A decohesion theory for hydrogen-induced crack propagation*. International Corrosion Conference Series, 1977. NACE-5(Stress Corros. Cracking Hydrogen Embrittlement Iron Base Alloys): p. 351-8.
-

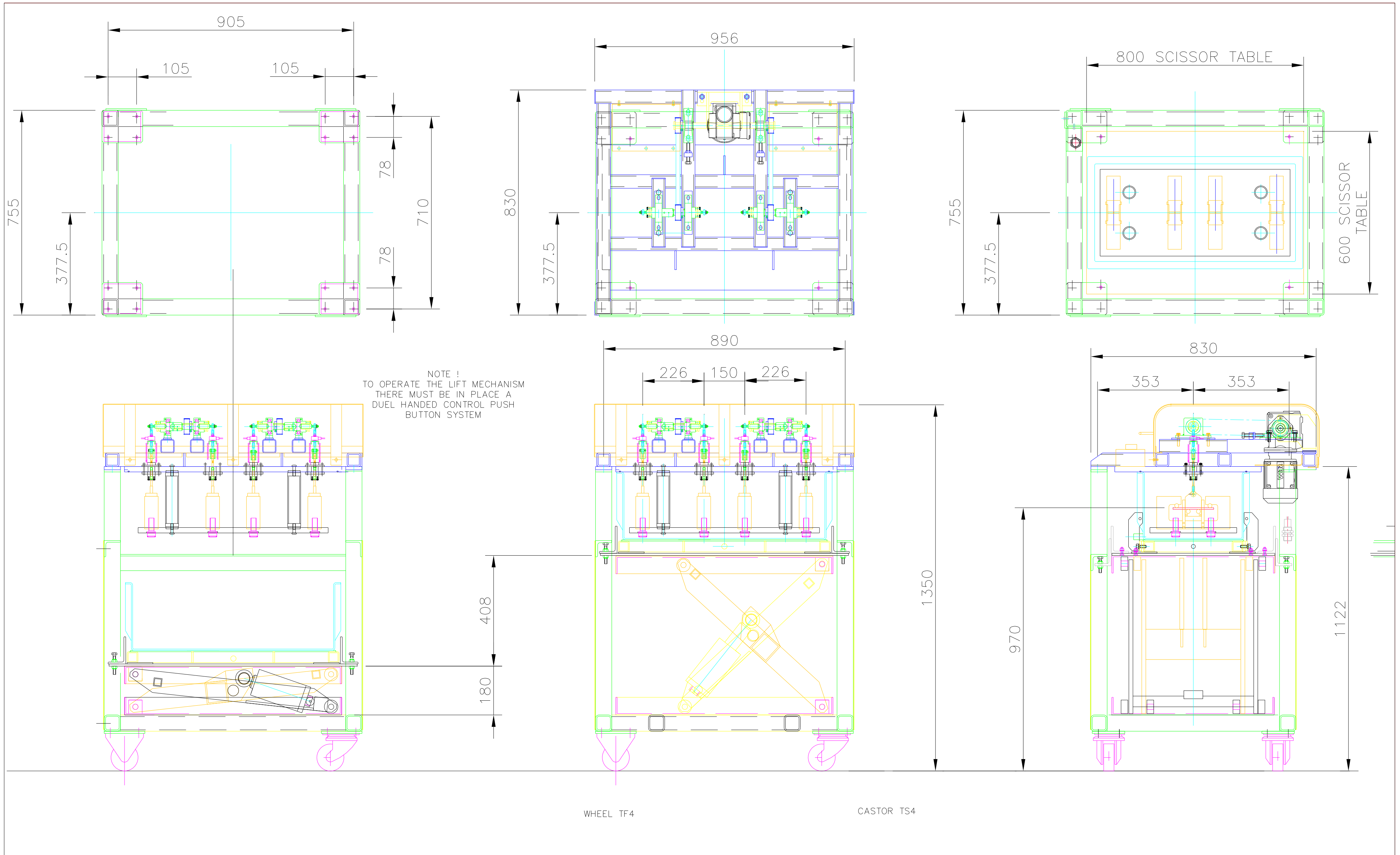
11. References

- ⁵⁴ Beachem, C.D., *New model for hydrogen- assisted cracking (hydrogen embrittlement')*. 1972. 3(2): p. 437-51.
- ⁵⁵ Birnbaum, H.K. *Hydrogen related fracture of metals*. 1983. Calacatoggio, Fr: Plenum Press, New York, NY, USA.
- ⁵⁶ Suresh, S., *Fatigue of Materials*. Second ed. 1998: Cambridge University Press.
- ⁵⁷ Pao, P.S., *Mechanisms of Corrosion Fatigue*. ASM Handbook Volume 19: Fatigue and Fracture, ed. N.D. Dimatteo. 1996: ASM International.
- ⁵⁸ Gangloff, R.P., *Corrosion Fatigue Cracking*. Second ed. Corrosion tests and standards: Application and Interpretation, ed. R. Baboian. 2005, West Conshohocken, PA: ASTM.
- ⁵⁹ Hagn, L., *Life Prediction Methods for Aqueous Environments*. Materials Science and Engineering a-Structural Materials Properties Microstructure and Processing, 1988. 103(1): p. 193-205
- ⁶⁰ Wei, R.P. and J.D. Landes, *Correlation between Sustained-Load and Fatigue Crack Growth in High-Strength Steels*. Materials Research and Standards, 1969. 9(7): p. 25-&.
- ⁶¹ Hertzberg, R.W., *Deformation and fracture mechanics of engineering materials*. Fourth ed. 1996: John Wiley & Sons, Inc.
- ⁶² Austen, I.M. and E.F. Walker, *Quantitative understanding of the effects of mechanical and environmental variables on corrosion fatigue crack growth behaviour*. I Mech E Conference Publications, 1977(4): p. 1-10.
- ⁶³ Andresen, P.L., *Corrosion fatigue testing*. ASM Handbook Volume 19: Fatigue and Fracture, ed. N.D. Dimatteo. 1996: ASM International
- ⁶⁴ Paris, P.C., M.P. Gomez, and W.E. Anderson, *A rational analytic theory of fatigue*. The Trend in Engineering at the University of Washington, 1961. 13(1): p. 9-14
- ⁶⁵ Gangloff, R.P., *Environmental effects on fatigue crack propagation*. 9th ed. ASM Metals Handbook: Volume 8: Mechanical Testing. 1985: ASM International.
- ⁶⁶ *ASTM Standard E 647 - 95a, Standard test method for measurement of fatigue crack growth rates*. Annual book of ASTM Standards. Vol. 11.03. 1995.
- ⁶⁷ *BS ISO 11782-2:1998 Corrosion of metal and alloys - Corrosion fatigue testing - Part 2: Crack propagation testing using precracked specimens*. British Standard. 1998
- ⁶⁸ American Petroleum Institute, Specification 17J, Specification for Unbonded Flexible Pipe, Second Edition (2002)
- ⁶⁹ Anderson, T.R. *Corrosion Fatigue of Steel Armour in Flexible Risers*, Proceedings of OMAE 2002, Paper 28052, Oslo
- ⁷⁰ Trillo. T., Kane. R.D., Ethridge. A, Clements. R, *Corrosion Fatigue Testing of Armor Wire Materials in Subsea Environments*. NACE Int. Conf. 2007, Paper 07103
- ⁷¹ ASTM D1141, *Standard Specification for Substitute Ocean Water*. (1980)
-

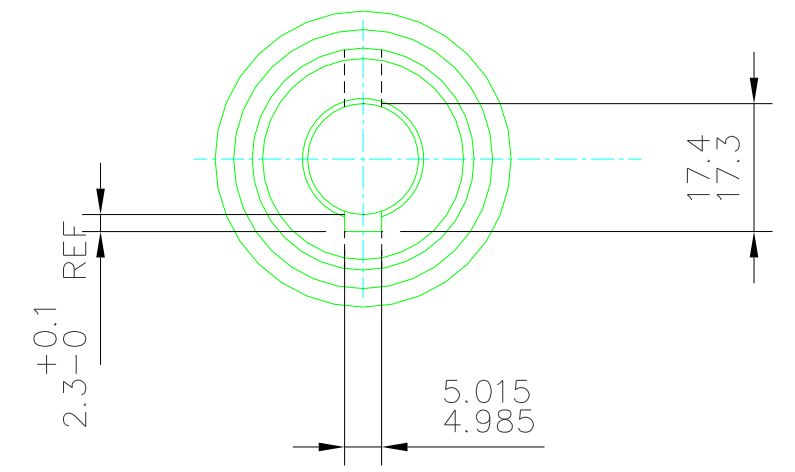
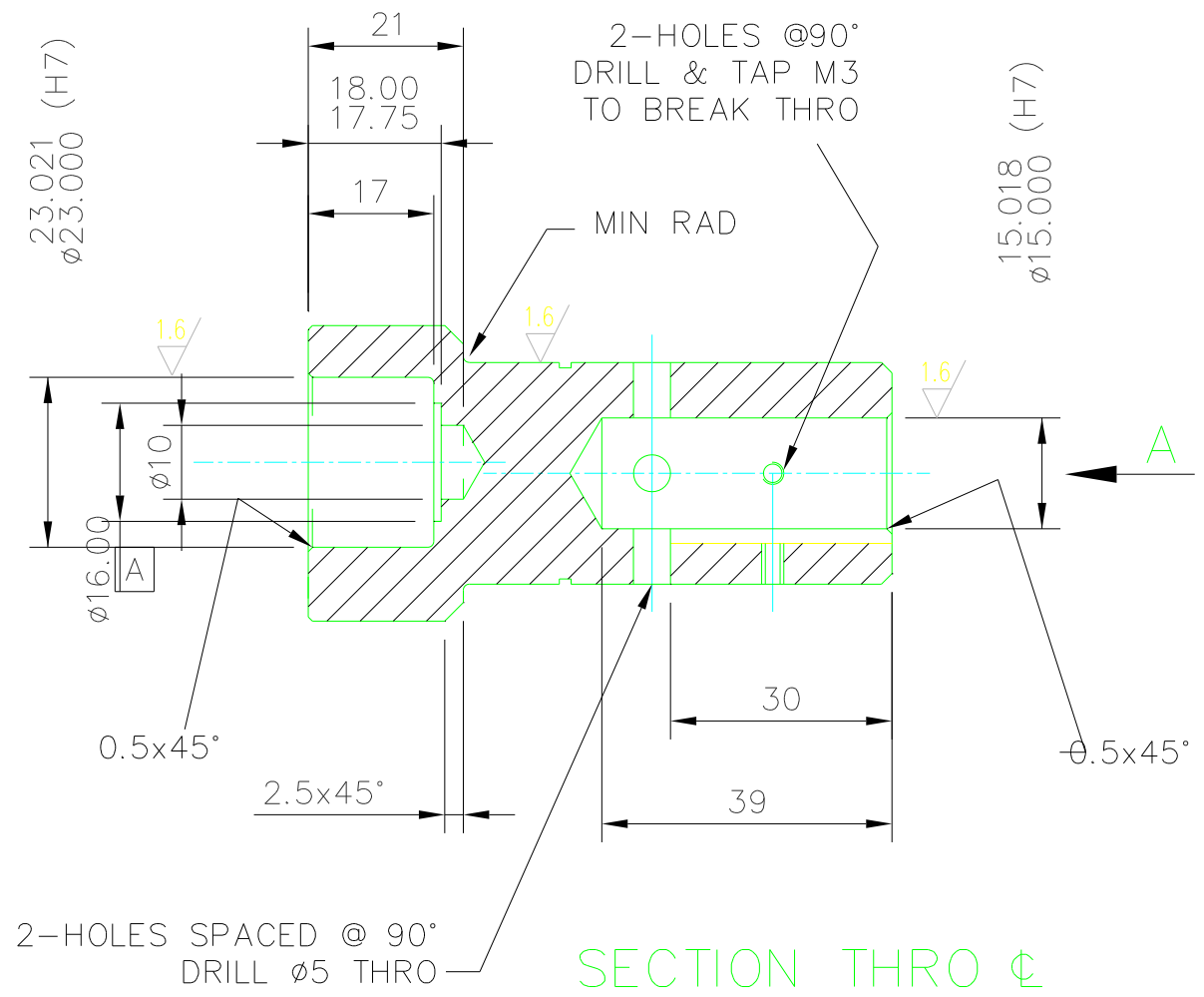
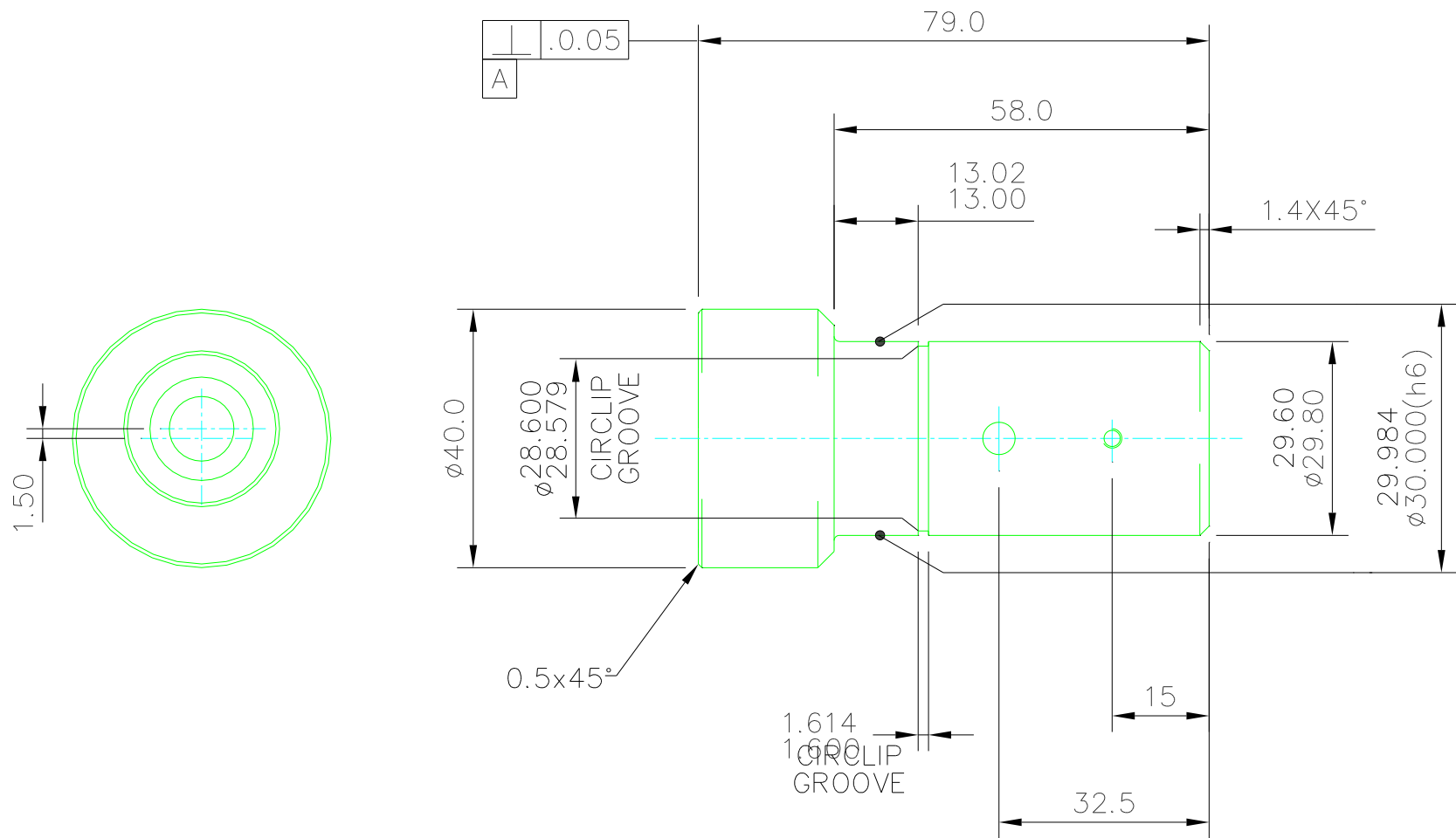
11. References

⁷² Dugstad, A. *Fundamental Aspects of CO₂ metal Loss Corrosion. Part 1: Mechanism*. NACE Int. Conf. 2006, Paper 06111

Appendix 1 – Atmospheric Pressure Corrosion Fatigue Test Machine Drawings



THIS DRAWING IS THE SOLE PROPERTY OF LANESFIELD ENGINEERING SEALS AND MUST NOT BE REPRODUCED NOR ITS CONTENTS DIVULGED WITHOUT WRITTEN PERMISSION	UNLESS OTHERWISE STATED		LANESFIELD ENGINEERING LTD.		DRAWN	DATE
	ALL DIMENSIONS IN MILLIMETERS		UNIT 11. SPRING ROAD IND ESTATE, LANESFIELD DRIVE. W'TON. WEST MIDLANDS. WV4 6UA FAX No 01902-405005 TELE No 01902 497777			
	TOLERANCES U0S		CUSTOMER		SCALE	
	MACHINING	+ 0.25MM	DRAWING TITLE		DRAWING No.	
FABRICATING	± 2.0MM	Layout of Test Machine		ISSUE No.		
		REMOVE ALL SHARP EDGES AND CORNERS				
		THIRD ANGLE PROJECTION				



OUTER DRIVE SPINDLE
 MATERIAL ST/STEEL
 2-OFF REQUIRED

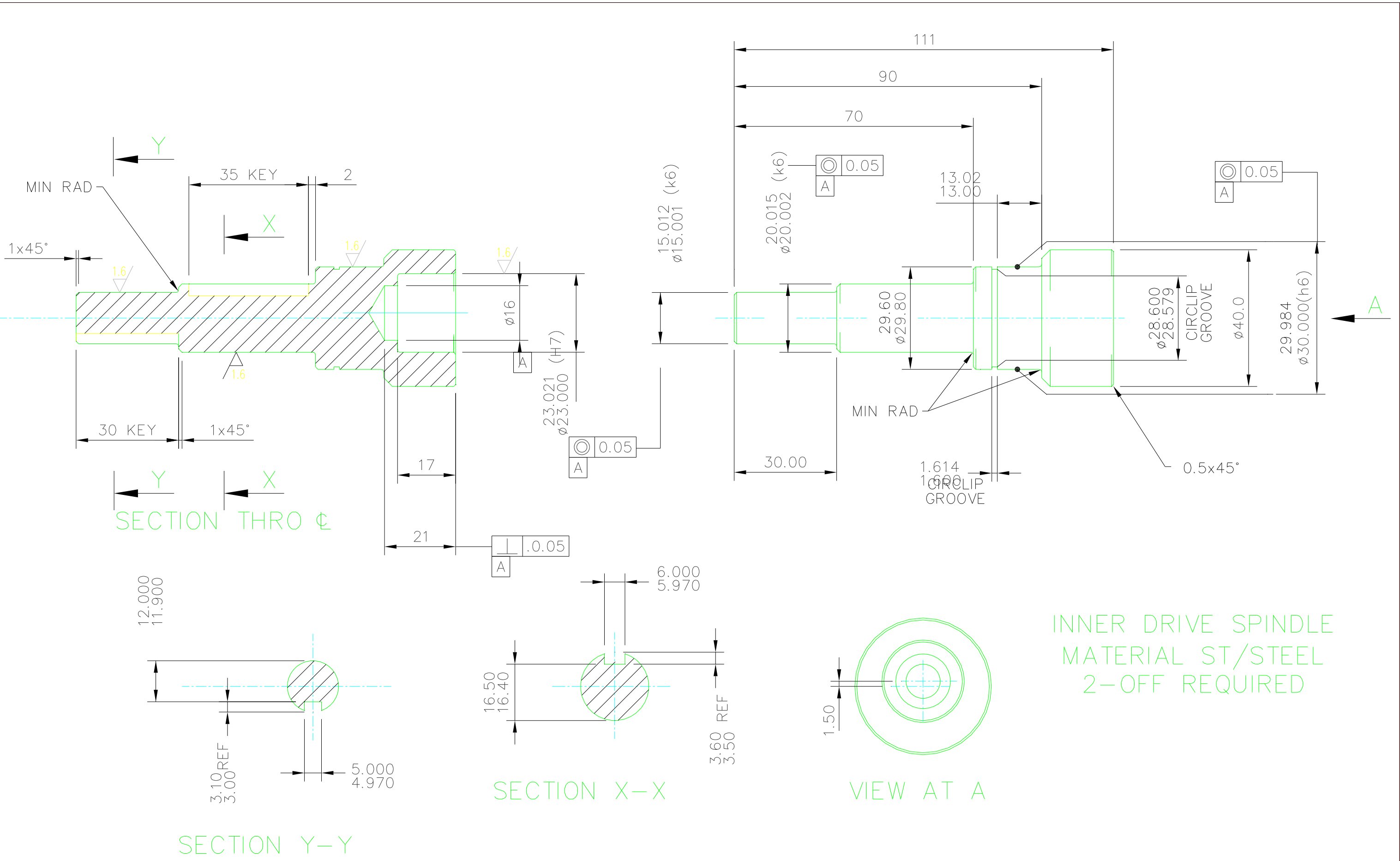
VIEW AT A

THIS DRAWING IS THE SOLE PROPERTY OF LANESFIELD ENGINEERING SEALS AND MUST NOT BE REPRODUCED NOR ITS CONTENTS DIVULGED WITHOUT WRITTEN PERMISSION

UNLESS OTHERWISE STATED	
ALL DIMENSIONS IN MILLIMETERS	REMOVE ALL SHARP EDGES AND CORNERS
TOLERANCES UOS	THIRD ANGLE PROJECTION
MACHINING	+ 0.25MM
FABRICATING	± 2.0MM

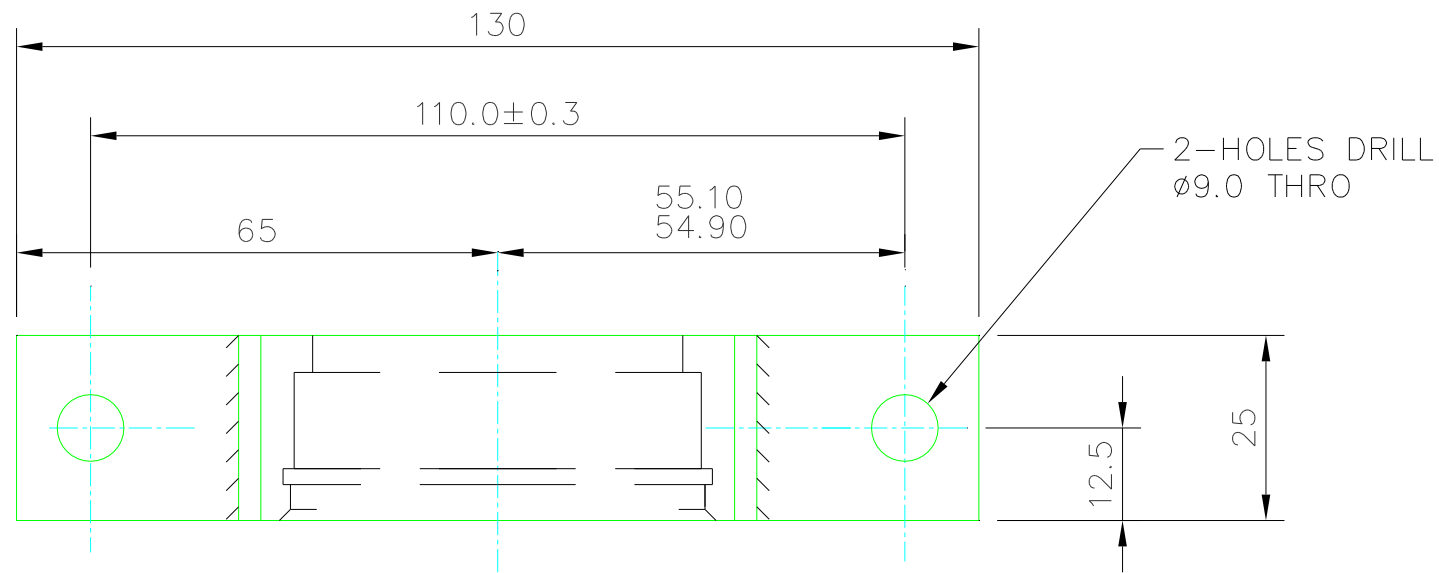
LANESFIELD ENGINEERING LTD. UNIT 11. SPRING ROAD IND ESTATE, LANESFIELD DRIVE. W/TON, WEST MIDLANDS. WV4 6UA FAX No 01902-405005 TELE No 01902 497777	
CUSTOMER	BODYCOTE
DRAWING TITLE	TEST MACHINE OUTER DRIVE SPINDLE DETAILS

DRAWN	R.K.C.	DATE	
SCALE	1:1 @ A3		
DRAWING No.	DR/1611-D1	ISSUE No.	

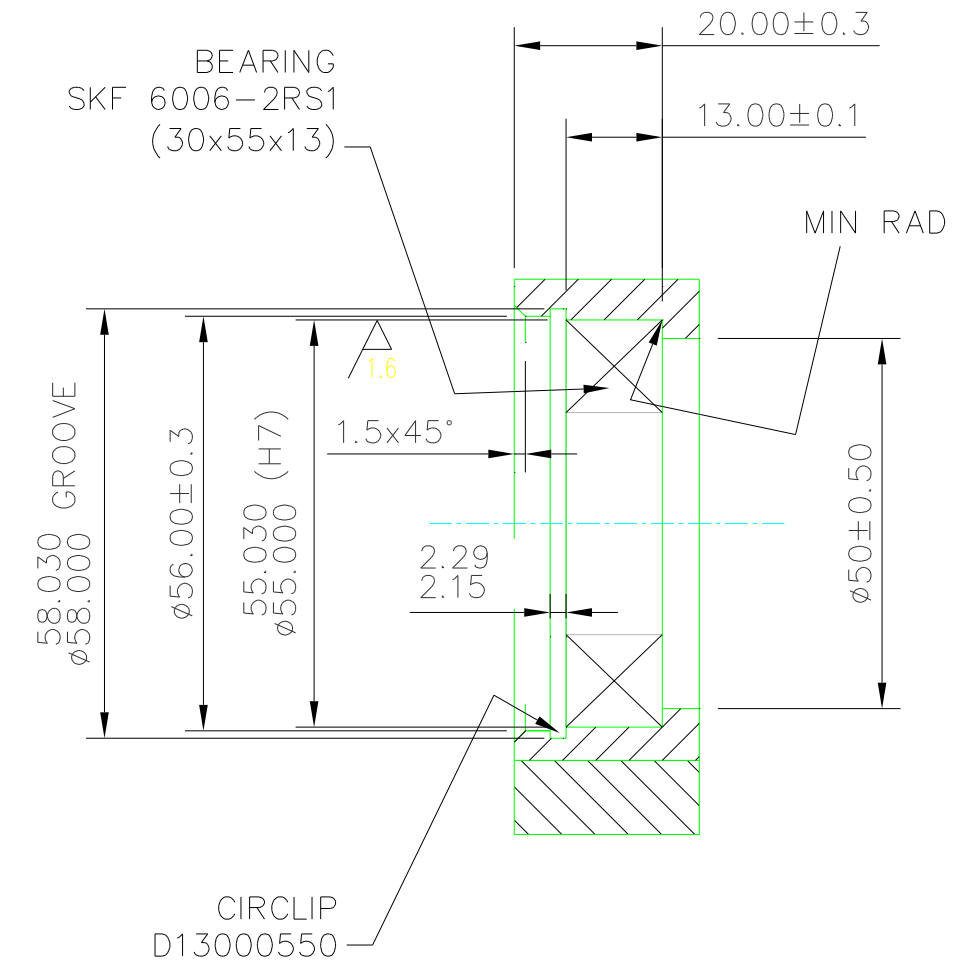
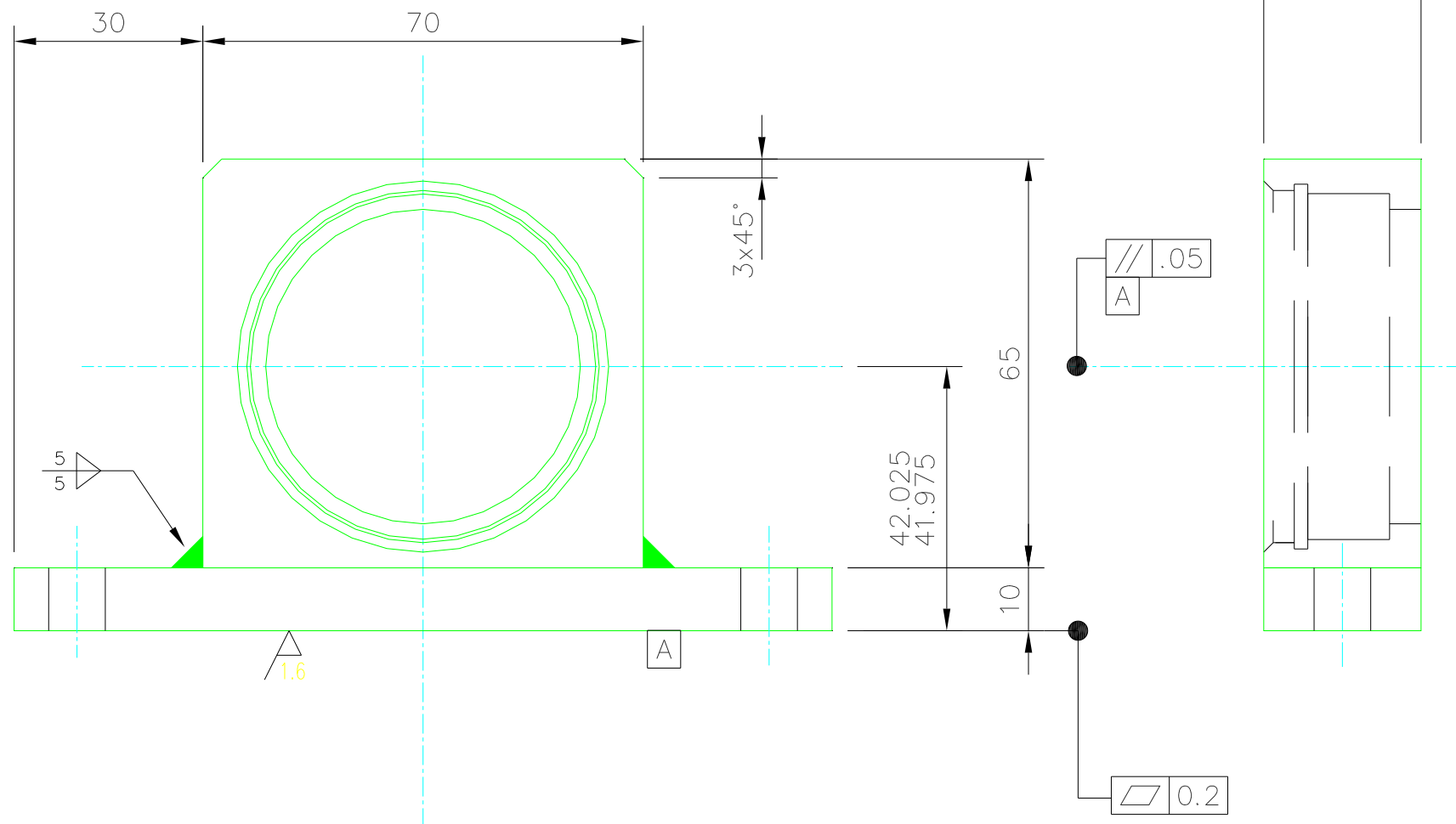


INNER DRIVE SPINDLE
 MATERIAL ST/STEEL
 2-OFF REQUIRED

THIS DRAWING IS THE SOLE PROPERTY OF LANESFIELD ENGINEERING SEALS AND MUST NOT BE REPRODUCED NOR ITS CONTENTS DIVULGED WITHOUT WRITTEN PERMISSION	UNLESS OTHERWISE STATED		LANESFIELD ENGINEERING LTD.		DRAWN	R.K.C.	DATE
	ALL DIMENSIONS IN MILLIMETERS		UNIT 11. SPRING ROAD IND ESTATE, LANESFIELD DRIVE. W'TON, WEST MIDLANDS. WV4 6UA				
	TOLERANCES UOS		FAX No 01902-405005 TELE No 01902 497777				
	MACHINING + 0.25MM		REMOVE ALL SHARP EDGES AND CORNERS				
FABRICATING ± 2.0MM		THIRD ANGLE PROJECTION		CUSTOMER	BODYCOTE		
				DRAWING TITLE	TEST MACHINE INNER DRIVE SPINDLE DETAILS		
				SCALE	1:1 @ A3		
				DRAWING No.	DR/1611-D2		ISSUE No.



PILLOW BLOCK
MATERIAL MILD STEEL
4-OFF REQUIRED



SECTION THRO ̢

THIS DRAWING IS THE SOLE PROPERTY OF LANESFIELD ENGINEERING SEALS AND MUST NOT BE REPRODUCED NOR ITS CONTENTS DIVULGED WITHOUT WRITTEN PERMISSION

UNLESS OTHERWISE STATED

ALL DIMENSIONS IN MILLIMETERS

TOLERANCES UOS

MACHINING + 0.25MM

FABRICATING ± 2.0MM

REMOVE ALL SHARP EDGES AND CORNERS

THIRD ANGLE PROJECTION



LANESFIELD ENGINEERING LTD.

UNIT 11, SPRING ROAD IND ESTATE, LANESFIELD DRIVE, W'TON, WEST MIDLANDS. WV4 6UA
FAX No 01902-405005 TELE No 01902 497777

CUSTOMER BODYCOTE

DRAWING TITLE TEST MACHINE
PILLOW BLOCK DETAILS

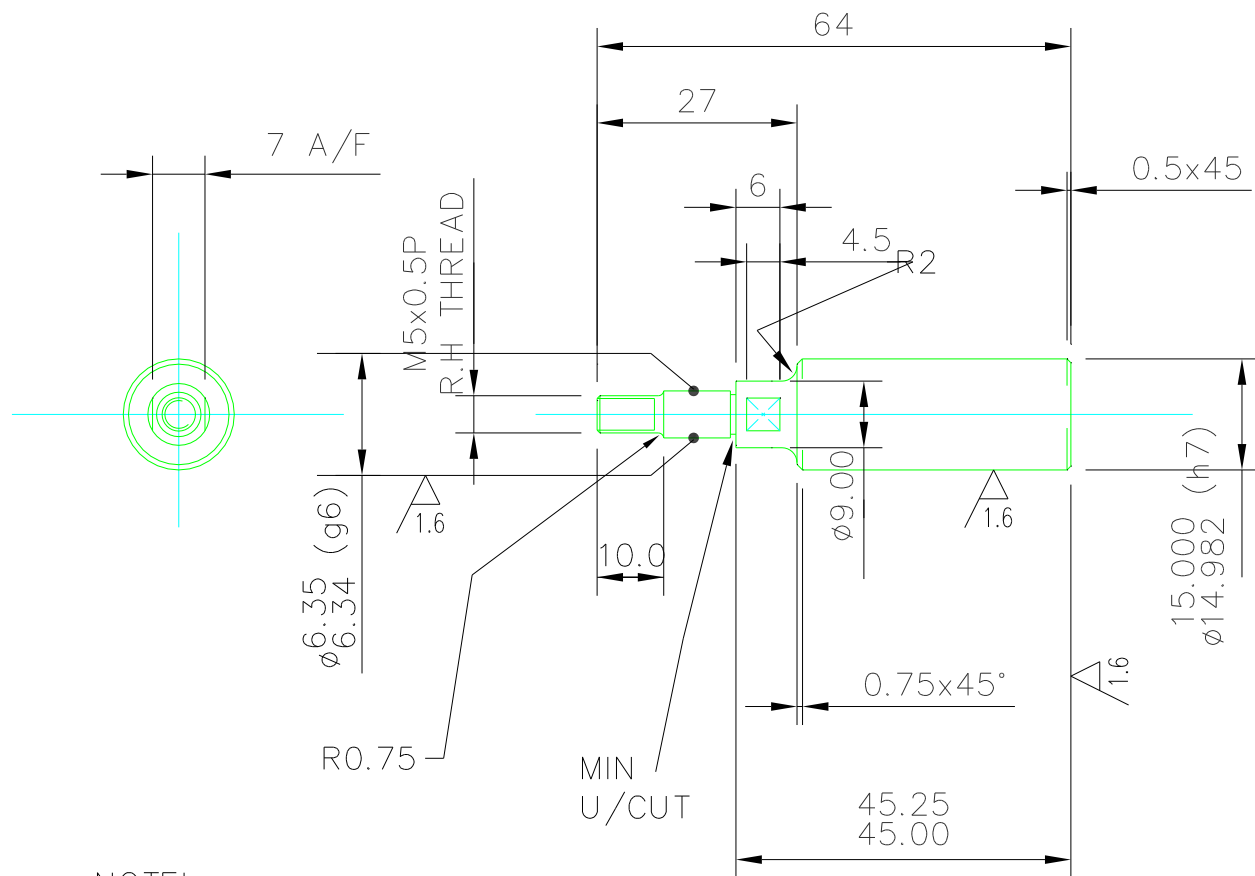
DRAWN R.K.C.

DATE

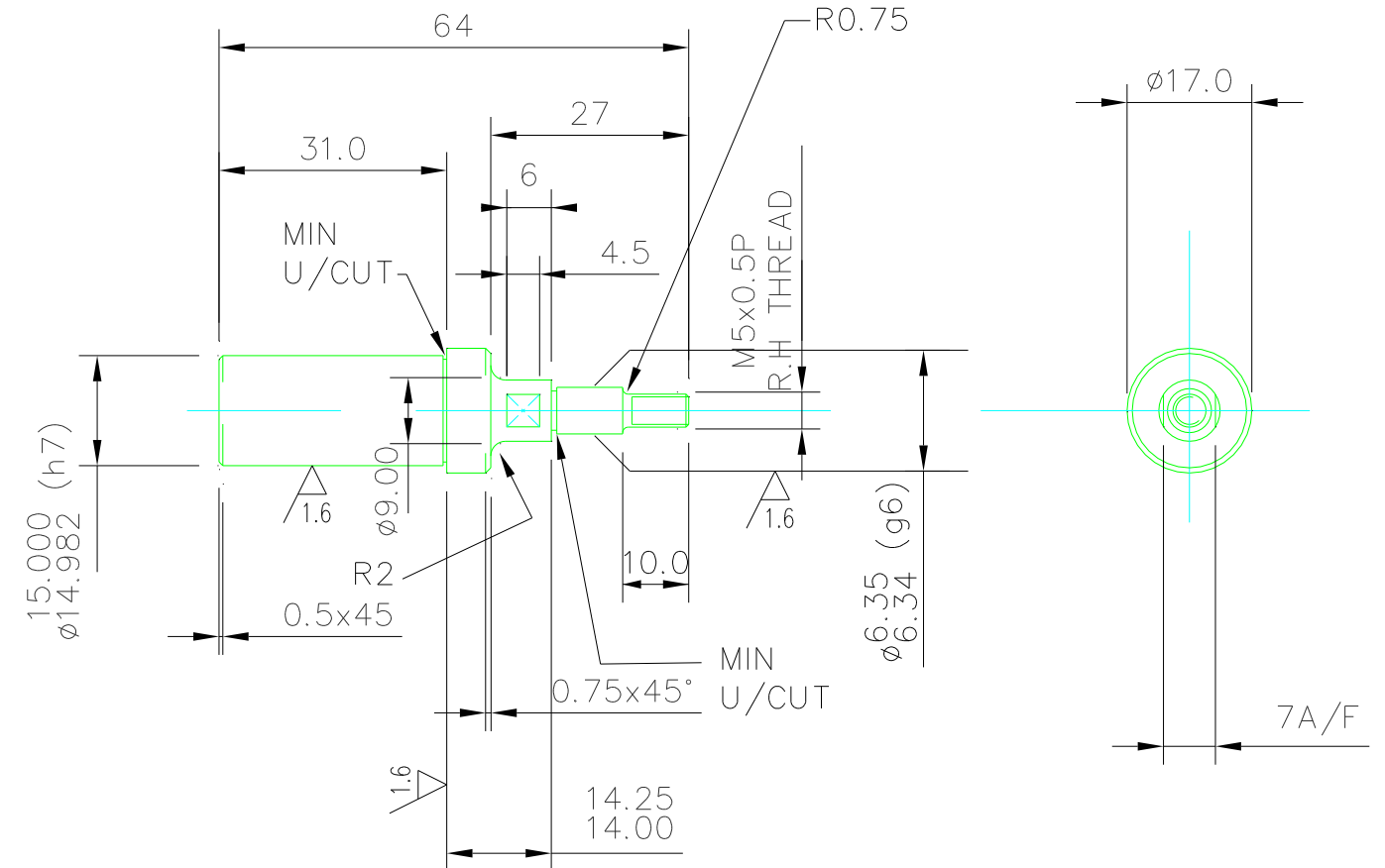
SCALE 1:1 @ A3

DRAWING No. DR/1611-D3

ISSUE No.



NOTE!
ALL DIAMETERS MUST
BE CONCENTRIC TO
WITHIN .02 OF TIR



NOTE!
ALL DIAMETERS MUST
BE CONCENTRIC TO
WITHIN .02 OF TIR

D4A

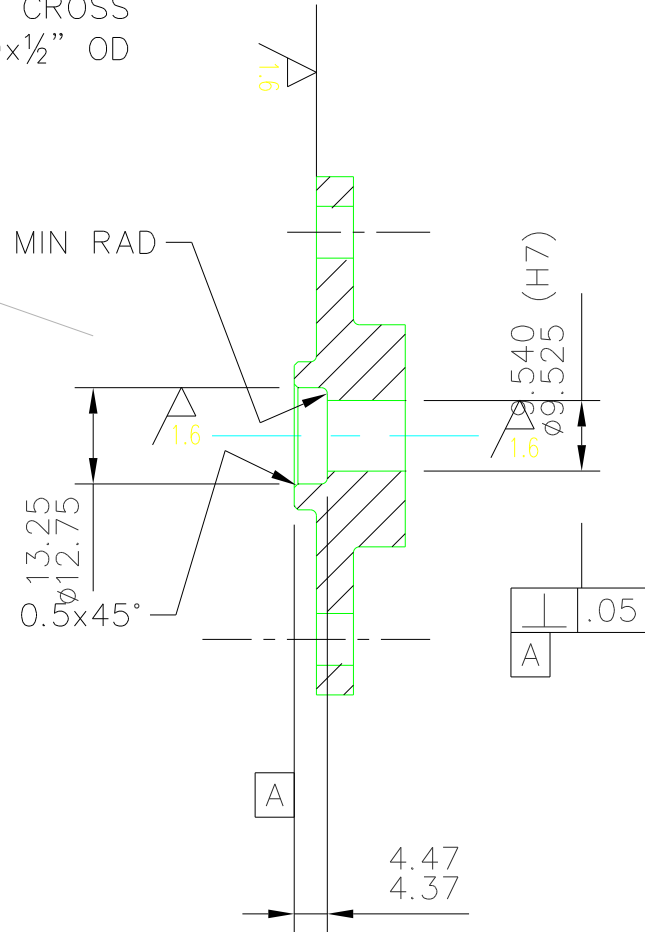
L.H DRIVE SPINDLE
MATERIAL ST/STEEL
2-OFF REQUIRED

D4B

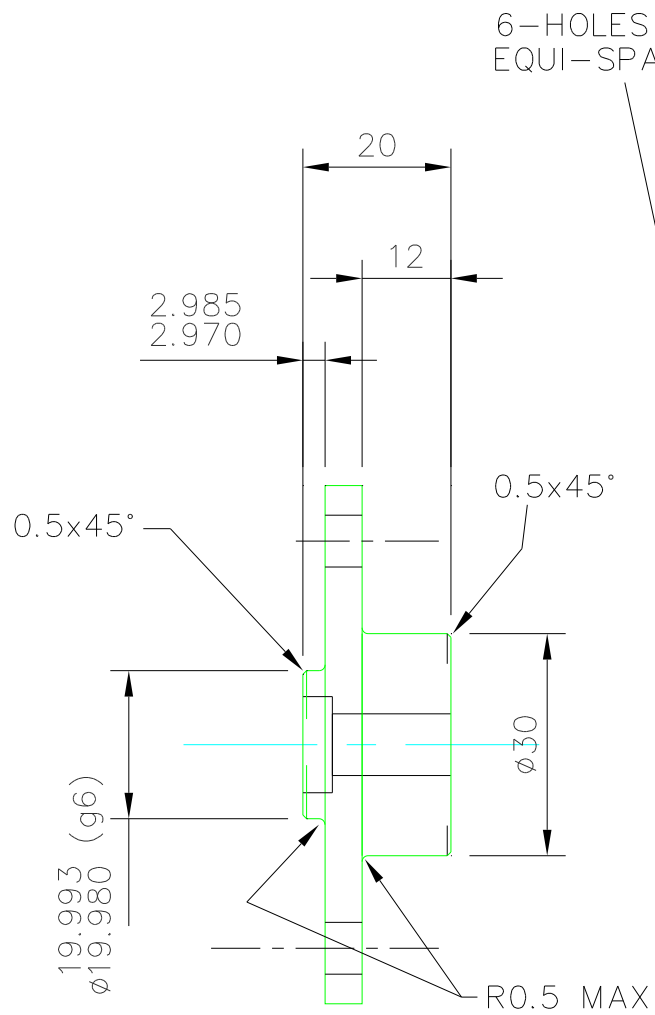
R.H DRIVE SPINDLE
MATERIAL ST/STEEL
2-OFF REQUIRED

THIS DRAWING IS THE SOLE PROPERTY OF LANESFIELD ENGINEERING SEALS AND MUST NOT BE REPRODUCED NOR ITS CONTENTS DIVULGED WITHOUT WRITTEN PERMISSION	UNLESS OTHERWISE STATED		LANESFIELD ENGINEERING LTD.		DRAWN	R.K.C.	DATE
	ALL DIMENSIONS IN MILLIMETERS		REMOVE ALL SHARP EDGES AND CORNERS		UNIT 11, SPRING ROAD IND ESTATE, LANESFIELD DRIVE, W'TON, WEST MIDLANDS. WV4 6UA		
	TOLERANCES UOS		THIRD ANGLE PROJECTION		FAX No 01902-405005 TELE No 01902 497777		
	MACHINING	+ 0.25MM			CUSTOMER		SCALE 1:1 @ A3
FABRICATING	± 2.0MM	DRAWING TITLE			DRAWING No.		ISSUE No.
				BODYCOTE		DR/1611-D4	
				TEST MACHINE DRIVE SHAFT DETAILS			

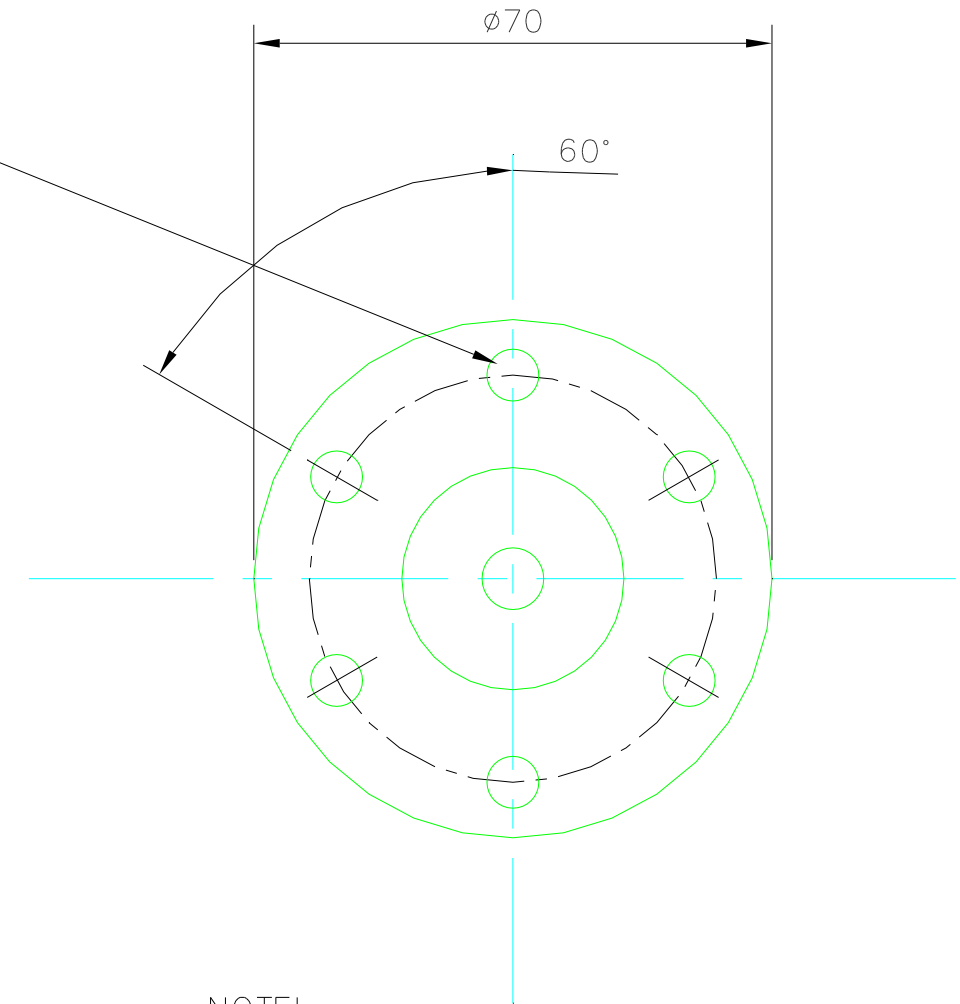
TO SUIT SILICONE 'O' RING
 SIZE REF 202 3,53mm CROSS
 SECTION ¼" IDx½" OD



SECTION THRO ϕ



6-HOLES DRILL ϕ 7 THRO
 EQUI-SPACED ON A ϕ 55.00 PC



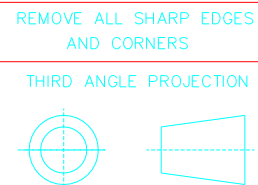
NOTE!
 ALL DIAMETERS MUST
 BE CONCENTRIC TO
 WITHIN .02 OF TIR

OUTER COVER GUIDE
 MATERIAL SUPER DUPLEX
 4-OFF REQUIRED

THIS DRAWING IS THE SOLE PROPERTY
 OF LANESFIELD ENGINEERING SEALS
 AND MUST NOT BE REPRODUCED NOR
 ITS CONTENTS DIVULGED WITHOUT
 WRITTEN PERMISSION

UNLESS OTHERWISE STATED

ALL DIMENSIONS IN MILLIMETERS	
TOLERANCES UOS	
MACHINING	+ 0.25MM
FABRICATING	± 2.0MM



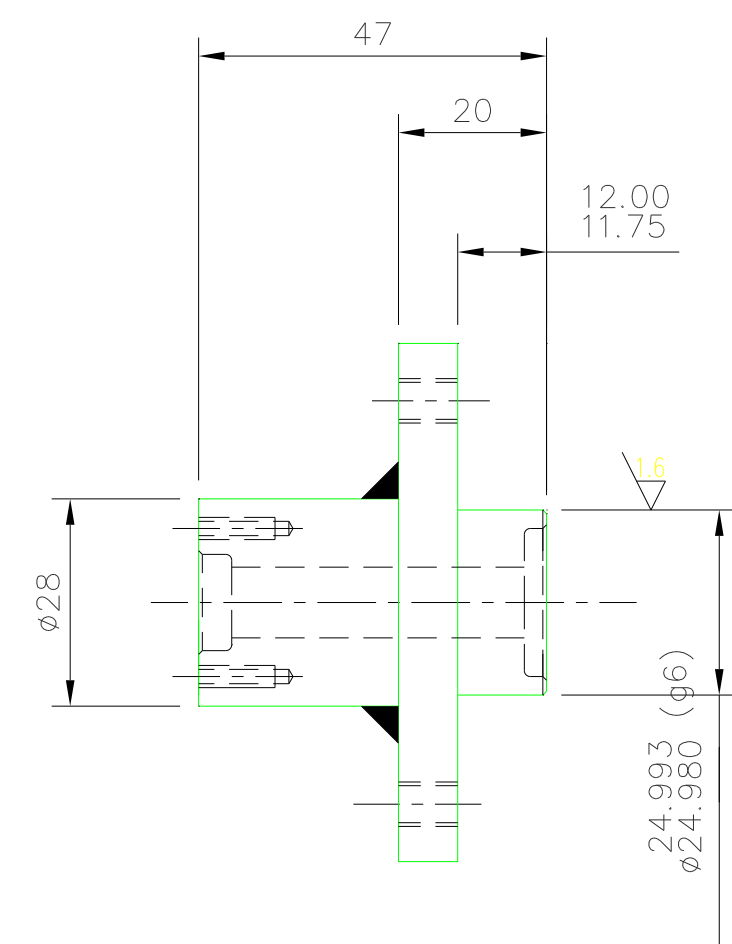
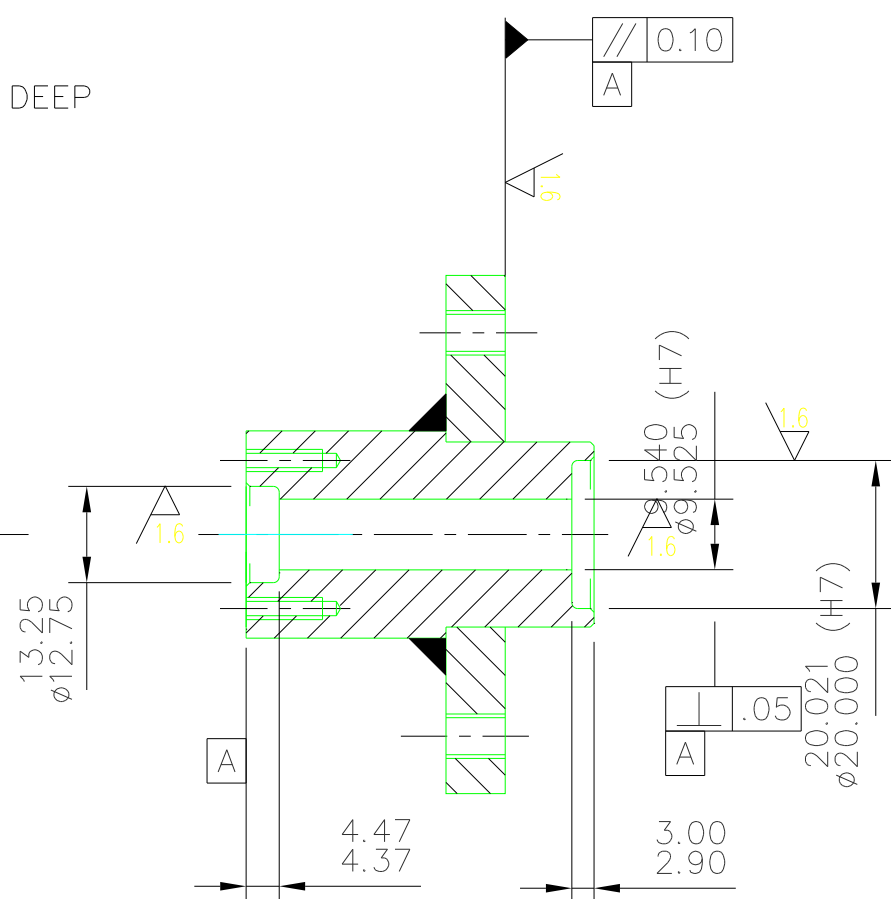
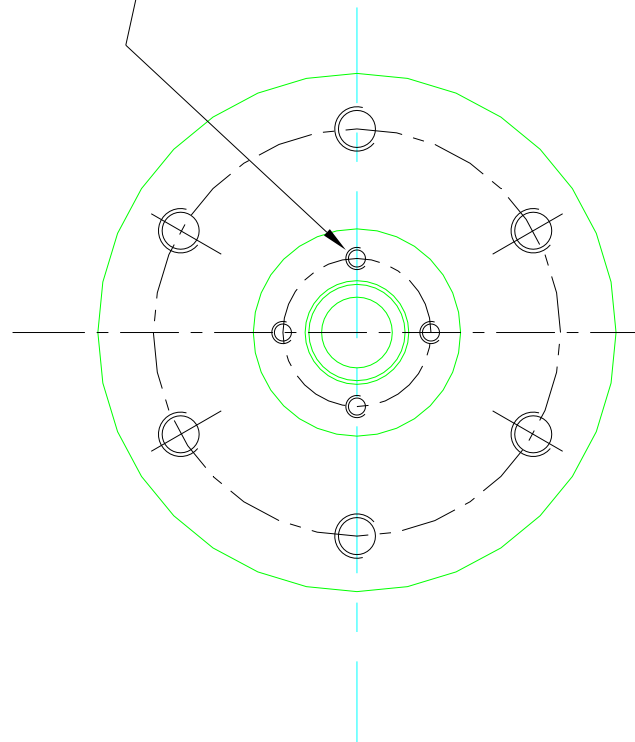
LANESFIELD ENGINEERING LTD.
 UNIT 11, SPRING ROAD IND ESTATE, LANESFIELD DRIVE, W'TON, WEST MIDLANDS. WV4 6UA
 FAX No 01902-405005 TELE No 01902 497777

CUSTOMER BODYCOTE

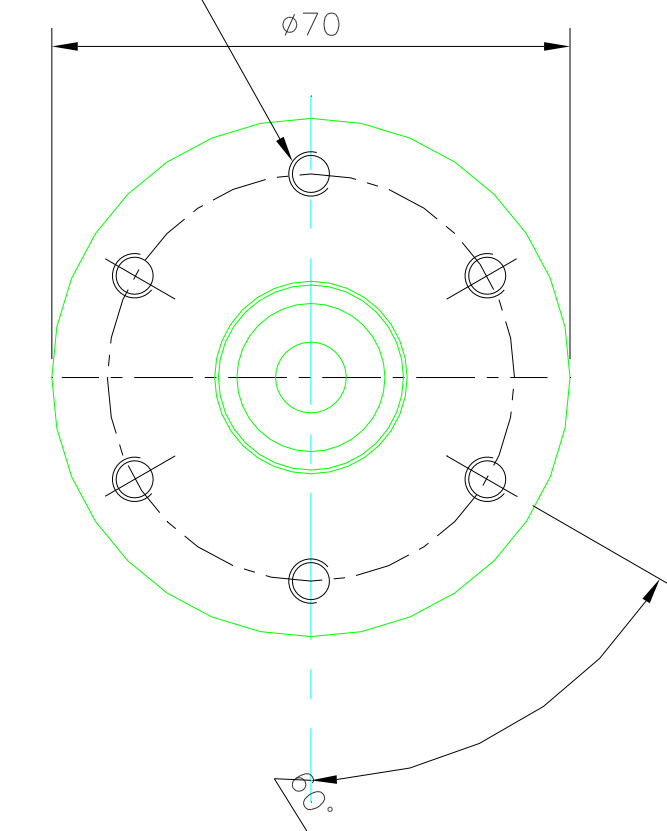
DRAWING TITLE TEST MACHINE
 OUTER COVER GUIDE DETAILS

DRAWN R.K.C.	DATE
SCALE 1:1 @ A3	
DRAWING No. DR/1611-D5	ISSUE No.

4-HOLES DRILL & TAP M3 x 10 DEEP
EQUI-SPACED ON A $\phi 20.00$ PC



6-HOLES DRILL & TAP M6 THRO
EQUI-SPACED ON A $\phi 55.00$ PC



SECTION THRO ϕ

GUIDE
MATERIAL SUPER DUPLEX
4-OFF REQUIRED

THIS DRAWING IS THE SOLE PROPERTY
OF LANESFIELD ENGINEERING SEALS
AND MUST NOT BE REPRODUCED NOR
ITS CONTENTS DIVULGED WITHOUT
WRITTEN PERMISSION

UNLESS OTHERWISE STATED

ALL DIMENSIONS IN
MILLIMETERS

TOLERANCES UOS

MACHINING + 0.25MM

FABRICATING ± 2.0 MM

REMOVE ALL SHARP EDGES
AND CORNERS

THIRD ANGLE PROJECTION



LANESFIELD ENGINEERING LTD.

UNIT 11, SPRING ROAD IND ESTATE, LANESFIELD DRIVE, W'TON, WEST MIDLANDS, WV4 6UA
FAX No 01902-405005 TELE No 01902 497777

CUSTOMER BODYCOTE

DRAWING TITLE TEST MACHINE
GUIDE DETAILS

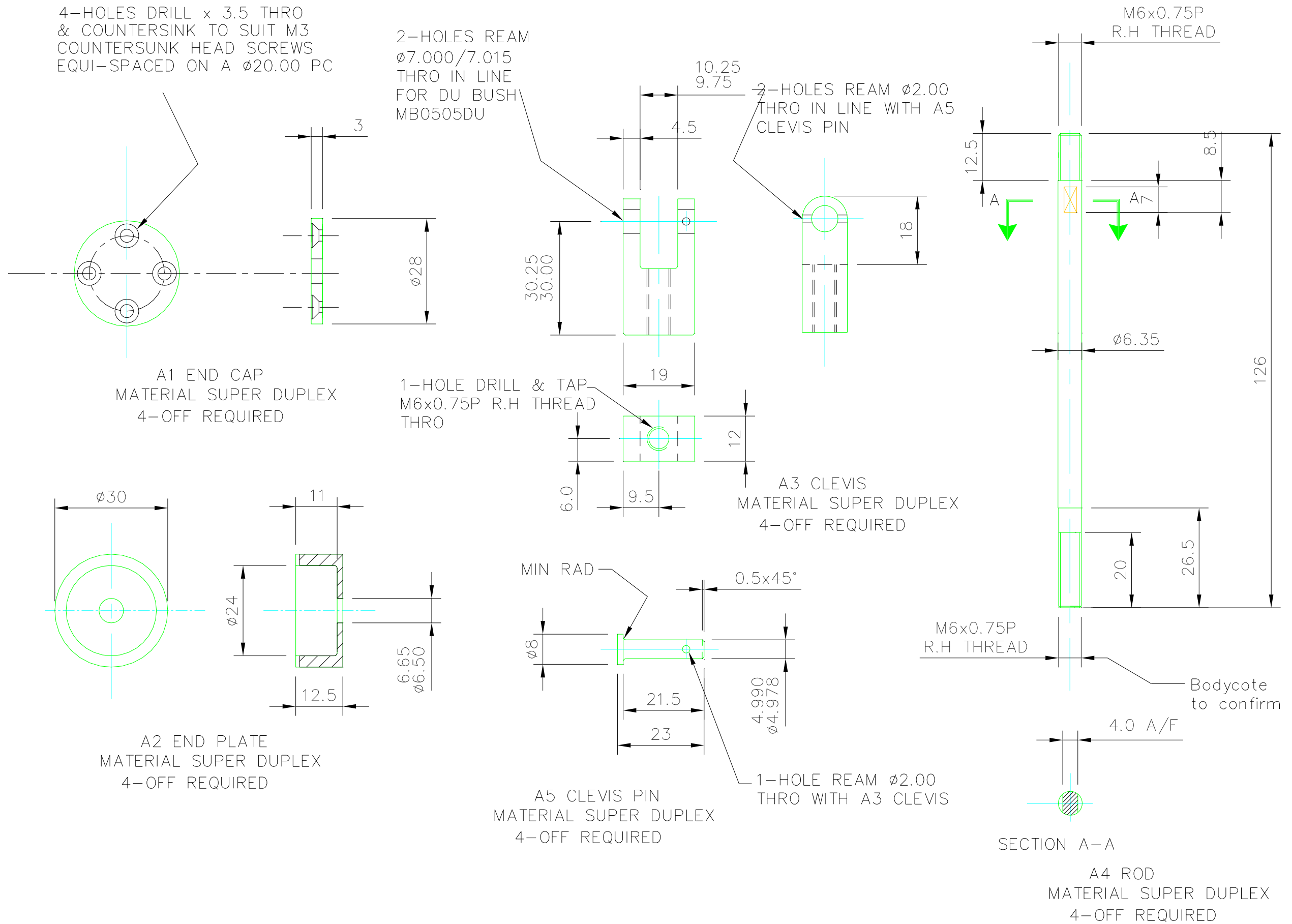
DRAWN R.K.C.

DATE

SCALE 1:1 @ A3

DRAWING No. DR/1611-D6

ISSUE No.



THIS DRAWING IS THE SOLE PROPERTY OF LANESFIELD ENGINEERING SEALS AND MUST NOT BE REPRODUCED NOR ITS CONTENTS DIVULGED WITHOUT WRITTEN PERMISSION

UNLESS OTHERWISE STATED

ALL DIMENSIONS IN MILLIMETERS

TOLERANCES UOS

MACHINING + 0.25MM

FABRICATING $\pm 2.0MM$

REMOVE ALL SHARP EDGES AND CORNERS

THIRD ANGLE PROJECTION



LANESFIELD ENGINEERING LTD.

UNIT 11, SPRING ROAD IND ESTATE, LANESFIELD DRIVE, W'TON, WEST MIDLANDS. WV4 6UA
 FAX No 01902-405005 TELE No 01902 497777

CUSTOMER BODYCOTE

DRAWING TITLE TEST MACHINE DETAILS

DRAWN R.K.C.

DATE

SCALE 1:1 @ A3

DRAWING No. DR/1611-D7

ISSUE No.

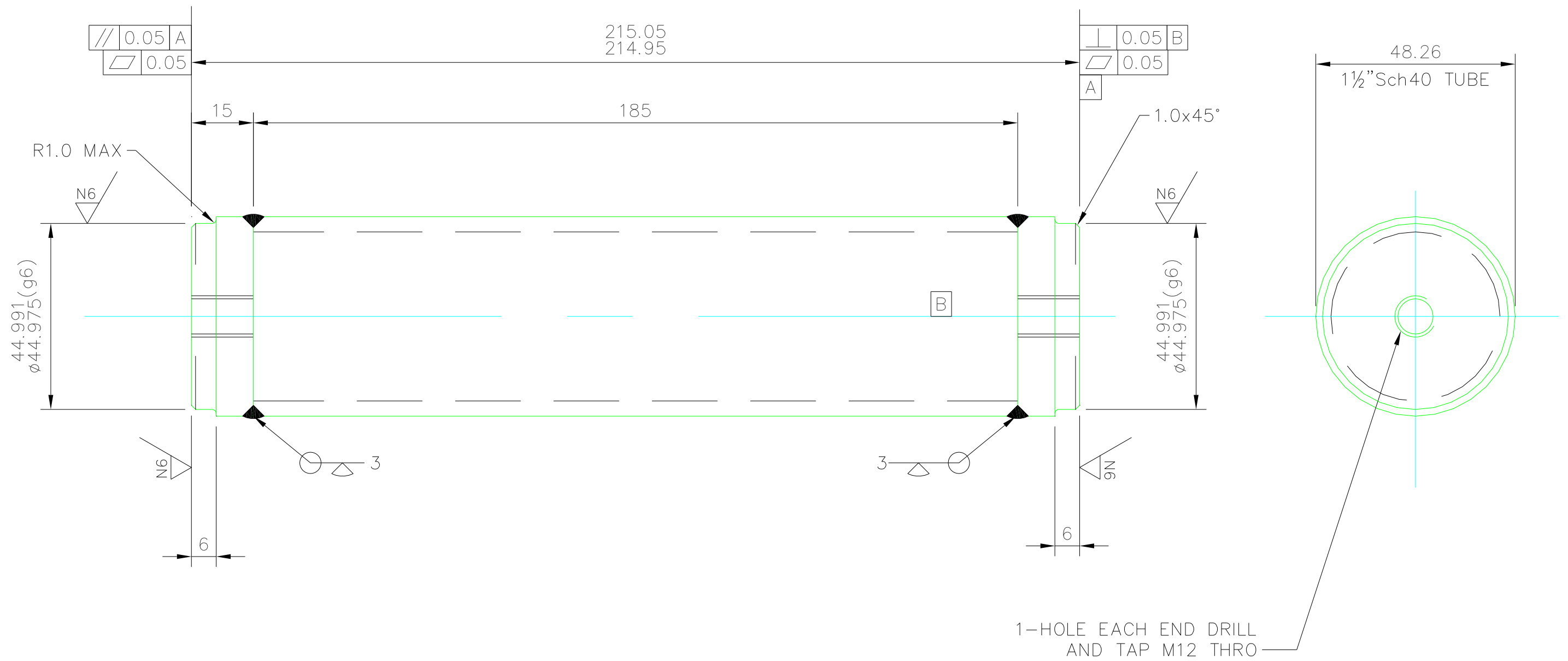


TABLE PILLAR
 MATERIAL SUPER DUPLEX
 4-OFF REQUIRED

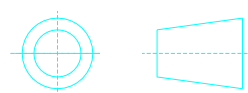
THIS DRAWING IS THE SOLE PROPERTY OF LANESFIELD ENGINEERING SEALS AND MUST NOT BE REPRODUCED NOR ITS CONTENTS DIVULGED WITHOUT WRITTEN PERMISSION

UNLESS OTHERWISE STATED

ALL DIMENSIONS IN MILLIMETERS	
TOLERANCES UOS	
MACHINING	+ 0.25MM
FABRICATING	± 2.0MM

REMOVE ALL SHARP EDGES AND CORNERS

THIRD ANGLE PROJECTION



LANESFIELD ENGINEERING LTD.

UNIT 11. SPRING ROAD IND ESTATE, LANESFIELD DRIVE. W'TON. WEST MIDLANDS. WV4 6UA
 FAX No 01902-405005 TELE No 01902 497777

CUSTOMER BODYCOTE

DRAWING TITLE TEST MACHINE TABLE SUPPORT DETAILS

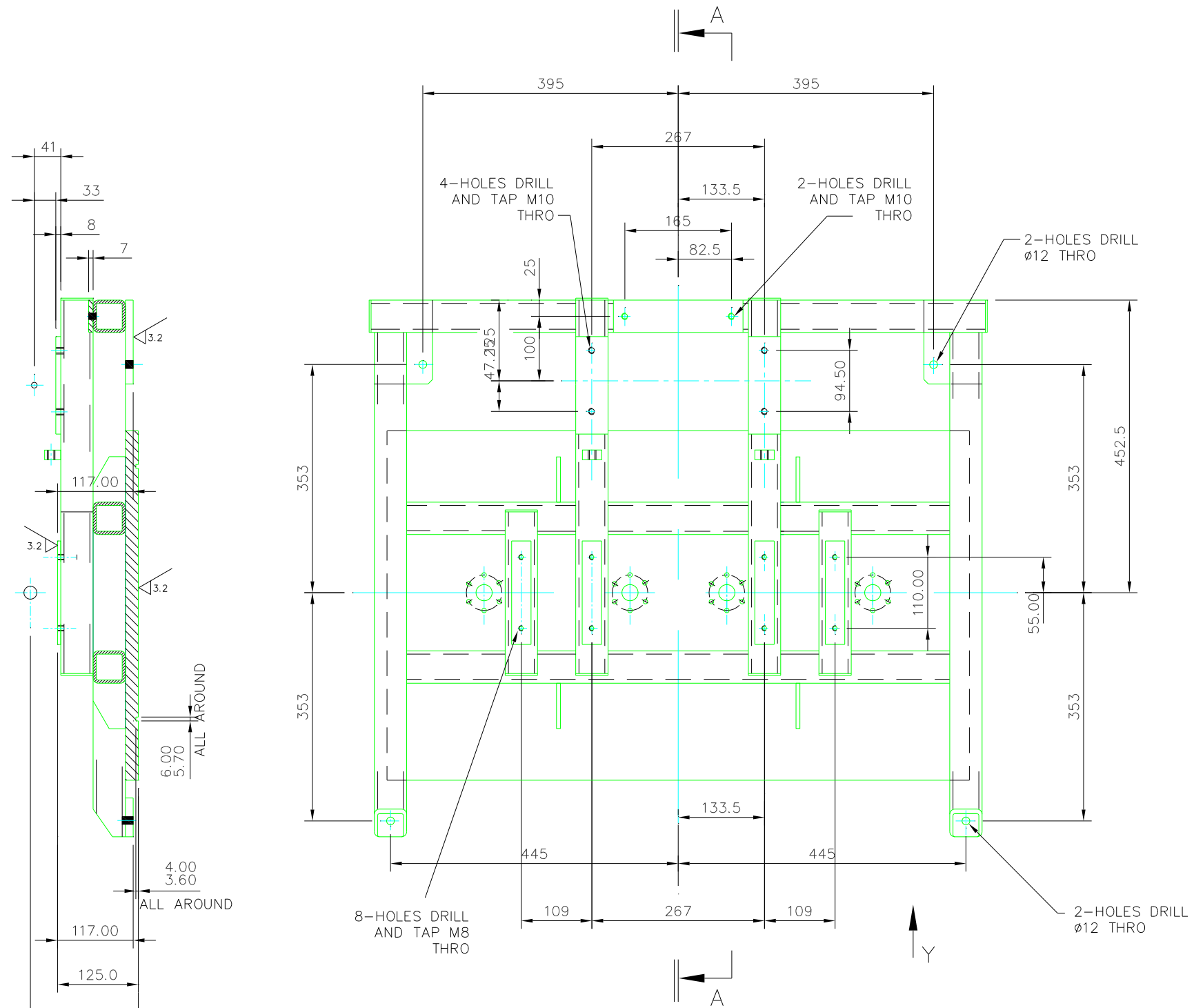
DRAWN R.K.C.

DATE

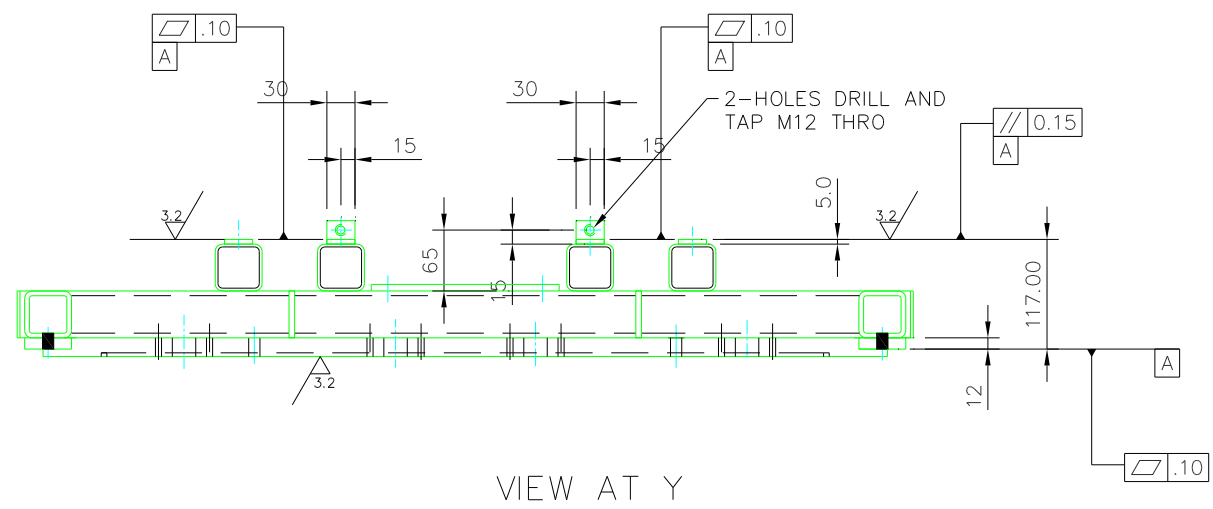
SCALE 1:1 @ A3

DRAWING No. DR/1611-D8

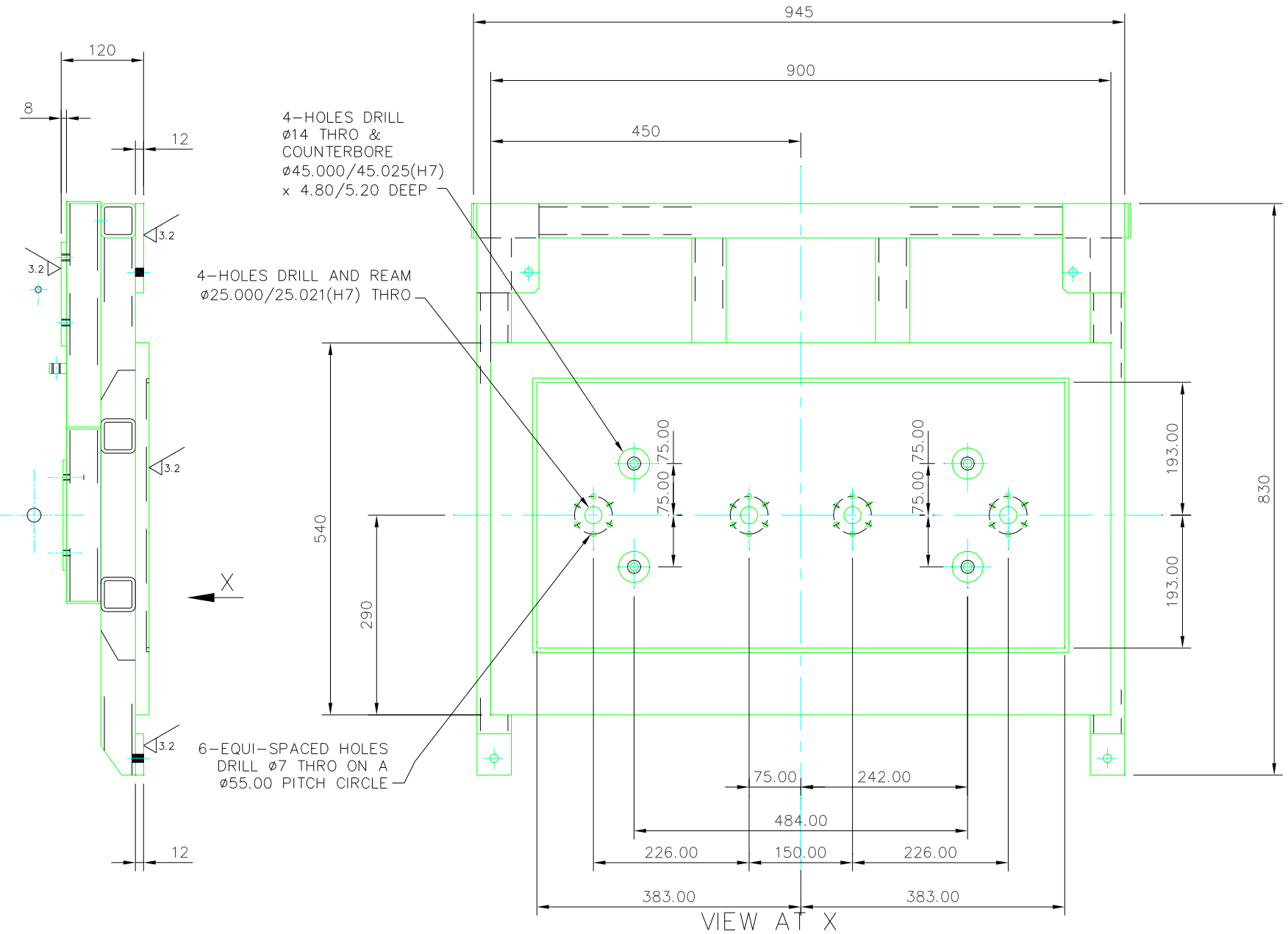
ISSUE No.



SECTION A-A



VIEW AT Y

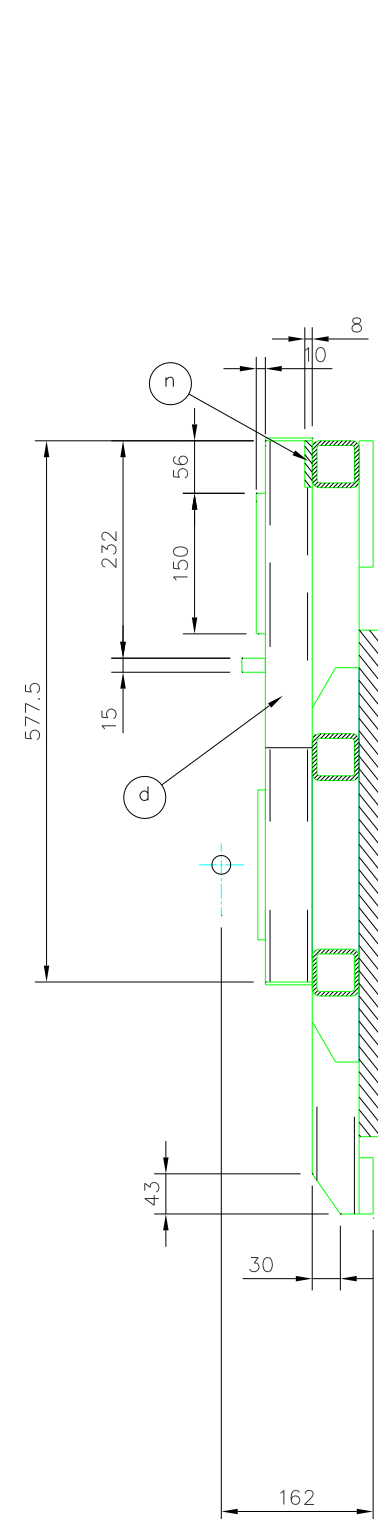


VIEW AT X

TOP PLATE
MATERIAL M.S FABRICATION
1-OFF REQUIRED

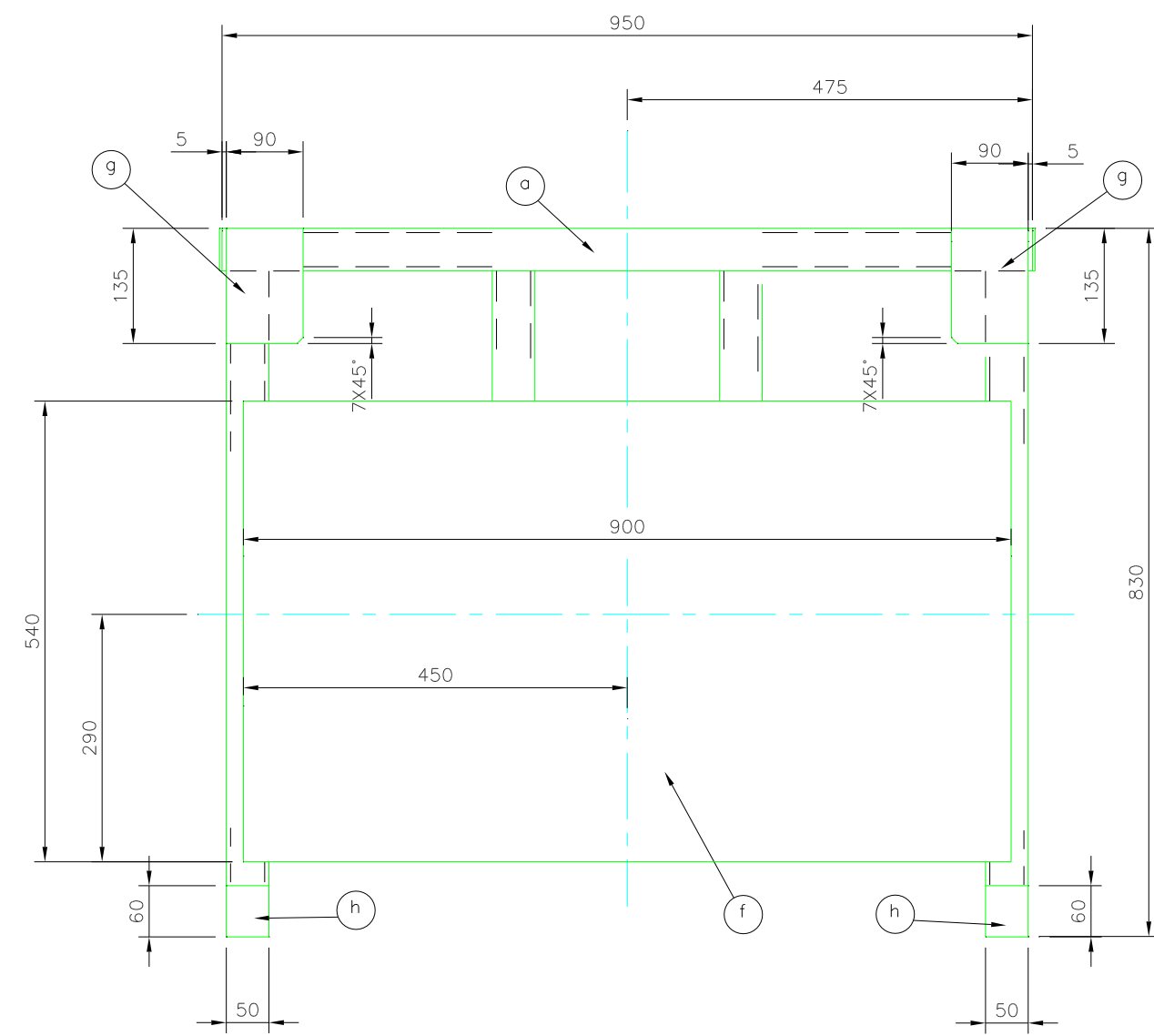
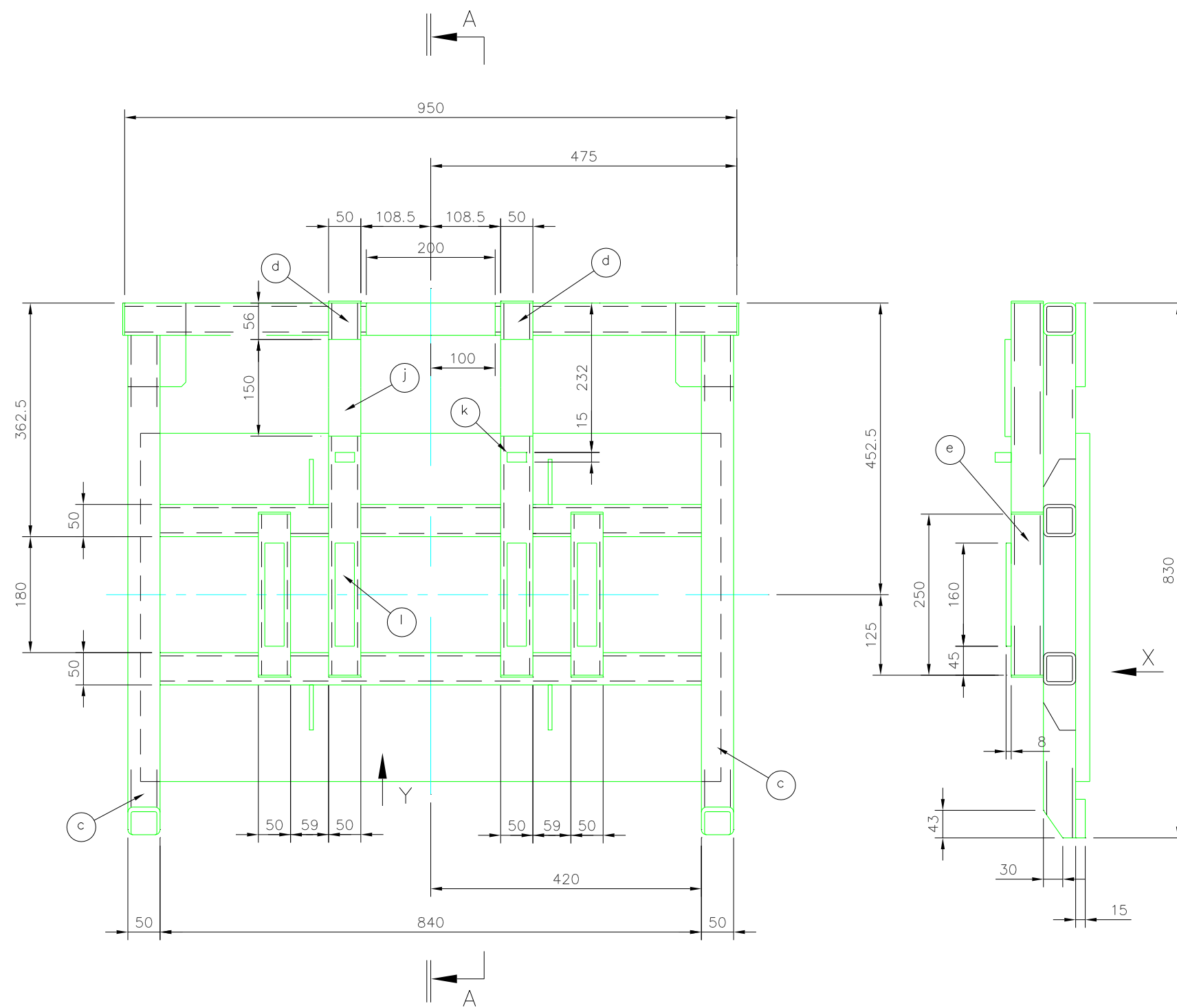
NOTE !
READ THIS DRAWING IN CONJUNCTION
WITH FABRICATION DRAWING D9/FAB

THIS DRAWING IS THE SOLE PROPERTY OF LANESFIELD ENGINEERING SEALS AND MUST NOT BE REPRODUCED NOR ITS CONTENTS DIVULGED WITHOUT WRITTEN PERMISSION	UNLESS OTHERWISE STATED		LANESFIELD ENGINEERING LTD. UNIT 11, SPRING ROAD IND. ESTATE, LANESFIELD DRIVE, W.TON, WEST MIDLANDS, WV4 6UA FAX No 01902-405005 TELE No 01902 497777		DRAWN R.K.C.	DATE
	ALL DIMENSIONS IN MILLIMETERS		REMOVE ALL SHARP EDGES AND CORNERS		SCALE 1:5 @ A1	
	TOLERANCES UDS		THIRD ANGLE PROJECTION		DRAWING No.	
	MACHINING	+ 0.25MM			TEST MACHINE TOP PLATE DETAIL	
FABRICATING	+ 2.0MM	DR/1611-D9 M/C				

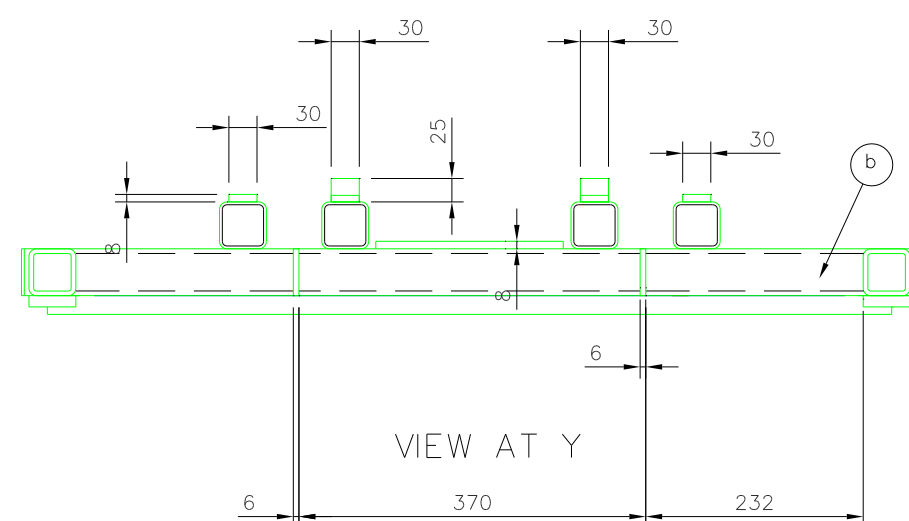


SECTION A-A

NOTE !
FULLY WELD ALL JOINTS
STRESS RELIEVE PRIOR TO M/C
BREAK ALL SHARP EDGES

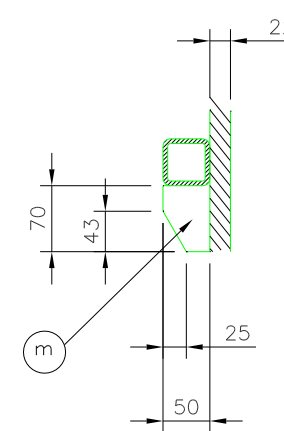


VIEW AT X



VIEW AT Y

SECTION THRO GUSSET
typ 4-places



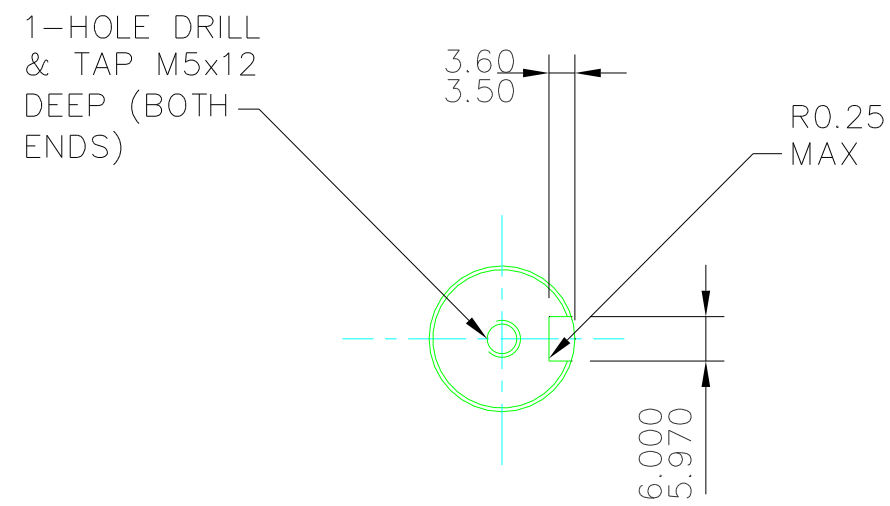
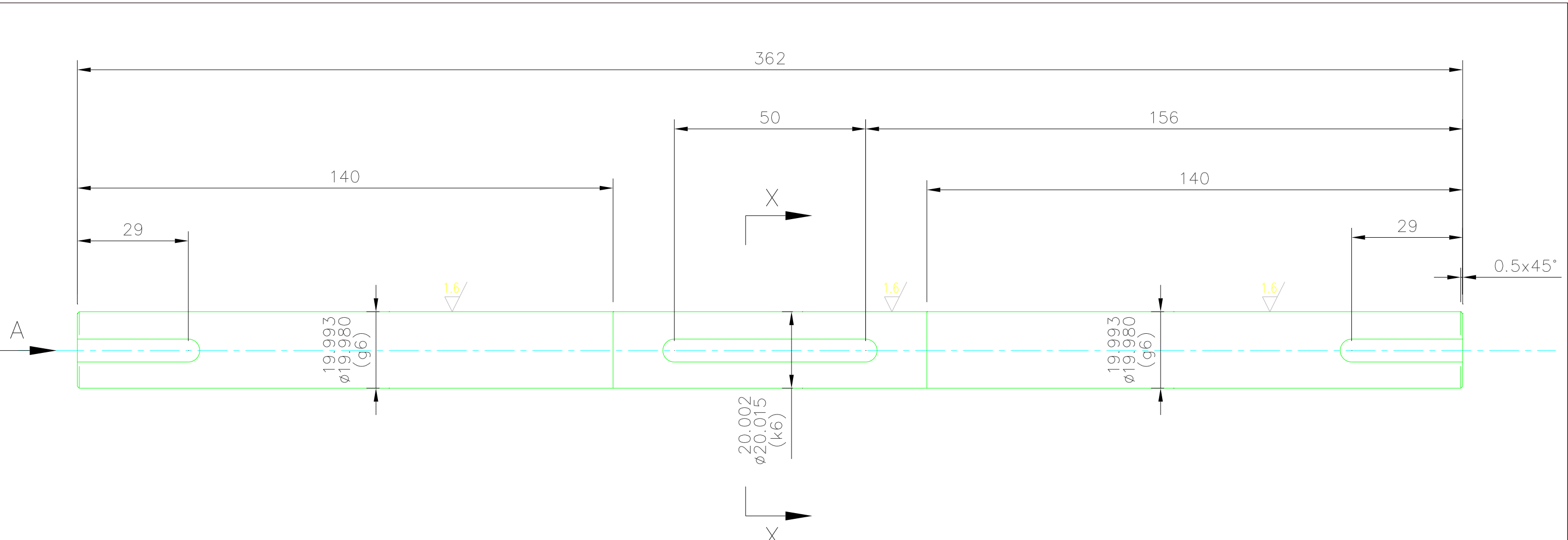
MATERIAL LIST

- a) 50x50x5 RHS x 980 LONG 1-OFF REQUIRED
- b) 50x50x5 RHS x 840 LONG 2-OFF REQUIRED
- c) 50x50x5 RHS x 825 LONG 2-OFF REQUIRED
- d) 50x50x5 RHS x 557.5 LONG 2-OFF REQUIRED
- e) 50x50x5 RHS x 250 LONG 2-OFF REQUIRED
- f) 900x540x22 thick SUPER DUPLEX PLATE 1-OFF REQUIRED
- g) 90x135x15 thick M.S PLATE 2-OFF REQUIRED
- h) 60x50x15 thick M.S PLATE 2-OFF REQUIRED
- j) 150x50x10 thick M.S PLATE 2-OFF REQUIRED
- k) 30x25x15 thick M.S PLATE 2-OFF REQUIRED
- l) 250x30x8 thick M.S PLATE 4-OFF REQUIRED
- m) 70x50x6 thick M.S PLATE 4-OFF REQUIRED
- n) 200x50x8 thick M.S PLATE 1-OFF REQUIRED
- o) 50x50 PLASTIC END COVERS 10-OFF REQUIRED

TOP PLATE
MATERIAL M.S FABRICATION
1-OFF REQUIRED

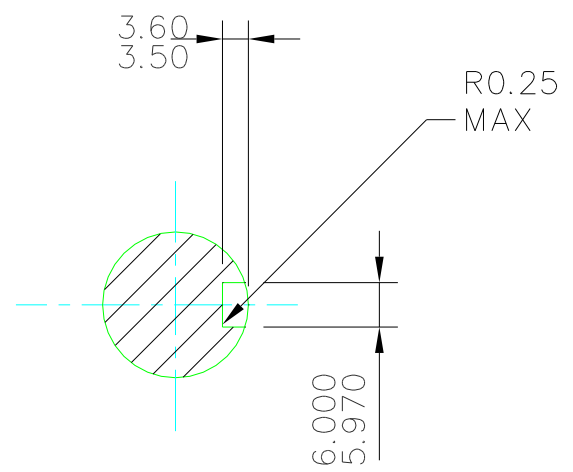
NOTE !
READ THIS DRAWING IN CONJUNCTION
WITH MACHINING DRAWING D9/MC

THIS DRAWING IS THE SOLE PROPERTY OF LANESFIELD ENGINEERING SEALS AND MUST NOT BE REPRODUCED NOR ITS CONTENTS DIVULGED WITHOUT WRITTEN PERMISSION	UNLESS OTHERWISE STATED		LANESFIELD ENGINEERING LTD. UNIT 11, SPRING ROAD IND. ESTATE, LANESFIELD DRIVE, W.TON, WEST MIDLANDS, WV4 6UA FAX No 01902-405005 TELE No 01902 497777	DRAWN	R.K.C.	DATE
	TOLERANCES UNLESS OTHERWISE STATED	REMOVE ALL SHARP EDGES AND CORNERS		CUSTOMER	BODYCOTE	
	MACHINING + 0.25MM FABRICATING + 2.0MM	THIRD ANGLE PROJECTION		DRAWING TITLE	TEST MACHINE TOP PLATE DETAIL	SCALE
				DRAWING No.	DR/1611-D9 FAB	ISSUE No.



VIEW AT 'A'
TYP BOTH ENDS

DRIVE SHAFT
MATERIAL EN8
1-OFF REQUIRED



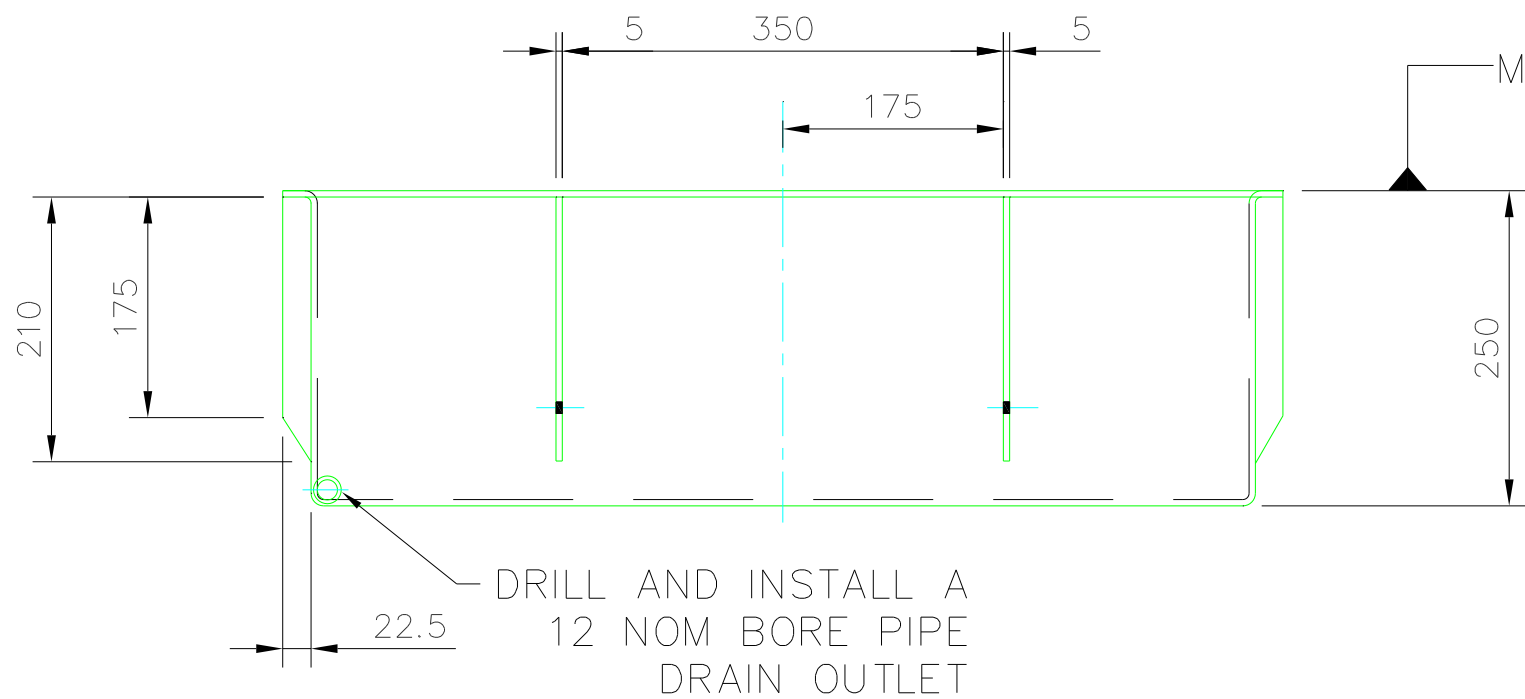
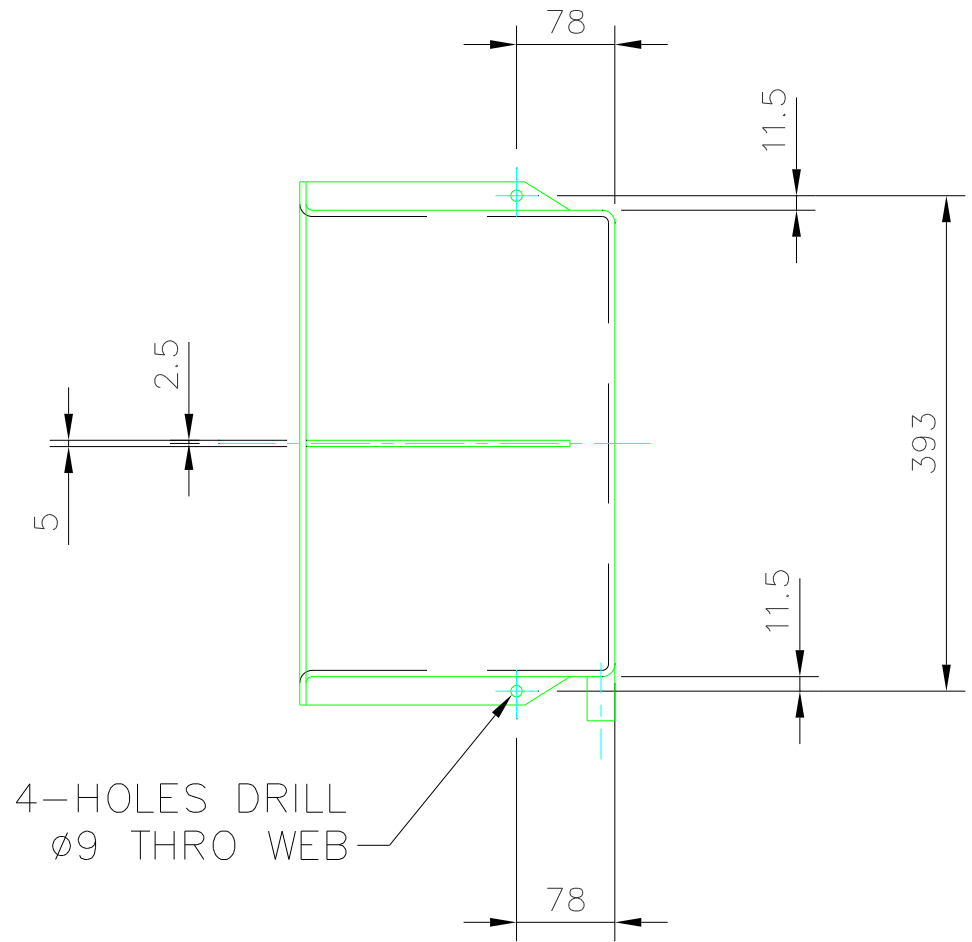
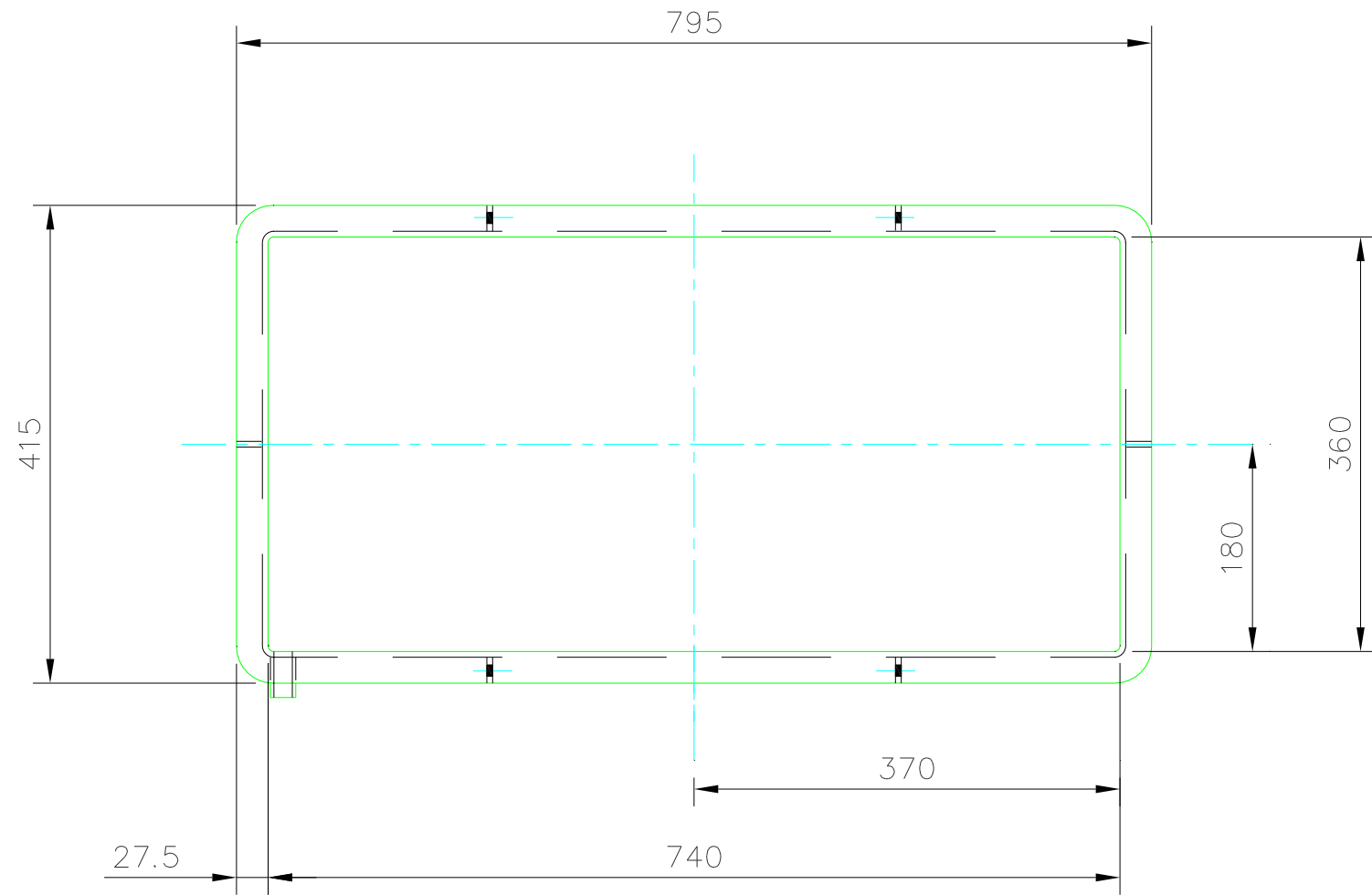
SECTION X-X

THIS DRAWING IS THE SOLE PROPERTY OF LANESFIELD ENGINEERING SEALS AND MUST NOT BE REPRODUCED NOR ITS CONTENTS DIVULGED WITHOUT WRITTEN PERMISSION

UNLESS OTHERWISE STATED	
ALL DIMENSIONS IN MILLIMETERS	REMOVE ALL SHARP EDGES AND CORNERS
TOLERANCES UOS	THIRD ANGLE PROJECTION
MACHINING	+ 0.25MM
FABRICATING	± 2.0MM

LANESFIELD ENGINEERING LTD. UNIT 11, SPRING ROAD IND ESTATE, LANESFIELD DRIVE, W'TON, WEST MIDLANDS. WV4 6UA FAX No 01902-405005 TELE No 01902 497777	
CUSTOMER	BODYCOTE
DRAWING TITLE	TEST MACHINE DRIVE SHAFT DETAILS

DRAWN	R.K.C.	DATE	
SCALE	1:1 @ A3		
DRAWING No.	DR/1611-D10	ISSUE No.	



TANK
MATERIAL 5mm THICK
PLASTIC SHEET
1-OFF REQUIRED

NOTE !
TANK MUST BE LEAK PROOF TESTED
PRIOR TO DELIVERY

THIS DRAWING IS THE SOLE PROPERTY
OF LANESFIELD ENGINEERING SEALS
AND MUST NOT BE REPRODUCED NOR
ITS CONTENTS DIVULGED WITHOUT
WRITTEN PERMISSION

UNLESS OTHERWISE STATED

ALL DIMENSIONS IN MILLIMETERS	
TOLERANCES UOS	
MACHINING	+ 0.25MM
FABRICATING	± 2.0MM

REMOVE ALL SHARP EDGES
AND CORNERS

THIRD ANGLE PROJECTION



LANESFIELD ENGINEERING LTD.

UNIT 11, SPRING ROAD IND ESTATE, LANESFIELD DRIVE, W'TON, WEST MIDLANDS, WV4 6UA
FAX No 01902-405005 TELE No 01902 497777

CUSTOMER BODYCOTE

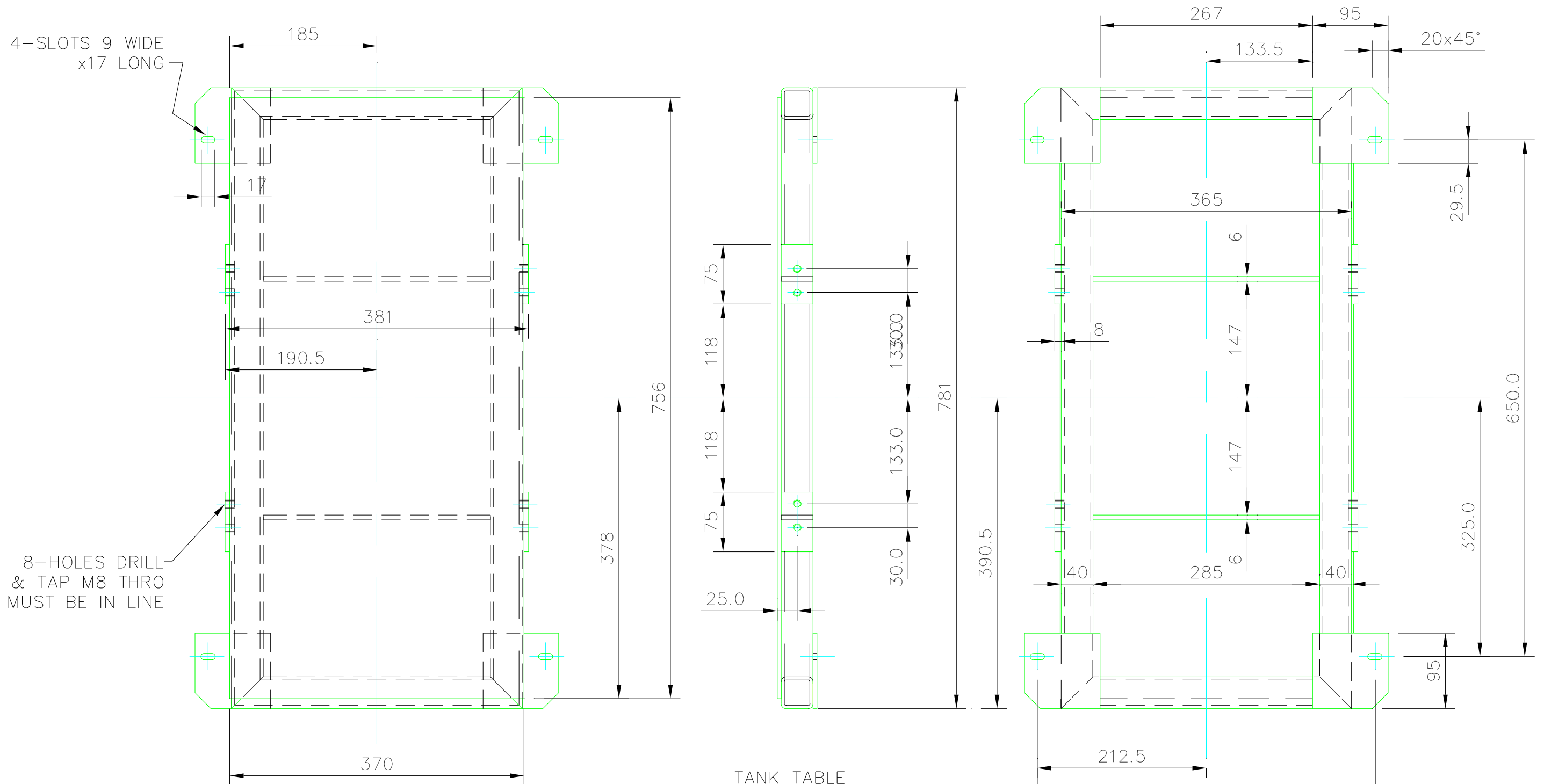
DRAWING TITLE TEST MACHINE
FLUID TANK

DRAWN R.K.C.

DATE

SCALE 1:7.5 @ A3

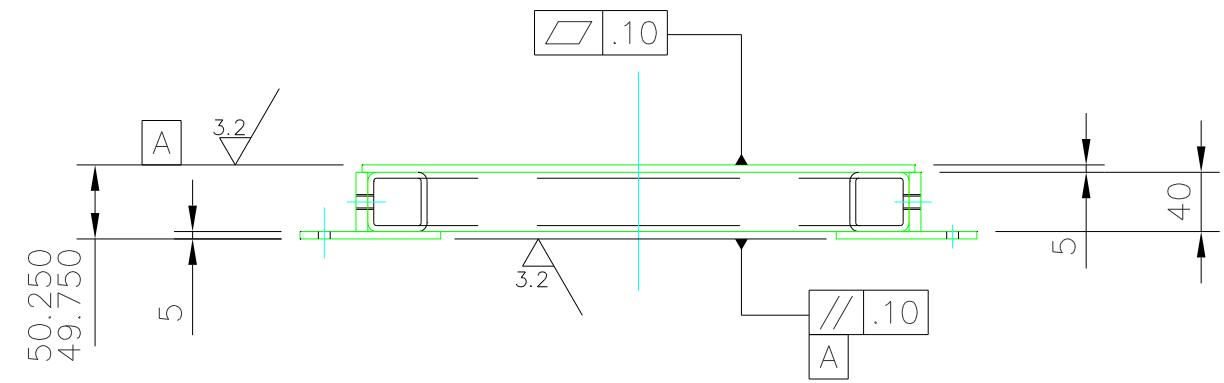
DRAWING No. DR/1611-D12
ISSUE No.



TANK TABLE
1-OFF REQUIRED
MATERIAL M.S FABRICATION

- MATERIAL LIST
- 40x40x5 THICK RHSx781 LONG - 2-OFF REQUD
 - 40x40x5 THICK RHSx365 LONG - 2-OFF REQUD
 - 40x8 THICK FLATx75 LONG - 4-OFF REQUD
 - 40x6 THICK FLATx285 LONG - 2-OFF REQUD
 - 756x370x6 THICK PLATE - 1-OFF REQUD
 - 96x95x6 THICK PLATE - 4-OFF REQUD

NOTE !
WELD ALL JOINTS

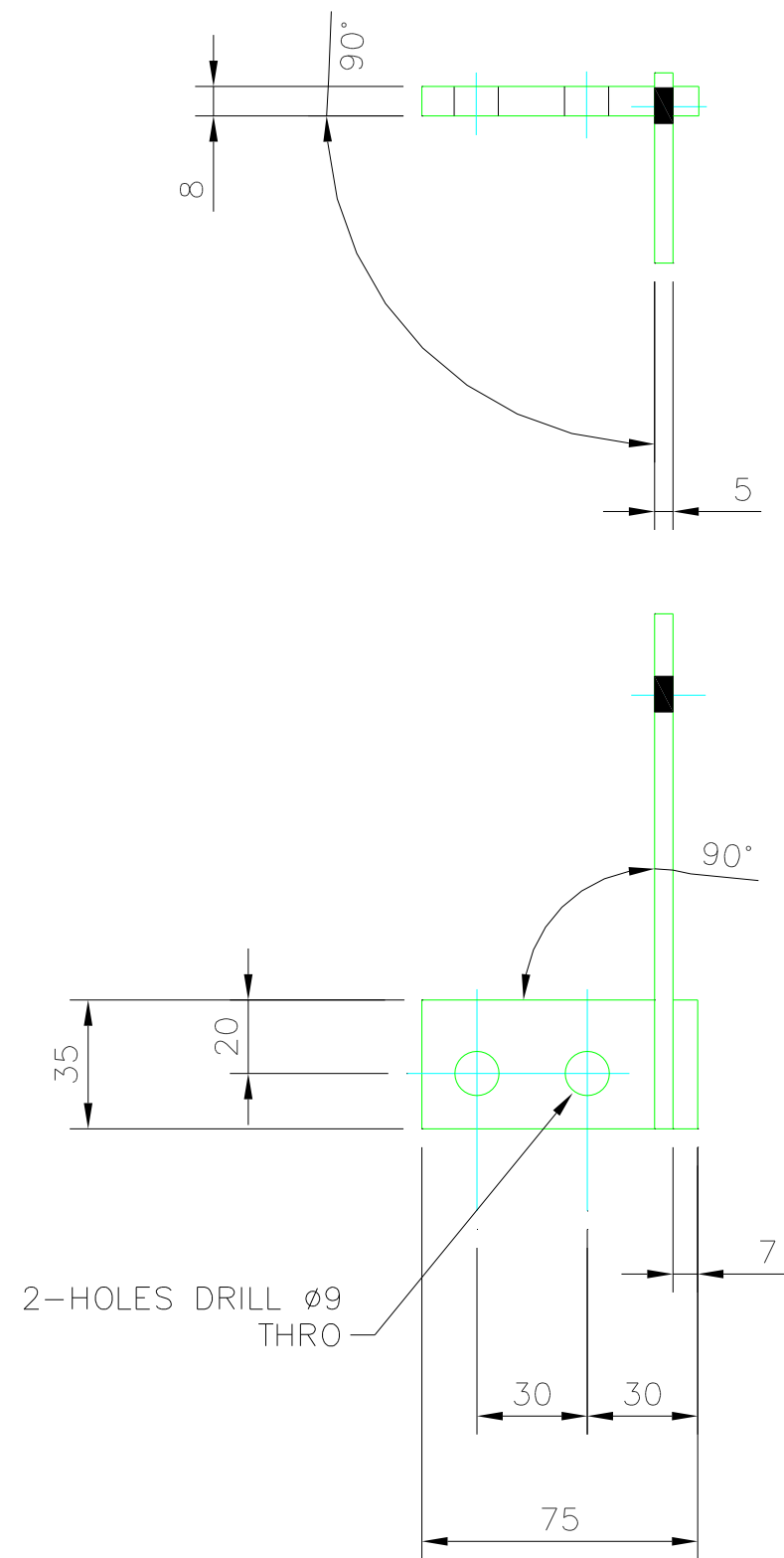


THIS DRAWING IS THE SOLE PROPERTY OF LANESFIELD ENGINEERING SEALS AND MUST NOT BE REPRODUCED NOR ITS CONTENTS DIVULGED WITHOUT WRITTEN PERMISSION

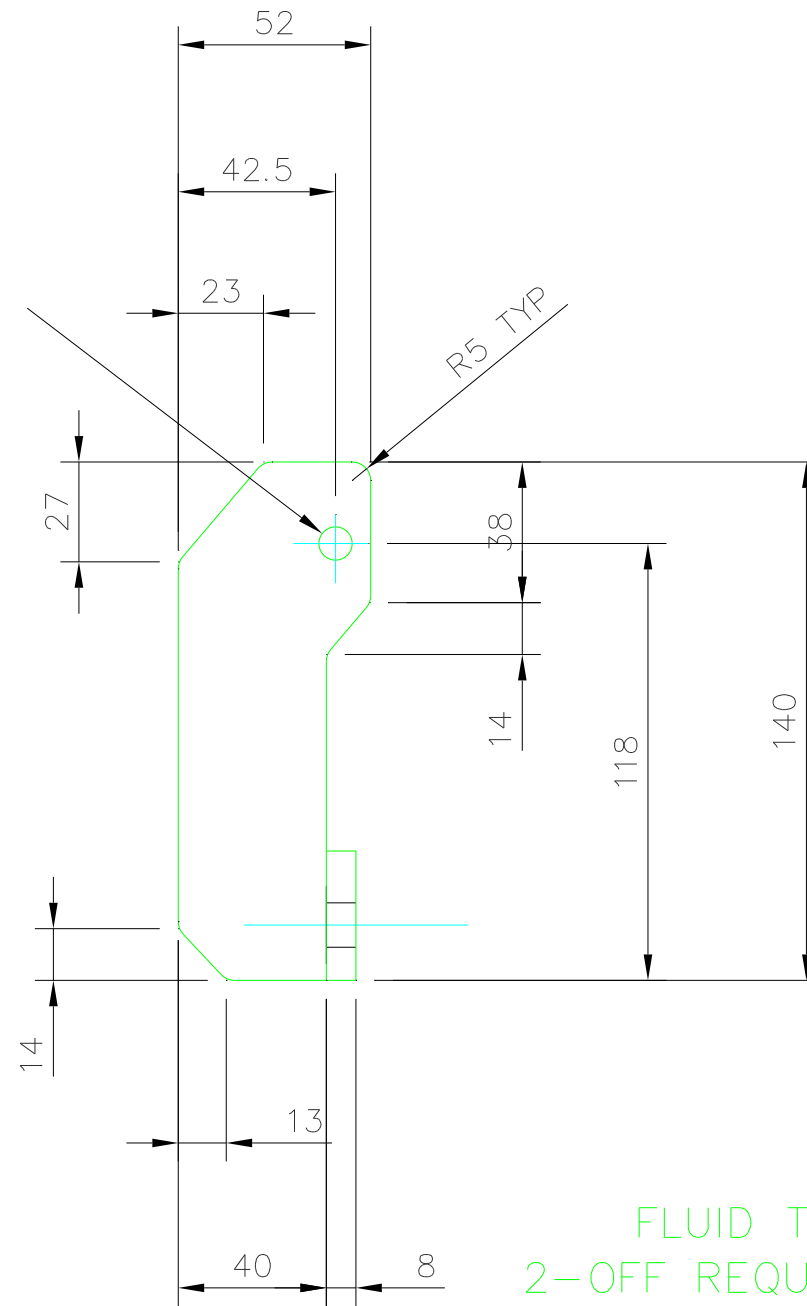
UNLESS OTHERWISE STATED	
ALL DIMENSIONS IN MILLIMETERS	REMOVE ALL SHARP EDGES AND CORNERS
TOLERANCES UOS	THIRD ANGLE PROJECTION
MACHINING	+ 0.25MM
FABRICATING	± 2.0MM

LANESFIELD ENGINEERING LTD. UNIT 11. SPRING ROAD IND ESTATE, LANESFIELD DRIVE. W'TON, WEST MIDLANDS. WV4 6UA FAX No 01902-405005 TELE No 01902 497777	
CUSTOMER	BODYCOTE
DRAWING TITLE	TEST MACHINE FLUID TANK TABLE

DRAWN	R.K.C.	DATE	
SCALE	1:5 @ A3		
DRAWING No.	DR/1611-D13	ISSUE No.	

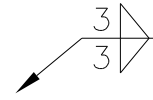


1-HOLE DRILL ø9 THRO



FLUID TANK BRACKET
 2-OFF REQUIRED (AS DRAWN)
 2-OFF REQUIRED (OPP HAND)
 MATERIAL M.S FABRICATION

NOTE !
 FULLY WELD JOINTS



THIS DRAWING IS THE SOLE PROPERTY OF LANESFIELD ENGINEERING SEALS AND MUST NOT BE REPRODUCED NOR ITS CONTENTS DIVULGED WITHOUT WRITTEN PERMISSION

UNLESS OTHERWISE STATED

ALL DIMENSIONS IN MILLIMETERS

TOLERANCES UOS

MACHINING + 0.25MM

FABRICATING ± 2.0MM

REMOVE ALL SHARP EDGES AND CORNERS

THIRD ANGLE PROJECTION



LANESFIELD ENGINEERING LTD.

UNIT 11, SPRING ROAD IND ESTATE, LANESFIELD DRIVE, W'TON, WEST MIDLANDS. WV4 6UA
 FAX No 01902-405005 TELE No 01902 497777

CUSTOMER

BODYCOTE

DRAWING TITLE

TEST MACHINE
 FLUID TANK BRACKET

DRAWN

R.K.C.

DATE

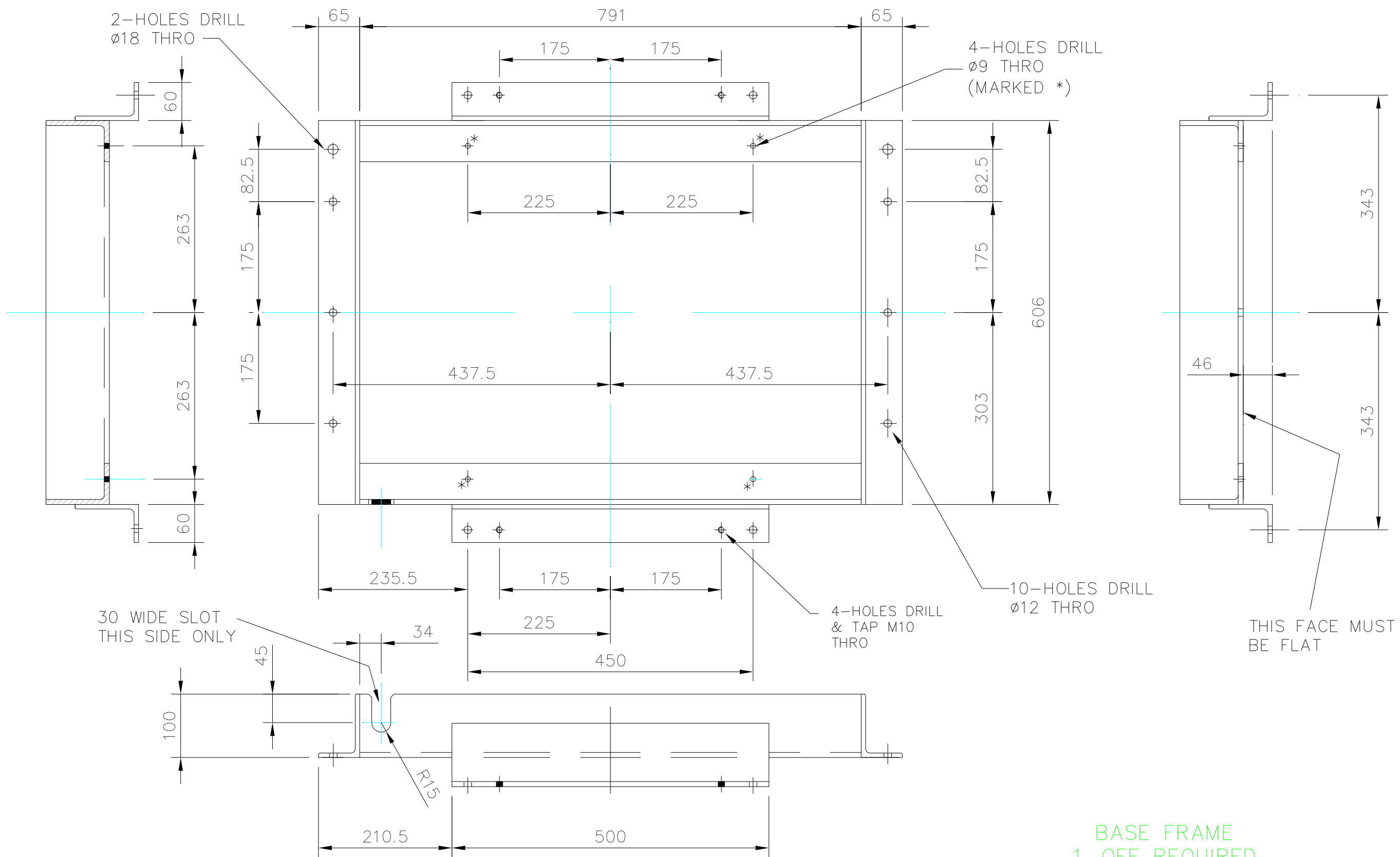
SCALE

1:2 @ A3

DRAWING No.

DR/1611-D14

ISSUE No.



BASE FRAME
 1-OFF REQUIRED
 MATERIAL 100x65x8 THICK R.S.ANGLE

THIS DRAWING IS THE SOLE PROPERTY OF LANESFIELD ENGINEERING SEALS AND MUST NOT BE REPRODUCED NOR ITS CONTENTS DIVULGED WITHOUT WRITTEN PERMISSION

UNLESS OTHERWISE STATED

ALL DIMENSIONS IN MILLIMETERS

TOLERANCES UOS

MACHINING + 0.25MM

FABRICATING ± 2.0MM

REMOVE ALL SHARP EDGES AND CORNERS

THIRD ANGLE PROJECTION



LANESFIELD ENGINEERING LTD.

UNIT 11, SPRING ROAD IND ESTATE, LANESFIELD DRIVE, W'TON, WEST MIDLANDS. WV4 6UA
 FAX No 01902-405005 TELE No 01902 497777

CUSTOMER BODYCOTE

DRAWING TITLE TEST MACHINE FLUID TANK BASE FRAME

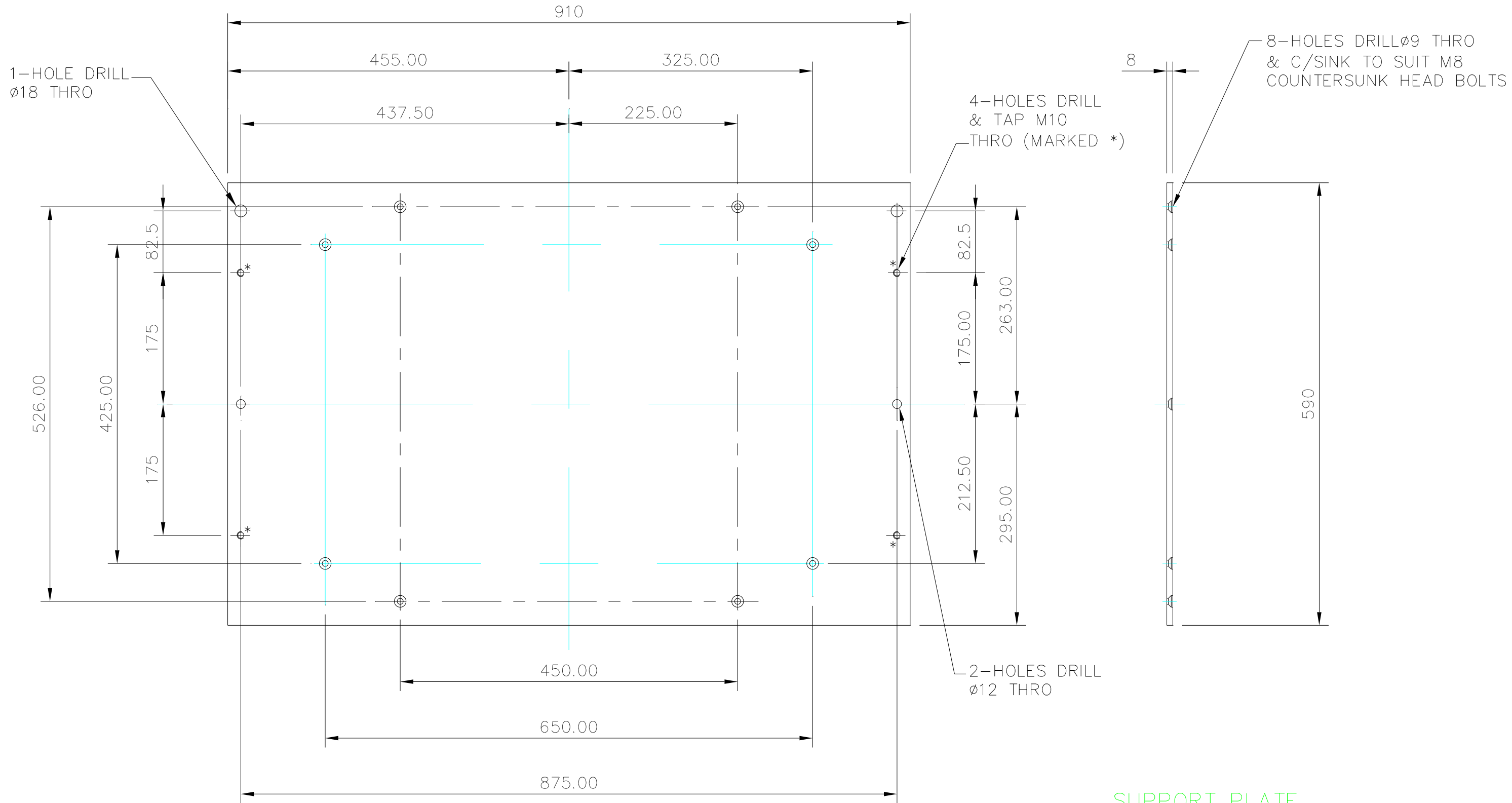
DRAWN R.K.C.

DATE

SCALE 1:7.5 @ A3

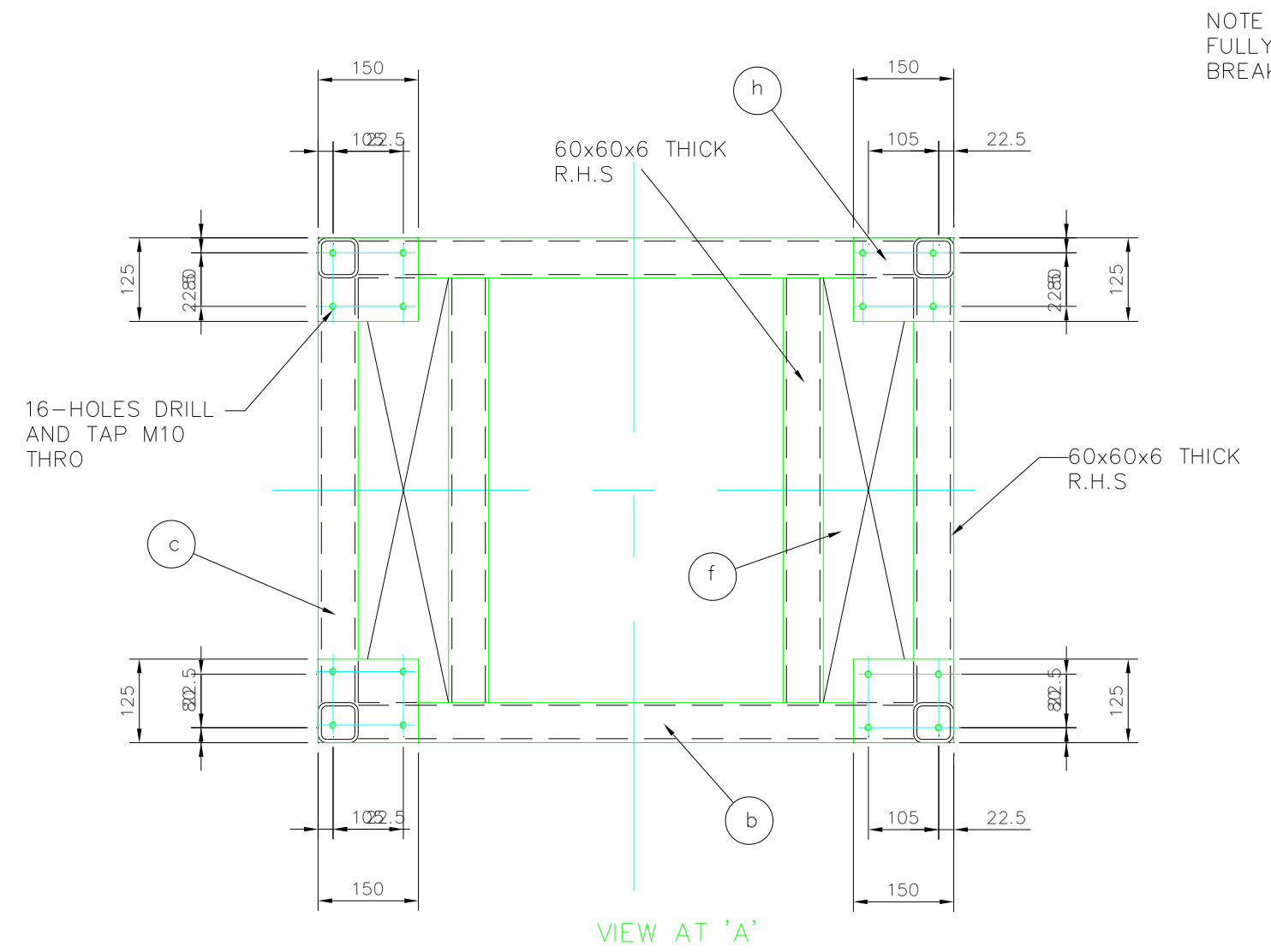
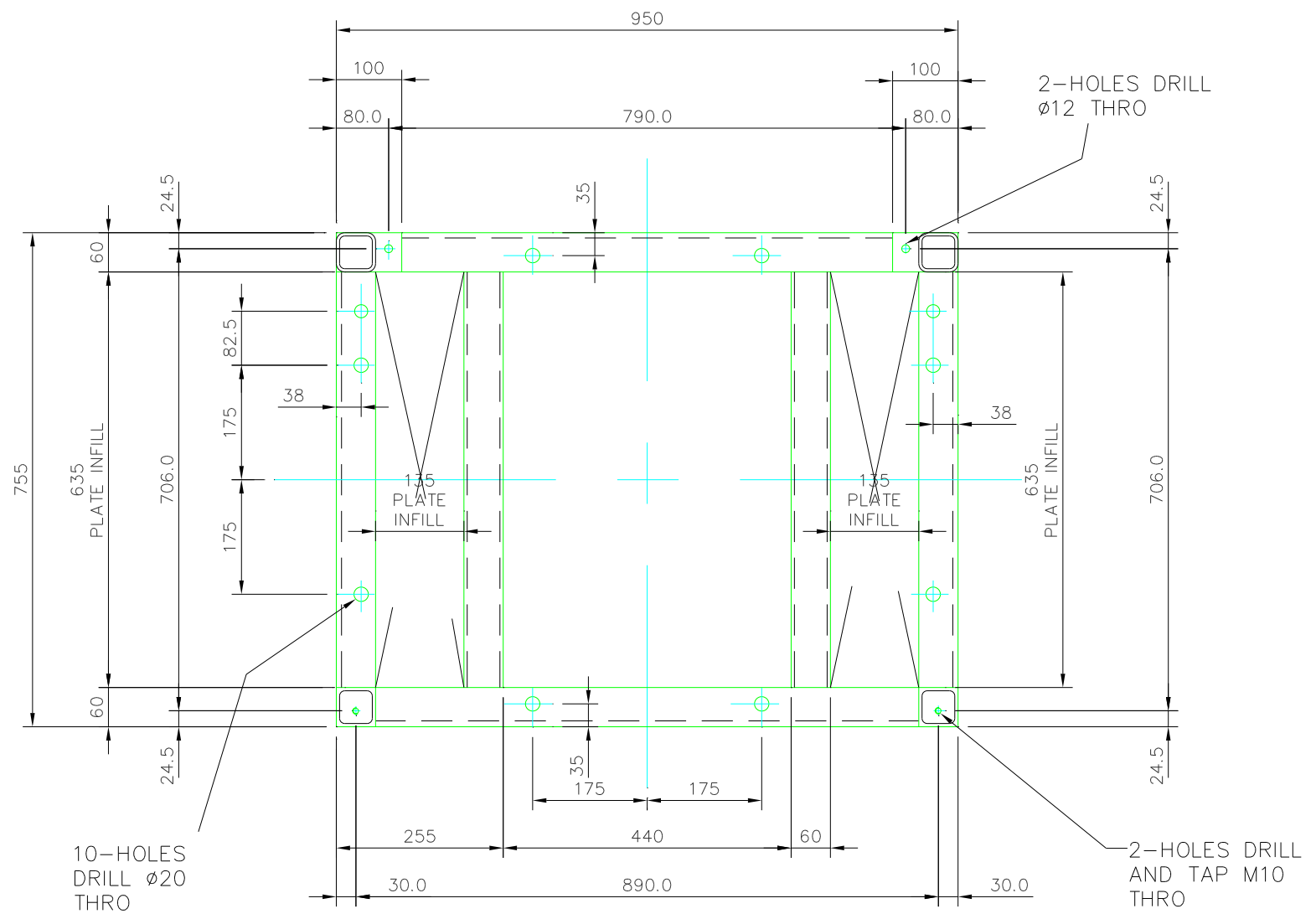
DRAWING No. DR/1611-D15

ISSUE No.

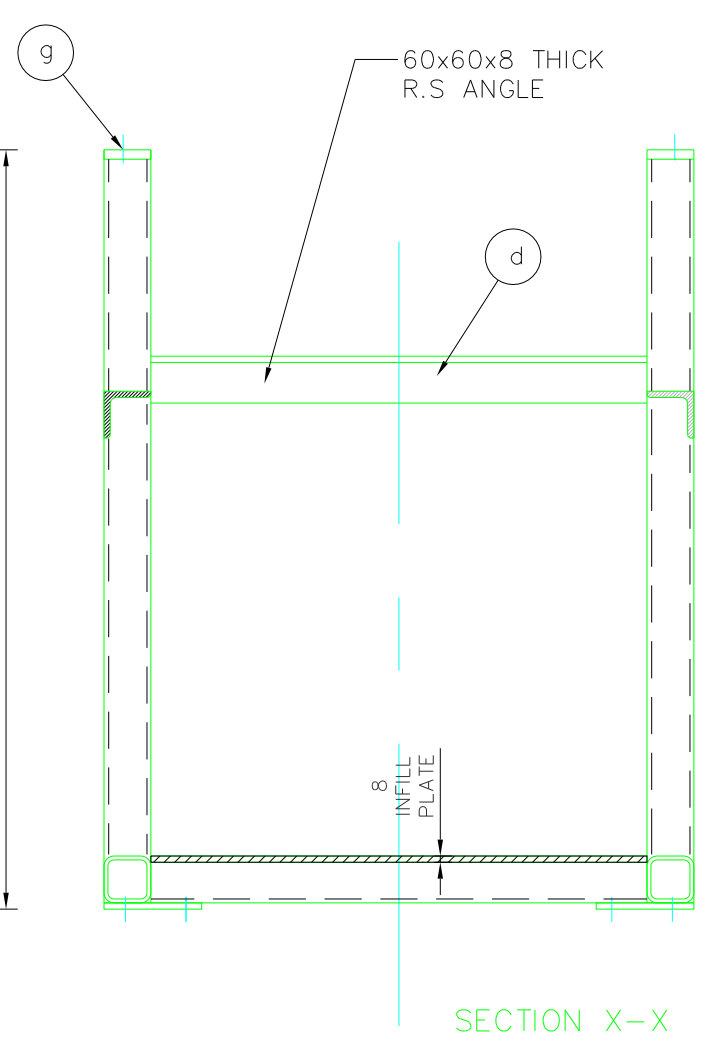
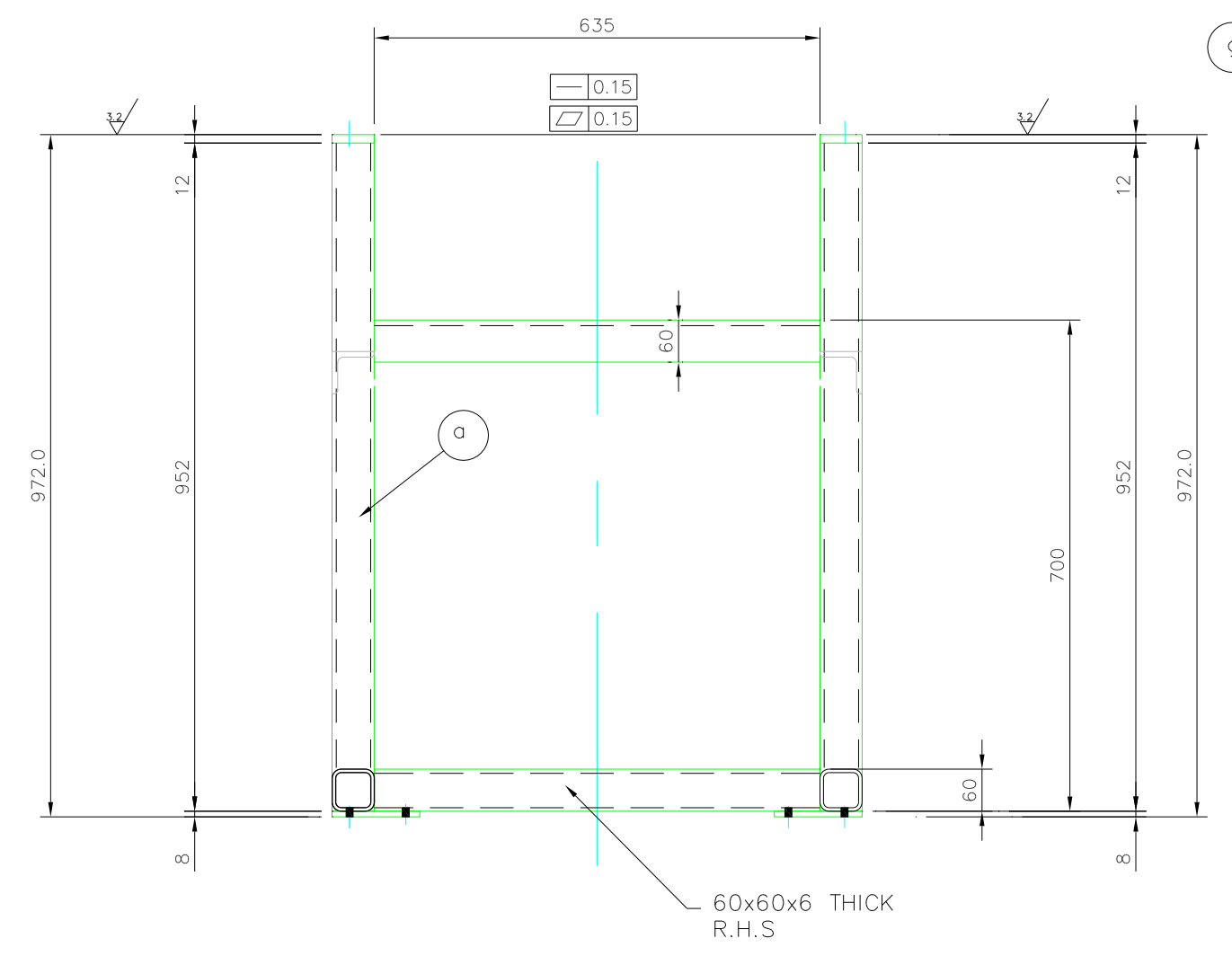
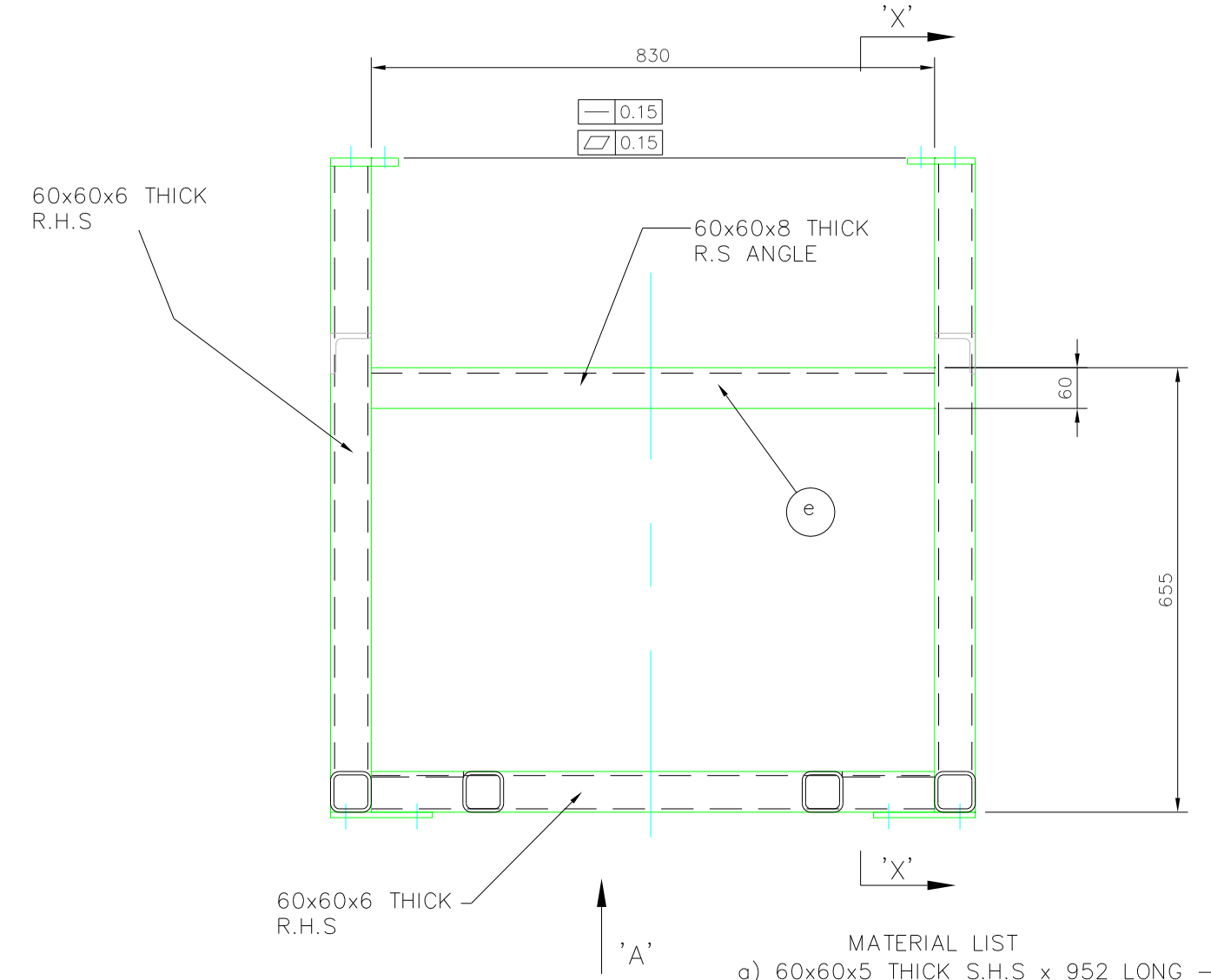


SUPPORT PLATE
 1-OFF REQUIRED
 MATERIAL FLASH GROUND PLATE

THIS DRAWING IS THE SOLE PROPERTY OF LANESFIELD ENGINEERING SEALS AND MUST NOT BE REPRODUCED NOR ITS CONTENTS DIVULGED WITHOUT WRITTEN PERMISSION	UNLESS OTHERWISE STATED		LANESFIELD ENGINEERING LTD.		DRAWN	R.K.C.	DATE	
	ALL DIMENSIONS IN MILLIMETERS		REMOVE ALL SHARP EDGES AND CORNERS		UNIT 11, SPRING ROAD IND ESTATE, LANESFIELD DRIVE, W'TON, WEST MIDLANDS. WV4 6UA FAX No 01902-405005 TELE No 01902 497777			
	TOLERANCES UOS		THIRD ANGLE PROJECTION		CUSTOMER			SCALE
	MACHINING	+ 0.25MM			BODYCOTE			1:5 @ A3
FABRICATING	± 2.0MM	DRAWING TITLE			DRAWING No.	ISSUE No.		
				TEST MACHINE FLUID TANK BASE PLATE			DR/1611-D16	



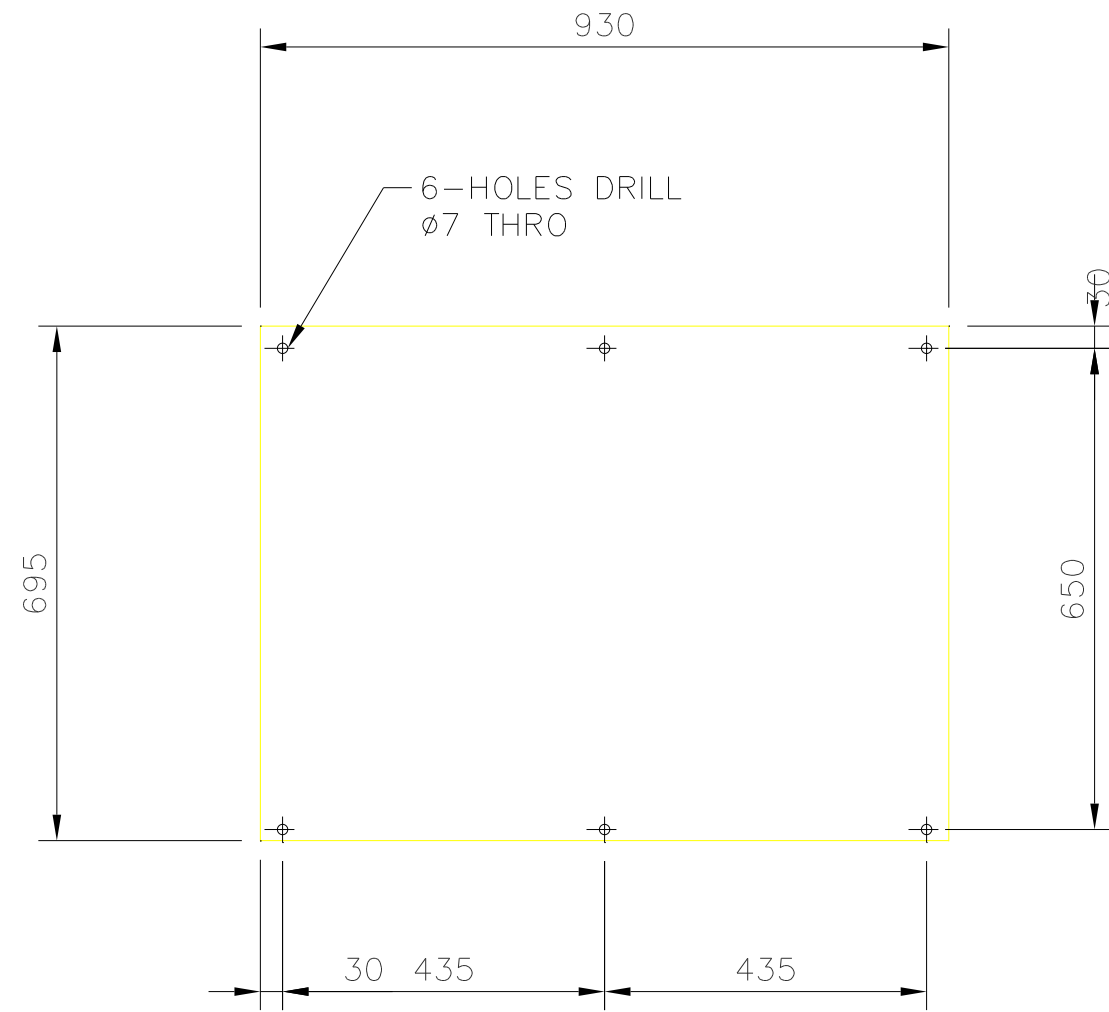
NOTE !
FULLY WELD ALL JOINTS
BREAK ALL SHARP EDGES



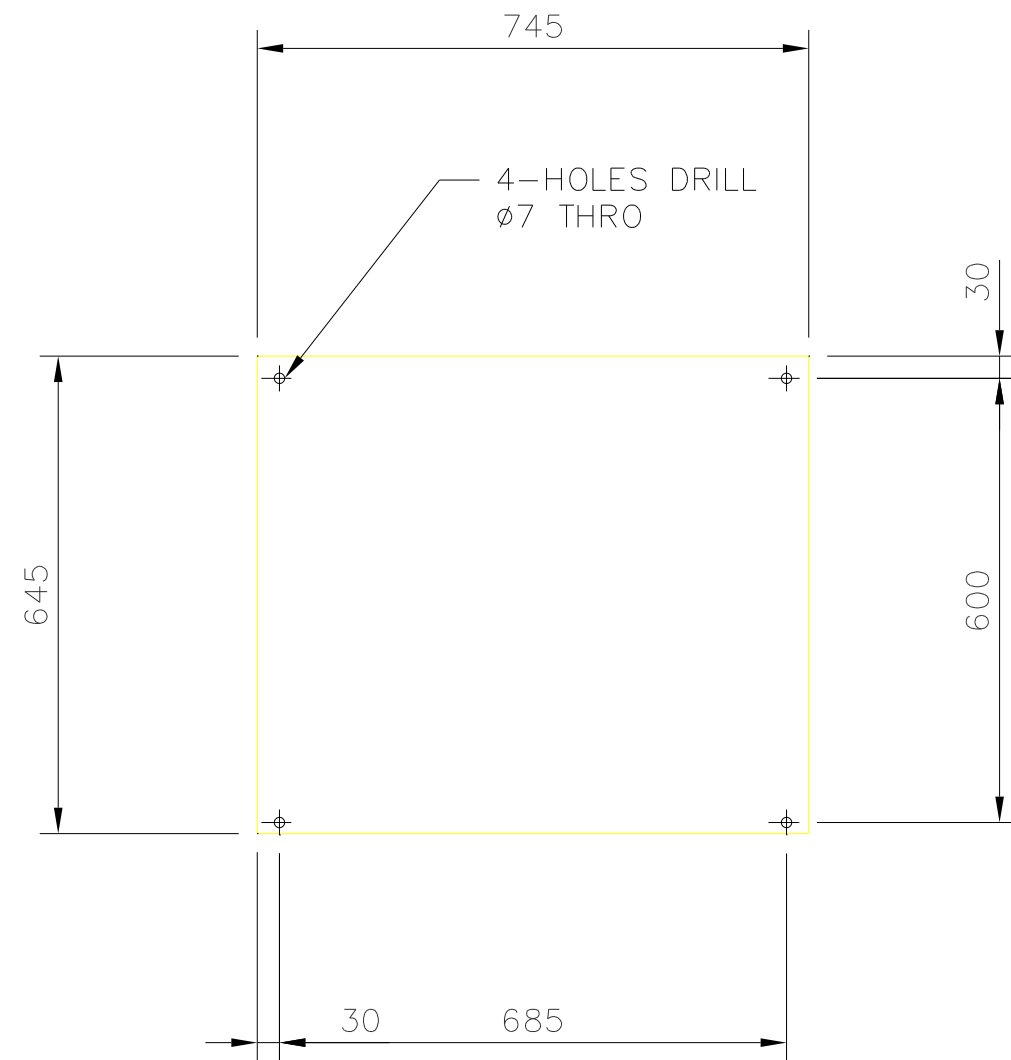
- MATERIAL LIST**
- a) 60x60x5 THICK S.H.S x 952 LONG - 4-OFF REQUIRED
 - b) 60x60x5 THICK S.H.S x 830 LONG - 2-OFF REQUIRED
 - c) 60x60x5 THICK S.H.S x 635 LONG - 4-OFF REQUIRED
 - d) 60x60x8 THICK R.S ANGLE x 830 LONG - 2-OFF REQUIRED
 - e) 60x60x8 THICK R.S ANGLE x 635 LONG - 2-OFF REQUIRED
 - f) 635x135x8 THICK M.S PLATE - 2-OFF REQUIRED
 - g) 60x60x15 THICK M.S PLATE - 2-OFF REQUIRED
 - h) 150x125x8 THICK M.S PLATE - 4-OFF REQUIRED
 - j) 100x60x15 THICK M.S PLATE - 2-OFF REQUIRED

BASE FRAME
1-OFF REQUIRED
MATERIAL M.S FABRICATION

THIS DRAWING IS THE SOLE PROPERTY OF LANESFIELD ENGINEERING SEALS AND MUST NOT BE REPRODUCED NOR ITS CONTENTS DIVULGED WITHOUT WRITTEN PERMISSION	UNLESS OTHERWISE STATED		LANESFIELD ENGINEERING LTD. UNIT 11, SPRING ROAD IND. ESTATE, LANESFIELD DRIVE, W.TON, WEST MIDLANDS, WV4 6UA FAX No 01902-405005 TELE No 01902 497777	DRAWN	R.K.C.	DATE
	TOLERANCES UNLESS OTHERWISE STATED	THIRD ANGLE PROJECTION		CUSTOMER	BODYCOTE	
	MACHINING: +0.25MM FABRICATING: +2.0MM			DRAWING TITLE	TEST MACHINE BASE FRAME DETAIL	SCALE
				DRAWING No.	DR/1611-D17	ISSUE No.



COVER PLATE
2-OFF REQUIRED
MATERIAL 2mm THICK M.S SHEET



COVER PLATE
2-OFF REQUIRED
MATERIAL 2mm THICK M.S SHEET

THIS DRAWING IS THE SOLE PROPERTY OF LANESFIELD ENGINEERING SEALS AND MUST NOT BE REPRODUCED NOR ITS CONTENTS DIVULGED WITHOUT WRITTEN PERMISSION

UNLESS OTHERWISE STATED

ALL DIMENSIONS IN MILLIMETERS

TOLERANCES UOS

MACHINING + 0.25MM

FABRICATING ± 2.0MM

REMOVE ALL SHARP EDGES AND CORNERS

THIRD ANGLE PROJECTION



LANESFIELD ENGINEERING LTD.

UNIT 11, SPRING ROAD IND ESTATE, LANESFIELD DRIVE, W'TON, WEST MIDLANDS. WV4 6UA
FAX No 01902-405005 TELE No 01902 497777

CUSTOMER

BODYCOTE

DRAWING TITLE

TEST MACHINE
BASE FRAME COVER DETAILS

DRAWN

R.K.C.

DATE

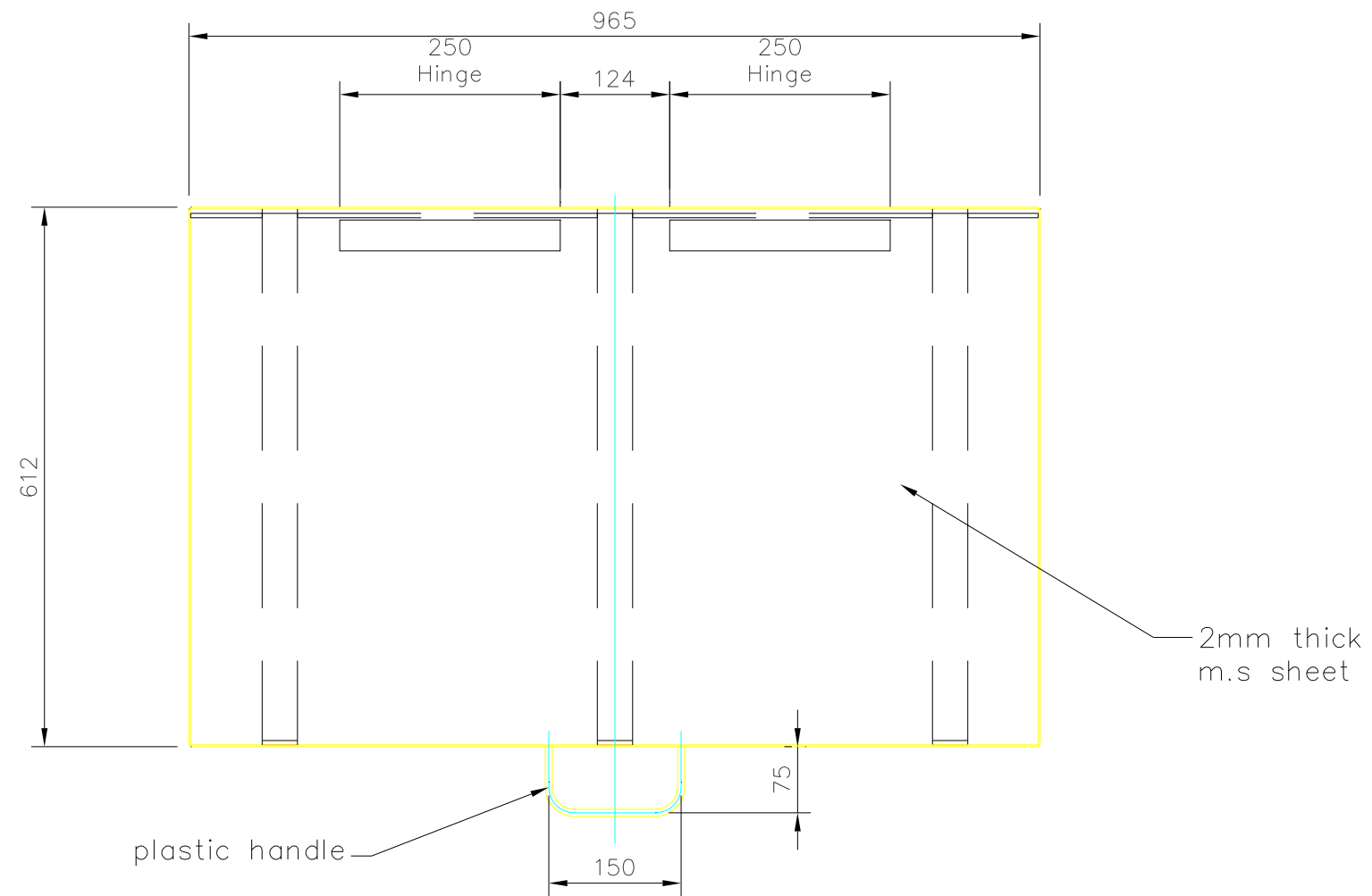
SCALE

1:10 @ A3

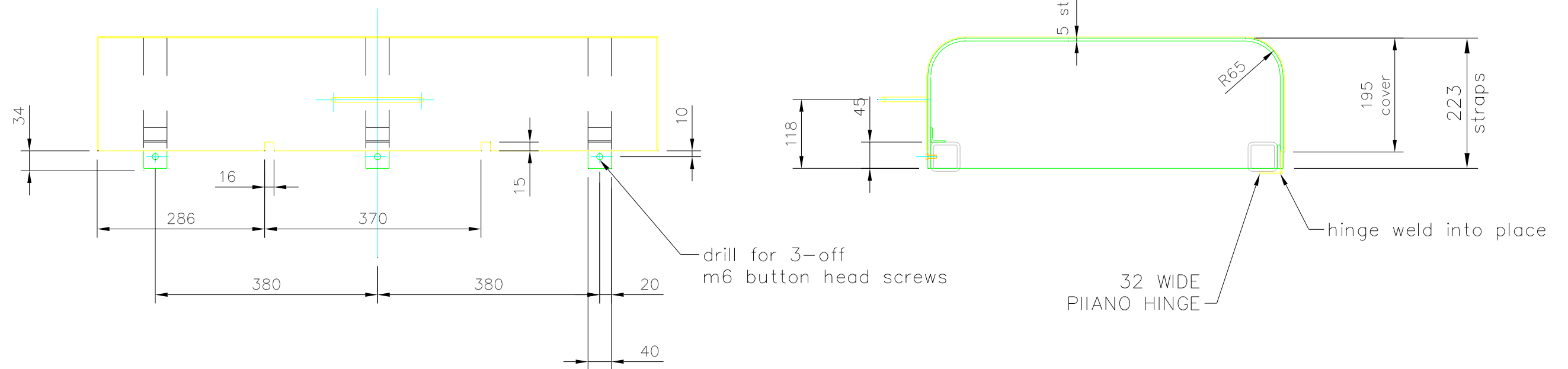
DRAWING No.

DR/1611-D18

ISSUE No.



DRIVE COVER
1-OFF REQUIRED
MATERIAL M.S SHEET



THIS DRAWING IS THE SOLE PROPERTY OF LANESFIELD ENGINEERING SEALS AND MUST NOT BE REPRODUCED NOR ITS CONTENTS DIVULGED WITHOUT WRITTEN PERMISSION

UNLESS OTHERWISE STATED

ALL DIMENSIONS IN MILLIMETERS

TOLERANCES UOS

MACHINING + 0.25MM

FABRICATING ± 2.0MM

REMOVE ALL SHARP EDGES AND CORNERS

THIRD ANGLE PROJECTION



LANESFIELD ENGINEERING LTD.

UNIT 11. SPRING ROAD IND ESTATE, LANESFIELD DRIVE. W'TON, WEST MIDLANDS. WV4 6UA
FAX No 01902-405005 TELE No 01902 497777

CUSTOMER BODYCOTE

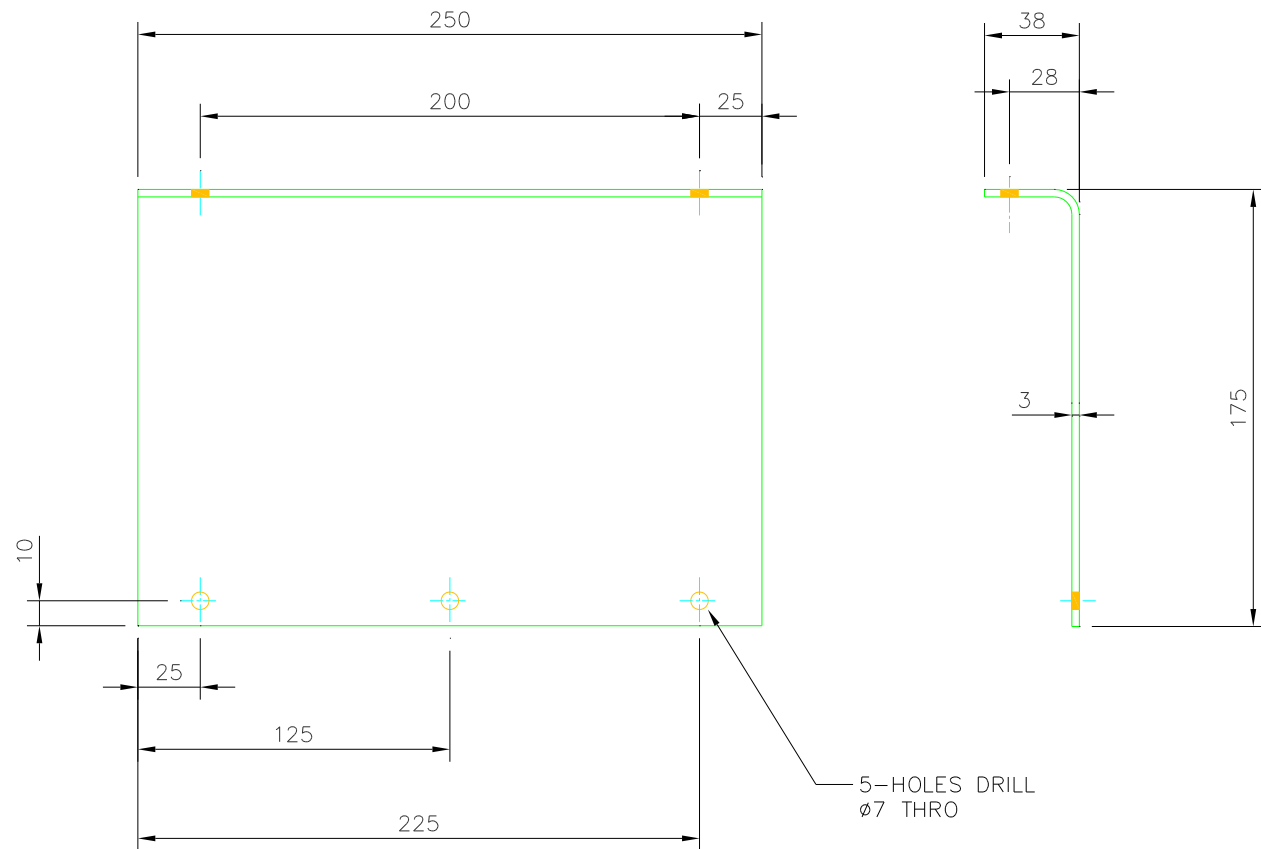
DRAWING TITLE TEST MACHINE DRIVE COVER DETAILS

DRAWN R.K.C.

DATE

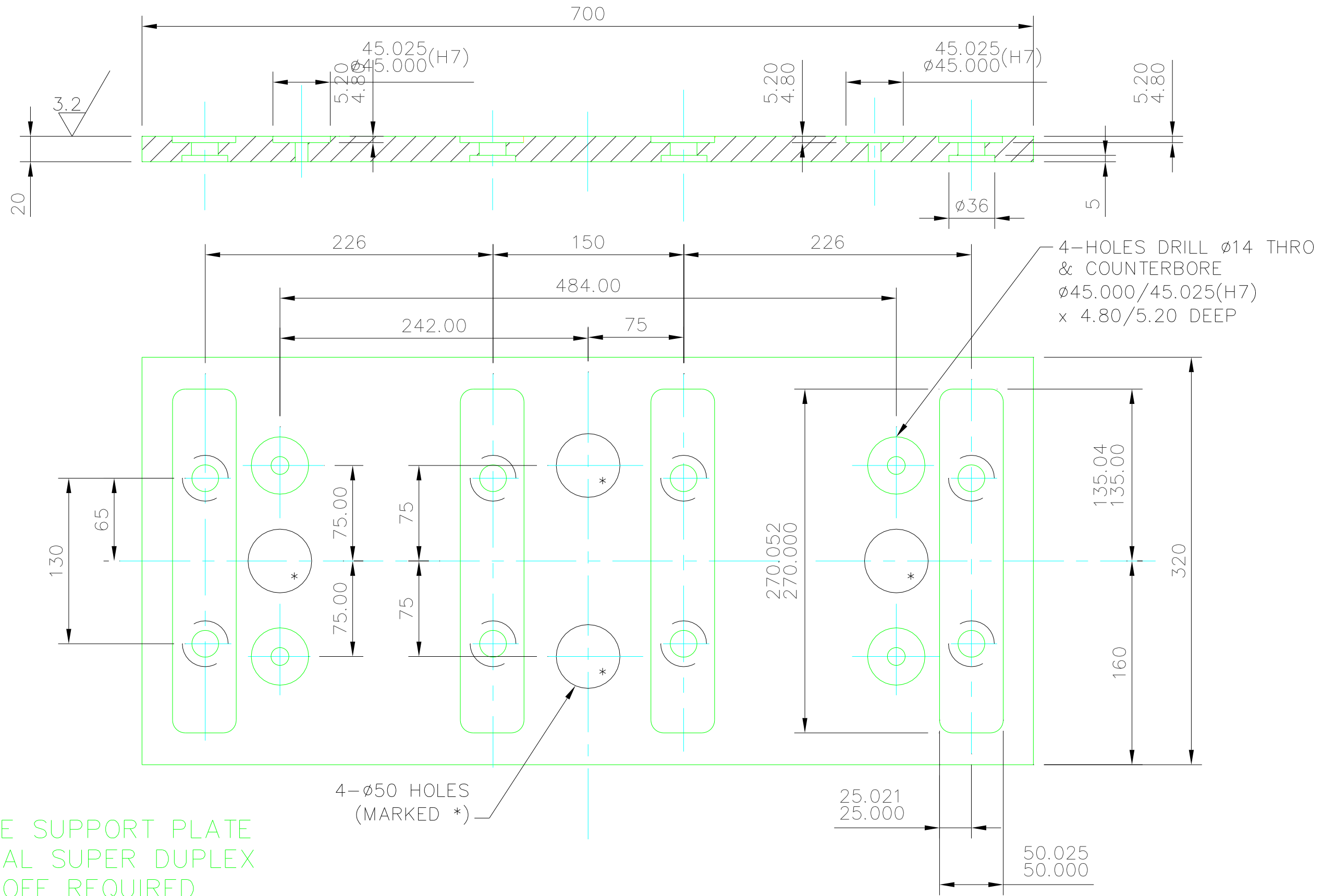
SCALE 1:7.5 @ A3

DRAWING No. DR/1611-D19
ISSUE No.



COVER GUARD
2-OFF REQUIRED
MATERIAL M.S SHEET

<p>THIS DRAWING IS THE SOLE PROPERTY OF LANESFIELD ENGINEERING SEALS AND MUST NOT BE REPRODUCED NOR ITS CONTENTS DIVULGED WITHOUT WRITTEN PERMISSION</p>	UNLESS OTHERWISE STATED		LANESFIELD ENGINEERING LTD.		DRAWN	R.K.C.	DATE		
	ALL DIMENSIONS IN MILLIMETERS		REMOVE ALL SHARP EDGES AND CORNERS		UNIT 11, SPRING ROAD IND ESTATE, LANESFIELD DRIVE, W'TON, WEST MIDLANDS. WV4 6UA FAX No 01902-405005 TELE No 01902 497777				
	TOLERANCES UOS		THIRD ANGLE PROJECTION		CUSTOMER	BODYCOTE		SCALE	1:2 @ A3
	MACHINING	+ 0.25MM			DRAWING TITLE	TEST MACHINE DRIVE COVER DETAILS		DRAWING No.	ISSUE No.
FABRICATING	+ 2.0MM						DR/1611-D20		



FIXTURE SUPPORT PLATE
 MATERIAL SUPER DUPLEX
 1-OFF REQUIRED

4-Ø50 HOLES
 (MARKED *)

4-HOLES DRILL Ø14 THRO
 & COUNTERBORE
 Ø45.000/45.025(H7)
 x 4.80/5.20 DEEP

THIS DRAWING IS THE SOLE PROPERTY
 OF LANESFIELD ENGINEERING SEALS
 AND MUST NOT BE REPRODUCED NOR
 ITS CONTENTS DIVULGED WITHOUT
 WRITTEN PERMISSION

UNLESS OTHERWISE STATED

ALL DIMENSIONS IN
 MILLIMETERS

TOLERANCES UOS

MACHINING + 0.25MM

FABRICATING ± 2.0MM

REMOVE ALL SHARP EDGES
 AND CORNERS

THIRD ANGLE PROJECTION



LANESFIELD ENGINEERING LTD.

UNIT 11, SPRING ROAD IND ESTATE, LANESFIELD DRIVE, W'TON, WEST MIDLANDS. WV4 6UA
 FAX No 01902-405005 TELE No 01902 497777

CUSTOMER BODYCOTE

DRAWING TITLE TEST MACHINE
 FIXTURE SUPPORT PLATE DETAILS

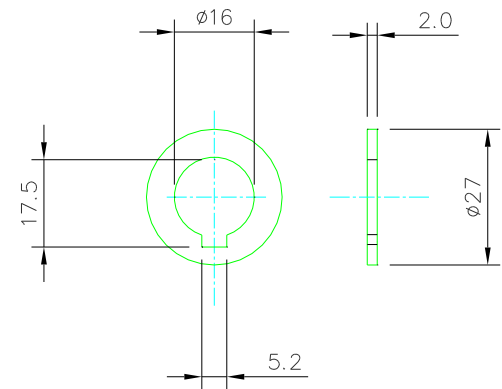
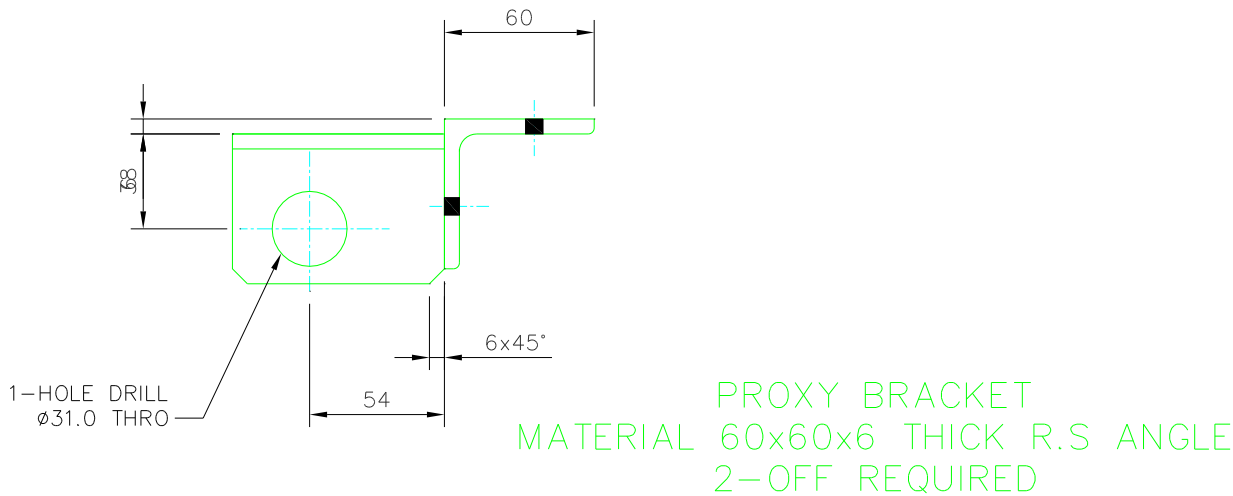
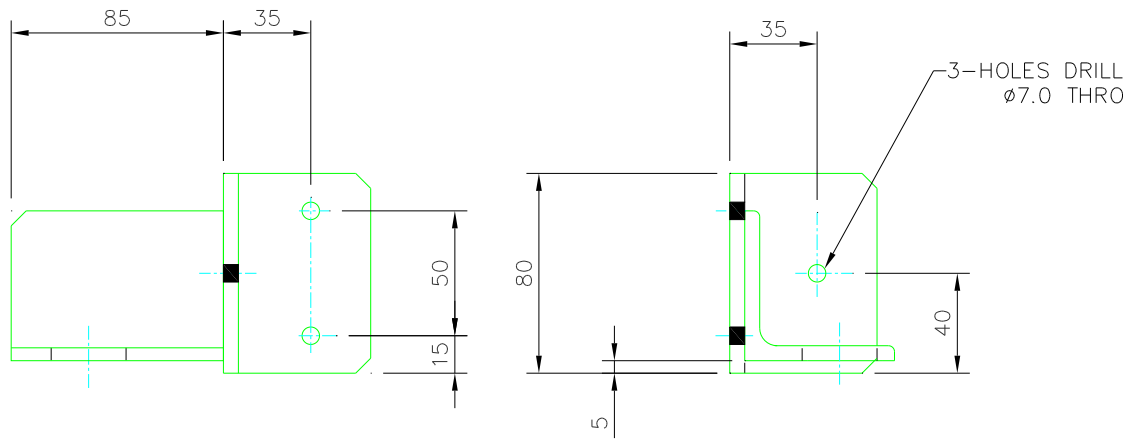
DRAWN R.K.C.

DATE

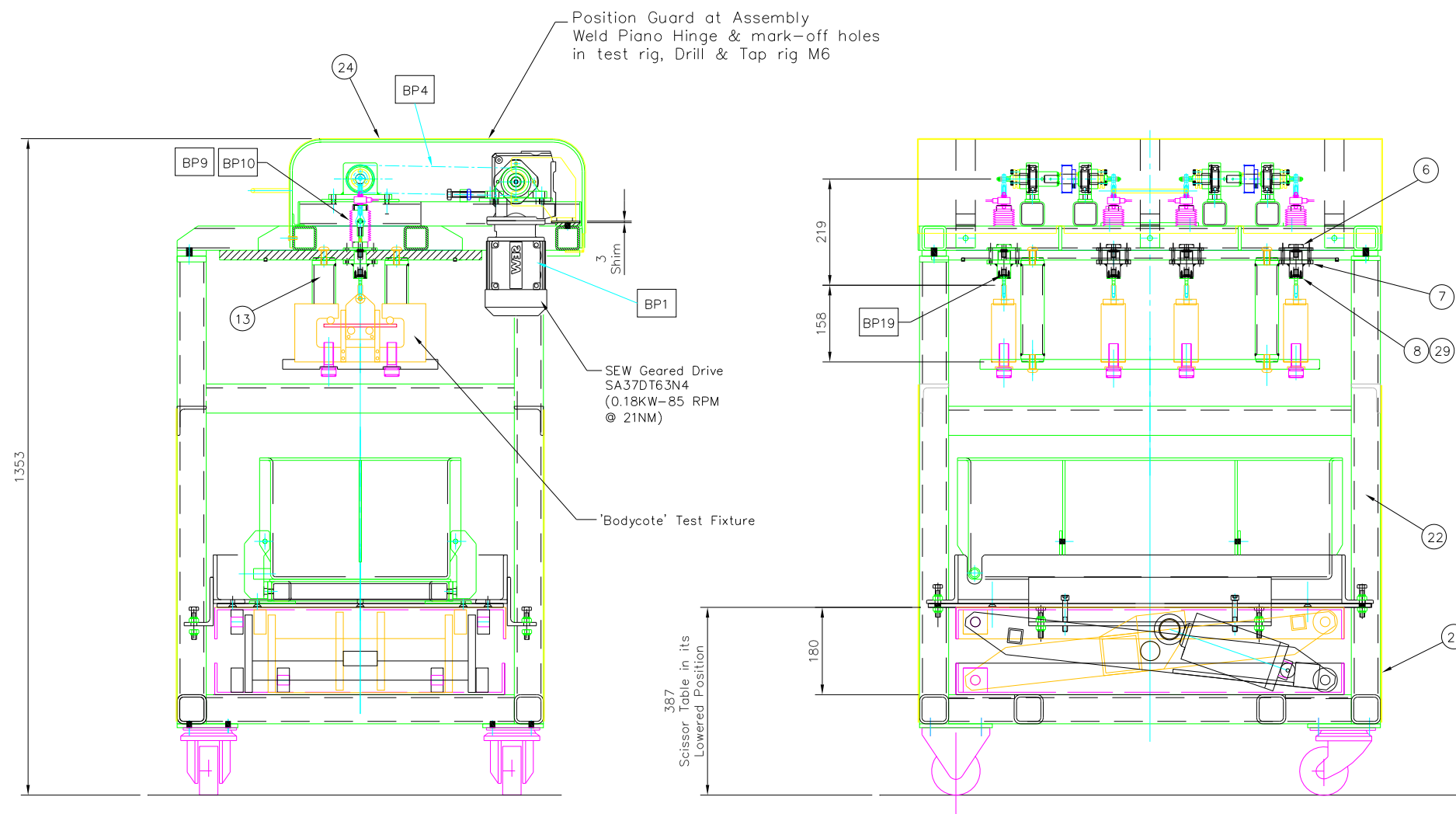
SCALE 1:2 @ A3

DRAWING No. ISSUE No.

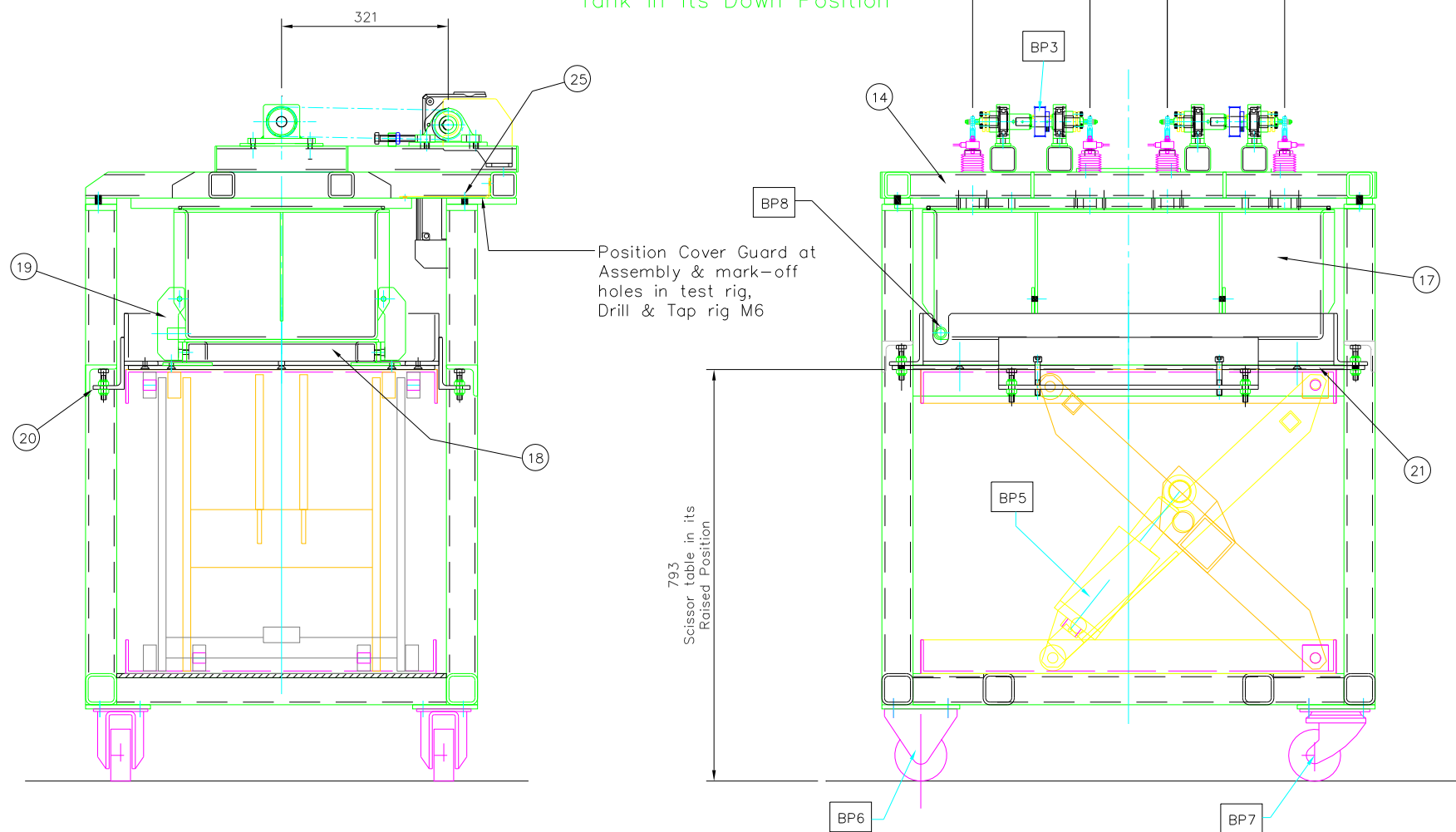
DR/1611-D21



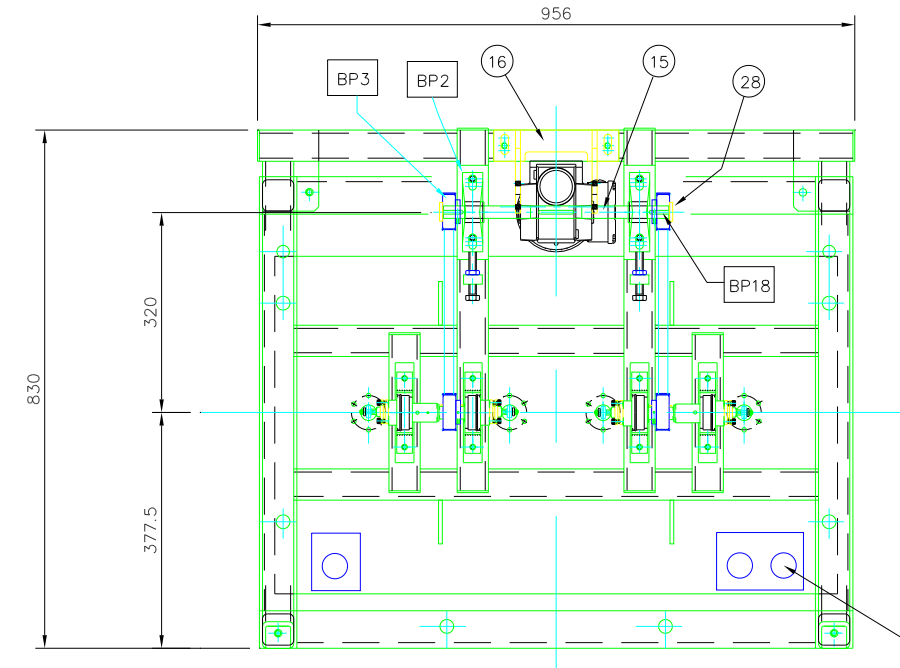
<p>THIS DRAWING IS THE SOLE PROPERTY OF LANESFIELD ENGINEERING SEALS AND MUST NOT BE REPRODUCED NOR ITS CONTENTS DIVULGED WITHOUT WRITTEN PERMISSION</p>	UNLESS OTHERWISE STATED		LANESFIELD ENGINEERING LTD.		DRAWN	R.K.C.	DATE
	ALL DIMENSIONS IN MILLIMETERS		REMOVE ALL SHARP EDGES AND CORNERS		UNIT 11, SPRING ROAD IND ESTATE, LANESFIELD DRIVE, W'TON, WEST MIDLANDS. WV4 6UA FAX No 01902-405005 TELE No 01902 497777		
	TOLERANCES UOS		THIRD ANGLE PROJECTION		CUSTOMER BODYCOTE		
	MACHINING	+ 0.25MM			SCALE 1:1 & 1:2 @ A3		
FABRICATING	+ 2.0MM	DRAWING TITLE TEST MACHINE PROXY SWITCH BRACKET DETAILS			DRAWING No.	DR/1611-D22	ISSUE No.



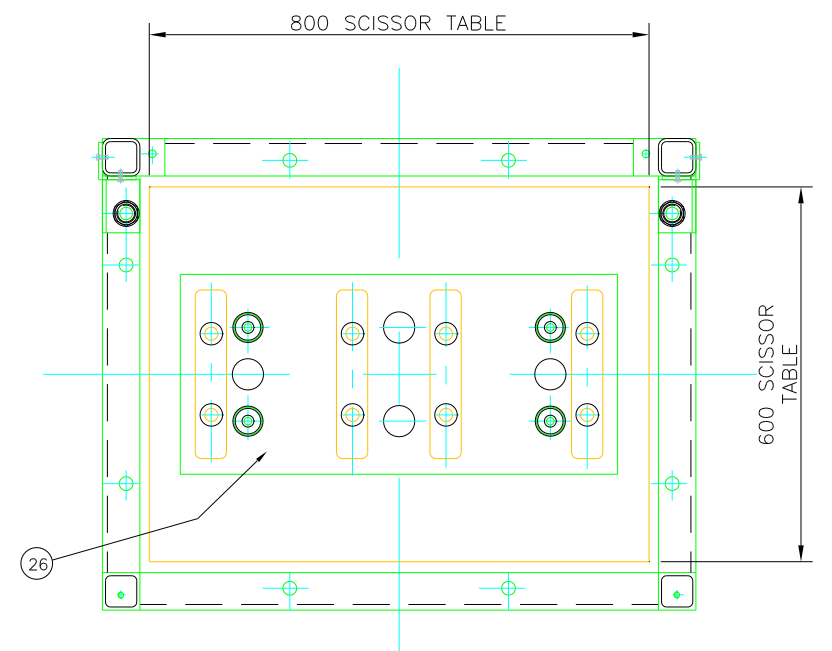
Elevations on Fixture Tank in its Down Position



Elevations on Fixture Tank in its Up Position

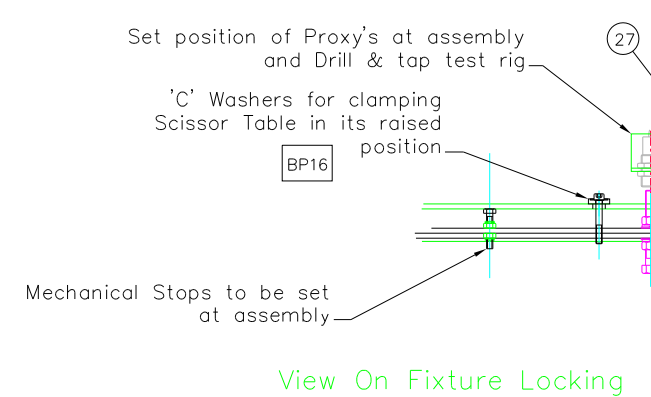


View at Arrow 'A'

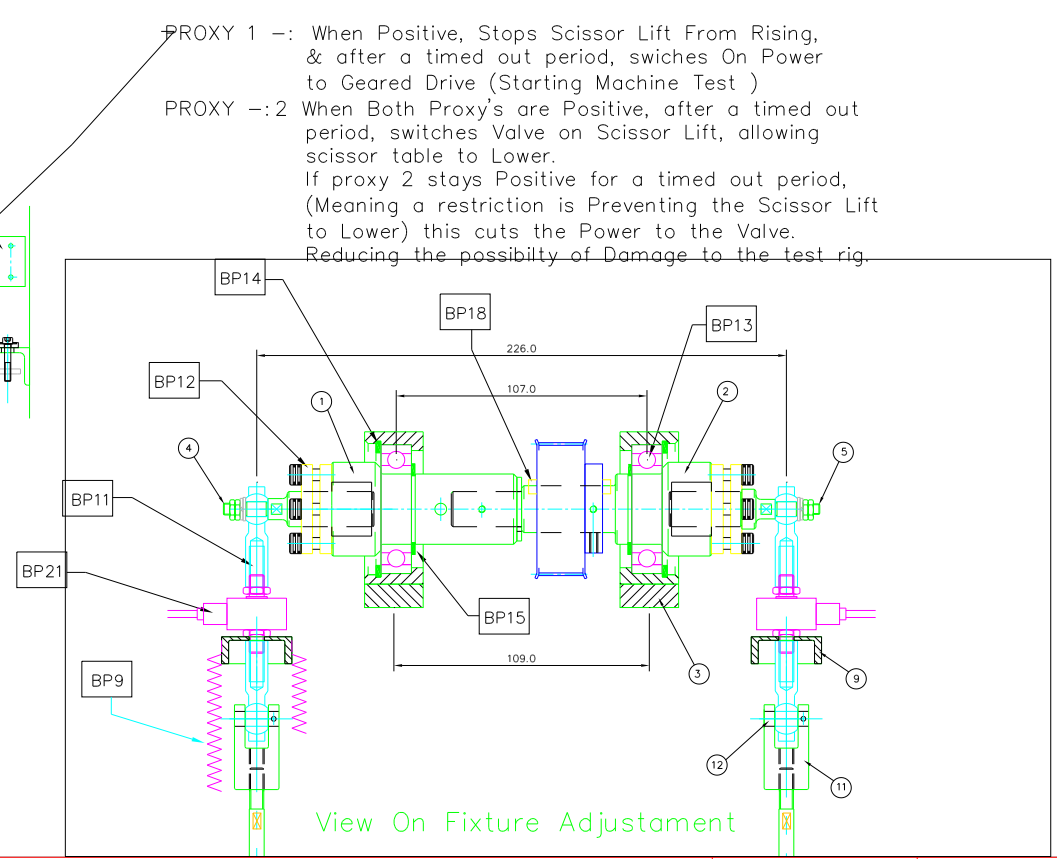


Plan View On Test Fixture Plate

Provide a TWO Handed Push button Arrangement to actuate Scissor Lift with a timed out safety feature preventing operation of the the scissor lift by using one hand only.



View On Fixture Locking



View On Fixture Adjustment

<p>THIS DRAWING IS THE SOLE PROPERTY OF LANESFIELD ENGINEERING SEALS AND MUST NOT BE REPRODUCED NOR ITS CONTENTS DIVULGED WITHOUT WRITTEN PERMISSION</p>	<p>UNLESS OTHERWISE STATED</p>		<p>LANESFIELD ENGINEERING LTD. UNIT 11, SPRING ROAD INDUSTRIAL ESTATE, LANESFIELD DRIVE, W.TON, WEST MIDLANDS, WV4 6UA FAX No 01902-405005 TELE No 01902 497777</p>	<p>DRAWN R.K.C. DATE</p>
	<p>ALL DIMENSIONS IN MILLIMETERS</p>	<p>REMOVE ALL SHARP EDGES AND CORNERS</p>	<p>CUSTOMER BODYCOTE</p>	<p>SCALE 1:7.5 @ A1</p>
	<p>TOLERANCES UDS</p> <p>MACHINING + 0.25MM</p> <p>FABRICATING + 2.0MM</p>	<p>THIRD ANGLE PROJECTION</p>	<p>DRAWING TITLE TEST MACHINE GENERAL ARRANGEMENT</p>	<p>DRAWING No. DR/1611-CA-1</p>

Appendix 2 –High Pressure Corrosion Fatigue Test Machine Drawings

UNLESS OTHERWISE SPECIFIED, DRAWING DIMENSIONS ARE TO BE TAKEN TO THE CENTER OF THE DIMENSION LINE. DIMENSIONS ARE TO BE TAKEN TO THE CENTER OF THE DIMENSION LINE. DIMENSIONS ARE TO BE TAKEN TO THE CENTER OF THE DIMENSION LINE.

IF IN DOUBT ASK

DO NOT SCALE

DO NOT SCALE

MATERIAL: ASME SB546 - HASTELLOY C276 SOLID BAR

MATERIAL: ASME SB546 - HASTELLOY C276 SOLID BAR

MATERIAL: ASTM A387 GR22 G31B MILL CERTIFIED

MATERIAL: ASME SB546 - HASTELLOY C276 SOLID BAR

CUSTOMER'S OWN DESIGN - DYNAMIC SEAL HOUSING

MATERIAL: ASME SB546 - HASTELLOY C276 SOLID BAR

ASSEMBLY NOTES

ENSURE ALL TAPPED HOLES ON TOP QUADRANT OF VESSEL AND SCREWED FLANGE ARE VERTICAL AND AXIALLY ALIGNED

8-HOLES $\phi 6.75 \times 22.00$ DP EQUI-SP ON A $\phi 76.0$ PCD (DO NOT BREAK THROUGH)

TAP M8x200 DP (DO NOT BREAK THROUGH)

PARTIAL VIEW DETAIL OF BOLT HOLES

BS141 (PTFE) 'O' RING

PTFE BS141

USE WHITWORTH THREAD FORM 6TPI

$\phi 17.58$ MID SEAL DIAMETER

$\phi 8.00$ IDT

$\phi 280$

$\phi 240.00$ BOLT PCD

$\phi 61.04$

$\phi 20.0$

$\phi 90.0$

$\phi 160.00$

$\phi 2300$

$\phi 76.0$ REF

$\phi 90.10$ REF

$\phi 50.10$ REF

R12

45

45

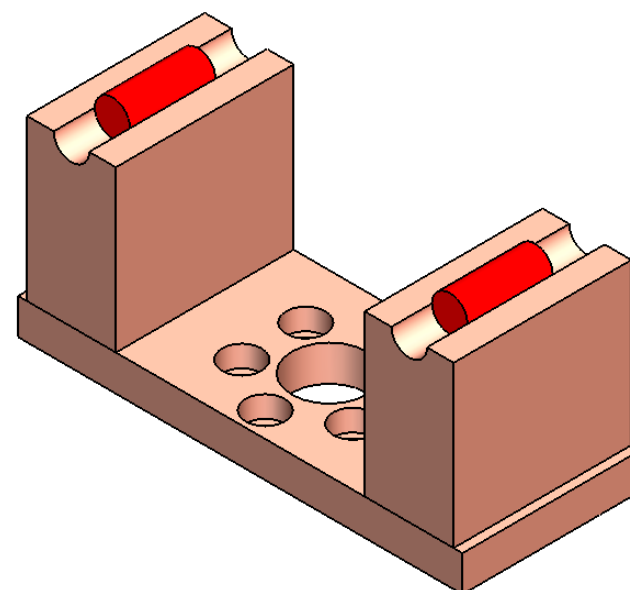
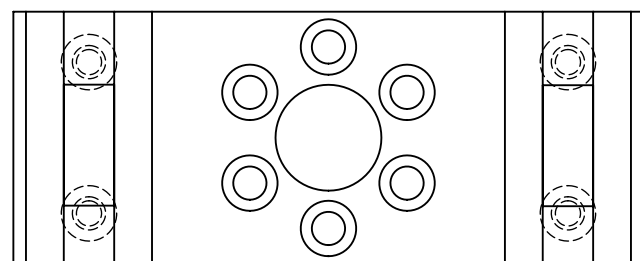
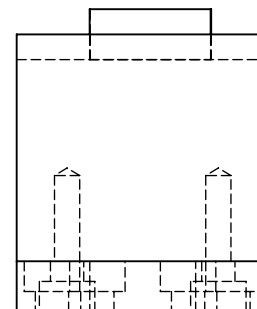
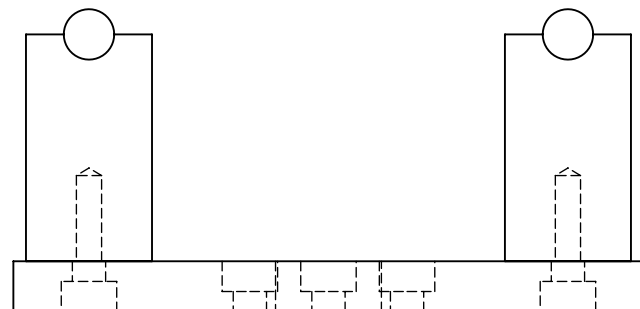
DO NOT SCALE

CHKD BY:	DATE:										
6		5		4		3		2		1	

QUANTITY: 8-OFF

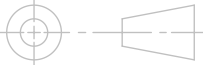
MATERIAL: ASME SB546 - HASTELLOY C276 SOLID BAR

DO NOT SCALE



MACHINING INSTRUCTIONS

NUMBER OFF: **2** MATERIAL: Nickel plated steel

THIRD ANGLE PROJECTION

 TOLERANCES:
 0: ±1
 0.0: ±0.5
 0.00: ±0.05
 (ANGULAR: ±1°)
 DEBUR AND BREAK SHARP EDGES UNLESS OTHERWISE SPECIFIED, ALL DIMENSIONS IN mm

Property of EXOVA (UK) LTD. The document contains proprietary and confidential information which may not, without the prior written consent of EXOVA (UK) LTD., be used or reproduced in whole or in part, or communicated to any person not employed by EXOVA (UK) LTD.

SCALE: 1:2	SHEET 1 OF 3	A4
TITLE:		
PART: Outer span rollers assembly		
DRWG No.: Bottom fixture - 01		
DRAWN	; 09/04/2010	
LAST REVISED	ravier.o - 09/04/2010 12:17:26	

Bottom fixture - 01
 DRWG No.:



1 Bottom fixture - 02

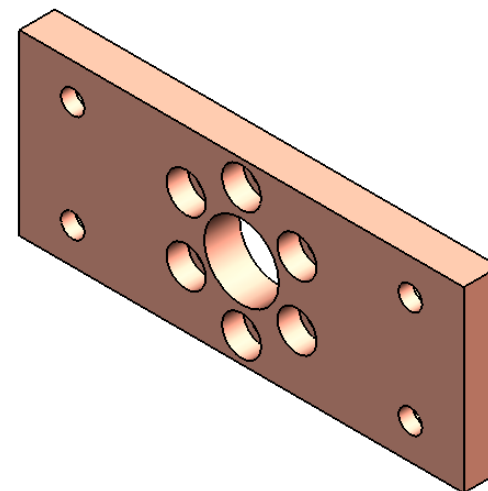
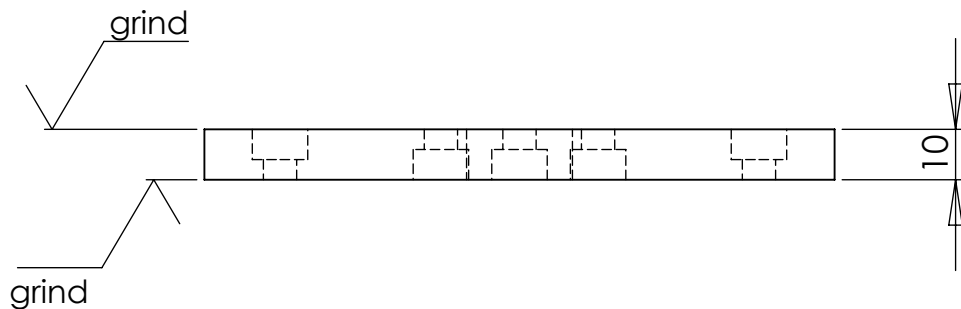
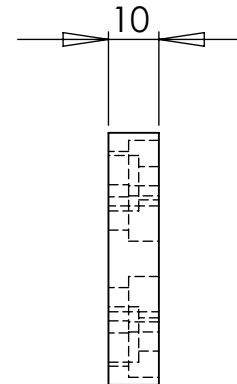
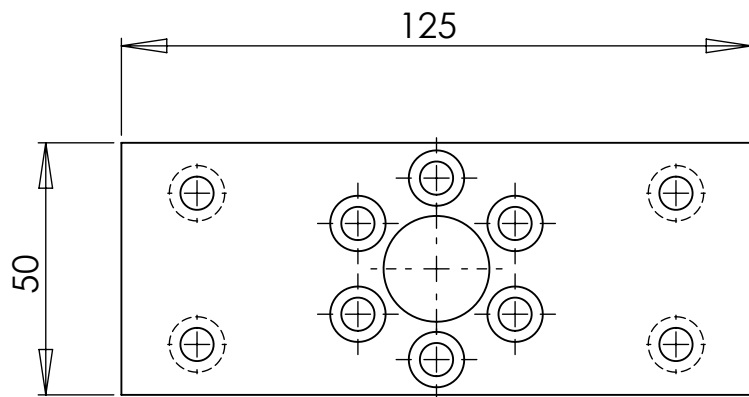
2 DRWG No.:

3

4

5

6



MACHINING INSTRUCTIONS

NUMBER OFF: 2	MATERIAL: Nickel plated steel
-------------------------	----------------------------------

THIRD ANGLE PROJECTION 	TOLERANCES: 0: ±1 0.0: ±0.5 0.00: ±0.05 (ANGULAR: ±1°)	DEBUR AND BREAK SHARP EDGES UNLESS OTHERWISE SPECIFIED, ALL DIMENSIONS IN mm
----------------------------	--	---

Property of EXOVA (UK) LTD. The document contains proprietary and confidential information which may not, without the prior written consent of EXOVA (UK) LTD., be used or reproduced in whole or in part, or communicated to any person not employed by EXOVA (UK) LTD.

SCALE: 1:2	SHEET 2 OF 3	A4
TITLE:		
PART: Outer span rollers base plate		
DRWG No.:		
Bottom fixture - 02		
DRAWN	; 09/04/2010	
LAST REVISED	ravier.o - 09/04/2010 12:17:26	

1

2

3

4

5

6



1 Bottom fixture - 03

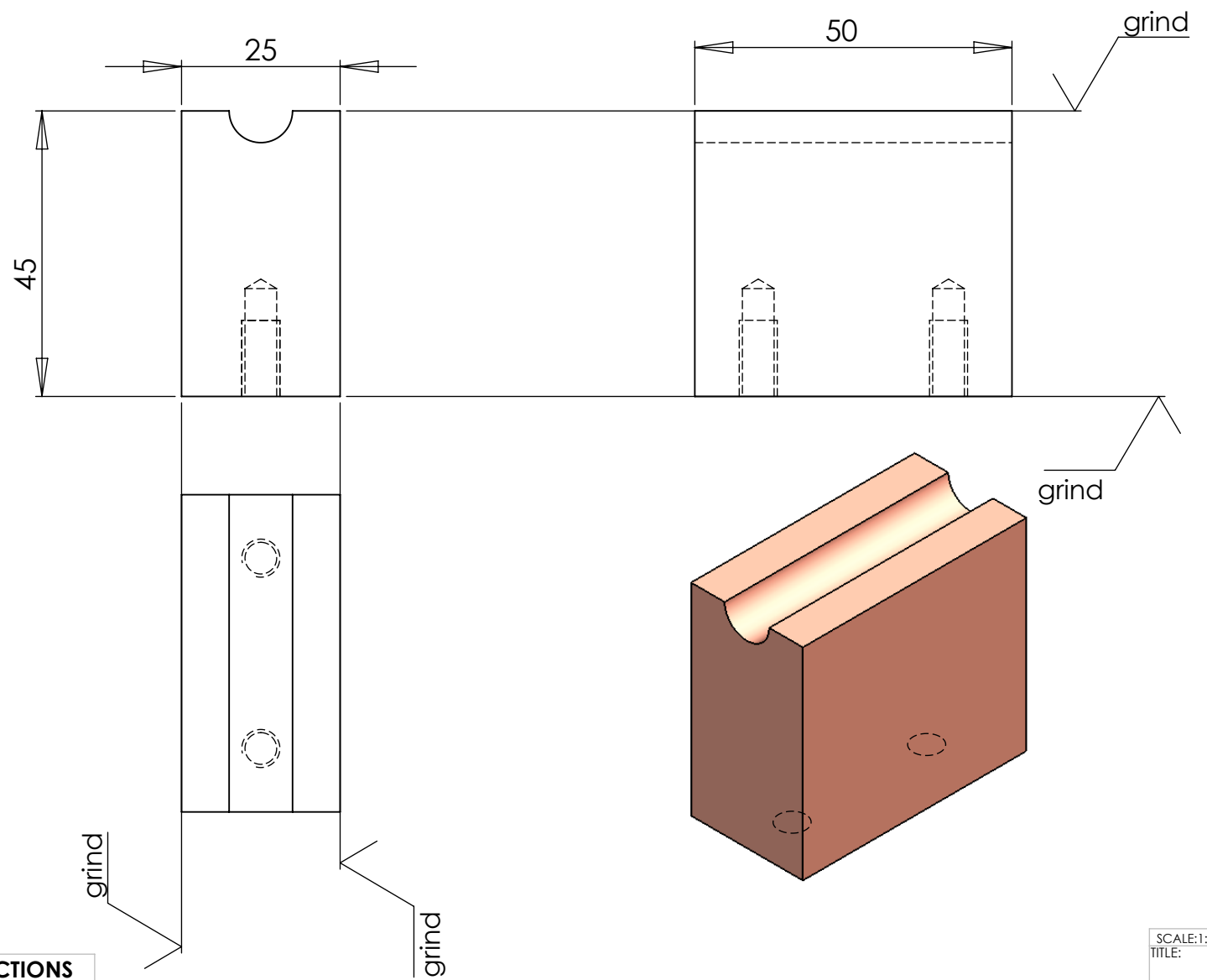
2 DRWG No.:

3

4

5

6



MACHINING INSTRUCTIONS

NUMBER OFF: **4** MATERIAL: Nickel plated steel

THIRD ANGLE PROJECTION

 TOLERANCES:
 0: ±1
 0.0: ±0.5
 0.00: ±0.05
 (ANGULAR: ±1°)
 DEBUR AND BREAK SHARP EDGES UNLESS OTHERWISE SPECIFIED, ALL DIMENSIONS IN mm

Property of EXOVA (UK) LTD. The document contains proprietary and confidential information which may not, without the prior written consent of EXOVA (UK) LTD., be used or reproduced in whole or in part, or communicated to any person not employed by EXOVA (UK) LTD.

SCALE: 1:2	SHEET 3 OF 3	A4
TITLE:		
PART: Outer span rollers side plates		
DRWG No.: Bottom fixture - 03		
DRAWN		: 09/04/2010
LAST REVISED		ravier.o - 09/04/2010 12:17:26

1

2

3

4

5

6

1

2

3

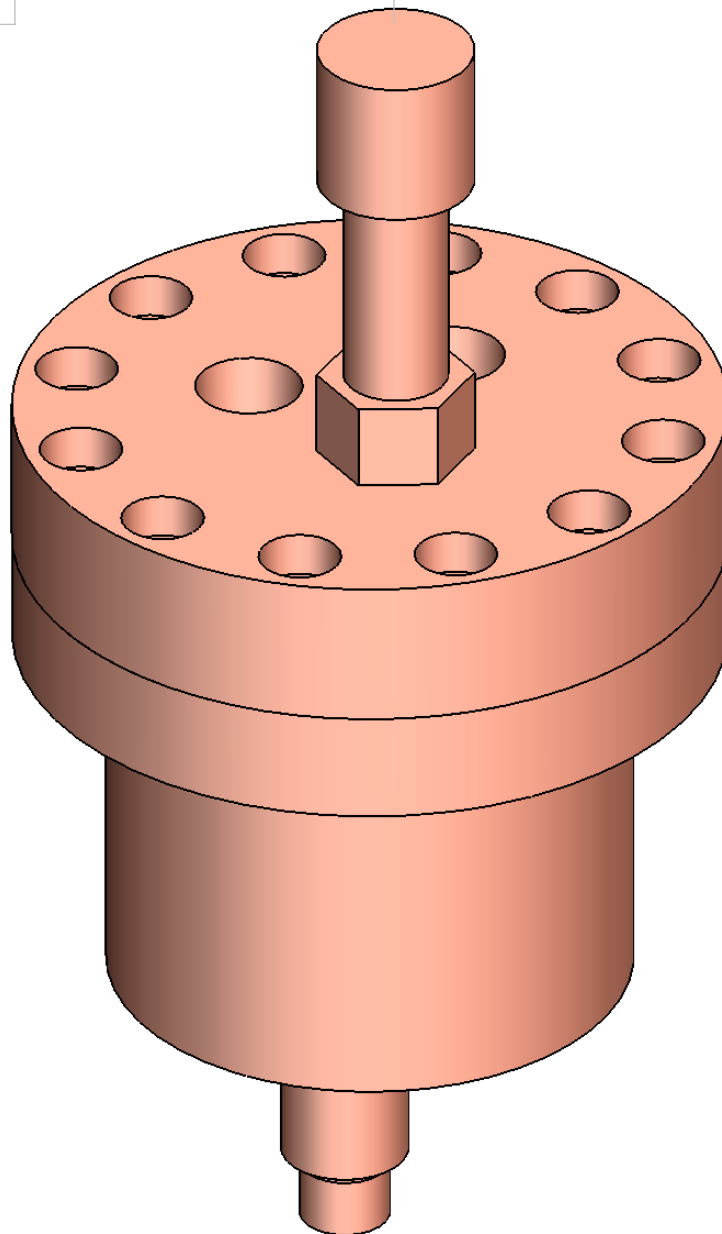
4

5

6

pH sampling vessel - 01

DRWG No.:



MACHINING INSTRUCTIONS

NUMBER OFF:	MATERIAL:
#	Stainless

THIRD ANGLE PROJECTION	TOLERANCES:	DEBUR AND BREAK SHARP EDGES
	0: ±1	UNLESS OTHERWISE SPECIFIED, ALL DIMENSIONS IN mm
	0.0: ± 0.5	
	0.00: ±0.05	
	(ANGULAR: ± 1°)	

Property of EXOVA (UK) LTD. The document contains proprietary and confidential information which may not, without the prior written consent of EXOVA (UK) LTD., be used or reproduced in whole or in part, or communicated to any person not employed by EXOVA (UK) LTD.

SCALE: 1:1.2	SHEET 1 OF 4	A4
TITLE:		
PART: pH sampling vessel		
DRWG No.: pH sampling vessel - 01		
DRAWN	: 09/12/2009	
LAST REVISED	ravier.o - 18/01/2010 10:09:55	

1

2

3

4

5

6

A

B

C

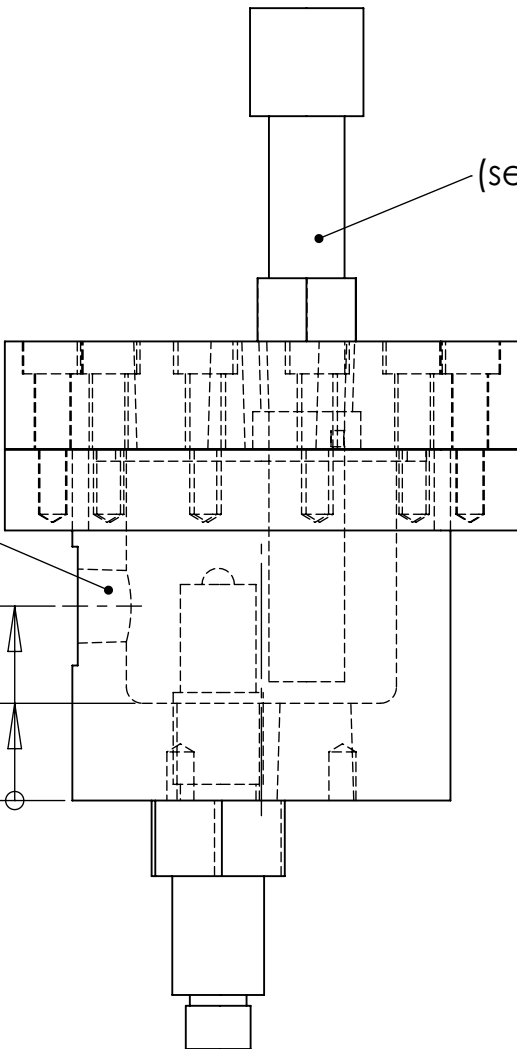
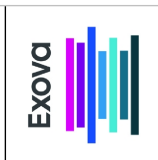
D

A

B

C

D



pH probe
(see attached drawing)

1/4" NPT
Sol in port

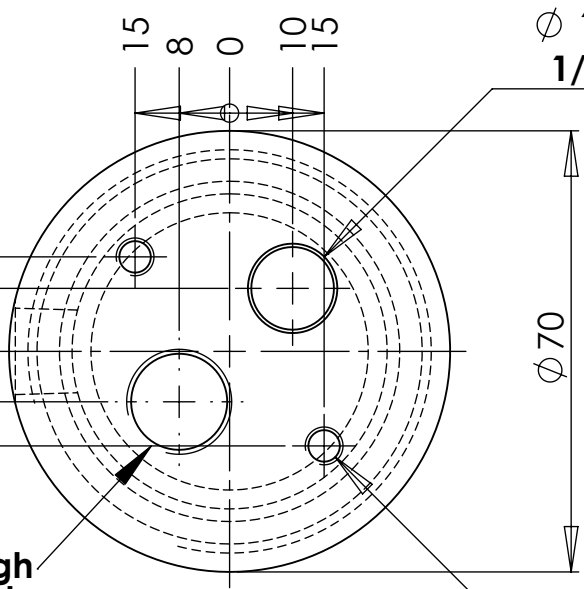
36
18
0

MACHINING INSTRUCTIONS

NUMBER OFF:	#	MATERIAL:	Stainless
THIRD ANGLE PROJECTION		TOLERANCES:	0: ±1 0.0: ±0.5 0.00: ±0.05 (ANGULAR: ±1°)
		DEBUR AND BREAK SHARP EDGES UNLESS OTHERWISE SPECIFIED, ALL DIMENSIONS IN mm	

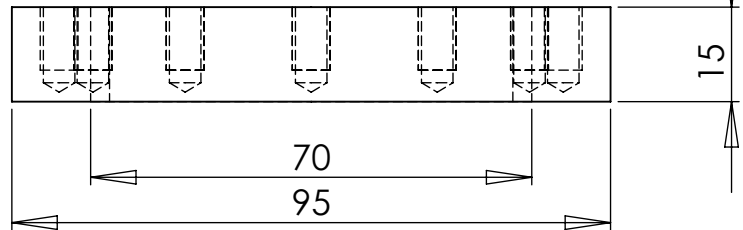
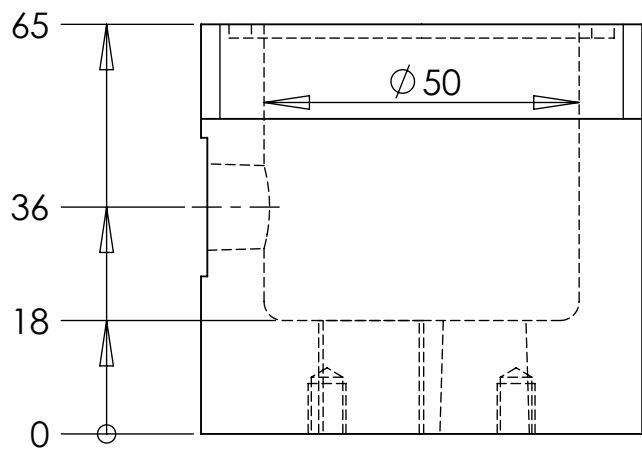
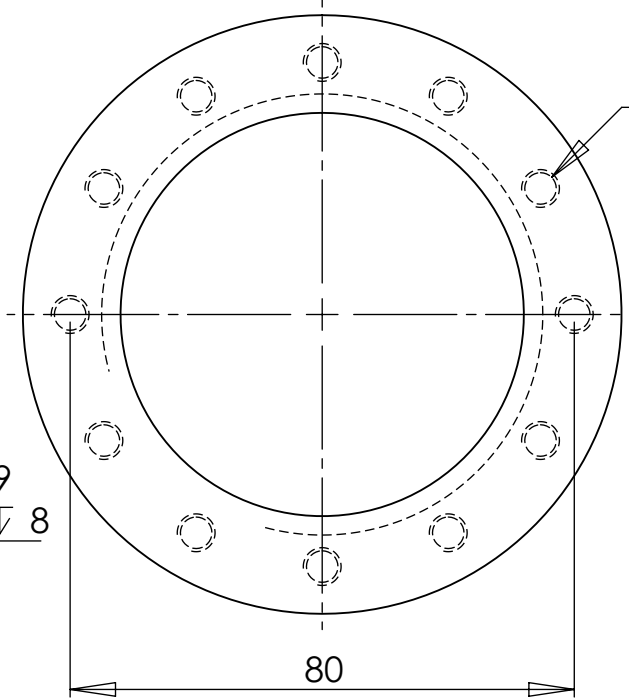
Property of EXOVA (UK) LTD. The document contains proprietary and confidential information which may not, without the prior written consent of EXOVA (UK) LTD., be used or reproduced in whole or in part, or communicated to any person not employed by EXOVA (UK) LTD.

SCALE: 1:1.2	SHEET 2 OF 4	A4
TITLE:		
PART: pH sampling vessel		
DRWG No.: pH sampling vessel - 02		
DRAWN		:09/12/2009
LAST REVISED	ravier.o - 18/01/2010 10:09:55	



3/8" BSP
Threaded through
Level sensor port

2 x $\varnothing 5 \downarrow 9$
M6x1.0 - 6H $\downarrow 8$

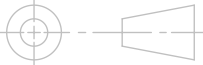


MACHINING INSTRUCTIONS

NUMBER OFF: **1**

MATERIAL: **Stainless**

THIRD ANGLE PROJECTION

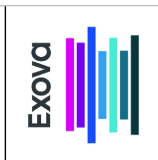


TOLERANCES:
0: ± 1
0.0: ± 0.5
0.00: ± 0.05
(ANGULAR: $\pm 1^\circ$)

DEBUR AND
BREAK SHARP
EDGES
UNLESS OTHERWISE
SPECIFIED, ALL
DIMENSIONS IN mm

Property of EXOVA (UK) LTD. The document contains proprietary and confidential information which may not, without the prior written consent of EXOVA (UK) LTD., be used or reproduced in whole or in part, or communicated to any person not employed by EXOVA (UK) LTD.

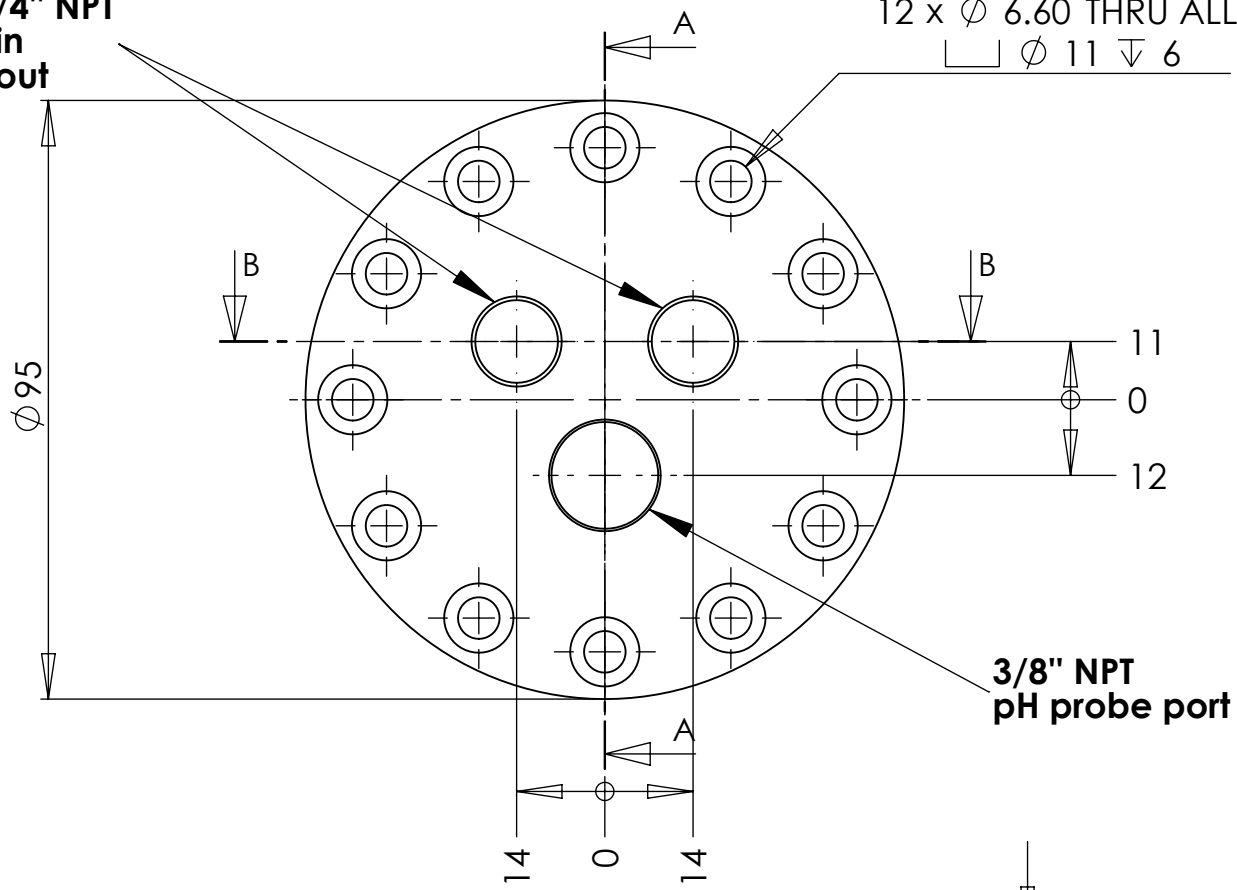
SCALE: 1:1.2	SHEET 3 OF 4	A4
TITLE:		
PART: Body		
DRWG No.: pH sampling vessel - 03		
DRAWN	: 09/12/2009	
LAST REVISED	ravier.o - 18/01/2010 10:09:55	



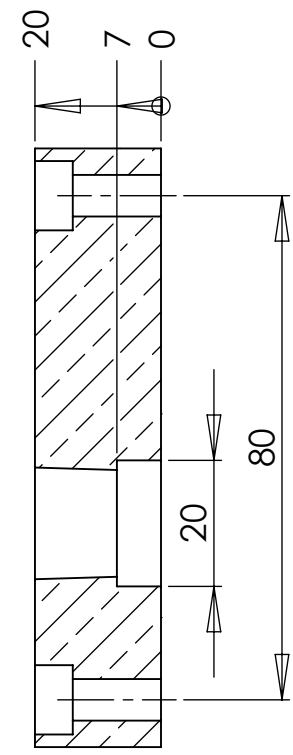
Top lid

2 off 1/4" NPT
 - Gas in
 - Gas out

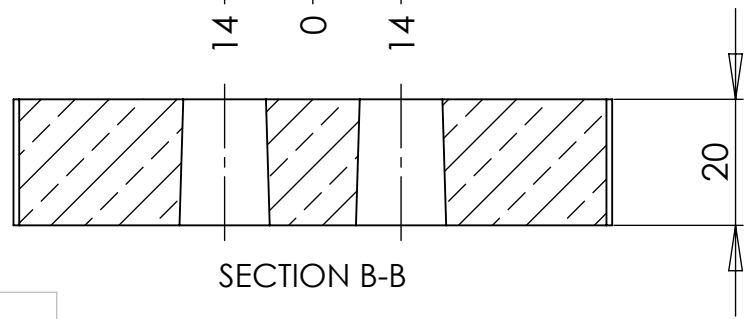
12 x ϕ 6.60 THRU ALL
 ϕ 11 ∇ 6



3/8" NPT
 pH probe port



SECTION A-A



SECTION B-B

MACHINING INSTRUCTIONS

NUMBER OFF: 1	MATERIAL: Ask
THIRD ANGLE PROJECTION 	TOLERANCES: 0: ± 1 0.0: ± 0.5 0.00: ± 0.05 (ANGULAR: $\pm 1^\circ$)
DEBUR AND BREAK SHARP EDGES UNLESS OTHERWISE SPECIFIED, ALL DIMENSIONS IN mm	

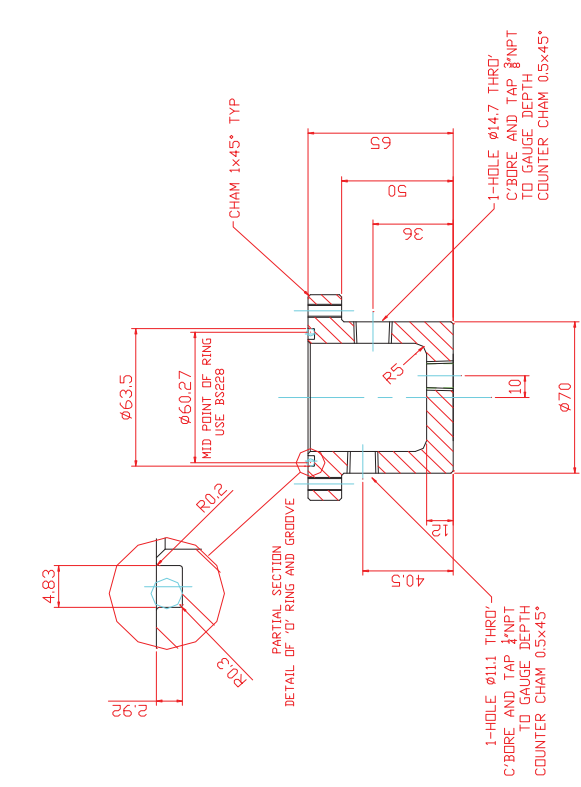
Property of EXOVA (UK) LTD. The document contains proprietary and confidential information which may not, without the prior written consent of EXOVA (UK) LTD., be used or reproduced in whole or in part, or communicated to any person not employed by EXOVA (UK) LTD.

SCALE: 1:1.2	SHEET 4 OF 4	A4
TITLE:		
PART: Part Name		
DRWG No.: pH sampling vessel - 04		
DRAWN	: 09/12/2009	
LAST REVISED	ravier.o - 18/01/2010 10:09:55	

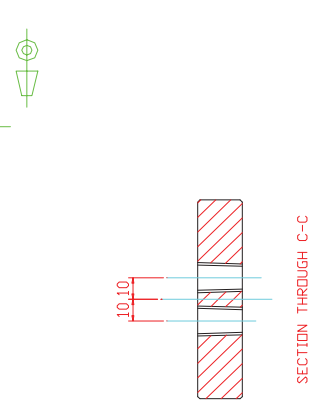
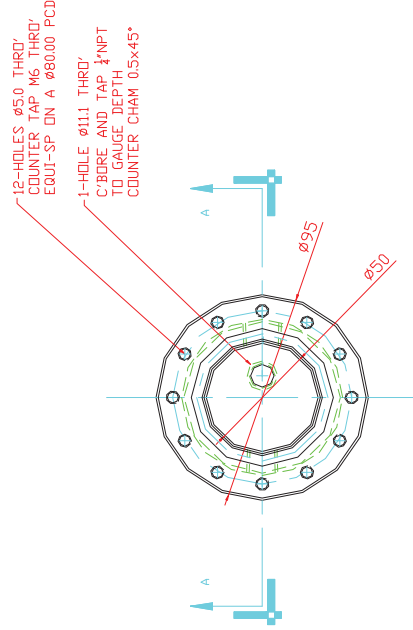
DO NOT SCALE

IF IN DOUBT ASK

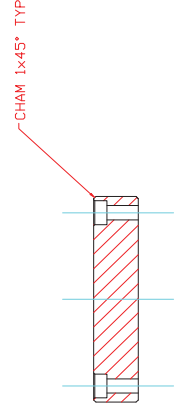
UNLESS OTHERWISE SPECIFIED, ALL DIMENSIONS ARE TO BE TAKEN TO THE CENTERLINE UNLESS INDICATED OTHERWISE. DIMENSIONS IN PARENTHESES ARE FOR INFORMATION ONLY. DIMENSIONS IN BRACKETS ARE FOR INFORMATION ONLY. DIMENSIONS IN PARENTHESES ARE FOR INFORMATION ONLY. DIMENSIONS IN PARENTHESES ARE FOR INFORMATION ONLY.



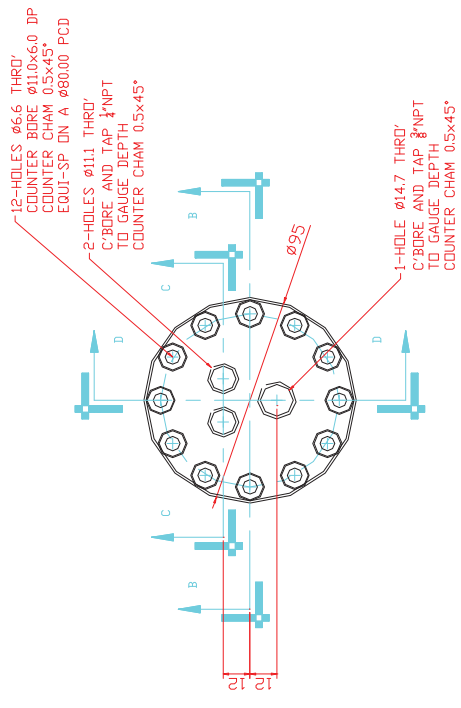
SECTION THROUGH A-A



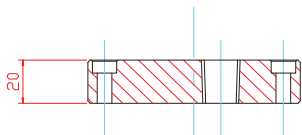
SECTION THROUGH C-C



SECTION THROUGH B-B



SECTION THROUGH D-D



ITEM 12 SAMPLING MICROCLAVE COVER

QUANTITY: 8-DFF
MATERIAL: ASME SA 479 - DUAL CERTIFIED 316-316L STAINLESS STEEL

ITEM 12 SAMPLING MICROCLAVE

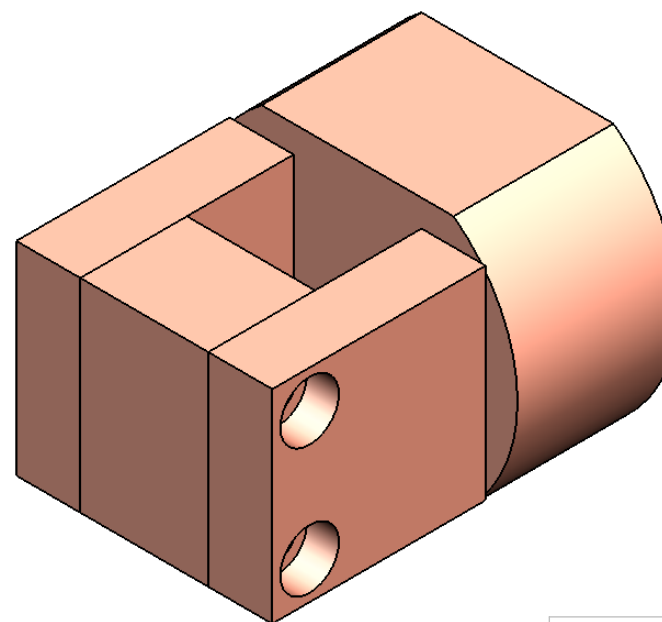
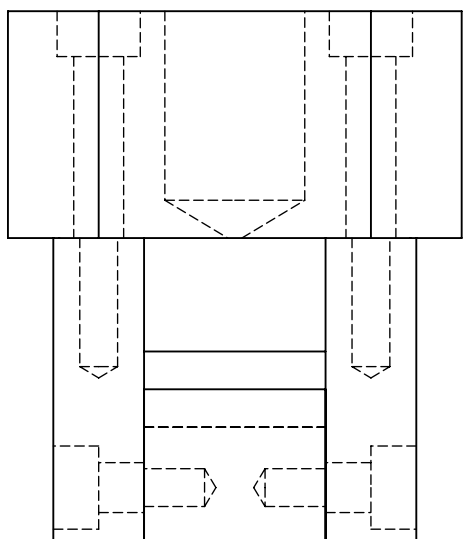
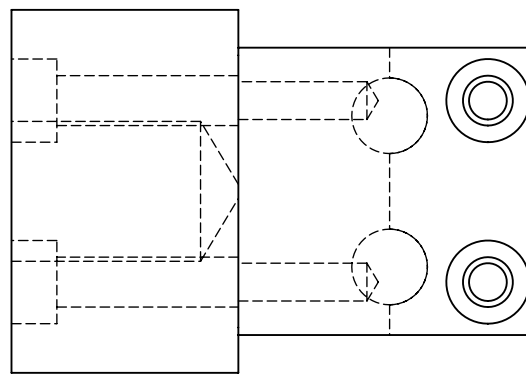
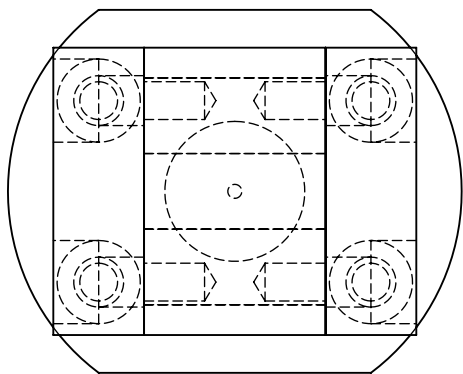
QUANTITY: 8-DFF
MATERIAL: ASME SA 479 - DUAL CERTIFIED 316-316L STAINLESS STEEL

DESIGN DATA		CHECK BY:		DATE:	
REV. CATEGORY:	MODULE 6	1			
DESIGN PRESSURE:	55 BAR (7.975 PSIG)	2			
TEST PRESSURE:	82.5 BAR (11.9625 PSIG)	3			
DESIGN TEMPERATURE:	150°C	4			
MATERIAL:	SA 479 (316L)	5			
VESSEL SHELL:	SA 479 (316L)	6			
VESSEL COVER:	SA 479 (316L)				
WELDING PROCEDURE:	SA 479 (316L)				
WELDING MATERIAL:	SA 479 (316L)				
WELDING POSITION:	SA 479 (316L)				
WELDING QUALITY:	SA 479 (316L)				
WELDING INSPECTION:	SA 479 (316L)				
WELDING RECORD:	SA 479 (316L)				
WELDING APPROVAL:	SA 479 (316L)				
WELDING DATE:	SA 479 (316L)				
WELDING TIME:	SA 479 (316L)				
WELDING COST:	SA 479 (316L)				
WELDING WEIGHT:	SA 479 (316L)				
WELDING VOLUME:	SA 479 (316L)				
WELDING AREA:	SA 479 (316L)				
WELDING PERIMETER:	SA 479 (316L)				
WELDING LENGTH:	SA 479 (316L)				
WELDING WIDTH:	SA 479 (316L)				
WELDING HEIGHT:	SA 479 (316L)				
WELDING DEPTH:	SA 479 (316L)				
WELDING TOLERANCE:	SA 479 (316L)				
WELDING FINISH:	SA 479 (316L)				
WELDING SURFACE:	SA 479 (316L)				
WELDING CORNER:	SA 479 (316L)				
WELDING EDGE:	SA 479 (316L)				
WELDING BEVEL:	SA 479 (316L)				
WELDING GROOVE:	SA 479 (316L)				
WELDING RING:	SA 479 (316L)				
WELDING GASKET:	SA 479 (316L)				
WELDING O-RING:	SA 479 (316L)				
WELDING SEAL:	SA 479 (316L)				
WELDING GROMMET:	SA 479 (316L)				
WELDING WEDGE:	SA 479 (316L)				
WELDING PIN:	SA 479 (316L)				
WELDING NUT:	SA 479 (316L)				
WELDING BOLT:	SA 479 (316L)				
WELDING SCREW:	SA 479 (316L)				
WELDING WASHER:	SA 479 (316L)				
WELDING LOCKWASHER:	SA 479 (316L)				
WELDING SPRING:	SA 479 (316L)				
WELDING SHIM:	SA 479 (316L)				
WELDING GASKET:	SA 479 (316L)				
WELDING O-RING:	SA 479 (316L)				
WELDING SEAL:	SA 479 (316L)				
WELDING GROMMET:	SA 479 (316L)				
WELDING WEDGE:	SA 479 (316L)				
WELDING PIN:	SA 479 (316L)				
WELDING NUT:	SA 479 (316L)				
WELDING BOLT:	SA 479 (316L)				
WELDING SCREW:	SA 479 (316L)				
WELDING WASHER:	SA 479 (316L)				
WELDING LOCKWASHER:	SA 479 (316L)				
WELDING SPRING:	SA 479 (316L)				
WELDING SHIM:	SA 479 (316L)				
WELDING GASKET:	SA 479 (316L)				
WELDING O-RING:	SA 479 (316L)				
WELDING SEAL:	SA 479 (316L)				
WELDING GROMMET:	SA 479 (316L)				
WELDING WEDGE:	SA 479 (316L)				
WELDING PIN:	SA 479 (316L)				
WELDING NUT:	SA 479 (316L)				
WELDING BOLT:	SA 479 (316L)				
WELDING SCREW:	SA 479 (316L)				
WELDING WASHER:	SA 479 (316L)				
WELDING LOCKWASHER:	SA 479 (316L)				
WELDING SPRING:	SA 479 (316L)				
WELDING SHIM:	SA 479 (316L)				
WELDING GASKET:	SA 479 (316L)				
WELDING O-RING:	SA 479 (316L)				
WELDING SEAL:	SA 479 (316L)				
WELDING GROMMET:	SA 479 (316L)				
WELDING WEDGE:	SA 479 (316L)				
WELDING PIN:	SA 479 (316L)				
WELDING NUT:	SA 479 (316L)				
WELDING BOLT:	SA 479 (316L)				
WELDING SCREW:	SA 479 (316L)				
WELDING WASHER:	SA 479 (316L)				
WELDING LOCKWASHER:	SA 479 (316L)				
WELDING SPRING:	SA 479 (316L)				
WELDING SHIM:	SA 479 (316L)				
WELDING GASKET:	SA 479 (316L)				
WELDING O-RING:	SA 479 (316L)				
WELDING SEAL:	SA 479 (316L)				
WELDING GROMMET:	SA 479 (316L)				
WELDING WEDGE:	SA 479 (316L)				
WELDING PIN:	SA 479 (316L)				
WELDING NUT:	SA 479 (316L)				
WELDING BOLT:	SA 479 (316L)				
WELDING SCREW:	SA 479 (316L)				
WELDING WASHER:	SA 479 (316L)				
WELDING LOCKWASHER:	SA 479 (316L)				
WELDING SPRING:	SA 479 (316L)				
WELDING SHIM:	SA 479 (316L)				
WELDING GASKET:	SA 479 (316L)				
WELDING O-RING:	SA 479 (316L)				
WELDING SEAL:	SA 479 (316L)				
WELDING GROMMET:	SA 479 (316L)				
WELDING WEDGE:	SA 479 (316L)				
WELDING PIN:	SA 479 (316L)				
WELDING NUT:	SA 479 (316L)				
WELDING BOLT:	SA 479 (316L)				
WELDING SCREW:	SA 479 (316L)				
WELDING WASHER:	SA 479 (316L)				
WELDING LOCKWASHER:	SA 479 (316L)				
WELDING SPRING:	SA 479 (316L)				
WELDING SHIM:	SA 479 (316L)				
WELDING GASKET:	SA 479 (316L)				
WELDING O-RING:	SA 479 (316L)				
WELDING SEAL:	SA 479 (316L)				
WELDING GROMMET:	SA 479 (316L)				
WELDING WEDGE:	SA 479 (316L)				
WELDING PIN:	SA 479 (316L)				
WELDING NUT:	SA 479 (316L)				
WELDING BOLT:	SA 479 (316L)				
WELDING SCREW:	SA 479 (316L)				
WELDING WASHER:	SA 479 (316L)				
WELDING LOCKWASHER:	SA 479 (316L)				
WELDING SPRING:	SA 479 (316L)				
WELDING SHIM:	SA 479 (316L)				
WELDING GASKET:	SA 479 (316L)				
WELDING O-RING:	SA 479 (316L)				
WELDING SEAL:	SA 479 (316L)				
WELDING GROMMET:	SA 479 (316L)				
WELDING WEDGE:	SA 479 (316L)				
WELDING PIN:	SA 479 (316L)				
WELDING NUT:	SA 479 (316L)				
WELDING BOLT:	SA 479 (316L)				
WELDING SCREW:	SA 479 (316L)				
WELDING WASHER:	SA 479 (316L)				
WELDING LOCKWASHER:	SA 479 (316L)				
WELDING SPRING:	SA 479 (316L)				
WELDING SHIM:	SA 479 (316L)				
WELDING GASKET:	SA 479 (316L)				
WELDING O-RING:	SA 479 (316L)				
WELDING SEAL:	SA 479 (316L)				
WELDING GROMMET:	SA 479 (316L)				
WELDING WEDGE:	SA 479 (316L)				
WELDING PIN:	SA 479 (316L)				
WELDING NUT:	SA 479 (316L)				
WELDING BOLT:	SA 479 (316L)				
WELDING SCREW:	SA 479 (316L)				
WELDING WASHER:	SA 479 (316L)				
WELDING LOCKWASHER:	SA 479 (316L)				
WELDING SPRING:	SA 479 (316L)				
WELDING SHIM:	SA 479 (316L)				
WELDING GASKET:	SA 479 (316L)				
WELDING O-RING:	SA 479 (316L)				
WELDING SEAL:	SA 479 (316L)				
WELDING GROMMET:	SA 479 (316L)				
WELDING WEDGE:	SA 479 (316L)				
WELDING PIN:	SA 479 (316L)				
WELDING NUT:	SA 479 (316L)				
WELDING BOLT:	SA 479 (316L)				
WELDING SCREW:	SA 479 (316L)				
WELDING WASHER:	SA 479 (316L)				
WELDING LOCKWASHER:	SA 479 (316L)				
WELDING SPRING:	SA 479 (316L)				
WELDING SHIM:	SA 479 (316L)				
WELDING GASKET:	SA 479 (316L)				
WELDING O-RING:	SA 479 (316L)				
WELDING SEAL:	SA 479 (316L)				
WELDING GROMMET:	SA 479 (316L)				
WELDING WEDGE:	SA 479 (316L)				
WELDING PIN:	SA 479 (316L)				
WELDING NUT:	SA 479 (316L)				
WELDING BOLT:	SA 479 (316L)				
WELDING SCREW:	SA 479 (316L)				
WELDING WASHER:	SA 479 (316L)				
WELDING LOCKWASHER:	SA 479 (316L)				
WELDING SPRING:	SA 479 (316L)				
WELDING SHIM:	SA 479 (316L)				
WELDING GASKET:	SA 479 (316L)				
WELDING O-RING:	SA 479 (316L)				
WELDING SEAL:	SA 479 (316L)				
WELDING GROMMET:	SA 479 (316L)				
WELDING WEDGE:	SA 479 (316L)				
WELDING PIN:	SA 479 (316L)				
WELDING NUT:	SA 479 (316L)				
WELDING BOLT:	SA 479 (316L)				
WELDING SCREW:	SA 479 (316L)				
WELDING WASHER:	SA 479 (316L)				
WELDING LOCKWASHER:	SA 479 (316L)				
WELDING SPRING:	SA 479 (316L)				
WELDING SHIM:	SA 479 (316L)				
WELDING GASKET:	SA 479 (316L)				
WELDING O-RING:	SA 479 (316L)				
WELDING SEAL:	SA 479 (316L)				
WELDING GROMMET:	SA 479 (316L)				
WELDING WEDGE:	SA 479 (316L)				
WELDING PIN:	SA 479 (316L)				
WELDING NUT:	SA 479 (316L)				
WELDING BOLT:	SA 479 (316L)				
WELDING SCREW:	SA 479 (316L)				
WELDING WASHER:	SA 479				



Top fixture - 01

DRWG No.:



MACHINING INSTRUCTIONS

NUMBER OFF:

2

MATERIAL:

Nickel plated steel

THIRD ANGLE PROJECTION



TOLERANCES:
0: ±1
0.0: ± 0.5
0.00: ±0.05
(ANGULAR: ± 1°)

DEBUR AND
BREAK SHARP
EDGES
UNLESS OTHERWISE
SPECIFIED, ALL
DIMENSIONS IN mm

Property of EXOVA (UK) LTD. The document contains proprietary and confidential information which may not, without the prior written consent of EXOVA (UK) LTD., be used or reproduced in whole or in part, or communicated to any person not employed by EXOVA (UK) LTD.

SCALE: 1:2 SHEET 1 OF 4 A4

TITLE:

PART:

Inner span (top) assembly

DRWG No.:

Top fixture - 01

DRAWN

; 09/04/2010

LAST REVISED

ravier.o - 09/04/2010 11:55:11



1
Top fixture - 02

2
DRWG No.:

3

4

5

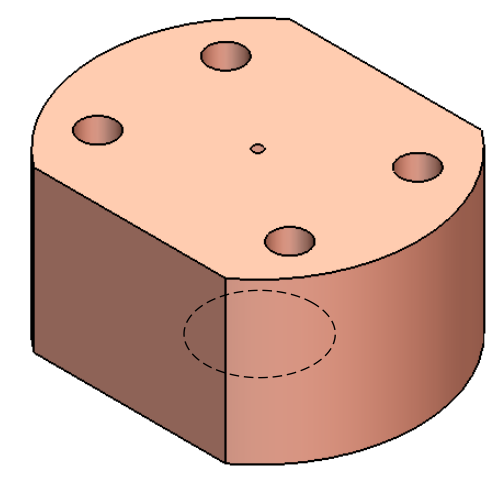
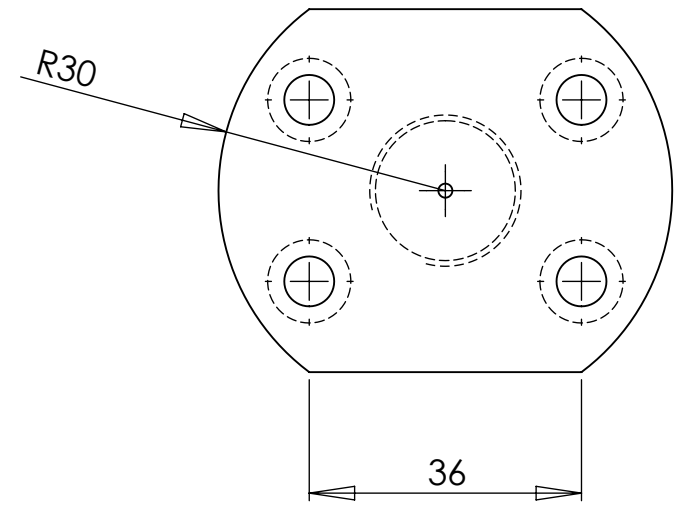
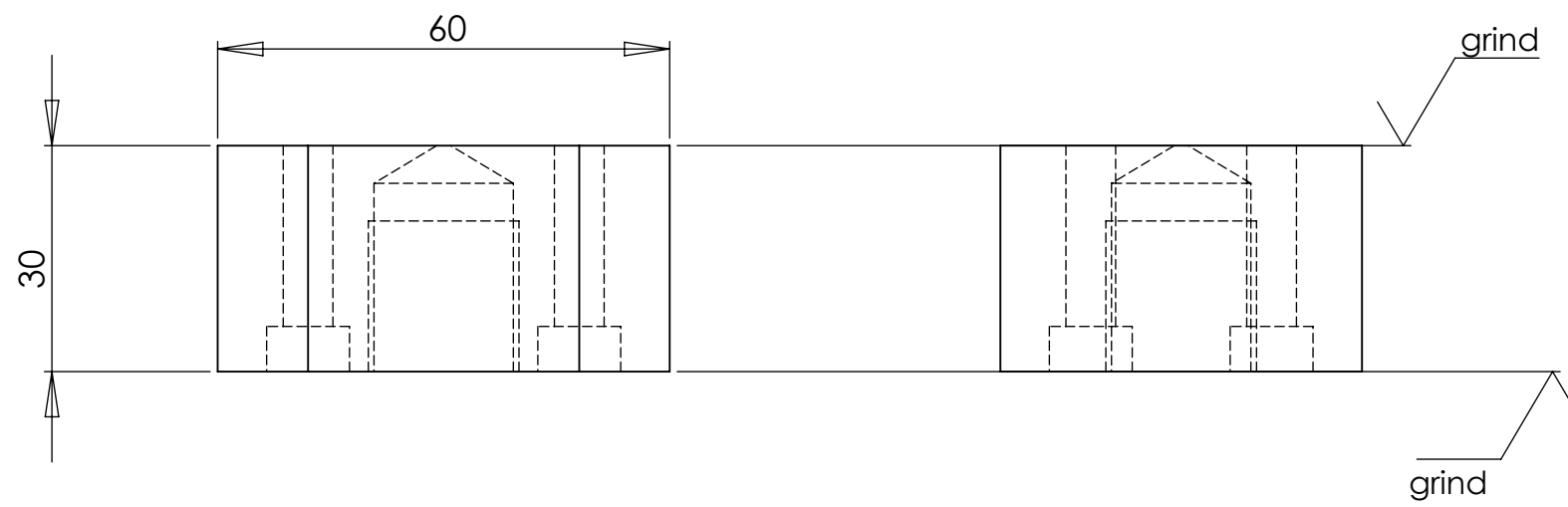
6

A

B

C

D



MACHINING INSTRUCTIONS

NUMBER OFF: **2**

MATERIAL: **Nickel plated steel**

THIRD ANGLE PROJECTION

TOLERANCES:
0: ±1
0.0: ±0.5
0.00: ±0.05
(ANGULAR: ±1°)

DEBUR AND BREAK SHARP EDGES UNLESS OTHERWISE SPECIFIED, ALL DIMENSIONS IN mm

Property of EXOVA (UK) LTD. The document contains proprietary and confidential information which may not, without the prior written consent of EXOVA (UK) LTD., be used or reproduced in whole or in part, or communicated to any person not employed by EXOVA (UK) LTD.

SCALE: 1:2	SHEET 2 OF 4	A4
TITLE:		
PART: Inner span rollers nut		
DRWG No.: Top fixture - 02		
DRAWN	: 09/04/2010	
LAST REVISED	ravier.o - 09/04/2010 11:55:11	

1

2

3

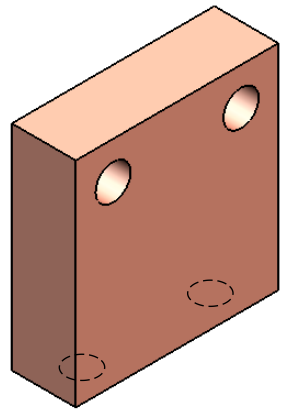
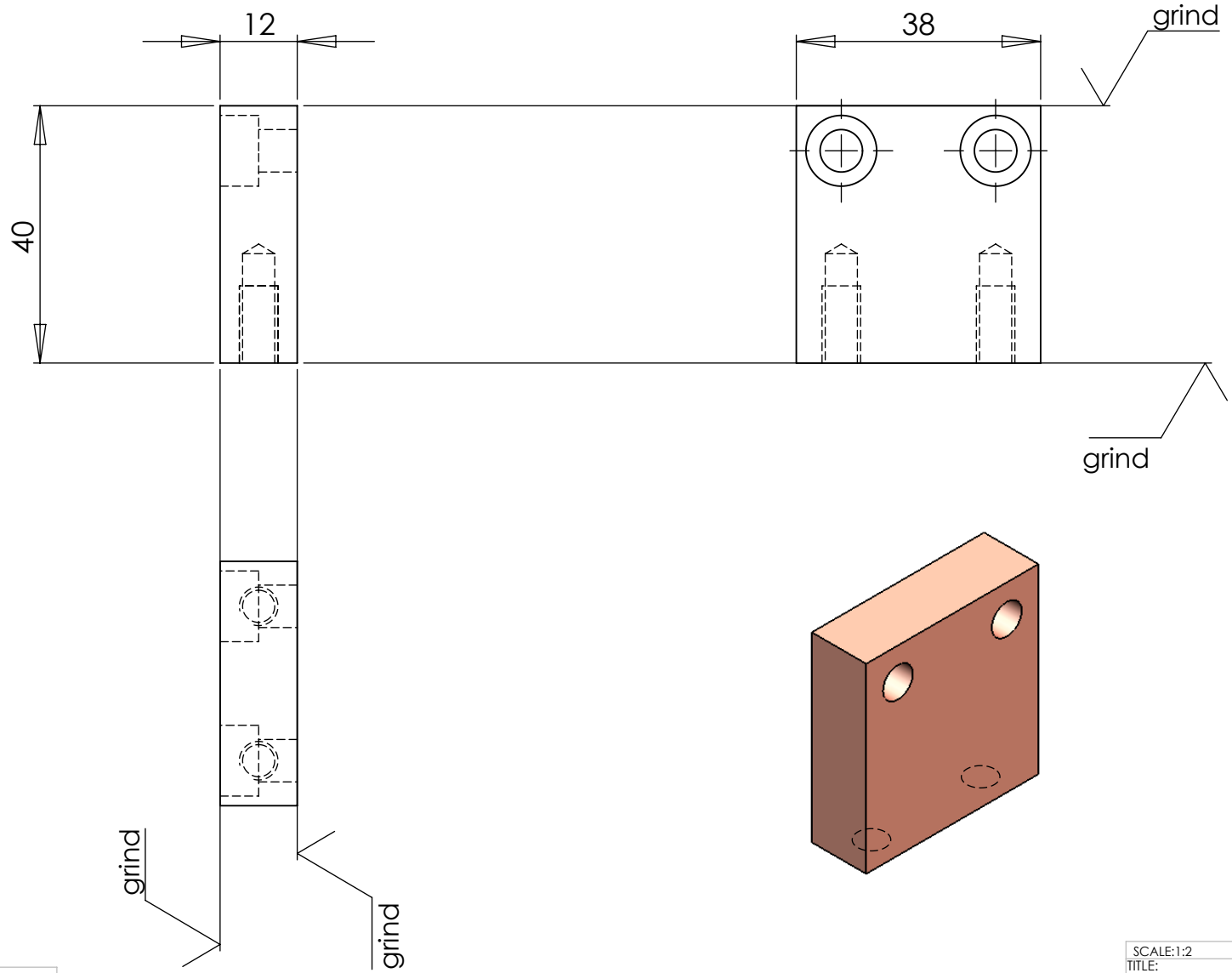
4

5

6



1 2 3 4 5 6
 Top fixture - 03 DRWG No.:



MACHINING INSTRUCTIONS

NUMBER OFF: **4** MATERIAL: Nickel plated steel

THIRD ANGLE PROJECTION

 TOLERANCES:
 0: ±1
 0.0: ± 0.5
 0.00: ±0.05
 (ANGULAR: ± 1°)
 DEBUR AND BREAK SHARP EDGES UNLESS OTHERWISE SPECIFIED, ALL DIMENSIONS IN mm

Property of EXOVA (UK) LTD. The document contains proprietary and confidential information which may not, without the prior written consent of EXOVA (UK) LTD., be used or reproduced in whole or in part, or communicated to any person not employed by EXOVA (UK) LTD.

SCALE: 1:2	SHEET 3 OF 4	A4
TITLE:		
PART: Inner span rollers side plates		
DRWG No.: Top fixture - 03		
DRAWN		: 09/04/2010
LAST REVISED		ravier.o - 09/04/2010 11:55:11

1 2 3 4 5 6



1
Top fixture - 04

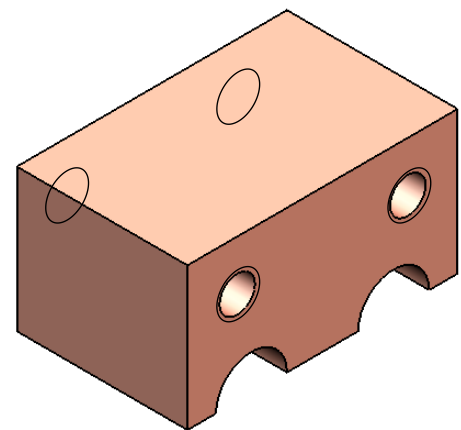
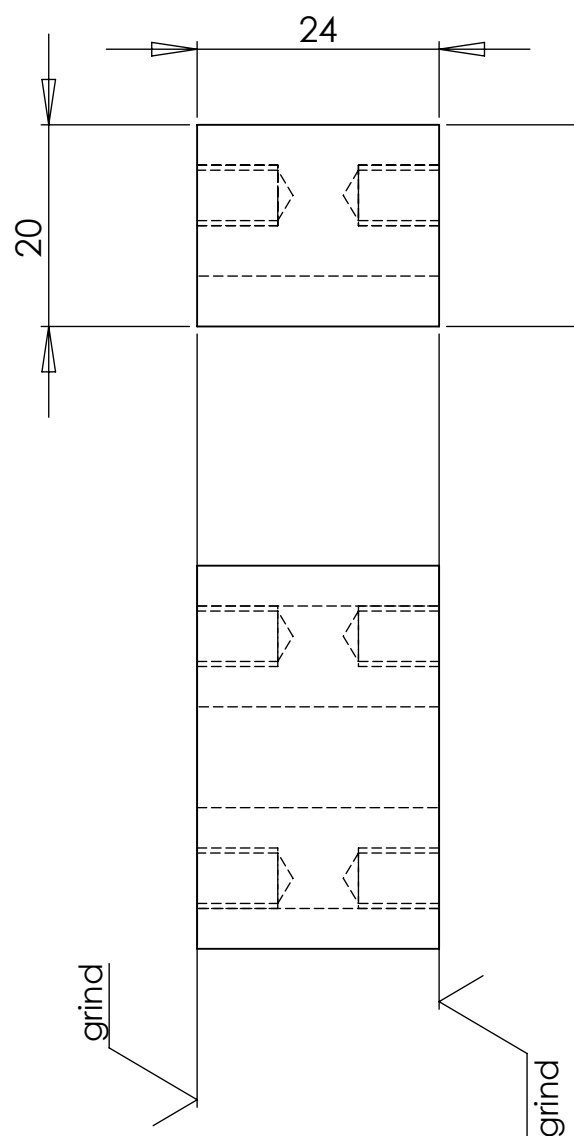
2
DRWG No.:

3

4

5

6



MACHINING INSTRUCTIONS

NUMBER OFF: **2**
MATERIAL: Nickel plated steel

THIRD ANGLE PROJECTION

 TOLERANCES:
 0: ±1
 0.0: ± 0.5
 0.00: ±0.05
 (ANGULAR: ± 1°)
 DEBUR AND BREAK SHARP EDGES UNLESS OTHERWISE SPECIFIED, ALL DIMENSIONS IN mm

Property of EXOVA (UK) LTD. The document contains proprietary and confidential information which may not, without the prior written consent of EXOVA (UK) LTD., be used or reproduced in whole or in part, or communicated to any person not employed by EXOVA (UK) LTD.

SCALE: 1:2	SHEET 4 OF 4	A4
TITLE:		
PART: Inner span rollers top plate		
DRWG No.: Top fixture - 04		
DRAWN	; 09/04/2010	
LAST REVISED	ravier.o - 09/04/2010 11:55:11	